FUNGAL PRIMARY AND SECONDARY METABOLISM AND ITS IMPORTANCE FOR VIRULENCE AND BIOMEDICAL APPLICATIONS

EDITED BY: Fernando Rodrigues, Laure Ries, Chengshu Wang and Koon Ho Wong

PUBLISHED IN: Frontiers in Microbiology and Frontiers in Fungal Biology

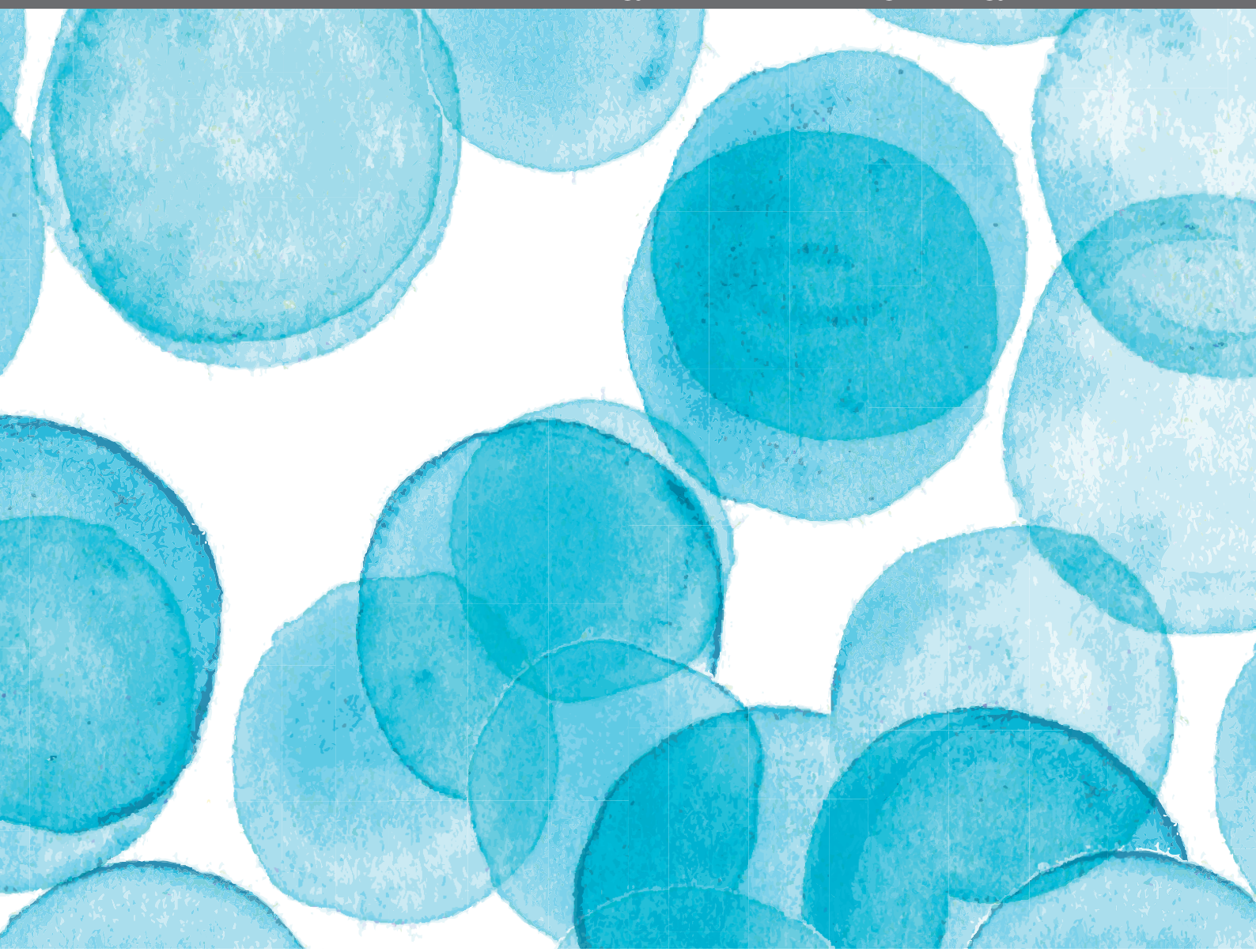

frontiers Research Topics

frontiers

ISSN 1664-8714
ISBN 978-2-88966-889-2
DOI 10.3389/978-2-88966-889-2

About Frontiers

Frontiers is more than just an open-access publisher of scholarly articles: it is a pioneering approach to the world of academia, radically improving the way scholarly research is managed. The grand vision of Frontiers is a world where all people have an equal opportunity to seek, share and generate knowledge. Frontiers provides immediate and permanent online open access to all its publications, but this alone is not enough to realize our grand goals.

Frontiers Journal Series

The Frontiers Journal Series is a multi-tier and interdisciplinary set of open-access, online journals, promising a paradigm shift from the current review, selection and dissemination processes in academic publishing. All Frontiers journals are driven by researchers for researchers; therefore, they constitute a service to the scholarly community. At the same time, the Frontiers Journal Series operates on a revolutionary invention, the tiered publishing system, initially addressing specific communities of scholars, and gradually climbing up to broader public understanding, thus serving the interests of the lay society, too.

Dedication to Quality

Each Frontiers article is a landmark of the highest quality, thanks to genuinely collaborative interactions between authors and review editors, who include some of the world's best academicians. Research must be certified by peers before entering a stream of knowledge that may eventually reach the public - and shape society; therefore, Frontiers only applies the most rigorous and unbiased reviews.
Frontiers revolutionizes research publishing by freely delivering the most outstanding research, evaluated with no bias from both the academic and social point of view. By applying the most advanced information technologies, Frontiers is catapulting scholarly publishing into a new generation.

What are Frontiers Research Topics?

Frontiers Research Topics are very popular trademarks of the Frontiers Journals Series: they are collections of at least ten articles, all centered on a particular subject. With their unique mix of varied contributions from Original Research to Review Articles, Frontiers Research Topics unify the most influential researchers, the latest key findings and historical advances in a hot research area! Find out more on how to host your own Frontiers Research Topic or contribute to one as an author by contacting the Frontiers Editorial Office: frontiersin.org/about/contact

FUNGAL PRIMARY AND SECONDARY METABOLISM AND ITS IMPORTANCE FOR VIRULENCE AND BIOMEDICAL APPLICATIONS

Topic Editors:
Fernando Rodrigues, University of Minho, Portugal
Laure Ries, University of São Paulo, Brazil
Chengshu Wang, Center for Excellence in Molecular Plant Sciences, Chinese Academy of Sciences (CAS), China
Koon Ho Wong, University of Macau, China

Citation: Rodrigues, F., Ries, L., Wang, C., Wong, K. H., eds. (2021). Fungal Primary and Secondary Metabolism and its Importance for Virulence and Biomedical Applications. Lausanne: Frontiers Media SA. doi: 10.3389/978-2-88966-889-2

Table of Contents

frontiers in Microbiology

ORIGINAL RESEARCH
published: 09 April 2020
doi: 10.3389/fmicb.2020.00610

New Insight Into Pathogenicity and Secondary Metabolism of the Plant Pathogen *Penicillium expansum* Through Deletion of the Epigenetic Reader SntB

Joanna Tannous[1†], Omer Barda[2†], Dianiris Luciano-Rosario[3], Dov B. Prusky[2,4], Edward Sionov[2] and Nancy P. Keller[1,5,6*]*

[1] Department of Medical Microbiology and Immunology, University of Wisconsin – Madison, Madison, WI, United States, [2] Institute of Postharvest and Food Sciences, The Volcani Center, Agricultural Research Organization, Rishon LeZion, Israel, [3] Department of Plant Pathology, University of Wisconsin – Madison, Madison, WI, United States, [4] College of Food Science and Engineering, Gansu Agricultural University, Lanzhou, China, [5] Food Research Institute, University of Wisconsin – Madison, Madison, WI, United States, [6] Department of Bacteriology, University of Wisconsin – Madison, Madison, WI, United States

OPEN ACCESS

Edited by:
Chengshu Wang,
Institute of Plant Physiology and Ecology (SIBS-CAS), China

Reviewed by:
Ana-Rosa Ballester,
Institute of Agrochemistry and Food Technology (IATA), Spain
Sandra Garrigues,
Westerdijk Fungal Biodiversity Institute, Netherlands

***Correspondence:**
Edward Sionov
edwardsio@volcani.agri.gov.il
Nancy P. Keller
npkeller@wisc.edu

[†] These authors have contributed equally to this work

Specialty section:
This article was submitted to Fungi and Their Interactions, a section of the journal Frontiers in Microbiology

Received: 21 January 2020
Accepted: 19 March 2020
Published: 09 April 2020

Citation:
Tannous J, Barda O, Luciano-Rosario D, Prusky DB, Sionov E and Keller NP (2020) New Insight Into Pathogenicity and Secondary Metabolism of the Plant Pathogen Penicillium expansum Through Deletion of the Epigenetic Reader SntB. Front. Microbiol. 11:610. doi: 10.3389/fmicb.2020.00610

Penicillium expansum is one of the most harmful post-harvest pathogens of pomaceous fruits and the causal agent of blue rot disease. During infection, *P. expansum* produces the toxic secondary metabolites patulin and citrinin that can impact virulence and, further, render the fruit inedible. Several studies have shown that epigenetic machinery controls synthesis of secondary metabolites in fungi. In this regard, the epigenetic reader, SntB, has been reported to govern the production of multiple toxins in *Aspergillus* species, and impact virulence of plant pathogenic fungi. Here we show that deletion of *sntB* in *P. expansum* results in several phenotypic changes in the fungus including stunted vegetative growth, reduced conidiation, but enhanced germination rates as well as decreased virulence on Golden Delicious apples. In addition, a decrease in both patulin and citrinin biosynthesis *in vitro* and patulin in apples, was observed. SntB positively regulates expression of three global regulators of virulence and secondary metabolism (LaeA, CreA, and PacC) which may explain in part some of the phenotypic and virulence defects of the PeΔ*sntB* strain. Lastly, results from this study revealed that the controlled environmental factors (low temperatures and high CO_2 levels) to which *P. expansum* is commonly exposed during fruit storage, resulted in a significant reduction of *sntB* expression and consequent patulin and citrinin reduction. These data identify the epigenetic reader SntB as critical factor regulated in post-harvest pathogens under storage conditions and a potential target to control fungal colonization and decaying of stored fruit.

Keywords: *Penicillium expansum*, epigenetic regulation, SntB, epigenetic reader, virulence, secondary metabolism, patulin, citrinin

INTRODUCTION

The ubiquitous fungus *Penicillium expansum* is the dominant post-harvest pathogen among fruits and vegetables, mainly pome fruits (Tannous et al., 2017a). Because of its ability to grow at low temperatures, *P. expansum* has also been associated with widespread spoilage of fruits during storage (Altunatmaz et al., 2012; Tannous et al., 2015). Besides the aesthetic aspect of its presence, contamination by *P. expansum* poses a health hazard due to the production of toxic secondary metabolites (mycotoxins) in contaminated fruit. Among the mycotoxins produced by *P. expansum*, the polyketide patulin is the most notable contaminant, given its long-established toxicity and prevalence during fruit infection (Puel et al., 2010; Tannous et al., 2017a). Citrinin is another polyketide mycotoxin reported to often co-occur with patulin on apples (Martins et al., 2002). This mycotoxin has been shown to be genotoxic and nephrotoxic (Flajs and Peraica, 2009). Due to the agricultural losses and serious health risks associated with the occurrence of these mycotoxins, a deeper understanding of what triggers their production is needed.

A few years ago, the complete genome sequence of *P. expansum* was unveiled by two research groups (Ballester et al., 2015; Li et al., 2015). Both papers provide new insights into secondary metabolism biosynthetic gene clusters, mainly those responsible for patulin and citrinin biosynthesis. Today, the biosynthetic pathways of patulin and citrinin synthesis are largely known (Artigot et al., 2009; Snini et al., 2014; Tannous et al., 2014, 2017b; He and Cox, 2016; Li et al., 2019). Recent studies were focused on the regulation of these two mycotoxins and other *P. expansum* secondary metabolites that could impact virulence and/or health hazards related to this pathogen. In this regard, the widely studied global regulator of secondary metabolism in fungi, LaeA, a member of the transcriptional Velvet Complex (Bayram et al., 2008), was shown to positively regulate patulin production (Kumar et al., 2016). Deletion of *laeA* in two *P. expansum* strains led to a significant decrease in patulin biosynthesis due to down-regulation of the expression of the patulin biosynthesis genes (Kumar et al., 2016). In contrast, citrinin biosynthesis was not subjected to *laeA* regulation in *P. expansum* (Kumar et al., 2016). Both patulin and citrinin synthesis were reduced as a result of deletion of *veA*, a second component of the Velvet Complex (El Hajj Assaf et al., 2018). Patulin was found to also be positively regulated by PacC, the pH regulatory transcription factor (Barad et al., 2014; Chen et al., 2018). Lastly, CreA, the carbon catabolite repressor has been reported to act as a positive regulator of both patulin and citrinin production (Tannous et al., 2018). In addition to their impact on secondary metabolism and some physiological traits, the loss of all these regulatory proteins resulted in attenuated virulence of *P. expansum* on apples (Kumar et al., 2016; El Hajj Assaf et al., 2018; Tannous et al., 2018).

In recent years, epigenetic and consequent histone post-translational modifications have been shown to play an important role in secondary metabolite production in fungi (Pfannenstiel and Keller, 2019), including regulation of several *Aspergillus* and *Fusarium* mycotoxins such as aflatoxin, fumonisin and trichothecenes (Visentin et al., 2012; Liu et al., 2015; Yang et al., 2016; Pfannenstiel et al., 2018). Most studies investigated the role of histone modifying enzymes, such as methylases or histone deacetylases in modulating secondary metabolite synthesis in fungi. However, more recently an additional histone modifying protein, the epigenetic reader SntB, was identified in *Aspergillus* species to regulate not only fungal development and secondary metabolism (Pfannenstiel et al., 2017) but also virulence in the aflatoxigenic fungus *A. flavus* (Pfannenstiel et al., 2018). SntB orthologs, called Snt2, had previously been described in the plant pathogens *Fusarium oxysporum* (Denisov et al., 2011) and *Magnaporthe oryzae* (He et al., 2018). These studies did not address the impact on secondary metabolism but found that the loss of *snt2* resulted in reduced virulence of both pathogens on their respective hosts. Additionally, both studies reported defects in autophagy-dependent cell death pathways in the *snt2* mutants.

To our knowledge, epigenetic control of mycotoxin production and virulence in *P. expansum* has not been addressed. Our work presents evidence that SntB regulates *P. expansum* development, patulin and citrinin production, and virulence on apples. SntB is a positive regulator of *laeA, creA,* and *pacC* expression, which may explain some of its impact on fungal biology. Moreover, this is the first report of epigenetic response(s) of a post-harvest pathogen to environmental stressors. Data from our study revealed a deregulation of *sntB* under low temperatures and high CO_2 levels, two conditions widely applied during fruit storage to limit *P. expansum* growth. These results allowed us to propose epigenetic responses as a potential modulator of virulence of storage pathogens.

MATERIALS AND METHODS

Strains and Growth Conditions

Penicillium expansum strain Pe-21 (also called Pe-d1) from Israel, was used to generate the Δ*ku70* knock-out strain that was used as the parental control strain for all subsequent experiments. Derivative strains from *P. expansum* Pe-21 are listed in **Supplementary Table S1**. Strains were cultivated in glucose minimal medium (GMM) at 25°C for 5 days to collect fresh spores. Conidia were collected and adjusted using a hemocytometer to the indicated concentrations. Screening of fungal transformants was done on sorbitol minimal medium (SMM) agar supplemented with the appropriate antibiotic (hygromycin or phleomycin at the respective concentrations of 100 and 50 μg/ml). For physiological experiments, GMM agar and broth were used. To screen for secondary metabolite production *in vitro*, strains were cultivated on four different agar media chosen to represent a broad range of nutrient source, which are: Potato Dextrose Agar (PDA), Yeast Extract Sucrose Agar (YES), Czapek Yeast Extract Agar (CYA) and GMM, at 25°C for 10 days. Each medium was prepared as shown in **Supplementary Table S2**.

Plasmid and Strain Construction and Confirmation

Competent cells of the yeast strain BJ5464 (*MATalpha*, *ura3-52*, *trp1*, *leu2-*Δ*1*, *his3-*Δ*200*, *pep4:HIS3*, *prb1-*Δ*1.6R*, *can1*, *GAL*) were used to facilitate appropriate plasmid construct assembly. The plasmids used in this study are listed in **Supplementary Table S3**.

Construction of the ku70 Gene Deletion Cassette

In our recent work, a Δ*ku70* strain of *P. expansum* Pe-21 was generated using hygromycin as a selectable marker (Tannous et al., 2018). Here a new *P. expansum* Δ*ku70* was created to allow recycling of the hygromycin resistance gene that can be re-used as a selectable marker in future transformations. The new *P. expansum* Δ*ku70*, hygromycin sensitive (Hyg^S) strain, termed TJT14.1, was constructed by employing the β-Rec/six site-specific recombination system described by Hartmann et al. (2010). The hygromycin recyclable marker used to construct the Δ*ku70* strain is based on site-specific recombination that allows repetitive gene targeting. The elements of the self-excising β-rec/*six* blaster cassette are shown in **Supplementary Figure S1A**. The Δ*ku70* knockout cassette was constructed using yeast recombination cloning (Wiemann et al., 2018). The three fragments (5′flank Ku70- hygromycin resistance cassette and 3′flank Ku70) were assembled into the pYHC-WA-pyrG plasmid. The plasmid was linearized by PCR using primers YS_F and YS_R (**Supplementary Table S4A**). After yeast recombinational cloning, the plasmid pJT1 was created and recovered from yeast DNA by transforming into *E. coli*. The nested primers Pe_KOKu70_NestedF and Pe_KOKu70_NestedR were used to amplify the entire deletion cassette from plasmid pJT1 using the Long Template Expand PCR System (Roche, Indianapolis, IN, United States). PCR reactions were performed according to the manufacturer's instructions, and the construct was eluted with a QIAquick PCR Purification Kit (Qiagen, Hilden, Germany). This construct was used to transform protoplasts of the parental strain Pe-21 (Barad et al., 2016b).

Construction of sntB Gene Deletion and Complementation Cassettes

The predicted sequence for the *P. expansum sntB* ortholog was obtained from GenBank (XM_016748327) by conducting a BLAST search with the *A. flavus sntB* gene sequence (AFLA_029990) against the *P. expansum* genome scaffolds. The generated Hyg^S Δ*ku70* strain, TJT14.1, was used to delete the *sntB* gene using the phleomycin resistance gene *ble* as a selectable marker (Silar, 1995). The resultant deletion strain was called TJT15.1. The schematic representation of the *sntB* gene replacement with the *ble* gene is depicted in **Supplementary Figure S2A**. The three amplified fragments (5′flank *sntB*, *ble* gene, and 3′flank *sntB*) were assembled using a double joint PCR protocol described by Lim et al. (2012). To confirm that the phenotype exhibited by the Δ*sntB* strain is caused by the deletion of this specific gene, TJT15.1 was complemented with a wild-type copy of the *sntB* gene using hygromycin as selectable marker to create TJT17.1. *Not*I and *Bsrg*I restriction sites introduced respectively at the predicted promoter and terminator of the *sntB* gene, using primers Pe_sntBcomp_F and Pe_sntBcomp_R, were used to subclone *sntB* downstream of the *hph* gene into the pJT1 plasmid (**Supplementary Figure S3A**). The ligation of the digested insert into the recipient plasmid was performed using the T4 DNA ligase from New England Biolabs, according to the manufacturer's instructions. The ligation reaction was later transformed into *E. coli* DH5alpha competent cells following the manufacturer's directions (Thermo Fisher Scientific). Five bacterial colonies were picked and screened for successful ligations by conducting a diagnostic restriction digest with the same enzymes used for the cloning. The correct plasmids were then grown in 50 ml LB supplemented with ampicillin (100 μg/ml), and the plasmid DNA was isolated using Quantum Prep® Plasmid Midiprep Kit (Biorad) according to the manufacturers' instructions. Ten micrograms of plasmid DNA was used for the transformation of the Δ*sntB* strain. The plasmid was linearized using *swa*I prior to fungal transformation.

Protoplast Transformation

To generate the different deletion and complement strains, the fungal transformation was performed following the polyethylene glycol-mediated protoplast transformation protocol described previously by Tannous et al. (2018). All transformants were screened by PCR and further subjected to southern blot to confirm the single insertion of the deletion cassette using [α32P] dCTP (PerkinElmer, United States) to label the DNA probes, following manufacturer's instructions. In order to recycle the *hph* resistance cassette and gain back the sensitivity to hygromycin B in the Δ*ku70* strain generated in this study, deletion strains were grown on minimal medium amended with 2% xylose to activate the ß-recombinase placed under the xylose-inducible promoter. The confirmation of the hygromycin sensitivity was done on GMM hygromycin plates and by PCR targeting the *hph* gene. Primers used for constructing the deletion cassettes, molecular cloning and mutants' confirmation are listed in **Supplementary Table S4A**.

Physiological Analysis

Both vegetative growth and conidial production were assessed on GMM agar. To measure the radial mycelial growth, agar plates were point-inoculated with 10^6 spores of each strain and incubated at 25°C. Radial growth was monitored by diameter measurements in the four cardinal directions. Measurements were recorded on alternate days for a 6 day period.

To quantify total conidia produced by the various strains, GMM top agar (0.7% (w/v) agar) containing 10^6 spores was overlaid on agar plates of the same media (20 ml) and incubated at 25°C in the dark. To accurately count conidia, 2 cm plugs from each plate were homogenized in 3 ml of 0.01% Tween 20 water, diluted and enumerated with a hemocytometer. Conidial production was quantified starting by the second day post-inoculation using three replicate plates per strain.

Germination assays were performed in sterile 12-well culture plates. The spore concentration of all strains was adjusted to 10^5 spores/ml in GMM broth, and one milliliter of each spore suspension was distributed into 3 replicate wells. Time-course microscopy was carried out over 24 h at 25°C using a Nikon Ti inverted microscope. Germination rate was monitored regularly by capturing images of each well hourly, beginning 4 h post-incubation. A number of spore germlings was counted for each strain and recorded. The percent of germinated spores was plotted against time, and the germination rates were determined.

Evans Blue Staining

Liquid cultures of *P. expansum* strains were grown in GMM supplemented with Yeast Extract (YE). The 25 ml cultures were inoculated using 10^8 spores and incubated for 14 h at 25°C under

250 rpm. After incubation, mycelia were harvested in 50 ml tubes and washed twice with Dulbecco's Phosphate-Buffered Saline (DPBS) lacking calcium and magnesium (Life Technologies, Carlsbad, CA, United States). For the negative control, mycelia were incubated at 100°C for 45 min before proceeding with the protocol. Mycelia were later incubated at 37°C for 10 min in a 0.1% Evans Blue (Sigma Aldrich, St Louis, MO, United States) solution. After incubation, three wash steps were performed using DPBS again. Samples were mounted using Ibidi mounting Medium (Ibidi, Fitchburg, WI, United States).

Imaging and Analysis

Fluorescence microscopy was performed using Axio Imager A10 Microscope EC Plan-NEOFLUAR 40x/1.3 Oil DIC/∞/0.17 objective and a series 120 X-Cite R light source (EXFO) (Olympus Corporation, Shinjuku, TYO, Japan). Micrographs were acquired using the DIC (Differential Interphase Contrast) and TRITC (Tetramethylrhodamine) channels with uniform exposure settings for all samples: 6 ms for the DIC channel and 40 ms for the TRITC channel. The mean gray value area per hyphae of 10 micrographs per strain was calculated using Fiji (Schindelin et al., 2012).

RNA Isolation and qRT-PCR Analyses

Cultures intended for RNA isolation were grown on sterile 0.45 μm nitrocellulose membrane circles (Whatman, Kent, United Kingdom) placed on top of solid YES medium (20 g bacto yeast extract, 150 g sucrose, 15 g bacto agar per liter). A 10^6 fungal spores/ml solution (100 μl) was inoculated onto 55 mm petri dishes containing 10 ml of media. To test the impact of abiotic stressors, the plates were incubated at 28°C for 48 h in the dark and then transferred to the appropriate stress conditions for additional 48 h. For comparison between the WT, Δ*sntB* and complement strains, the plates were grown at 28°C for 4 days. After incubation, total RNAs were extracted from 100 mg of lyophilized mycelia using the Hybrid-R RNA isolation kit (GeneAll, Seoul, South Korea) according to the manufacturer protocol. The DNase and reverse-transcription reactions were performed on 1 μg of total RNA with the Maxima First-Strand cDNA Synthesis Kit (Thermo Fisher Scientific, Waltham, MA, United States) according to the manufacturer protocol. The cDNA samples were diluted 1:20 (v/v) with ultrapure water. Real time quantitative PCR was performed with the StepOnePlus system (Applied Biosystems, Waltham, MA, United States). PCR amplifications were performed with 3 μl of cDNA template in 10 μl of a reaction mixture containing 7 μl mix from the Fast SYBR green Master Mix (Applied Biosystems, Waltham, MA, United States) and 200 nM primers. PCRs were carried out with the following cycling program: 20 s at 95°C, followed by 40 cycles of 95°C for 3 s and 60°C for 20 s. The samples were normalized using β-*tubulin* gene (PEXP_025370) as endogenous control and the relative expression levels were measured using the $2^{(-\Delta\Delta Ct)}$ analysis method (Livak and Schmittgen, 2001). Primers used for qRT-PCR analyses are listed in **Supplementary Table S4B**. Results were analyzed with StepOne software v2.3.

Mycotoxin Analysis

Agar plugs with fungal mycelia from gene expression experiments were used to evaluate mycotoxin production. For patulin analysis, 1 g agar was added to 2 ml of HPLC grade ethyl acetate (Bio-Lab, Jerusalem, Israel) and crushed to homogeneity. Patulin was extracted by shaking for 30 min at 150 RPM on an orbital shaking platform. The supernatant was transferred to a clean glass tube and was evaporated to dryness under a stream of gaseous nitrogen at 50°C. The residues were re-dissolved in 1 ml of the mobile phase (0.02 M ammonium acetate:acetonitrile 9:1), filtered through a 0.22 μm PTFE syringe filter (Agela Technologies, Tianjin, China) and kept at −20°C prior to HPLC analysis. For citrinin analysis, 1 g agar plug with fungal mycelia was added to 1 ml of methanol and crushed. The mycotoxin was extracted by shaking for 30 min at 150 RPM and centrifuged for 10 min at 6000 × g. The supernatant was filtered through a 0.22 μm PTFE syringe filter and kept at −20°C prior to HPLC analysis. The citrinin mobile phase consisted of acidified water (adjusted to pH 2.5 with acetic acid) and acetonitrile (50:50). Both mycotoxins were quantitatively analyzed by injection of 20 μl into a reverse phase UHPLC system (Waters ACQUITY Arc, FTN-R, Milford, MA, United States) using a Kinetex 3.5 μm XB-C18 (150 × 4.6 mm) column (Phenomenex, Torrance, CA, United States). The column temperature was maintained at 30°C and the flow rate was 1 ml/min. The patulin peak was detected with a photodiode array (PDA) detector at 280 nm; citrinin was detected with a fluorescence detector (331 nm excitation, 500 nm emission). Both mycotoxins were quantified by comparing with a calibration curve of the standard mycotoxins (Fermentek, Jerusalem, Israel).

Virulence Assessment of *P. expansum* Strains

SntB deletion and complement mutants confirmed by Southern blot analysis were tested on apples cv. Golden Delicious, obtained from a local orchard, to evaluate the role of *sntB* in the virulence process of *P. expansum*. As described previously by Tannous et al. (2018), apples were surface sterilized with 2% sodium hypochlorite solution and thoroughly rinsed with sterile distilled water. A single uniform 5 mm deep wound was made at the equator of each apple (put on its side) using sterile toothpicks. For each strain, 10 μl of a spore suspension at a concentration of 10^8 spores/ml were deposited into the wound. Apples were incubated at 25°C in the dark for 11 days. The diameter of the rotten spots were recorded every other day. Three technical replicates were performed for each strain, and the entire experiment was repeated twice for confirmation of the observed results. At the end of the incubation period, patulin was extracted from apples and quantified by HPLC as described earlier by Tannous et al. (2018). Moreover, to eliminate the effect of variability between apples and to compare the fruit colonization, the three strains (control, Δ*sntB*, and *sntB*C) were inoculated twice on the same apple. Six technical replicates were performed and the whole experiment was repeated three times for confirmation of the observed results. Representative images were taken 5 days post-inoculation.

Statistical Analyses

For all experiments, values are stated as the mean ± standard error of the mean (SEM) of three independent replicates unless otherwise indicated. The statistical analysis of the data was performed using the one-way ANOVA. If one-way ANOVA reports a p value of < 0.05 further analyses were performed using Tukey's single-step multiple comparison test to determine significant difference between the strains. Analyses were done using R Studio (R Studio Team, 2015, Boston, MA, United States) and GraphPad Prism software (GraphPad, San Diego, CA, United States).

RESULTS

Multi-Species Comparison of SntB Protein Sequences

The deduced amino acid sequence of SntB in *P. expansum* (XP_016595169) showed a high degree of identity with orthologous sequences from species of *Aspergillus* (ranging from 60 to 64%), whereas a lower percentage of identity was scored with the orthologous sequences from *M. oryzae* (around 46%) and *F. oxysporum* (around 42%). The sequence identity with the Snt2 of *Saccharomyces cerevisiae* was even lower (around 32%), and therefore it was excluded from the multisequence alignment. Alignment of deduced amino acid sequences of SntB revealed the presence of five highly conserved domains (boxes A–E) that are considered to be essential for the activity of this protein (**Supplementary Figure S4**). The first conserved domain (box A) consists of the Bromo adjacent homology (BAH) domain that may be involved in protein-protein interaction specialized in gene silencing (Callebaut et al., 1999). Box B carries the first plant homeodomain (PHD) finger which is a C_4HC_3 zinc-finger-like motif thought to be involved in epigenetics and chromatin-mediated transcriptional regulation (Aasland et al., 1995; Fair et al., 2001). The third domain (box C) contains the SANT (SWI3, ADA2, N-CoR, and TFIIIB) DNA-binding domains, belonging to a various set of proteins that share a common 3 alpha-helix bundle. Recent studies suggested that SANT domains might be a histone-tail-binding module (Boyer et al., 2004). In boxes D and E, are found two other plant homeodomain (PHD) fingers.

Strains Construction and Validation by Southern Blotting Analysis

To identify the Hyg^S Δ*ku70:hph* transformants, fifty colonies obtained using the pJT1 vector were found resistant to hygromycin. Monosporic transformants were further checked by direct specific PCR analysis targeting the *ku70* gene using the primer set Pe_Ku70orf_F and Pe_Ku70orf_R. Amplification of the ORF was not observed in twenty three transformants, which were then analyzed by southern blotting. Only five out of twenty three transformants showed a single insertion of the cassette at the *ku70* locus. To recycle the *hph* resistance cassette and gain back the sensitivity to hygromycin B, these five transformants were grown on minimal medium amended with 2% xylose. Four of these transformants were not able to grow on plates supplemented with hygromycin B after this treatment. The absence of *hph* gene was further confirmed by PCR using the primer set hph_F and hph_R (data not shown). A single Δ*ku70*, Hyg^S strain labeled TJT14.1 was used for the following experiments as a control strain. Southern blot confirmation for the selected Δ*ku70* is shown in **Supplementary Figure S1B**.

To determine the effects of *sntB* on growth, conidiation, and other cellular processes, *sntB* deletion (*Pe*Δ*sntB*) and complementation strains were generated. For *sntB* deletion, ten single transformants were initially selected on SMM agar supplemented with phleomycin (50 μg/ml). The phleomycin resistant strains were later confirmed by PCR for the absence of the ORF amplification (data not shown) and subjected to a final confirmation by southern blot analysis using probes specific for flanking regions of the *sntB* gene (**Supplementary Figure S2B**). Two DNA fragments of 1216 and 1189 kb corresponding respectively to the 5′ and 3′flanking regions of *sntB* were used to generate the radioactive probes utilized in this hybridization. Genomic DNA from both the control and *Pe*Δ*sntB* strains were digested separately with *Eco*RI and *Ban*II. The presence of 5.4 and 2.5 kb bands in the Southern blot analysis confirmed the *sntB* deletion, while 4.2 and 1.6 kb bands corresponded to the control (**Supplementary Figure S2B**). One of the correct *Pe*Δ*sntB* deletion strains was used for the following experiments and was called TJT15.1.

With respect to the *sntB* complement strain, diagnostic PCR was performed to confirm the integration of the wild type allele in the Δ*sntB* strain using the same set of primers that amplify the *sntB* ORF (data not shown). The positive strains were later subjected to southern blot analysis using the *sntB* gene as a probe (**Supplementary Figure S3B**). Genomic DNA from both *sntB* deletion and complement strains were digested with *Not*I and *Bsrg*I. As expected, the Δ*sntB* strain did not show any band, whereas the *sntBc* strain revealed the expected band of 6.3 kb (**Supplementary Figure S3B**). One of the correct *sntBc* strain was used for the following experiments and was labeled TJT17.1.

P. expansum Δ*sntB* Is Aberrant in Spore Production, Germination, and Growth Morphology

The impact of *sntB* deletion on *P. expansum* physiology was evaluated by virtue of four different determinants: pigmentation, radial growth, spore production and germination rate. Visual observation of growth plates showed distinct pigmentation patterns correlating with *sntB* loss on all media examined after 72 h of growth at 25°C (**Figure 1A**). Radial growth data collected on GMM agar after 6 days of culture at 25°C revealed a significant reduction of growth diameter when *sntB* is deleted in *P. expansum* (**Figure 1B**). While the Δ*sntB* strain (TJT15.1) reached an approximate growth diameter of 25 mm, the control strain (TJT14.1) grew to an area of 30 mm, 6 days post-inoculation. However, the *sntB* complement strain (TJT17.1) was 1 mm greater in growth diameter compared to the control strain at the end of the incubation period (**Figure 1B**). A similar pattern

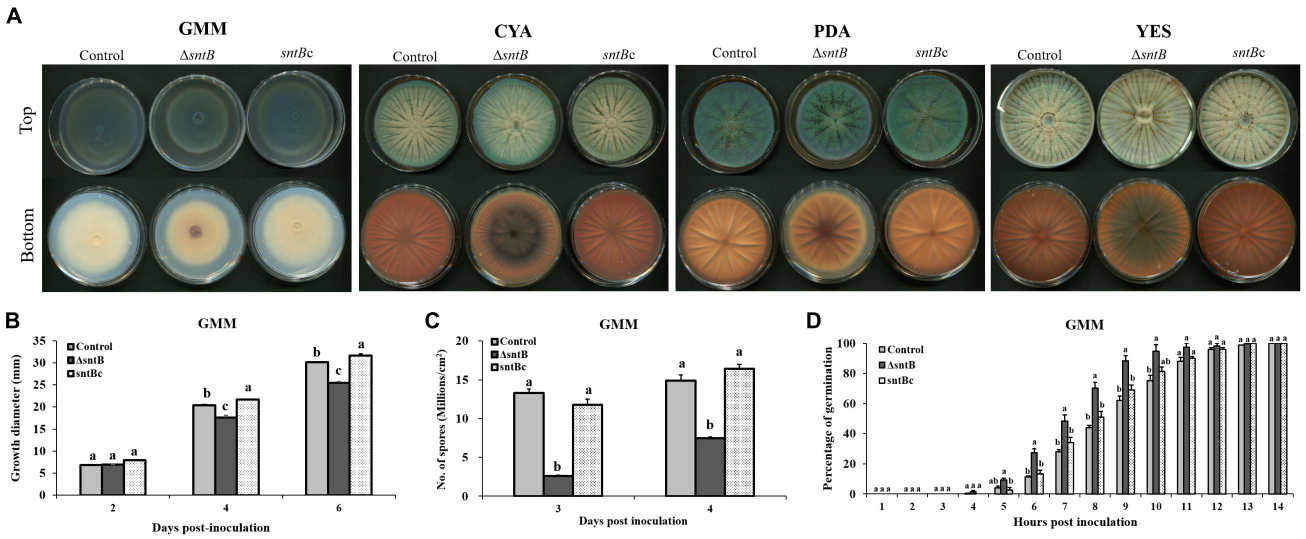

FIGURE 1 | Physiological analysis of the control, *sntB* deletion and complement strains of *P. expansum* Pe-21. **(A)** Growth phenotype of *P. expansum* strains monitored on four different media (GMM, Glucose Minimal Medium; CYA, Czapek Yeast Extract Agar; PDA, Potato Dextrose Agar; YES, Yeast Extract Sucrose Agar) for 72 h at 25°C. **(B)** Radial growth, **(C)** conidia production were monitored on GMM agar, and **(D)** germination rate of *P. expansum* strains was measured on GMM broth. One-way ANOVA differences were considered significant when $p < 0.05$. Different letters above the columns indicate statistically significant differences between the strains as determined using Tukey's single-step multiple comparison test.

was observed on the three other tested media (**Supplementary Figures S5A–C**). Sporulation data gathered on the second and third days post-inoculation on GMM agar showed decreased spore production by the Δ*sntB* mutant compared to both the control and the *sntB* complement strains (**Figure 1C**). It remains unclear if the reduced spore count in the Δ*sntB* strain is due to growth impairment. However, the *Pe*Δ*sntB* mutant spores showed a faster germination rate compared to the control strains, starting 4 h post-inoculation. All strains reached equivalent germination rates 11 h post-inoculation (**Figure 1D**).

SntB Does Not Affect Cell Viability *in vitro*

Other studies have reported SntB homologs to be involved in autophagy mediated programed cell death (Denisov et al., 2011; He et al., 2018). To investigate if *P. expansum* SntB plays a role in cell death pathways, we first assessed *in vitro* cell viability of WT, Δ*sntB*, and *sntB* complement strains using Evans Blue Dye (**Supplementary Figure S6A**). Dead cells are permeable to this dye. Moreover, this staining fluoresces upon excitation with green light providing the opportunity to have quantitative data. After quantification and comparison of fluorescence using the average mean gray area for 10 micrographs per strain, we found no significant difference in cell viability between the assessed samples (**Supplementary Figure S6B**).

SntB Modulates Mycotoxin Biosynthesis

Loss of *sntB* resulted in significant reduction of patulin and citrinin levels in the mutant strain compared to the control strain when grown in YES media (**Figures 2A,B**). To determine if the changes in patulin and citrinin levels were correlated with transcript levels, the expression levels of selected biosynthetic genes in both patulin and citrinin gene clusters were analyzed and compared between the control, *sntB* deletion and complement strains. Comparison of gene expression between the control and Δ*sntB* mutant revealed that deletion of *sntB* resulted in a reduced expression level of the specific transcription factor of the patulin gene cluster, *patL*, and the polyketide synthase (PKS) gene, *patK* (**Figure 2C**). Similarly, *sntB* deletion resulted in a significant reduction of the expression level of the citrinin gene cluster transcription factor, *ctnA*, and *citC*, which encodes an oxidoreductase in citrinin biosynthetic pathway (**Figure 2D**). Production of both mycotoxins was recovered by the complement strain, although not to the level of the control strain, which was in agreement with gene expression analysis (**Figures 2A–D**). These results were not totally unexpected considering that previous publications have reported similar outcomes, where the complement strains partially restored the parental phenotype (Carvalho et al., 2010; Kwon et al., 2011; Pfannenstiel et al., 2017).

Moreover, we also asked if loss of *sntB* influenced expression of regulatory genes known to regulate both metabolites. Expression of *creA* encoding the transcription factor regulating carbon catabolite repression (Tannous et al., 2018), *pacC* encoding the pH regulatory transcription factor (Chen et al., 2018) and *laeA* encoding a methyltransferase involved in global regulation of fungal secondary metabolism (Kumar et al., 2016), were markedly downregulated in the knockout strain (>2-fold, $p < 0.001$) (**Figure 2E**). Overall, the complement strain expressed similar levels of the global regulatory genes compared to the control strain (**Figure 2E**).

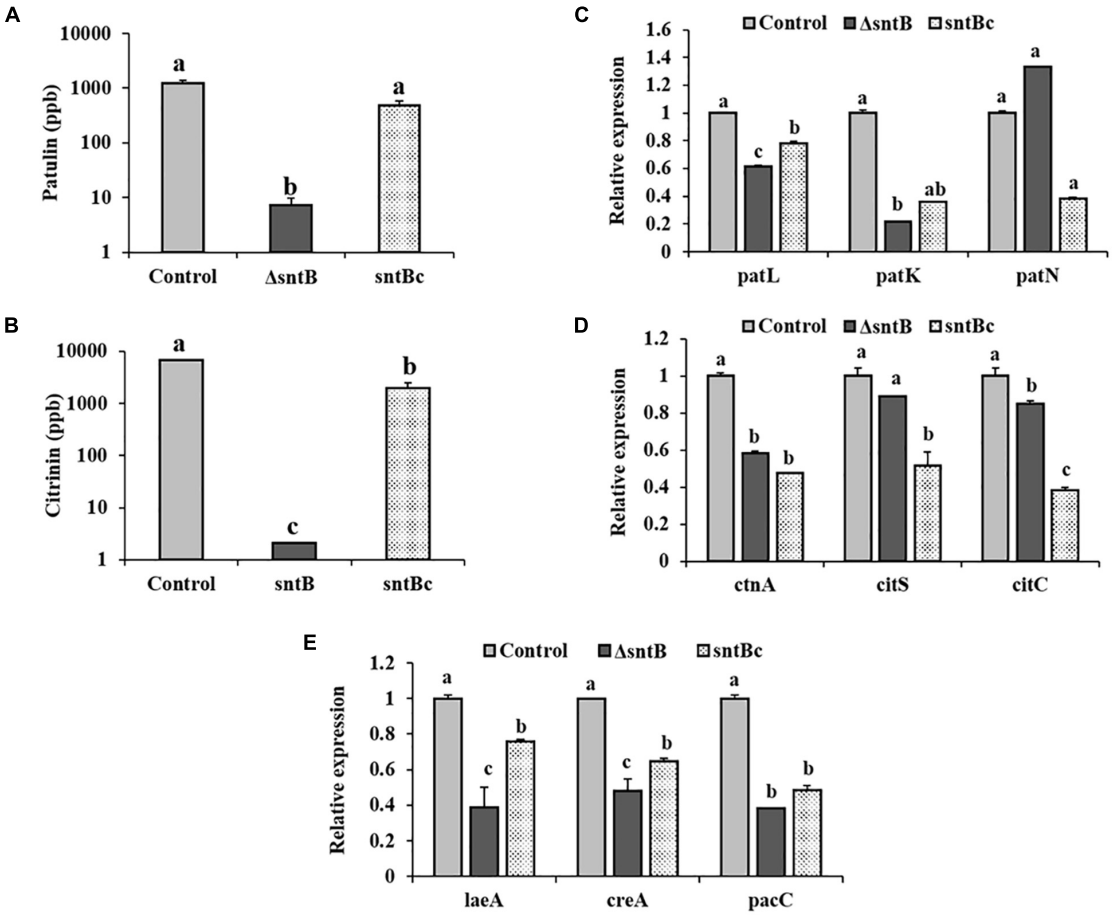

FIGURE 2 | SntB-associated regulation of patulin and citrinin biosynthesis. The three *Penicillium* strains (control, Δ*sntB*, and *sntB*c) were grown on solidified YES media at 28°C. Patulin **(A)** and citrinin **(B)** levels, relative expressions of patulin **(C)** and citrinin cluster genes **(D)**, and global transcription factors **(E)** were evaluated at 4 days post-inoculation. Error bars represent the standard error of the mean (SEM) across three technical replicates. One-way ANOVA differences were considered significant when $p < 0.05$. Different letters above the columns indicate statistically significant differences between the strains as determined using Tukey's single-step multiple comparison test.

SntB Deletion Mutant Exhibits Reduced Virulence and Patulin Production on Apples

Next, we analyzed the ability of the *Pe*Δ*sntB* mutant to infect apple cv. Golden Delicious. Apple fruits were inoculated with a conidial suspension of Δ*sntB, sntB*c, and the *P. expansum* control strains. Lesion development was monitored every 2 days, and the diameter was measured. As shown in **Figures 3A,B**, *sntB* disruption resulted in a significant reduction of decay development as the lesion diameter caused by Δ*sntB* was about 37% smaller than that of the control and *sntB* complement strains on day 11 post-inoculation. Similar to the results described *in vitro*, the production of patulin by the Δ*sntB* mutant was significantly reduced compared to the control and the *sntB* complement strain on apples (**Figure 3C**). As described in our previous work (Tannous et al., 2018), citrinin was not detectable on apples.

sntB and Subsequent Patulin and Citrinin Synthesis Is Regulated by Storage Environments

To gain an understanding on how SntB itself may be regulated and possibly affect subsequent patulin and citrinin synthesis in conditions associated with fruit storage, we assessed the impact of temperature, light and CO_2 levels on gene expression and mycotoxin synthesis. qRT-PCR analyses showed a significant downregulation of *sntB* when *P. expansum* was exposed to high CO_2 levels and low temperatures (18 and 5°C) (**Figure 4A**). Metabolite analysis showed that patulin and citrinin levels were reduced after incubation at 5°C and high CO_2, while their synthesis was significantly upregulated under continuous white light (**Figures 4B,C**). Interestingly, incubation of the control strain at 18°C resulted in a dramatic increase in patulin accumulation of more than 130 ppm compared to 1.2 ppm at 28°C (control condition). In contrast, citrinin production

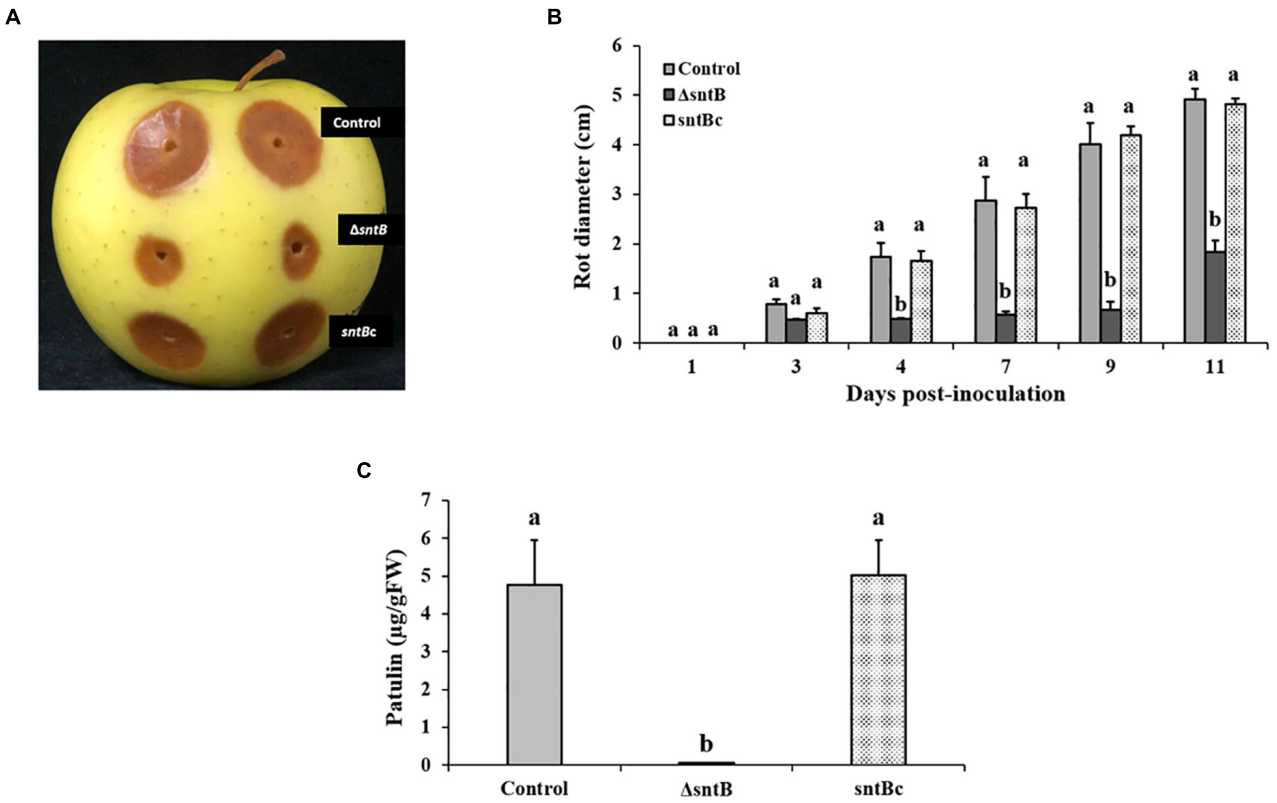

FIGURE 3 | SntB is required for *P. expansum* pathogenicity and patulin production on apples. **(A)** Apples were inoculated with 10^6 spores and incubated at 25°C in the dark for 5 days. **(B)** Histogram showing the rot diameter on apples inoculated with the three *Penicillium* strains (control, Δ*sntB*, *sntB*c). **(C)** Histogram displaying patulin production on apples analyzed by HPLC. Each strain was inoculated with 3 reps. One-way ANOVA differences were considered significant when $p < 0.05$. Different letters above the columns indicate statistically significant differences between the strains as determined using Tukey's single-step multiple comparison test.

by the control strain was markedly inhibited at 18°C to a concentration of 0.014 ppm compared to 6.8 ppm under control condition (**Figures 4B,C**). The *sntB* deletion strain produced significantly lower amounts of both mycotoxins compared to the control strain, while their accumulation was recovered by the complement strain, under all tested conditions (**Figures 4B,C**). A similar pattern was observed for the relative expression of the two key genes in the patulin biosynthetic pathway, *patK* and *patN* (**Figure 5A**). However, the transcript level of the patulin specific transcription factor (*patL*) was significantly decreased at 18°C and under white light, in contrary to the aforementioned increase of the mycotoxin level under the same conditions. The expression levels of the citrinin transcription factor (*ctnA*) and another two keys genes involved in citrinin biosynthesis (*citS* and *citC*) correlated with the mycotoxin production under all tested conditions except white light, under which a downregulation of the tested genes was observed (**Figure 5B**).

DISCUSSION

Due to its cytotoxic, genotoxic and teratogenic properties, its wide presence in fruits and its virulence-associated function (Snini et al., 2015), patulin synthesis by the fruit pathogen *P. expansum* has been the topic of research of many studies resulting in an excellent understanding of the biosynthetic pathway of this mycotoxin (Li et al., 2019). Emphasis has also been recently focused on citrinin, another nephrotoxic mycotoxin of *P. expansum*, reported to often co-occur with patulin (Gimeno, 2005). The biosynthetic steps leading to citrinin and the gene cluster responsible for its production are currently known (He and Cox, 2016; Schmidt-Heydt et al., 2019). Yet, the regulatory pathways underlying the production of both mycotoxins are still not completely resolved, and concurrent research is dedicated to expanding current knowledge.

This paper reports on the identification of a new protein in *P. expansum* that adds to the short list of proteins recognized to play a role in the virulence of this pathogen (Barad et al., 2016a; Kumar et al., 2016; Chen et al., 2018; El Hajj Assaf et al., 2018; Tannous et al., 2018; Li et al., 2019). This current study is the first to explore a novel response of the post-harvest pathogen *P. expansum* to epigenetic perturbations through the deletion of the epigenetic reader SntB. In addition to its impact on the ability of the fungus to cause infection and proliferate within apple tissue, SntB also regulates secondary metabolism in *P. expansum* with negative effects on patulin and citrinin production *in vitro* (**Figures 2A,B**).

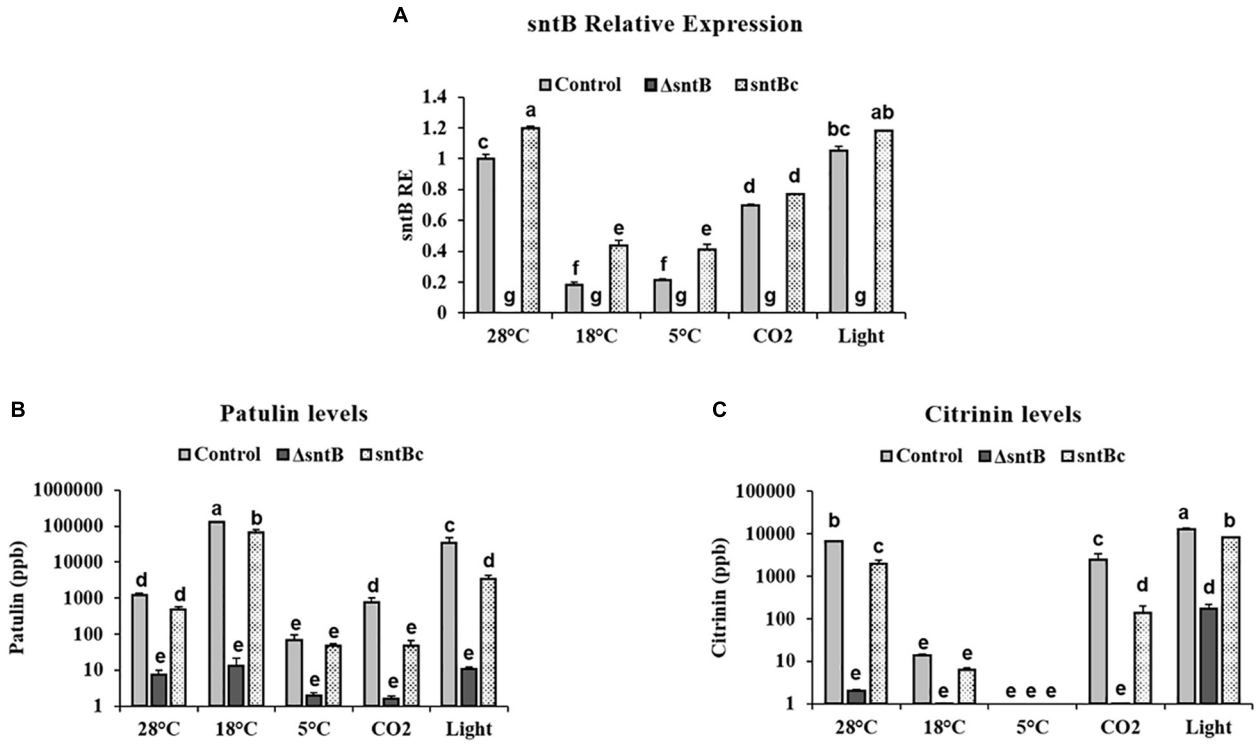

FIGURE 4 | Effect of abiotic factors on *sntB* expression and mycotoxin accumulation. The three *Penicillium* strains (control, Δ*sntB*, and *sntBc*) were grown on YES agar media at 28°C for 48h in the dark and then subjected to different treatment conditions for additional 48 h. Control – 28°C incubation in the dark; 18–18°C incubation in the dark; 5–5°C incubation in the dark; light – 28°C incubation under continuous white fluorescent lighting; CO_2 – 28°C incubation at 20% CO_2 in the dark. **(A)** Total RNA was extracted and the relative expression of *sntB* was evaluated. **(B)** Patulin and **(C)** citrinin were extracted and subjected to HPLC analysis. Each strain was inoculated with 3 reps. One-way ANOVA differences were considered significant when $p < 0.05$. Different letters above the columns indicate statistically significant differences between the strains as determined using Tukey's single-step multiple comparison test.

Penicillium expansum sntB encodes a protein with several histone interacting domains: a BAH domain, a SANT domain and three plant homeodomain (PHD) fingers. SntB is homologous to Snt2 in *Saccharomyces cerevisiae* and *Schizosaccharomyces pombe* (Roguev et al., 2004; Baker et al., 2013). In the latter, Snt2 was shown to be a member of a protein complex called Lid2C that includes the proteins Lid2, Ash2, Sdc1, and Jmj3 (Roguev et al., 2004). A different complex was found in *S. cerevisiae,* and this includes the subunits Ecm5 and Rpd3 (Shevchenko et al., 2008). Originally reported to be simply involved in the regulation of chromatin remodeling (Roguev et al., 2004), subsequent research has shown that the protein reader SntB is a putative virulence factor and a major regulator of fungal secondary metabolism (Denisov et al., 2011; Baker et al., 2013; He et al., 2018; Pfannenstiel et al., 2018). Loss of *sntB* in the mycotoxigenic seed pathogen *A. flavus* resulted in global misregulation of secondary metabolism, where some metabolites were up- and some down-regulated such as aflatoxin (Pfannenstiel et al., 2018; Greco et al., 2019). We see a similar global misregulation in the *P. expansum*Δ*sntB* mutant.

The effect of SntB on various secondary metabolites may in part lay in its regulation of transcriptional complexes/transcription factors (**Figure 2E**). LaeA, a member of the Velvet Complex (VC) linking secondary metabolism to development (Bayram et al., 2008), regulates the expression of 12 putative backbone genes in *P. expansum* including patulin genes (Kumar et al., 2016). Along the same line, the carbon catabolite repressor, CreA, was proposed to post-transcriptionally regulate patulin and citrinin biosynthesis (Tannous et al., 2018). Similarly, deletion of *sntB* resulted in decreased biosynthesis of both mycotoxins (**Figures 2A,B**). Lastly, the reduced production of mycotoxins can also be potentially linked to the deregulation of the gene encoding the regulatory protein PacC (**Figure 2E**). Previous works have established that the pH-responsive zinc finger transcription factor PacC is essential for patulin biosynthesis in *P. expansum*. Barad et al. (2016a) provided the first evidence for the pivotal role of PacC in regulating patulin production in *P. expansum*. This paper showed that ammonia secretion by *P. expansum* during fruit colonization resulted in the activation of PacC and the subsequent increase of patulin accumulation (Barad et al., 2016a). These findings have later been confirmed by Chen et al. (2018) that showed a loss of patulin production by the Δ*pacC* mutant of *P. expansum* at pH values above 6.0 due to the significant down-regulation of all the genes in this cluster.

Whilst the deletion of *sntB* in *P. expansum* was not lethal, a large set of physiological characteristics were disturbed. This included decreased radial growth on all tested media, reduced

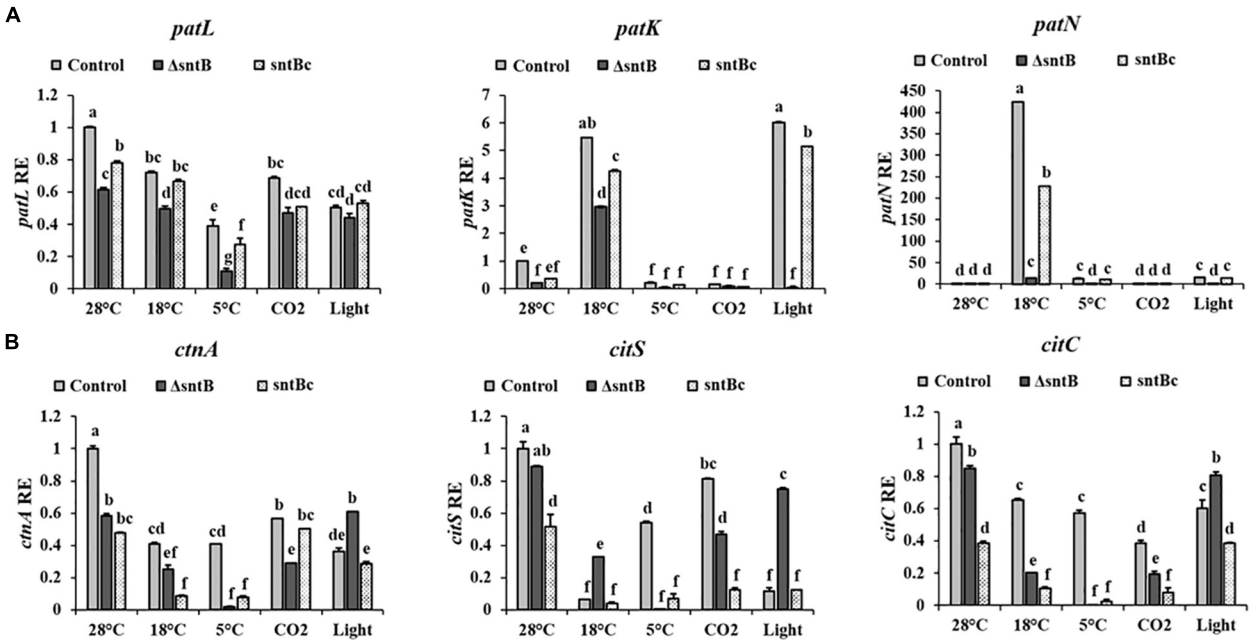

FIGURE 5 | Effect of abiotic factors on relative expression of mycotoxin cluster genes. The three *Penicillium* strains (control, Δ*sntB*, and *sntBc*) were grown on YES agar media at 28°C for 48 h in the dark and then subjected to different treatment conditions as mentioned in **Figure 4**. RNA was extracted and the relative expression of patulin cluster genes **(A)**, and citrinin cluster genes **(B)** was evaluated. Error bars represent the standard error of the mean (SEM) across three technical replicates. One-way ANOVA differences were considered significant when $p < 0.05$. Different letters above the columns indicate statistically significant differences between the strains as determined using Tukey's single-step multiple comparison test.

conidial formation and accelerated spore germination (**Figure 1**). To the best of our knowledge, this is the first report to show the physiological effects of the epigenetic reader SntB in *Penicillium*. However, those findings were not unexpected as similar outcomes for *sntB* loss were observed in other ascomycetes. In *A. flavus*, the deletion of *sntB* has led to various morphological phenotypes, such as reduced radial growth and reduced sclerotia formation (Pfannenstiel et al., 2018). Along the same line, *snt2* deletion mutants of *Fusarium oxysporum* and *Neurospora crassa*, displayed morphological aberrations, including a drop in conidia formation and biomass accumulation, delayed vegetative growth and recurrent hyphal septation (Denisov et al., 2011; Kronholm et al., 2016). Although there have been several studies involved with SntB in ascomycetes, further data are needed to establish a congruent storyline about the impact of SntB on fungal development. Several previous reports described the role of epigenetics in the regulation of phenotypic alterations in filamentous fungi. Epigenetic mechanisms, e.g., histone modifications and RNA interference pathway, were found to be involved in phenotypic plasticity (i.e., phenotypic changes in the colony morphology) of *N. crassa* across an array of controlled environments including temperature, pH, osmotic stress and sugar content (Kronholm et al., 2016). Comparable results were previously gathered in the dimorphic yeast *Aureobasidium pullulans*, where phenotypic switches from yeast to mycelial form are likely to be an epigenetic phenomenon (Slepecky and Starmer, 2009).

Apart from their impact on fungal morphology and secondary metabolism, a number of studies highlighted the crucial role of epigenetic modifications in the success of fungal plant pathogens. Virulence assays performed on apples showed that the deletion of the *sntB* gene had a profound effect on lesion development during infection as lesion diameter caused by Δ*sntB* was smaller than that of the control strain (**Figure 3**). Complementation of the deletion strain with the wild type copy of *sntB* restored the parental virulence phenotype (**Figure 3**). Our results were in agreement with previous reports on three other plant pathogens, *A. flavus* (Pfannenstiel et al., 2018), *M. oryzae* (He et al., 2018), and *F. oxysporum* (Denisov et al., 2011), where the deletion and/or disruption of *sntB* reduced virulence on the respective plant hosts.

How SntB regulates *P. expansum* virulence is still unknown. The studies of both *M. oryzae* and *F. oxysporum* suggested that decrease in virulence could be mediated by the autophagic programmed cell death. However, our results did not support a role for SntB in PCD in *P. expansum* (**Supplementary Figure S6**). One possible explanation for these results is the difference in protein architecture of *P. expansum* SntB compared to other reported species. In *M. oryzae*, MoSnt2 contains an ELM2 domain that *P. expansum* SntB lacks (He et al., 2018). In a similar manner, *F. oxysporum* f. sp. *melonis* Snt2 contains a GATA-Zn domain that is not present in *P. expansum* SntB (Denisov et al., 2011). The reported functional difference may also be explained by the distinctive lifestyles of plant pathogenic

fungi. In *M. oryzae*, autophagy mediated cell death and MoSnt2 are required for appressoria formation, an essential penetration structure present in *M. oryzae* but not in *P. expansum* (Veneault-Fourrey et al., 2006; He et al., 2018).

Penicillium expansum sntB was found to be regulated by different environmental factors, such as temperature and CO_2 levels, that are usually used to modulate the physiology of stored fruits (Hulme, 1971). Moreover our data revealed that the down regulation of *sntB* observed at low temperatures and high CO_2 levels (**Figure 4A**) is accompanied by a significant decrease of patulin and citrinin production (**Figures 4B,C**). However, we found a negative correlation between patulin accumulation and *patL* expression in the WT under certain environmental conditions (incubation at 18°C and under light; **Figure 5A**). In addition to transcription factor of the patulin gene cluster (PatL), other regulatory proteins known to impact patulin biosynthesis in *P. expansum*, including transcription factors LaeA, CreA, and PacC associated with production of secondary metabolites and broad responses to carbon availability and pH, respectively (Kumar et al., 2016, 2018; Chen et al., 2018; Tannous et al., 2018). At the same time, patulin accumulation under all tested conditions is positively correlated with the transcript level of one of the key genes in the patulin biosynthetic pathway, *patK* (PKS). Those results are of great importance as they point out that the same environmental factors that regulate the host physiological response also regulate the expression of *P. expansum sntB* and mycotoxin production simultaneously. Therefore, the epigenetic reader SntB opens up new avenues of study in order to thoroughly understand *P. expansum* biology and virulence. This will allow better regulation of fungal decaying of stored fruit as well as mycotoxin contamination by *P. expansum* during fruit storage.

CONCLUSION

An increasing body of evidence points toward epigenetic mechanisms being responsible for a wide array of biological phenomena, including morphological development, virulence and secondary metabolism. This work represents the first step in the exploration of epigenetic regulation of development and pathogenesis in the post-harvest plant pathogen *P. expansum*. The present data shows that SntB is necessary for the biosynthesis of several secondary metabolites, including patulin and citrinin, and is required for full virulence on apples. *sntB* expression responds to environmental factors modulated during host storage and thus may provide clues to incorporate epigenetic control strategies against this storage disease.

DATA AVAILABILITY STATEMENT

All datasets generated for this study are included in the article/**Supplementary Material**.

AUTHOR CONTRIBUTIONS

NK, DP, ES, OB, and JT conceived the presented idea and designed the study. JT, OB, and DL-R carried out the experiments, collected, analyzed the data and designed the figures. JT wrote the manuscript with support from OB and DL-R on specific sections. NK, DP, and ES edited the manuscript. All authors discussed the results, commented on the manuscript, conceived, and planned the experiments.

FUNDING

This research was supported by Research Grant Award No. IS-5042-17C from BARD, the United States – Israel Binational Agricultural Research and Development Fund and in part by the Food Research Institute of the University of Wisconsin, Madison.

SUPPLEMENTARY MATERIAL

The Supplementary Material for this article can be found online at: https://www.frontiersin.org/articles/10.3389/fmicb.2020.00610/full#supplementary-material

REFERENCES

Aasland, R., Gibson, T. J., and Stewart, A. F. (1995). The PHD finger: implications for chromatin-mediated transcriptional regulation. *Trends Biochem. Sci.* 20, 56–59. doi: 10.1016/s0968-0004(00)88957-4

Altunatmaz, S. S., Issa, G., and Aydin, A. (2012). Detection of airborne psychrotrophic bacteria and fungi in food storage refrigerators. *Braz. J. Microbiol.* 43, 1436–1443. doi: 10.1590/s1517-83822012000400027

Artigot, M. P., Loiseau, N., Laffitte, J., Mas-Reguieg, L., Tadrist, S., Oswald, I. P., et al. (2009). Molecular cloning and functional characterization of two CYP619 cytochrome P450s involved in biosynthesis of patulin in *Aspergillus clavatus*. *Microbiology* 155, 1738–1747. doi: 10.1099/mic.0.024836-0

Baker, L. A., Ueberheide, B. M., Dewell, S., Chait, B. T., Zheng, D., and Allis, C. D. (2013). The yeast Snt2 protein coordinates the transcriptional response to hydrogen peroxide-mediated oxidative stress. *Mol. Cell. Biol.* 33, 3735–3748. doi: 10.1128/mcb.00025-13

Ballester, A.-R., Marcet-Houben, M., Levin, E., Sela, N., Selma-Lázaro, C., Carmona, L., et al. (2015). Genome, transcriptome, and functional analyses of *Penicillium expansum* provide new insights into secondary metabolism and pathogenicity. *Mol. Plant Microbe Interact.* 28, 232–248. doi: 10.1094/mpmi-09-14-0261-fi

Barad, S., Espeso, E. A., Sherman, A., and Prusky, D. (2016a). Ammonia activates pacC and patulin accumulation in an acidic environment during apple colonization by *Penicillium expansum*. *Mol. Plant. Pathol.* 17, 727–740. doi: 10.1111/mpp.12327

Barad, S., Sionov, E., and Prusky, D. (2016b). Role of patulin in post-harvest diseases. *Fungal Biol. Rev.* 30, 24–32. doi: 10.1016/j.fbr.2016.02.001

Barad, S., Horowitz, S. B., Kobiler, I., Sherman, A., and Prusky, D. (2014). Accumulation of the mycotoxin patulin in the presence of gluconic acid contributes to pathogenicity of *Penicillium expansum*. *Mol. Plant Microbe Interact.* 27, 66–77. doi: 10.1094/mpmi-05-13-0138-r

Bayram, Ö, Krappmann, S., Ni, M., Bok, J. W., Helmstaedt, K., Valerius, O., et al. (2008). VelB/VeA/LaeA complex coordinates light signal with fungal development and secondary metabolism. *Science* 320, 1504–1506. doi: 10.1126/science.1155888

Boyer, L. A., Latek, R. R., and Peterson, C. L. (2004). The SANT domain: a unique histone-tail-binding module? *Nat. Rev. Mol. Cell Biol.* 5, 158–163. doi: 10.1038/nrm1314

Callebaut, I., Courvalin, J.-C., and Mornon, J.-P. (1999). The BAH (bromo-adjacent homology) domain: a link between DNA methylation, replication and transcriptional regulation. *FEBS Lett.* 446, 189–193. doi: 10.1016/s0014-5793(99)00132-5

Carvalho, N. D., Arentshorst, M., Kwon, M. J., Meyer, V., and Ram, A. F. (2010). Expanding the ku70 toolbox for filamentous fungi: establishment of complementation vectors and recipient strains for advanced gene analyses. *Appl. Microbiol. Biotechnol.* 87, 1463–1473. doi: 10.1007/s00253-010-2588-1

Chen, Y., Li, B., Xu, X., Zhang, Z., and Tian, S. (2018). The pH-responsive PacC transcription factor plays pivotal roles in virulence and patulin biosynthesis in *Penicillium expansum*. *Environ. Microbiol.* 20, 4063–4078. doi: 10.1111/1462-2920.14453

Denisov, Y., Freeman, S., and Yarden, O. (2011). Inactivation of Snt2, a BAH/PHD-containing transcription factor, impairs pathogenicity and increases autophagosome abundance in *Fusarium oxysporum*. *Mol. Plant Pathol.* 12, 449–461. doi: 10.1111/j.1364-3703.2010.00683.x

El Hajj Assaf, C., Snini, S., Tadrist, S., Bailly, S., Naylies, C., et al. (2018). Impact of *veA* on the development, aggressiveness, dissemination and secondary metabolism of *Penicillium expansum*. *Mol. Plant Pathol.* 19, 1971–1983. doi: 10.1111/mpp.12673

Fair, K., Anderson, M., Bulanova, E., Mi, H., Tropschug, M., and Diaz, M. O. (2001). Protein interactions of the MLL PHD fingers modulate MLL target gene regulation in human cells. *Mol. Cell. Biol.* 21, 3589–3597. doi: 10.1128/mcb.21.10.3589-3597.2001

Flajs, D., and Peraica, M. (2009). Toxicological properties of citrinin. *Arh. Hig Rada Toksikol.* 60, 457–464.

Gimeno, A. (2005). Patulin and citrinin in Portuguese apples with rotten spots. *J. Food Protect.* 68, 1–7.

Greco, C., Pfannenstiel, B. T., Liu, J. C., and Keller, N. P. (2019). Depsipeptide *Aspergillicins* revealed by chromatin reader protein deletion. *ACS Chem. Biol.* 14, 1121–1128. doi: 10.1021/acschembio.9b00161

Hartmann, T., Dümig, M., Jaber, B. M., Szewczyk, E., Olbermann, P., Morschhäuser, J., et al. (2010). Validation of a self-excising marker in the human pathogen *Aspergillus fumigatus* by employing the β-rec/six site-specific recombination system. *Appl. Environ. Microbiol.* 76, 6313–6317. doi: 10.1128/aem.00882-10

He, M., Xu, Y., Chen, J., Luo, Y., Lv, Y., Su, J., et al. (2018). MoSnt2-dependent deacetylation of histone H3 mediates MoTor-dependent autophagy and plant infection by the rice blast fungus *Magnaporthe oryzae*. *Autophagy* 14, 1543–1561. doi: 10.1080/15548627.2018.1458171

He, Y., and Cox, R. J. (2016). The molecular steps of citrinin biosynthesis in fungi. *Chem. Sci.* 7, 2119–2127. doi: 10.1039/c5sc04027b

Hulme, A. C. (1971). *The Biochemistry of Fruits and Their Products*. London: Academic Press.

Kronholm, I., Johannesson, H., and Ketola, T. (2016). Epigenetic control of phenotypic plasticity in the filamentous fungus *Neurospora crassa*. *G3* 6, 4009–4022. doi: 10.1534/g3.116.033860

Kumar, D., Barad, S., Chen, Y., Luo, X., Tannous, J., Dubey, A., et al. (2016). LaeA regulation of secondary metabolism modulates virulence in *Penicillium expansum* and is mediated by sucrose. *Mol. Plant Pathol.* 18, 1150–1163. doi: 10.1111/mpp.12469

Kumar, D., Tannous, J., Sionov, E., Keller, N., and Prusky, D. (2018). Apple intrinsic factors modulating the global regulator, LaeA, the Patulin gene cluster and patulin accumulation during fruit colonization by *Penicillium expansum*. *Front. Plant Sci.* 9:1094. doi: 10.3389/fpls.2018.01094

Kwon, M. J., Arentshorst, M., Roos, E. D., van den Hondel, C. A., Meyer, V., and Ram, A. F. (2011). Functional characterization of Rho GTPases in *Aspergillus niger* uncovers conserved and diverged roles of Rho proteins within filamentous fungi. *Mol. Microbiol.* 79, 1151–1167. doi: 10.1111/j.1365-2958.2010.07524.x

Li, B., Chen, Y., Zong, Y., Shang, Y., Zhang, Z., Xu, X., et al. (2019). Dissection of patulin biosynthesis, spatial control and regulation mechanism in *Penicillium expansum*. *Environ. Microbiol.* 21, 1124–1139. doi: 10.1111/1462-2920.14542

Li, B., Zong, Y., Du, Z., Chen, Y., Zhang, Z., Qin, G., et al. (2015). Genomic characterization reveals insights into patulin biosynthesis and pathogenicity in *Penicillium* species. *Mol. Plant Microbe Interact.* 28, 635–647. doi: 10.1094/mpmi-12-14-0398-fi

Lim, F. Y., Sanchez, J. F., Wang, C. C., and Keller, N. P. (2012). Toward awakening cryptic secondary metabolite gene clusters in filamentous fungi. *Methods Enzymol.* 517:303. doi: 10.1016/b978-0-12-404634-4.00015-2

Liu, Y., Liu, N., Yin, Y., Chen, Y., Jiang, J., and Ma, Z. (2015). Histone H3K4 methylation regulates hyphal growth, secondary metabolism and multiple stress responses in *Fusarium graminearum*. *Environ. Microbiol.* 17, 4615–4630. doi: 10.1111/1462-2920.12993

Livak, K. J., and Schmittgen, T. D. (2001). Analysis of relative gene expression data using real-time quantitative PCR and the 2- Δ ΔCT method. *Methods* 25, 402–408. doi: 10.1006/meth.2001.1262

Martins, M. L., Gimeno, A., Martins, H. M., and Bernardo, F. (2002). Co-occurrence of patulin and citrinin in Portuguese apples with rotten spots. *Food Addit. Contam.* 19, 568–574. doi: 10.1080/02652030210121320

Pfannenstiel, B. T., Greco, C., Sukowaty, A. T., and Keller, N. P. (2018). The epigenetic reader SntB regulates secondary metabolism, development and global histone modifications in *Aspergillus flavus*. *Fungal Genet. Biol.* 120, 9–18. doi: 10.1016/j.fgb.2018.08.004

Pfannenstiel, B. T., and Keller, N. P. (2019). On top of biosynthetic gene clusters: how epigenetic machinery influences secondary metabolism in fungi. *Biotechnol. Adv.* 37:107345. doi: 10.1016/j.biotechadv.2019.02.001

Pfannenstiel, B. T., Zhao, X., Wortman, J., Wiemann, P., Throckmorton, K., Spraker, J. E., et al. (2017). Revitalization of a forward genetic screen identifies three new regulators of fungal secondary metabolism in the genus *Aspergillus*. *MBio* 8:e1246-17.

Puel, O., Galtier, P., and Oswald, I. P. (2010). Biosynthesis and toxicological effects of patulin. *Toxins* 2, 613–631. doi: 10.3390/toxins2040613

Roguev, A., Shevchenko, A., Schaft, D., Thomas, H., Stewart, A. F., and Shevchenko, A. (2004). A comparative analysis of an orthologous proteomic environment in the yeasts *Saccharomyces cerevisiae* and *Schizosaccharomyces* pombe. *Mol. Cell. Proteom.* 3, 125–132.

R Studio Team (2015). *RStudio: Integrated Development for R*. Boston, MA: RStudio, Inc. Available at: http://www.rstudio.com

Schindelin, J., Arganda-Carreras, I., Frise, E., Kaynig, V., Longair, M., Pietzsch, T., et al. (2012). Fiji: an open-source platform for biological-image analysis. *Nat. Methods* 9, 676–682. doi: 10.1038/nmeth.2019

Schmidt-Heydt, M., Stoll, D., and Geisen, R. (2019). Whole-genome sequencing of the fungus *Penicillium citrinum* reveals the biosynthesis gene cluster for the mycotoxin citrinin. *Microbiol. Resour. Announc.* 8, e1419–e1418.

Shevchenko, A., Roguev, A., Schaft, D., Buchanan, L., Habermann, B., Sakalar, C., et al. (2008). Chromatin Central: towards the comparative proteome by accurate mapping of the yeast proteomic environment. *Genome Biol.* 9:R167.

Silar, P. (1995). Two new easy to use vectors for transformations. *Fungal Genet. Rep.* 42:73. doi: 10.4148/1941-4765.1353

Slepecky, R. A., and Starmer, W. T. (2009). Phenotypic plasticity in fungi: a review with observations on *Aureobasidium pullulans*. *Mycologia* 101, 823–832. doi: 10.3852/08-197

Snini, S. P., Tadrist, S., Laffitte, J., Jamin, E. L., Oswald, I. P., and Puel, O. (2014). The gene *PatG* involved in the biosynthesis pathway of patulin, a food-borne mycotoxin, encodes a 6-methylsalicylic acid decarboxylase. *Int. J. Food Microbiol.* 171, 77–83. doi: 10.1016/j.ijfoodmicro.2013.11.020

Snini, S. P., Tannous, J., Heuillard, P., Bailly, S., Lippi, Y., Zehraoui, E., et al. (2015). The patulin is a cultivar dependent aggressiveness factor favoring the colonization of apples by *Penicillium expansum*. *Mol. Plant Pathol.* 17, 920–930. doi: 10.1111/mpp.12338

Tannous, J., Atoui, A., El Khoury, A., Francis, Z., Oswald, I. P., Puel, O., et al. (2015). A study on the physicochemical parameters for *Penicillium expansum* growth and patulin production: effect of temperature, pH, and water activity. *Food Sci. Nutr.* 4, 611–622. doi: 10.1002/fsn3.324

Tannous, J., El Khoury, R., Snini, S. P., Lippi, Y., El Khoury, A., Atoui, A., et al. (2014). Sequencing, physical organization and kinetic expression of the patulin biosynthetic gene cluster from *Penicillium expansum*. *Int. J. Food Microbiol.* 189, 51–60. doi: 10.1016/j.ijfoodmicro.2014.07.028

Tannous, J., Keller, N. P., Atoui, A., El Khoury, A., Lteif, R., Oswald, I. P., et al. (2017a). Secondary metabolism in *Penicillium expansum*: emphasis on recent

advances in patulin research. *Crit. Rev. Food Sci. Nutr.* 58, 2082–2098. doi: 10.1080/10408398.2017.1305945

Tannous, J., Snini, S. P., El Khoury, R., Canlet, C., Pinton, P., Lippi, Y., et al. (2017b). Patulin transformation products and last intermediates in its biosynthetic pathway, E-and Z-ascladiol, are not toxic to human cells. *Arch. Toxicol.* 91, 2455–2467. doi: 10.1007/s00204-016-1900-y

Tannous, J., Kumar, D., Sela, N., Sionov, E., Prusky, D., and Keller, N. P. (2018). Fungal attack and host defense pathways unveiled in near avirulent interactions of *Penicillium expansum* creA mutants on apples. *Mol. Plant Pathol.* 19, 2635–2650. doi: 10.1111/mpp.12734

Veneault-Fourrey, C., Barooah, M., Egan, M., Wakley, G., and Talbot, N. J. (2006). Autophagic fungal cell death is necessary for infection by the rice blast fungus. *Science* 312, 580–583. doi: 10.1126/science.1124550

Visentin, I., Montis, V., Döll, K., Alabouvette, C., Tamietti, G., Karlovsky, P., et al. (2012). Transcription of genes in the biosynthetic pathway for fumonisin mycotoxins is epigenetically and differentially regulated in the fungal maize pathogen *Fusarium verticillioides*. *Eukaryot. Cell* 11, 252–259. doi: 10.1128/ec.05159-11

Wiemann, P., Soukup, A. A., Folz, J. S., Wang, P.-M., Noack, A., and Keller, N. P. (2018). CoIN: co-inducible nitrate expression system for secondary metabolites in *Aspergillus nidulans*. *Fungal Biol. Biotechnol.* 5:6.

Yang, K., Liang, L., Ran, F., Liu, Y., Li, Z., Lan, H., et al. (2016). The DmtA methyltransferase contributes to *Aspergillus flavus* conidiation, sclerotial production, aflatoxin biosynthesis and virulence. *Sci. Rep.* 6:23259.

Conflict of Interest: The authors declare that the research was conducted in the absence of any commercial or financial relationships that could be construed as a potential conflict of interest.

frontiers in Microbiology

ORIGINAL RESEARCH
published: 07 May 2020
doi: 10.3389/fmicb.2020.00811

The Pheromone Module SteC-MkkB-MpkB-SteD-HamE Regulates Development, Stress Responses and Secondary Metabolism in *Aspergillus fumigatus*

*Dean Frawley[1], Maria C. Stroe[2], Berl R. Oakley[3], Thorsten Heinekamp[2], Maria Straßburger[4], Alastair B. Fleming[5], Axel A. Brakhage[2,6] and Özgür Bayram[1]**

[1] Department of Biology, Fungal Genetics and Secondary Metabolism Laboratory, Maynooth University, Maynooth, Ireland, [2] Department of Molecular and Applied Microbiology, Hans Knöll Institute (HKI), Leibniz Institute for Natural Product Research and Infection Biology, Jena, Germany, [3] Department of Molecular Biosciences, University of Kansas, Lawrence, KS, United States, [4] Transfer Group Antiinfectives, Leibniz Institute for Natural Product Research and Infection Biology, Hans Knöll Institute (HKI), Jena, Germany, [5] Department of Microbiology, School of Genetics and Microbiology, Moyne Institute of Preventive Medicine, Trinity College Dublin, Dublin, Ireland, [6] Department of Microbiology and Molecular Biology, Institute of Microbiology, Friedrich Schiller University, Jena, Germany

OPEN ACCESS

Edited by:
Laure Ries,
University of São Paulo, Brazil

Reviewed by:
Daisuke Hagiwara,
University of Tsukuba, Japan
Eduardo Antonio Espeso,
Consejo Superior de Investigaciones Científicas (CSIC), Spain

***Correspondence:**
Özgür Bayram
ozgur.bayram@mu.ie

Specialty section:
This article was submitted to Fungi and Their Interactions, a section of the journal Frontiers in Microbiology

Received: *27 February 2020*
Accepted: *06 April 2020*
Published: *07 May 2020*

Citation:
Frawley D, Stroe MC, Oakley BR, Heinekamp T, Straßburger M, Fleming AB, Brakhage AA and Bayram Ö (2020) The Pheromone Module SteC-MkkB-MpkB-SteD-HamE Regulates Development, Stress Responses and Secondary Metabolism in Aspergillus fumigatus. Front. Microbiol. 11:811. doi: 10.3389/fmicb.2020.00811

In order for eukaryotes to efficiently detect and respond to environmental stimuli, a myriad of protein signaling pathways are utilized. An example of highly conserved signaling pathways in eukaryotes are the mitogen-activated protein kinase (MAPK) pathways. In fungi, MAPK pathways have been shown to regulate a diverse array of biological processes, such as asexual and sexual development, stress responses and the production of secondary metabolites (SMs). In the model fungus *Aspergillus nidulans*, a MAPK pathway known as the pheromone module is utilized to regulate both development and SM production. This signaling cascade consists of the three kinases SteC, MkkB, and MpkB, as well as the SteD adaptor protein and the HamE scaffold. In this study, homologs of each of these proteins have been identified in the opportunistic human pathogen *A. fumigatus.* By performing epitope tagging and mass spectrometry experiments, we have shown that these proteins form a pentameric complex, similar to what is observed in *A. nidulans.* This complex has been shown to assemble in the cytoplasm and MpkB enters the nucleus, where it would presumably interact with various transcription factors. Pheromone module mutant strains exhibit drastic reductions in asexual sporulation, vegetative growth rate and production of SMs, such as gliotoxin. Mutants also display increased sensitivity to cell wall and oxidative stress agents. Overall, these data provide evidence of the existence of a conserved MAP kinase signaling pathway in *Aspergillus* species and suggest that this pathway is critical for the regulation of fungal development and secondary metabolism.

Keywords: *Aspergillus fumigatus*, gliotoxin, pheromone module, secondary metabolism, MAP Kinases, stress responses, asexual sporulation

INTRODUCTION

Aspergillus fumigatus is a saprophytic fungus that is ubiquitous in the environment and is an opportunistic human pathogen (Latge, 1999). This species reproduces predominately via the production of hydrophobic conidia that can easily spread throughout the air, allowing for the rapid colonization of new environments (Dagenais and Keller, 2009). The conidia of this fungus can pose severe threats to human health, as these spores are commonly inhaled daily and can germinate in the alveoli in the lungs (Latge, 1999). Within 4–6 h of colonization, conidia can spread throughout the lungs, resulting in the development of invasive pulmonary aspergillosis (van de Veerdonk et al., 2017). Immunocompromised individuals, such as patients that are undergoing chemotherapy or organ transplantations have a much higher risk of developing pulmonary aspergillosis and the mortality rate in these individuals is generally over 50%, reaching as high as 95% in specific situations (Latge, 1999, 2001; Maschmeyer et al., 2007; Balloy and Chignard, 2009; McCormick et al., 2010).

A myriad of virulence factors contribute to the survival and spread of *A. fumigatus* spores in the human body, making *A. fumigatus* a highly adaptable pathogen. For example, *A. fumigatus* utilizes various systems that aid in the detoxification of reactive oxygen species that are produced by phagocytic immune cells like neutrophils and macrophages (Abad et al., 2010; Hillmann et al., 2016). Another virulence factor is the fungal cell wall, which is the main defense and source of structural integrity for *A. fumigatus* cells as they colonize the lungs (Abad et al., 2010). The cell wall retains high plasticity and its composition is readily altered to adapt to various environmental conditions and cell stressors, allowing for *A. fumigatus* spores to avoid the body's natural defense mechanisms (van de Veerdonk et al., 2017). *A. fumigatus* growth and virulence is greatly influenced by the ability of this species to produce various bioactive compounds known as secondary metabolites (SMs), which can possess a myriad of properties. *A. fumigatus* has 40 predicted SM core synthase enzyme-encoding genes, 19 of which have been shown to produce downstream products (Romsdahl and Wang, 2019). The production of gliotoxin, a SM with immunosuppressive properties is a major contributor to virulence (Hof and Kupfahl, 2009) and is implicated in 96% of cases of *A. fumigatus* infections (Ghazaei, 2017). Gliotoxin inhibits the activity of various enzymes including nicotinamide adenine dinucleotide phosphate (NADPH) oxidases and alcohol dehydrogenases. Gliotoxin is also capable of inducing apoptosis and inhibiting various functions of macrophages and neutrophils (Gardiner et al., 2005; Spikes et al., 2008). As a result, gliotoxin production enables fungal growth and colonization of host tissue *via* suppression of the immune system (Ghazaei, 2017).

In order for fungal species like *A. fumigatus* to regulate their development, stress responses and secondary metabolism in response to external stimuli, a variety of protein signaling pathways are utilized (Bayram et al., 2008, 2012; Elramli et al., 2019). Mitogen-activated protein kinase (MAPK) pathways are highly conserved signaling cascades in eukaryotes that are critical for the regulation of various biological processes such as cell growth and immune responses, to name a few (Marshall, 1994; Schaeffer and Weber, 1999; Widmann et al., 1999; Shaul and Seger, 2007; Rincon and Davis, 2009). In a general MAPK pathway, stimulus detection at a receptor leads to the activation of three protein kinases, often termed MAPKKK/MAP3K, MAPKK/MAP2K, and MAPK, which phosphorylate each other sequentially. The MAPK translocates into the nucleus when phosphorylated and activates various transcription factors and regulators, which in turn, modulate numerous biological processes (Marshall, 1994; Widmann et al., 1999; Saito, 2010).

In the model ascomycete fungus *A. nidulans*, a MAPK pathway known as the pheromone module has been characterized (Bayram et al., 2012; Frawley et al., 2018). This pathway consists of three kinases, known as SteC (MAP3K), MkkB (MAP2K), and MpkB (MAPK), as well as the SteD adaptor protein and the HamE scaffold protein. These proteins form a pentameric complex that assembles at the plasma membrane and hyphal tips in response to pheromone signaling. Once assembled, kinase phosphorylation enables transduction of a signal downstream, via translocation of MpkB into the nucleus where it interacts with various transcription factors such as SteA and the velvet protein VeA to modulate biological processes. Activation of the SteA transcription factor results in the positive regulation of hyphal fusion and formation of cleistothecia, which are sexual reproductive structures. VeA activation results in assembly of the trimeric velvet complex (VeA-VelB-LaeA) which regulates secondary metabolism (Vallim et al., 2000; Atoui et al., 2008; Bayram et al., 2008, 2012; Sarikaya Bayram et al., 2010). Characterization of this pheromone module signaling pathway led to the identification of a homologous signaling module in the saprophytic fungus *A. flavus* (Frawley et al., 2020). This species is a prolific producer of the carcinogen aflatoxin B1 and causes contamination of a wide array of agricultural crops (Lewis et al., 2005; Yu et al., 2005; Amare and Keller, 2014; Rushing and Selim, 2019). The *A. flavus* pheromone module consists of SteC, MkkB, MpkB, and SteD. However, HamE was not shown to interact with the proteins of this pathway. This tetrameric complex was shown to assemble in the cytoplasm and is essential for the regulation of asexual sporulation, sclerotia formation and aflatoxin B1 production (Frawley et al., 2020).

Both secondary metabolism and various methods of fungal development are co-regulated *via* pheromone module signaling in *A. nidulans* (Bayram et al., 2012; Frawley et al., 2018) and *A. flavus* (Frawley et al., 2020). This information, coupled with the recent identification of the MpkB homolog in *A. fumigatus* (Manfiolli et al., 2019), led to the proposal that *A. fumigatus* may also utilize a similar mechanism of regulation to control its developmental programs and SM production. In this work, homologs of the remaining pheromone module proteins (SteC, MkkB, SteD, and HamE) have been identified in *A. fumigatus.* Using a genetic and proteomic approach, we detected physical interactions between these proteins. In combination with confocal imaging, these data suggest that these proteins form a MAP kinase pheromone module in the cytoplasm and that MpkB enters the nucleus, similar to what is observed in both

A. nidulans (Bayram et al., 2012; Frawley et al., 2018) and *A. flavus* (Frawley et al., 2020). This work also provides evidence that the pheromone module is critical for the regulation of asexual sporulation, cell stress responses and secondary metabolism. Overall, the data from this study suggests that the pheromone module is a highly conserved signaling pathway that is critical for the regulation of development and secondary metabolism in *Aspergillus* species.

MATERIALS AND METHODS

Strains, Growth Media and Culturing Conditions

Fungal strains used in this study are listed in **Supplementary Table S1**. The *Aspergillus fumigatus* CEA17 (*pyrG*+) and CEA17 (*pyrG*Δ) strains served as wild-type hosts for all deletions and epitope taggings. Various plasmids used for the knock-out and epitope tagging experiments are listed in **Supplementary Table S2**. Plasmids were cloned into Stellar (Clontech) competent *Escherichia coli* cells and these cells were cultured in LB medium (supplemented with 100 μg/ml ampicillin) and SOC media. To induce asexual sporulation of fungal strains, Glucose Minimal Medium (GMM) agar plates were used. To promote vegetative growth, liquid complete medium, Czapek-Dox medium and Sabouraud medium were used. Details of the ingredients of each medium are provided in the **Supplementary Information**.

Phenotypic Assays

Strains were point inoculated (5×10^3 spores) in triplicate on GMM agar plates containing appropriate supplements. Plates were incubated in the presence of light for 4 days to induce asexual sporulation. All incubations were performed at 37°C. Stereomicroscopic images were captured using an Olympus szx16 microscope with Olympus sc30 camera. Digital pictures were taken and processed with the Cell Sens Standard software (Olympus). Quantifications of colony diameter and asexual conidiation were performed using three independent biological replicates. Bar charts represent the mean values ± s.d. *P*-values were calculated by performing unpaired Student's *t*-tests ($^*P < 0.05$; $^{**}P < 0.01$; $^{***}P < 0.001$), using Graphpad Prism Version 6.

For testing the stress responses of *A. fumigatus* strains, strains were inoculated on GMM agar plates containing appropriate supplements and the following stress agents were used: Congo Red (20, 30, 50 μg/ml), H_2O_2 (2, 3, 4 mM) and NaCl (0.5, 1 and 1.5 M). All plates were incubated at 37°C for 3 days.

GFP/HA-Trap and Sample Preparation for LC-MS Protein Identification

Isolation and preparation of GFP and HA fusion proteins for mass spectrometry analysis was performed as explained in detail (Bayram et al., 2008). Detailed descriptions of methods used are given in the provided **Supplementary Information**.

RP-HPLC Analysis of Gliotoxin Levels

Detailed information on culturing conditions and preparation of samples for RP-HPLC analysis is provided in **Supplementary Information**. 3 biological replicates were prepared per strain and data is presented as a bar chart, with the bars representing the mean ± s.d. *P*-values were calculated by performing unpaired Student's *t*-tests ($^*P < 0.05$; $^{**}P < 0.01$), using the Graphpad Prism Version 6.

Extraction of Fungal Compounds and LC-MS Analysis

Strains were inoculated in triplicate in 40 ml of liquid GMM at a concentration of 5 million spores/ml and incubated for 48 h on a shaker at 37°C. The culture broth containing fungal mycelium was homogenized using an ULTRA-TURRAX (IKA-Werke, Staufen, Germany). Homogenized cultures were extracted twice with a total of 100 ml ethyl acetate, dried with sodium sulfate and concentrated under reduced pressure. For LC-MS analysis, the dried extracts were dissolved in 1 ml of methanol and loaded onto an ultrahigh-performance liquid chromatography (LC)–MS system consisting of an UltiMate 3000 binary rapid-separation liquid chromatograph with photodiode array detector (Thermo Fisher Scientific, Dreieich, Germany) and an LTQ XL linear ion trap mass spectrometer (Thermo Fisher Scientific, Dreieich, Germany) equipped with an electrospray ion source. The extracts (injection volume, 10 μl) were analyzed on a 150 mm by 4.6-mm Accucore reversed-phase (RP)-MS column with a particle size of 2.6 μm (Thermo Fisher Scientific, Dreieich, Germany) at a flow rate of 1 ml/min, with the following gradient over 21 min: initial 0.1% (v/v) HCOOH-MeCN/0.1% (v/v) HCOOH-H_2O 0/100, which was increased to 80/20 in 15 min and then to 100/0 in 2 min, held at 100/0 for 2 min, and reversed to 0/100 in 2 min.

Confocal Microscopy

Conidia were cultured in eight-chambered cover glasses (Lab-Tek; Thermo Fisher Scientific) and incubated at 30°C for various durations in 400 μL of liquid GMM, containing appropriate supplements. Additional details for DAPI staining, immunostaining and confocal imaging are provided in the **Supplementary Information**.

RESULTS

The SteC, MkkB, MpkB, SteD, and HamE Homologs Physically Interact in *A. fumigatus*

To determine whether *A. fumigatus* possesses homologs of the pheromone module proteins that are present in *A. nidulans*, reciprocal BLAST searches (Altschul et al., 1990) were performed and the ASPGD website was utilized[1]. Homologs of all five members of the *A. nidulans* pheromone module were found to exist in the *A. fumigatus* genome. According to BLAST and ASPGD, the *A. fumigatus* SteC homolog

[1]http://www.aspgd.org

(Afu5g06420) exhibits 78.04% sequence similarity to the *A. nidulans* protein, while *A. fumigatus* MkkB (Afu3g05900), MpkB (Afu6g12820) (Manfiolli et al., 2019), SteD (Afu2g17130) and HamE (Afu5g13970) exhibit 80.19, 98.59, 75.65, and 64.57% sequence similarity, respectively. To determine the sizes of these *A. fumigatus* proteins and the domains they possess in comparison to the *A. nidulans* proteins, "ScanProsite" (de Castro et al., 2006) and "InterPro" (Mitchell et al., 2019) software was used (**Figures 1A,B**).

It was found that SteC in both *A. nidulans* and *A. fumigatus* possesses a SAM domain at the N-terminus. In *A. nidulans*, this SAM domain is located between amino acid residues 63 and 126, while for *A. fumigatus*, it is present between amino acids 98 and 161. SteC in both species also contains a RA domain and a protein kinase domain. The RA domain in *A. nidulans* is located between amino acids 248 and 351, while the RA domain in *A. fumigatus* is located at amino acids 311 and 414. The protein kinase domain is located at amino acids 607 and 881 in *A. nidulans*, while the protein kinase domain in *A. fumigatus* is located at amino acids 672 and 947. According to ASPGD, the sequence provided for *A. fumigatus* SteC is 1,007 amino acids in length, considerably larger than the *A. nidulans* sequence (886 amino acids). However, attempts at tagging this sequence at the C-terminus with various epitope tags proved to be unsuccessful. This suggested that the sequence provided on ASPGD is incorrect. Pair-wise sequence alignment of the *A. nidulans* and *A. fumigatus* protein sequences using the Smith-Waterman algorithm (Madeira et al., 2019) led to the determination of the extent of homology (**Supplementary Figure S3**). This alignment revealed the presence of an alternate stop codon, ahead of the stop codon predicted on ASPGD. Tagging of the SteC sequence from this stop codon proved to be successful (**Supplementary Figure S1B**). This leads us to conclude that the *A. fumigatus* protein sequence is 952 amino acids in length, as opposed to 1,007 amino acids.

MkkB in both *A. nidulans* and *A. fumigatus* possesses a protein kinase domain. This domain extends from amino acids 67–334 in both of these species, signifying high conservation between these two orthologs. MpkB in both species also possesses a protein kinase domain at very similar residues. In *A. nidulans,* this domain is present at amino acids 22–310, while in *A. fumigatus,* this domain extends from amino acids 21–309. The SteD adaptor in both species contains SAM and RA domains. The SAM domains in *A. nidulans* and *A. fumigatus* are located at amino acids 66–129 and 67–130, respectively. The RA domains are located at amino acids 370–459 and 365–455 in *A. nidulans*, and *A. fumigatus*, respectively. Lastly, the HamE protein consists of WD40 repeats at the N-terminus of both proteins between amino acids 30–300 and 38–348 in *A. nidulans* and *A. fumigatus*, respectively.

To assess protein-protein interactions between these pheromone module proteins, the C-terminal ends of the *steC, mkkB, mpkB*, and *steD* genes were fused to an *sgfp* epitope tag (**Supplementary Figure S1**). All attempts to successfully detect the *hamE* gene tagged with *sgfp via* western blotting and mass spectrometry (MS) failed. We therefore coupled the C-terminus of the *hamE* gene to a *3xha* epitope tag (**Supplementary Figure S2**). Each tagged protein was immunoprecipitated from strains that had undergone vegetative growth for 24 h. These samples were run on a MS to detect the tagged proteins and their interaction partners (**Figure 1C**). It was found that SteC-GFP pulldowns co-purified the adaptor protein SteD (**Supplementary Table S4**), MkkB-GFP pulldowns co-purified SteC, MpkB, SteD, and HamE (**Supplementary Table S5**), MpkB-GFP pulldowns co-purified MkkB and SteD (**Supplementary Table S6**) and SteD-GFP pulldowns co-purified SteC (**Supplementary Table S7**). Despite HamE being detectable in purifications of MkkB-GFP, HamE-HA pulldowns did not co-purify any pheromone module components (**Supplementary Table S8**) and so this interaction may be transient or the binding affinity may be too low to allow co-purifications under the conditions we used. Taken together, this interactome data provides evidence that a complex of at least four proteins is assembled in *A. fumigatus* (**Figure 1D**). This complex consists of the three kinases SteC, MkkB, and MpkB, as well as the adaptor protein SteD and possibly the HamE scaffold protein.

Each Pheromone Module Protein Is Critical for the Regulation of Asexual Sporulation and Vegetative Growth

In order to assess whether the pheromone module protein homologs in *A. fumigatus* contribute to the regulation of asexual sporulation, mutant strains were generated. The respective *steC, mkkB, mpkB, steD*, and *hamE* gene open reading frames were deleted (**Supplementary Figures S1**, **S2**) by replacing these genomic regions with either the pyrithiamine resistance gene (*ptrA*) or the *A. fumigatus pyrG* gene. To determine whether phenotypic differences observed in the mutant strains were due to the deletion of specific genes and not secondary abnormalities, complementation strains were made. A functional copy of each gene open reading frame, including the promoter and terminator regions were reinserted into the respective mutant strains to restore the wild-type phenotype.

Each mutant and complementation strain were spot inoculated on GMM agar plates. These plates were incubated in the presence of light for 4 days to induce asexual reproduction and production of conidia (**Figure 2A**). For each of the five mutant strains, a dramatic reduction in sporulation was observed, similar to what is observed in both *A. nidulans* (Bayram et al., 2012; Frawley et al., 2018) and *A. flavus* (Frawley et al., 2020), with the exception of the *A. flavus hamE* mutant, which did not show any defects in asexual reproduction. For the *A. fumigatus* mutants, the average values of conidia produced were expressed as a percentage of the CEA17 wild-type average, which was chosen to represent 100% production (**Figure 2C**). The average percentage range for these mutants was between 10.16 and 27.02%. The complementation of each gene restored the ability of these strains to undergo asexual sporulation to a similar degree to that of the wild type. The average percentage range of sporulation for the complementation strains was between 63.06 and 102.89%.

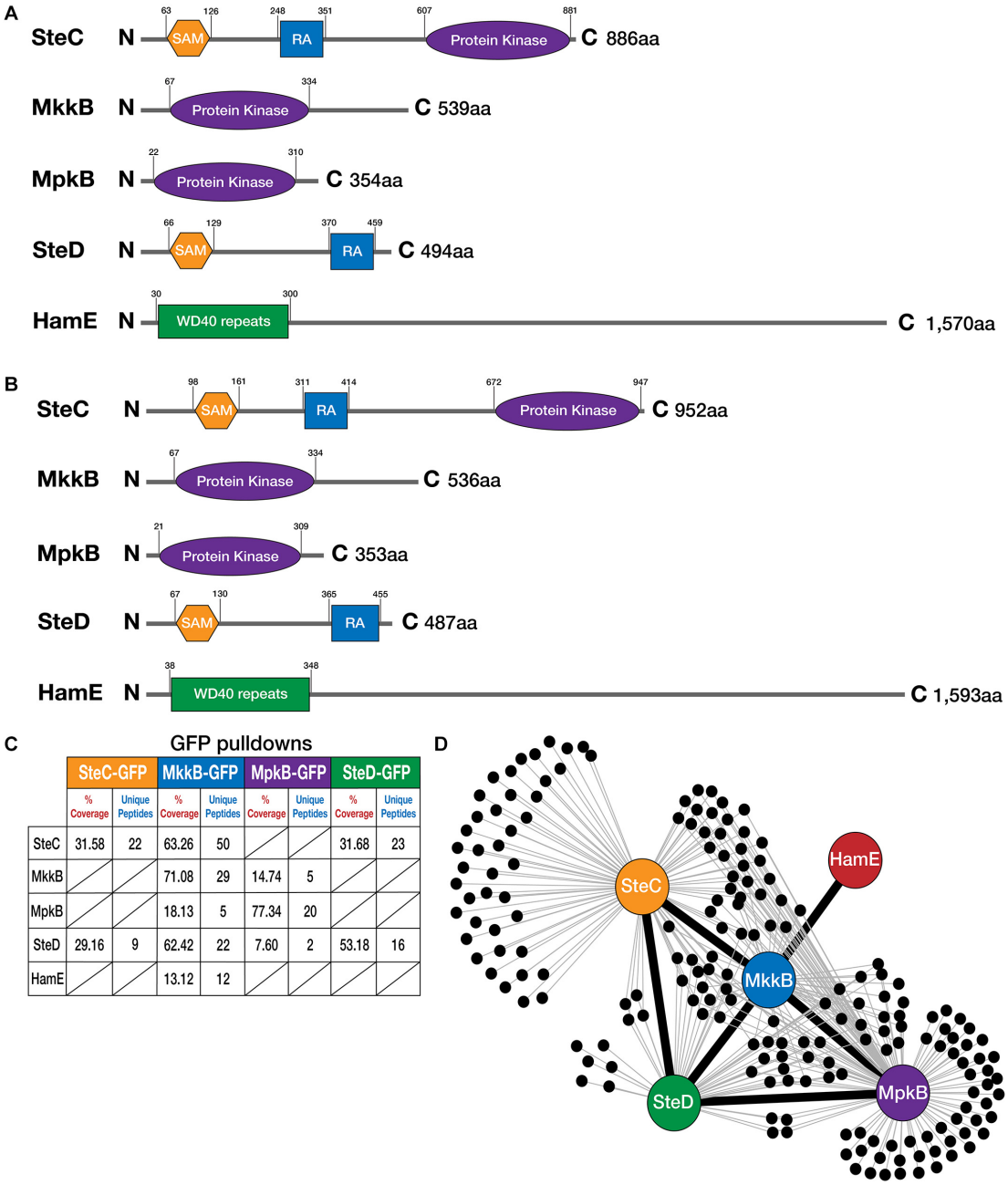

	SteC-GFP		MkkB-GFP		MpkB-GFP		SteD-GFP	
	% Coverage	Unique Peptides	% Coverage	Unique Peptides	% Coverage	Unique Peptides	% Coverage	Unique Peptides
SteC	31.58	22	63.26	50			31.68	23
MkkB			71.08	29	14.74	5		
MpkB			18.13	5	77.34	20		
SteD	29.16	9	62.42	22	7.60	2	53.18	16
HamE			13.12	12				

FIGURE 1 | Detection of interactions between pheromone module proteins in *A. fumigatus*. **(A)** Schematic diagrams illustrating the structures of the pheromone module proteins in *A. nidulans*. Amino acids (aa). N (N-terminal), C (C-terminal). SAM (Sterile Alpha Motif), RA (Ras-associated). Detection of protein sizes and domains were performed using a combination of ScanProsite (de Castro et al., 2006) and InterPro software (Mitchell et al., 2019). **(B)** Schematics illustrating the structures of the pheromone module proteins in *A. fumigatus*. Reciprocal BLAST searches were performed to detect protein homologs (Altschul et al., 1990). **(C)** GFP-pulldowns and LC-MS/MS analysis of the pheromone module kinases and SteD. GFP-tagged proteins are given at the top of the table and co-purified proteins are given on the left-hand side. The percentage of coverage and unique peptides of each detected protein are displayed. Two biological replicates of each strain were used. Strains were cultured vegetatively for 24 h in complete media. **(D)** Interaction network of the pheromone module components based on unique peptides detected in each GFP pulldown. Each black dot represents a protein detected in two independent biological replicates but not in the wild type.

To determine whether the pheromone module proteins contribute to regulating vegetative growth in *A. fumigatus*, the colony diameters of each strain were measured (**Figure 2B**). It was observed that each mutant exhibited a significantly smaller colony diameter in comparison to the CEA17 strain, with the *hamE* mutant displaying the highest degree of reduction. Aside from the *hamE* mutant phenotype, these data support the findings in *A. nidulans*, where the deletion of either *steC, mkkB,*

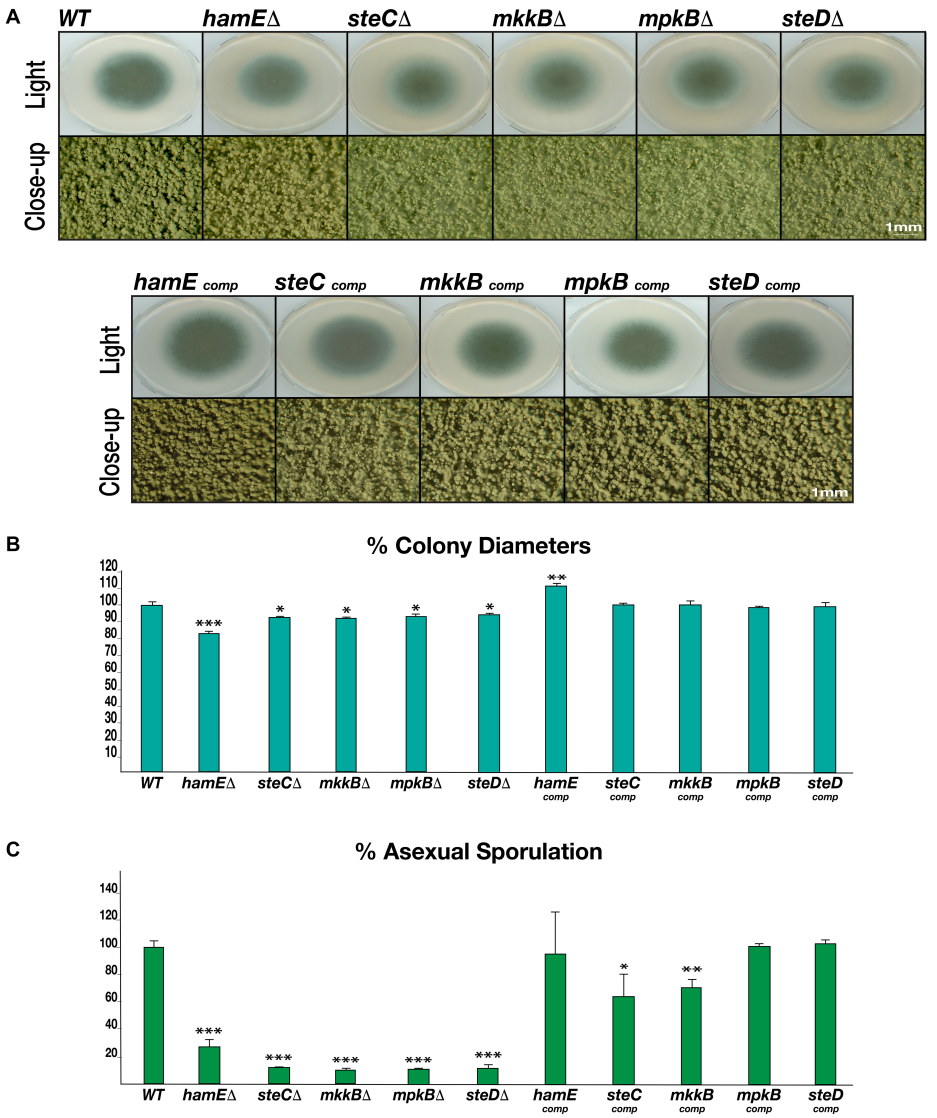

FIGURE 2 | Rates of asexual sporulation and vegetative growth in deletion and complementation strains. **(A)** Asexual phenotypes of deletion and complementation strains. Each strain was spot inoculated (5×10^3 spores) in triplicate on GMM agar plates containing appropriate supplements. Wild type refers to the CEA17 strain. All plates were incubated at 37∘C for 4 days. The Olympus szx16 microscope with an Olympus sc30 camera was used to capture close-up images at $2 \times$ magnification. **(B)** Rates of vegetative growth for each strain. The average values from three independent biological replicates were plotted ± s.d. as a percentage of the WT strain. *P*-values were calculated by performing unpaired Student's *t*-tests (*$P < 0.05$; **$P < 0.01$; ***$P < 0.001$). **(C)** Rates of asexual sporulation for each strain calculated by performing spore counts of colonies on plates.

mpkB, or *steD* results in a dramatic reduction in vegetative growth (Frawley et al., 2018). However, these results contradict the findings in *A. flavus* since no reductions in the rates of hyphal extension were observed in any of these mutants (Frawley et al., 2020). For the *A. fumigatus* deletion strains, the average percentage range of colony diameters was between 83.22–94.61%. Complementation of each gene restored the wild type phenotype and the average percentage range of hyphal extension was 98.2–111.37%.

Taken together, these data suggest that the pheromone module proteins are essential for the regulation of both asexual sporulation and vegetative hyphal growth. These findings also suggest that these five proteins may act as a complex to regulate these processes due to the similarities of the mutant phenotypes.

The Pheromone Module Proteins Contribute to the Regulation of Cell Wall and Oxidative Stress Responses

Fungi like *A. fumigatus* utilize multiple MAPK pathways to respond to various cell stressors, such as cell wall, osmotic and oxidative stresses (Rispail et al., 2009; Hamel et al., 2012). To determine the relevance of the pheromone module proteins with respect to the responses to cell stressors, each mutant

and complementation strain was spot inoculated on GMM agar plates containing various exogenous stress agents. The radial growth phenotypes of each strain were compared to the wild-type phenotypes. In order to assess whether the pheromone module proteins play a role in the response to osmotic stress, each strain was inoculated on plates containing various concentrations of the osmotic stress agent NaCl (**Supplementary Figure S4**). It was observed that in the presence of 0.5 M NaCl, the radial growth of all strains, including the wild type was not inhibited. At higher concentrations of NaCl (1 M and 1.5 M), the radial growth of all strains, including the wild type was significantly reduced. At 1.5 M NaCl, growth of all strains was minimal but overall, no differences were observed between strains with regards to the rates of vegetative growth in the presence of osmotic stress. The complementation of each gene resulted in similar phenotypes as those observed for the mutant strains and wild type (**Supplementary Figure S5**).

To assess the influence of the pheromone module proteins in the response to cell wall stress specifically, each strain was inoculated on plates containing various concentrations (20, 30, and 50 μg/ml) of the cell wall stressor Congo Red (**Figure 3A**). It was observed that the CEA17 wild-type strain exhibited significant sensitivity to Congo Red at higher concentrations (50 μg/ml). However, it was evident that the deletion of *steC,*

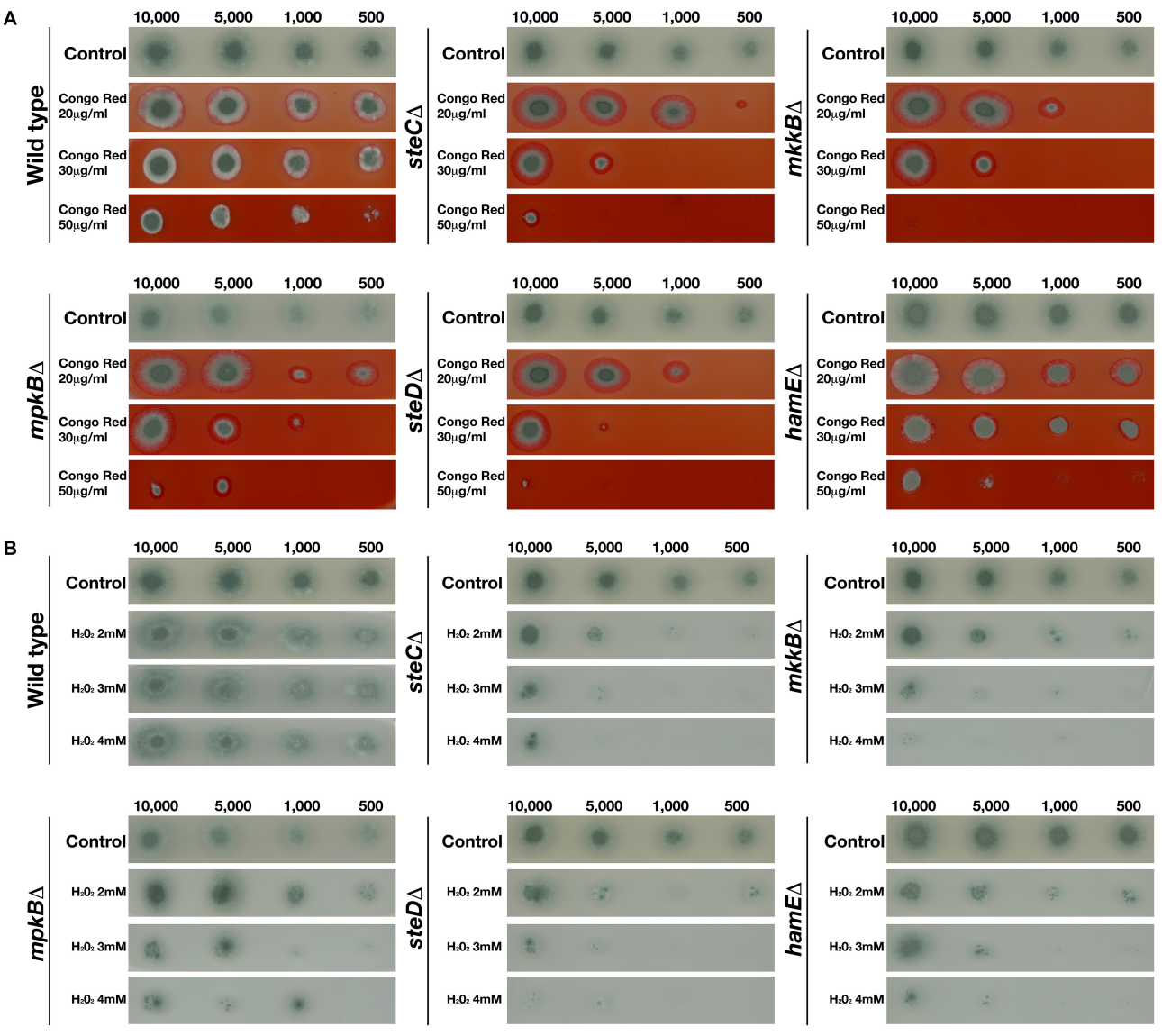

FIGURE 3 | Growth phenotypes of mutant strains in the presence of various concentrations of Congo Red and H_2O_2. Strains were point-inoculated on GMM agar plates containing exogenous stress agents and left to incubate at 37°C for 3 days. The number of spores used for inoculation are listed above each panel. "Control" refers to strains point inoculated on GMM agar plates that did not contain any stress agents. **(A)** Growth phenotypes of the CEA17 wild-type strain and each mutant strain in the presence of 20, 30, and 50 μg Congo Red. **(B)** Growth phenotypes of the CEA17 wild-type strain and each mutant strain in the presence of 2, 3, or 4 mM H_2O_2.

mkkB, mpkB, steD, and *hamE* resulted in increased sensitivity to all Congo Red concentrations tested. Each of these mutant strains displayed significant growth defects in the presence of each concentration of Congo Red, suggesting that these proteins may play a role in cell wall biosynthesis or maintenance. Complementation of each gene resulted in increased radial growth when compared to the respective mutants and the phenotypes of each complementation strain more closely resembled the wild-type phenotypes (**Supplementary Figure S6**).

To determine whether the pheromone module proteins contribute to the response to oxidative stress, each strain was inoculated on plates containing various concentrations (2, 3, and 4 mM) of the oxidative stress agent H_2O_2 (**Figure 3B**). It was observed that the CEA17 wild-type strain did not exhibit any significant growth impairments in the presence of any of the H_2O_2 concentrations tested. The radial growth of each inoculated CEA17 colony in the presence of H_2O_2 was similar to the growth on the control plates. However, it was observed that the wild-type colonies inoculated in the presence of H_2O_2 displayed significantly reduced sporulation levels in comparison to colonies on the control plates. For each of the mutant strains, it was apparent that the presence of H_2O_2 significantly impaired radial growth. The growth of each strain was reduced in the presence of all H_2O_2 concentrations tested and minimal growth was observed for each strain in the presence of 4mM H_2O_2. The complementation of each gene resulted in the restoration of radial growth, comparable to the rates observed for the wild-type colonies, albeit slightly smaller (**Supplementary Figure S7**). In the presence of each H_2O_2 concentration, these complementation strains closely resembled the wild-type colonies with regards to both radial growth and levels of sporulation.

Taken together, the results of these stress tests indicate that the pheromone module proteins contribute to the regulation of cellular responses to cell wall and oxidative stressors but do not influence sensitivity to osmotic stress. The deletion of any of the five members of the pheromone module results in increased sensitivity to both the cell wall stress agent Congo Red and the oxidative stressor H_2O_2.

The Levels of Secondary Metabolite Production Are Reduced in Pheromone Module Mutant Strains

In order to determine the roles of the pheromone module proteins with regards to the regulation of secondary metabolism in *A. fumigatus*, the levels of various SMs produced by the pheromone module mutants were determined by LC-MS analysis (**Figure 4** and **Supplementary Table S9**). *A. fumigatus* is capable of producing a myriad of SMs, many of which are uncharacterized. The most notable SM is the immunosuppressive agent gliotoxin, which is a major contributor to *A. fumigatus* virulence (Hof and Kupfahl, 2009; Ghazaei, 2017). Other notable SMs produced by *A. fumigatus* include (i) pseurotin A, a competitive inhibitor of chitin synthase which is also an inducer of nerve cell proliferation and acts as an immunosuppressive agent (Maiya et al., 2007; Ishikawa et al., 2009), (ii) pseurotin D, which exhibits apomorphine-antagonistic activity (Ishikawa and Ninomiya, 2008), (iii) fumagillin, an anti-angiogenic compound (Mc et al., 1951; Sin et al., 1997) and (iv) pyripyropene A, which exhibits insecticidal properties (Horikoshi et al., 2017).

By performing LC-MS analysis, the levels of each of the compounds listed above were determined in the pheromone module mutant strains and complementation strains. Gliotoxin was detected in all strains (**Figure 4A**). It was found that each mutant produces significantly less gliotoxin than the wild type. The average reductions in gliotoxin production for the mutant strains were between 63 and 80%. It was observed that the complementation of each gene restored the ability of these strains to produce gliotoxin to a level similar to that observed for the wild-type strain. The average levels of gliotoxin production for the complementation strains ranged between 87 and 145% of the wild-type average. Pseurotin A, pseurotin D, fumagillin and pyripyropene A were detected in the wild type, *hamE* mutant, *mkkB* mutant and respective complementation strains. Interestingly, the *hamE* mutant and the *mkkB* mutant exhibited different trends in production of all four metabolites tested. It was observed that pseurotin A production (**Figure 4B**) is increased in the *hamE* mutant (63% increase) and significantly decreased in the *mkkB* mutant (65% decrease). For pseurotin D (**Figure 4C**), the levels showed a similar trend, with an increase in production being observed in the *hamE* mutant (37% increase) and a significant decrease being evident in the *mkkB* mutant (69% decrease). Fumagillin production (**Figure 4D**) shows no significant difference between the wild type and *hamE* mutant, whereas in the *mkkB* mutant, the levels of production are dramatically reduced (31% decrease). Lastly, the levels of pyripyropene A (**Figure 4E**) were slightly increased in the *hamE* mutant (20% increase), whereas production of this compound was significantly decreased in the *mkkB* mutant (50% decrease).

Overall, these data suggest that MkkB is critical for the positive regulation of gliotoxin, pseurotin A, pseurotin D, fumagillin and pyripyropene A. However, HamE is required for the positive regulation of gliotoxin and negative regulation of pseurotin A, pseurotin D and pyripyropene A, whilst having no apparent effects in the regulation of fumagillin production. This could suggest that HamE may also act independently of the pheromone module to regulate secondary metabolism, perhaps in a similar manner to what is observed in *A. flavus* (Frawley et al., 2020).

The Deletion of *mkkB* and *hamE* Does Not Reduce Virulence in a Murine Infection Model

To assess the influence of both *mkkB* and *hamE* in the regulation of *A. fumigatus* virulence, both mutant strains and the respective complementation strains were inoculated in mice to test the infectivity of these strains in a murine infection model of invasive aspergillosis (**Supplementary Figure S8**). When compared to the wild-type strain, it was evident that the deletion of both *mkkB* and *hamE* did not influence virulence, which complements the

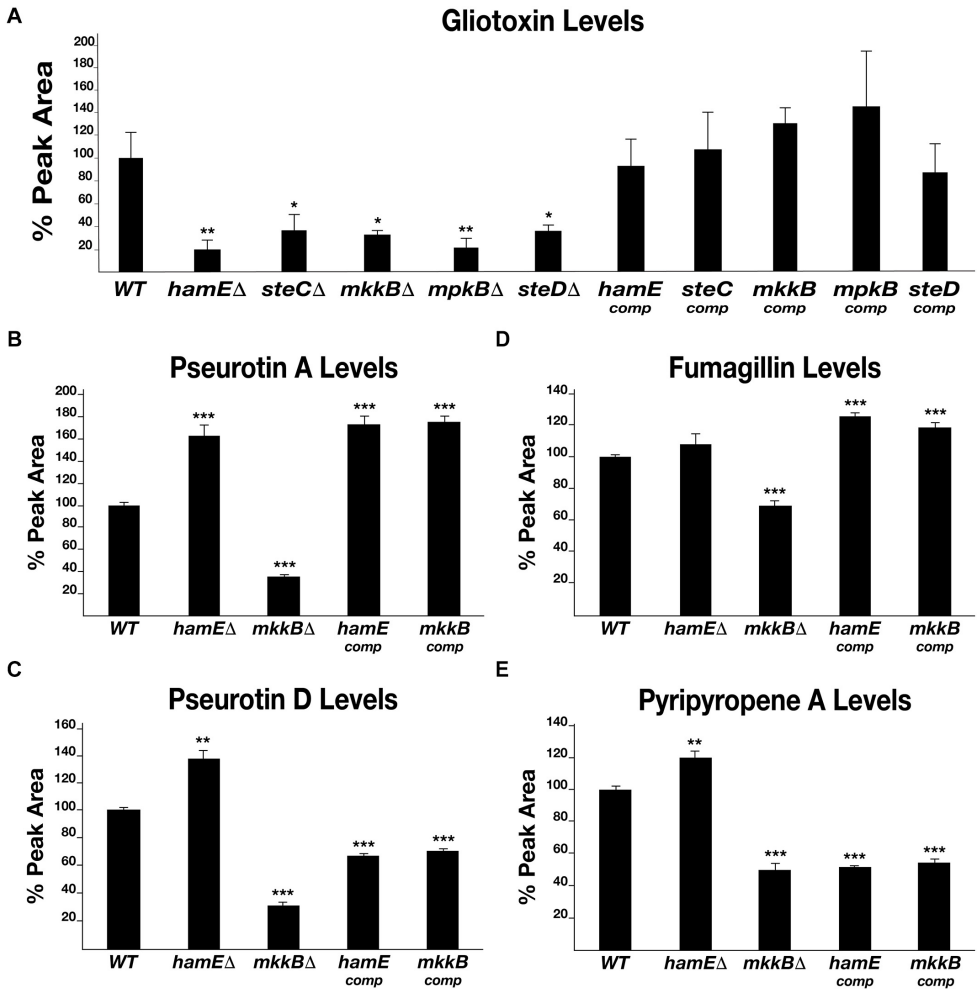

FIGURE 4 | Levels of production of various metabolites in pheromone module mutant strains. **(A)** HPLC detection of gliotoxin levels in deletion and complementation strains. Each strain was inoculated (10^7 spores/ml) in triplicate in 40 ml Czapek-Dox medium and left to incubate on a shaker at 37°C for 72 h. Average peak area values were plotted as a percentage of the wild type ± s.d. *P*-values were calculated by performing unpaired Student's *t*-tests (*$P < 0.05$; **$P < 0.01$). For panels (B–E), strains were inoculated in triplicate in 40 ml of liquid GMM (5 million spores/ml) and incubated for 48 h at 37°C. Statistical calculations were performed as described for panel **(A)**. **(B)** Graphical representation of the pseurotin A levels in each strain. (**$P < 0.01$; ***$P < 0.01$). **(C)** Graphical representation of the pseurotin D levels in each strain. **(D)** Graphical representation of the fumagillin levels in each strain. **(E)**. Graphical representation of the pyripyropene A levels in each strain.

findings for *mpkB* (Manfiolli et al., 2019). This suggests that the pheromone module pathway is not required for the regulation of fungal virulence in murine infection models.

The Localization of the Pheromone Module Is Cytoplasmic and MpkB Is the Only Protein That Translocates Into the Nucleus

Confocal microscopy imaging was performed to determine the sub-cellular localizations of the pheromone module proteins *in vivo* (**Figure 5**). To monitor the localizations of these proteins in living material, strains were initially imaged without DAPI staining. To then compare the localizations of these proteins with respect to the nuclei, samples were subsequently fixed and stained with DAPI. Confocal microscopy imaging revealed that SteC-GFP displayed cytoplasmic fluorescence that was uniform throughout hyphae. This fusion protein was also shown to be excluded from interphase nuclei (**Figure 5A**). MkkB-GFP fluorescence was uniformly distributed throughout fungal hyphae. It was observed that this fusion protein is mostly cytoplasmic and is excluded from interphase nuclei and vacuoles. This protein was also observed to be enriched at the central portion of some septa and hyphal tips (**Figure 5B**). MpkB-GFP exhibited mostly uniform cytoplasmic distribution throughout fungal hyphae. However, MpkB was also observed to be slightly more concentrated in interphase nuclei and at the hyphal apices (**Figure 5C**). SteD-GFP fluorescence was faint and mostly uniform throughout the fungal hyphae. This fusion protein was found to be cytoplasmic and is excluded from interphase nuclei and vacuoles (**Figure 5D**). To observe the sub-cellular localization of HamE *in vivo*, immunostaining

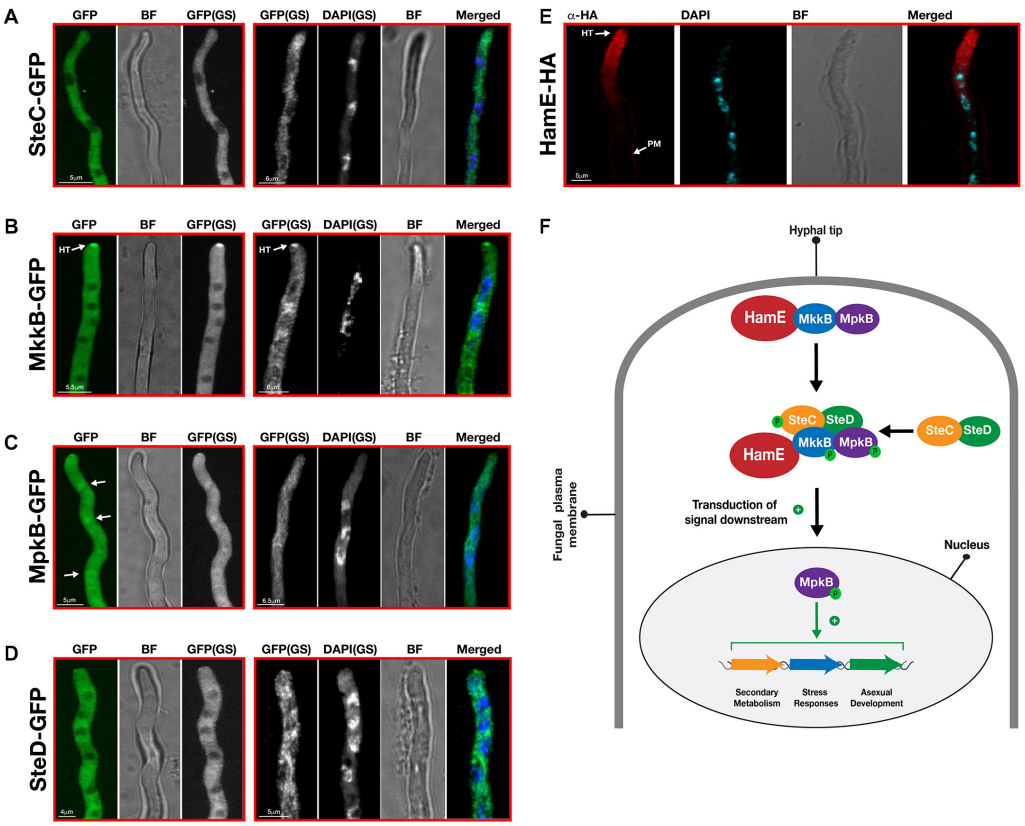

FIGURE 5 | Sub-cellular localization patterns of the pheromone module proteins *in vivo*. **(A)** Sub-cellular localization of SteC-GFP. Strains from panels A–D were incubated at 30°C for various durations in 400 μL of liquid GMM, containing appropriate supplements. "BF" (brightfield images). "GS" (grayscale images). To visualize the nuclei, DAPI staining was performed. White arrows depict the accumulation of fusion protein in the nuclei. "HT" refers to accumulation of protein at hyphal tips. **(B)** Sub-cellular localization of MkkB-GFP. **(C)** Sub-cellular localization of MpkB-GFP. **(D)** Sub-cellular localization of SteD-GFP. **(E)** Sub-cellular localization of HamE-HA. The HamE-HA strain was inoculated (5×10^3 spores) on sterile coverslips, covered in 450 μL of Sabouraud media, containing supplements. This strain were left to incubate at 30°C for 16 h. **(F)** Schematic model of the pheromone module in *A. fumigatus*. MkkB, MpkB, and HamE localize to the hyphal tips. These three proteins interact with the SteC-SteD dimer in the cytoplasm to form a pentameric complex which results in MpkB activation and transduction of a signal downstream to the nucleus. MpkB translocates into the nucleus, where it presumably interacts with transcription factors to positively regulate asexual sporulation, vegetative growth, stress responses and production of various SMs. "P" represents phosphate groups.

was performed, using the HamE-HA strain. It was observed that the HamE protein becomes enriched at the hyphal tips and the plasma membrane and is absent from interphase nuclei (**Figure 5E**).

Overall, these data complement findings in both *A. nidulans* (Bayram et al., 2012; Frawley et al., 2018) and *A. flavus* (Frawley et al., 2020), suggesting that a conserved mechanism of complex assembly and signaling exists in *A. fumigatus*. The kinases MkkB and MpkB may accumulate and interact with HamE at the hyphal tips, in response to pheromone signaling between neighboring hyphae. Signal detection could lead to the interaction of this trimer with the cytoplasmic SteC-SteD dimer to form a pentameric complex which enables efficient kinase phosphorylation and MpkB activation. Presumably, MpkB then translocates into the nucleus, where it interacts with various transcription factors to regulate a myriad of biological processes, such as vegetative growth, asexual sporulation, stress responses and secondary metabolism (**Figure 5F**). However, the exact molecular mechanism of signal transduction from hyphal tip to the nuclear envelope, as well as the direct targets of MpkB in the nucleus are currently unknown.

DISCUSSION

Eukaryotic organisms utilize a myriad of MAP kinase pathways to regulate a diverse range of biological processes (Schaeffer and Weber, 1999). The pheromone module in the model ascomycete fungus *A. nidulans* is a MAPK cascade that is activated in response to pheromone signaling, which occurs between neighboring hyphae and is critical for initiating hyphal fusion events (Bayram et al., 2012; Frawley et al., 2018). In this pathway, the three kinases SteC, MkkB, and MpkB are tethered to the membrane and hyphal tips via SteD adaptor interactions. MkkB and MpkB are bound by the HamE scaffold protein and this allows for efficient kinase phosphorylation in response to a detected stimulus. MpkB phosphorylation and translocation into the nucleus results in the activation

of various transcription factors. Consequently, the pheromone module is involved in the regulation of asexual and sexual development, as well as secondary metabolism (Bayram et al., 2012; Frawley et al., 2018). The pheromone module is a highly conserved pathway that has been shown to exist in many organisms. For example, the homologous yeast Fus3 pathway is extensively studied and is responsible for promoting cell fusion and sexual development in response to pheromone signaling (Bardwell, 2005). The homologous MAK-2 pathway in the model filamentous fungus *Neurospora crassa* regulates germling and hyphal fusion (Pandey et al., 2004; Li et al., 2005). Recently, we have identified a homologous pheromone module in the plant and human pathogen *A. flavus*. This complex consists of the three kinases SteC, MkkB and MpkB, as well as the SteD adaptor. This pathway was shown to be critical for the regulation of asexual sporulation, sclerotia development and aflatoxin B1 production (Frawley et al., 2020).

Due to the high degree of conservation of the pheromone module, it was hypothesized that a similar mechanism of signaling could be utilized by the opportunistic human pathogen *A. fumigatus* to regulate development and secondary metabolism. This work highlights the identification of four homologous pheromone module proteins in *A. fumigatus* (SteC, MkkB, SteD and HamE). The *A. fumigatus* MpkB homolog has been previously identified and characterized (Manfiolli et al., 2019) but has not been studied within the context of the pheromone signaling pathway. In this study, we have shown, *via* a genetic and proteomic approach that these *A. fumigatus* homologous proteins physically interact to form a complex (**Figures 1C,D** and **Supplementary Tables S4–S8**), similar to what is observed in both *A. nidulans* (Bayram et al., 2012; Frawley et al., 2018) and *A. flavus* (Frawley et al., 2020). This complex could potentially consist of two sub-complexes. MkkB, MpkB and HamE have been shown to become enriched at the hyphal tips (**Figures 5B,C,E**, respectively) and thus, it is possible that they form a trimeric complex. Both SteC and SteD were dispersed throughout the fungal hyphae, indicating that they may form a dimer in the cytoplasm (**Figures 5A,D**, respectively). Interactions between these two sub-complexes could lead to assembly of the pentameric pheromone module in the cytoplasm, which complements the findings in *A. flavus* (Frawley et al., 2020). This would allow for MpkB activation and translocation into the nucleus, where it could interact with various transcription factors to modulate a diverse range of biological processes.

This work provides evidence that the pheromone module proteins are required for the positive regulation of both asexual sporulation and vegetative growth rate (**Figure 2**). All pheromone module mutants exhibited dramatically reduced sporulation levels (**Figures 2A,C**), as well as reduced colony diameters (**Figure 2B**). These data support the findings in *A. nidulans,* in which each mutant produced fewer conidia and the rates of hyphal growth were hindered in all mutants, aside from the *hamE* deletion strain (Frawley et al., 2018). These results do not fully duplicate the phenotypes observed in *A. flavus*, however, as the deletion of *hamE* in this species did not result in any defects in asexual sporulation or vegetative growth rate. Also, the deletion of *steC, mkkB, mpkB* or *steD* does not hinder the rates of hyphal growth in *A. flavus* (Frawley et al., 2020). Interestingly, in the study by Manfiolli et al. the deletion of *A. fumigatus mpkB* did not cause any defects in radial growth rate (Manfiolli et al., 2019). However, this mutant did exhibit significantly reduced levels of sporulation. The discrepancies in vegetative growth of the *mpkB* mutant in our study could be due to factors such as differences in the composition of the media used, the quantity of spores used for inoculation and the duration of incubation. Overall, our phenotypic data suggest that each of the pheromone module proteins contribute to the regulation of asexual development and hyphal growth in *A. fumigatus*. Due to the similarities in phenotypes observed for each mutant, these data provide evidence that each of these proteins function within the same pathway to regulate fungal development.

The influence of the pheromone module proteins in the regulation of various cell stress responses was also examined. Three main MAPK pathways become activated in *A. fumigatus* in response to stress. The CWI pathway is activated in response to cell wall stress agents and signals via the MAPK MpkA (Valiante et al., 2015; van de Veerdonk et al., 2017). The HOG pathway is required for the response to osmotic stressors and signals via the MAPK SakA (Du et al., 2006; Martinez-Montanes et al., 2010; de Nadal and Posas, 2015). Lastly, the HOG pathway, in cooperation with the MAPK MpkC have been shown to regulate cellular responses to osmotic, oxidative and cell wall stresses (Bruder Nascimento et al., 2016). It was observed that each pheromone module mutant strain exhibited significant defects in growth when cultured in the presence of exogenous stress agents such as the cell wall stressor Congo Red (**Figure 3A**) and the oxidative stressor H_2O_2 (**Figure 3B**). In relation to stress tests performed by Manfiolli et al., it was found that MpkB localization is increased in the nucleus in the presence of cell wall, oxidative and osmotic stress agents (Manfiolli et al., 2019). The *A. fumigatus mpkB* mutant also exhibited increased sensitivity to H_2O_2 as sporulation was drastically reduced in the presence of all H_2O_2 concentrations tested, which complements our findings. Interestingly, the presence of Congo Red did not impair vegetative growth of the wild type or the *mpkB* mutant. However, addition of the cell wall perturbing agent caspofungin caused significant reductions in the radial growth rates of this mutant. While this does not fully complement our findings, it does provide further evidence that MpkB plays a role in either the response to cell wall stressors or in cell wall biosynthesis. It appears that the strains used in the study by Manfiolli et al. (2019) exhibited increased resistance to Congo red as the growth of the wild type was not significantly impaired, even at 150 μg/ml concentration.However, in our study, a dramatic reduction in vegetative growth is evident for the wild type strain in the presence of 50 μg/ml Congo red. This could explain why the *mpkB* mutant in our study exhibits significantly reduced growth in the presence of Congo Red. Overall, these data provide evidence that the pheromone module proteins contribute to the regulation of cellular responses to stress, particularly cell wall and oxidative stress.

LC-MS analysis revealed that the pheromone module proteins are required for the regulation of SM production (**Figure 4**). *A. fumigatus* is a prolific producer of SMs, most notably the

immunosuppressive agent gliotoxin (Hof and Kupfahl, 2009; Romsdahl and Wang, 2019). It was evident that the deletion of any of the five pheromone module genes results in dramatic reductions in gliotoxin production in comparison to a wild type strain (**Figure 4A**). It was also observed that the deletion of *mkkB* results in significantly reduced levels of pseurotin A, pseurotin D, fumagillin and pyripyropene A (**Figures 4B–E**). However, the deletion of *hamE* resulted in increased production of each of these compounds, with the exception of fumagillin, which showed no significant differences in comparison to the wild-type. Taken together, these data suggest that the pheromone module proteins contribute to the positive regulation of SM production, which complement the findings observed in both *A. nidulans* (Bayram et al., 2012; Frawley et al., 2018) and *A. flavus* (Frawley et al., 2020). However, these data also propose that HamE may exert regulatory roles that are independent of the pheromone module signalling pathway, which supports findings in *A. flavus* (Frawley et al., 2020).

In summary, this study has identified pheromone module homologs in the opportunistic human pathogen *A. fumigatus* and has provided evidence of the existence of a cytoplasmic pentameric complex, similar to what is observed in both *A. nidulans* (Bayram et al., 2012; Frawley et al., 2018) and *A. flavus* (Frawley et al., 2020). This complex consists of the three kinases SteC, MkkB and MpkB, as well as the SteD adaptor and the scaffold HamE, which together, enable transduction of a signal downstream and translocation of MpkB into the nucleus. MpkB would then presumably interact with transcription factors to regulate asexual sporulation, vegetative growth, stress responses and secondary metabolism (**Figure 5F**). According to the IP-MS data for MpkB-GFP (**Supplementary Table S6**), it was found that MpkB interacts with the SteA transcription factor, similar to what is observed in *A. nidulans* (Bayram et al., 2012). This transcription factor has been shown to be involved in the regulation of sexual development and hyphal fusion in various fungal species (Wong Sak Hoi and Dumas, 2010). MpkB was also found to interact with DvrA which is a C2H2 transcription factor. Orthologs of DvrA are predicted to play roles in the suppression of the host inflammatory response. Interestingly, MpkB was also found to interact with Afu1g04550. This is an uncharacterized protein in *A. fumigatus*, however, the ortholog of this protein in *A. nidulans* is HmbC. HmbC is a high mobility group box (HMGB) protein which is a chromatin-associated protein that has also been shown to interact with VeA, allowing for the regulation of development and secondary metabolism (Bokor et al., 2019). This could explain why MpkB in *A. fumigatus* was not found to interact directly with any of the velvet complex components, yet defects in both development and SM production were observed in the pheromone module mutant strains. However, despite the roles of the pheromone module in the regulation of both development and secondary metabolism, it was evident that this pathway is not essential for *A. fumigatus* virulence in a murine model, suggesting that compensatory mechanisms may also be utilized by this species to promote its virulence. These data also suggest that HamE may perform functions that are not associated with the pheromone module. Future studies will focus on characterizing the molecular roles of HamE to determine its functions within the context of the pheromone module signaling pathway as well as possible independent functions.

Overall, this work has provided insight on the molecular roles of the pheromone module in *A. fumigatus* and has contributed to the understanding of how MAPK signaling is utilized by filamentous fungal species to regulate their development and secondary metabolism in response to environmental stimuli.

DATA AVAILABILITY STATEMENT

All datasets generated for this study are included in the article/**Supplementary Material**.

ETHICS STATEMENT

The animal study was reviewed and approved by Federal State authority: Thüringer Landesamt für Verbraucherschutz Ethics committee: Beratende Komission nach §15 Abs. 1 Tierschutzgesetz Permit number: 03-027/16.

AUTHOR CONTRIBUTIONS

Project conceptualisation, experimental design, data analysis and preparation of the manuscript was performed by DF. Preparation of samples for LC-MS analysis and formatting of results was performed by MCS. Confocal microscopy imaging was performed by BO. Murine infection models were performed by MS and TH. AF and AB were responsible for reviewing and editing the manuscript and provided resources for the experiments. ÖB was responsible for project conceptualisation, experimental design, supervision of the project, reviewing and editing the manuscript.

FUNDING

This study was funded by a Maynooth University John and Pat Hume Scholarship and an IRC postgraduate scholarship (GOIPG/2018/35) to DF and a Science Foundation Ireland grant (Grant No: 13/CDA/2142) to ÖB. MS facility in Maynooth University was funded by SFI Grant No: 12/RI/2346(3). MS and AB were funded by the Federal Ministry of Education and Research (BMBF, grant number 03ZZ0803A).

ACKNOWLEDGMENTS

The authors would like to thank Dr. Özlem Sarikaya-Bayram for providing the pOSB113 plasmid.

SUPPLEMENTARY MATERIAL

The Supplementary Material for this article can be found online at: https://www.frontiersin.org/articles/10.3389/fmicb.2020.00811/full#supplementary-material

REFERENCES

Abad, A., Fernandez-Molina, J. V., Bikandi, J., Ramirez, A., Margareto, J., Sendino, J., et al. (2010). What makes *Aspergillus fumigatus* a successful pathogen? Genes and molecules involved in invasive aspergillosis. *Rev. Iberoam. Micol.* 27, 155–182. doi: 10.1016/j.riam.2010.10.003

Altschul, S. F., Gish, W., Miller, W., Myers, E. W., and Lipman, D. J. (1990). Basic local alignment search tool. *J. Mol. Biol.* 215, 403–410.

Amare, M. G., and Keller, N. P. (2014). Molecular mechanisms of *Aspergillus flavus* secondary metabolism and development. *Fungal Genet. Biol.* 66, 11–18. doi: 10.1016/j.fgb.2014.02.008

Atoui, A., Bao, D., Kaur, N., Grayburn, W. S., and Calvo, A. M. (2008). *Aspergillus nidulans* natural product biosynthesis is regulated by mpkB, a putative pheromone response mitogen-activated protein kinase. *Appl. Environ. Microbiol.* 74, 3596–3600. doi: 10.1128/AEM.02842-07

Balloy, V., and Chignard, M. (2009). The innate immune response to *Aspergillus fumigatus*. *Microb. Infect.* 11, 919–927. doi: 10.1016/j.micinf.2009.07.002

Bardwell, L. (2005). A walk-through of the yeast mating pheromone response pathway. *Peptides* 26, 339–350. doi: 10.1016/j.peptides.2004.10.002

Bayram, O., Bayram, O. S., Ahmed, Y. L., Maruyama, J., Valerius, O., Rizzoli, S. O., et al. (2012). The *Aspergillus nidulans* MAPK module AnSte11-Ste50-Ste7-Fus3 controls development and secondary metabolism. *PLoS Genet.* 8:e1002816. doi: 10.1371/journal.pgen.1002816

Bayram, O., Krappmann, S., Ni, M., Bok, J. W., Helmstaedt, K., Valerius, O., et al. (2008). VelB/VeA/LaeA complex coordinates light signal with fungal development and secondary metabolism. *Science* 320, 1504–1506. doi: 10.1126/science.1155888

Bokor, E., Amon, J., Keisham, K., Karacsony, Z., Vagvolgyi, C., and Hamari, Z. (2019). HMGB proteins are required for sexual development in *Aspergillus nidulans*. *PLoS One* 14:e0216094. doi: 10.1371/journal.pone.0216094

Bruder Nascimento, A. C., Dos Reis, T. F., De Castro, P. A., Hori, J. I., Bom, V. L., De Assis, L. J., et al. (2016). Mitogen activated protein kinases SakA(HOG1) and MpkC collaborate for *Aspergillus fumigatus* virulence. *Mol. Microbiol.* 100, 841–859. doi: 10.1111/mmi.13354

Dagenais, T. R., and Keller, N. P. (2009). Pathogenesis of *Aspergillus fumigatus* in invasive aspergillosis. *Clin. Microbiol. Rev.* 22, 447–465. doi: 10.1128/CMR.00055-08

de Castro, E., Sigrist, C. J., Gattiker, A., Bulliard, V., Langendijk-Genevaux, P. S., Gasteiger, E., et al. (2006). ScanProsite: detection of PROSITE signature matches and ProRule-associated functional and structural residues in proteins. *Nucleic Acids Res.* 34, W362–W365. doi: 10.1093/nar/gkl124

de Nadal, E., and Posas, F. (2015). Osmostress-induced gene expression–a model to understand how stress-activated protein kinases (SAPKs) regulate transcription. *FEBS J.* 282, 3275–3285. doi: 10.1111/febs.13323

Du, C., Sarfati, J., Latge, J. P., and Calderone, R. (2006). The role of the sakA (Hog1) and tcsB (sln1) genes in the oxidant adaptation of *Aspergillus fumigatus*. *Med. Mycol.* 44, 211–218. doi: 10.1080/13693780500338886

Elramli, N., Karahoda, B., Sarikaya-Bayram, O., Frawley, D., Ulas, M., Oakley, C. E., et al. (2019). Assembly of a heptameric STRIPAK complex is required for coordination of light-dependent multicellular fungal development with secondary metabolism in *Aspergillus nidulans*. *PLoS Genet.* 15:e1008053. doi: 10.1371/journal.pgen.1008053

Frawley, D., Greco, C., Oakley, B., Alhussain, M. M., Fleming, A. B., Keller, N. P., et al. (2020). The tetrameric pheromone module SteC-MkkB-MpkB-SteD regulates asexual sporulation, sclerotia formation and aflatoxin production in *Aspergillus flavus*. *Cell Microbiol.* e13192. doi: 10.1111/cmi.13192

Frawley, D., Karahoda, B., Sarikaya Bayram, O., and Bayram, O. (2018). The HamE scaffold positively regulates MpkB phosphorylation to promote development and secondary metabolism in *Aspergillus nidulans*. *Sci. Rep.* 8:16588. doi: 10.1038/s41598-018-34895-6

Gardiner, D. M., Waring, P., and Howlett, B. J. (2005). The epipolythiodioxopiperazine (ETP) class of fungal toxins: distribution, mode of action, functions and biosynthesis. *Microbiology* 151, 1021–1032. doi: 10.1099/mic.0.27847-0

Ghazaei, C. (2017). Molecular insights into pathogenesis and infection with *Aspergillus fumigatus*. *Malays. J. Med. Sci.* 24, 10–20. doi: 10.21315/mjms2017.24.1.2

Hamel, L. P., Nicole, M. C., Duplessis, S., and Ellis, B. E. (2012). Mitogen-activated protein kinase signaling in plant-interacting fungi: distinct messages from conserved messengers. *Plant Cell* 24, 1327–1351. doi: 10.1105/tpc.112.096156

Hillmann, F., Bagramyan, K., Strassburger, M., Heinekamp, T., Hong, T. B., Bzymek, K. P., et al. (2016). The crystal structure of peroxiredoxin Asp f3 provides mechanistic insight into oxidative stress resistance and virulence of *Aspergillus fumigatus*. *Sci. Rep.* 6:33396. doi: 10.1038/srep33396

Hof, H., and Kupfahl, C. (2009). Gliotoxin in *Aspergillus fumigatus*: an example that mycotoxins are potential virulence factors. *Mycotoxin Res.* 25, 123–131. doi: 10.1007/s12550-009-0020-4

Horikoshi, R., Goto, K., Mitomi, M., Oyama, K., Sunazuka, T., and Omura, S. (2017). Identification of pyripyropene A as a promising insecticidal compound in a microbial metabolite screening. *J. Antibiot. (Tokyo)* 70, 272–276. doi: 10.1038/ja.2016.155

Ishikawa, M., and Ninomiya, T. (2008). Chemical modification of pseurotin A: one-pot synthesis of synerazol and pseurotin E and determination of absolute stereochemistry of pseurotin E. *J. Antibiot.* 61, 692–695. doi: 10.1038/ja.2008.99

Ishikawa, M., Ninomiya, T., Akabane, H., Kushida, N., Tsujiuchi, G., Ohyama, M., et al. (2009). Pseurotin A and its analogues as inhibitors of immunoglobulin E [correction of immunoglobuline E] production. *Bioorg. Med. Chem. Lett.* 19, 1457–1460. doi: 10.1016/j.bmcl.2009.01.029

Latge, J. P. (1999). *Aspergillus fumigatus* and aspergillosis. *Clin. Microbiol. Rev.* 12, 310–350.

Latge, J. P. (2001). The pathobiology of *Aspergillus fumigatus*. *Trends Microbiol.* 9, 382–389.

Lewis, L., Onsongo, M., Njapau, H., Schurz-Rogers, H., Luber, G., Kieszak, S., et al. (2005). Aflatoxin contamination of commercial maize products during an outbreak of acute aflatoxicosis in eastern and central Kenya. *Environ. Health Perspect.* 113, 1763–1767. doi: 10.1289/ehp.7998

Li, D., Bobrowicz, P., Wilkinson, H. H., and Ebbole, D. J. (2005). A mitogen-activated protein kinase pathway essential for mating and contributing to vegetative growth in *Neurospora crassa*. *Genetics* 170, 1091–1104. doi: 10.1534/genetics.104.036772

Madeira, F., Park, Y. M., Lee, J., Buso, N., Gur, T., Madhusoodanan, N., et al. (2019). The EMBL-EBI search and sequence analysis tools APIs in 2019. *Nucleic Acids Res.* 47, W636–W641. doi: 10.1093/nar/gkz268

Maiya, S., Grundmann, A., Li, X., Li, S. M., and Turner, G. (2007). Identification of a hybrid PKS/NRPS required for pseurotin A biosynthesis in the human pathogen *Aspergillus fumigatus*. *Chembiochem* 8, 1736–1743. doi: 10.1002/cbic.200700202

Manfiolli, A. O., Siqueira, F. S., Dos Reis, T. F., Van Dijck, P., Schrevens, S., Hoefgen, S., et al. (2019). Mitogen-activated protein kinase cross-talk interaction modulates the production of melanins in *Aspergillus fumigatus*. *mBio* 10:e00215-19. doi: 10.1128/mBio.00215-19

Marshall, C. J. (1994). MAP kinase kinase kinase, MAP kinase kinase and MAP kinase. *Curr. Opin. Genet. Dev.* 4, 82–89.

Martinez-Montanes, F., Pascual-Ahuir, A., and Proft, M. (2010). Toward a genomic view of the gene expression program regulated by osmostress in yeast. *Omics* 14, 619–627. doi: 10.1089/omi.2010.0046

Maschmeyer, G., Haas, A., and Cornely, O. A. (2007). Invasive aspergillosis: epidemiology, diagnosis and management in immunocompromised patients. *Drugs* 67, 1567–1601. doi: 10.2165/00003495-200767110-00004

Mc, C. M., Callender, M. E., and Lawlis, J. F. Jr. (1951). Fumagillin (H-3), a new antibiotic with amebicidal properties. *Science* 113, 202–203. doi: 10.1126/science.113.2930.202

McCormick, A., Loeffler, J., and Ebel, F. (2010). *Aspergillus fumigatus*: contours of an opportunistic human pathogen. *Cell Microbiol.* 12, 1535–1543. doi: 10.1111/j.1462-5822.2010.01517.x

Mitchell, A. L., Attwood, T. K., Babbitt, P. C., Blum, M., Bork, P., Bridge, A., et al. (2019). InterPro in 2019: improving coverage, classification and access to protein sequence annotations. *Nucleic Acids Res.* 47, D351–D360. doi: 10.1093/nar/gky1100

Pandey, A., Roca, M. G., Read, N. D., and Glass, N. L. (2004). Role of a mitogen-activated protein kinase pathway during conidial germination and hyphal fusion in *Neurospora crassa*. *Eukaryot. Cell* 3, 348–358. doi: 10.1128/ec.3.2.348-358.2004

Rincon, M., and Davis, R. J. (2009). Regulation of the immune response by stress-activated protein kinases. *Immunol. Rev.* 228, 212–224. doi: 10.1111/j.1600-065X.2008.00744.x

Rispail, N., Soanes, D. M., Ant, C., Czajkowski, R., Grunler, A., Huguet, R., et al. (2009). Comparative genomics of MAP kinase and calcium-calcineurin signalling components in plant and human pathogenic fungi. *Fungal Genet. Biol.* 46, 287–298. doi: 10.1016/j.fgb.2009.01.002

Romsdahl, J., and Wang, C. C. C. (2019). Recent advances in the genome mining of *Aspergillus* secondary metabolites (covering 2012-2018). *Medchemcomm* 10, 840–866. doi: 10.1039/c9md00054b

Rushing, B. R., and Selim, M. I. (2019). Aflatoxin B1: a review on metabolism, toxicity, occurrence in food, occupational exposure, and detoxification methods. *Food Chem. Toxicol.* 124, 81–100. doi: 10.1016/j.fct.2018.11.047

Saito, H. (2010). Regulation of cross-talk in yeast MAPK signaling pathways. *Curr. Opin. Microbiol.* 13, 677–683. doi: 10.1016/j.mib.2010.09.001

Sarikaya Bayram, O., Bayram, O., Valerius, O., Park, H. S., Irniger, S., Gerke, J., et al. (2010). LaeA control of velvet family regulatory proteins for light-dependent development and fungal cell-type specificity. *PLoS Genet.* 6:e1001226. doi: 10.1371/journal.pgen.1001226

Schaeffer, H. J., and Weber, M. J. (1999). Mitogen-activated protein kinases: specific messages from ubiquitous messengers. *Mol. Cell. Biol.* 19, 2435–2444. doi: 10.1128/mcb.19.4.2435

Shaul, Y. D., and Seger, R. (2007). The MEK/ERK cascade: from signaling specificity to diverse functions. *Biochim. Biophys. Acta* 1773, 1213–1226. doi: 10.1016/j.bbamcr.2006.10.005

Sin, N., Meng, L., Wang, M. Q., Wen, J. J., Bornmann, W. G., and Crews, C. M. (1997). The anti-angiogenic agent fumagillin covalently binds and inhibits the methionine aminopeptidase. MetAP-2. *Proc. Natl. Acad. Sci. U.S.A.* 94, 6099–6103. doi: 10.1073/pnas.94.12.6099

Spikes, S., Xu, R., Nguyen, C. K., Chamilos, G., Kontoyiannis, D. P., Jacobson, R. H., et al. (2008). Gliotoxin production in *Aspergillus fumigatus* contributes to host-specific differences in virulence. *J. Infect. Dis.* 197, 479–486. doi: 10.1086/525044

Valiante, V., Macheleidt, J., Foge, M., and Brakhage, A. A. (2015). The *Aspergillus fumigatus* cell wall integrity signaling pathway: drug target, compensatory pathways, and virulence. *Front. Microbiol.* 6:325. doi: 10.3389/fmicb.2015.00325

Vallim, M. A., Miller, K. Y., and Miller, B. L. (2000). *Aspergillus* SteA (sterile12-like) is a homeodomain-C2/H2-Zn+2 finger transcription factor required for sexual reproduction. *Mol. Microbiol.* 36, 290–301. doi: 10.1046/j.1365-2958.2000.01874.x

van de Veerdonk, F. L., Gresnigt, M. S., Romani, L., Netea, M. G., and Latge, J. P. (2017). *Aspergillus fumigatus* morphology and dynamic host interactions. *Nat. Rev. Microbiol.* 15, 661–674. doi: 10.1038/nrmicro.2017.90

Widmann, C., Gibson, S., Jarpe, M. B., and Johnson, G. L. (1999). Mitogen-activated protein kinase: conservation of a three-kinase module from yeast to human. *Physiol. Rev.* 79, 143–180. doi: 10.1152/physrev.1999.79.1.143

Wong Sak Hoi, J., and Dumas, B. (2010). Ste12 and Ste12-like proteins, fungal transcription factors regulating development and pathogenicity. *Eukaryot. Cell* 9, 480–485. doi: 10.1128/EC.00333-09

Yu, J., Cleveland, T. E., Nierman, W. C., and Bennett, J. W. (2005). *Aspergillus flavus* genomics: gateway to human and animal health, food safety, and crop resistance to diseases. *Rev. Iberoam. Micol.* 22, 194–202. doi: 10.1016/s1130-1406(05)70043-7

Conflict of Interest: The authors declare that the research was conducted in the absence of any commercial or financial relationships that could be construed as a potential conflict of interest.

The handling editor declared a past co-auhorship with one of the authors ÖB.

frontiers in Microbiology

ORIGINAL RESEARCH
published: 19 May 2020
doi: 10.3389/fmicb.2020.00935

Transcriptome Analysis Uncovers a Link Between Copper Metabolism, and Both Fungal Fitness and Antifungal Sensitivity in the Opportunistic Yeast *Candida albicans*

*Inès Khemiri[1], Faiza Tebbji[1] and Adnane Sellam[1,2]**

[1] CHU de Québec Research Center, Université Laval, Quebec City, QC, Canada, [2] Department of Microbiology, Infectious Diseases and Immunology, Faculty of Medicine, Université Laval, Quebec City, QC, Canada

OPEN ACCESS

Edited by:
Laure Ries,
University of São Paulo, Brazil

Reviewed by:
Changbin Chen,
Institut Pasteur of Shanghai (CAS), China
Delma S. Childers,
University of Aberdeen, United Kingdom

***Correspondence:**
Adnane Sellam
Adnane.sellam.1@ulaval.ca;
adnane.sellam@gmail.com

Specialty section:
This article was submitted to Fungi and Their Interactions, a section of the journal Frontiers in Microbiology

Received: *11 February 2020*
Accepted: *20 April 2020*
Published: *19 May 2020*

Citation:
Khemiri I, Tebbji F and Sellam A (2020) Transcriptome Analysis Uncovers a Link Between Copper Metabolism, and Both Fungal Fitness and Antifungal Sensitivity in the Opportunistic Yeast Candida albicans. Front. Microbiol. 11:935. doi: 10.3389/fmicb.2020.00935

Copper homeostasis is an important determinant for virulence of many human pathogenic fungi such as the highly prevalent yeast *Candida albicans*. However, beyond the copper transporter Ctr1, little is known regarding other genes and biological processes that are affected by copper. To gain insight into the cellular processes that are modulated by copper abundance in *C. albicans*, we monitored the global gene expression dynamic under both copper depletion and excess using RNA-seq. Beyond copper metabolism, other different transcriptional programs related to fungal fitness such as stress responses, antifungal sensitivity, host invasion and commensalism were modulated in response to copper variations. We have also investigated the transcriptome of the mutant of the copper utilization regulator, *mac1,* and identified potential direct targets of this transcription factor under copper starvation. We also showed that Mac1 was required for the invasion and adhesion to host cells and antifungal tolerance. This study provides a framework for future studies to examine the link between copper metabolism and essential functions that modulate fungal virulence and fitness inside the host.

Keywords: *Candida albicans*, RNA-seq, copper metabolism, fungal fitness, antifungal sensitivity

INTRODUCTION

The redox properties of copper (Cu) make this trace element crucial for biological systems as it serves as an essential cofactor of enzymes that function in many biological processes including iron acquisition, antioxidative defense, and energy metabolism (Festa and Thiele, 2011). Cu is also toxic for the cell and its accumulation should be tightly monitored and kept at homeostatic levels. In the context of host-pathogen interaction, Cu is thought to be elemental for what is known as nutritional immunity of host cells during fungal infections (Hood and Skaar, 2012; Samanovic et al., 2012; Djoko et al., 2015). Cu is differentially distributed across different anatomical sites of the human body where it is mostly abundant in skeleton and bone marrow, skeletal muscle, liver, brain, and blood (Linder et al., 1998). Host cells seems to use both Cu-sequestration and Cu-poisoning to limit

fungal pathogens from proliferating in different niches. In the case of the meningitis causing agent *Cryptococcus neoformans*, Cu is available at limiting concentrations in the brain interstitium while it is highly abundant in lung airways (Ballou and Wilson, 2016). For the highly prevalent human pathogenic yeast *Candida albicans*, Cu availability is highly dynamic for the same anatomical niche within the host. For instance, upon earlier phase of kidney colonization, *C. albicans* is confronted by high levels of Cu which is considered as a host-imposed Cu-poisoning strategy (Mackie et al., 2016; Culbertson et al., 2020). This earlier Cu spike is followed by a rapid sequestration by renal tissues to probably limit fungal growth as *C. albicans* activates its own Cu utilization machinery to promote its fitness.

Our current knowledge on regulatory mechanisms of Cu homeostasis of eukaryotic cells came mainly from works in the model yeast *Saccharomyces cerevisiae*. When Cu becomes limiting, *S. cerevisiae* promotes Cu import through the activation of the transcription factor Mac1 that induces the transcription of the high affinity Cu membrane transporters Ctr1 and Ctr3 (González et al., 2008). Transcript levels of the ferric reductase Fre1 and Fre7 that reduces Cu ($Cu^{2+} \rightarrow Cu^{+}$) prior to its uptake by Ctr1 is also activated by Mac1 (van Bakel et al., 2005). Response to Cu excess is primarily controlled by the transcription factor Cup2 that activates different Cu-chaperones such as Cup1-1, Crs5 and Ccc2 in addition to the Cu-transporting P-type ATPase that are required for Cu tolerance (González et al., 2008).

Pathogenic fungi are exposed to a labile pool of Cu within the human host and has consequently evolved a tight regulatory control to ensure cellular homeostasis of this trace element. As in *S. cerevisiae*, *C. albicans* uses Mac1 to mediate the activation of both the Cu transporter Ctr1 and the ferric reductase Fre7 under Cu starvation (Marvin et al., 2003; Woodacre et al., 2008). Furthermore, *C. albicans* uses the P-type ATPase Crp1 that function as a Cu extrusion pump to survive in high Cu environments (Weissman et al., 2000). *C. albicans* has an ortholog of Cup2 that is required for Cu tolerance (Homann et al., 2009), however, its role as a transcriptional modulator of Cu detoxification has not been explored so far. Interestingly, under Cu excess, *C. albicans* activates the Cu-dependent superoxide dismutase Sod1 (Cu-Sod1) to neutralize the superoxide anion while it uses the Mn-requiring Sod3 (Mn-Sod3) under Cu limitation (Li et al., 2015). As Sod enzymes use metals as cofactors to convert superoxide to oxygen and hydrogen peroxide, *C. albicans* shifts metal co-factors for superoxide dismutase depending on Cu abundance in the colonized niches. *C. neoformans* depends on the Cu-transporters Ctr1 and Ctr4 for Cu uptake and on the Cu-metallothioneins MT1 and MT2 for Cu detoxification (Ding et al., 2011, p. 99). In this pathogenic fungus, both Cu uptake and detoxification are governed by the same transcriptional regulator Cuf1 (Ding et al., 2011, p. 99; Garcia-Santamarina et al., 2018). In *Aspergillus fumigatus*, intracellular Cu uptake relies on the Cu-transporters *ctrA2* and *ctrC* that are both under the control of the transcriptional factor *Afmac1* (Cai et al., 2017). Alteration of either uptake or detoxification processes in *C. albicans*, *A. fumigatus*, *C. neoformans* and the dimorphic fungus *Histoplasma capsulatum* impairs fungal virulence and fitness (Waterman et al., 2007; Ding et al., 2013; Sun et al., 2014; Mackie et al., 2016; Cai et al., 2017) suggesting that Cu metabolism might be a promising therapeutic targeted to treat fungal infections.

While Cu homeostasis is an important virulence determinant in *C. albicans* (Mackie et al., 2016), the impact of Cu availability on the transcriptome of this important human pathogen remain unexplored. Furthermore, beyond the Cu transporter Ctr1, little is known regarding other genes or biological process that are affected by Cu abundance or modulated by Mac1 at the genome level in *C. albicans*. To gain insight into the cellular processes that are modulated by Cu abundance in *C. albicans*, we monitored the global gene expression dynamic under both Cu depletion and excess using RNA-seq. Our data uncovered that, in addition to Cu utilization genes, other different cellular processes related to fungal fitness were modulated in response to Cu fluctuations. We have also investigated the transcriptome of *mac1* mutant and identified potential direct targets of this transcription factor under Cu starvation. We also showed that Mac1 was required for the invasion and the adhesion to human enterocytes and antifungal tolerance. Thus, this study provides a framework for future studies to examine the link between Cu metabolism and essential functions that modulate fungal virulence and fitness inside the host.

MATERIALS AND METHODS

Fungal Strains and Media

Candida albicans was routinely maintained at 30°C on YPD (1% yeast extract, 2% peptone, 2% dextrose, with 50 mg/ml uridine). The *C. albicans* WT strain SN250 (*ura3*/:imm434/*URA3 iro1*:*IRO1*/*iro1*:imm434 *his1*:*hisG*/*his*:*hisG leu2*:Cd*HIS1*/*leu2*:Cm*LEU2 arg4*/*arg4*) (Noble et al., 2010) used in this study derives from the SC5314 clinical strain. *mac1* (*mac1*:*LEU2*/*mac1*:*HIS1*) deletion mutant come from the transcription factor deletion collection (Homann et al., 2009) that was constructed in SN125 (*his1*/*his1*, *leu2*/*leu2*, *arg4*/*arg4*, *URA3*/*ura3*:imm434, *IRO1*/*iro1*:imm434).

To build the *mac1* complemented strain, the *MAC1* gene was reintegrated into the null mutant *mac1* strain using pDUP3 plasmid (Gerami-Nejad et al., 2013). Briefly, the *MAC1* locus containing its endogenous promoter [(−678,0) intergenic region] was amplified by PCR using primers containing flanking sequences homologous to pDUP3. The resulting pDUP3-*MAC1* construct was digested by *Sfi*I and integrated into the *NEU5L* genomic site of the *mac1* strain as previously described (Gerami-Nejad et al., 2013) using lithium acetate transformation (Wilson et al., 2000). Transformants were selected on YPD plates supplemented with 200 μg/ml nourseothricin and correct integration was verified by PCR. Primers used for *MAC1* cloning in pDUP3 plasmid and for the diagnosis of pDUP3-*MAC1* integration are listed in the **Supplementary Table S1**.

Growth Inhibition Assays

All chemicals used in this study were provided by Sigma-Aldrich (St. Louis, MO, United States). Working stock solutions of

Copper (II) Sulfate ($CuSO_4$; 532 mM), Bathocuproinedisulfonic acid disodium salt (BCS; 8 mM), Bathophenanthrolinedisulfonic acid (BPS; 8 mM) and fluconazole (3.3 mM) were prepared using Milli-Q sterile water. Amphotericin B and miconazole stock solutions were prepared using dimethyl sulfoxide (DMSO; Sigma-Aldrich) at a concentration of 1 mM and 2 mM, respectively.

For growth assays in liquid YPD medium, overnight cultures of *C. albicans* were resuspended in fresh YPD medium at an OD_{600} of 0.05 and added to a flat-bottom 96-well plate in a total volume of 100 µl per well in addition of the tested compounds. For each experiment, a compound-free positive growth control and a cell-free negative control were included. Growth assay curves were performed in triplicate in 96-well plates using a Sunrise plate-reader (Tecan) at 30°C under constant agitation with OD_{600} readings taken every 10 min for 48 h.

For spot dilution assays, overnight cultures were diluted to an OD_{600} of 0.1 and fivefold serial dilutions were prepared in distilled water. A total of 4 µl of each dilution were spotted on YP-agar with different carbon sources (glucose, maltose, glycerol, and ethanol) at 2% or on YPD plates with the different antifungals: amphotericin B (1 µg/ml), miconazole (0.5 µg/ml), and fluconazole (0.5 µg/ml). Plates were incubated at 30°C for 3 days and imaged using the SP-imager system.

Expression Analysis by RNA-Seq and qPCR

Overnight cultures of *mac1* mutant and WT (SN250) strains were diluted to an OD_{600} of 0.1 in 40 ml of fresh YPD-uridine medium and grown at 30°C under agitation (200 rpm) to an OD_{600} of 0.4. Cultures were then either left untreated or exposed to either $CuSO_4$ (2 mM) or BCS (400 µM), and incubated at 30°C for 30 min. For each condition, a total of two biological replicates were considered for RNA-seq analysis. Cells were then harvested by centrifugation at 3,000 × *g* for 5 min and the pellets were quick-frozen and stored at −80°C. Total RNA was extracted using an RNAeasy purification kit (Qiagen) and glass bead lysis in a Biospec Mini 24 bead-beater. Total RNA was eluted, assessed for integrity on an Agilent 4200 TapeStation System prior to cDNA library preparation. The NEBNext UltraTM II RNA Library Prep Kit for Illumina was used to construct the RNA-seq library following the manufacturer's instruction. The quality, quantity and the size distribution of the libraries were determined using an Agilent Bioanalyzer. A 2 × 100 paired-end sequencing of cDNAs were performed using an Illumina Novaseq6000 sequencing system.

For qPCR confirmation experiments, a total of three biological and three assay replicates were performed. cDNA was synthesized from 1 µg of total RNA using High-Capacity cDNA Reverse Transcription kit (Applied Biosystems). The mixture was incubated at 25°C for 10 min, 37°C for 120 min and 85°C for 5 min. Two units per microliter of RNAse H (NEB) was added to remove RNA and samples were incubated at 37°C for 20 min. qPCR was performed using a LightCycler 480 Instrument (Roche Life Science) for 40 amplification cycles with the PowerUp SYBR Green master mix (Applied Biosystems). The reactions were incubated at 50°C for 2 min, 95°C for 2 min and cycled for 40 times at 95°C, 15 s; 54°C, 30 s; 72°C, 1 min. Fold-enrichment of each tested transcripts was estimated using the comparative ΔΔCt method. To evaluate the gene expression level, the results were normalized using Ct values obtained from Actin (*ACT1*, C1_13700W_A). Primer sequences used for this analysis are summarized in **Supplementary Table S1**.

RNA-Sequencing Data Analysis

Adaptor sequences and low quality score bases (Phred score < 30) were first trimmed using Trimmomatic (Bolger et al., 2014). The resulting reads were aligned to the *C. albicans* reference assembly SC5314 from Ensembl[1], using STAR (Dobin et al., 2013). Read counts are obtained using HTSeq (Anders et al., 2015) and are represented as a table which reports, for each sample (columns), the number of reads mapped to a given gene (rows). For all downstream analyses, we excluded lowly expressed genes with an average read count lower than 1 across all samples, resulting in 5,942 genes in total. The R package *limma* (Ritchie et al., 2015) was used to identify differences in gene expression levels between treated and non-treated samples. Nominal *p*-values were corrected for multiple testing using the Benjamini–Hochberg method. Differentially expressed transcripts in the **Supplementary Tables S2, S4** were identified using a false-discovery rate (FDR) of 5% and twofold enrichment cut-off. Gene ontology (GO) analysis was performed using GO Term Finder of the Candida Genome Database (Skrzypek et al., 2017). The GSEA Pre-Ranked tool[2] (Subramanian et al., 2005) was used to determine statistical significance of correlations between the characterized transcriptomes with a ranked gene list or GO biological process terms as described by Sellam et al. (2014). All RNA-seq raw data are available in the **Supplementary Table S5** and also at Gene Expression Omnibus (GEO) with the accession number GSE147697.

HT-29 Adherence and Damage Assay

Damage to the human colon epithelial cell line HT-29 was assessed using a lactate dehydrogenase (LDH) cytotoxicity detection kit^{PLUS} (Roche), which measures the release of the LDH enzyme in the growth medium. HT-29 cells were grown in 96-well plate as monolayers in McCoy's medium supplemented with 10% FBS at 1×10^4 cells per well and incubated at 37°C with 5% CO_2 overnight. HT-29 cells were then infected with *C. albicans* cells at MOI cell:yeast of 1:2 in the presence or the absence of BCS (100 µM or 800 µM), for 24 h at 37°C with 5% CO_2. HT-29 cells were also incubated with 100 µM or 800 µM BCS alone to rule out any toxic effect of this compound on HT-29 cells. No discernable growth defect of HT-29 cells was noticed with both BCS concentrations. Following incubation, 100 µl of supernatant was removed from each experimental well and LDH activity in this supernatant was determined by measuring the absorbance at 490 nm (OD_{490}) following the manufacturer's instructions.

For the adherence assay, *C. albicans* cells were co-incubated with HT-29 cells at 37°C and 5% CO_2 for 1 h. Non-adherent

[1]http://fungi.ensembl.org/Candida_albicans_sc5314_gca_000182965/Info/Index
[2]http://www.broadinstitute.org/gsea/

cells were removed by rinsing five times with 1 ml PBS and cells were then fixed with 4% paraformaldehyde. HT-29 cells were permeabilized with 0.5% Triton X-100 and adherent fungal cells were stained with 2 μM calcofluor white during 30 min in the dark at room temperature. Adherent cells were visualized using Cytation 5 high-content microscope with 20× magnification and DAPI filter. For each well, at least 10 fields were photographed.

RESULTS

Global Transcriptional Responses to Copper Depletion and Repletion in *C. albicans*

To gain insight into the cellular processes that are modulated by Cu abundance in the pathogenic yeast *C. albicans*, we monitored the global gene expression dynamic under both Cu depletion (400 μM BCS) and excess (2 mM $CuSO_4$) using RNA-seq. Transcripts associated with both Cu utilization and detoxification were identified by comparing the transcriptional profiles of WT cells treated with BCS and $CuSO_4$, respectively, to that of non-treated WT cells. In response to Cu excess, *C. albicans* activated transcripts associated with Cu detoxification and transport including the cytosolic small chaperone *ATX1*, the metallothionein *CUP1*, the P-type ATPase *CCC2* and the Cu efflux pump *CRP1* (**Figures 1A,B**). We also found that genes of Cu uptake such as the Cu transporter *CTR1*, the transcription factor *MAC1* and the cupric reductase *FRE7* were downregulated (**Figure 1A**). Transcripts involved in iron uptake, and both cytosolic and mitochondrial ribosome biogenesis were activated whereas those related to glycolysis, energy and, NAD and hexose/glucose metabolisms were repressed (**Figure 1B**). Genes related to drug response and detoxification such as the MFS transporter *MDR1,* as well as its transcriptional activator *MRR1*, together with other MFS (*FLU1*, *NAG3*, *NAG4*, *TPO3*, *TPO4*), ABC (*MLT1*), and MaTE (*ERC1*, *ERC3*) transporters were significantly induced. Among repressed transcripts, we also found many genes of the ergosterol biosynthesis pathway (*ERG1*, *ERG3*, *ERG11*, *ARE2*) in addition to their *bona fide* transcriptional regulator Upc2 (**Supplementary Table S2**).

Under Cu deprivation, as in other fungi, *C. albicans* upregulated genes required for Cu internalization including the Cu transporter Ctr1 and the ferric reductases Fre7, Fre30, and orf19.7077 that reduce Cu to facilitate its uptake by Ctr1 (**Figures 1A,C** and **Supplementary Table S2**). Other transcripts including the manganese transporter *SMF12* and the ABC transporter *SNQ2* were also activated. We also found that under Cu depletion, *C. albicans* upregulated the Mn-dependant superoxide dismutase *SOD3* (Mn-*SOD3*) and repressed the Cu-dependant *SOD1* (Cu-*SOD1*). Reversely, under Cu excess, Cu-*SOD1* were activated and Mn-*SOD3* repressed. This switch from Cu to Mn cofactors of Sods is an adaptative strategy for *C. albicans* cells to resist to reactive oxygen species (ROS) inside the host when Cu become limiting (Li et al., 2015). Taken together, our data suggest that Cu abundance did not affect exclusively Cu detoxification and utilization pathways but also other biological processes that might require this essential micronutrient to fulfill their functions.

qPCR confirmed gene expression alterations as shown by RNA-seq for both Cu utilization (*MAC1, CTR1, FRE7*, and *SOD3*) and detoxification (*CUP1*, *CRP1*, *SOD1*, and *CUP2*) genes under both Cu deprivation and excess, respectively (**Figure 1D**).

Gene Set Enrichment Analysis of the *C. albicans* Cu-Sensitive Transcriptomes

Gene set enrichment analysis (GSEA) was used to mine the transcriptomes associated with both Cu starvation and excess, to uncover potential resemblance with *C. albicans* genome annotations and other experimental large-scale omics data (Subramanian et al., 2005; Sellam et al., 2014; **Supplementary Table S3**). **Figures 2A,C** summarize the significant correlations of the Cu-responsive transcriptomes with either functional GO categories, *C. albicans* transcriptional signatures in different physiological conditions or in specific mutant background, and also with genome-wide promoter occupancies data. For both Cu availability conditions, GSEA recapitulated most of the GO correlations as identified by the conventional methodology. Cells growing in Cu excess exhibited a transcriptional profile similar to that of different mutants of transcription factors such as *upc2*, *efg1*, and *ace2* and to mutants of different signaling pathways including Ras1-cAMP-PKA (*ras1*) and the AGC protein kinase Sch9 pathways in addition to a significant correlation with a set of genes with protomers enriched in Cat8 binding motif (**Figures 2A,B** and **Supplementary Table S3**).

Under Cu deprivation, upregulated transcripts were significantly similar to the *C. albicans* transcriptional programs expressed during the colonization of the murine gut (Pierce et al., 2013), and the interaction with host cells including the human oral epithelial cells (Spiering et al., 2010) and the bone marrow-derived mouse macrophages (Marcil et al., 2008). This similarity suggests that, during the interaction with the host, *C. albicans* might be confronted by a Cu-deprived environment that the host might generate as an immune strategy to sequester this essential metal. Transcriptional similarities were also observed with the transcriptomes associated with fungal fitness and virulence traits including persistence under hypoxia and biofilm formation or during exposures to antifungal molecules (ketoconazole, rapamycin, and geldanamycin) (**Figures 2C,D** and **Supplementary Table S3**). As in other human pathogenic fungi, *C. albicans* might connect the control of fitness and virulence attributes to the Cu cellular adaptive machinery as a cue to promote either commensalism or pathogenicity (Ballou and Wilson, 2016).

Mac1-Mediated Control of Copper Deprivation

Prior to assessing the contribution of the transcription factor Mac1 to the global response of *C. albicans* to Cu deprivation, we first tested and confirmed the growth defect of *mac1* mutant under different conditions including Cu deprivation, utilization of non-fermentable carbon sources and iron chelation as previously reported (Marvin et al., 2004, p. 1;

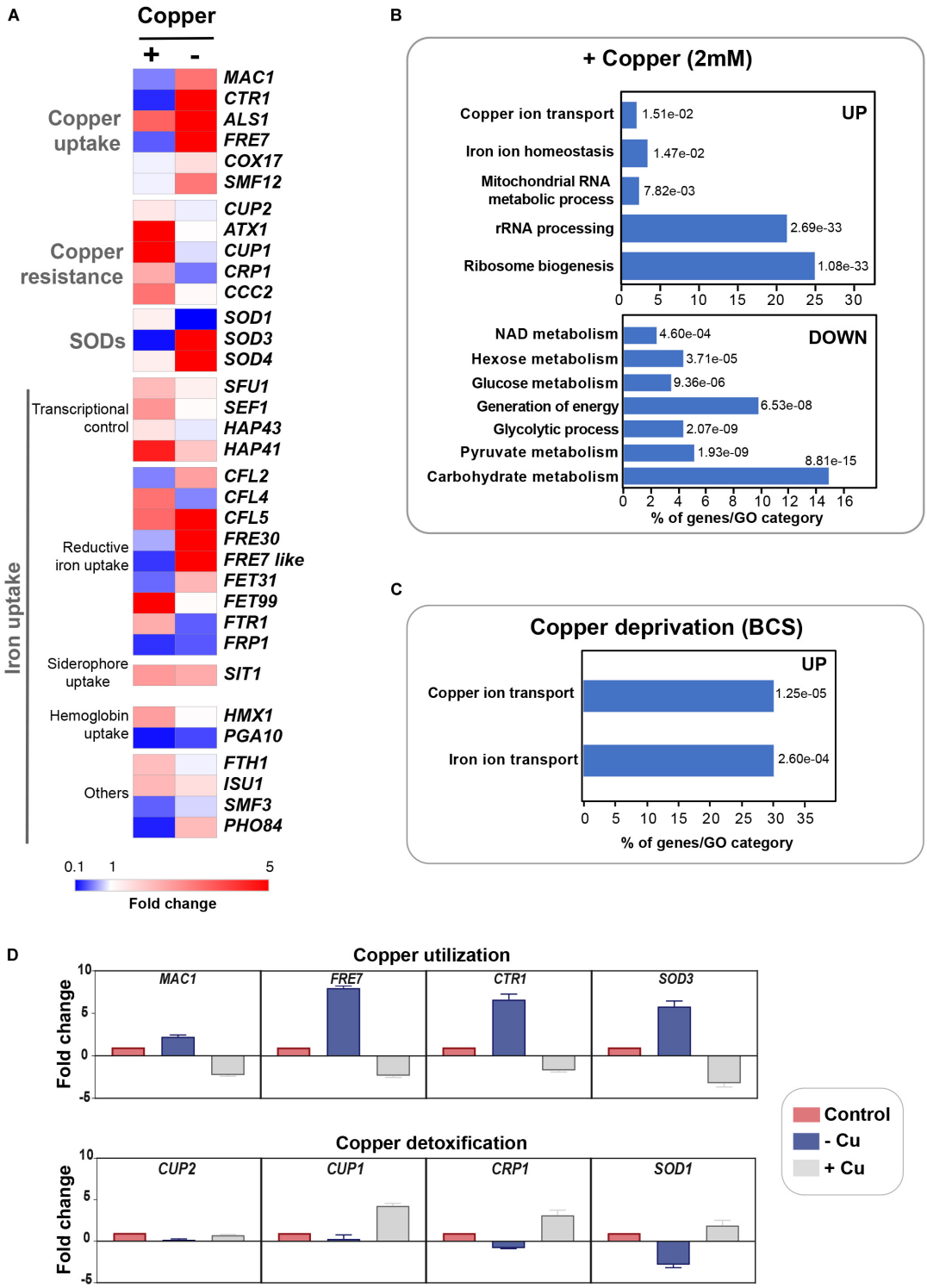

FIGURE 1 | Genome-wide transcriptional profiling of *C. albicans* to Cu variations by RNA-seq. **(A)** Heat map visualization of the transcript levels of the Cu homeostasis pathway in *C. albicans* in response to Cu excess and deprivation. *C. albicans* WT cells were exposed to either 2 mM $CuSO_4$ or 400 μM BCS, and incubated at 30°C for 30 min. Transcripts associated with both Cu utilization (copper "–") and detoxification (copper "+") were identified by comparing the transcriptional profiles of WT cells treated with BCS and CuSO4, respectively, to that of non-treated WT cells. **(B,C)** Gene function and biological process enriched in the transcriptional profiles of *C. albicans* growing under Cu excess **(B)** and limitation **(C)**. **(D)** qPCR validation of RNA-seq data. Transcript levels of both Cu utilization (*MAC1, CTR1, FRE7*, and *SOD3*) and detoxification (*CUP1*, *CRP1*, *SOD1*, and *CUP2*) genes were assessed and fold-changes were calculated using the comparative ΔΔCt method. Data were normalized using Ct values obtained from actin gene in each condition.

A

	Description	NES
Up-regulated transcripts		
GO Terms	Transition metal ion transport	2.90
	Iron ion transport	2.87
	rRNA metabolic process	2.71
Transcriptional profiles	Nitrosative stress Up	2.62
	upc2 Do	2.59
Transcription factor	Cat8_TF	2.59
Down-regulated transcripts		
GO Terms	Cytosolic ribosome	-4.69
	Pyruvate metabolism	-2.65
	Glycolysis	-2.58
	Mitochondrial membrane part	-3.05
Transcriptional profiles	*ace2* Do	-3.73
	efg1 Do	-3.53
	ras1 Do	-3.11
	sch9 Do	-2.99

B

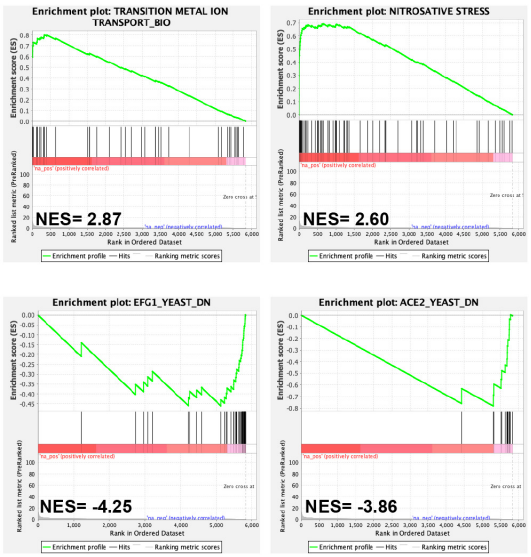

C

	Description	NES
Up-regulated transcripts		
GO Terms	Mitochondrion	6.42
	Mitochondrial ribosome	4.78
	Hexose transport	3.14
	Metal ion transport	4.11
Transcriptional profiles	BMDM Phagocytosis Up	6.25
	Ketoconazole Up	6.45
	RHE90 Up	5.25
	sch9 Up	4.27
	GI colonization Up	3.53
	upc2 Up	3.49
	Geldanamycin Up	3.50
	Rapamycin Up	3.09
	sef1 (+BPS) Up	3.25
Transcription factor	Zap1_ChIP	3.31
	Cup2 motif	3.31
Down-regulated transcripts		
GO Terms	Cytosolic ribosome	-4.95
	Sulfur amino acid metabolism	-2.96
	Glycolysis	-3.80
	Methionine metabolic process	-3.72
Transcriptional profiles	*tye7* Do	-6.41
	Hypoxia Up	-7.49
	Heat shock Up	-3.84
	Hyphae Do	-4.32
Transcription factor	Tye7_TF	-6.46
	Gal4_TF	-3.40
	Tbf1_TF	-3.84

D

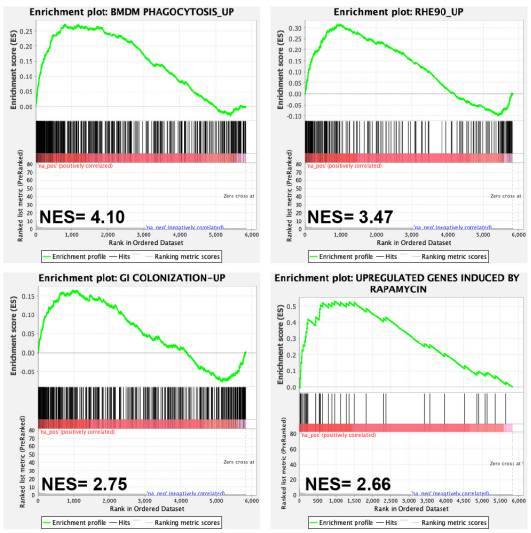

FIGURE 2 | Gene set enrichment analysis of RNA-seq data. RNA-seq data of Cu excess **(A,B)** and deprivation **(C,D)** were analyzed using gene set enrichment analysis (GSEA). Relevant correlations between *C. albicans* transcriptome under Cu excess **(A)** and limitation **(C)** and other gene sets and functions are summarized. The complete GSEA correlations are listed in **Supplementary Table S3**. Graphs of GSEA for both Cu abundance conditions were also shown **(B,D)**. NES, normalized enrichment score.

Homann et al., 2009; Khamooshi et al., 2014; **Figure 3**). To identify Mac1-dependant transcripts associated with Cu utilization, we compared the transcriptional profile of *mac1* cells exposed to BCS to that of non-treated *mac1* cells. Overall, our RNA-seq data showed that the inducibility of genes of Cu uptake and utilization including *CTR1*, *ALS1*, *FRE17, COX17* in addition to the Mn-*SOD3* and many iron uptake transcripts (*CFL2*, *CFL5*, *FRE30*, *FET31*, and orf19.7077) were lost in *mac1* mutant under Cu depleted conditions (**Figure 4A**). This data confirmed the role of Mac1 as the *bona fide* transcriptional regulator of Cu homeostasis in *C. albicans*.

Other cellular processes were also altered in *mac1* mutant as compared to the WT under Cu deprivation (**Figure 4B** and **Supplementary Table S4**) including the repression of respiratory electron transport chain genes and the upregulation of iron homeostasis processes (**Figures 4A–C**). This transcriptional

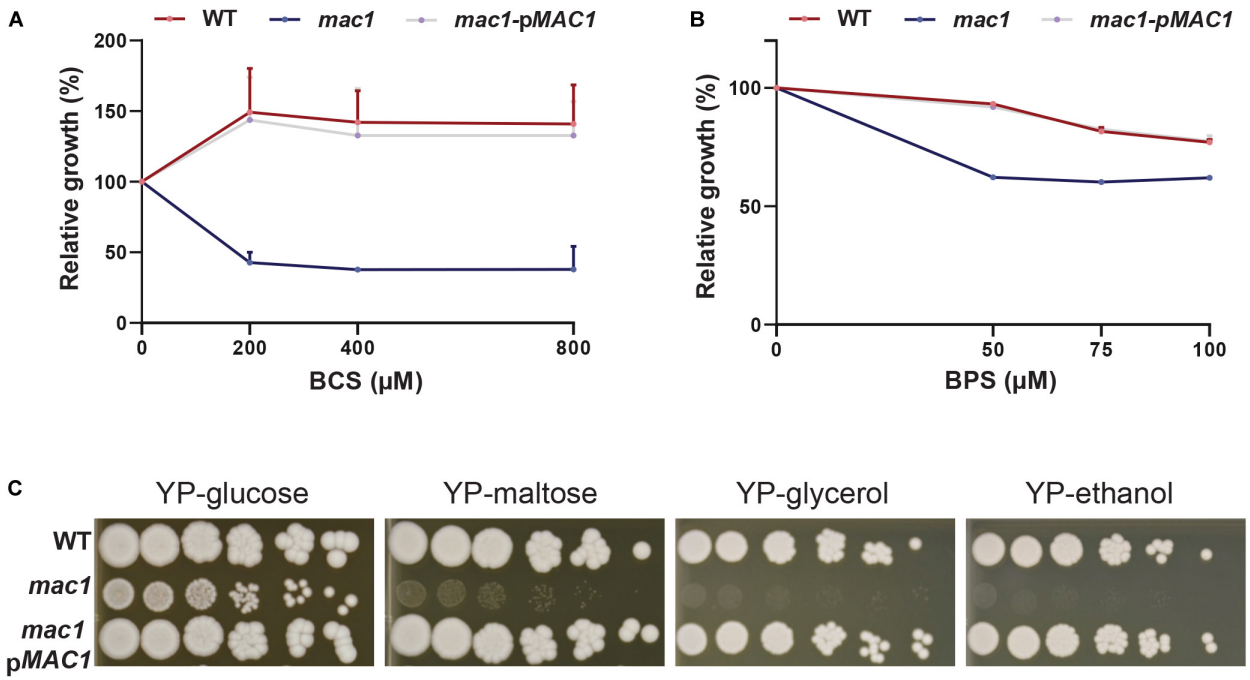

FIGURE 3 | Phenotypic characterization of *mac1* mutant. **(A,B)** The *C. albicans* WT, *mac1* and the *mac1* complemented strains were grown at 30°C in YPD supplemented with different concentrations of BCS or BPS. $OD_{600\ nm}$ reading was taken after 48 h of incubation. ODs measurements for each concentration of BCS and BPS are the mean of triplicate. **(C)** *mac1* is required for the utilization of alternative and non-fermentable carbon sources. The *C. albicans* WT, *mac1* and the *mac1* complemented strains were serially diluted, spotted on media with the indicated carbon sources and incubated for 3 days at 30°C.

signature is reminiscent of an iron deprived environment that is most likely due to the fact that many iron uptake and utilization proteins depend on Cu for their functionality (Knight et al., 2002). Accordingly, a total of 34 among the 55 upregulated transcripts in *mac1* were also upregulated in *C. albicans* cells under iron starvation as previously shown (Chen et al., 2011) and most of those genes are under the control of the Sfu1-Sef1-Hap43 iron transcriptional control axis (**Figure 4C**). Of note, we found that the transcriptional level of Sef1 and the CCAAT-binding factors Hap3, Hap1, and Hap43 were activated in *mac1* mutant.

We also analyzed the 50 gene promoters that *mac1* failed to activate for potential consensus binding motifs and identified two enriched mini-sequences one of which is the well-known Mac1 binding site (McDaniels et al., 1999; Garcia-Santamarina et al., 2018; **Figure 4D**). Mac1 binding motif was found in the promoters of Ctr1 and Sod3, as previously reported (Woodacre et al., 2008; Li et al., 2015), in addition to the ferric reductases Fre30 and Fre7 (**Table 1**). Mac1-regulatory motif was also found in 5′ cis-regulatory regions of genes that are not related directly to Cu metabolism such as electron transport chain (Sdh2, Sdh4, Cyb2), nitrosative stress response (Yhb1) and, manganese (Smf12) and iron transport (Ftr1) genes.

Copper Modulates Antifungal Sensitivity and Virulence

Gene set enrichment analysis of the *C. albicans* transcripts modulated by Cu limitation uncovered a significant correlation with the transcriptional program expressed when cells are challenged with the azole antifungal, ketoconazole (**Figure 2C**). This led to hypothesize that both stresses affect similar cellular processes in *C. albicans* or that Cu homeostasis modulates drug sensitivity. We found that genetic inactivation of *MAC1* rendered *C. albicans* cells hypersensitive to both polyene (amphotericin B) and azole (fluconazole and miconazole) antifungals (**Figure 5A**). Antifungal sensitivity of *mac1* was reversed by supplementing the growth medium by $CuSO_4$ which suggests that Cu homeostasis modulates antifungal tolerance in *C. albicans* (**Figure 5B**).

As the transcriptional profile of *C. albicans* cells under Cu deprivation is similar to that experienced during the interaction with the human host (**Figures 2C,D**), we tested whether Mac1 is required to damage the HT-29 human enterocytes using the LDH release assay. *mac1* mutant exhibited a reduced ability to damage HT-29 cells as compared to the WT and the revertant strains (**Figure 5C**). HT-29 damage by *mac1* mutant was further attenuated when both *C. albicans* and host cells were cocultured in the presence of BCS. Interestingly, Cu chelation exerts a protective antifungal activity since supplementation of the culture medium with 100 and 800 μM of BCS prevented 20 and 62% of HT-29 damage by the *C. albicans* WT strain, respectively. Together these data suggest that Cu homeostasis in *C. albicans* and the availability of this metal in host niches is essential for fungal virulence.

The adherence of *mac1* mutant to the HT-29 enterocytes was also tested and the obtained data indicate a significant

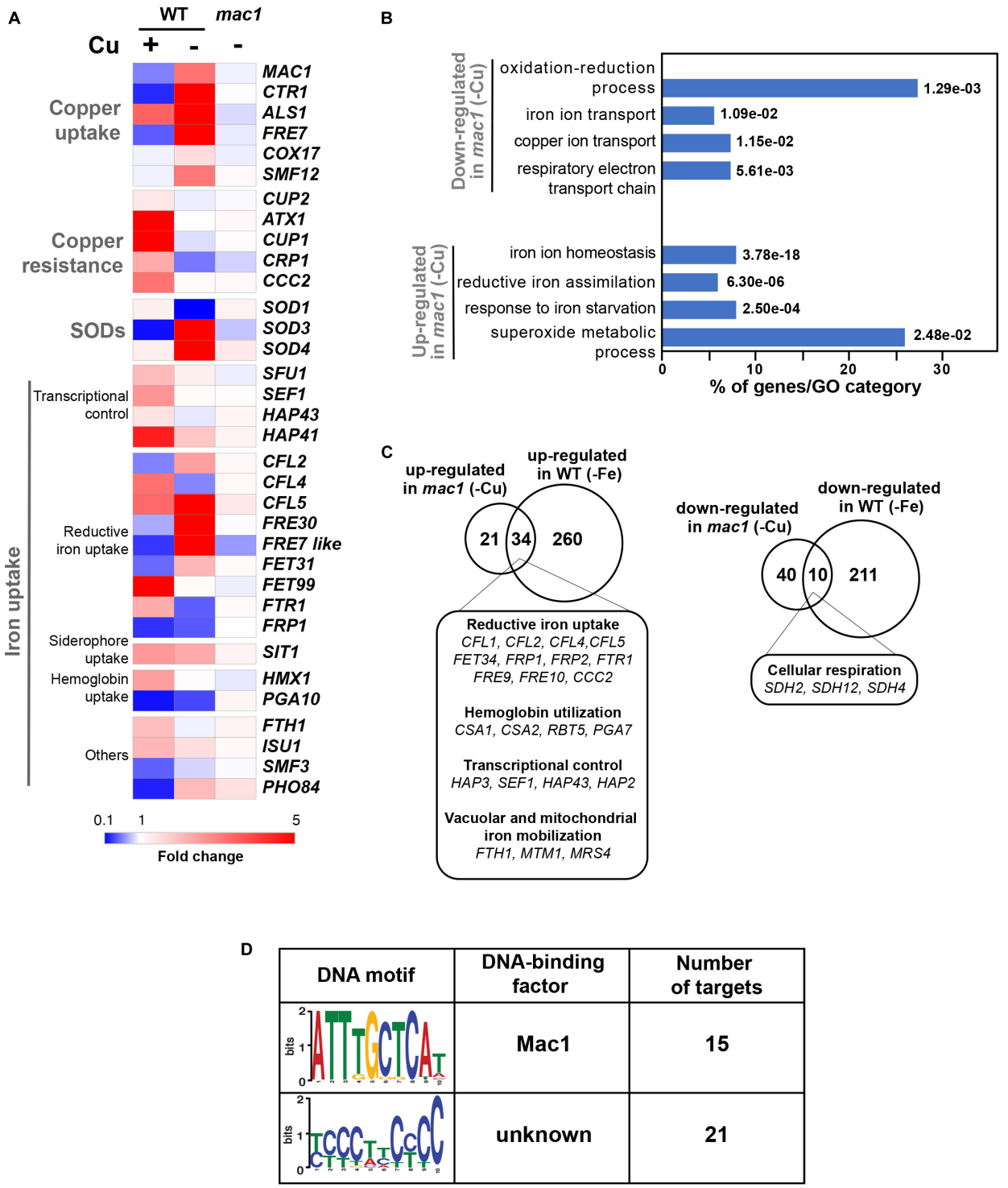

FIGURE 4 | The Mac1-dependant control of Cu deprivation transcriptome. **(A)** Transcriptional alterations of Cu homeostasis genes in both WT and *mac1*. Heatmap visualization was presented as in **Figure 1A** for the WT and includes *mac1* RNA-seq data. As the WT strain, *mac1* mutant were exposed to 400 μM BCS, and incubated at 30°C for 30 min. Mac1-dependant transcripts associated with Cu utilization were identified by comparing the transcriptional profile of *mac1* cells exposed to BCS to that of non-treated *mac1* cells. **(B)** Gene ontology analysis of upregulated and downregulated transcripts in *mac1* in response to BSC. The *p*-values were calculated using hypergeometric distribution. **(C)** Comparison of the Cu- and the iron-depletion transcriptomes of *C. albicans* (from Chen et al., 2011). Venn diagrams summarize the similarity between up- and downregulated transcripts under both iron and Cu starvations. Functional gene categories enriched in both conditions are indicated. **(D)** *De novo* prediction of DNA cis-regulatory motif enriched in the 50 gene promoters that *mac1* failed to activate using MEME analysis tool (http://meme-suite.org).

TABLE 1 | List of genes with putative Mac1 cis-regulatory motif.

Gene name	Orf19 ID	Motif location		Description
		Start	End	
CTR1	orf19.3646	−274	−266	Copper transporter
FTR2	orf19.7231	−501	−493	High-affinity iron permease
FRE30	orf19.6140	−237	−229	Protein with similarity to ferric reductases
	orf19.7078	−893	−885	Ortholog of *S. cerevisiae* YCL012C, proteins localize to the endoplasmic reticulum and vacuole
FRE7 like	orf19.7077	−133	−125	Putative ferric reductase
CWH43	orf19.3225	−261	−253	Putative sensor/transporter protein with a predicted role in cell wall biogenesis
TIM12	orf19.4620	−202	−194	Component of the Tim22 complex, involved in protein import into mitochondrial inner membrane
	orf19.1409.2	−668	−660	Protein of unknown function with predicted transmembrane domain
		−949	−941	
FDH1	orf19.638	−243	−235	Formate dehydrogenase; oxidizes formate to CO_2
YHB1	orf19.3707	−834	−824	Nitric oxide dioxygenase; acts in nitric oxide scavenging/detoxification
	orf19.6277	−423	−415	Protein of unknown function, has a PhoX domain with phosphoinositide-binding activity
SDH4	orf19.4468	−265	−257	Succinate dehydrogenase
SMF12	orf19.2270	−279	−271	Manganese transporter
CYB2	orf19.5000	−138	−130	Putative cytochrome b2 precursor
SOD3	orf19.7111.1	−153	−145	Cytosolic manganese-containing superoxide dismutase
SDH2	orf19.637	−297	−289	Succinate dehydrogenase, Fe-S subunit

reduction of *mac1* attachment as compared to the WT and the complemented strain (**Figure 5D**). Moreover, adding or depriving Cu from the growth medium reduced significantly the WT adherence to the HT-29. *mac1* adherence defect to HT-29 was not reverted by Cu supplementation or phenocopied by Cu chelation in the WT strain (**Figure 5D**). This suggests that Mac1 might control other biological processes independently from its *bona fide* role as Cu metabolism modulator.

DISCUSSION

So far, the global response of *C. albicans* to Cu availability remain unexplored. Previous works have focused only on known Cu metabolic genes that are homologous to *S. cerevisiae* such as the Cu transporter Ctr1 (Marvin et al., 2004, 1), the transcription factor Mac1 (Woodacre et al., 2008) and the Cu efflux pump Crp1 (Weissman et al., 2000). Here, we explored the genome-wide transcriptional response of *C. albicans* to elevated Cu or Cu deprivation in order to unbiasedly assess cellular processes associated with fungal fitness that are modulated by Cu availability (**Figure 6**).

Our RNA-seq data recapitulated the *bona fide* fungal response to Cu. When grown under limiting concentrations, *C. albicans* activate Cu utilization genes such as the Cu transporter Ctr1 while under Cu excess genes involved in Cu detoxification (Crp1) and relocalization (Atx1, Cup1, Ccc2) were induced. As in other fungi (van Bakel et al., 2005; Rustici et al., 2007; Garcia-Santamarina et al., 2018), we also found that iron utilization genes were differentially modulated by Cu depletion which might reflect a situation of iron deficiency as well. Indeed, iron uptake depends on the multicopper ferroxidases and consequently Cu deprivation engender a subordinate iron depletion in *C. albicans* cells. Intriguingly, upon Cu excess, transcript levels of the transcription factor Sef1 and its direct target genes related to iron uptake and utilization such as the high affinity iron permease Ftr1, the ferric reductase Cfl5, the siderophore transporter Sit1 and the heme oxygenase Hmx1 were upregulated. This transcriptional signature reflects a defect in iron internalization as was also noticed under Cu limitation. This is similar to what was observed in yeast and mammalian cells where Cu overload deplete intracellular iron levels (Arredondo et al., 2004; Jo et al., 2008). This phenomenon could be explained by the fact that, as eukaryotic cells try to detoxify Cu by efflux, this essential metal become limiting for the Cu-dependent iron uptake machinery which led to iron deficiency.

The main goal of the current study was to uncover, beyond the Cu homeostatic routes, other biological processes that are modulated by Cu. Mining the *C. albicans* Cu transcriptome uncovered significant similarities with transcriptional programs activated by this opportunistic yeast in different niches within the host or during the interaction with immune cells. This highlight the importance of Cu for both fungal fitness and survival to immune response. Accordingly, our data showed that depriving *C. albicans* cells from Cu or inactivating the master transcriptional regulator of Cu uptake *MAC1* both led to decreased damage and adherence to human enterocytes. Virulence defect in these conditions could be attributed to the fact that Cu is important for *C. albicans* to express its virulence factors such as metabolic flexibility and stress resistance. As shown previously (Marvin et al., 2004, p. 1; Mackie et al., 2016) and confirmed by our work, a homeostatic level of Cu is essential for *C. albicans* to metabolize different carbon sources, an important attribute for this yeast to colonize diverse niches with contrasting nutrients (Miramon and Lorenz, 2017; Burgain et al., 2019). Furthermore, as Sod1 requires Cu for the disproportionation

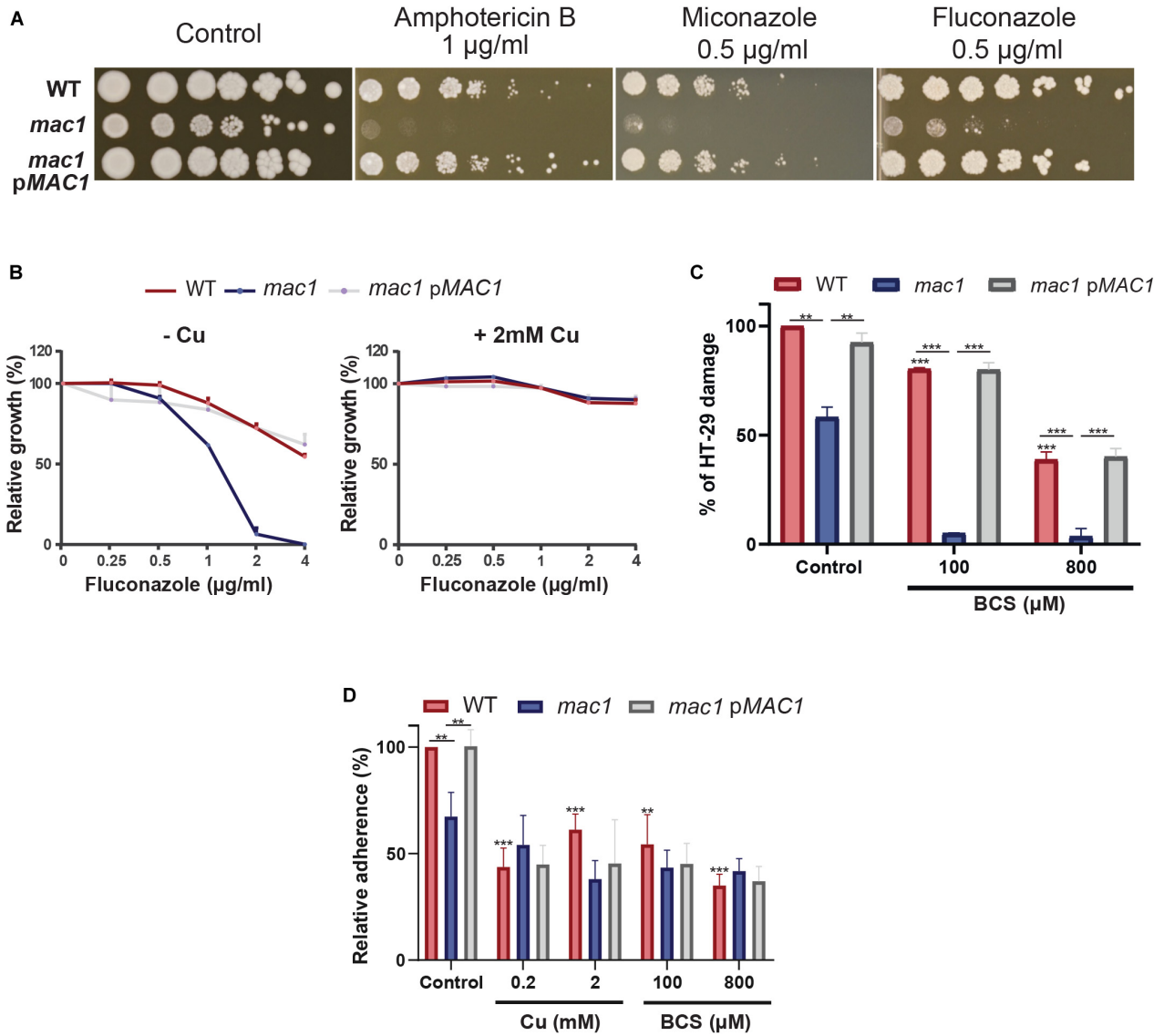

FIGURE 5 | Copper modulates antifungal sensitivity and host invasion. **(A)** Mac1 modulates antifungal sensitivity. *C. albicans* WT, *mac1* and *mac1* complemented strains were serially diluted, spotted on media with different antifungals (amphotericin B, miconazole, and fluconazole) and incubated for 3 days at 30°C. **(B)** Cu supplementation restore *mac1* growth inhibition by fluconazole. The *C. albicans* WT, *mac1* and the *mac1* complemented strains were grown at 30°C on YPD with different concentrations of fluconazole with or without 2 mM $CuSO_4$. OD_{600} reading was taken after 48 h of incubation. **(C)** *MAC1* inactivation and Cu depletion attenuate damage of the human colon epithelial HT-29 cells. HT-29 cell damage was assessed using the lactate dehydrogenase (LDH) release assay and was calculated as percentage of LDH activity in cell infected by *mac1* and the revertant strains, with or without BCS, relatively to cells infected by the WT (SN250) strain. At least four biological replicates were obtained for each experiment. **(D)** *mac1* mutant had a reduced adherence to HT-29 cells. *C. albicans* WT, *mac1* and *mac1* complemented strains were co-incubated with HT-29 for 1 h at 37°C and 5% CO_2. Fungal cells were stained with 2 µM calcofluor white and counted. Data are presented as means ± SD from at least three independent experiments performed in triplicate. The statistical difference for each condition vs. WT control or between conditions was determined by two-tailed Student's *t*-test. $^{**}p < 0.01$, $^{***}p < 0.005$.

of superoxide into peroxide and oxygen, Cu depletion might deteriorate the ability of *C. albicans* to resist the oxidative burst killing by phagocytic immune cells (Kang et al., 2002; Frohner et al., 2009).

At the genome level, our data uncovered that *C. albicans* cells grown in BCS exhibited a transcriptional pattern similar to that of cells challenged with ketoconazole. This suggest that Cu starvation, as azoles, might lead to sterol depletion. In accordance with that, we have shown that the Cu deficient mutant *mac1* was hypersensitive to the ergosterol inhibitors (miconazole, fluconazole, and amphotericin B) as did sterol deficient mutants such as *upc2* (Silver et al., 2004; MacPherson et al., 2005; Hoot et al., 2011). The opposite is also possible where sterol decrease might lead to Cu deprivation. However, a recent study had shown that ergosterol depletion by fluconazole do not affect the intracellular amount of Cu in *C. albicans* (Hunsaker and Franz, 2019).

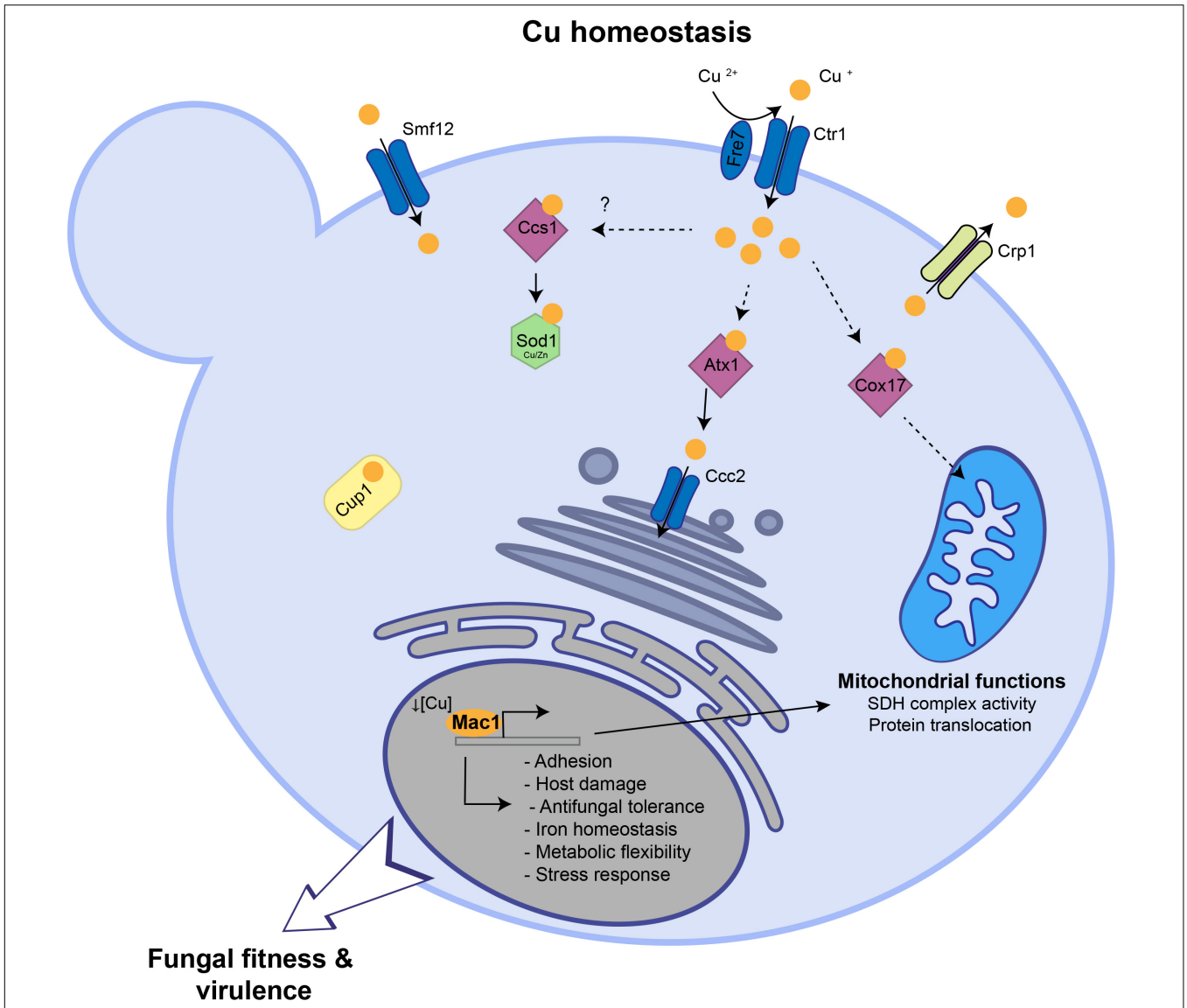

FIGURE 6 | Summary of Cu homeostasis and Cu-modulated processes in *C. albicans*. Under Cu excess, transcripts associated with Cu detoxification and transport including the cytosolic small chaperone *ATX1*, the metallothionein *CUP1*, the P-type ATPase *CCC2* and the Cu efflux pump *CRP1* are upregulated. Under Cu deprivation, *C. albicans* activated genes required for Cu uptake including the transporter Ctr1 and the ferric reductases Fre7 that reduce Cu to facilitate its uptake by Ctr1. Other transcripts including the Cu metallochaperone *COX17*, the manganese transporter *SMF12,* with a potential role in Cu uptake, and the superoxide dismutase *SOD3* were activated. Key *C. albicans* fitness and virulence processes that are modulated by Cu abundance and Mac1 activity were shown.

The growth defect of *mac1* mutant in the presence of fluconazole was reverted by Cu supplementation suggesting that Cu might correct ergosterol depletion by promoting *de novo* synthesis of this fungal sterol. In a support of such hypothesis, studies in *S. cerevisiae* has shown that Cu promote ergosterol biosynthesis by promoting the transcription of *ERG* genes which led to the rescue of growth inhibition by lovastatin, an inhibitor of the ergosterol biosynthetic enzyme Hmg1 (Fowler et al., 2011).

This current investigation provides a rich framework for future work to uncover novel candidates for Cu homeostasis. For instance, under Cu excess, different categories of transporters were induced suggesting their contribution to Cu efflux. Under Cu starvation, the manganese transporter *SMF12* were induced and it is a potential target of Mac1 as its promoter has a putative Mac1-binding motif. Thus, in addition to manganese, Smf12 might serve as a Cu transporter as was suggested also in *S. cerevisiae* (Liu et al., 1997). Furthermore, our data indicate that in addition to the *bona fide* Cu uptake genes, Mac1 might have other potential new targets and modulate other biological functions (**Table 1** and **Figure 6**) such as the succinate dehydrogenase complex activity (*SDH12*, *SDH2*, *SDH4*), mitochondrial protein translocation and insertion in inner membrane (*TIM12*) and adhesion (*ALS1*). Why Mac1 might link Cu metabolism to those functions remains to be

determined. Taken together, these assumptions should provide a fertile area for future investigations.

DATA AVAILABILITY STATEMENT

The datasets generated for this study can be found in the datasets generated for this study are available at Figshare: https://figshare.com/s/98f0075055b2737ad1f5.

AUTHOR CONTRIBUTIONS

IK, FT, and AS contributed to the design, execution, and/or data collection, and analysis of the experiments of this work. AS drafted the manuscript. All authors contributed to revision and final approval of the manuscript.

FUNDING

Work in Sellam's group is supported by funds from the Canadian Institutes for Health Research project grant (CIHR, IC118460). AS is a recipient of the Fonds de Recherche du Québec-Santé (FRQS) J2 salary award. IK received Ph.D. scholarships from Universiteì Laval (bourse Pierre-Jacob Durand) and the CHU de Québec Foundation.

SUPPLEMENTARY MATERIAL

The Supplementary Material for this article can be found online at: https://www.frontiersin.org/articles/10.3389/fmicb.2020.00935/full#supplementary-material

REFERENCES

Anders, S., Pyl, P. T., and Huber, W. (2015). HTSeq—a Python framework to work with high-throughput sequencing data. *Bioinformatics* 31, 166–169. doi: 10.1093/bioinformatics/btu638

Arredondo, M., Cambiazo, V., Tapia, L., González-Agüero, M., Núñez, M. T., Uauy, R., et al. (2004). Copper overload affects copper and iron metabolism in Hep-G2 cells. *Am. J. Physiol. Gastrointest. Liver Physiol.* 287, G27–G32. doi: 10.1152/ajpgi.00297.2003

Ballou, E. R., and Wilson, D. (2016). The roles of zinc and copper sensing in fungal pathogenesis. *Curr. Opin. Microbiol.* 32, 128–134. doi: 10.1016/j.mib.2016.05.013

Bolger, A. M., Lohse, M., and Usadel, B. (2014). Trimmomatic: a flexible trimmer for Illumina sequence data. *Bioinformatics* 30, 2114–2120. doi: 10.1093/bioinformatics/btu170

Burgain, A., Pic, É, Markey, L., Tebbji, F., Kumamoto, C. A., and Sellam, A. (2019). A novel genetic circuitry governing hypoxic metabolic flexibility, commensalism and virulence in the fungal pathogen *Candida albicans*. *PLoS Pathog.* 15:e1007823. doi: 10.1371/journal.ppat.1007823

Cai, Z., Du, W., Zeng, Q., Long, N., Dai, C., and Lu, L. (2017). Cu-sensing transcription factor Mac1 coordinates with the Ctr transporter family to regulate Cu acquisition and virulence in *Aspergillus fumigatus*. *Fungal Genet. Biol.* 107, 31–43. doi: 10.1016/j.fgb.2017.08.003

Chen, C., Pande, K., French, S. D., Tuch, B. B., and Noble, S. M. (2011). An iron homeostasis regulatory circuit with reciprocal roles in *Candida albicans* commensalism and pathogenesis. *Cell Host Microbe* 10, 118–135. doi: 10.1016/j.chom.2011.07.005

Culbertson, E., Khan, A., Muchenditsi, A., Lutsenko, S., Sullivan, D., Petris, M., et al. (2020). Changes in mammalian copper homeostasis during microbial infection. *Metallomics* 12, 416–426. doi: 10.1039/C9MT00294D

Ding, C., Festa, R. A., Chen, Y.-L., Espart, A., Palacios, Ò, Espín, J., et al. (2013). *Cryptococcus neoformans* copper detoxification machinery is critical for fungal virulence. *Cell Host Microbe* 13, 265–276. doi: 10.1016/j.chom.2013.02.002

Ding, C., Yin, J., Tovar, E. M. M., Fitzpatrick, D. A., Higgins, D. G., and Thiele, D. J. (2011). The copper regulon of the human fungal pathogen *Cryptococcus neoformans* H99. *Mol. Microbiol.* 81, 1560–1576. doi: 10.1111/j.1365-2958.2011.07794.x

Djoko, K. Y., Ong, C. Y., Walker, M. J., and McEwan, A. G. (2015). The role of copper and zinc toxicity in innate immune defense against bacterial pathogens. *J. Biol. Chem.* 290, 18954–18961. doi: 10.1074/jbc.R115.647099

Dobin, A., Davis, C. A., Schlesinger, F., Drenkow, J., Zaleski, C., Jha, S., et al. (2013). STAR: ultrafast universal RNA-seq aligner. *Bioinformatics* 29, 15–21. doi: 10.1093/bioinformatics/bts635

Festa, R. A., and Thiele, D. J. (2011). Copper: an essential metal in biology. *Curr. Biol.* 21, R877–R883. doi: 10.1016/j.cub.2011.09.040

Fowler, D. M., Cooper, S. J., Stephany, J. J., Hendon, N., Nelson, S., and Fields, S. (2011). Suppression of statin effectiveness by copper and zinc in yeast and human cells. *Mol. Biosyst.* 7, 533–544. doi: 10.1039/C0MB00166J

Frohner, I. E., Bourgeois, C., Yatsyk, K., Majer, O., and Kuchler, K. (2009). *Candida albicans* cell surface superoxide dismutases degrade host-derived reactive oxygen species to escape innate immune surveillance. *Mol. Microbiol.* 71, 240–252. doi: 10.1111/j.1365-2958.2008.06528.x

Garcia-Santamarina, S., Festa, R. A., Smith, A. D., Yu, C.-H., Probst, C., Ding, C., et al. (2018). Genome-wide analysis of the regulation of Cu metabolism in *Cryptococcus neoformans*. *Mol. Microbiol.* 108, 473–494. doi: 10.1111/mmi.13960

Gerami-Nejad, M., Zacchi, L. F., McClellan, M., Matter, K., and Berman, J. (2013). Shuttle vectors for facile gap repair cloning and integration into a neutral locus in *Candida albicans*. *Microbiology* 159, 565–579. doi: 10.1099/mic.0.064097-0

González, M., Reyes-Jara, A., Suazo, M., Jo, W. J., and Vulpe, C. (2008). Expression of copper-related genes in response to copper load. *Am. J. Clin. Nutr.* 88, 830S–834S. doi: 10.1093/ajcn/88.3.830S

Homann, O. R., Dea, J., Noble, S. M., and Johnson, A. D. (2009). A phenotypic profile of the *Candida albicans* regulatory network. *PLoS Genet.* 5:e1000783. doi: 10.1371/journal.pgen.1000783

Hood, M. I., and Skaar, E. P. (2012). Nutritional immunity: transition metals at the pathogen-host interface. *Nat. Rev. Microbiol.* 10, 525–537. doi: 10.1038/nrmicro2836

Hoot, S. J., Smith, A. R., Brown, R. P., and White, T. C. (2011). An A643V amino acid substitution in Upc2p contributes to azole resistance in well-characterized clinical isolates of *Candida albicans*. *Antimicrob. Agents Chemother.* 55, 940–942. doi: 10.1128/AAC.00995-10

Hunsaker, E. W., and Franz, K. J. (2019). *Candida albicans* reprioritizes metal handling during fluconazole stress. *Metallomics* 11, 2020–2032. doi: 10.1039/C9MT00228F

Jo, W. J., Loguinov, A., Chang, M., Wintz, H., Nislow, C., Arkin, A. P., et al. (2008). Identification of genes Involved in the toxic response of *Saccharomyces cerevisiae* against iron and copper overload by parallel analysis of deletion mutants. *Toxicol. Sci.* 101, 140–151. doi: 10.1093/toxsci/kfm226

Kang, S.-O., Oh, J.-H., Yim, H.-S., Rhie, G., Huh, W.-K., and Hwang, C.-S. (2002). Copper- and zinc-containing superoxide dismutase (Cu/ZnSOD) is required for the protection of *Candida albicans* against oxidative stresses and the expression of its full virulence. *Microbiology* 148, 3705–3713. doi: 10.1099/00221287-148-11-3705

Khamooshi, K., Sikorski, P., Sun, N., Calderone, R., and Li, D. (2014). The Rbf1, Hfl1 and Dbp4 of *Candida albicans* regulate common as well as transcription factor-specific mitochondrial and other cell activities. *BMC Genomics* 15:56. doi: 10.1186/1471-2164-15-56

Knight, S. A. B., Lesuisse, E., Stearman, R., Klausner, R. D., and Dancis, A. (2002). Reductive iron uptake by *Candida albicans*: role of copper, iron and the TUP1 regulator. *Microbiology* 148, 29–40. doi: 10.1099/00221287-148-1-29

Li, C. X., Gleason, J. E., Zhang, S. X., Bruno, V. M., Cormack, B. P., and Culotta, V. C. (2015). *Candida albicans* adapts to host copper during infection by swapping metal cofactors for superoxide dismutase. *Proc. Natl. Acad. Sci. U.S.A.* 112, E5336–E5342. doi: 10.1073/pnas.1513447112

Linder, M. C., Wooten, L., Cerveza, P., Cotton, S., Shulze, R., and Lomeli, N. (1998). Copper transport. *Am. J. Clin. Nutr.* 67, 965S–971S. doi: 10.1093/ajcn/67.5.965S

Liu, X. F., Supek, F., Nelson, N., and Culotta, V. C. (1997). Negative control of heavy metal uptake by the *Saccharomyces cerevisiae* BSD2 gene. *J. Biol. Chem.* 272, 11763–11769. doi: 10.1074/jbc.272.18.11763

Mackie, J., Szabo, E. K., Urgast, D. S., Ballou, E. R., Childers, D. S., MacCallum, D. M., et al. (2016). Host-imposed copper poisoning impacts fungal micronutrient acquisition during systemic *Candida albicans* infections. *PLoS One* 11:e0158683. doi: 10.1371/journal.pone.0158683

MacPherson, S., Akache, B., Weber, S., De Deken, X., Raymond, M., and Turcotte, B. (2005). *Candida albicans* zinc cluster protein Upc2p confers resistance to antifungal drugs and is an activator of ergosterol biosynthetic genes. *Antimicrob. Agents Chemother.* 49, 1745–1752. doi: 10.1128/AAC.49.5.1745-1752.2005

Marcil, A., Gadoury, C., Ash, J., Zhang, J., Nantel, A., and Whiteway, M. (2008). Analysis of PRA1 and its relationship to *Candida albicans*- macrophage interactions. *Infect. Immun.* 76, 4345–4358. doi: 10.1128/IAI.00588-07

Marvin, M. E., Mason, R. P., and Cashmore, A. M. (2004). The CaCTR1 gene is required for high-affinity iron uptake and is transcriptionally controlled by a copper-sensing transactivator encoded by CaMAC1. *Microbiol. Read. Engl.* 150, 2197–2208. doi: 10.1099/mic.0.27004-0

Marvin, M. E., Williams, P. H., and Cashmore, A. M. (2003). The *Candida albicans* CTR1 gene encodes a functional copper transporter. *Microbiol. Read. Engl.* 149, 1461–1474. doi: 10.1099/mic.0.26172-0

McDaniels, C. P. J., Jensen, L. T., Srinivasan, C., Winge, D. R., and Tullius, T. D. (1999). The yeast transcription factor Mac1 binds to DNA in a modular fashion. *J. Biol. Chem.* 274, 26962–26967. doi: 10.1074/jbc.274.38.26962

Miramon, P., and Lorenz, M. C. (2017). A feast for *Candida*: metabolic plasticity confers an edge for virulence. *PLoS Pathog.* 13:e1006144. doi: 10.1371/journal.ppat.1006144

Noble, S. M., French, S., Kohn, L. A., Chen, V., and Johnson, A. D. (2010). Systematic screens of a *Candida albicans* homozygous deletion library decouple morphogenetic switching and pathogenicity. *Nat. Genet.* 42, 590–598. doi: 10.1038/ng.605

Pierce, J. V., Dignard, D., Whiteway, M., and Kumamoto, C. A. (2013). Normal adaptation of *Candida albicans* to the murine gastrointestinal tract requires Efg1p-dependent regulation of metabolic and host defense genes. *Eukaryot. Cell* 12, 37–49. doi: 10.1128/EC.00236-12

Ritchie, M. E., Phipson, B., Wu, D., Hu, Y., Law, C. W., Shi, W., et al. (2015). limma powers differential expression analyses for RNA-sequencing and microarray studies. *Nucleic Acids Res.* 43:e47. doi: 10.1093/nar/gkv007

Rustici, G., van Bakel, H., Lackner, D. H., Holstege, F., Wijmenga, C., Bahler, J., et al. (2007). Global transcriptional responses of fission and budding yeast to changes in copper and iron levels: a comparative study. *Genome Biol.* 8:R73. doi: 10.1186/gb-2007-8-5-r73

Samanovic, M. I., Ding, C., Thiele, D. J., and Darwin, K. H. (2012). Copper in microbial pathogenesis: meddling with the metal. *Cell Host Microbe* 11, 106–115. doi: 10.1016/j.chom.2012.01.009

Sellam, A., van het Hoog, M., Tebbji, F., Beaurepaire, C., Whiteway, M., and Nantel, A. (2014). Modeling the transcriptional regulatory network that controls the early hypoxic response in *Candida albicans*. *Eukaryot. Cell* 13, 675–690. doi: 10.1128/EC.00292-13

Silver, P. M., Oliver, B. G., and White, T. C. (2004). Role of *Candida albicans* transcription factor Upc2p in drug resistance and sterol metabolism. *Eukaryot. Cell* 3, 1391–1397. doi: 10.1128/EC.3.6.1391-1397.2004

Skrzypek, M. S., Binkley, J., Binkley, G., Miyasato, S. R., Simison, M., and Sherlock, G. (2017). The *Candida* genome database (CGD): incorporation of assembly 22, systematic identifiers and visualization of high throughput sequencing data. *Nucleic Acids Res.* 45, D592–D596. doi: 10.1093/nar/gkw924

Spiering, M. J., Moran, G. P., Chauvel, M., Maccallum, D. M., Higgins, J., Hokamp, K., et al. (2010). Comparative transcript profiling of *Candida albicans* and *Candida dubliniensis* identifies SFL2, a *C. albicans* gene required for virulence in a reconstituted epithelial infection model. *Eukaryot. Cell* 9, 251–265. doi: 10.1128/EC.00291-09

Subramanian, A., Tamayo, P., Mootha, V. K., Mukherjee, S., Ebert, B. L., Gillette, M. A., et al. (2005). Gene set enrichment analysis: a knowledge-based approach for interpreting genome-wide expression profiles. *Proc. Natl. Acad. Sci. U.S.A.* 102, 15545–15550. doi: 10.1073/pnas.0506580102

Sun, T.-S., Ju, X., Gao, H.-L., Wang, T., Thiele, D. J., Li, J.-Y., et al. (2014). Reciprocal functions of *Cryptococcus neoformans* copper homeostasis machinery during pulmonary infection and meningoencephalitis. *Nat. Commun.* 5:5550. doi: 10.1038/ncomms6550

van Bakel, H., Strengman, E., Wijmenga, C., and Holstege, F. C. P. (2005). Gene expression profiling and phenotype analyses of *S. cerevisiae* in response to changing copper reveals six genes with new roles in copper and iron metabolism. *Physiol. Genomics* 22, 356–367. doi: 10.1152/physiolgenomics.00055.2005

Waterman, S. R., Hacham, M., Hu, G., Zhu, X., Park, Y.-D., Shin, S., et al. (2007). Role of a CUF1/CTR4 copper regulatory axis in the virulence of *Cryptococcus neoformans*. *J. Clin. Invest.* 117, 794–802. doi: 10.1172/JCI30006

Weissman, Z., Berdicevsky, I., Cavari, B.-Z., and Kornitzer, D. (2000). The high copper tolerance of *Candida albicans* is mediated by a P-type ATPase. *Proc. Natl. Acad. Sci. U.S.A.* 97, 3520–3525. doi: 10.1073/pnas.97.7.3520

Wilson, R. B., Davis, D., Enloe, B. M., and Mitchell, A. P. (2000). A recyclable *Candida albicans* URA3 cassette for PCR product-directed gene disruptions. *Yeast* 16, 65–70. doi: 10.1002/(SICI)1097-0061(20000115)16:1<65::AID-YEA508<3.0.CO;2-M

Woodacre, A., Mason, R. P., Jeeves, R. E., and Cashmore, A. M. (2008). Copper-dependent transcriptional regulation by *Candida albicans* Mac1p. *Microbiology* 154, 1502–1512. doi: 10.1099/mic.0.2007/013441-0 doi: 10.1099/mic.0.2007/013441-0

Conflict of Interest: The authors declare that the research was conducted in the absence of any commercial or financial relationships that could be construed as a potential conflict of interest.

frontiers in Microbiology

ORIGINAL RESEARCH
published: 25 June 2020
doi: 10.3389/fmicb.2020.01337

MAT1-1-3, a Mating Type Gene in the *Villosiclava virens*, Is Required for Fruiting Bodies and Sclerotia Formation, Asexual Development and Pathogenicity

*Mingli Yong[1], Junjie Yu[1], Xiayan Pan[1], Mina Yu[1], Huijuan Cao[1], Zhongqiang Qi[1], Yan Du[1], Rongsheng Zhang[1], Tianqiao Song[1], Xiaole Yin[1], Zhiyi Chen[1], Wende Liu[2] and Yongfeng Liu[1]**

[1] Institute of Plant Protection, Jiangsu Academy of Agricultural Sciences, Nanjing, China, [2] State Key Laboratory for Biology of Plant Diseases and Insect Pests, Institute of Plant Protection, Chinese Academy of Agricultural Sciences, Beijing, China

OPEN ACCESS

Edited by:
Laure Ries,
University of São Paulo, Brazil

Reviewed by:
Kin-Ming (Clement) Tsui,
Weill Cornell Medicine - Qatar, Qatar
Jing Fan,
Sichuan Agricultural University, China
Zide Jiang,
South China Agricultural University, China

***Correspondence:**
Yongfeng Liu
liuyf@jaas.ac.cn

Specialty section:
This article was submitted to Fungi and Their Interactions, a section of the journal Frontiers in Microbiology

Received: *27 February 2020*
Accepted: *25 May 2020*
Published: *25 June 2020*

Citation:
Yong M, Yu J, Pan X, Yu M, Cao H, Qi Z, Du Y, Zhang R, Song T, Yin X, Chen Z, Liu W and Liu Y (2020) MAT1-1-3, a Mating Type Gene in the Villosiclava virens, Is Required for Fruiting Bodies and Sclerotia Formation, Asexual Development and Pathogenicity. Front. Microbiol. 11:1337. doi: 10.3389/fmicb.2020.01337

Villosiclava virens is the prevalent causative pathogen of rice false smut, a destructive rice disease. Mating-type genes play a vital role in the evolution of mating systems in fungi. Some fungi have lost *MAT1-1-3*, one of the mating-type genes, during evolution, whereas others still retain *MAT1-1-3*. However, how *MAT1-1-3* regulates the sexual development of heterothallic *V. virens* remains unknown. Here, we generated the *MAT1-1-3* mutants, which exhibited defects in vegetative growth, stress response, pathogenicity, sclerotia formation and fruiting body maturation. An artificial outcrossing inoculation assay showed that the Δ*mat1-1-3* mutant was unable to produce sclerotia. Unexpectedly, the Δ*mat1-1-3* mutant could form immature fruiting bodies without mating on potato sucrose agar medium (PSA) compared with the wild-type strain, most likely by activating the truncated *MAT1-2-1* transcription to regulate the sexual development. Moreover, RNA-seq data showed that knockout of *MAT1-1-3* results in misregulation of a subset of genes involved in sexual development, MAPK signaling, cell wall integrity, autophagy, epigenetic modification, and transcriptional regulation. Collectively, this study reveals that *MAT1-1-3* is required for asexual and sexual development, and pathogenicity of *V. virens*, thereby provides new insights into the function of mating-type genes in the fungi life cycle and infection process.

Keywords: mating type gene, *Villosiclava virens*, *MAT1-1-3*, sexual development, pathogenicity

INTRODUCTION

Villosiclava virens (Anamorph, *Ustilaginoidea virens*) is a plant pathogen that causes rice false smut (RFS), which results in substantial rice yield losses worldwide (Brooks et al., 2010; Ladhalakshmi et al., 2012; Jecmen and Tebeest, 2015; Fan et al., 2016). *V. virens* infects rice florets to produce the RFS balls, which can generate sclerotia on their surface (Ashizawa et al., 2012; Tang et al., 2013; Hu et al., 2014; Song et al., 2016; Yong et al., 2018). Additionally, *V. virens* directly affects the rice

food safety by producing mycotoxins, which are harmful to humans and animals (Li et al., 2008; Fu et al., 2017; Wang et al., 2017). In addition to the completion of genome sequencing and the available transcriptome data (Zhang et al., 2014), the recently established clustered regularly interspaced short palindromic repeats (CRISPR) mediated gene knockout system provides an effective tool to study the gene function in *V. virens* (Liang et al., 2018; Fang et al., 2019; Guo et al., 2019; Yu et al., 2019). During the pathogen's sexual life cycle, *V. virens* can produce ascospores by sexual reproduction (Zhang et al., 2014; Yong et al., 2018), which, through invasion of rice spikelets, are considered to be one of the primary infection sources of rice false smut (RFS) (Ikegami, 1960; Wang, 1995). Genetic recombination occurs during sexual reproduction when two compatible strains mate, thereby playing a vital role in expanding *V. virens* genetic diversity (Sun et al., 2013; Wang et al., 2014). Thus, the sexual reproduction plays an important role in the prevalence of RFS and genetic diversity in *V. virens*.

Sexual reproduction is a key step for fungi to complete their life cycle (Zhang et al., 2014). In ascomycetous fungi, sexual reproduction, controlled by mating type alleles/idiomorphs (*MAT*) (Yun et al., 1999; Zheng and Wang, 2013), is divided into three major modes: heterothallic, homothallic and pseudohomothallic (or secondary homothallic) (Whittle et al., 2011; Zheng and Wang, 2013). The two opposite idiomorphs are named *MAT1-1* (or *MATA*) and *MAT1-2* (or *MATa*) (Alby et al., 2009; Whittle et al., 2011). Homothallic (self-compatible) species carry both *MAT1-1* and *MAT1-2* idiomorph genes in a single nucleus, usually closely linked or fused (Nelson, 1996; Wilken et al., 2012). In contrast, heterothallic (self-incompatible) species have alternate *MAT* idiomorph in different nuclei (Coppin et al., 1997; Yun et al., 1999). Extensive evidences showed that these mating modes could exist in different fungi belong to the same genus and play an important role in evolutionary biology. For example, the *Neurospora* species employ these three mating modes to complete the process of sexual reproduction, and multiple switches in the mating systems have occurred in the genus' evolutionary history (Nygren et al., 2011; Whittle et al., 2011). For ascomycete *Cordyceps* sensu lato (sl), there are also reproductive switches between homothallic and heterothallic modes (Hu et al., 2013; Zheng et al., 2013). In addition, some studies supported the hypothesis that the sexual reproduction of *Aspergillus* genus may evolve from homothallic to heterothallic mode (Galagan et al., 2005; Paoletti et al., 2005), but still need more evidences to prove in the future. However, some studies supported the hypothesis that the ancestral mating system in *Neurospora* was heterothallic (Gioti et al., 2012). Compared with heterothallism, homothallism is more likely to accumulate deleterious genomic mutations (Whittle et al., 2011). To avoid self-crossing, genetic barriers have evolved sexual dimorphism to prevent selfing (Klix et al., 2010). Therefore, as one of the factors of species evolution, these studies indicate that heterothallism plays a more important role than homothallism during species evolution (Lee et al., 2010; Zheng and Wang, 2013).

Villosiclava virens has a heterothallic sexual reproduction system controlled by *MAT1-1* and *MAT1-2* idiomorphs (Yu J. J. et al., 2015). The *MAT1-1* idiomorph includes *MAT1-1-1*, *MAT1-1-2*, *MAT1-1-3*, and a truncated *MAT1-2-1*, and the *MAT1-2* idiomorph includes *MAT1-2-1* and *MAT1-2-8* (Yu J. J. et al., 2015). Extensive studies show that *MAT1-1* and *MAT1-2* in fungi have different functions to regulate sexual reproduction. For example, in heterothallic *N. crassa*, *matA-1* (*MAT1-1-1*) mutant is sterile but *matA-2* (*MAT1-1-2*) and *matA-3* (*MAT1-1-3*) mutants have slightly reduced fertility (Ferreira et al., 1998). In heterothallic *Podospora anserina*, *SMR2* (*MAT1-1-3*) mutant can produce asci, but the number is reduced (Zickler et al., 1995). However, in homothallic *Fusarium graminearum*, *mat1-1-2* and *mat1-1-3* mutants are fertile, *mat1-1-1* and *mat1-2-1* mutants display male- and female-specific defects, respectively (Zheng et al., 2015). In addition, in homothallic *Sordaria macrospora*, *SmtA-3* (*MAT1-1-3*) is not required for fruiting body development and also has no effect on vegetative morphology (Klix et al., 2010). In filamentous ascomycetes, *MAT1-1-1* and *MAT1-2-1* encode α-box domain proteins and high mobility group (HMG) domain transcription factors, respectively (Turgeon et al., 1993b). *MAT1-1-3* also encodes an HMG domain transcription factor (Coppin et al., 1997; Debuchy and Turgeon, 2006). In contrast to SmtA-3 (MAT1-1-3) and SMR2 (MAT1-1-3) proteins, the HMG motif is lacking in the putative SmtA-3 protein (Klix et al., 2010). Different functional requirements for *MAT1-1-3* in sexual development between homothallic *F. graminearum* and *S. macrospora* imply that some of the regulatory networks controlled by MAT proteins may not be conserved across filamentous ascomycetes (Kim et al., 2012). Thus, the function of *MAT1-1-3* homologs in sexual reproduction is variable (Yokoyama et al., 2005), and little is known about *MAT1-1-3* function in *V. virens*.

In this study, *MAT1-1-3* was characterized using Δ*mat1-1-3* mutant generated with the CRISPR/Cas9 system. We performed phylogenetic comparisons of *V. virens* with other fungi and the MAT1-1-3 proteins from different species. We have demonstrated that the transcription factor *MAT1-1-3* is required for vegetative growth, stress response, pathogenicity and sexual development in *V. virens*. The Δ*mat1-1-3* mutant could form an immature fruiting body without mating in PSA medium plate. Transcriptome analysis of Δ*mat1-1-3* mutant and wild-type strains revealed differential expression of a subset of genes. In addition, the expression level of truncated *MAT1-2-1* was up-regulated in Δ*mat1-1-3* mutant. Collectively, our study demonstrates that *MAT1-1-3* plays a vital role in sexual and asexual development in *V. virens*.

MATERIALS AND METHODS

Strains and Growth Conditions

Villosiclava virens WT strains Uv1-56 (*MAT1-1* mating-type) and Uv2-51 (*MAT1-2* mating-type) and all transformants generated in this study were cultured and maintained on potato sucrose agar (PSA) plates (200 g/L potato, 20 g/L sucrose, 15 g/L agar) at 28°C in the dark. *Agrobacterium*

tumefaciens strain AGL1 was incubated on LB medium (0.5% yeast extract, 1% tryptone, 1% NaCl) at 28°C. Yeast strain AH109 was incubated on YPDA medium (1% yeast extract, 2% peptone, 2% glucose, 0.003% adenine hemisulfate, 2% agar) at 30°C. All strains used are listed in **Supplementary Table S1**. For DNA extraction, hyphae were harvested after growth in PSA at 28°C for 7 days in the dark. Conidiation in potato sucrose broth (PSB) medium (200 g/L potato and 20 g/L sucrose) and fungal growth on PSA plates were measured using protocols from a previous study (Xie et al., 2019). Colony diameters of Uv1-56, indicated mutant and complemented strains were measured on PSA medium after 15 days at 28°C.

For conidiation, Uv1-56, mutant or complemented strains were cultured in PSB medium with shaking at 150 rpm at 28°C for 7 days. Then, the cultured mixtures were filtered, and the concentrations of conidia were measured using a hemocytometer. For the germination test, conidial suspension droplets were added to water agar plates, incubated at 28°C for 12 h and photographed with an Olympus BX-53 microscope. For stress tests, Uv1-56, mutant and complemented strains were incubated on PSA at 28°C for 15 days with different concentrations of stress agents, including 0.5 M NaCl, 0.7 M Sorbitol, 0.07% H_2O_2, 600 μg/ml congo red (CR), 600 μg/ml calcofluor white (CFW) and 0.03% sodium dodecyl sulfate (SDS). The inhibition rates were calculated as described previously (Xie et al., 2019). Three biological replicates were performed to assess conidiation, germination and stress tests.

Orthology and Phylogenetic Analysis

A multisequence phylogenetic tree was constructed using the concatenated sequences of core genes identified by the default parameters of the CEGMA (v2.5) pipeline. Briefly, the CEGMA software contains the core eukaryotic genes dataset, which has 458 core genes. We searched the homologous genes in different fungal genome database using CEGMA software based on these 458 core genes. The phylogenetic tree was constructed using the homologous proteins encoded by the core homologous genes. Multiple sequence alignments of proteins were made by muscle, and then a neighbor-joining tree was built using MEGA7 with 1000 bootstrap repeats for distance estimation. The similarity of MAT1-1-3 homologs from different fungi was analyzed with MEGA7 software. The sequences of MAT1-1-3 homologous proteins in different fungi proteome database was obtained from National Center for Biotechnology Information (NCBI) with specific accession number as below: *Villosiclava virens* (*Ustilaginoidea virens*, AKE48501.1), *Metarhizium anisopliae* (BAE93596.1), *Metarhizium robertsii* (XP_007819908.2), *Ephelis japonica* (BAD72606.2), *Epichloe typhina* (BAD72610.2), *Claviceps purpurea* (BAD72602.2), *Ophiocordyceps sinensis* (AGW27558.1), *Tolypocladium inflatum* (BAE93600.1), *Pyrenopeziza brassicae* (CAA06846.1), *Fusarium graminearum* (AAG42812.1), *Fusarium fujikuroi* (AAC71053.1), *Fusarium oxysporum* (AEO15073.1), *Sordaria macrospora* (KAA8630682.1), *Neurospora crassa* (AAC37476.1), *Podospora anserina* (CAA52051.1).

Plasmid Construction and Transformant Generation

For constructing gene replacement plasmids, the *MAT1-1-3* gene replacement vector (*pMD19-MAT1-1-3*) was obtained using previously reported methods (Li et al., 2019). Briefly, upstream and downstream flanking sequences (∼1 kb) of *MAT1-1-3* were cloned using primers *MAT1-1-3*-upF/upR and *MAT1-1-3*-doF/doR, respectively. The *hygromycin B-resistance* (*HYG*) gene fragment was amplified from the *SK1044-hyg* plasmid using primers F3/R3. The upstream, downstream and *HYG* fragments were inserted into vector T-Vector *pMD19*. To generate the *Cas9-gRNA* vector, gene gRNA spacers were designed with the gRNA designer website for best on-target scores[1]. Synthetic sgRNA oligos were annealed and inserted into *Bsm*BI-digested *pmCas9:tRp-gRNA* (Liang et al., 2018) to generate *pmCas9:tRp-gRNA-MAT1-1-3* constructs. The *pMD19-MAT1-1-1*, *pMD19-MAT1-1-2*, *pmCas9:tRp-gRNA-MAT1-1-1* and *pmCas9:tRp-gRNA-MAT1-1-2* constructs were generated in a similar manner. All constructs were confirmed by sequencing.

To generate knockout mutants, replacement *pMD19-MAT1-1-3* vector and *pmCas9:tRp-gRNA-MAT1-1-3* were co-transformed into strain Uv1-56 protoplasts using the PEG-mediated method as described previously (Li et al., 2019). *HYG* gene was used to screen for knockout transformants. *MAT1-1-3* was verified by PCR with primer pair *MAT1-1-3*-F2/R2, and the *HYG* gene was verified by PCR with primers F1/R3 and F3/R1. Primers F1/R1 were used to amplify the inserted fragment by PCR, and sequencing traces of junction regions confirmed that *MAT1-1-3* was replaced by the *HYG* gene in mutants. The *MAT1-1-1* and *MAT1-1-2* knockout mutants were also generated using the same method.

For complementation assays, the *MAT-1-1-3* gene, including its 1.5 kb promoter, was amplified with primers C-*MAT-1-1-3*-F/R. The amplified fragment was cloned into *Bam*HI and *Hin*dIII digested *pKO1-NEO-Uv* vector and was verified by sequencing analysis. The complementary vector was transformed into *A. tumefaciens* strain AGL1 and complementation transformants generated by the Agrobacterium-mediated (ATMT) were screened with geneticin selection using methods described previously (Yu M. N. et al., 2015). All primers used in this study are listed in **Supplementary Table S2**.

Pathogenicity and Sclerotia Formation Assays

To detect pathogenicity, the rice susceptible cultivar Liangyoupeijiu was artificially inoculated with *V. virens* as described previously (Tang et al., 2013; Yu J. J. et al., 2015) with minor modifications. Briefly, the rice plants grown in a greenhouse were used to inoculate with *V. virens*. Uv1-56, Uv2-51, complemented and mutant strains were cultured in PSB at 28°C for 7 days with rotary shaking at 150 rpm/min. Mixtures of hyphae and conidia were created with a blender, and the conidia concentration was adjusted to 1×10^6/mL

[1] http://grna.ctegd.uga.edu/

with PSB. Seven days before the heading stage, about 1–2 mL of inoculum suspension was injected into 15 swollen flag leaf sheaths of rice using sterilized syringes. Inoculated rice was cultured in the greenhouse for 6 days at 25°C at 95%–100% humidity (RH) and then were placed at 28°C and about 80% RH. The rice false smut balls were counted after 30 dpi. The average diseased grain rate was calculated as previously described (Hu et al., 2014) and modified as follows: average diseased grain rate = (average of the number of false smut balls per panicle/average of the total number of rice grains per panicle) × 100%.

For sclerotia formation assays, the hyphae and conidia suspension of Uv1-56 and Uv2-51 prepared as above were mixed in a 1:1 ratio to generate the mixed inoculum suspension. The mixed inoculum suspension of Δ*mat1-1-3* and Uv2-51 (or complemented strain and Uv2-51) was also prepared using the same method. The mixed inoculum suspension was inoculated the rice swollen flag leaf sheath of rice on the seventh day before heading stage using a needle syringe. The inoculated rice plants were grown in a greenhouse at 25°C and 95%–100% RH for 6 days. Then these plants were transferred to another growth room under normal conditions (25°C-30°C, 80% RH, and 12-hr light/12-hr dark photoperiod) for 24 days of growth. Finally, these plants were further transferred to a growth incubator at a day-and-night temperature of 25°C/15°C and 70% RH for another 15 days of growth before counting the sclerotia. The sclerotium formation rate was calculated as follows: sclerotium formation rate = (average of the number of sclerotia/average of the number of false smut balls) × 100%. The sclerotia germination assay was performed according to previous methods (Yong et al., 2018). The statistical analyses were performed by Student's t-test. All experiments were repeated three times.

Confrontation Assay

The WT Uv1-56, Uv2-51 and mutant strains were cultured on PSA plates for 15 days. The mycelium plugs from 15-day-old PSA cultures were placed onto the right and left sides of the PSA plates, respectively. Thirty plates replicates were performed in each experimental treatment. Hyphae of Uv1-56 and Δ*mat1-1-3* were harvested at 10 and 15 days for RNA extraction. Meanwhile, the cell fusion of opposing mating type strains was observed and photographed with an Olympus BX-53 microscope. In order to observe the formation of fruiting bodies, the strain culture time was extended to 60 days and photographed with a digital camera. Three biological replicates were performed.

qRT-PCR and RNA-seq Analysis

Gene expression was evaluated by quantitative real-time PCR with specific primers. For the confrontation assay, Uv1-56 or Δ*mat1-1-3* was crossed with Uv2-51. Samples of confrontation culture strains were harvested at 10 and 15 days. RNA was extracted with the BioTeKe RNA reagent Kit and cDNA reverse transcription was performed using the PrimeScript RT reagent Kit with gDNA Eraser (Perfect Real Time, Takara). An ABI PRISM 7000 Sequence Detection System (Applied Biosystems, United States) with SYBR® Premix Ex Taq (Tli RNaseH Plus) (Takara, Japan) was used. The reactions were conducted as described previously (Fang et al., 2019). β-*tubulin* was used as the internal reference for measuring gene expression. Relative expression was determined using the $2^{-\Delta\Delta Ct}$ method (Livak and Schmittgen, 2001). For detecting the transcript level of *MAT1-1-3* and truncated *MAT1-2-1* in wild-type Uv1-56, mycelia were harvested after incubation in PSB at 28°C for 7 days for RNA extraction. Transcript amounts were calculated using the $2^{-\Delta CT}$ method in ABI 7000 System Sequence Detection Software. Three biological replicates were performed and the results showed similar trends.

RNA from wild-type Uv1-56 and Δ*mat1-1-3* mutant, which were harvested after incubation on PSB at 28°C for 7 days, was extracted using Trizol® Reagent. RNA-seq libraries were prepared with the ScriptSeq v2 kit (Epicentre SSV21124) following a published method (Jiao et al., 2018). Transcriptome sequencing was performed by Illumina HiSeq 2500 with the paired-end 2 × 150 bp model at the Majorbio biomedical technology Co., Ltd. (Shanghai, China). RNA-seq data from each sample were aligned to version 1 of the *Villosiclava virens* reference genome (Zhang et al., 2014) using Hisat2. Transcript assembly was performed using Cufflinks (Trapnell et al., 2012). Analysis of the difference in gene expression was performed using DEGseq. The cutoff for differential expression was transcripts per million reads (TPM) adjusted $p < 0.05$ and $|\log2FC| \geq 1$.

Generation of *MAT1-1-3-GFP* Fusion Transformants and Subcellular Localization

To obtain the *MAT1-1-3-GFP* construct, a cDNA fragment of the *MAT1-1-3* gene was amplified from strain Uv1-56 cDNA template with primers *MAT1-1-3*-GFP-F/R and cloned into *Bam*HI and *Sma*I digested *pKD1GFP* with the ClonExpress II One Step Cloning Kit (Vazyme, China). The resulting plasmid was confirmed by sequencing analysis. The *pKD1GFP* plasmid was transformed into *A. tumefaciens* strain AGL1 using the freeze-thaw method (Weigel and Glazebrook, 2006) and was then transformed into *V virens* via ATMT transformation as described previously (Yu M. N. et al., 2015). After 7 days of *A. tumefaciens* strain and *V. virens* co-culturing, transformants were picked and observed under a fluorescence microscope. *MAT1-1-3-GFP* fusion transformants were incubated on PSB at 28°C for 7 days. The hyphae and conidia were harvested and stained with 4′, 6-diamidino-2-phenylindole (DAPI) (Sigma-Aldrich, United States) to visualize nuclei as described previously (Li et al., 2015). A rotary laser confocal microscope (Ultra View VoX, PerkinElmer, United States) was used to observe MAT1-1-3 colonization.

4′,6-Diamidino-2-Phenylindole (DAPI) and Calcofluor White Staining

The conidia and hyphae of indicated strains were harvested after 7 days in PSB. Staining was conducted as described previously (Li et al., 2015). To observe the septum of hyphae, the indicated strains were stained with 20 μg/ml calcofluor white (CFW), which was used to stain the cellulose and chitin in the cell wall (Roncero and Durán, 1985), for 5–15 min,

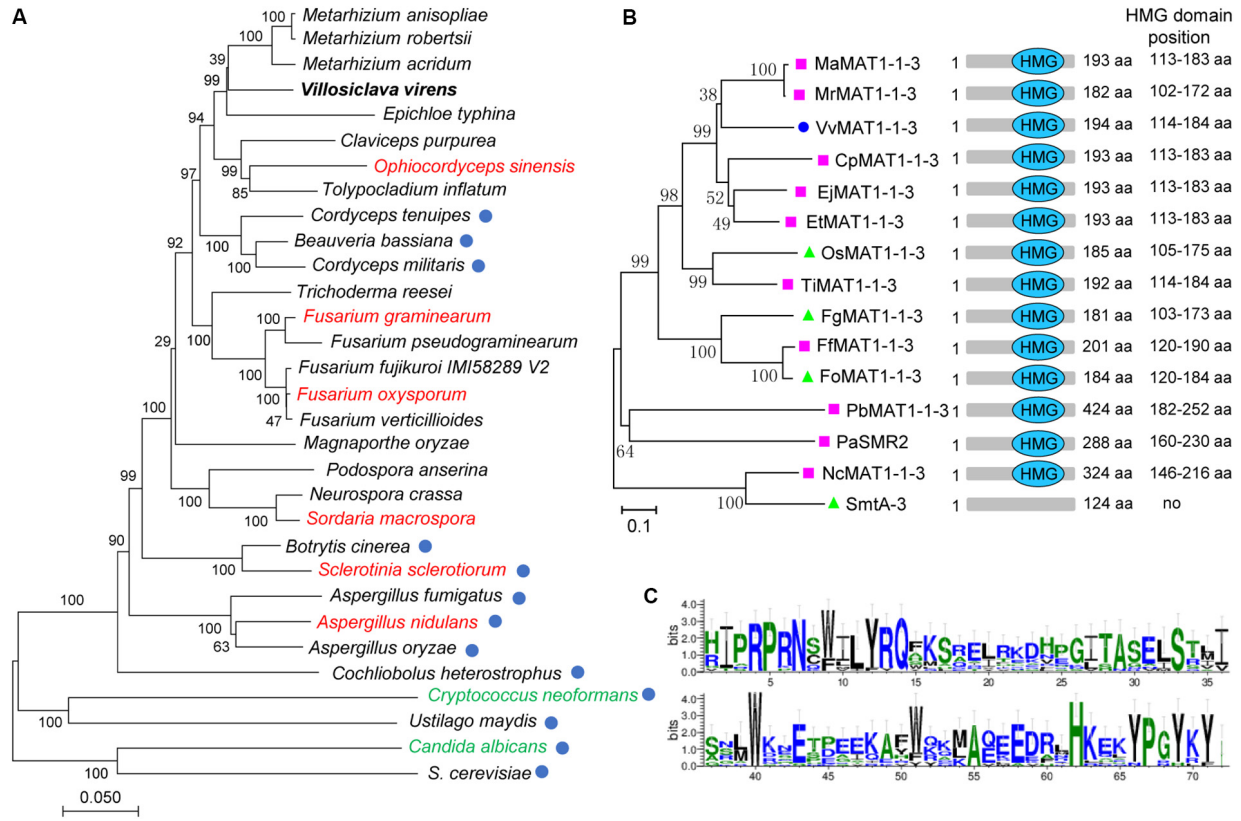

FIGURE 1 | Phylogenetic analysis of *Villosiclava virens* with other fungi and VvMAT1-1-3 protein with MAT1-1-3 from various fungi. **(A)** The multisequence phylogenetic tree was constructed by MEGA7 with core eukaryotic genes identified using the CEGMA (v2.5) pipeline to show the evolutionary relationship of *V. virens* with different fungal species. Blue circles indicate species that do not have a *MAT1-1-3* gene. The red names indicate fungi that undergo homothallic sexual reproduction, the green names indicate fungi that undergo sexual reproduction that is homothallic and heterothallic. The black names indicated fungi that are heterothallic and possess a *MAT1-1-3* gene. **(B)** Phylogenetic tree of fungal *MAT1-1-3* genes and the position of the high mobility group (HMG) domain in different fungal *MAT1-1-3* genes. Pink squares indicate heterothallic fungi; green triangles indicate homothallic fungi; the blue circle indicates *V. virens*. **(C)** The weblogo depicts the multiple sequence alignment of HMG domains from the 14 protein sequences in **(B)**. The logo shows the conservation of various residues. The *y*-axis represents the bit score. A score of 4 on the *y*-axis means 100% conservation. The *x*-axis displays the amino acid position.

and the pictures were taken by a fluorescence microscope (Nikon Eclipse 80i, Japan). The hyphae and conidia were and stained with 20 μg/mL 4′, 6-diamidino-2-phenylindole (DAPI) (Sigma-Aldrich, United States) for 1 h to visualize nucleus under the PerkinElmer UltraView VoX confocal (PerkinElmer, United States).

Yeast Two-Hybrid Assay

Protein-protein interactions were performed by the yeast two-hybrid system (Clontech, Laboratories, Inc.). *MAT1-1-3* ORF was amplified using primers BD113-F/R, from the cDNA of Uv1-56, and then was cloned into the *Sma*I-digested *pGBKT7* vector using the ClonExpress II One Step Cloning Kit (Vazyme, Nanjing, China). The same method was used to clone *MAT1-1-1* and *MAT1-1-2* ORFs into the *Sma*I-digested *pGADT7* vector to make prey constructs. The resulting bait and prey constructs were confirmed by sequencing analysis and co-transformed into yeast strain AH109. The transformants were grown on the SD-Trp-Leu and SD-Trp-Leu-His-Ade medium plates at 30°C for 3–5 days. This experiment was repeated three times.

RESULTS

Phylogenetic Analyses of *V. virens* and MAT1-1-3 Proteins With Other Fungi

To explore the evolutionary relationships of *V. virens* with other fungi, we selected 31 representative members of fungi, including heterothallic, homothallic and combined species. Phylogenetic analysis established that *V. virens* is more closely related to Clavicipitaceae although received weak bootstrap support (i.e., *Metarhizium* spp. *Epichloe typhina*, *Claviceps purpurea*), followed by Ophiocordycipitaceae (i.e., *Ophiocordyceps* and *Tolypocladium*), then Cordycipitaceae (i.e., *Cordyceps spp. Beauveria bassiana*) (**Figure 1A**). The Clavicipitaceae, Ophiocordycipitaceae and Cordycipitaceae all belong to Hypocreales (Bushley et al., 2013). In **Figure 1A**, fungi indicated with red undergo homothallic sexual reproduction,

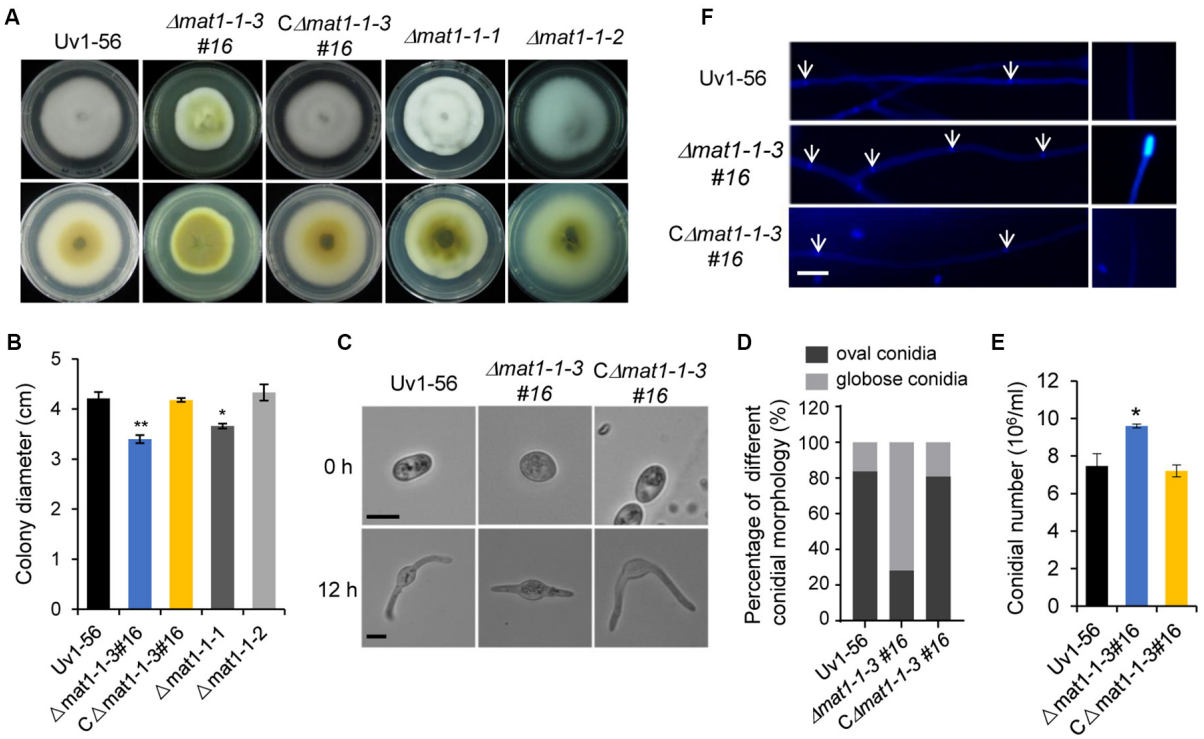

FIGURE 2 | *MAT1-1-3* affects mycelial growth, conidial morphology and production. **(A)** Colony morphology of wild-type (Uv1-56), Δ*mat1-1-3#16* deletion mutant, complemented strain CΔ*mat1-1-3#16*, Δ*mat1-1-1* and Δ*mat1-1-2* deletion mutants on PSA medium after 15 days of incubation at 28°C. **(B)** Quantified growth rate of wild type, mutant and complemented strain in **(A)**. Colony diameter was statistically analyzed, and error bars represent SD. The asterisks indicate significant differences (one-way ANOVA, $^*p < 0.05$, $^{**}p < 0.01$). **(C)** The conidial morphology and germination of wild-type, mutant and complemented strains were photographed after culturing on water agar plates for 0 h and 12 h. Scale bars, 5 μm. **(D)** Statistical analysis of the percentage of different conidial morphology in wild-type, mutant and complemented strains. **(E)** Statistical analysis of conidia production on PSB medium after 7 days of culturing with 150 rpm shaking at 28°C. Data are shown as mean ± SD from three independent replicates. Asterisks indicate significant differences (one-way ANOVA, $^*p < 0.05$). **(F)** Hyphae of wild-type, mutant and complemented strains were stained with calcofluor white, which detects chitin and cellulose in the cell wall, and fluorescence is shown in blue color. The hyphal septum of the Δ*mat1-1-3* mutant was shorter than that of wild type and complemented strains. Deletion of MAT1-1-3 altered the distribution of chitin in the cell wall. Arrows indicate the hyphal septa. Scale bars, 10 μm.

fungi indicated with green undergo homothallic and heterothallic sexual reproduction, and the remaining fungi are heterothallic (**Figure 1A**). However, the sexual reproductive mode of Ophiocordycipitaceae switches between homothallism and heterothallism. For example, *Tolypocladium inflatum* is heterothallic, but *Ophiocordyceps sinensis* is homothallic (Hu et al., 2013). As shown by the blue circle in **Figure 1A**, some fungi have lost the *MAT1-1-3* gene during Hypocreales evolution. For example, *E. typhina* and *O. sinensis* have the *MAT1-1-3* gene, while *C. tenuipes*, *C. militaris* and *B. bassiana* have lost the *MAT1-1-3* gene and their sexual reproduction is heterothallic (**Figure 1A**). *V. virens* also has *MAT1-1-3*, suggesting that the gene plays an important role in the evolution of sexual reproduction. Phylogenetic analysis further showed that the MAT1-1-3 protein from *V. virens* is clustered with those from *Metarhizium* spp. (**Figure 1B**). In addition, all of the sequences from 15 diverse fungi were found to contain the high mobility group (HMG) domain, except SmtA-3 (**Figure 1B**). Thus, we further compared the HMG domain sequences of 14 fungi species using WebLogo. Multiple sequence alignment of these proteins showed that the HMG domain is conserved among different fungi (**Figure 1C**). Collectively, the results suggest that MAT1-1-3 is a conserved protein among different fungi.

MAT1-1-3 Affects *V. virens* Mycelial Growth, Conidial Morphology and Production

To investigate the function of *V. virens MAT1-1-3*, we generated Δ*mat1-1-3* mutants in strain Uv1-56 (wild type) by using the CRISPR/Cas9 system (Liang et al., 2018; Li et al., 2019) to replace *MAT1-1-3* with an *HYG* gene (*hygromycin B-resistance*) (**Supplementary Figure S1A**). Genome DNA PCR and sequencing analysis of three Δ*mat1-1-3* mutants (#8, #16 and #20) confirmed that *MAT1-1-3* was successfully replaced (**Supplementary Figures S1B,C**). These mutants had similar phenotypes, so mutant #16 was selected for additional study. A complementation assay was carried out with Δ*mat1-1-3#16* to generate the CΔ*mat1-1-3#16* complemented strain (**Supplementary Figures S1B,C**). The *MAT1-1-3* is located at the *MAT1-1* idiomorph of *V. virens*,

which also contains two other mating type genes *MAT1-1-1* and *MAT1-1-2*. Thus, to assess whether *MAT1-1-1* and *MAT1-1-2* have the same phenotype with *MAT1-1-3*, we also generated Δ*mat1-1-1* and Δ*mat1-1-2* mutants using the same method.

The Δ*mat1-1-3* and Δ*mat1-1-1* mutants, but not Δ*mat1-1-2* mutant, exhibited a reduction in mycelial growth rate compared with those of the WT Uv1-56 and complemented strain (CΔ*mat1-1-3#16*) (**Figures 2A,B**). Moreover, the colony of Δ*mat1-1-3* mutant exhibited deeper pigmentation on PSA medium plate compared with those of the WT Uv1-56, Δ*mat1-1-1*, Δ*mat1-1-2* mutants and complemented strain (**Figures 2A,B**). Based on the difference in colony morphology between Δ*mat1-1-3* mutant and the other two mutants (Δ*mat1-1-1* and Δ*mat1-1-2*), we only focused on studying the function of *MAT1-1-3* in this study. The Δ*mat1-1-3* mutant produced more globose conidia compared with WT and complemented strain, which produced more oval conidia (**Figures 2C–E**). The conidia produced by Δ*mat1-1-3* mutant geminated slower than that of produced by WT and complemented strain (**Figure 2C**). CFW staining showed that the hyphal septa of the Δ*mat1-1-3* mutant increased and chitin accumulated on the tip of mycelium in the Δ*mat1-1-3* mutant compared with WT (**Figure 2F**), indicating that *MAT1-1-3* involved in regulating cell wall chitin and cellulose synthesis. Mycelial growth and hyphal septa defects of the mutant were rescued in the complemented strain CΔ*mat1-1-3#16* (**Figure 2**). Together, these results indicated that *MAT1-1-3* was required for conidial morphogenesis, conidia production, germination and cell wall integrity.

MAT1-1-3 Regulates *V. virens* in Response to Different Abiotic Stresses

To test whether knockout of *MAT1-1-3* affects *V. virens* responses to the osmotic, oxidative stress and cell wall integrity. The WT, mutant and complemented strains were cultured on PSA medium containing different stress agents. The growth inhibition rate of mycelial growth was calculated after 15 days of culture at 28°C. Our results demonstrated that the growth inhibition rate of mycelial growth of mutant displays significant difference, the Δ*mat1-1-3* mutant exhibited increases in the tolerance to NaCl, Sorbitol, H_2O_2, CR and CFW, but more sensitive to SDS compared with WT and complemented strain CΔ*mat1-1-3#16* (**Figure 3**). Taken together, these results indicated that *MAT1-1-3* is required for regulating the *V. virens* responses to osmotic stress and oxidation stress as well as cell wall integrity.

MAT1-1-3 Is Required for the Pathogenicity of *V. virens*

To further evaluate the role of *MAT1-1-3* in fungal pathogenicity, suspensions of shattered hyphae and conidia from various strains were individually inoculated into booting stage rice panicles. At 30 days post-inoculation (dpi), the false smut balls produced on rice spikelets were counted to evaluate *V. virens* pathogenicity. Rice panicles infected by the Δ*mat1-1-3* mutant produced significantly fewer false smut balls than those infected by WT and complemented CΔ*mat1-1-3#16* strains (**Figure 4**). This result suggested that *MAT1-1-3* was required for the pathogenicity of *V. virens*.

MAT1-1-3 Is Required for Sclerotia Formation

We next investigated whether *MAT1-1-3* regulated sclerotia formation of *V. virens*. On the seventh day before heading stage, the swollen flag leaf sheath of rice was inoculated with the mixed suspension of conidia and hyphae of Uv1-56 & Uv2-51, Δ*mat1-1-3* & Uv2-51, and CΔ*mat1-1-3#16* & Uv2-51. As shown in **Figure 5**, Δ*mat1-1-3* mutant could not produce the sclerotia, whereas the wild-type Uv1-56 could produce the sclerotia on the surface of false smut balls, which were marked by the red arrows. Apparently, the complemented strain CΔ*mat1-1-3#16* restored the sclerotia production to the WT level (**Figure 5**). Together, the results suggested that *MAT1-1-3* was required for sclerotia formation and sexual development of *V. virens*.

MAT1-1-3 Is a Negative Regulator of the Immature Fruiting Body in *V. virens*

The fertile sclerotia play an important role in the sexual cycle and development of *V. virens*, but current research shows that it is only produced in rice spikelets infected by two opposite mating-type strains in the field. The sclerotia can germinate and form different sexual structures, such as primordia, fruiting body, asci and ascospores. The germination of sclerotia collected from the field was observed in the laboratory. Germination assays showed that the sclerotia began to germinate at 50 days, primordia emerged at 55 to 65 days, and mature fruiting bodies, filled with asci containing ascospores, appeared at 75 days (**Figure 6A**). Although Δ*mat1-1-3* mutant could not produce sclerotia after outcrossing with Uv2-51 in the field (**Figure 5**), the Δ*mat1-1-3* mutant alone formed the fruiting body primordium and germinated on the PSA medium (**Figure 6B**). The mycelium of Δ*mat1-1-3* mutant began to grow densely at 20 days and a large number of hyphae differentiated into filaments at 30 days (**Figure 6B**). Then the primordia appeared at 35 days (**Figure 6B**). At 40 days, the primordia of fruiting body appeared (**Figure 6B**). However, the fruiting body could not reach maturity and the immature stromata had no ascospores (marked with red squares), even though extended the growth time in PSA medium plate (**Figure 6B**), indicating that the Δ*mat1-1-3* mutant alone can form similar sexual structures. Conversely, wild-type Uv1-56 and CΔ*mat1-1-3#16* could not form fruiting body primordia and the colonies began to dry and shrink after 40 days on PSA medium (**Figure 6C**). After crossing with Uv2-51, only the Δ*mat1-1-3* mutant could form the primordia at 35 days compared with WT and CΔ*mat1-1-3#16* (**Figure 6D**). Taken together, these results indicate that *MAT1-1-3* negatively regulates the formation and development of immature fruiting bodies during the sexual development of *V. virens*.

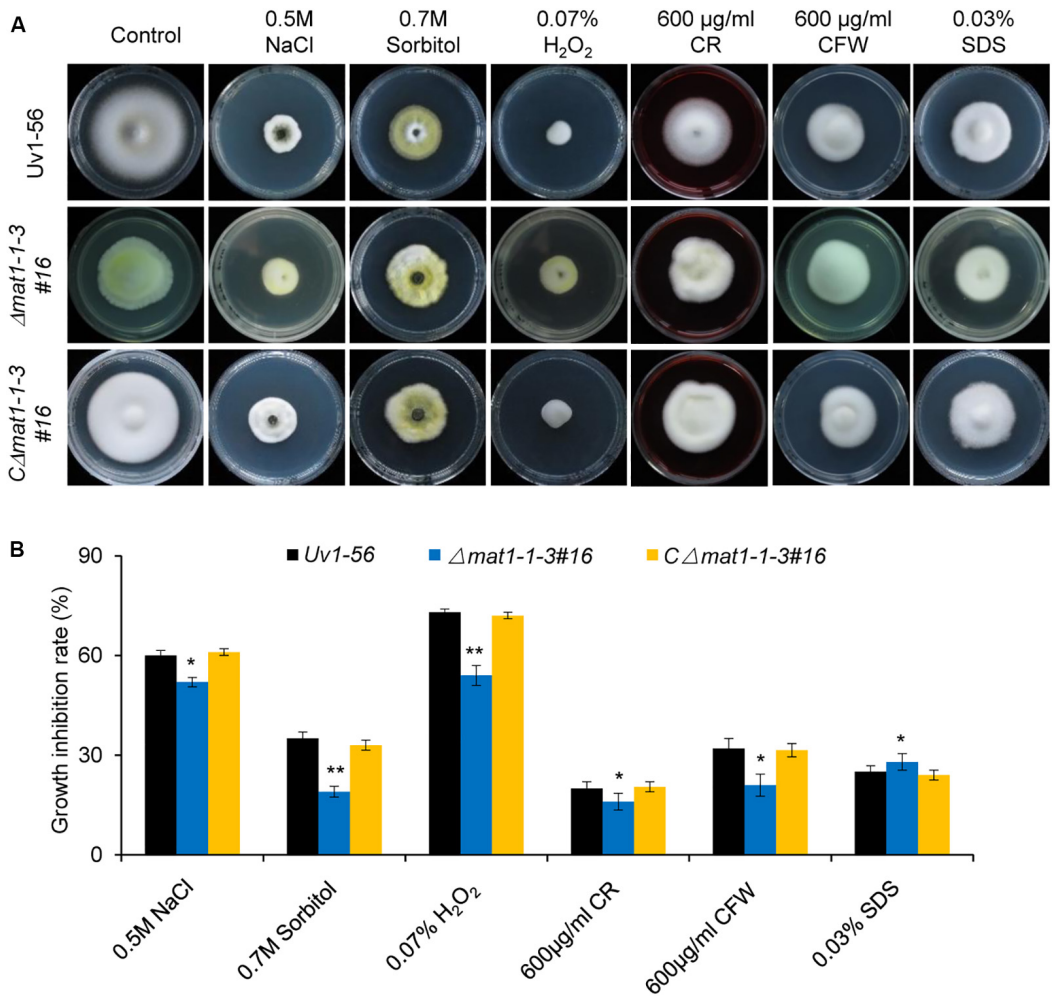

FIGURE 3 | *MAT1-1-3* is involved in regulating pathogen stress responses. **(A)** Mycelial radial growth of the indicated wild-type, Δ*mat1-1-3#16* and complemented CΔ*mat1-1-3#16* strains on PSA medium supplemented with salt stress agent (0.5 M NaCl), osmotic stress agent (0.7 M Sorbitol), oxidative-stress agent (0.07% H_2O_2), and cell wall disturbing agents Congo Red (CR, 600 μg/mL), calcofluor white (CFW, 600 μg/mL) and sodium dodecyl sulfate (0.03% SDS). Photographs were taken after 15 days of incubation at 28°C. **(B)** Statistical analysis of the indicated strains growth inhibition rate under different stress conditions. Colony diameters of the indicated strains were measured. Data are shown as mean ± SD of three independent replicates. Asterisks indicate significant differences (one-way ANOVA, $*p < 0.05$, $**p < 0.01$).

Deletion of *MAT1-1-3* Affects Expression of Pheromone Precursor and Pheromone Receptor Genes and Mating Hyphae Growth

The expression level of pheromone precursor and pheromone receptor genes are strictly regulated during sexual reproduction. Yu et al. (2016) identified several genes homologous to pheromone precursor (*PPG1*, a homolog of *ccg-4* in *N. crassa*) and pheromone receptors (*PRE1* and *PRE2*, homolog of *pre-1* and *pre-2* in *N. crassa*, respectively) in *V. virens* (Yu et al., 2016). Given that *MAT1-1-3* regulated the sexual development of *V. virens*, we investigated the expression of pheromone precursor and pheromone receptors genes after confronting mutant or WT strains with the *MAT1-2* strain Uv2-51 for 10 days or 15 days. Compared with the WT, qRT-PCR results showed decreased *PPG1* expression and increased *PRE1* and *PRE2* expression in the Δ*mat1-1-3* mutant at 10 days and 15 days, and the expression level of *PRE1* and *PRE2* at 10 days was higher than at 15 days (**Figure 7A**), suggesting that *MAT1-1-3* can regulate transcription of these genes. It has been known that pheromone-related genes also regulate the cell fusion of opposing mating type strains before mating (Jones and Bennett, 2011). To test if the cell fusion was affected in the Δ*mat1-1-3* mutant, we employed a confrontation assay (Snetselaar et al., 1996). In the control, mating hyphae formed normally when Uv1-56 was confronted with Uv2-51 at 10 days (**Figure 7B**). However, when the Δ*mat1-1-3* mutant was confronted with Uv2-51, both strains had longer mating hyphae than those in the control, and the hyphae of Δ*mat1-1-3* mutant were more frequently fused with Uv2-51 than with WT strain at 15 days (**Figure 7B**). At 20 days, the Δ*mat1-1-3* mutant colony fused better with Uv2-51 than with

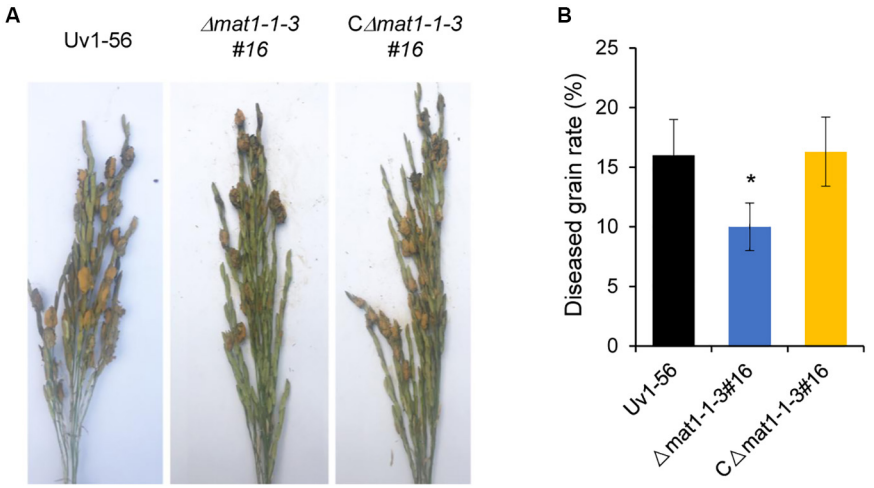

FIGURE 4 | *MAT1-1-3* is required for *Villosiclava virens* full pathogenicity in rice. **(A)** Rice spikelets were infected with an inoculum of wild-type Uv1-56, Δ*mat1-1-3#16* mutant and complemented strains. Pictures were taken 30 days post-inoculation. **(B)** Statistical analysis of the average diseased grains rate in the infected spikelets. False smut balls were counted from each single rice panicle as described in materials and methods. Data represent means ± SD from three independent experiments. Asterisks indicate significant differences (one-way ANOVA, $^*p < 0.05$).

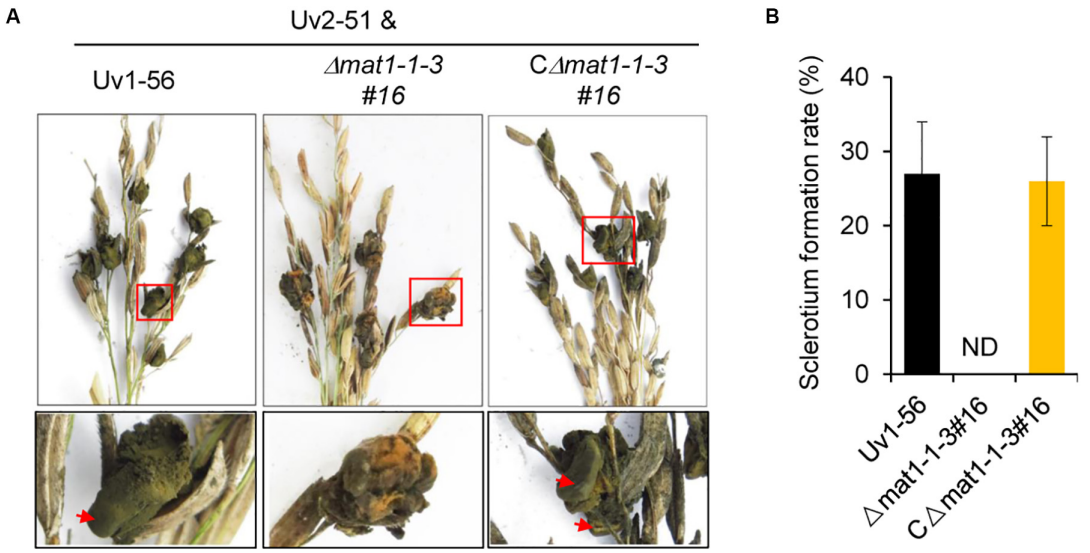

FIGURE 5 | *MAT1-1-3* is indispensable for *Villosiclava virens* sclerotia formation and sexual development. **(A)** In contrast with Uv1-56 and complemented strains, the Δ*mat1-1-3#16* mutant was unable to produce sclerotia. Pictures were photographed 45 days post-inoculation (dpi). The enlarged regions marked with squares were shown at the bottom. **(B)** Statistical analysis of sclerotium formation rates of wild-type, mutant or complemented strains crossed with Uv2-51 at 45 dpi. Data are shown as means ± SD of three independent replicates. ND, not detection.

the wild-type strain (**Figure 7B**). Taken together, these results demonstrate that *MAT1-1-3* is likely to regulate the expression of *PPG1*, *PRE1* and *PRE2* to affect mating hyphae growth and hyphae fusion.

Subcellular Localization and the Interacting Protein of MAT1-1-3

To better understand the biological function of *MAT1-1-3*, we examined the localization of MAT1-1-3 fused with green fluorescence protein (GFP) by a confocal microscope. The transformants expressing MAT1-1-3-GFP were generated in the background of WT Uv1-56. We observed that MAT1-1-3-GFP signal accumulated in the nucleus and cytoplasm of the conidia and hyphae (**Figure 8A**). The nuclear signal was confirmed by nuclear dye DAPI. The proteins encoded by mating-type genes can form a heterodimer, which is involved in morphological changes and spore development in fungi (Kämper et al., 1995; Lee et al., 2010; Kües et al., 2011). To investigate the relationship between the MAT1-1-3 and

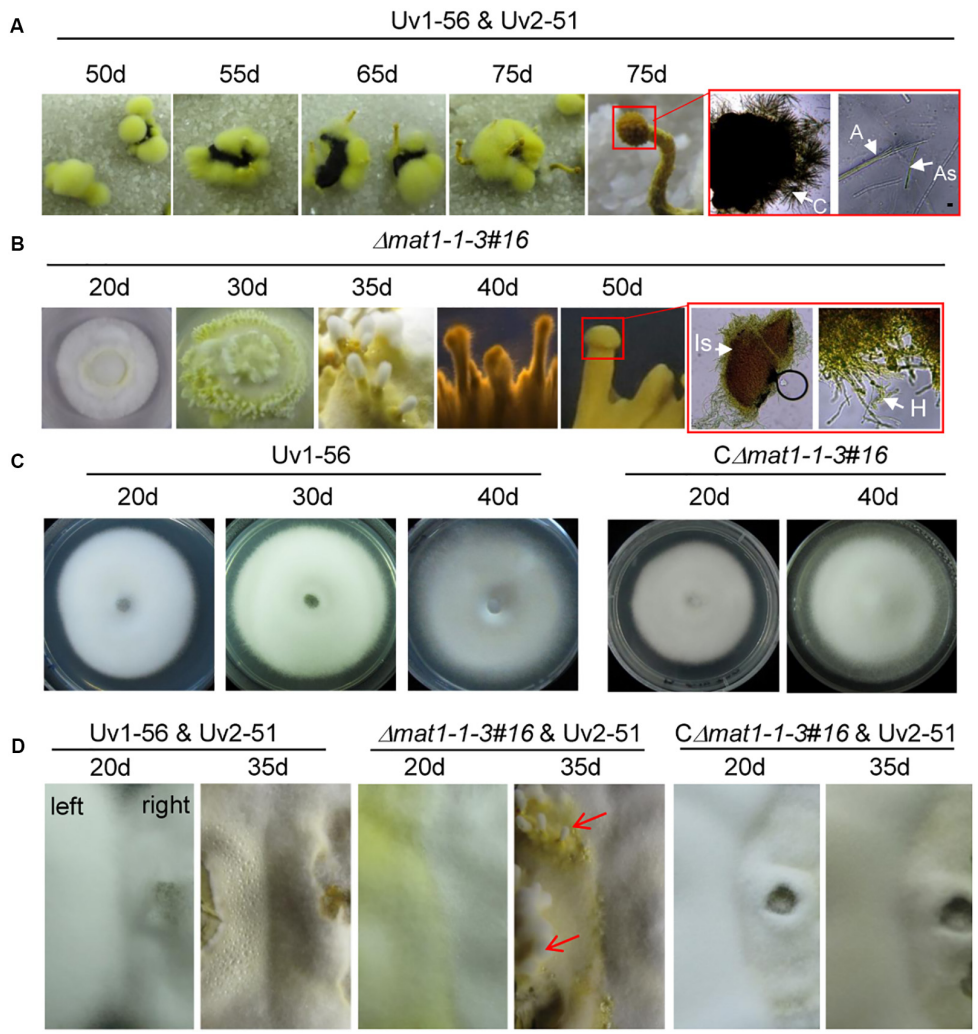

FIGURE 6 | *MAT1-1-3* negatively regulates the formation of fruiting bodies in *Villosiclava virens*. **(A)** Inoculum of wild-type Uv1-56 mixed with Uv2-51 infected the rice panicle to form fertile sclerotia. Wild-type sclerotia germination formed different sexual structures at different periods. The magnified red square region indicates that mature fruiting bodies could form a cavity and ascospores. **(B)** Sexual structures for the Δ*mat1-1-3* mutant formed after different periods on the PSA medium. The magnified red square region shows that the fruiting body was immature, no ascospores were produced and only hypha formed. **(C)** Wild-type Uv1-56 and complemented CΔ*mat1-1-3#16* strains could not form the sexual structure on PSA plates. **(D)** For the confrontation assay, wild-type Uv1-56, complemented strain or mutant Δ*mat1-1-3* were confronted with wild-type Uv2-51 and cultured at 28°C for 20 days and 35 days on PSA medium. The colony growing on the right in the plate represents the Uv2-51 strain. The Δ*mat1-1-3* mutant, but not WT Uv1-56 and complemented strains, formed sexual structures at 35 days after confronting culture with Uv2-51. Is, Immature stroma; H, hypha; C, cavity; A, asci; As, ascospores.

other mating-type proteins in *V. virens*, we performed a yeast two-hybrid (Y2H) assay to examine the interaction. Y2H assay showed that MAT1-1-3 interacted with MAT1-1-1, but could not interact with MAT1-1-2 (**Figure 8B**), indicating that MAT1-1-3 and MAT1-1-1 may form a complex to regulate sexual reproduction of *V. virens*.

MAT1-1-3 Deletion Affects the Transcription of a Subset of Genes

To further study *MAT1-1-3* regulation mechanisms in *V. virens*, we performed transcriptome sequencing (RNA-seq) analysis of the Δ*mat1-1-3* mutant. The transcripts of *MAT1-1-3* could be detected when WT cultured in potato sucrose broth (PSB) medium (**Supplementary Figure S2A**). Thus, the samples for RNA-seq were extracted from mycelia of Δ*mat1-1-3* mutant and WT cultured in PSB for 7 days. We prepared three biological replicates samples for Δ*mat1-1-3* (Δ*mat1-1-3_1/2/3*) mutant and WT (WT_1/2/3), respectively, though one sample from Δ*mat1-1-3* and another sample from WT were contaminated and discarded. The correlation coefficients (0.8954 and 0.8098) for the expression profiles of all transcripts between two wild-type (WT-1 and WT-3) or two mutant (Δ*mat1-1-3_1* and Δ*mat1-1-3_3*) samples, respectively (**Figure 9A**), suggested that the RNA-seq data were credible. Analysis of the differentially expressed genes (DEG) revealed that the *MAT1-1-3* knockout

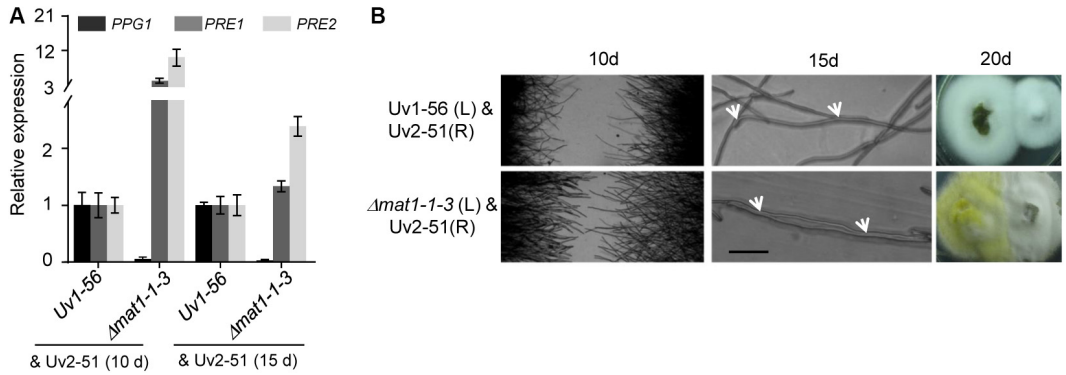

FIGURE 7 | *MAT1-1-3* affects the expression of pheromone and pheromone receptor genes. **(A)** qRT-PCR analysis of *PPG1*, *PRE1* and *PRE2* in wild-type Uv1-56 and Δ*mat1-1-3* mutant. The wild-type and mutant strains were confronted with the *MAT1-2* type strain Uv2-51 after 10 days or 15 days on PSA medium. **(B)** Mating hyphae formation assay with wild-type and mutant strains confronted with Uv2-51. After 10 days, when Δ*mat1-1-3* crossed with Uv2-51, both strains formed mating hyphae that were longer than those of control Uv1-56 crossed with Uv2-51. After 15 days, hyphal fusions, indicated by arrows, appeared between Uv1-56 and Δ*mat1-1-3* mutant crossed with Uv2-51. The Δ*mat1-1-3* mutant fused earlier than wild-type with the Uv2-51 strain at 20 days. Scale bars, 10 μm.

affected the transcription of a subset of genes (**Supplementary Table S3**). In comparison with WT, 1001 genes showed increased expression and 651 genes showed decreased expression in the Δ*mat1-1-3* mutant (**Figures 9B,C** and **Supplementary Table S4**). Enrichment analysis of Gene Ontology (GO) categories indicated that all significantly differentially expressed genes involved in regulation of molecular function, biosynthetic process, response to stress, regulation of cellular process, cellular metabolic and cell cycle process were significantly enriched (**Figure 9D**).

Extensive evidence has shown that genes involved in fungal cell wall integrity, MAPK signaling, sexual development, autophagy process, transcription factors and epigenetic modification are involved in fungal pathogenicity, growth and development. We further analyzed 1652 up- and down-regulated genes and found that a subset of genes involved in these processes was misregulated in the Δ*mat1-1-3* mutant (**Figure 9E** and **Supplementary Table S5**). The cell wall is essential for growth and participates in morphogenetic and differentiation processes in fungi (de Medina-Redondo et al., 2008). qRT-PCR results confirmed increased expression in Δ*mat1-1-3* mutant of genes encoding beta-1,3-glucanosyltransferase (*Gel3*), cell wall protein (CWP1) and adhesin protein Mad2 (*Mad2*) (**Figure 9F**). Several genes involved in the MAPK signaling pathway, which is essential for mating (Herskowitz, 1995; Banuett, 1998), including encoding the mitogen-activated protein kinase (*MAF1*), mitogen-activated protein kinase kinase (*MAPKK*) and G-protein coupled receptor (*GPCR*) increased expression in Δ*mat1-1-3* mutant; however, the expression was reduced for two genes encoding G protein alpha and beta subunit (*Ga* and *Gb*) (**Figure 9F** and **Supplementary Table S5**). Additionally, in the mutant, the expression levels of several genes involved in sexual development increased, like *PRE2*, or decreased, like *PPG1* (**Figure 9F**), which is consistent with our previous results (**Figure 7A**). Studies have reported that genes encoding transcription factors (*bZIP-1*, *bZIP-2*, *MADS-box* and *TF25*) involved in fruiting body development (Zheng and Wang, 2013; Yu et al., 2016), with significantly increased expression in the Δ*mat1-1-3* mutant (**Figures 9E,F**). In addition, all seven autophagy-related genes were up-regulated in the mutant, and several epigenetic modification related genes, such as DNA methyltransferase (*DIM-2*), histone methyltransferase (*HMT*) and GNAT family acetyltransferase, were misregulated in the mutant (**Figures 9E,F** and **Supplementary Table S5**). Taken together, these results suggest that *MAT1-1-3* regulates the expression of a subset of genes to control related functions in *V. virens*.

Our previous study showed that the truncated *MAT1-2-1* down-stream of the *MAT1-1-3* is part of the *MAT1-2-1* located on *MAT1-2* idiomorph (**Supplementary Figure S2B**) (Yu J. J. et al., 2015). The length of truncated *MAT1-2-1* is 273 bp without ATG, which shares 87% identities with the 273 bp at 3′ end of *MAT1-2-1* in the nucleotide sequence (**Supplementary Figure S2C**). The encoding protein with an HMG domain was predicted according to the 3′ end of MAT1-2-1 sequence, which shares 77% identities with the corresponding sequences in MAT1-2-1 (**Supplementary Figure S2**). RNA-seq data showed that the expression of truncated *MAT1-2-1* gene increased about 9-fold in the Δ*mat1-1-3* mutant, which was confirmed by qRT-PCR (**Figures 9E,F**). However, fewer transcripts of truncated *MAT1-2-1* are detected in WT compared with *MAT1-1-3* (**Supplementary Figure S2A**). The results suggest that *MAT1-1-3* negatively regulates the expression level of truncated *MAT1-2-1*.

DISCUSSION

Sexual cycle plays a crucial role in *V. virens* overwintering and genetic diversity (Sun et al., 2013; Wang et al., 2014; Deng et al., 2015; Yong et al., 2018). The sclerotia produced during the sexual cycle can survive in winter and produce a large number of ascospores in the coming year, which are considered as the primary infection source (Yong et al., 2018). Genetic

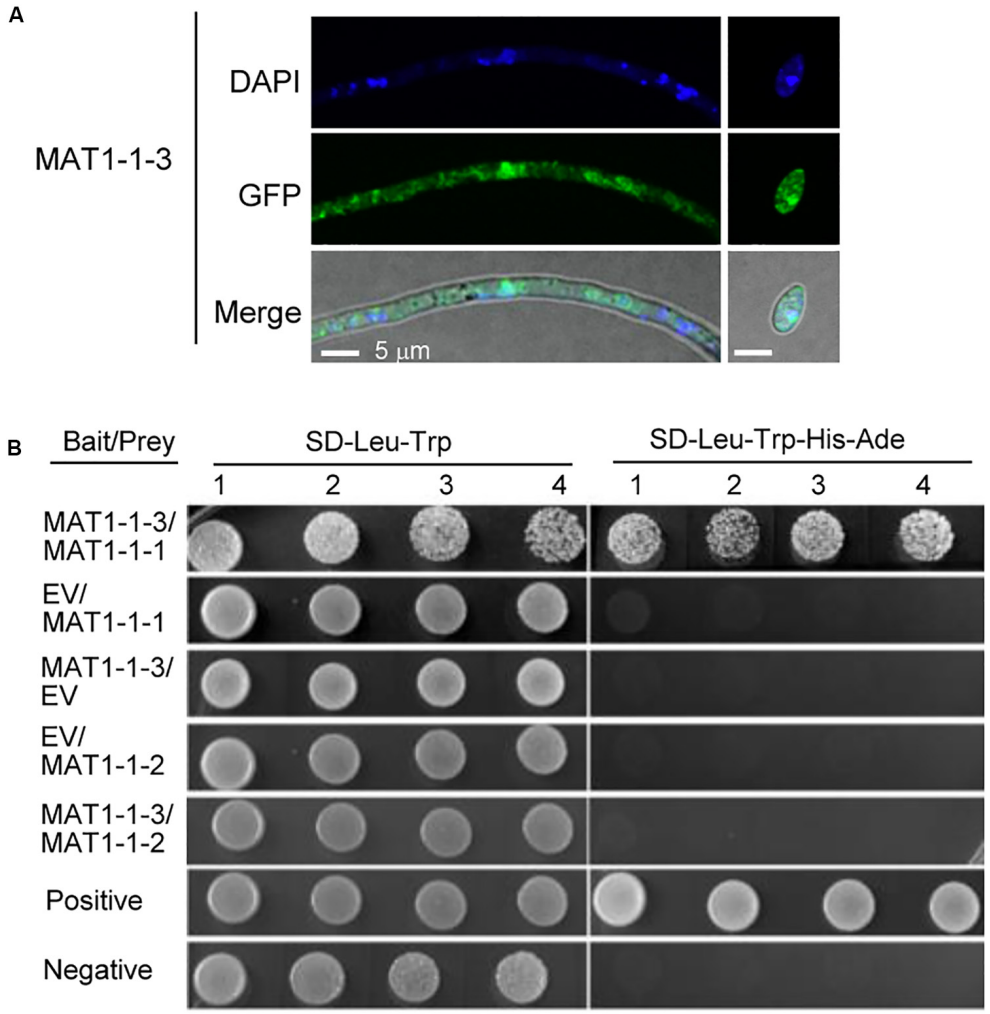

FIGURE 8 | Subcellular localization and the interacting protein of MAT1-1-3 in *Villosiclava virens*. **(A)** The subcellular localization of MAT1-1-3-GFP in the hyphae and conidia of *V. virens*. The hyphae and conidia were stained with DAPI before the signal was observed with a confocal microscope. Scale bars, 5 μm. **(B)** The yeast two-hybrid (Y2H) assay was used to examine interactions between MAT1-1-1, MAT1-1-2 and MAT1-1-3. EV, empty vector; SD/-Leu-Trp-His-Ade, synthetic dropout (SD) media lacking leucine, tryptophan, histidine and Adenine; SD/-Leu-Trp, SD media lacking leucine and tryptophan. Numbers indicate repeats using different single colonies.

recombination occurs during sexual reproduction and expands *V. virens* genetic diversity (Sun et al., 2013; Wang et al., 2014). Mating type genes play crucial roles in sexual reproduction (Zheng and Wang, 2013). Here, to better understand the genetic basis of sexual reproduction in *V. virens*, we characterized a mating type gene *MAT1-1-3* in *V. virens*. We found that MAT1-1-3 is a negative regulator of the immature fruiting body in *V. virens*, meanwhile, it is required for the asexual development and pathogenicity.

The Evolution of *V. virens* and MAT1-1-3 Proteins

The study of evolutionary relationships contributes to better understand the fungal origin and the relationships between different fungi. Previously, Zhang et al. (2014) systematically analyzed the evolutionary relationship of *V. virens* with other eleven fungi (ten Ascomycota and one Basidiomycota outgroup), including *Metarhizium* spp. via comparative genomic analyses and proteome comparisons. This study showed that *V. virens* is more closely to *Metarhizium* spp. than to other species including the plant pathogen *Claviceps purpurea* and the insect pathogenic fungus *Cordyceps militaris*. Our phylogenetic analysis data also showed that *V. virens* and *Metarhizium* spp. are in the same cluster, implying that the evolutionary relationship is close. The sexual reproduction mode of *Metarhizium* spp. is heterothallic (Zheng et al., 2011), which is consistent with *V. virens*. In addition, phylogenetic analysis data also showed that MAT1-1-3 proteins of *V. virens* and *Metarhizium* spp. are also in the same cluster. Among 31 fungi that we analyzed, some fungi (*C. tenuipes, C. militaris* and *B. bassiana*) have lost the *MAT1-1-3* gene, however, most fungi still have it. Several researches showed

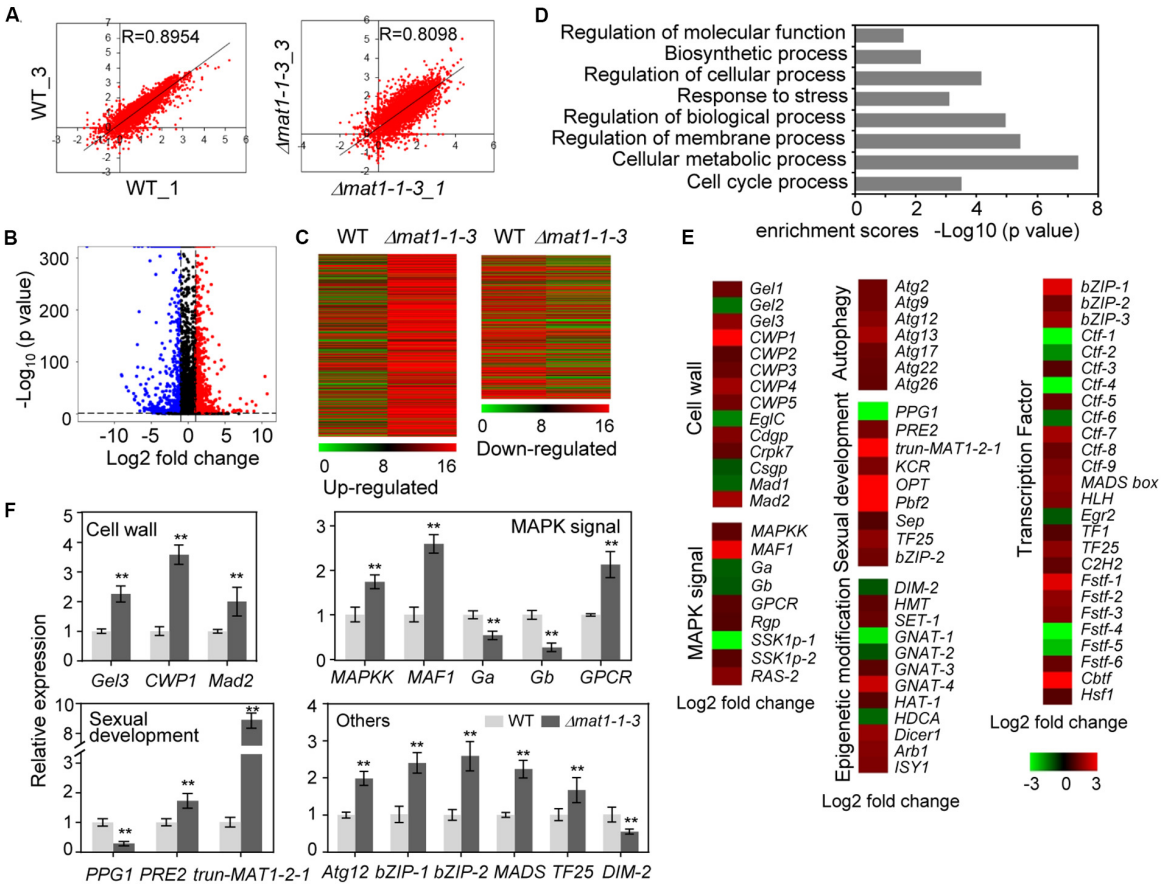

FIGURE 9 | *MAT1-1-3* regulates the expression of a subset of genes. **(A)** Scatter plots showing correlation of whole-genome expression measured as transcripts per million reads (TPM) between two WT samples (WT_1 versus WT_3, left) or two Δ*mat1-1-3* mutant samples (Δ*mat1-1-3_1* versus Δ*mat1-1-3_3*, right). Gene expression levels were measured for mycelium grown in PSB for 7 days. The x-axis indicates gene expression in WT_1 or Δ*mat1-1-3_1*, and the *y*-axis indicates gene expression in WT_3 or Δ*mat1-1-3_3* mutant. **(B)** Volcano map of differently expressed genes between WT and Δ*mat1-1-3* mutant. The *x*-axis indicates relative gene expression (log2 fold change between WT and Δ*mat1-1-3* mutant), and the *y*-axis indicates the mean of normalized counts [–$\log_{10}$ (*p*-value)]. Genes with significantly up-regulated expression ($p < 0.05$ and $\log_2$ fold change ≥ 1) are shown in red. Genes with significantly down-regulated expression ($p < 0.05$ and $\log_2$ fold change ≤ 1) are shown in blue. **(C)** Heatmaps of genes up-regulated and down-regulated in the Δ*mat1-1-3* mutant compared with WT. The original means of reading counts were adjusted by $\log_2$ transformation using MeV4.0. **(D)** Gene ontology (GO) enrichment analysis of significantly differentially expressed genes in Δ*mat1-1-3* compared with WT. The *x*-axis indicates enrichment scores [–log10 (*p*-value)] (the *P*-value indicates the possibility of significant enrichment) for each GO item on the *y*-axis. The fold enrichment was calculated based on the frequency of genes annotated to the term compared to their frequency in all transcripts detected. **(E)** Differentially expressed genes in the Δ*mat1-1-3* mutant might indicate involvement in pathogenesis and sexual development. Regulated genes include genes involved in cell wall integrity, MAPK signaling, sexual development, autophagy, and epigenetic modification. Some genes encoding transcription factors were also regulated by *MAT1-1-3*. The full names of abbreviated genes are shown in **Supplementary Table S5**. **(F)** qRT-PCR analysis of *MAT1-1-3* regulated genes. Relative expression levels were normalized with β-*tubulin* as the internal standard and presented as means ± SD from three biological replicates. Asterisks indicate significant differences (Student's *t*-test, $^*p < 0.05$, $^{**}p < 0.01$).

that *MAT1-1-3* may have been lost during the shift from plant to insect hosts, and could be a good indicator of Clavicipitaceae evolution (Yokoyama et al., 2006; Zheng et al., 2013). Our results showed that *MAT1-1-3* of *V. virens* is required for sclerotia formation and sexual development.

The Relationship Between Truncated Mating Type Genes and Mating Type Genes

Increasing studies show that unequal recombination/crossover and transposable elements (TE)-mediated translocations play an important role in the evolution of mating loci (Gioti et al., 2012; Dyer et al., 2016). In *Grosmannia clavigera*, the *MAT1-2* idiomorph contained a truncated *MAT1-1-1* located up-stream of the *MAT1-2-1* gene, which is homologous to the *MAT1-1-1* gene in the *MAT1-1* idiomorph (Tsui et al., 2013). Moreover, this truncated *MAT1-1-1* is present in multiple *G. clavigera* isolates. And they found that the unequal recombination/crossover event likely accounted for the truncated *MAT1-1-1*. Because the unequal recombination/crossover events have occurred in many fungal *MAT* idiomorphs. For example, the truncated *MAT1-1-1* gene was found in the *MAT1-2* idiomorph of *Hypocrea jecorina* (Seidl et al.,

2009) and also was identified in the *MAT1-2* idiomorph of at least five *Phialocephala* species (Zaffarano et al., 2010). In contrast, a partial *MAT1-2-1* sequence (360bp) located in the *MAT1-1* idiomorph of *Aspergillus fumigatus* (Paoletti et al., 2005). Our study here also showed that a truncated *MAT1-2-1* was found in *MAT1-1* idiomorph of *V. virens*. The length of truncated *MAT1-2-1* is 273 bp without start codon, but contains stop codon, which shares 87% identities with the 273 bp at 3′ end of *MAT1-2-1* in the nucleotide sequence. The encoding protein with an HMG domain was predicted according to the 3′ end of MAT1-2-1 sequence. The encoding protein shares 77% identities with the corresponding amino acid sequences in MAT1-2-1. Thus, we also think that the truncated *MAT1-2-1* organization is due to unequal recombination/crossover events during sexual reproduction.

Several studies showed that recombination/crossover event caused the truncated genes (*MAT1-1-1* or *MAT1-2-1*) to be non-functional or inactive in mating, thereby being called pseudogenes. For example, the truncated *MAT1-1-1* gene in *Ophiostoma montium* is highly eroded and possible is a pseudogene (Tsui et al., 2013). Similarly, the truncated *MAT1-1-1* gene in *Cordyceps takamontana* (known as *Isaria tenuipes*) was a pseudogene due to accumulated mutations and stop codons (Yokoyama et al., 2003). Our previous study showed that the truncated *MAT1-2-1* of *V. virens* was also named a pseudogene due to no start codon and very low detectable transcripts. However, the transcripts of truncated *MAT1-2-1* increased about 9-fold after knockout *MAT1-1-3*, indicating that it may have function, thereby being named truncated *MAT1-2-1* here. These data also suggest that *MAT1-1-3* suppresses the expression of truncated *MAT1-2-1* to regulate the mating of *V. virens*. Consistently, the transgenic strains, carrying both mating type genes, are unable to produce progeny in isolates of *N. crassa* (Glass et al., 1990), *Podospora anserina* (Coppin and Debuchy, 2000) and *Cochliobolus heterostrophus* (Turgeon et al., 1993a). These results, including our data, suggest that the truncated genes may interfere or compete with the signal from the "resident/original" HMG domain at the same locus. It is also possible that the truncated genes have evolved new functions through adaptive evolution (Tsui et al., 2013). Therefore, it will be important for future studies to investigate whether the truncated genes have functions and the mechanisms of how it regulates sexual reproduction.

Function of *MAT1-1-3* in Asexual Development, Sexual Cycle and Pathogenicity

In heterothallic *N. crassa*, the *matA-3* (*MAT1-1-3*) is dispensable for vegetative growth and sexual reproduction, such as asci production (Ferreira et al., 1998). However, the mutant A^{IIRIP}, which contains mutations in both *mat A-2* and *mat A-3* (Glass and Lee, 1992; Ferreira et al., 1996), normally mates as a *mat A* strain, but produces very few asci with ascospores (Ferreira et al., 1998). The *FMR1*, *SMR1* and *SMR2* (*MAT1-1-3*) are required for the development of fertilized female organs in *P. anserine*, *SMR2* (*MAT1-1-3*) was not essential for vegetative growth (Debuchy et al., 1993). However, the homothallic *S. macrospora SmtA-3* (*MAT1-1-3*) is not essential for fertility and vegetative growth (Klix et al., 2010), and *F. graminearum MAT1-1-3* is not essential for perithecium formation and vegetative growth, but is required for ascosporogenesis in self-crosses (Zheng et al., 2015). In our study, we demonstrated that knockout of *MAT1-1-3* caused obvious growth and conidial morphology defects compared to wild type. Additionally, the Δ*mat1-1-3* mutant could not form sclerotia after infecting rice spikelets. Meanwhile, *MAT1-1-3* is required for mating hyphae growth. A recent study showed that the *MAT1-1-3* of *F. graminearum* is not required for virulence (Zheng et al., 2015). However, *MAT1-1-3* was essential for the full pathogenicity of *V. virens*. Fungal sclerotia, which usually form in response to adverse environments like winter, germinate to form hyphae that serve as specific structures to start sexual reproduction under suitable conditions, thereby acting as the primary inoculum in the disease cycle (Yong et al., 2018; Liu et al., 2019). In outcrosses, the Δ*mat1-1-3* mutant was unable to produce sclerotia and could not initiate sexual reproduction. In addition, MAT1-1-3 interacted with MAT1-1-1, which is consistent with the MAT proteins in *Saccharomyces cerevisiae* and *Phaffia rhodozyma* to form complexes to regulate function (Haber, 2012; David-Palma et al., 2016). Thus, the *MAT1-1-3* plays a key role in asexual development, sexual reproduction and pathogenicity of *V. virens*.Fungal fruiting bodies are important structures for fungi development. The fruiting bodies formed by *Cordyceps. spp*. have an important value as edible and medicinal mushrooms (Zheng et al., 2011, 2013). Several studies reported that the mechanisms of regulating fungal fruiting body formation are different. For example, the *MAT1-2* single mating-type strain of *Ophiocordyceps xuefengensis* could form sterile fruiting bodies, with a *MAT1-2* locus that is only *MAT1-2-1* (Zou et al., 2017). The heterothallic *C. militaris* still can produce perithecia and ascospores although the loss of *MAT1-1-3* in the genome in outcrosses (Zheng et al., 2011). The mature fruiting bodies were formed after being crossed with two opposite strains. However, this is the first ascomycete species reported that the *C. militaris* Cm01 stain with only a *MAT1-1* single mating-type idiomorph also can produce stroma (fruiting body) without mature perithecia and ascospores on caterpillar pupae (Zheng et al., 2011). This is consistent with our result that the Δ*mat1-1-3* mutant can produce fruiting body primordium on PSA medium plate, but the fruiting body could not reach maturity and produce ascospores. Altogether, the result indicates that *MAT1-1-3* is required for regulating fruiting bodies development in *V. virens*. Furthermore, a recent study showed that during outcrossing in *C. militaris*, *MAT1-2-1* is required for fruiting body formation, and *MAT1-1-2* mutant could produce fruiting body but with sterile perithecia (Lu et al., 2016). These results suggest that the fruiting body also can be regulated by other mating-type genes, which provides an important basis for us to study the function of other mating-type genes in different fungi.

MAT1-1-3 Regulates the Expression of a Subset Genes Involved in MAPK Pathway, Cell Wall Integrity, Epigenetic Modification and Autophagy

Mitogen-activated protein kinase (MAPK) cascades are a conserved signal pathway that has been shown to play a key role in transduction extracellular signals to cellular responses (Gustin et al., 1998; Goldsmith and Dhanasekaran, 2007). Meanwhile, the G proteins perceive the extracellular signal through cell surface receptors, such as G-protein-coupled receptor (GPCR), which are critically involved in the regulation of different MAPK networks (Goldsmith and Dhanasekaran, 2007). MAPK modules regulate many important signaling pathways including cell proliferation, differentiation and apoptosis (Chang and Karin, 2001). Extensive studies showed that MAPK encoding genes are required for sexual reproduction in fungi (Herskowitz, 1995; Banuett, 1998). For example, the MAPK genes are required for fruiting body formation in *Aspergillus* (AN1017) and *Neurospora* (NC02393) (Pöggeler et al., 2006). In yeast, MAPK Slt2p, also called Mpk1p, involved in the regulation of many cellular events including the sexual cycle (Gustin et al., 1998). Moreover, a recent study showed that the blue-light receptor gene white collar-1 (*CmWC-1*) from *C. militaris* mediated the fruiting body development most likely via regulating G protein-coupled receptors (Yang et al., 2016). Strikingly, our RNA-seq and qRT-PCR data showed that the expression levels of *MAF1*, encoding a mitogen-activated protein kinase, *MAPKK* and *GPCR* increased in Δ*mat1-1-3* mutant. Furthermore, *Ga* and *Gb*, encoding G protein alpha and beta subunit respectively, exhibited reduced expression in Δ*mat1-1-3* mutant. Thus, the results indicate that the MAPK signal pathway also participates in the *V. virens* sexual reproduction, although the mechanism of MAPK regulation remains unclear. In addition, *MAT1-1-3* of *V. virens* is also required for regulating the expression of *PRE2* and *PPG1*, encoding pheromone receptor and pheromone precursor, respectively, which are important for fungal sexual reproduction (Pöggeler et al., 2006). Thus, it will contribute to better understand the *V. virens* sexual cycle via studying the function of these genes regulated by *MAT1-1-3*.

The cell wall is essential for growth, signal transduction and participates in morphogenetic and differentiation processes in yeast and fungi (de Medina-Redondo et al., 2008). We found that knockout of *MAT1-1-3* affected the *V. virens* cell wall integrity. Furthermore, *MAT1-1-3* also regulated abiotic stress, such as salt, osmotic- and oxidatives tress. Notably, many genes involved in cell wall integrity and stress response were misregulated in Δ*mat1-1-3* mutant. The *Gel1*, encoding the 1, 3-b-glucanosyltransferase, is required for maintaining the cell wall integrity of *F. graminearum* (Bolouri et al., 2017). Similarly, *Gel2* is required for cell wall morphogenesis and virulence in *Aspergillus fumigatus* (Mouyna et al., 2005). Apparently, these two genes are up-regulated and down-regulated in Δ*mat1-1-3* mutant, respectively. In addition, several genes involved in epigenetic modification can be regulated by MAT1-1-3, such as *DIM-2*, *HMT*, *SET-1* (encoding SET domain-containing protein), *HAT-1* (encoding histone acetyltransferase) and *HDCA* (encoding histone deacetylase A). *SET-2* (a homolog of *HMT* in *V. virens)* is essential for normal growth and development in *Neurospora* (Adhvaryu et al., 2005). Zheng et al. (2011) reported that *C. militaris* fruiting without mating also induced expression of several epigenetic genes. Epigenetic modification plays important roles in silencing and activating different gene clusters, including virulence genes, secondary metabolism and development related genes (Cichewicz, 2010). Thus, the future research on how *MAT1-1-3* regulates these genes expression will expand the sexual development networks. Our RNA-seq and qRT-PCR data also show that the expression of all 7 autophagy-related genes, including *ATG2*, *ATG9*, *ATG12*, *ATG13*, *ATG17*, *ATG22* and *ATG26*, was increased in Δ*mat1-1-3* mutant. The autophagy is an evolutionarily conserved cellular transport pathway involved in many cellular processes (Mizushima et al., 2011). For example, Atg22 plays a vital role in the development and virulence of *F. oxysporum* (Khalid et al., 2019). However, the function of these autophagy-related genes in *V. virens* is still unknown. Taken together, the RNA-seq data indicated that *MAT1-1-3* may regulate developmental processes and virulence by regulating the function of epigenetic modification and autophagy-related genes, which provides a clue for future research on how *MAT1-1-3* regulates the function of these genes.

DATA AVAILABILITY STATEMENT

All datasets generated for this study are included in the article/**Supplementary Material**.

AUTHOR CONTRIBUTIONS

MYo, JY, and YL designed the study. MYo, XP, MYu, HC, and ZQ performed the experiments. YD, RZ, TS, XY, and ZC helped to analyze the data. MYo, WL, and YL wrote the manuscript. YL contributed to reagents, materials, and analysis tools. All authors contributed to the article and approved the submitted version.

FUNDING

This work was supported by the National Natural Science Foundation of China (No. 31571961) and the China Postdoctoral Science Foundation (2018M632257).

ACKNOWLEDGMENTS

We thank Jin-Rong Xu (Purdue University, United States) for providing the CRISPR-Cas9 system plasmid. We also thank Dr. Liang Kong for helpful advice.

SUPPLEMENTARY MATERIAL

The Supplementary Material for this article can be found online at: https://www.frontiersin.org/articles/10.3389/fmicb.2020.01337/full#supplementary-material

REFERENCES

Adhvaryu, K. K., Morris, S. A., Strahl, B. D., and Selker, E. U. (2005). Methylation of histone H3 lysine 36 is required for normal development in *Neurospora crassa*. *Eukaryot. Cell* 4, 1455–1464. doi: 10.1128/EC.4.8.1455-1464.2005

Alby, K., Schaefer, D., and Bennett, R. J. (2009). Homothallic and heterothallic mating in the opportunistic pathogen *Candida albicans*. *Nature* 460, 890–893. doi: 10.1038/nature08252

Ashizawa, T., Takahashi, M., Arai, M., and Arie, T. (2012). Rice false smut pathogen, *Ustilaginoidea virens*, invades through small gap at the apex of a rice spikelet before heading. *J. Gen. Plant Pathol.* 78, 255–259. doi: 10.1007/s10327-012-0389-3

Banuett, F. (1998). Signalling in the yeasts: an informational cascade with links to the filamentous fungi. *Microbiol. Mol. Biol. Rev.* 62, 249–274.

Bolouri, M. M. R., Vilcinskas, A., and Rahnamaeian, M. (2017). The insect-derived antimicrobial peptide metchnikowin targets *Fusarium graminearum* β (1,3)glucanosyltransferase Gel1, which is required for the maintenance of cell wall integrity. *Biol. Chem.* 398, 491–498. doi: 10.1515/hsz-2016-0295

Brooks, S. A., Anders, M. M., and Yeater, K. M. (2010). Effect of furrow irrigation on the severity of false smut in susceptible rice varieties. *Plant Dis.* 94, 570–574. doi: 10.1094/pdis-94-5-0570

Bushley, K. E., Li, Y., Wang, W. J., Wang, X. L., Jiao, L., Spatafora, J. W., et al. (2013). Isolation of the MAT1-1 mating type idiomorph and evidence for selfing in the Chinese medicinal fungus *Ophiocordyceps sinensis*. *Fungal Biol.* 117, 599–610. doi: 10.1016/j.funbio.2013.06.001

Chang, L., and Karin, M. (2001). Mammalian MAP kinase signalling cascades. *Nature* 410, 37–40. doi: 10.1038/35065000

Cichewicz, R. H. (2010). Epigenome manipulation as a pathway to new natural product scaffolds and their congeners. *Nat. Prod. Rep.* 27, 11–22. doi: 10.1039/b920860g

Coppin, E., and Debuchy, R. (2000). Co-expression of the mating-type genes involved in internuclear recognition is lethal in *Podospora anserina*. *Genetics* 155, 657–669.

Coppin, E., Debuchy, R., Arnaise, S., and Picard, M. (1997). Mating types and sexual development in filamentous ascomycetes. *Microbiol. Mol. Biol. Rev.* 61, 411–428.

David-Palma, M., Sampaio, J. P., and Gonçalves, P. (2016). Genetic dissection of sexual reproduction in a primary homothallic basidiomycete. *PLoS Genet.* 12:e1006110. doi: 10.1371/journal.pgen.1006110

Debuchy, R., Arnaise, S., and Lecellier, G. (1993). The mat- allele of *Podospora anserina* contains three regulatory genes required for the development of fertilized female organs. *Mol. Gen. Genet.* 241, 667–673. doi: 10.1007/BF00279909

Debuchy, R., and Turgeon, B. G. (2006). "Mating-type structure, evolution, and function in euascomycetes," in *Growth, Differentiation and Sexuality. The Mycota (A Comprehensive Treatise On Fungi As Experimental Systems For Basic And Applied Research)*, Vol. 1, eds U. Kües and R. Fischer (Berlin: Springer), 293–323.

de Medina-Redondo, M., Arnáiz-Pita, Y., Fontaine, T., Del Rey, F., Latgé, J. P., and Vázquez De Aldana, C. R. (2008). The β-1,3-glucanosyltransferase gas4p is essential for ascospore wall maturation and spore viability in *Schizosaccharomyces pombe*. *Mol. Microbiol.* 68, 1283–1299. doi: 10.1111/j.1365-2958.2008.06233.x

Deng, Q. D., Yong, M. L., Li, D. Y., Lai, C. H., Chen, H. M., Fan, J., et al. (2015). Survey and examination of the potential alternative hosts of *Villosiclava virens*, the pathogen of rice false smut, in China. *J. Integr. Agr.* 14, 1332–1337. doi: 10.1016/S2095-3119(15)61030-9

Dyer, P. S., Inderbitzin, P., and Debuchy, R. (2016). "14 Mating-type structure, function, regulation and evolution in the pezizomycotina," in *Growth, Differentiation and Sexuality. The Mycota (A Comprehensive Treatise on Fungi as Experimental Systems for Basic and Applied Research)*, Vol. I, ed. J. Wendland (Cham: Springer).

Fan, J., Yang, J., Wang, Y. Q., Li, G. B., Li, Y., Huang, F., et al. (2016). Current understanding on *Villosiclava virens*, a unique flower-infecting fungus causing rice false smut disease. *Mol. Plant Pathol.* 17, 1321–1330. doi: 10.1111/mpp.12362

Fang, A. F., Gao, H., Zhang, N., Zheng, X. H., Qiu, S. S., Li, Y. J., et al. (2019). A novel effector gene SCRE2 contributes to full virulence of *Ustilaginoidea virens* to rice. *Front. Microbiol.* 10:845. doi: 10.3389/fmicb.2019.00845

Ferreira, A. V., An, Z., Metzenberg, R. L., and Glass, N. L. (1998). Characterization of mat A-2, mat A-3 and deltamatA mating-type mutants of *Neurospora crassa*. *Genetics* 148, 1069–1079.

Ferreira, A. V. B., Saupe, S., and Glass, N. L. (1996). Transcriptional analysis of the mt A idiomorph of *Neurospora crassa* identifies two genes in addition to mt A-1. *Mol. Gen. Genet.* 250, 767–774. doi: 10.1007/bf02172989

Fu, X., Xie, R., Wang, J., Chen, X., Wang, X., Sun, W., et al. (2017). Development of colloidal gold-based lateral flow immunoassay for rapid qualitative and semiquantitative analysis of ustiloxins A and B in rice samples. *Toxins* 9:79. doi: 10.3390/toxins9030079

Galagan, J. E., Calvo, S. E., Cuomo, C., Ma, L. J., Wortman, J. R., Batzoglou, S., et al. (2005). Sequencing of *Aspergillus nidulans* and comparative analysis with A. fumigatus and A. oryzae. *Nature* 438, 1105–1115. doi: 10.1038/nature04341

Gioti, A., Mushegian, A. A., Strandberg, R., Stajich, J. E., and Johannesson, H. (2012). Unidirectional evolutionary transitions in fungal mating systems and the role of transposable elements. *Mol. Biol. Evol.* 29, 3215–3226. doi: 10.1093/molbev/mss132

Glass, N. L., Grotelueschen, J., and Metzenberg, R. L. (1990). *Neurospora crassa* A mating-type region. *Proc. Natl. Acad. Sci. U.S.A.* 87, 4912–4916. doi: 10.1073/pnas.87.13.4912

Glass, N. L., and Lee, L. (1992). Isolation of *Neurospora crassa* A mating type mutants by repeat induced point (Rip) mutation. *Genetics* 132, 125–133.

Goldsmith, Z., and Dhanasekaran, D. N. (2007). G Protein regulation of MAPK networks. *Oncogene* 26, 3122–3142. doi: 10.1038/sj.onc.1210407

Guo, W., Gao, Y., Yu, Z., Xiao, Y., Zhang, Z., and Zhang, H. (2019). The adenylate cyclase UvAc1 and phosphodiesterase UvPdeH control the intracellular cAMP level, development, and pathogenicity of the rice false smut fungus *Ustilaginoidea virens*. *Fungal Genet. Biol.* 129, 65–73. doi: 10.1016/j.fgb.2019.04.017

Gustin, M. C., Albertyn, J., Alexander, M., and Davenport, K. (1998). MAP kinase pathways in the yeast *Saccharomyces cerevisiae*. *Microbiol. Mol. Biol. Rev.* 62, 1264–1300.

Haber, J. E. (2012). Mating-type genes and MAT switching in *Saccharomyces cerevisiae*. *Genetics* 191, 33–64. doi: 10.1534/genetics.111.134577

Herskowitz, I. (1995). MAP kinase pathways in yeast: for mating and more. *Cell* 80, 187–197. doi: 10.1016/0092-8674(95)90402-6

Hu, M. L., Luo, L. X., Wang, S., Liu, Y. F., and Li, J. Q. (2014). Infection processes of *Ustilaginoidea virens* during artificial inoculation of rice panicles. *Eur. J. Plant Pathol.* 139, 67–77. doi: 10.1007/s10658-013-0364-7

Hu, X., Zhang, Y. J., Xiao, G. H., Zheng, P., Xia, Y. L., Zhang, X. Y., et al. (2013). Genome survey uncovers the secrets of sex and lifestyle in caterpillar fungus. *Chin. Sci. Bull.* 58, 2846–2854. doi: 10.1007/s11434-013-5929-5

Ikegami, H. (1960). Studies on the false smut of rice IV. Infection of the false smut due to inoculation with chlamydospores and ascospores at the booting stage of rice plants. *Res. Bull. Fac. Agric. Gifu Univ.* 12, 45–51.

Jecmen, A. C., and Tebeest, D. O. (2015). First report of the occurrence of a white smut infecting rice in Arkansas. *J. Phytopathol.* 163, 138–143. doi: 10.1111/jph.12263

Jiao, Y. Q., Lee, Y. K., Gladman, N., Chopra, R., Christensen, S. A., Regulski, M., et al. (2018). MSD1 regulates pedicellate spikelet fertility in sorghum through the jasmonic acid pathway. *Nat. Commun.* 9:822. doi: 10.1038/s41467-018-03238-4

Jones, S. K. Jr., and Bennett, R. J. (2011). Fungal mating pheromones: choreographing the dating game. *Fungal Genet. Biol.* 48, 668–676. doi: 10.1016/j.fgb.2011.04.001

Kämper, J., Reichmann, M., Romeis, T., Bolker, M., and Kahmann, R. (1995). Multiallelic recognition: nonself-dependent dimerization of the bE and bW homeodomain proteins in *Ustilago maydis*. *Cell* 81, 73–83. doi: 10.1016/0092-8674(95)90372-0

Khalid, A. R., Zhang, S., Luo, X., Mehmood, K., Rahim, J., Shaheen, H., et al. (2019). Role of autophagy-related gene atg22 in developmental process and virulence of *Fusarium oxysporum*. *Genes* 10:365. doi: 10.3390/genes10050365

Kim, H. K., Cho, E. J., Lee, S., Lee, Y. S., and Yun, S. H. (2012). Functional analyses of individual mating-type transcripts at MAT loci in *Fusarium graminearum*

and *Fusarium asiaticum*. *FEMS Microbiol. Lett.* 337, 89–96. doi: 10.1111/1574-6968.12012

Klix, V., Nowrousian, M., Ringelberg, C., Loros, J. J., Dunlap, J. C., and Pöggeler, S. (2010). Functional characterization of MAT1-1-specifc mating-type genes in the homothallic ascomycete *Sordaria macrospora* provides new insights into essential and nonessential sexual regulators. *Eukaryot Cell* 9, 894–905. doi: 10.1128/EC.00019-10

Kües, U., James, T., and Heitman, J. (2011). "6 Mating type in basidiomycetes: unipolar, bipolar, and tetrapolar patterns of sexuality," in *Evolution of Fungi and Fungal-Like Organisms*, eds S. Pöggeler and J. Wöstemeyer (Berlin: Springer), 97–160. doi: 10.1007/978-3-642-19974-5_6

Ladhalakshmi, D., Laha, G. S., Singh, R., Karthikeyan, A., Mangrauthia, S. K., Sundaram, R. M., et al. (2012). Isolation and characterization of *Ustilaginoidea virens* and survey of false smut disease of rice in India. *Phytoparasitica* 40, 171–176. doi: 10.1007/s12600-011-0214-0

Lee, S. C., Ni, M., Li, W. J., Cecelia, S., and Heitman, J. (2010). The evolution of sex: a perspective from the fungal kingdom. *Microbiol. Mol. Biol. Rev.* 74, 298–340. doi: 10.1128/MMBR.00005-10

Li, C. H., Melesse, M., Zhang, S. J., Hao, C. F., Wang, C. F., Zhang, H. C., et al. (2015). FgCDC14 regulates cytokinesis, morphogenesis, and pathogenesis in *Fusarium graminearum*. *Mol. Microbiol.* 98, 770–786. doi: 10.1111/mmi.13157

Li, P. X., Evans, C. D., Wu, Y. Z., Cao, B., Hamel, E., and Joullié, M. M. (2008). Evolution of the total syntheses of ustiloxin natural products and their analogues. *J. Am. Chem. Soc.* 130, 2351–2364. doi: 10.1021/ja710363p

Li, Y. J., Wang, M., Liu, Z. H., Zhang, K., Cui, F. H., and Sun, W. X. (2019). Towards understanding the biosynthetic pathway for ustilaginoidin mycotoxins in *Ustilaginoidea virens*. *Environ. Microbiol.* 21, 2629–2643. doi: 10.1111/1462-2920.14572

Liang, Y. F., Han, Y., Wang, C. F., Jiang, C., and Xu, J. R. (2018). Targeted deletion of the USTA and UvSLT2 genes efficiently in *Ustilaginoidea virens* with the CRISPR-Cas9 system. *Front. Plant Sci.* 9:699. doi: 10.3389/fpls.2018.00699

Liu, Y., Liu, J. K., Li, G. H., Zhang, M. Z., Zhang, Y. Y., Wang, Y. Y., et al. (2019). A novel Botrytis cinerea-specific gene BcHBF1 enhances virulence of the grey mould fungus via promoting host penetration and invasive hyphal development. *Mol. Plant Pathol.* 20, 731–747. doi: 10.1111/mpp.12788

Livak, K. J., and Schmittgen, T. D. (2001). Analysis of relative gene expression data using real time quantitative PCR and the $2^{-\Delta\Delta C_T}$ method. *Methods* 25, 402–408. doi: 10.1006/meth.2001.1262

Lu, Y. Z., Xia, Y. L., Luo, F. F., Dong, C. H., and Wang, C. S. (2016). Functional convergence and divergence of mating-type genes fulfilling in *Cordyceps militaris*. *Fungal Genet. Biol.* 88, 35–43. doi: 10.1016/j.fgb.2016.01.013

Mizushima, N., Yoshimori, T., and Ohsumi, Y. (2011). The role of Atg proteins in autophagosome formation. *Annu. Rev. Cell Dev. Biol.* 27, 107–132. doi: 10.1146/annurev-cellbio-092910-154005

Mouyna, I., Morelle, W., Vai, M., Monod, M., and Latgé, J. P. (2005). Deletion of gel2 encoding for a β (1-3)glucanosyltransferase affects morphogenesis and virulence in *Aspergillus fumigatus*. *Mol. Microbiol.* 56, 1675–1688. doi: 10.1111/j.1365-2958.2005.04654.x

Nelson, M. A. (1996). Mating systems in ascomycetes: a romp in the sac. *Trends Genet.* 12, 69–74. doi: 10.1016/0168-9525(96)81403-x

Nygren, K., Strandberg, R., Wallberg, A., Nabholz, B., Gustafsson, T., García, D., et al. (2011). A comprehensive phylogeny of *Neurospora* reveals a link between reproductive mode and molecular evolution in fungi. *Mol. Phylogenet. Evol.* 59, 649–663. doi: 10.1016/j.ympev.2011.03.023

Paoletti, M., Rydholm, C., Schwier, E., Anderson, M. J., Szakacs, G., Lutzoni, F., et al. (2005). Evidence for sexuality in the opportunistic fungal pathogen *Aspergillus fumigatus*. *Curr. Biol.* 15, 1242–1248. doi: 10.1016/j.cub.2005.05.045

Pöggeler, S., Nowrousian, M., Ringelberg, C., Loros, J. J., Dunlap, J. C., and Kück, U. (2006). Microarray and real-time PCR analyses reveal mating type-dependent gene expression in a homothallic fungus. *Mol. Genet. Genom.* 275, 492–503. doi: 10.1007/s00438-006-0107-y

Roncero, C., and Durán, A. (1985). Effect of calcofluor white and congo red on fungal cell wall morphogenesis: *in vivo* activation of chitin polymerization. *J. Bacteriol.* 163, 1180–1185.

Seidl, V., Seibel, C., Kubicek, C. P., and Schmoll, M. (2009). Sexual development in the industrial workhorse *Trichoderma reesei*. *Proc. Natl. Acad. Sci. U.S.A.* 106, 13909–13914. doi: 10.1073/pnas.0904936106

Snetselaar, K. M., Bölker, M., and Kahmann, R. (1996). *Ustilago maydis* mating hyphae orient their growth toward pheromone sources. *Fungal Genet. Biol.* 20, 299–312. doi: 10.1006/fgbi.1996.0044

Song, J. H., Wei, W., Lv, B., Lin, Y., Yin, W. X., Peng, Y. L., et al. (2016). Rice false smut fungus hijacks the rice nutrients supply by blocking and mimicking the fertilization of rice ovary. *Environ. Microbiol.* 18, 3840–3849. doi: 10.1111/1462-2920.13343

Sun, X. Y., Kang, S., Zhang, Y. J., Tan, X. Q., Yu, Y. F., He, H. Y., et al. (2013). Genetic diversity and population structure of rice pathogen *Ustilaginoidea virens* in China. *PLoS One* 8:e76879. doi: 10.1371/journal.pone.0076879

Tang, Y. X., Jin, J., Hu, D. W., Yong, M. L., Xu, Y., and He, L. P. (2013). Elucidation of the infection process of *Ustilaginoidea virens* (teleomorph: *Villosiclava virens*) in rice spikelets. *Plant Pathol.* 62, 1–8. doi: 10.1111/j.1365-3059.2012.02629.x

Trapnell, C., Roberts, A., Goff, L., Pertea, G., Kim, D., Kelley, D. R., et al. (2012). Differential gene and transcript expression analysis of RNA-seq experiments with TopHat and Cufflinks. *Nat. Protoc.* 7, 562–578. doi: 10.1038/nprot.2012.016

Tsui, C. K., DiGuistini, S., Wang, Y., Feau, N., Dhillon, B., Bohlmann, J., et al. (2013). Unequal recombination and evolution of the mating-type (MAT) loci in the pathogenic fungus *Grosmannia clavigera* and relatives. *G3* 3, 465–480. doi: 10.1534/g3.112.004986

Turgeon, B. G., Bohlmann, H., Ciuffetti, L. M., Christiansen, S. K., Yang, G., Schäfer, W., et al. (1993a). Cloning and analysis of the mating type genes from *Cochliobolus heterostrophus*. *Mol. Gen. Genet.* 238, 270–284. doi: 10.1007/bf00279556

Turgeon, B. G., Christiansen, S. K., and Yoder, O. C. (1993b). "Mating type genes in ascomycetes and their imperfect relatives," in *The Fungal Holomorph: Mitotic, Meiotic And Pleomorphic Speciation In Fungal Systematics*, eds D. R. Reynolds and J. W. Taylor (Wallingford: CABI Publishing), 199–215.

Wang, F., Zhang, S., Liu, M. G., Lin, X. S., Liu, H. J., Peng, Y. L., et al. (2014). Genetic diversity analysis reveals that geographical environment plays a more important role than rice cultivar in *Villosiclava virens* population selection. *Appl. Environ. Microbiol.* 80, 2811–2820. doi: 10.1128/AEM.03936-13

Wang, G. (1995). The sexual stage of *Ustilaginoidea virens* and the infection process of ascospores on rice. *J. Zhejiang Wanli Univ. Z* 1, 3–9.

Wang, X., Wang, J., Lai, D., Wang, W., Dai, J., Zhou, L., et al. (2017). Ustiloxin G, a new cyclopeptide mycotoxin from rice false smut balls. *Toxins* 9:54. doi: 10.3390/toxins9020054

Weigel, D., and Glazebrook, J. (2006). Transformation of *Agrobacterium* using the freeze-thaw method. *CSH Protoc.* 7, 1031–1036. doi: 10.1101/pdb.prot4666

Whittle, C. A., Nygren, K., and Johannesson, H. (2011). Consequences of reproductive mode on genome evolution in fungi. *Fungal Genet. Boil.* 48, 661–667. doi: 10.1016/j.fgb.2011.02.005

Wilken, P. M., Steenkamp, E. T., Hall, T. A., Beer, Z. W. D., Wingfield, M. J., and Wingfield, B. D. (2012). Both mating types in the heterothallic fungus *Ophiostoma quercus* contain MAT1-1 and MAT1-2 genes. *Fungal Biol.* 116, 427–437. doi: 10.1016/j.funbio.2012.01.002

Xie, S. L., Wang, Y. F., Wei, W., Li, C. Y., Liu, Y., Qu, J. S., et al. (2019). The Bax inhibitor UvBI-1, a negative regulator of mycelial growth and conidiation, mediates stress response and is critical for pathogenicity of the rice false smut fungus *Ustilaginoidea virens*. *Curr. Genet.* 65, 1185–1197. doi: 10.1007/s00294-019-00970-2

Yang, T., Guo, M., Yang, H., Guo, S., and Dong, C. (2016). The blue-light receptor CmWC-1 mediates fruit body development and secondary metabolism in *Cordyceps militaris*. *Appl. Microbiol. Biotechnol.* 100, 743–755. doi: 10.1007/s00253-015-7047-6

Yokoyama, E., Arakawa, M., Yamagishi, K., and Hara, A. (2006). Phylogenetic and structural analyses of the mating-type loci in *Clavicipitaceae*. *FEMS Microbiol. Lett.* 264, 182–191. doi: 10.1111/j.1574-6968.2006.00447.x

Yokoyama, E., Yamagishi, K., and Hara, A. (2003). Structures of the mating-type loci of *Cordyceps takaomontana*. *Appl. Environ. Microbiol.* 69, 5019–5022. doi: 10.1128/AEM.69.8.5019-5022.2003

Yokoyama, E., Yamagishi, K., and Hara, A. (2005). Heterothallism in *Cordyceps takaomontana*. *FEMS Microbiol. Lett.* 250, 145–150. doi: 10.1016/j.femsle.2005.07.004

Yong, M. L., Deng, Q. D., Fan, L. L., Miao, J. K., Lai, C. H., Chen, H. M., et al. (2018). The role of *Ustilaginoidea virens* sclerotia in increasing incidence of rice

false smut disease in the subtropical zone in China. *Eur. J. Plant Pathol.* 150, 669–677. doi: 10.1007/s10658-017-1312-8

Yu, J., Yu, M., Song, T., Cao, H., Pan, X., Yong, M., et al. (2019). A homeobox transcription factor UvHOX2 regulates chlamydospore formation, conidiogenesis, and pathogenicity in *Ustilaginoidea virens*. *Front. Microbiol.* 10:1071. doi: 10.3389/fmicb.2019.01071

Yu, J. J., Sun, W. X., Yu, M. N., Yin, X. L., Meng, X. K., Zhao, J., et al. (2015). Characterization of mating-type loci in rice false smut fungus *Villosiclava virens*. *FEMS Microbiol. Lett.* 362:fnv014. doi: 10.1093/femsle/fnv014

Yu, J. J., Yu, M. N., Nie, Y. F., Sun, W. X., Yin, X. L., Zhao, J., et al. (2016). Comparative transcriptome analysis of fruiting body and sporulating mycelia of *Villosiclava virens* reveals genes with putative functions in sexual reproduction. *Curr. Genet.* 62, 575–584. doi: 10.1007/s00294-015-0563-1

Yu, M. N., Yu, J. J., Hu, J. K., Huang, L., Wang, Y. H., Yin, X. L., et al. (2015). Identification of pathogenicity-related genes in the rice pathogen *Ustilaginoidea virens* through random insertional mutagenesis. *Fungal Genet. Biol.* 76, 10–19. doi: 10.1016/j.fgb.2015.01.004

Yun, S. H., Berbee, M. L., Yoder, O. C., and Turgeon, B. G. (1999). Evolution of the fungal self-fertile reproductive life style from self-sterile ancestors. *Proc. Natl. Acad. Sci. U.S.A.* 96, 5592–5597. doi: 10.1073/pnas.96.10.5592

Zaffarano, P. L., Duò, A., and Grünig, C. R. (2010). Characterization of the mating type (MAT) locus in the *Phialocephala fortinii* s. l. – *Acephala applanata* species complex. *Fungal Genet. Biol.* 47, 761–772. doi: 10.1016/j.fgb.2010.06.001

Zhang, Y., Zhang, K., Fang, A. F., Han, Y. Q., Yang, J., Xue, M. F., et al. (2014). Specific adaptation of *Ustilaginoidea virens* in occupying host florets revealed by comparative and functional genomics. *Nat. Commun.* 5:3849. doi: 10.1038/ncomms4849

Zheng, P., and Wang, C. S. (2013). Sexuality control and sex evolution in fungi. *Sci. Sin. Vitae.* 43, 1090–1097. doi: 10.1360/052013-317

Zheng, P., Xia, Y., Xiao, G., Xiong, C., Hu, X., Zhang, S., et al. (2011). Genome sequence of the insect pathogenic fungus *Cordyceps militaris*, a valued traditional chinese medicine. *Genome Biol.* 12:R116. doi: 10.1186/gb-2011-12-11-r116

Zheng, P., Xia, Y. L., Zhang, S. W., and Wang, C. S. (2013). Genetics of *Cordyceps* and related fungi. *Appl. Microbiol. Biotechnol.* 97, 2797–2804. doi: 10.1007/s00253-013-4771-7

Zheng, Q., Hou, R., Zhang, J. Y., Ma, J. W., Wu, Z. S., Wang, G. H., et al. (2015). The MAT locus genes play different roles in sexual reproduction and pathogenesis in *Fusarium graminearum*. *PLoS One* 10:e0131623. doi: 10.1371/journal.pone.0131623

Zickler, D., Arnaise, S., Coppin, E., Debuchy, R., and Picard, M. (1995). Altered mating-type identity in the fungus *Podospora anserina* leads to selfish nuclei, uniparental progeny, and haploid meiosis. *Genetics* 140, 493–503.

Zou, J., Wu, L., He, Z. M., Zhang, P., and Chen, Z. H. (2017). Biological characteristics and cultivation of *Ophiocordyceps xuefengensis*. *Mycosystema* 36, 1104–1110. doi: 10.13346/j.mycosystema.170008

Conflict of Interest: The authors declare that the research was conducted in the absence of any commercial or financial relationships that could be construed as a potential conflict of interest.

frontiers in Microbiology

ORIGINAL RESEARCH
published: 26 June 2020
doi: 10.3389/fmicb.2020.01495

Antifungal Nafuredin and Epithiodiketopiperazine Derivatives From the Mangrove-Derived Fungus *Trichoderma harzianum* D13

Dong-Lin Zhao[1†], Xi-Fen Zhang[1†], Rui-Huan Huang[1], Dan Wang[1,2], Xiao-Qiang Wang[1], Yi-Qiang Li[1], Cai-Juan Zheng[3], Peng Zhang[1] and Cheng-Sheng Zhang[1]**

[1] Tobacco Research Institute, Chinese Academy of Agricultural Sciences, Qingdao, China, [2] Plant Protection Station of Shandong Province, Jinan, China, [3] Key Laboratory of Tropical Medicinal Resource Chemistry of Ministry of Education, Hainan Normal University, Haikou, China

OPEN ACCESS

Edited by:
Laure Ries,
University of São Paulo, Brazil

Reviewed by:
Linghong Meng,
Institute of Oceanology (CAS), China
Junfeng Wang,
South China Sea Institute of Oceanology (CAS), China

***Correspondence:**
Peng Zhang
zhangpeng@caas.cn
Cheng-Sheng Zhang
zhchengsheng@126.com

[†]These authors have contributed equally to this work

Specialty section:
This article was submitted to Fungi and Their Interactions, a section of the journal Frontiers in Microbiology

Received: *07 May 2020*
Accepted: *08 June 2020*
Published: *26 June 2020*

Citation:
Zhao D-L, Zhang X-F, Huang R-H, Wang D, Wang X-Q, Li Y-Q, Zheng C-J, Zhang P and Zhang C-S (2020) Antifungal Nafuredin and Epithiodiketopiperazine Derivatives From the Mangrove-Derived Fungus Trichoderma harzianum D13. Front. Microbiol. 11:1495. doi: 10.3389/fmicb.2020.01495

A new polyketide derivative, nafuredin C (**1**), a novel heterocyclic dipeptide, trichodermamide G (**3**), together with four known biogenetically related compounds nafuredin A (**2**), trichodermamide A (**4**), aspergillazin A (**5**), and peniisocoumarin H (**6**), were isolated from the mangrove-derived fungus *Trichoderma harzianum* D13. Their structures, including their absolute configurations, were determined by spectroscopic analysis and time-dependent density functional theory-electronic circular dichroism (ECD) calculations. Trichodermamide G was found to be a novel epithiodiketopiperazine derivative with an unprecedented cyclic system containing a sulfur bridge, and nafuredin C represented the third nafuredin derivative of these homologous compounds. The new compound nafuredin C exhibited obvious antifungal activity against *Magnaporthe oryzae* with a minimum inhibitory concentration (MIC) of 8.63 μM, which is on the same order of magnitude as the positive control carbendazim (MIC = 3.27 μM).

Keywords: nafuredins, epithiodiketopiperazines, *Magnaporthe oryzae*, antifungal activity, *Trichoderma harzianum*

INTRODUCTION

Rice blast disease is the most serious disease affecting cultivated rice, a staple food for nearly 50% of the world's population, and seriously threatens global food security. Each year, rice blast disease is responsible for the loss of 10–30% of the rice harvest, which is enough to feed more than 60 million people (Martin-Urdiroz et al., 2016; Zhou, 2016). Rice blast is caused by *Magnaporthe oryzae*, an ascomycete fungus that causes diseases in a wide range of economically important crops including barley, oats, rye grass, and millets. It was first reported in Brazil in 1985 and then rapidly spread to other South American countries, causing significant yield losses. The disease captured public attention in 2016 when it appeared in Bangladesh, resulting in thousands of rice fields being burned to prevent further spread of the disease (Ma and Xu, 2019). In China, rice blast occurs everywhere rice is cultivated, particularly in hilly areas. In epidemic years of the disease, yield loss can reach 40–50% and in severe cases can result in complete losses in major rice production areas (Zhao X. X. et al., 2019). Therefore, searching for new biological pesticides to control rice blast is necessary for sustainable development of the rice industry and food security worldwide.

Beneficial microbes can function as biocontrol organisms that help plants defend themselves from attack by pathogens. Fungi in the genus *Trichoderma* are excellent mycoparasites of plant pathogens and directly protect plants against them. In addition, *Trichoderma* spp. can enhance the plant defense system, which enables the plant to respond in a fast and strong manner to pathogen attack (Guzman-Guzman et al., 2019). These fungi are also prolific producers of numerous secondary metabolites with pharmaceutical and biotechnological importance, including polyketides, non-ribosomal peptides, siderophores, peptaibols, and volatile and non-volatile terpenes (Contreras-Cornejo et al., 2016). Several studies have focused on the application of *Trichoderma* spp. for controlling rice blast disease with apparent effects; however, marine-derived *Trichoderma* spp. have not been evaluated for use in plant protection, and few studies have reported their antifungal effects against *M. oryzae*.

During our ongoing search for new anti-phytopathogenic fungal secondary metabolites from marine-derived fungi in the Yellow Sea and South China Sea (Huang et al., 2018; Zhao et al., 2018; Zhao D. L. et al., 2019), we found that the extract of mangrove-derived fungus *Trichoderma harzianum* D13, collected from Hainan province, China, displayed a strong activity against fungal plant pathogens. Further chemical investigation of the ethyl acetate (EtOAc) extracts led to the isolation of six compounds (**Figure 1**), including two nafuredin derivatives, nafuredins C and A (**1** and **2**); three epithiodiketopiperazine derivatives, trichodermamide G (**3**), trichodermamide A (**4**), and aspergillazin A (**5**); and one isocoumarin, peniisocoumarin H (**6**). Among them, nafuredin C and trichodermamide G are new compounds. Herein, we report the isolation, structural elucidation, and antifungal activities of these compounds.

MATERIALS AND METHODS

General Experimental Procedures

Specific rotations were measured on a JASCO P-1020 digital polarimeter (Tokyo, Japan). ECD spectra were obtained on a JASCO J-815-150S spectropolarimeter. UV spectra were recorded on a Techcomp UV2310II spectrophotometer (Shanghai, China). The 1D (^{1}H, ^{13}C, and NOE) and 2D NMR spectra [HMQC, correlation spectroscopy (COSY), heteronuclear multiple bond correlation (HMBC), and nuclear Overhauser effect spectroscopy (NOESY)] were acquired on a DD2 500 MHz NMR spectrometer (Agilent Technologies, Santa Clara, CA, United States). A Micromass Q-TOF spectrometer (Waters, Milford, MA, United States) and Thermo Scientific LTQ Orbitrap XL spectrometer (Waltham, MA, United States) was used to measure the electrospray ionization mass spectrometry (ESIMS) and HRESIMS. High-performance liquid chromatography (HPLC) was performed using a Waters e2695 separation module with a Waters 2998 detector and Waters X-Bridge C_{18} (5 μm, 10 × 250 mm) column. Column chromatography (CC) was performed over silica gel (200–300 mesh; Qing Dao Hai Yang Chemical Group Co., Qingdao, China), octadecylsilyl silica (ODS) gel (RP18, 40–63 μm; Merck, Billerica, MA, United States), and Sephadex LH-20 (GE Healthcare, Little Chalfont, United Kingdom). Precoated silica gel plates (G60, F-254; Yan Tai Zi Fu Chemical Group Co., Yantai, China) were used for analytical thin-layer chromatography. Analytical and HPLC-grade solvents were used for isolation.

Fungal Material

The fungus was isolated from the internal tissues of the root of mangrove plant *Excoecaria agallocha* Linn. collected from Hainan province, China, in 2016, and was identified as *T. harzianum* (GenBank accession number MG827165) by sequence analysis of the internal transcribed spacer region of the rDNA. A voucher strain of this fungus was deposited in the Marine Agriculture Research Center, Tobacco Research Institute of Chinese Academy of Agricultural Sciences, Qingdao, China.

Extraction and Isolation

The fungus *T. harzianum* D13 was cultured on plates of potato dextrose agar medium at 28°C for 3 days. Plugs of agar supporting mycelium growth were cut and transferred aseptically into 200 × 1000-mL Erlenmeyer flasks each containing 400 mL of potato dextrose water liquid medium. The flasks were incubated at 28°C under static conditions for 30 days. The cultures (80 L) were filtered through gauze to separate the mycelial layer from the aqueous layer. The filtrate was then extracted twice with EtOAc, whereas the mycelium were mechanically broken and ultrasonically disrupted for 10 min and then extracted twice with CH_2Cl_2:MeOH (1:1, v/v). After removing CH_2Cl_2 and MeOH by evaporation under vacuum, the remaining aqueous solution was extracted three times with EtOAc. The combined EtOAc extracts were concentrated under reduced pressure to yield the total EtOAc extract (13.8 g). This extract was subjected to vacuum liquid chromatography on silica gel for elution with a gradient of EtOAc in petroleum ether (EtOAc/petroleum ether, 0–100%), and then with MeOH in EtOAc ranging from 10 to 50% to give eight fractions (Fractions 1–8). Fraction 3 was initially fractionated using an ODS gel column with a step gradient elution of MeOH–H_2O (60–90%) to afford Fr. 3-1 and Fr. 3-2. Fraction 3-1 was subsequently applied to a Sephadex LH-20 CC (CH_2Cl_2/MeOH, v/v, 1/1), and finally purified by reversed-phase-HPLC eluting with 80% MeOH–H_2O to obtain compound **2** (10.6 mg). Fraction 4 was separated on an ODS column eluting with 50–90% MeOH–H_2O to obtain Fr. 4-1 and Fr. 4-2. Fraction 4-1 was then afforded to silica gel CC (EtOAc/petroleum ether, 5% to 35%), followed by purification by HPLC (MeOH/H_2O, 80/20) to yield **1** (10.0 mg). Fraction 6 was subjected to ODS CC using a gradient elution of 30–90% MeOH–H_2O, followed by separation on Sephadex LH-20 (CH_2Cl_2–MeOH, v/v, 1/1) to afford subfractions Fr. 6-1–6-3. Fraction 6-1 was subjected to silica gel CC (MeOH/CH_2Cl_2, v/v, 1/50 to 1/10), and finally purified by semipreparative HPLC eluting with 35% MeCN–H_2O to give **6** (4.0 mg). Fractions 6-2–6-4 were purified by HPLC using 40, 40, and 35% MeOH–H_2O to give **5** (9.0 mg), **4** (68.5 mg), and **3** (32.0 mg), respectively.

Nafuredin C (**1**): white, amorphous powder; $[\alpha]^{20}_{D}$ +40.0 (*c* 0.37, MeOH); UV (MeOH) λ_{max} (log ε) 240 (4.38) nm; ECD

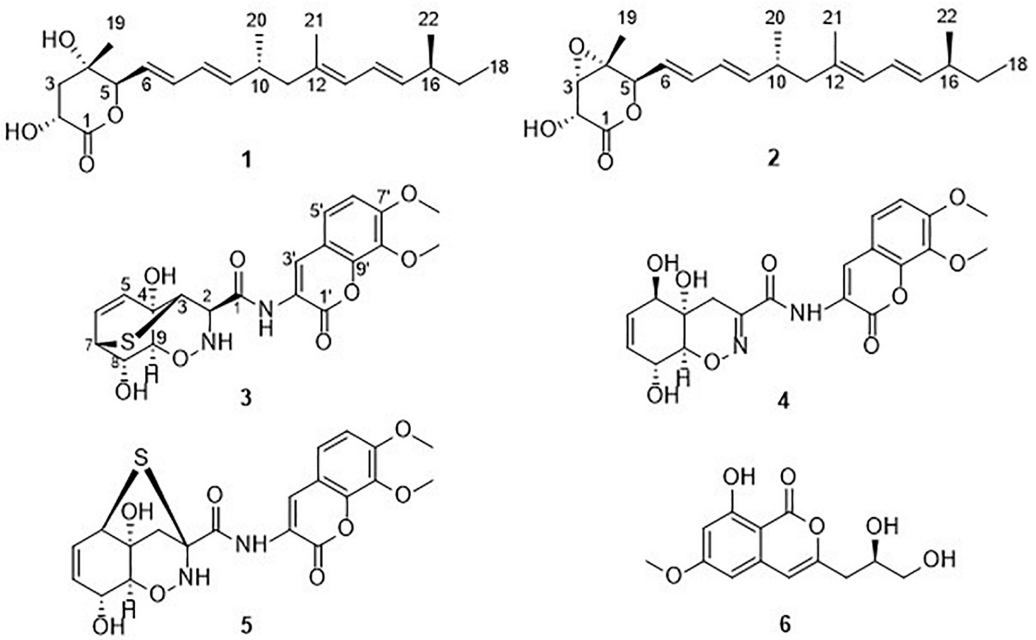

FIGURE 1 | Chemical structures of compounds **1–6**.

(0.93 mM, MeOH) λ_{max} ($\Delta\varepsilon$) 222 (-17.40), 244 (+21.99) nm; ^{1}H and ^{13}C NMR data, see **Table 1**; HRESIMS *m/z* 385.2349 [M +Na]$^+$ (calculated for $C_{22}H_{38}O_4Na$, 380.2795).

Trichodermamide G (**3**): yellow, amorphous powder; $[\alpha]^{20}_D$ −116.5 (*c* 0.50, MeOH); UV (MeOH) λ_{max} (log ε) 204 (4.40), 274 (3.96), 324 (4.28) nm; ECD (1.55 mM, MeOH) λ_{max} ($\Delta\varepsilon$) 226 (−3.08), 243 (+1.09), 325 (−5.07) nm; ^{1}H and ^{13}C NMR data, see **Table 2**; HRESIMS *m/z* 449.1026 [M +H]$^+$ (calculated for $C_{20}H_{21}O_8N_2S$, 449.1013).

Antifungal Assays

Antifungal activities were evaluated using the conventional broth dilution assay (Appendino et al., 2008). Five phytopathogenic fungal strains, including *Botrytis cinerea*, Magnaporthe *grisea*, *Phytophthora parasitica*, *Pestallozzia theae*, and *Valsa mali* were used. Carbendazim was used as a positive control.

RESULTS AND DISCUSSION

Structural Elucidation of the Isolated Compounds

Nafuredin C (**1**) was isolated as a white, amorphous powder. Its molecular formula, $C_{22}H_{34}O_4$, was established from high-resolution ESIMS (HRESIMS), ^{1}H and ^{13}C nuclear magnetic resonance (NMR) data (**Supplementary Figures S1, S2, S7**), indicating six indexes of hydrogen deficiency. The ^{1}H NMR (**Table 1**) spectrum displayed seven olefinic protons at δ_H 6.24 (1H, dd, *J* = 15.0, 10.5 Hz), 6.17 (1H, dd, *J* = 15.0, 11.0 Hz), 6.04 (1H, dd, *J* = 15.0, 10.5 Hz), 5.74 (1H, d, *J* = 11.0 Hz), 5.64 (1H, dd, *J* = 15.0, 7.5 Hz), 5.59 (1H, dd, *J* = 15.0, 6.0 Hz), and 5.43 (1H, dd, *J* = 15.0, 8.0 Hz), two hydroxyl signals at δ_H 5.82 (1H, d, *J* = 6.5 Hz) and 5.50 (1H, d, *J* = 5.0 Hz), two oxygenated methines at δ_H 4.46 (1H, m) and 3.95 (1H, t, *J* = 6.0 Hz), and five methyls at δ_H 1.67 (3H, s), 1.24 (3H, s), 0.95 (3H, d, *J* = 7.0 Hz), 0.92 (3H, d, *J* = 6.5 Hz), and 0.82 (3H, t, *J* = 7.0 Hz). The ^{13}C NMR and distortionless enhancement by polarization transfer (DEPT) spectra revealed 22 carbon signals, including one ester carbonyl group (δ_C 177.2), two quaternary carbons (one oxygenated, one olefinic), three methylene groups, 11 methines (seven olefinic, two oxygenated), and five methyl groups. These spectroscopic data are similar to those of nafuredin B, isolated from a mixed culture of the deep-sea-derived fungus *Talaromyces aculeatus* and mangrove-derived fungus *Penicillium variabile* (Zhang et al., 2017). The major differences were replacement of the sp^2 double bond at C-2 and C-3 in nafuredin B by a hydroxyl group at C-2 in **1**, which were consistent with the downfield shifts of C-1/C-4 (δ_C 163.3/68.0 in nafuredin B *vs* 177.2/84.8 in **1**) and upfield shifts of C-2/C-3 (δ_C 118.0/156.3 in nafuredin B *vs* 68.4/37.9 in **1**), supported by the COSY correlations of H-2/H-3, and key HMBC from H-2 to C-1/C-4, from H-3 to C-1/C-5, from H-5 to C-3/C-4, from 2-OH to C-1/C-2/C-3, and from H_3-19 to C-3/C-4/C-5 (**Figure 2** and **Supplementary Figures S4, S5**).

The relative configuration of the δ-lactone ring was established based on the NOESY spectrum (**Figure 2** and **Supplementary Figure S6**). The correlations of 4-OH with 2-OH and H-5 and of H-6 with H_3-19 indicated a cofacial relationship among 4-OH, 2-OH, and H-5. The geometry of double bonds in the olefinic chain was *E* elucidated from the *J* values and NOESY correlations (**Table 1** and **Figure 2**). Considering the biosynthesis and coisolation of nafuredin A (**2**), whose absolute configuration was determined based on asymmetric synthesis

TABLE 1 | ^{1}H NMR data (500 MHz, DMSO-d_6, δ in ppm, *J* in Hz) and ^{13}C NMR data (125 MHz, DMSO-d_6, δ in ppm) for **1**.

Position	δ_H (*J* in Hz)	δ_C, type
1		177.2, C
2	4.46, m	68.4, CH
3	2.57, dd (17.5, 9.0) 1.58, dd (13.0, 9.0)	37.9, CH_2
4		84.8, C
5	3.95, t (6.0)	75.5, CH
6	5.59, dd (15.0, 6.0)	129.6, CH
7	6.24, dd (15.0, 10.5)	132.6, CH
8	6.04, dd (15.0, 10.5)	127.5, CH
9	5.64, dd (15.0, 7.5)	140.4, CH
10	2.39, m	34.2, CH
11	2.06, m 1.95, dd (13.0, 7.5)	46.9, CH_2
12		134.1, C
13	5.74, d (11.0)	126.4, CH
14	6.17, dd (15.0, 11.0)	124.8, CH
15	5.43, dd (15.0, 8.0)	138.0, CH
16	2.06, m	37.9, CH
17	1.29, m	29.3, CH_2
18	0.82, t (7.0)	11.7, CH_3
19	1.24, s	24.5, CH_3
20	0.92, d (6.5)	19.8, CH_3
21	1.67, s	16.3, CH_3
22	0.95, d (7.0)	20.1, CH_3
2-OH	5.82, d (6.5)	
4-OH	5.50, d (5.0)	

TABLE 2 | ^{1}H NMR data (500 MHz, DMSO-d_6, δ in ppm, *J* in Hz) and ^{13}C NMR data (125 MHz, DMSO-d_6, δ in ppm) for **3**.

Position	δ_H (*J* in Hz)	δ_C, type
1		162.7, C
2	5.18, s	58.9, CH
3	3.29, s	44.6, CH
4		70.3, C
5	6.04, d (8.0)	132.9, CH
6	6.50, t (8.0)	134.7, CH
7	3.42, m	37.8, CH
8	4.02, brs	,72.1, CH
9	3.63, brs	87.0, CH
1′		155.8, C
2′		121.8, C
3′	6.77, s	112.7, C
4′		114.6, C
5′	7.04, d (9.0)	126.7, CH,
6′	6.61, d (9.0)	104.4, CH
7′		153.5, C
8′		136.5, C
9′		147.6, C
7′-OMe	3.81, s	55.9, CH_3
8′-OMe	3.69, s	60.3, CH_3
1-NH	10.09, s	

(Takano et al., 2001; Zhang et al., 2017), the chirality of C-10 and C-16 was determined to be 10*R* and 16*S*, which was supported by the identical NMR data. Comparing the computed ECD spectra with experimental results is a valid method of assigning the absolute configurations of natural products (Cao et al., 2020). To determine the absolute configuration of the δ-lactone ring in **1**, ECD computations for all B3LYP/6-311+G(d)-optimized conformers (50 structures) were carried out at the B3LYP/6-311++G(2d,p) level, and six structures with relative energy less than 2.5 kcal/mol were obtained. Boltzmann statistics were performed for ECD simulations with a standard deviation of σ 0.25 eV. The experimental and calculated ECD spectra for the (2*R*,4*S*,5*R*,10*R*,16*S*)-**1** showed good agreement (**Figure 3** and **Supplementary Table S1**), thus suggesting the absolute configuration.

Trichodermamide C (**3**) was obtained as a yellow, amorphous powder, with the molecular formula $C_{20}H_{20}N_2O_8S$ based on its HRESIMS, ^{1}H and ^{13}C NMR data, indicating 12 degrees of unsaturation (**Supplementary Figures S8, S9, S15**). The ^{13}C NMR and DEPT spectroscopic data (**Table 2**) revealed 20 carbon signals containing two carbonyl groups, two methoxyl groups, 10 methines (with five olefinic or aromatic, two thiogenated, one nitrogenated, two oxygenated), and six quaternary carbons

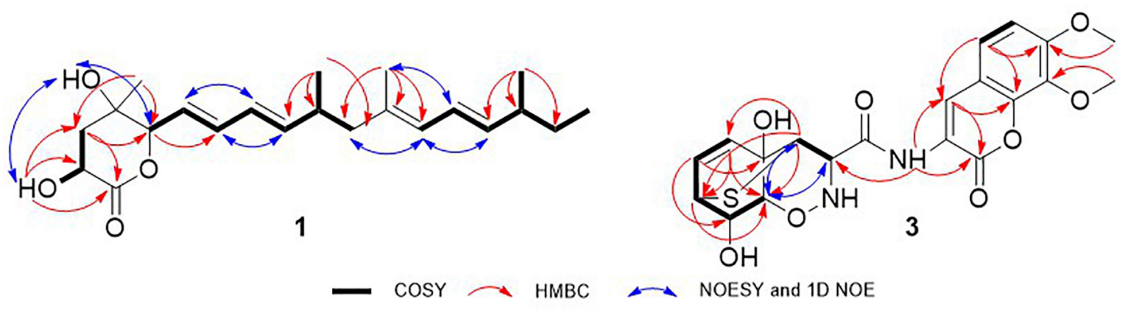

FIGURE 2 | COSY, key HMBC, 1D NOE, and NOESY correlations of **1** and **3**.

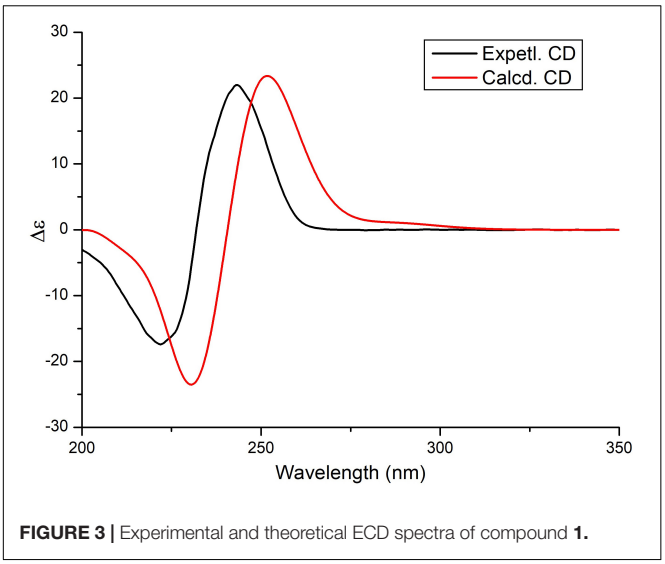

FIGURE 3 | Experimental and theoretical ECD spectra of compound **1.**

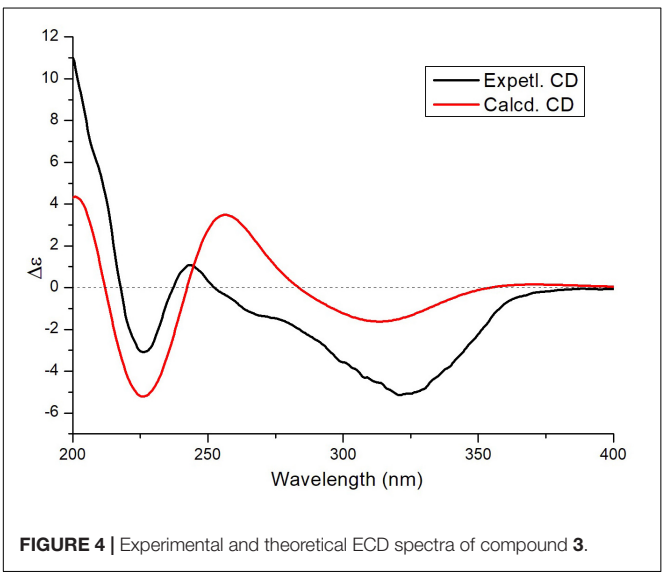

FIGURE 4 | Experimental and theoretical ECD spectra of compound **3**.

(with five sp^2 and one sp^3). In examining the ^{1}H NMR and HSQC data (**Supplementary Figures S8, S10**), an amide proton at δ_H 10.09, two *ortho*-aromatic protons attributed to a 1,2,3,4-tetrasubstituted phenyl unit at δ_H 7.04 (1H, d, J = 9.0 Hz) and 6.61 (1H, d, J = 9.0 Hz), and three olefinic protons including two derived from a *cis*-coupled double bond at δ_H 6.50 (1H, t, J = 8.0 Hz) and 6.04 (1H, d, J = 8.0 Hz) were observed in the deshielded region of the spectrum, whereas shielded signals for five methines at δ_H 5.18 (1H, s), 4.02 (1H, s), 3.63 (1H, s), 3.42 (1H, d, J = 9.5 Hz), and 3.29 (1H, s) were also present. Additionally, two *O*-methyl groups (δ_H 3.81 and 3.69) were observed in the ^{1}H NMR spectrum of **3**. Inspection of the above NMR data indicated that the isocoumarin portion of **3** was similar to that of aspergillazine A, a modified dipeptide isolated from the marine-derived fungus *Spicaria elegans* (Liu et al., 2005), whereas the signals of oxazine were obviously changed, possibly because of the different location of the sulfur bridge. The characteristic NMR data of C-3 (δ_H 3.29, δ_C 44.6) and C-7 (δ_H 3.42, δ_C 37.8) indicated they were linked by a sulfur atom, which was confirmed from the COSY correlation of H5/H6/H7/H8/H9 and HMBC correlations from H-3 to C-5/C-7/C-9, from H-5 to C-7/C-9, from H-6 to C-4/C-8, and from H-7 to C-9 (**Figure 2** and **Supplementary Figures S11, S12**). In the NOE difference spectra (**Figure 2** and **Supplementary Figures S13, S14**), irradiation of H-2 and H-3 enhanced the resonance of H-9. This information, in addition to the similar coupling constant of H8/H-9 (brs) to trichodermamide A and aspergillazine A (Capon et al., 2005; Liu et al., 2005), indicates a *syn* relationship among H-2, H-3, H-9, and 8-OH. 4-OH was assigned on the opposite face of the sulfur bridge, as the *cis* relationship did not lead to a reasonable model according to 3D simulations.

To determine the absolute configuration of **3**, ECD calculations were carried out. Monte Carlo conformational searches were applied using Spartan's 10 software with the Merck molecular force field. Conformers with a Boltzmann-population of over 10% were selected for ECD calculations and were initially optimized at the B3LYP/6-31g (d,p) level in MeOH using the conductor-like polarizable continuum calculation model. Theoretical calculation of the ECD was conducted in MeOH using time-dependent density functional theory at the B3LYP/6-31+g (d,p) level for all conformers of compound (2*R*,3*S*,4*S*,7*S*,8*S*,9*S*)-**3**. Rotatory strengths for a total of 30 excited states were calculated. ECD spectra were generated using the programs SpecDis 1.6 (University of Würzburg, Würzburg, Germany) and GraphPad Prism 5 (GraphPad, Inc., La Jolla, CA, United States) from dipole-length rotational strengths by applying Gaussian band shapes with sigma = 0.3 eV. The predicted ECD spectrum agreed well with the experimental result (**Figure 4** and **Supplementary Tables S2, S3**), indicating that the absolute configuration of **3** was 2*R*,3*S*,4*S*,7*S*,8*S*,9*S*.

Epipolythiodiketopiperazine alkaloids are fungal metabolites with a highly complex molecular architecture comprising a densely functionalized core structure with many stereogenic centers. In the past decade, an increasing number of studies have discovered powerful new biological processes involving these molecules, including cytotoxic, antileukemic, antiviral, antibiotic, and antinematodal activities (Kim and Movassaghi, 2015); however, epithiodiketopiperazines have not been widely examined. Notably, trichodermamide G is a novel epithiodiketopiperazine derivative with an unprecedented cyclic system containing a sulfur bridge.

Compounds **2** and **4**–**6** were identified as nafuredin A (Ui et al., 2001), trichodermamide A (Liu et al., 2005), aspergillazine

TABLE 3 | Antifungal activity of **1** and **2**.

Compounds	MIC (μM)		
	M. oryzae	*P. theae*	*V. mali*
1	8.63	553	34.5
2	17.4	-	16.7
Carbendazim	3.27	0.82	0.82

"–" means no antifungal activity.

A (Liu et al., 2005), and peniisocoumarin H (Cai et al., 2018) by comparison of their spectroscopic data with those in the literature.

Antifungal Activity

In the present study, all isolated compounds were evaluated to determine their anti-phytopathogenic fungal activities against *B. cinerea*, *M. oryzae*, *P. theae*, *P. parasitica*, and *V. mali*. The nafuredin derivatives **1** and **2** exhibited obvious antifungal activities against *M. oryzae*, with minimum inhibitory concentrations (MICs) of 8.63 and 17.4 μM, respectively. These data indicate that the antifungal activity toward *M. oryzae* of new compound **1** was the same magnitude as that of the positive control carbendazim (MIC = 3.27 μM). Compounds **1** and **2** also displayed weak antifungal activity against *V. mali* and *P. theae* compared to carbendazim (**Table 3**).

CONCLUSION

In summary, we report three polyketide derivatives, nafuredin C (**1**), nafuredin A (**2**), and peniisocoumarin H (**6**), and three epithiodiketopiperazine derivatives, trichodermamide G (**3**), trichodermamide A (**4**), and aspergillazin A (**5**), isolated from the mangrove-derived fungus *T. harzianum* D13. Among them, nafuredin C (**1**) and trichodermamide G (**3**) are new compounds. Their structures were assigned based on extensive NMR spectroscopic data, time-dependent density functional theory ECD calculations together with comparison of their ECD spectra. Trichodermamide G contains a unique sulfur bridge compared to the homologous compounds. The polyketide derivatives nafuredin C (**1**) and nafuredin A (**2**) exhibited distinct antifungal activity against *M. oryzae*. *T. harzianum* have been widely used as biocontrol agents and commercially marketed as biopesticides. Our study expands the source of *Trichoderma* which used for biocontrol, and provides basic material for the discovery of new antifungal pesticides.

DATA AVAILABILITY STATEMENT

The raw data supporting the conclusions of this article will be made available by the authors, without undue reservation, to any qualified researcher.

AUTHOR CONTRIBUTIONS

D-LZ and C-SZ conceived and designed the experiments. X-FZ R-HH, DW, X-QW, and PZ performed the experiments. Y-QL, C-JZ, and PZ analyzed the data. D-LZ wrote the manuscript. All authors reviewed the manuscript.

FUNDING

This work was supported by the National Natural Science Foundation of China (41806194), the Major Agricultural Application Technology Innovation Projects of Shandong Province (SD2019ZZ002), and the Foundation of Key Laboratory of Tropical Medicinal Resource Chemistry of Ministry of Education (RDZH2019001).

ACKNOWLEDGMENTS

We thank Dr. Fei Cao (College of Pharmaceutical Sciences, Hebei University) and Dr. Chao Liu (Sun Yat-sen University Cancer Center) for their efforts in the ECD analysis.

SUPPLEMENTARY MATERIAL

The Supplementary Material for this article can be found online at: https://www.frontiersin.org/articles/10.3389/fmicb.2020.01495/full#supplementary-material

REFERENCES

Appendino, G., Gibbons, S., Giana, A., Pagani, A., Grassi, G., Stavri, M., et al. (2008). Antibacterial cannabinoids from *Cannabis sativa*: a structure-activity study. *J. Nat. Prod.* 71, 1427–1430. doi: 10.1021/np8002673

Cai, R. L., Wu, Y. N., Chen, S. H., Cui, H., Liu, Z. M., Li, C. Y., et al. (2018). Peniisocoumarins A–J: isocoumarins from *Penicillium commune* QQF-3, an endophytic fungus of the mangrove plant *Kandelia candel*. *J. Nat. Prod.* 81, 1376–1383. doi: 10.1021/acs.jnatprod.7b01018

Cao, F., Meng, Z. H., Wang, P., Luo, D. Q., and Zhu, H. J. (2020). Dipleosporalones A and B, dimeric azaphilones from a marine-derived *Pleosporales* sp. fungus. *J. Nat. Prod.* 83, 1283–1287. doi: 10.1021/acs.jnatprod.0c00132

Capon, R. J., Ratnayake, R., Stewart, M., Lacey, E., Tennant, S., and Gill, J. H. (2005). Aspergillazines A–E: novel heterocyclic dipeptides from an Australian strain of *Aspergillus unilateralis*. *Org. Biomol. Chem.* 3, 123–129. doi: 10.1039/b413440k

Contreras-Cornejo, H. A., Macias-Rodriguez, L., del-Val, E., and Larsen, J. (2016). Ecological functions of *Trichoderma* spp. and their secondary metabolites in the rhizosphere: interactions with plants. *FEMS Microbiol. Ecol.* 92:fw036. doi: 10.1093/femsec/fw036

Guzman-Guzman, P., Porras-Troncoso, M. D., Olmedo-Monfil, V., and Herrera-Estrella, A. (2019). *Trichoderma* species: versatile plant symbionts. *Phytopathology* 109, 6–16. doi: 10.1094/PHYTO-07-18-0218-RVW

Huang, R. H., Gou, J. Y., Zhao, D. L., Wang, D., Liu, J., Ma, G. Y., et al. (2018). Phytotoxicity and anti-phytopathogenic activities of marine-derived fungi and their secondary metabolites. *RSC Adv.* 8, 37573–37580. doi: 10.1039/c8ra08047j

Kim, J., and Movassaghi, M. (2015). Biogenetically-inspired total synthesis of epidithiodiketopiperazines and related alkaloids. *Acc. Chem. Res.* 48, 1159–1171. doi: 10.1021/ar500454v

Liu, R., Gu, Q. Q., Zhu, W. M., Cui, C. B., and Fan, G. T. (2005). Trichodermamide A and aspergillazine A, two cytotoxic modified dipeptides from a marine-derived fungus *Spicaria elegans*. *Arch. Pharmacal Res.* 28, 1042–1046. doi: 10.1007/bf02977399

Ma, L. J., and Xu, J. R. (2019). Shuffling effector genes through mini-chromosomes. *PLos Genet.* 15:e1003826. doi: 10.1371/journal.pgen.1008345

Martin-Urdiroz, M., Oses-Ruiz, M., Ryder, L. S., and Talbot, N. J. (2016). Investigating the biology of plant infection by the rice blast fungus *Magnaporthe oryzae*. *Fungal Genet. Biol.* 90, 61–68. doi: 10.1016/j.fgb.2015.12.009

Takano, D., Nagamitsu, T., Ui, H., Shiomi, K., Yamaguchi, Y., Masuma, R., et al. (2001). Absolute configuration of nafuredin, a new specific NADH-fumarate

reductase inhibitor. *Tetrahedron Lett.* 42, 3017–3020. doi: 10.1002/chin.200129194

Ui, H., Shiomi, K., Yamaguchi, Y., Masuma, R., Nagamitsu, T., Takano, D., et al. (2001). Nafuredin, a novel inhibitor of NADH-fumarate reductase, produced by *Aspergillus niger* FT-0554. *J. Antibiot.* 54, 234–238. doi: 10.7164/antibiotics.54.234

Zhang, Z. Z., He, X. Q., Zhang, G. J., Che, Q., Zhu, T. J., Gu, Q. Q., et al. (2017). Inducing secondary metabolite production by combined culture of *Talaromyces aculeatus* and *Penicillium variabile*. *J. Nat. Prod.* 80, 3167–3171. doi: 10.1021/acs.jnatprod.7b00417

Zhao, D. L., Han, X. B., Wang, D., Liu, M. H., Gou, J. Y., Peng, Y. L., et al. (2019). Bioactive 3-decalinoyltetramic acids derivatives from a marine-derived strain of the fungus *Fusarium equiseti* D39. *Front. Microbiol.* 10:1285. doi: 10.3389/fmicb.2019.01285

Zhao, D. L., Wang, D., Tian, X. Y., Cao, F., Li, Y. Q., and Zhang, C. S. (2018). Anti-phytopathogenic and cytotoxic activities of crude extracts and secondary metabolites of marine-derived fungi. *Mar. Drugs* 16:36. doi: 10.3390/md16010036

Zhao, X. X., Wang, X. M., Xu, P., Zhao, L. N., Hu, Y., Chen, J. Y., et al. (2019). Research and prospect of rice blast resistance. *Hubei Agr. Sci.* 58, 5–9. doi: 10.14088/j.cnki.issn0439-8114.2019.11.001

Zhou, J. M. (2016). Plant pathology: a life and death struggle in rice blast disease. *Curr. Biol.* 26, 843–845. doi: 10.1016/j.cub.2016.08.038

Conflict of Interest: The authors declare that the research was conducted in the absence of any commercial or financial relationships that could be construed as a potential conflict of interest.

frontiers in Microbiology

ORIGINAL RESEARCH
published: 03 July 2020
doi: 10.3389/fmicb.2020.01113

Triterpenoids Extracted From *Antrodia cinnamomea* Mycelia Attenuate Acute Alcohol-Induced Liver Injury in C57BL/6 Mice *via* Suppression Inflammatory Response

Yange Liu[1,2], *Zhuqian Wang*[1], *Fange Kong*[1], *Lesheng Teng*[1], *Xiaoyi Zheng*[3], *Xingkai Liu*[4]* *and Di Wang*[1]*

[1] School of Life Sciences, Jilin University, Changchun, China, [2] School of Basic Medical Sciences, Nanchang University, Nanchang, China, [3] Division of Nephrology, Stanford University School of Medicine, Stanford, CA, United States, [4] Hepatobiliary and Pancreatic Surgery, The First Hospital of Jilin University, Jilin University, Changchun, China

OPEN ACCESS

Edited by:
Fernando Rodrigues, University of Minho, Portugal

Reviewed by:
Ricardo Silvestre, University of Minho, Portugal
Weilin Xu, Zhejiang University, China
Zhong Wang, Soochow University, China

***Correspondence:**
Xingkai Liu
xingkailiu@foxmail.com
Di Wang
jluwangdi@outlook.com

Specialty section:
This article was submitted to Fungi and Their Interactions, a section of the journal Frontiers in Microbiology

Received: *18 January 2020*
Accepted: *04 May 2020*
Published: *03 July 2020*

Citation:
Liu Y, Wang Z, Kong F, Teng L, Zheng X, Liu X and Wang D (2020) Triterpenoids Extracted From Antrodia cinnamomea Mycelia Attenuate Acute Alcohol-Induced Liver Injury in C57BL/6 Mice via Suppression Inflammatory Response. Front. Microbiol. 11:1113. doi: 10.3389/fmicb.2020.01113

Excessive alcohol consumption causes liver injury–induced mortality. Here we systematically analyzed the structure of triterpenoids extracted from *Antrodia cinnamomea* mycelia (ACT) and investigated their protective effects against acute alcohol-induced liver injury in mice. Liquid chromatography–mass spectrometry and liquid chromatography with tandem mass spectrometry were performed to determine the structures of ACT constituents. Alcohol-induced liver injury was generated in C57BL/6 mice by oral gavage of 13 g/kg white spirit (a wine at 56% ABV). Mice were treated with either silibinin or ACT for 2 weeks. Liver injury markers and pathological signaling were then quantified with enzyme-linked immunosorbent assays, antibody array assays, and Western blots, and pathological examinations were performed using hematoxylin-eosin staining and periodic acid–Schiff staining. Triterpenoids extracted from *A. cinnamomea* mycelia contain 25 types of triterpenoid compounds. A 2-weeks alcohol consumption treatment caused significant weight loss, liver dyslipidemia, and elevation of alanine aminotransferase, aspartate aminotransferase, γ-glutamyl transferase, and alkaline phosphatase activities in the serum and/or liver. These effects were markedly reversed after 2-weeks ACT administration. Triterpenoids extracted from *A. cinnamomea* mycelia alleviated the organ structural changes and inflammatory infiltration of alcohol-damaged tissues. Triterpenoids extracted from *A. cinnamomea* mycelia inhibited proinflammatory cytokine levels and enhanced anti-inflammatory cytokine levels. Acute alcohol treatment promoted inflammation with significant correlations to hypoxia-inducible factor 1α (HIF-1α), which was reduced by ACT and was partially related to modulation of the protein kinase B (Akt)/70-kDa ribosomal protein S6 kinase phosphorylation (p70S6K) and Wnt/β-catenin signaling pathways. In conclusion, ACT protected against acute alcohol-induced liver damage in mice mainly through its suppression of the inflammatory response, which may be related to HIF-1α signaling.

Keywords: ***Antrodia cinnamomea*** **mycelia, triterpenoids, alcohol, liver injury, inflammatory response**

INTRODUCTION

According to a World Health Organization report on alcohol and health in 2018, alcohol abuse kills more than three million people each year. Excessive alcohol consumption is the most frequent cause of alcoholic liver disease (ALD), which involves alcoholic hepatitis, steatosis, steatohepatitis, fibrosis, and cirrhosis (Gonçalves et al., 2017). Acute alcoholic hepatitis and liver cirrhosis are associated with a high mortality rate, which can reach 50% in acute alcohol hepatitis. Although low-grade fatty liver disease can be alleviated after alcohol withdrawal, 35% of heavy alcohol drinkers will develop more severe forms of liver injury (Lucey et al., 2009). Alcoholic liver disease imposes a significant and increasing treatment burden on society.

Excessive levels of alcohol and alcohol metabolites upregulate the levels of cytokine/chemokine receptors and proinflammatory cytokines including tumor necrosis factor (TNF), interferons (IFNs), and interleukins (ILs) (Gao and Bataller, 2011; Wang et al., 2018). The spleen, an important source of proinflammatory cytokines, is consistently damaged in patients with ALD (Cesta, 2006). Alcohol metabolism causes central venous hypoxia, which results from increased oxygen consumption and decreased oxygen delivery to the liver (Tsukamoto and Xi, 2010). Under hypoxic conditions, hypoxia-inducible factor 1α (HIF-1α) facilitates the synthesis of nitric oxide (NO), increases the expression of cytokines such as TNF-α, and promotes inflammation and cell death (Pan et al., 2018). All of these processes are involved in ALD and especially in alcoholic hepatitis. Depletion of HIF-1α in hepatocytes can alleviate alcohol-induced fat accumulation and inflammation in the liver (Nath et al., 2011). This evidence indicates that there is an association between inflammation and HIF-1α and that HIF-1α may be a potential therapeutic target for ALD treatment.

Medicines commonly used to treat acute alcoholic hepatitis, such as metadoxine, s-ademetionine, and silibinin, exert various side effects that limit their efficacies (Ambade et al., 2018). Certain fungi and their natural products can potentially function as novel medicines because of their pharmacological effectiveness and reduced side effects. We have previously demonstrated that *Antrodia cinnamomea*, an edible fungus used in traditional medicine, exerts hepatoprotective effects by modulating oxidative stress (Liu et al., 2017b). More than 78 compounds, including terpenoids, have been extracted from *A. cinnamomea* mycelium through submerged fermentation, and the potential pharmaceutical activities of some of these compounds have been evaluated (Ma et al., 2014). Triterpenoids are derived from squalene or related acyclic 30-carbon precursors, are the largest and most structurally diverse group of natural products, and are regarded as the most important biologically active natural products besides polysaccharides (Yu et al., 2010). The hepatoprotective qualities of *A. cinnamomea* and its triterpenoid compounds against CCl_4- and N-nitrosodiethylamine–induced liver injury in mice have been studied (Tien et al., 2017). Although the hepatoprotective qualities of *A. cinnamomea* against alcohol-induced liver injury have been reported, only antrosterol (Chang et al., 2017) and antroquinonol (Kumar et al., 2011) have been extracted from *A. cinnamomea* and its fruiting body (Lu et al., 2007; Huang et al., 2010). The secondary metabolites of petri dish–cultured *A. cinnamomea* can reduce aspartate aminotransferase (AST)– and alanine aminotransferase (ALT)–related pathologies and hepatic fat accumulation upon alcohol-induced liver injury (Wu et al., 2019). However, an association between the triterpenes contained in cultured mycelia of *A. cinnamomea* and hepatoprotection has not yet been established.

In this study, we aimed to systemically determine the structure of triterpenoids extracted from *A. cinnamomea* mycelia grown by submerged fermentation and to investigate the hepatoprotective properties and underlying mechanisms of action in mice with acute alcohol injury.

MATERIALS AND METHODS

A. cinnamomea Culture and Sample Preparation

Antrodia cinnamomea mycelia were obtained by submerged fermentation as previously described (Liu et al., 2017a). Triterpenoids were extracted in 80% ethanol twice at 80°C for 100 min. After centrifugation, the supernatant was collected and concentrated at 50°C. After being diluted ninefold in D.D. water, the samples were loaded onto an AB-8 type Amberlyst column (3 × 45 cm) and eluted with D.D. water and 40, 80, and 100% ethanol, respectively, at a flow rate of 0.8 mL/min. The eluent fractions from 80 and 100% ethanol elutions were collected. The triterpenoids of *A. cinnamomea* mycelia (ACT) were prepared by removing the ethanol from wash solution. Vanillin-glacial acetic acid and perchloric acid colorimetric spectrophotometry was performed to analyze the concentrations of the triterpenoids as previously described (Ma et al., 2014).

Liquid Chromatography–Mass Spectrometry and Liquid Chromatography With Tandem Mass Spectrometry Analysis

Approximately 50 mg of ACT was extracted with 800 μL of methanol and 10 μL of internal standard (2.9 mg/mL, DL-*o*-chlorophenylalanine). The solution was ground using a grinding mill at 65 Hz for 45 s, vortexed for 30 s, and then centrifuged at 12,000 revolutions/min for 15 min at 4°C. Subsequently, 200 μL of supernatant was transferred to a vial for liquid chromatography–mass spectrometry (LC-MS) analysis (UltiMate 3000LC, Orbitrap Elite; Thermo Fisher Scientific, Waltham, MA, USA) with a Hypersil GOLD C18 column (100 × 2.1 mm, 1.9 μm; Thermo Fisher Scientific, Waltham MA, USA). Chromatographic separation conditions were as follows: column temperature: 40°C; flow rate: 0.3 mL/mL; mobile phase A: water + 0.1% formic acid; mobile phase B: acetonitrile + 0.1% formic acid; injection volume: 4 μL; automatic injector temperature: 4°C. ESI–: ESI-heater temperature: 300°C; sheath gas flow rate: 45 arb; aux gas flow rate: 15 arb; sweep gas flow rate; 1 arb; spray voltage: 3.2 kV; capillary temperature: 350°C; S-Lens RF level: 60%; liquid chromatography with tandem mass spectrometry (LC-MS/MS): high-energy collision dissociation, 40 V; resolution: 17,500. The gradient of the mobile phase is

shown in **Table 1S**. The details of mass spectra detected by LC-MS/MS from the ACT sample are shown in **Figure 1S**.

Animal Experiment Design

The study protocol was approved by the Institutional Animal Ethics Committee of Jilin University (no. SY0605). The model development of alcohol-induced liver injury was similar to that described in previous studies with some modification (Huang et al., 2015; Lim et al., 2015; Massey et al., 2018). Eight-weeks-old C57BL/6 male mice (18–22 g) were purchased from Liaoning Changsheng Biotechnology Co., Ltd. [SCXK (Liao)-2015-0001, Liaoning, China] and housed in a controlled room with a relative humidity of 50 ± 5%, a temperature of 23 ± 1°C, and a 12-h light/dark cycle. After 7-days acclimatization, all mice were randomized into six groups ($n = 8$/group). One group of mice (control group, $n = 8$) was treated (oral gavage) with 10 mL/kg normal saline (0.9% NaCl), and the other five groups of mice were treated (oral gavage) with 13 g/kg of white spirit (a wine at 56% ABV; Beijing Shunxin Agricultural Co. Ltd., Beijing, China) at 9:00 AM once per day. At 4:00 P.M, on the same day, the control group ($n = 8$) and one experimental group ($n = 8$) were treated (oral gavage) with 10 mL/kg normal saline; one group ($n = 8$) was additionally treated (oral gavage) with 63 mg/kg of silibinin (Sil group) (Tianjin Tasly Sants Pharmaceutical Co. Ltd., Tianjin, China), used as a positive control; and three groups were additionally orally gavaged with 5 mg/kg ($n = 8$), 15 mg/kg ($n = 8$), or 45 mg/kg ($n = 8$) of ACT. The treatment period lasted for 14 days, and all mice were weighed every 3 days. A detailed experimental protocol and drug administration specifics are shown in **Figure 2A**.

Sample Collection

After the last administration, the mice were fasted for 8 h. Blood was collected from the retrobulbar plexus/sinus. Tissues including those of the liver, kidney, spleen, and heart were quickly harvested after euthanasia.

Histology Assay

The collected tissues were fixed in 10% buffered formalin overnight, dehydrated in an ethanol series, cleared with dimethyl benzene, embedded in paraffin, and cut into 5-μm-thick sections. To assess pathological changes, sections of all organs were stained with hematoxylin-eosin (H&E), and the sections of the kidneys were further stained with periodic acid–Schiff (PAS) stain. All stained slides were examined using an IX73 inverted microscope (400×; Olympus, Tokyo, Japan).

Antibody Array Assay

A total of 111 cytokines, chemokines, and growth factors were detected in the liver of mice with acute alcohol injury using the Proteome Profiler Mouse XL Cytokine Array kit (ARY028; R&D Systems, Minneapolis, MN, USA) according to the manufacturer's protocols. Briefly, 200 μg of each sample was diluted with the array buffer. The membranes were blocked with 2 mL of array buffer for 1 h and then incubated with the prepared samples overnight at 4°C with rocking. After washing, the membranes were incubated with primary antibody for 1 h, followed by incubation with streptavidin/horseradish peroxidase for 30 min at room temperature. The membranes were then exposed using the developing substrate solution under the chemiluminescence imager (Chemi Scope 6300; Clinx Science Instruments, Shanghai, China).

Enzyme-Linked Immunosorbent Assay

Based on cytokine screening from the antibody array, the levels of the following cytokines and enzymes in the serum, liver, and/or spleen were measured using an enzyme-linked immunosorbent assay (ELISA) kit (Shanghai Yuanye Bio-Technology Co. Ltd., Shanghai, China) according to the manufacturer's instructions: human cartilage glycoprotein 39 (YKL-40, CK-E95772), plasminogen activator inhibitor 1 (PAI-1, CK-E93562), ALT (CK-E90314), AST (CK-E90386), chemokine (C-X-C motif) ligand 13 (CXCL13, CK-E95658), thrombopoietin (TPO, CK-E93965), retinol-binding protein 4 (RBP4, CK-E20170), γ-glutamyl transferase (GGT, CK-E94933), alkaline phosphatase (ALP, CK-E20105), IL-7 (CK-E20125), IL-22 (CK-E93411), IL-33 (CK-E94161), IL-1α (CK-E20009), vascular endothelial growth factor (VEGF, CK-E20260), regulated upon activation normal T cell expressed and secreted (RANTES, CK-E20198), P-selectin (CK-E20212), intercellular cell adhesion molecule 1 (ICAM-1, CK-E11381), neutrophil gelatinase-associated lipocalin (NGAL, CK-E20174), vascular cell adhesion molecule 1 (VCAM-1, CK-E20253), NO (CK-E20293), reactive oxygen species (ROS, CK-E91516), TNF-α (CK-E20220), IFN-α (CK-E20311), IFN-β (CK-E20334), triglyceride (TG, CK-E91733), total cholesterol (TCHO, CK-E91839), and low-density lipoprotein (LDL, CK-E91911).

Western Blot Analysis

Liver and spleen tissues were homogenized in cold radioimmunoprecipitation assay (Sigma-Aldrich, St. Louis, MO, USA) buffer containing 1% protease inhibitor cocktail (Sigma-Aldrich) and 2% phenylmethanesulfonyl fluoride (Sigma-Aldrich). The protein concentrations of lysed tissues were analyzed using a bicinchoninic acid protein assay kit (Merck Millipore, Burlington, MA, USA). Subsequently, 40–50 μg of protein was separated using 10–12% sodium dodecyl sulfate–polyacrylamide gel electrophoresis and transferred to polyvinylidene difluoride membranes. After blocking with 5% bovine serum albumin, the membranes were incubated at 4°C overnight with the following antibodies: phosphorylated (P)-protein kinase B (Akt, ab131443), total (T)-Akt (ab200195), P-mammalian target of rapamycin (mTOR, ab109268), T-mTOR (ab32028), P-glycogen synthase kinase 3β (GSK-3β, ab75745), T-GSK-3β (ab93926), T-70-kDa ribosomal protein S6 kinase (p70S6K, ab184551), P-β-catenin (ab27798), T-β-catenin (ab32572), Wnt 1 (ab85060), Wnt 3+3α (ab172612), HIF-1α (ab16066) (Abcam, Cambridgeshire, UK), P-p70S6K (#9234; CST, Boston, USA), and glyceraldehyde-3-phosphate dehydrogenase (GAPDH, ABS16; Merck Millipore). After washing, the membranes were incubated with horseradish

peroxidase–conjugated goat anti–rabbit secondary antibodies (bs-0295G; Beijing Biosynthesis Biotechnology Co. Ltd., Beijing, China). Proteins were visualized using a Gel Imaging System (UVP, Upland, CA, USA), and the band intensities were quantified using Image J (National Institutes of Health, Bethesda, MD, USA).

Statistical Analysis

Data are expressed as the means ± *SD* and were analyzed using SPSS 16.0 software (IBM, Armonk, NY, USA). Comparisons between groups were performed using a one-way analysis of variance with parametric test, following by *post-hoc* multiple comparisons (Dunn test). $P < 0.05$ was considered as statistically significant.

Liquid chromatography–MS data analysis for feature extraction was performed and preprocessed with Compound Discoverer software (Thermo Fisher Scientific) and then normalized and edited.

RESULTS

Major Triterpenoid Types in ACT

As determined by LC-MS data (**Figure 1**) and according to the United Network of Human Metabolome Database, 25 major types of triterpenoids were found in ACT (**Table 1**). Their detailed mass spectra from LC-MS/MS are shown in **Figure 1S**.

Protection by ACT Against Alcohol-Induced Liver Injury

ACT treatment in mice reversed the body weight loss induced by excessive alcohol, especially on the fourth, and 7th day ($P < 0.05$; **Table 2S**).

Alcohol increased the activity of ALT ($P < 0.05$, **Figures 2B,C**) and AST (**Figures 2D,E**) in both the serum and liver and increased the levels of GGT ($P < 0.05$; **Figure 2F**) and ALP ($P < 0.05$; **Figure 2G**) in the liver, indicating early liver injuries. Alcohol treatment in mice increases the levels of TG ($P < 0.05$; **Figure 2H**), TCHO ($P < 0.05$; **Figure 2I**), and LDL ($P < 0.05$; **Figure 2J**), suggesting alcohol-driven dyslipidemia. Only ACT, but not Sil, attenuated these upregulated lipid metabolism products in mice with acute alcohol injuries ($P < 0.001$; **Figures 2H–J**). Triterpenoids extracted from *A. cinnamomea* mycelia administered at 15 and 45 mg/kg showed similar efficacy on pathological changes after a 14-days administration ($P < 0.05$; **Figures 2B–J**). However, ACT at 15 mg/kg failed to influence the hepatic levels of ALT (**Figure 2C**).

Compared with the control mice, the alcohol-injured mice exhibited characteristic damage to the liver including lipid droplets, inflammatory infiltration, and necrosis (**Figure 3A**), symptoms that were relieved by ACT administration (**Figure 3A**). Triterpenoids extracted from *A. cinnamomea* mycelia treatment also alleviated alcohol-induced injuries such as thickening of the basement membrane, narrowing of the capsular space (**Figure 3B**), a high rate of PAS-positive

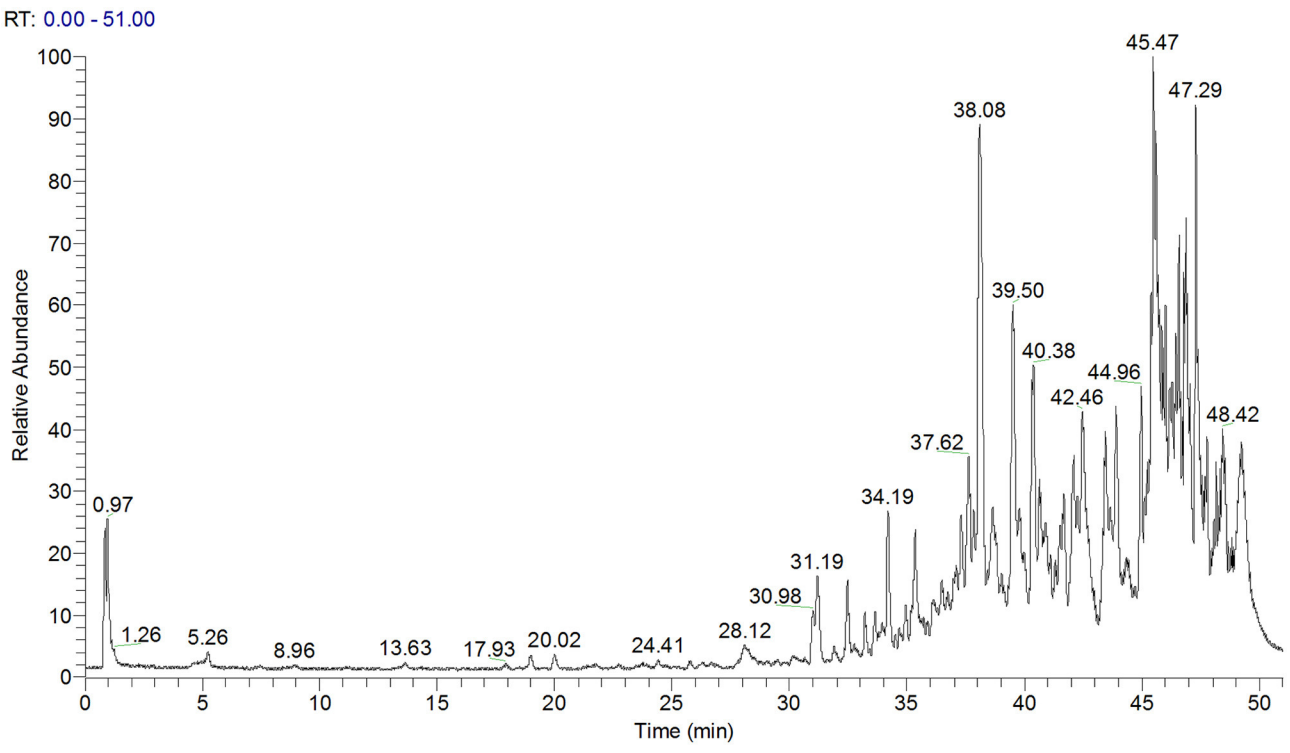

FIGURE 1 | Total ion chromatogram of ACT as obtained by LC-MS. ACT, triterpenoids separated from *A. cinnamomea* mycelia.

TABLE 1 | Twenty-five major types of triterpenoids extracted from ACT and analyzed by LC-MS and LC-MS/MS.

No.	Molecular weight	Name	CAS	MZ	RT (min)	Area: ACT.raw (F1)
1	436.3339	Ganoderal A	104700-98-3	435.3266	45.63	1535.710215
2	438.3496	Ganoderol A	104700-97-2	437.3423	45.631	44145.19097
3	440.3278	Camelledionol	81426-90-6	439.3205	47.147	1041.589219
4	440.3655	Ganoderol B	104700-96-1	439.3582	45.374	538.4306751
5	442.3439	Camellenodiol	81426-91-7	441.3366	48.075	4116.106675
6	448.3180	Porrigenin A	196607-75-7	447.3107	46.447	982.1673132
7	452.3290	Tyromycic acid	104759-35-5	451.3217	45.169	3005.389475
8	454.3437	Ganoderal B	114020-55-2	453.3364	48.011	811.0190589
9	456.3599	Ganodermanondiol	/	455.3526	48.549	8811.756089
10	460.2807	Lucidenic acid N	364622-33-3	459.2735	45.964	298.8221905
11	462.2977	Lucidenic acid M	110241-33-3	461.2904	35.382	1294.49912
12	468.3242	Glabrolide	10401-33-9	467.3169	45.541	1176.825686
13	469.2101	**Desoxylimonin**	/	468.2028	45.448	645.6217662
14	470.3392	Rubinic acid	94662-96-1	469.3319	45.187	20425.83661
15	470.3755	Momoridcin	/	469.3683	47.359	43707.50927
16	484.3182	Ganolucidic acid E	114567-50-9	483.3109	38.929	2069.389669
17	488.3495	Ganoderiol D	114567-45-2	487.3422	38.393	29266.99928
18	490.3653	Ganoderiol H	114612-72-5	489.3580	46.104	1090.990007
19	502.3293	Ganolucidic acid B	98683-75-1	501.3221	46.002	4160.083098
20	502.3652	**Ganoderiol I**	114567-49-6	501.3579	40.078	24539.03582
21	504.3446	Protobassic acid	37905-13-8	503.3373	47.996	19431.66385
22	504.3813	**Ganoderiol G**	114567-48-5	503.3741	37.971	1841.985826
23	516.3445	Phytolaccinic acid	54928-05-1	515.3372	46.269	733.9864822
24	528.3808	Tsugaric acid B	201045-20-7	527.3735	46.134	2656.340618
25	544.1966	**Physalin D**	54980-22-2	543.1893	38.42	1721.83703

Bold text indicates no found fragment ion. ACT, triterpenoids separated from A. cinnamomea mycelia; CAS, chemical abstracts service; MZ, mass-to-charge ratio; RT, retention time.

spots (**Figure 3C**) in the kidney, and an increased ratio of inflammatory infiltration in the spleen (**Figure 3D**) and heart (**Figure 3E**). Compared with the healthy control mice, 45 mg/kg of ACT administration showed no effect on the pathological features of the liver, spleen, kidney, or heart, suggesting that the use of ACT is safe for these organs (**Figure 2S**).

Effects of ACT on the Inflammatory Response in Acute Alcohol-Injured Mice

ACT administered at 15 and 45 mg/kg showed similar efficacies on the pathological changes in cytokines and organ structures. According to the recommended dosage of *A. cinnamomea* for human consumption and the extraction ratio of triterpenoids in this study, we chose liver samples obtained from mice treated with 15 mg/kg ACT for analysis by cytokine screening.

Using the data obtained from the antibody array assay, 21 of the 111 target cytokines were chosen for further analysis based on their correlation with ALD and their changes among experimental groups (**Figure 4** and **Table 3S**). Compared with the acute alcohol-injured mice, Sil-treated mice showed increased levels of 14 cytokines and reduced levels of seven cytokines, whereas ACT-treated mice (15 mg/kg) showed increased levels of 20 cytokines and reduced level of one cytokine in the liver tissues (**Figure 4** and **Table 3S**).

The ELISA method was used to validate the changes in cytokines identified by the cytokine array. Compared with the acute alcohol-injured mice, ACT-treated mice showed reduced levels of 12 cytokines including IL-1α ($P < 0.05$), IL-7 ($P < 0.05$), IL-33 ($P < 0.05$), TNF-α ($P < 0.05$), IFN-α ($P < 0.01$), IFN-β ($P < 0.05$), VEGF ($P < 0.05$), RANTES ($P < 0.01$), P-selectin ($P < 0.05$), CXCL13 ($P < 0.05$), YKL-40 ($P < 0.05$), and PAI-1 ($P < 0.05$) and increased levels of IL-22 ($P < 0.05$) in the liver (**Table 2**).

Furthermore, a 14-days treatment of ACT at 45 mg/kg resulted in 22.5, 19.3, 28.5, 23.7, 40.9, and 36.9% reductions in the levels of IL-1α ($P < 0.05$), IL-7 ($P < 0.05$), IL-33 ($P < 0.05$), TNF-α ($P < 0.05$), IFN-α ($P < 0.01$), and IFN-β ($P < 0.05$), respectively, compared with their levels in acute alcohol-injured mice, with the exception of IL-22 in the spleen (**Table 3**).

NO and ROS are major molecules involved in the pathogenesis of inflammatory diseases (Liu et al., 2018b), and the hepatic and splenic levels of NO and ROS were significantly reduced by ACT treatment at 45 mg/kg in acute alcohol-injured mice ($P < 0.01$; **Tables 2**, **3**).

ACT and Sil failed to affect the hepatic levels of TPO, RBP4, IL-23, ICAM-1, NGAL, and VCAM-1 in acute alcohol-injured mice compared with the model group (**Table 4S**).

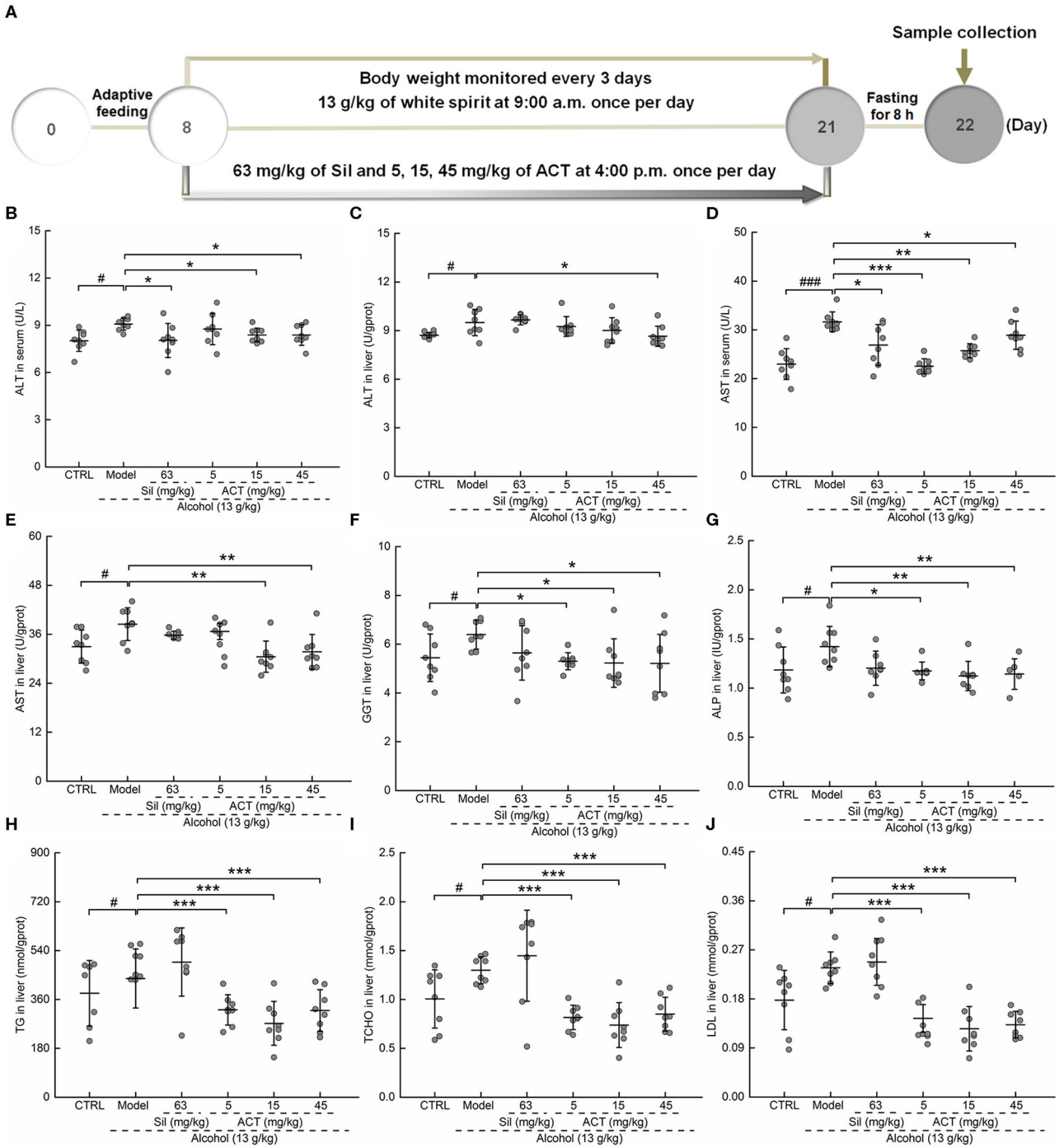

FIGURE 2 | ACT treatment decreases liver injury markers and lipid abnormalities. Mice were treated with ACT for 14 days, and their liver injury markers were quantified with enzyme-linked immunosorbent assay. **(A)** The experimental protocol and drug administration. **(B–F)** The levels of **(B,C)** alanine aminotransferase and **(D,E)** aspartate aminotransferase in both the serum and liver, respectively, and the levels of **(F)** γ-glutamyl transferase, **(G)** alkaline phosphatase, **(H)** triglyceride, **(I)** total cholesterol, and **(J)** low-density lipoprotein in the liver. Data are expressed as the means ± *SD* ($n = 8$) and were analyzed using a one-way analysis of variance with parametric tests. $^{\#}P < 0.05$ and $^{\#\#\#}P < 0.001$ vs. the control group; $^{*}P < 0.05$, $^{**}P < 0.01$, and $^{***}P < 0.001$ vs. the model group. ACT, triterpenoids separated from *A. cinnamomea* mycelia; Sil, silibinin.

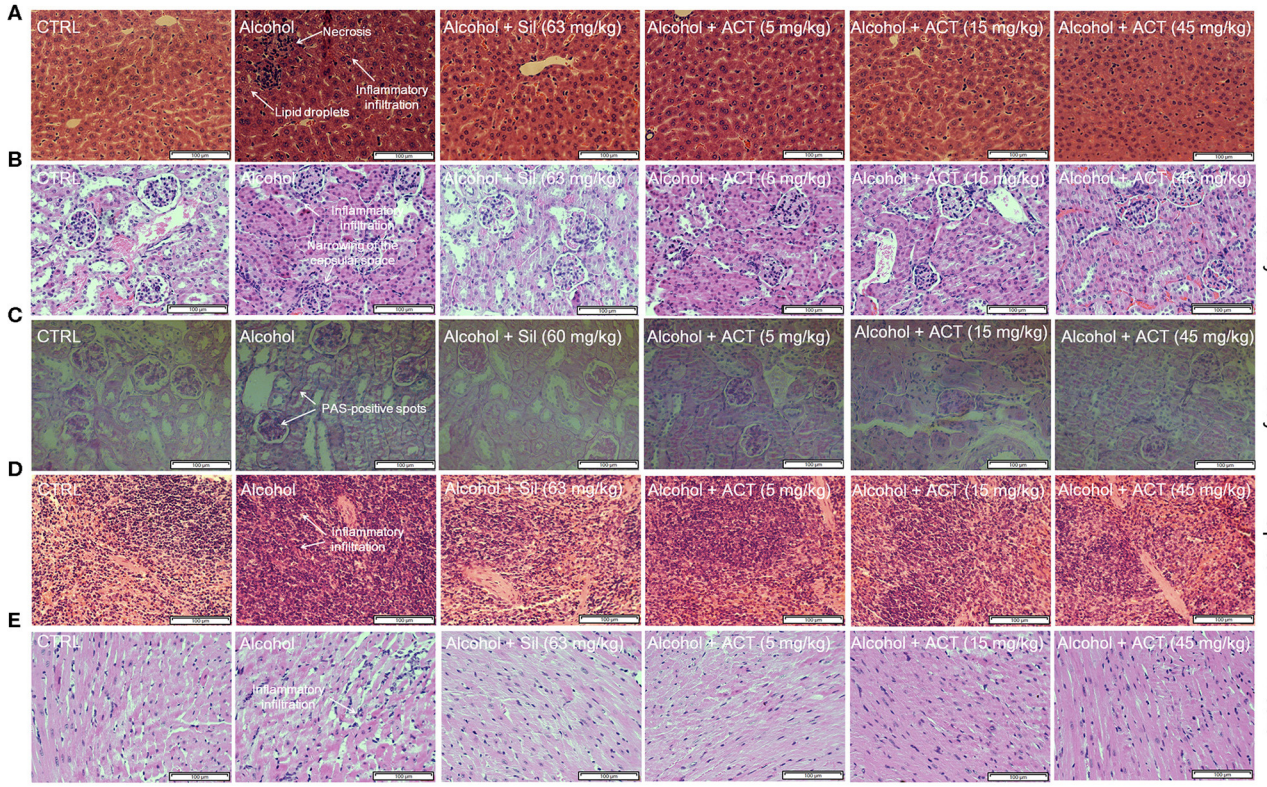

FIGURE 3 | ACT treatment alleviates structural organ changes and hepatocyte apoptosis. Histopathological analyses of the **(A)** liver, **(B)** kidney, **(D)** spleen, and **(E)** heart by H&E staining, and of the **(C)** kidney by PAS staining (scale bar 100 μm; magnification × 400). ACT, triterpenoids separated from *A. cinnamomea* mycelia; Sil, silibinin; H&E, hematoxylin and eosin; PAS, periodic acid–Schiff.

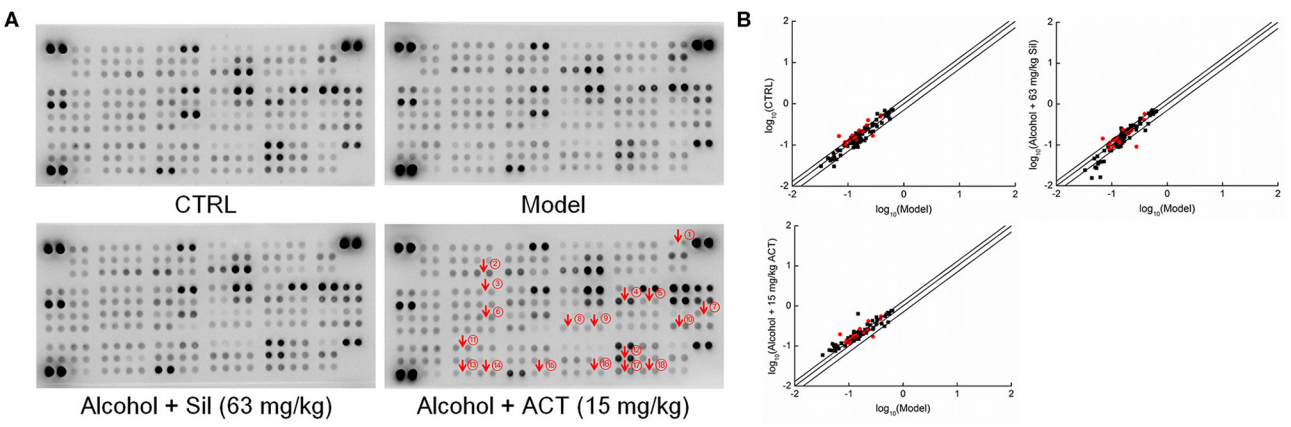

FIGURE 4 | Antibody array assay. The effects of ACT and Sil on 111 cytokines in the livers of mice with acute alcohol-induced liver injury were detected using the Proteome Profiler Mouse XL Cytokine Array kit ($n = 3$). **(A)** The array graph represents the cytokine expressions. **(B)** Scatter diagram of the 111 cytokines. The relative density is the ratio of the absolute value and the reference spot value. The red dots indicate the proteins validated by enzyme-linked immunosorbent assay. ACT, triterpenoids separated from *A. cinnamomea* mycelia; Sil, silibinin. ① RANTES, regulated upon activation normal T cell expressed and secreted; ② YKL-40, human cartilage glycoprotein 39; ③ CXCL13, chemokine (C-X-C motif) ligand 13; ④ ICAM-1, intercellular cell adhesion molecule 1; ⑤ IFN-γ, interferon γ; ⑥ IL-1α, interleukin 1α; ⑦ IL-7, interleukin 7; ⑧ IL-22, interleukin 22; ⑨ IL-23, interleukin 23; ⑩ IL-33, interleukin 33; ⑪ NGAL, neutrophil gelatinase-associated lipocalin; ⑫ RBP4, retinol-binding protein 4; ⑬ P-selectin; ⑭ PAI-1, plasminogen activator inhibitor 1; ⑮ TPO, thrombopoietin; ⑯ TNF-α, tumor necrosis factor α; ⑰ VCAM-1, vascular cell adhesion molecule 1; ⑱ VEGF, vascular endothelial growth factor.

TABLE 2 | ACT and Sil regulates the expression level of inflammatory cytokines in liver of mice with acute alcohol exposure.

	CTRL	Alcohol	Alcohol + Sil (mg/kg)	Alcohol + ACT (mg/kg)		
			63	5	15	45
NO (μmol/gprot)	7.7 ± 2.5	10 ± 2.3$^{\#}$	9 ± 4.9	6.6 ± 1.5*	4.1 ± 1.1**	5.6 ± 1.1**
ROS (U/mgprot)	353.2 ± 35.7	392.8 ± 38.2$^{\#}$	353.9 ± 18.2*	371.8 ± 29.7	336.9 ± 32**	342.9 ± 21**
IL-1α (pg/mgprot)	5.7 ± 1.5	6.3 ± 0.8	5.4 ± 1.6	4.5 ± 0.2**	4.8 ± 0.4**	5 ± 1*
IL-7 (pg/mgprot)	30 ± 2.2	32.6 ± 1.8$^{\#}$	30.6 ± 2.6	30.9 ± 2.2	28.9 ± 1.6*	30.5 ± 2.8
IL-22(pg/mgprot)	5.3 ± 0.8	4.6 ± 0.4$^{\#}$	5.5 ± 1.7	4.6 ± 0.1	5.1 ± 0.8	5.3 ± 0.7*
IL-33 (pg/mgprot)	15.5 ± 2.9	22.9 ± 4.4$^{\#\#}$	16.4 ± 4.1**	15.9 ± 1.6**	17.3 ± 2.6*	18.6 ± 4.8*
TNF-α (pg/mgprot)	69.4 ± 12.7	81.7 ± 6.8$^{\#}$	74.7 ± 17.5	75.8 ± 7.2	67.1 ± 15.2*	68.6 ± 12.4*
IFN-α (pg/mgprot)	6.1 ± 1.3	7.2 ± 0.7$^{\#}$	5.7 ± 1.2*	5.7 ± 0.4**	5.4 ± 0.9**	5.4 ± 0.7***
IFN-β (pg/mgprot)	69.6 ± 6.9	88.8 ± 14.9$^{\#\#}$	80.2 ± 23.7	75.2 ± 7.8	79 ± 8.2	72 ± 7.9*
VEGF (pg/mgprot)	29.6 ± 5.3	39 ± 10.1$^{\#}$	32.6 ± 7.5	32.7 ± 4.3	33.2 ± 4.1	30.7 ± 3.9*
RANTES (pg/mgprot)	70.1 ± 13.2	83.9 ± 6.5$^{\#}$	68.5 ± 7.9**	67 ± 5.4**	70.1 ± 15.6	60.1 ± 7.2**
P-selectin (pg/mgprot)	22 ± 5.4	31 ± 5.2$^{\#\#}$	25.2 ± 7.4	31.4 ± 1.6	25.3 ± 2*	27.8 ± 2.4
CXCL13 (pg/mgprot)	142.9 ± 15.5	158.5 ± 16.4$^{\#}$	147.2 ± 23.2	145.5 ± 10.9	149.5 ± 12.5	138.7 ± 14.1*
YKL-40 (ng/mgprot)	14.5 ± 0.8	15.2 ± 0.6$^{\#}$	14.4 ± 0.8*	14.9 ± 0.3	14.3 ± 1.1*	14.2 ± 0.6**
PAI-1 (pg/mgprot)	175.3 ± 24.9	194.7 ± 14.1$^{\#}$	184 ± 18.3	179.5 ± 13.1	182.2 ± 13.1	177.5 ± 18.7*

*Data are expressed as the means ± SD (n = 8) and were analyzed using a one-way analysis of variance (ANOVA) with parametric tests. $^{\#}P < 0.05$ and $^{\#\#}P < 0.01$ vs. the control group (one-way ANOVA); *P < 0.05, **P < 0.01, and ***P < 0.001 vs. the model group (one-way ANOVA). ACT, triterpenoids separated from A. cinnamomea mycelia; Sil, silibinin.*

TABLE 3 | ACT and Sil regulates the expression level of inflammatory cytokines in the spleen of mice with acute alcohol-exposure.

	CTRL	Alcohol	Alcohol + Sil (mg/kg)	Alcohol + ACT (mg/kg)		
			63	5	15	45
NO (μmol/gprot)	5.9 ± 1.5	9.4 ± 1.6$^{\#\#}$	7.1 ± 1.8*	7.8 ± 0.9	7.9 ± 1.2	6.1 ± 1.7**
ROS (U/mgprot)	170.9 ± 23.7	218.7 ± 79.2$^{\#}$	240.9 ± 51.4	201.3 ± 31	155 ± 36*	122.3 ± 13.4**
IL-1α (pg/mgprot)	12.3 ± 3.5	16 ± 3.2$^{\#}$	14 ± 3.4	16.1 ± 1.2	15 ± 3	12.4 ± 3.3*
IL-7 (pg/mgprot)	34.6 ± 7	49.2 ± 7.8$^{\#\#\#}$	40.3 ± 9.2*	43.4 ± 8.2	49 ± 8.2	39.7 ± 8.3*
IL-22 (pg/mgprot)	13.2 ± 3.3	10.2 ± 0.9	8.8 ± 2.4	10 ± 2.4	9.9 ± 2.6	10.1 ± 2.5
IL-33 (pg/mgprot)	35.6 ± 9	52.7 ± 12$^{\#\#}$	41.3 ± 12	40.7 ± 7.2	43 ± 6	37.7 ± 9.2*
TNF-α (pg/mgprot)	11.6 ± 1.9	15.6 ± 3.7$^{\#\#}$	11.7 ± 3.3	11.9 ± 1.5*	14.4 ± 2	11.9 ± 1.7*
IFN-α (pg/mgprot)	12.2 ± 1.5	16.4 ± 5.8$^{\#}$	12.5 ± 3.9	12.9 ± 2.2	11 ± 2.8	9.7 ± 2.7**
IFN-β (pg/mgprot)	163.7 ± 15.5	286.2 ± 93.9$^{\#\#}$	217.7 ± 28	184.9 ± 17.7	201.9 ± 41.4	180.6 ± 26.5*

*Data are expressed as the means ± SD (n = 8) and were analyzed using a one-way analysis of variance (ANOVA) with parametric tests. $^{\#}P < 0.05$, $^{\#\#}P < 0.01$ and $^{\#\#\#}P < 0.001$ vs. the control group (one-way ANOVA); *P < 0.05 and **P < 0.01 vs. the model group. ACT, triterpenoids separated from A. cinnamomea mycelia; Sil, silibinin.*

Effects of ACT on the Expression of HIF-1α, Akt, and Wnt1/β-Catenin Signaling-Related Proteins

Based on the data obtained from the antibody array assay, we hypothesized that the HIF-1α expression may be involved in ACT-mediated hepatoprotection against acute alcohol-induced liver injury. We then analyzed the protein expression levels of HIF-1α and its important upstream regulators Akt/p70S6K and Wnt/β-catenin. Alcohol consumption significantly increased the protein levels of HIF-1α ($P < 0.05$) and the phosphorylation levels of Akt ($P < 0.05$), mTOR ($P < 0.05$), p70S6K ($P < 0.05$), and GSK-3β ($P < 0.01$) (**Figures 5A,B**). Triterpenoids extracted from *A. cinnamomea* mycelia treatment also reduced the protein levels of Wnt1 ($P < 0.05$) and Wnt 3+3α ($P < 0.01$) and the phosphorylation levels of β-catenin ($P < 0.01$) in the liver (**Figure 5A**) and spleen (**Figure 5B**) of mice with acute alcohol injury. These pathological alterations in the protein levels and phosphorylation statuses were remarkably alleviated over 14 days of ACT administration, especially at doses of 15 and 45 mg/kg. Comparatively, Sil failed to regulate the expression levels of Wnt 3+3α in the liver (**Figure 5A**) of mice with acute alcohol injuries.

DISCUSSION

The triterpenoids are a large and structural diverse group of important natural compounds that are abundant in *A. cinnamomea* and have well-established biological activities (Yu et al., 2010). We elucidated the structures of these chemical

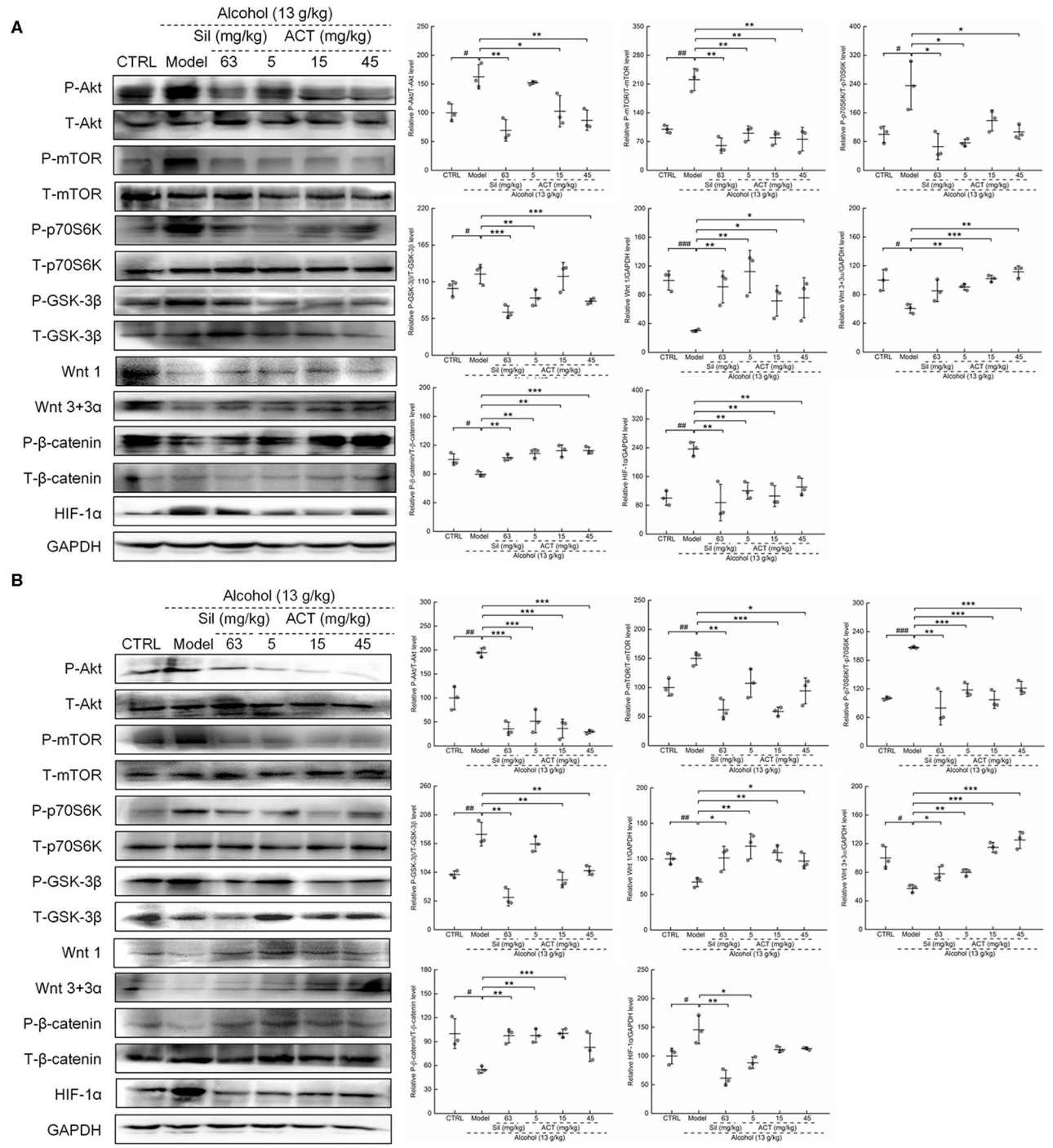

FIGURE 5 | ACT treatment regulates HIF-1α *via* Akt/p70S6K and Wnt/β-catenin signaling in the liver and spleen. Fourteen-day ACT administration regulated the phosphorylation levels of Akt, mTOR, GSK-3β, p70S6K, and β-catenin and the expression levels of Wnt 1, Wnt3, and HIF-1α in the liver **(A)** and spleen **(B)** of mice with acute alcohol-induced injuries. Quantified protein expression was normalized by related total protein expression and/or GAPDH expression. Data are expressed as the means ± *SD* ($n = 3$) and were analyzed using a one-way analysis of variance with parametric tests. $^{\#}P < 0.05$ and $^{\#\#}P < 0.01$ vs. the control group; $^{*}P < 0.05$, $^{**}P < 0.01$, and $^{***}P < 0.001$ vs. the model group. ACT, Triterpenoids separated from *A. cinnamomea* mycelia; Sil, silibinin; Akt, protein kinase B; mTOR, mammalian target of rapamycin; GSK-3β, glycogen synthase kinase 3 beta; p70S6K, 70-kDa ribosomal protein S6 kinase; GAPDH, glyceraldehyde-3-phosphate dehydrogenase.

constituents by LC-MS and LC-MS/MS and confirmed the presence of 25 types of triterpenoid compounds in ACT. Some types of triterpenoids have been confirmed to show protective effects on liver cells. Ganodermanondiol has shown beneficial effects on t-BHP–induced hepatotoxicity through an AMPK- and Nrf2-mediated pathway in human liver-derived HepG2 cells (Li et al., 2013). Ganoderol B has also shown inhibitory effects in HepG2 cells against H_2O_2-induced increases in ALT and AST levels (Peng et al., 2013), and physalin D has been shown to effectively clear 1,1-diphenyl-2-picrylhydrazyl radicals and exert antioxidant activity (Helvaci et al., 2010). Our data provide a complete list of ACT triterpenoids, which may be potential medicines to treat liver diseases in the future.

Alcohol consumption results in changes in the cell membrane permeability, leading to the leakage of hepatic ALT and AST into the blood. The occurrence of liver damage is often accompanied by abnormal increases in ALT, AST, GGT, and ALP activities (Zhang et al., 2017), which serve as the clinical indicators to determine the liver function status (Nada et al., 2010). Lipid metabolism disorders in the liver, such as pathological changes in the levels of TG, TCHO, and LDL, can also be used for the diagnosis of ALD (Zheng et al., 2014). In our study, ACT treatment suppressed the high levels of ALT and AST, remedied the defects of liver lipid metabolism, and alleviated the pathological changes in liver tissues, thus confirming its protective activity against acute alcohol-induced liver injury. Our data suggest that ACT is a candidate medicine to restore hepatocyte membrane permeability and lipid metabolism in cases of alcohol-induced liver injury.

Furthermore, ACT relieved the alcohol-induced inflammatory cell infiltration of organs in our ALD mice, suggesting that it plays an important role against inflammatory responses. According to the antibody array assay, 15 mg/kg ACT treatment strongly influenced the levels of 21 cytokines, most of which are associated with inflammatory responses. Indeed, studies have also reported that the alcohol metabolites acetaldehyde and acetate can directly induce an inflammatory response (Wang et al., 2012) *via* TNF-α overexpression and cause mitochondrial electron transport chain dysfunction, leading to the production of ROS as a by-product (Shanmugam et al., 2003; Shen et al., 2009). The generation of ROS induces the secretion of YKL-40 (Gerin et al., 2016), which is highly expressed in patients with liver fibrosis and cirrhosis (Shen et al., 2009). Reactive oxygen species and TNF-α can promote the release of PAI-1 (Zagotta et al., 2013) and promote cell necrosis *via* the activation of inflammatory responses (Wang et al., 2012), which further helps in the release of IL-1α (Iyer et al., 2009), a factor responsible for neutrophil infiltration (Eigenbrod et al., 2008; Hajime et al., 2010). P-selectin, the expression of which is also controlled by TNF and IL-1, predominantly mediates venular leukocyte recruitment to the sites of inflammation in the liver, similar to the progression of acute allergic responses (Klintman et al., 2004; Sun et al., 2012). The production of NO can be stimulated by IL-33, which is highly expressed in patients with ALD and serves as an alarm during severe tissue injury (Wang et al., 2017), and is responsible for the formation of hydroxyl radicals (Liu et al., 2017b) that impair mitochondrial respiration during alcohol-induced liver damage (Hao et al., 2018). Patients with ALD also show high levels of RANTES and CXCL13. RANTES is involved in the inflammatory processes during the progression of liver fibrosis (Karatayli et al., 2018), and CXCL13 controls circulation and redistribution of B cells in lymphoid organs (Murray et al., 2017). In our study, the anti-inflammatory effects of ACT were confirmed by the suppression of these proinflammatory cytokines, selectins, and ROS after ACT treatment in acute alcohol-injured mice, and these effects may play important roles in hepatoprotection against alcohol-induced acute liver injury.

Alcohol consumption induces hypoxia in the centrilobular area of the liver (French, 2004), which has been considered to promote cellular inflammatory responses, toxicity, and apoptosis (Yun et al., 2014). Interferon α and TNF-α control the expression level of hypoxia-stabilized HIF-1α (Tsapournioti et al., 2013; Yeh et al., 2018), which further regulates the levels of ROS (Yu et al., 2018) and PAI-1 (Zagotta et al., 2013). In addition, under hypoxic conditions, ROS produced from complex III of the respiratory chain are mediated by HIF-1α *via* the reduction of prolyl hydroxylase activity (Chua et al., 2010). Notably, HIF-1α binds to the hypoxia-responsive element in the promoters of target genes to mediate the inflammatory response (Wang et al., 2013) and promote alcohol-induced lipid accumulation (Nath et al., 2011), which can worsen liver injury. Our results showed that the HIF-1α expression was markedly elevated after alcohol administration, similarly to the previous findings (Yun et al., 2014), and was inhibited by 14-days ACT treatment.

Hypoxia activates mTOR signaling, which is triggered by phosphorylation *via* the Akt pathway. Upregulation of mTOR and its downstream target gene p70S6K, which in turn activates HIF-1α, exacerbates ischemia/reperfusion-induced liver inflammation (Zhu et al., 2018). Increased phosphorylation of Akt can suppress the activation of GSK-3β by upregulating its phosphorylation (Huang et al., 2015), and the inhibited activation of GSK-3β is responsible for the accumulation of HIF-1α (Cheng et al., 2014). Activated GSK-3β can regulate β-catenin ubiquitination and degradation, which in turn can be disabled by Wnt ligand binding. Alcohol consumption induces hepatocyte damage by promoting the upregulation of Foxo3A, which suppresses Wnt/β-catenin signaling (Huang et al., 2015), and the activation of Wnt/β-catenin promotes hepatocyte survival under hypoxic conditions (Liu et al., 2018a). Our results suggest that ACT mediates these changes in the expression of proteins involved in the Akt/p70S6K and Wnt/β-catenin pathways, which together regulate the HIF-1α expression. Additionally, hypoxia is considered to promote cellular inflammatory responses. In this study, ACT exerted protective effects against acute alcohol-induced liver injury mainly by preventing inflammatory responses, which may be related to the reduction of the overexpression of HIF-1α signaling.

There are certain limitations to this investigation. First, ACT treatment at 15 and 45 mg/kg showed similar efficacy in regulating the levels of cytokines and proteins in the livers of alcohol-treated mice. Triterpenoids extracted from *A. cinnamomea* mycelia treatment at 45 mg/kg showed greater effects on the levels of cytokines in the spleen than that at 15 mg/kg. Two-weeks administration of ACT at 45 mg/kg

also showed few adverse effects on healthy mice, indicating its safety for use in treating liver injury. More experiments are warranted to determine the optimal dosage of ACT treatment for hepatoprotection against alcohol damage. Second, ACT contains 25 types of triterpenoids, and we did not determine which specific ACT triterpenoids caused the hepatoprotective effects observed in this study. Preliminary results from *in vitro* analysis suggest that the hepatoprotective effects may be caused by several types of triterpenoids working together. Third, HIF-1α serves as a junction between alcohol-induced hypoxia and the inflammatory response. However, we analyzed the expression changes in proteins related only to HIF-1α signaling. Further experiments are warranted in HIF-1α siRNA-transfected cells and knockout mice to further confirm the relationship between Wnt/β-catenin, Akt/p70S6K, and HIF-1α.

By systematic determination of the triterpenoids contained in ACT, we verified the protective properties of ACT against alcohol-induced liver injury in mice, which may be related to the ACT-induced modulation of the HIF-1α expression. These data establish that the hepatoprotective effects of ACT occur mainly through the suppression of the inflammatory response, which may be related to HIF-1α signaling.

DATA AVAILABILITY STATEMENT

All datasets generated for this study are included in the article/ **Supplementary Material**.

ETHICS STATEMENT

The animal study was reviewed and approved by the Institution Animal Ethics Committee of Jilin University (NO. SY0605).

AUTHOR CONTRIBUTIONS

DW and XL conceived and design of research. DW and XZ edited and revised manuscript. XL approved final version of manuscript. YL performed experiments and drafted manuscript. ZW analyzed data and prepared figures. FK and LT interpreted results of experiments. All authors contributed to the article and approved the submitted version.

FUNDING

This work was supported by the Natural Science Foundation of China (Grant No. 81801904), and the Special Projects of Cooperation between Jilin University and Jilin Province in China (SXGJSF2017-1).

SUPPLEMENTARY MATERIAL

The Supplementary Material for this article can be found online at: https://www.frontiersin.org/articles/10.3389/fmicb.2020.01113/full#supplementary-material

REFERENCES

Ambade, A., Lowe, P., Kodys, K., Catalano, D., Gyongyosi, B., Cho, Y., et al. (2018). Pharmacological inhibition of CCR2/5 signaling prevents and reverses alcohol-induced liver damage, steatosis and inflammation in mice. *Hepatology* 69, 1105–1121. doi: 10.1002/hep.30249

Cesta, M. F. (2006). Normal structure, function, and histology of the spleen. *Toxicol. Pathol.* 34, 455–465. doi: 10.1080/01926230600867743

Chang, Y.-Y., Liu, Y.-C., Kuo, Y.-H., Lin, Y.-L., Wu, Y.-H. S., Chen, J.-W., et al. (2017). Effects of antrosterol from *Antrodia camphorata* submerged whole broth on lipid homeostasis, antioxidation, alcohol clearance, and anti-inflammation in livers of chronic-alcohol fed mice. *J. Ethnopharmacol.* 202, 200–207. doi: 10.1016/j.jep.2017.03.003

Cheng, D. D., Zhao, H. G., Yang, Y. S., Hu, T., and Yang, Q. C. (2014). GSK3beta negatively regulates HIF1alpha mRNA stability via nucleolin in the MG63 osteosarcoma cell line. *Biochem. Biophys. Res. Commun.* 443, 598–603. doi: 10.1016/j.bbrc.2013.12.020

Chua, Y. L., Dufour, E., Dassa, E. P., Rustin, P., Jacobs, H. T., Taylor, C. T., et al. (2010). Stabilization of hypoxia-inducible factor-1α protein in hypoxia occurs independently of mitochondrial reactive oxygen species production. *J. Biol. Chem.* 285, 31277–31284. doi: 10.1074/jbc.M110.158485

Eigenbrod, T., Park, J. J., Iwakura, Y., and Nunez, G. (2008). Cutting edge: critical role for mesothelial cells in necrosis-induced inflammation through the recognition of IL-1alpha released from dying cells. *J. Immunol.* 181, 8194–8198. doi: 10.4049/jimmunol.181.12.8194

French, S. W. (2004). The role of hypoxia in the pathogenesis of alcoholic liver disease. *Hepatol. Res.* 29, 69–74. doi: 10.1016/j.hepres.2004.02.006

Gao, B., and Bataller, R. (2011). Alcoholic liver disease: pathogenesis and new therapeutic targets. *Gastroenterology* 141, 1572–1585. doi: 10.1053/j.gastro.2011.09.002

Gerin, F., Erman, H., Erboga, M., Sener, U., Yilmaz, A., Seyhan, H., et al. (2016). The effects of ferulic acid against oxidative stress and inflammation in formaldehyde-induced hepatotoxicity. *Inflammation* 39, 1377–1386. doi: 10.1007/s10753-016-0369-4

Gonçalves, J. L., Lacerda-Queiroz, N., Sabino, J. F., Marques, P. E., Galvão, I., Gamba, C. O., et al. (2017). Evaluating the effects of refined carbohydrate and fat diets with acute ethanol consumption using a mouse model of alcoholic liver injury. *J. Nutr. Biochem.* 39, 93–100. doi: 10.1016/j.jnutbio.2016.08.011

Hajime, K., Dipti, K., Yoichiro, I., and Rock, K. L. (2010). Identification of the cellular sensor that stimulates the inflammatory response to sterile cell death. *J. Immunol.* 184:4470. doi: 10.4049/jimmunol.0902485

Hao, L., Sun, Q., Zhong, W., Zhang, W., Sun, X., and Zhou, Z. (2018). Mitochondria-targeted ubiquinone (MitoQ) enhances acetaldehyde clearance by reversing alcohol-induced posttranslational modification of aldehyde dehydrogenase 2: a molecular mechanism of protection against alcoholic liver disease. *Redox Biol.* 14, 626–636. doi: 10.1016/j.redox.2017.11.005

Helvaci, S., Kokdil, G., Kawai, M., Duran, N., Duran, G., and Guvenc, A. (2010). Antimicrobial activity of the extracts and physalin D from *Physalis alkekengi* and evaluation of antioxidant potential of physalin D. *Pharm. Biol.* 48, 142–150. doi: 10.3109/13880200903062606

Huang, C.-H., Chang, Y.-Y., Liu, C.-W., Kang, W.-Y., Lin, Y.-L., Chang, H.-C., et al. (2010). Fruiting body of niuchangchih (*Antrodia camphorata*) protects livers against chronic alcohol consumption damage. *J. Agric. Food Chem.* 58, 3859–3866. doi: 10.1021/jf100530c

Huang, C. K., Yu, T., de la Monte, S. M., Wands, J. R., Derdak, Z., and Kim, M. (2015). Restoration of Wnt/beta-catenin signaling attenuates alcoholic liver disease progression in a rat model. *J. Hepatol.* 63, 191–198. doi: 10.1016/j.jhep.2015.02.030

Iyer, S. S., Pulskens, W. P., Sadler, J. J., Butter, L. M., Teske, G. J., Ulland, T. K., et al. (2009). Necrotic cells trigger a sterile inflammatory response through the Nlrp3 inflammasome. *Proc. Natl. Acad. Sci. U. S. A.* 106, 20388–20393. doi: 10.1073/pnas.0908698106

Karatayli, E., Hall, R. A., Weber, S. N., Dooley, S., and Lammert, F. (2018). Effect of alcohol on the interleukin 6-mediated inflammatory response in a new mouse model of acute-on-chronic liver injury. *Biochim. Biophys. Acta Mol. Basis Dis.* 1865, 298–307. doi: 10.1016/j.bbadis.2018.11.008

Klintman, D., Li, X., and Thorlacius, H. (2004). Important role of P-selectin for leukocyte recruitment, hepatocellular injury, and apoptosis in endotoxemic mice. *Clin. Diagn. Lab. Immunol.* 11:56. doi: 10.1128/CDLI.11.1.56-62.2004

Kumar, K. J. S., Chu, F.-H., Hsieh, H.-W., Liao, J.-W., Li, W.-H., Lin, J. C.-C., et al. (2011). Antroquinonol from ethanolic extract of mycelium of *Antrodia cinnamomea* protects hepatic cells from ethanol-induced oxidative stress through Nrf-2 activation. *J. Ethnopharmacol.* 136, 168–177. doi: 10.1016/j.jep.2011.04.030

Li, B., Lee, D. S., Kang, Y., Yao, N. Q., An, R. B., and Kim, Y. C. (2013). Protective effect of ganodermanondiol isolated from the Lingzhi mushroom against tert-butyl hydroperoxide-induced hepatotoxicity through Nrf2-mediated antioxidant enzymes. *Food Chem. Toxicol.* 53, 317–324. doi: 10.1016/j.fct.2012.12.016

Lim, J. D., Lee, S. R., Kim, T., Jang, S. A., Kang, S. C., Koo, H. J., et al. (2015). Fucoidan from Fucus vesiculosus protects against alcohol-induced liver damage by modulating inflammatory mediators in mice and HepG2 cells. *Mar. Drugs* 13, 1051–1067. doi: 10.3390/md13021051

Liu, S., Yin, Y., Yu, R., Li, Y., and Zhang, W. (2018a). R-spondin3-LGR4 signaling protects hepatocytes against DMOG-induced hypoxia/reoxygenation injury through activating β-catenin. *Biochem. Biophys. Res. Commun.* 499, 59–65. doi: 10.1016/j.bbrc.2018.03.126

Liu, Y., Li, L., An, S., Zhang, Y., Feng, S., Lu, Z., et al. (2017a). Antifatigue effects of *Antrodia cinnamomea* cultured mycelium via modulation of oxidative stress signaling in a mouse model. *BioMed Res. Int.* 2017:9374026. doi: 10.1155/2017/9374026

Liu, Y., Wang, J., Li, L., Hu, W., Qu, Y., Ding, Y., et al. (2017b). Hepatoprotective effects of *Antrodia cinnamomea*: the modulation of oxidative stress signaling in a mouse model of alcohol-induced acute liver injury. *Oxid. Med. Cell. Longev.* 2017:7841823. doi: 10.1155/2017/7841823

Liu, Z., Ren, Z., Zhang, J., Chuang, C. C., Kandaswamy, E., Zhou, T., et al. (2018b). Role of ROS and nutritional antioxidants in human diseases. *Front. Physiol.* 9:477. doi: 10.3389/fphys.2018.00477

Lu, Z.-M., Tao, W.-Y., Zou, X.-L., Fu, H.-Z., and Ao, Z.-H. (2007). Protective effects of mycelia of *Antrodia camphorata* and *Armillariella tabescens* in submerged culture against ethanol-induced hepatic toxicity in rats. *J. Ethnopharmacol.* 110, 160–164. doi: 10.1016/j.jep.2006.09.029

Lucey, M. R., Mathurin, P., and Morgan, T. R. (2009). Alcoholic hepatitis. *N. Engl. J. Med.* 360, 1512–1513. doi: 10.1056/NEJMc091513

Ma, T. W., Lai, Y., and Yang, F. C. (2014). Enhanced production of triterpenoid in submerged cultures of *Antrodia cinnamomea* with the addition of citrus peel extract. *Bioprocess. Biosyst. Eng.* 37, 2251–2261. doi: 10.1007/s00449-014-1203-8

Massey, V. L., Qin, L., Cabezas, J., Caballeria, J., Sancho-Bru, P., Bataller, R., et al. (2018). TLR7-let-7 signaling contributes to ethanol-induced hepatic inflammatory response in mice and in alcoholic hepatitis. *Alcohol. Clin. Exp. Res.* 42, 2107–2122. doi: 10.1111/acer.13871

Murray, H. W., Luster, A. D., Zheng, H., and Ma, X. (2017). Gamma interferon-regulated chemokines in leishmania donovani infection in the liver. *Infect. Immun.* 85:e00824–e00916. doi: 10.1128/IAI.00824-16

Nada, S. A., Omara, E. A., Abdel-Salam, O. M. E., and Zahran, H. G. (2010). Mushroom insoluble polysaccharides prevent carbon tetrachloride-induced hepatotoxicity in rat. *Food Chem. Toxicol.* 48, 3184–3188. doi: 10.1016/j.fct.2010.08.019

Nath, B., Levin, I., Csak, T., Petrasek, J., Mueller, C., Kodys, K., et al. (2011). Hepatocyte-specific hypoxia-inducible factor-1 alpha is a determinant of lipid accumulation and liver injury in alcohol-induced steatosis in mice. *Hepatology* 53, 1526–1537. doi: 10.1002/hep.24256

Pan, W., Wang, L., Zhang, X. F., Zhang, H., Zhang, J., Wang, G., et al. (2018). *Hypoxia-induced microRNA-191 contributes to hepatic ischemia/reperfusion injury through the ZONAB/Cyclin D1 axis. Cell Death Differ.* 26, 291–305. doi: 10.1038/s41418-018-0120-9

Peng, X. R., Liu, J. Q., Han, Z. H., Yuan, X. X., Luo, H. R., and Qiu, M. H. (2013). Protective effects of triterpenoids from *Ganoderma resinaceum* on H(2)O(2)-induced toxicity in HepG2 cells. *Food Chem.* 141, 920–926. doi: 10.1016/j.foodchem.2013.03.071

Shanmugam, N., Reddy, M. A., Guha, M., and Natarajan, R. (2003). High glucose-induced expression of proinflammatory cytokine and chemokine genes in monocytic cells. *Diabetes* 52, 1256–1264. doi: 10.2337/diabetes.52.5.1256

Shen, Z., Ajmo, J. M., Rogers, C. Q., Liang, X., Le, L., Murr, M. M., et al. (2009). Role of SIRT1 in regulation of LPS- or two ethanol metabolites-induced TNF-α production in cultured macrophage cell lines. *Am. J. Physiol. Gastrointest. Liver Physiol.* 296:G1047. doi: 10.1152/ajpgi.00016.2009

Sun, W. Y., Abeynaike, L. D., Escarbe, S., Smith, C. D., Pitson, S. M., Hickey, M. J., et al. (2012). Rapid histamine-induced neutrophil recruitment is sphingosine kinase-1 dependent. *Am. J. Pathol.* 180, 1740–1750. doi: 10.1016/j.ajpath.2011.12.024

Tien, A.-J., Chien, C.-Y., Chen, Y.-H., Lin, L.-C., and Chien, C.-T. (2017). Fruiting bodies of *Antrodia cinnamomea* and its active ariterpenoid, antcin K, ameliorates N-nitrosodiethylamine-induced hepatic inflammation, fibrosis and carcinogenesis in rats. *Am. J. Chin. Med.* 45, 173–198. doi: 10.1142/S0192415X17500124

Tsapournioti, S., Mylonis, I., Hatziefthimiou, A., Ioannou, M. G., Stamatiou, R., Koukoulis, G. K., et al. (2013). TNFalpha induces expression of HIF-1alpha mRNA and protein but inhibits hypoxic stimulation of HIF-1 transcriptional activity in airway smooth muscle cells. *J. Cell. Physiol.* 228, 1745–1753. doi: 10.1002/jcp.24331

Tsukamoto, H., and Xi, X. P. (2010). Incomplete compensation of enhanced hepatic oxygen consumption in rats with alcoholic centrilobular liver necrosis. *Hepatology* 9, 302–306. doi: 10.1002/hep.1840090223

Wang, H. J., Gao, B., Zakhari, S., and Nagy, L. E. (2012). Inflammation in alcoholic liver disease. *Annu. Rev. Nutr.* 32, 343–368. doi: 10.1146/annurev-nutr-072610-145138

Wang, M., Shen, G., Xu, L., Liu, X., Brown, J. M., Feng, D., et al. (2017). *IL-1 receptor like 1 protects against alcoholic liver injury by limiting NF-κB activation in hepatic macrophages. J. Hepatol.* S0168-8278, 32263–32268. doi: 10.1016/j.jhep.2017.08.023

Wang, X., Lan, Y., Zhu, Y., Li, S., Liu, M., Song, X., et al. (2018). Hepatoprotective effects of *Auricularia cornea* var. Li. polysaccharides against the alcoholic liver diseases through different metabolic pathways. *Sci. Rep.* 8:7574. doi: 10.1038/s41598-018-25830-w

Wang, X., Wu, D., Yang, L., Gan, L., and Cederbaum, A. I. (2013). Cytochrome P450 2E1 potentiates ethanol induction of hypoxia and HIF-1alpha *in vivo*. *Free Radic. Biol. Med.* 63, 175–186. doi: 10.1016/j.freeradbiomed.2013.05.009

Wu, Y., Tian, W.-D., Gao, S., Liao, Z.-J., Wang, G.-H., Lo, J.-M., et al. (2019). Secondary metabolites of petri-dish cultured *Antrodia camphorata* and their hepatoprotective activities against alcohol-induced liver injury in mice. *Chin. J. Nat. Med.* 17, 33–42. doi: 10.1016/S1875-5364(19)30007-X

Yeh, Y. H., Hsiao, H. F., Yeh, Y. C., Chen, T. W., and Li, T. K. (2018). Inflammatory interferon activates HIF-1alpha-mediated epithelial-to-mesenchymal transition via PI3K/AKT/mTOR pathway. *J. Exp. Clin. Cancer Res.* 37:70. doi: 10.1186/s13046-018-0730-6

Yu, Q., Dong, L., Li, Y., and Liu, G. (2018). SIRT1 and HIF1alpha signaling in metabolism and immune responses. *Cancer Lett.* 418, 20–26. doi: 10.1016/j.canlet.2017.12.035

Yu, Y. L., Chen, I. K., Huang, R. Y., Wang, W. R., Chou, C. J., Chang, T. T., et al. (2010). A triterpenoid methyl antcinate K isolated from *Antrodia cinnamomea* promotes dendritic cell activation and Th2 differentiation. *Eur. J. Immunol.* 39, 2482–2491. doi: 10.1002/eji.200839039

Yun, J. W., Son, M. J., Abdelmegeed, M. A., Banerjee, A., Morgan, T. R., Yoo, S. H., et al. (2014). Binge alcohol promotes hypoxic liver injury through a CYP2E1-HIF-1alpha-dependent apoptosis pathway in mice and humans. *Free Radic. Biol. Med.* 77, 183–194. doi: 10.1016/j.freeradbiomed.2014.08.030

Zagotta, I., Dimova, E. Y., Funcke, J. B., Wabitsch, M., Kietzmann, T., and Fischer-Posovszky, P. (2013). Resveratrol suppresses PAI-1 gene expression in a human *in vitro* model of inflamed adipose tissue. *Oxid. Med. Cell. Longev.* 2013:793525. doi: 10.1155/2013/793525

Zhang, L., Zhao, Q., Wang, L., Zhao, M., and Zhao, B. (2017). Protective effect of polysaccharide from maca *(Lepidium meyenii)* on Hep-G2 cells

and alcoholic liver oxidative injury in mice. *Int. J. Biol. Macromol.* 99:63. doi: 10.1016/j.ijbiomac.2017.01.125

Zheng, L., Zhai, G., Zhang, J., Wang, L., Ma, Z., Jia, M., et al. (2014). Antihyperlipidemic and hepatoprotective activities of mycelia zinc polysaccharide from Pholiota nameko SW-02. *Int. J. Biol. Macromol.* 70, 523–529. doi: 10.1016/j.ijbiomac.2014.07.037

Zhu, Q., Wang, H., Jiang, B., Ni, X., Jiang, L., Li, C., et al. (2018). Loss of ATF3 exacerbates liver damage through the activation of mTOR/p70S6K/ HIF-1alpha signaling pathway in liver inflammatory injury. *Cell Death Dis.* 9:910. doi: 10.1038/s41419-018-0894-1

Conflict of Interest: The authors declare that the research was conducted in the absence of any commercial or financial relationships that could be construed as a potential conflict of interest.

frontiers in Microbiology

ORIGINAL RESEARCH
published: 17 July 2020
doi: 10.3389/fmicb.2020.01641

Mycovirus-Induced Tenuazonic Acid Production in a Rice Blast Fungus *Magnaporthe oryzae*

*Akihiro Ninomiya[1], Syun-ichi Urayama[1,2], Rei Suo[3], Shiro Itoi[3], Shin-ichi Fuji[4], Hiromitsu Moriyama[5] and Daisuke Hagiwara[1,2]**

[1] Faculty of Life and Environmental Sciences, University of Tsukuba, Tsukuba, Japan, [2] Microbiology Research Center for Sustainability, University of Tsukuba, Tsukuba, Japan, [3] College of Bioresource Sciences, Nihon University, Fujisawa, Japan, [4] Faculty of Bioresource Sciences, Akita Prefectural University, Akita, Japan, [5] Department of Applied Biological Sciences, Tokyo University of Agriculture and Technology, Fuchu, Japan

Fungi are a rich source of natural products with biological activities. In this study, we evaluated viral effects on secondary metabolism of the rice blast fungus *Magnaporthe oryzae* using an isolate of APU10-199A co-infected with three types of mycoviruses: a totivirus, a chrysovirus, and a partitivirus. Comparison of the secondary metabolite profile of APU10-199A with that of the strain lacking the totivirus and chrysovirus showed that a mycotoxin tenuazonic (TeA) acid was produced in a manner dependent on the mycoviruses. Virus reinfection experiments verified that TeA production was dependent on the totivirus. Quantitative reverse transcription PCR and RNA-sequencing analysis indicated the regulatory mechanism underlying viral induction of TeA: the totivirus activates the TeA synthetase gene *TAS1* by upregulating the transcription of the gene encoding a $Zn(II)_2$-Cys_6-type transcription factor, *TAS2*. To our knowledge, this is the first report that confirmed mycovirus-associated regulation of secondary metabolism at a transcriptional level by viral reinfection. Because only treatment with dimethyl sulfoxide has been reported to trigger TeA production in this fungus without gene manipulation, our finding highlights the potential of mycoviruses as an epigenomic regulator of fungal secondary metabolism.

Keywords: mycovirus, *Magnaporthe oryzae*, secondary metabolism, mycotoxin, tenuazonic acid

OPEN ACCESS

Edited by:
Chengshu Wang, Institute of Plant Physiology and Ecology (CAS), China

Reviewed by:
Syed Riyaz-ul-Hassan, Indian Institute of Integrative Medicine (CSIR), India
Takayuki Motoyama, RIKEN, Japan

****Correspondence:***
Daisuke Hagiwara
hagiwara.daisuke.gb@u.tsukuba.ac.jp

Specialty section:
This article was submitted to Fungi and Their Interactions, a section of the journal Frontiers in Microbiology

Received: *03 March 2020*
Accepted: *24 June 2020*
Published: *17 July 2020*

Citation:
Ninomiya A, Urayama S, Suo R, Itoi S, Fuji S, Moriyama H and Hagiwara D (2020) Mycovirus-Induced Tenuazonic Acid Production in a Rice Blast Fungus Magnaporthe oryzae. Front. Microbiol. 11:1641. doi: 10.3389/fmicb.2020.01641

INTRODUCTION

Fungi produce structurally diverse secondary metabolites (SMs), and thus are a rich source of compounds for drug discovery. Since discovery of the first antibiotic penicillin, thousands of bioactive compounds, such as cyclosporine and lovastatin, have been found in fungi and reported (Bérdy, 2005). In contrast, some fungi can produce mycotoxins, which are a great threat to human health. For example, aflatoxins, carcinogenic mycotoxins produced by certain *Aspergillus* species, cause poisoning of grains (Bennett and Klich, 2003). A human fungal pathogen, *Aspergillus fumigatus*, produces a mycotoxin gliotoxin, which is implicated in the virulence of the fungus (Sugui et al., 2007). Studies of fungal genomes have revealed that fungi have the potential to produce more SMs than expected, as they have a large number of genes for secondary metabolism

(Khaldi et al., 2010; Sanchez et al., 2012). To broaden the fungal chemical space, several studies have attempted to trigger the silent secondary metabolism (Brakhage and Schroeckh, 2011).

As is often the case with bacteria, fungi are infected with viruses called mycoviruses. Unlike bacterial phages, mycoviruses do not lyse the cells of their host but are transmitted intracellularly, and they are thus considered to behave as a symbiont. Most of the known mycoviruses are RNA viruses with an RNA-dependent RNA polymerase (RdRp) encoded in their genome, which is used for phylogenetic classification of mycoviruses. In the history of mycovirus research, the influence of mycoviruses on plant pathogenic fungi have been intensively analyzed because such viruses have potential as pest control agents. For example, cryphonectria hypovirus 1 reduces the pathogenicity of its host, a chestnut blight fungus, *Cryphonectria parasitica* (Nuss, 2005). *C. parasitica* harboring cryphonectria hypovirus 1 has been used for the control of chestnut blight in Europe. In addition to reduced virulence, mycoviruses cause their hosts to undergo a characteristic change of phenotype, such as colony morphology, mycelial growth, and sexual reproduction (Ghabrial et al., 2015). Thus, mycoviruses are considered to be epigenomic factors that expand the physiological diversity of their hosts.

The effect of mycoviruses on fungal secondary metabolism has been investigated in particular on mycotoxin production. In an early study, aflatoxin production by *Aspergillus flavus* is repressed by a mycovirus (Schmidt et al., 1986). Kim and co-workers revealed a decrease of trichothecene production in *Fusarium graminearum* induced by a double-stranded RNA virus (Chu et al., 2002), and Okada et al. (2018) reported chrysovirus-induced enhancement of phytotoxin production in *Alternaria alternata*. Recently, Nerva et al. (2019) reported overproduction of a carcinogenic mycotoxin, ochratoxin A (OTA) in *Aspergillus ochraceus* induced by a partitivirus. Curiously, a gene encoding polyketide synthase (PKS) for OTA biosynthesis was absent in the strain used in the study. Thus, the regulation mechanism of OTA production by partitiviruses remains unclear. So far, although some reports provided data showing that mycoviruses affect host fungal mycotoxin production, the induction mechanism has been poorly understood.

To gain more insight into mycovirus regulation of fungal secondary metabolism, more studies are needed. In a previous study, a rice blast fungus, *Magnaporthe oryzae* APU10-199A, which was co-infected with three types of viruses, a totivirus, a chrysovirus, and a partitivirus, was isolated and characterized (Higashiura et al., 2019). Although the three types of RNA viruses are widely distributed in filamentous fungi and are well studied (Ghabrial et al., 2015), the effects on secondary metabolism have been poorly understood. Here, we demonstrate totivirus-induced production of a mycotoxin tenuazonic acid (TeA) in the *M. oryzae* strain. We also report induced expression of the biosynthetic gene for TeA. To the best of our knowledge, this is the first report that indicates the molecular mechanism underlying regulation of fungal secondary metabolism by a mycovirus. We point out the potential of mycoviruses as an agent that controls fungal secondary metabolism.

MATERIALS AND METHODS

Microorganisms and Culture Conditions

The *M. oryzae* APU10-199A was isolated from symptomatic leaves of the japonica rice cultivar Akitakomachi in Akita Prefecture, Japan in our previous work (Higashiura et al., 2019). The *M. oryzae* APU10-199A strain harbors a totivirus, chrysovirus, and partitivirus. A strain that lacks the totivirus and chrysovirus (here we named the strain APU10-199A_P) was obtained from *M. oryzae* APU10-199A during single conidia isolation. Co-infection of three viruses (APU10-199A) and loss of totivirus and chrysovirus (APU10-199A_P) were confirmed by gel electrophoresis of dsRNA extracted from the strains and RT-PCR in the previous research (Higashiura et al., 2019). *M. oryzae* strains were grown on potato dextrose agar (PDA; BD, Franklin Lakes, NJ, United States), and agar plugs were inoculated into liquid media. Liquid culture was performed using potato dextrose broth (PDB) (BD), soy sauce-sucrose (SS) medium (5% soy sauce; Shiboritate Nama Shoyu, Kikkoman, Chiba, Japan; 5% sucrose in tap water) (Nukina, 1999), or IPN medium (20% vegetable juice; Yasai Ichinichi Kore Ippon, Kagome Co., Ltd., Aichi, Japan; 0.3% $CaCO_3$).

Analysis of Secondary Metabolite Profile

The strains were cultured in 60 mL PDB, SS, and IPN media in a 200 mL Erlenmeyer flask at 25°C with agitation at 40 rpm for 2 weeks or with agitation at 150 rpm for 5 days. After filtration of the culture broth through miracloth (Merck Millipore, Burlington, MA, United States), the filtrate was extracted by an equivalent volume of ethyl acetate, which was dried *in vacuo*. The extracts were dissolved in dimethyl sulfoxide (DMSO) and analyzed using a 1260 Infinity LC system (Agilent Technologies, Inc., Santa Clara, CA, United States) with a Poroshell 120 EC-C18 column (ϕ3.0 mm × 100 mm, particle size 2.7 μm; Agilent). The high-performance liquid chromatography (HPLC) analytical condition was a gradient elution of 5–100% acetonitrile containing 0.5% acetic acid for 18 min.

Isolation of Tenuazonic Acid

Magnaporthe oryzae infected with totivirus was cultured in SS medium (1.2 L) for 5–7 days at 25°C with agitation at 150 rpm. The culture supernatant was extracted with ethyl acetate, and the dried extract was subjected to octadecylsilane flash chromatography, which yielded 0, 20, 40, 60, and 100% methanol fractions. The 20 and 40% methanol fractions were purified using the above-mentioned HPLC system with a COSMOSIL $5C_{18}$-AR-II column (ϕ10 mm × 250 mm; Nacalai Tesque, Kyoto, Japan) to supply TeA (6.0 mg). The HPLC analytical condition was an isocratic elution of 32% acetonitrile containing 0.5% acetic acid for 20 min.

NMR and HRESIMS Analysis

Nuclear magnetic resonance (NMR) spectra were recorded on a 500-MHz ECA500 NMR spectrometer (JEOL Ltd., Tokyo, Japan) at 293 K. The NMR chemical shifts ^{1}H and ^{13}C were referenced to the solvent peaks: δ_H 3.30 and δ_C 49.0

for CD_3OD (Eurisotop, Saint-Aubin, France). High-resolution electrospray ionization mass spectrometry (HRESIMS) analysis was performed using UPLC-SYNAPT G2 HDMS (Waters, Milford, MA, United States).

Tenuazonic acid (compound **1**): ^1H and ^{13}C NMR data – see **Supplementary Table S1**; HRESIMS *m/z*: $[M + H]^+$; calculated for $C_{10}H_{16}NO_3$ 198.1130, result was 198.1127.

qRT-PCR Analysis

Magnaporthe oryzae APU10-199A and APU10-199A_P were cultured for 7 days at 25°C in SS medium with agitation at 150 rpm. Mycelia were ground to a fine powder with a mortar and pestle. Total RNA was extracted by TRIzol Reagent (Thermo Fisher Scientific, Waltham, MA, United States), purified by PureLink RNA Mini Kit (Thermo Fisher), treated with DNase I (Thermo Fisher), and then purified by RNA Clean & Concentrator (Zymo Research, Irvine, CA, United States). cDNA was synthesized using ReverTra Ace qPCR RT Master Mix with gDNA Remover (TOYOBO, Osaka, Japan), and quantitative reverse transcription polymerase chain reaction (qRT-PCR) was performed using Brilliant III Ultra-Fast SYBR Green QPCR Master Mix (Agilent). The expression levels of the genes of interest were normalized against those of the β-tubulin gene. Sequences of primers used in this study are given in **Supplementary Table S2**.

Reinfection of Mycovirus

Virus infection was performed via hyphal anastomosis between the virus-infected original isolate APU10-199A as a donor and APU10-199A_P as described previously (Yaegashi et al., 2011). First, the APU10-199A_P was transformed with the *hph* gene as described previously (Higashiura et al., 2019). To proceed anastomosis, the donor and recipient strains were co-inoculated with 1 cm distance on a PDA plate and incubated at 25°C for 14 days. Then, several plugs picked up from the border of two colonies were subcultured four times on PDA plates containing hygromycin B (200 μg/mL) to recover the strains derived from APU10-199A_P with *hph* gene. The recovered hygromycin-resistant strains were confirmed to harbor viruses by RT-PCR by using primers specific to each virus (for sequences of primers see **Supplementary Table S2**).

RNA-Sequencing Analysis

Each *M. oryzae* strain was cultured for 5 days at 25°C in SS medium with agitation at 150 rpm. Total RNA was extracted and purified as described above. Novogene (Beijing, China) supported library preparation, sequencing, and partial data analysis. The reads were mapped to reference genomes of *M. oryzae* 70-15 (GCA_000002495.2), and the read count per gene was performed by CLC Genomics Workbench (QIAGEN, Hilden, Germany).

Data Availability

The datasets generated for this study can be found in the DDBJ DRA under accession number SSUB014300.

RESULTS

Mycoviruses Affected Tenuazonic Acid Production

First, we compared the SM profiles of APU10-199A with those of APU10-199A_P, the strain lacking the totivirus and chrysovirus. Because fungal secondary metabolism is influenced by nutrient regimes and physical parameters (Bode et al., 2002), we cultured *M. oryzae* in three different media: SS, PDB, and IPN (for composition, see section "Materials and Methods") with agitation at two different rates (40 and 150 rpm). As a result, we found three major peaks in the culture from APU10-199A_P, which were hardly detectable in APU10-199A when cultured at 40 rpm (**Figure 1**). When cultured in SS medium at 150 rpm, the production of compound **1** was observed in the culture of APU10-199A but not in that of APU10-199A_P. Metabolite analysis was not performed in PDB and IPN at 150 rpm due to their slow growth. These data showed that the production of compounds was affected by the mycoviruses. Hereinafter we focus on the virus-induced production of **1**.

To identify compound **1**, we cultured APU10-199A in SS medium (1.2 L) with agitation at 150 rpm, and isolated 6.0 mg of **1** from the culture supernatant. The molecular formula of **1** was determined by HRESIMS to be $C_{10}H_{15}NO_3$ (**Supplementary Figure S1**). On the basis of NMR analysis (**Supplementary Table S1**), we assigned the planar structure of **1** as TeA (**Figure 2A**). Finally, we identified **1** as TeA because the chemical shifts of **1** were in good agreement with the reported value (Nolte et al., 1980), and **1** was coeluted with the TeA standard in HPLC (**Figure 2B**). TeA is a mycotoxin reported from several filamentous fungi (Rosett et al., 1957), such as *Alternaria* and *Magnaporthe* species. TeA inhibits protein synthesis in mammalian cells by preventing peptide bond formation (Carrasco and Vazquez, 1973).

Mycoviruses Affected Expression of Biosynthetic and Regulator Genes for TeA

It has been reported that TeA is biosynthesized by a non-ribosomal peptide synthetase (NRPS) and PKS hybrid enzyme, TeA synthetase 1 (TAS1) in *M. oryzae* (Yun et al., 2015). The expression of *TAS1* is regulated by a $Zn(II)_2$-Cys_6-type transcription factor, TAS2 (Yun et al., 2017). To analyze the influence of the mycovirus(es) on the transcription of *TAS1* and *TAS2*, we determined the expression levels of these genes in APU10-199A and APU10-199A_P by qRT-PCR. The expression levels of both *TAS1* and *TAS2* were higher in APU10-199A than those in APU10-199A_P (**Figure 3**). These data suggested that a mycovirus enhances TeA production in *M. oryzae* by upregulating the transcription factor gene *TAS2*. Yun et al. (2015) also reported that 1% DMSO addition to culture induces TeA production in *M. oryzae*. Under our conditions, however, DMSO addition did not induce TeA production or enhance expression of *TAS1* and *TAS2* in APU10-199A or APU10-199A_P (**Supplementary Figure S2** and **Figure 3**).

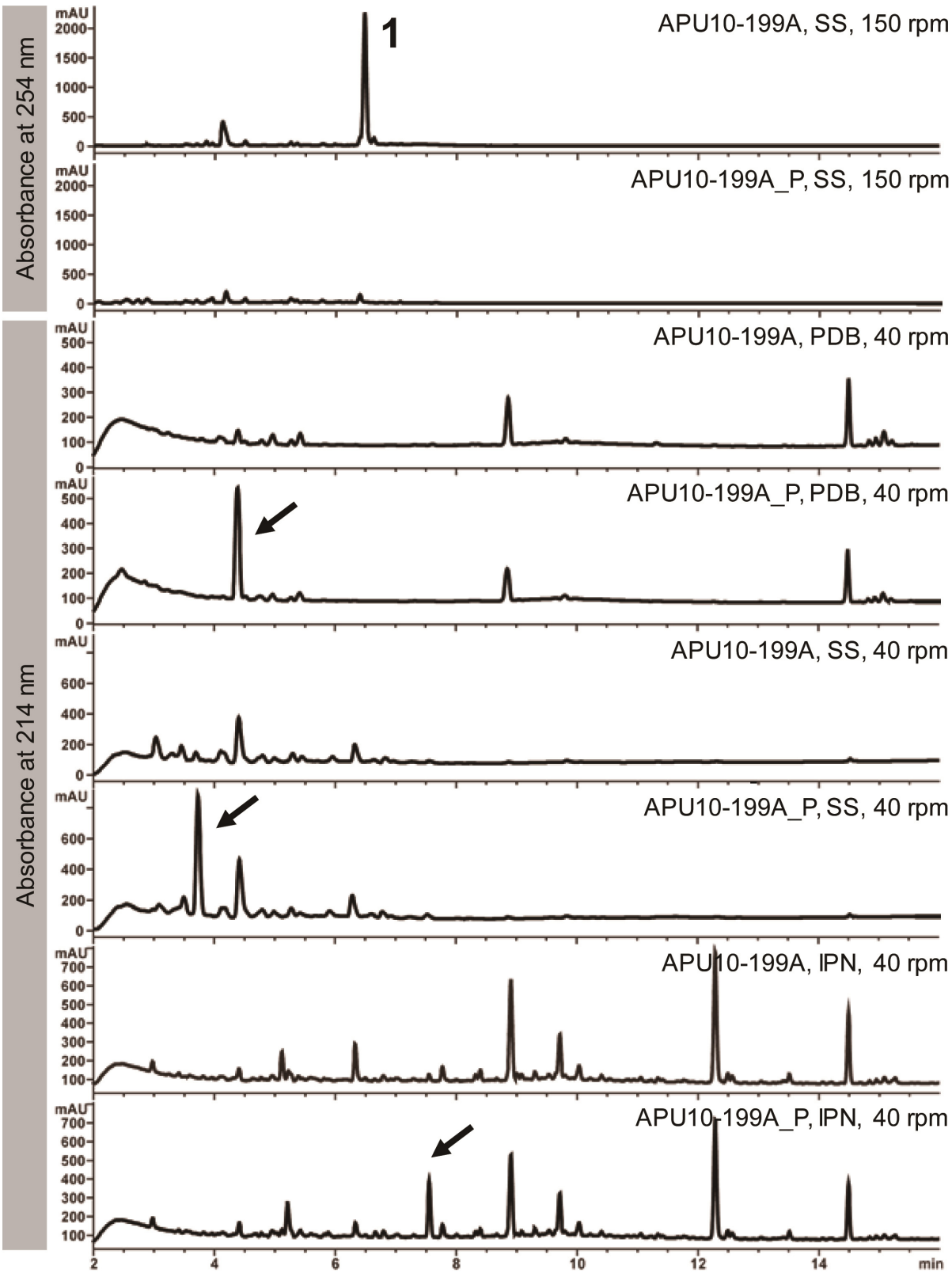

FIGURE 1 | Secondary metabolite profiles of APU10-199A and APU10-199A_P. Each strain was cultured in three different media – soy sauce-sucrose (SS) medium, potato dextrose broth (PDB), and lPN medium – with agitation at two different rates (40 and 150 rpm). Production levels of the compounds shown by the arrows were higher in APU10-199A_P than in APU10-199A. These data show a representative profile from three independent culture experiments.

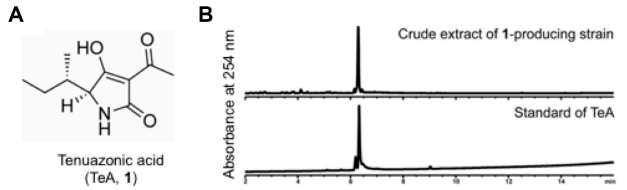

FIGURE 2 | (A) Chemical structure of tenuazonic acid (TeA). For spectroscopic data, see the **Supplementary Data**. **(B)** HPLC chart of the extract of the TeA-producing strain and TeA standard.

Totivirus-Induced TeA Production Proved by Reinfection Experiment

The APU10-199A_P strain that did not produce TeA lacks the totivirus and chrysovirus. The next question is which mycovirus induces TeA production. To identify the TeA inducer, we established several re-infected virus strains derived from APU10-199A_P with the *hph* gene introduced as a selective marker through the hyphal anastomosis method (see section "Materials and Methods"). As a result, six reinfected (RI) strains (RI-1-60, RI-4-49, RI-4-51, RI-4-53, RI-4-59, and RI-4-61) were obtained (**Supplementary Figure S3**). The virus infection profiles of RI strains were checked by RT-PCR (**Figure 4**) and agarose gel electrophoresis of the dsRNA (**Supplementary Figure S4**). RI-4-49 and RI-4-53, infected with all three viruses, produced TeA (**Figure 4**; for the HPLC chart, see **Supplementary Figure S5**), which indicated that the introduction of the *hph* gene and reinfection manipulation do not affect the TeA production. RI-4-51 and RI-4-59, infected with the totivirus and the partitivirus, also produced TeA, which indicated that TeA production was not dependent on the chrysovirus. RI-4-61, infected with the

FIGURE 4 | Virus infection profiles and tenuazonic acid production of the strains obtained by virus reinfection experiments. The presence of the totivirus, chrysovirus, and partitivirus was confirmed by RT-PCR using primers specific to each virus (for sequences of primers see **Supplementary Table S2**). Tenuazonic acid (TeA) productivity in each strain is shown by + or –.

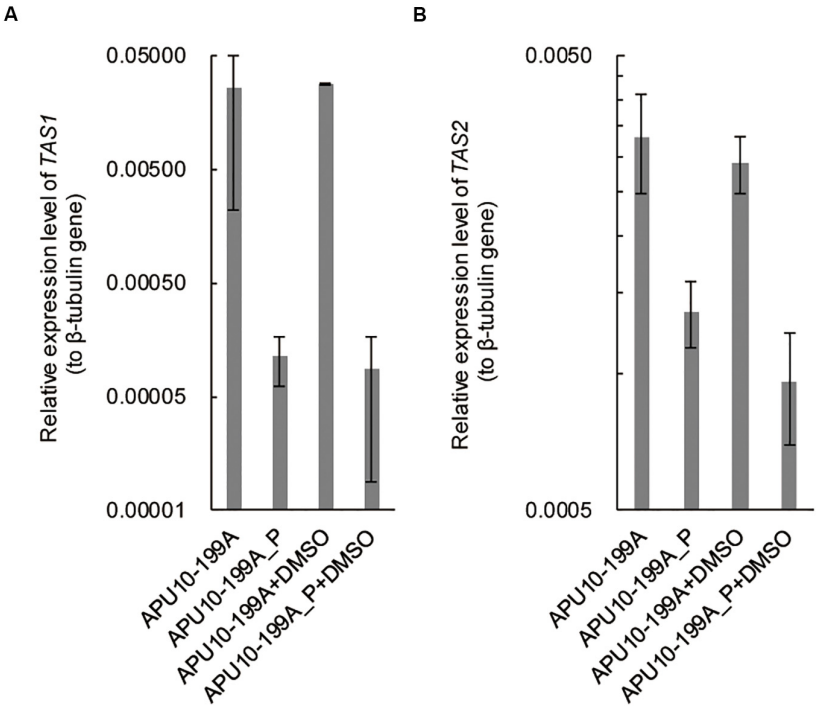

FIGURE 3 | Expression levels of *TAS1* and *TAS2* in APU10-199A and APU10-199A_P. Each strain was cultured in SS medium, and the expression levels of **(A)** *TAS1* and **(B)** *TAS2* were determined by qRT-PCR. This experiment was performed on three independent biological replicates each containing three technical replicates. Error bars represent the standard deviation.

chrysovirus and the partitivirus, did not produce TeA under our conditions. Thus, we concluded that TeA production depended on infection with a totivirus.

Mycoviruses Affected Multiple SM Core Genes

For comprehensive understanding of the viral effects on secondary metabolism of *M. oryzae*, we performed RNA sequencing for the APU10-199A, APU10-199A_P, RI-4-49, and RI-4-51 strains. RI-4-49 is reinfected with both the totivirus and chrysovirus, while RI-4-51 is reinfected with only the former. The genome sequence of *M. oryzae* 70-15 (GCA_000002495.2) was searched for genes responsible for formation of core structures of SMs (hereinafter referred to as "core genes") by antiSMASH 5.0 (Blin et al., 2019). Accordingly, 7 terpene synthases, 16 NRPSs, 21 PKSs, and 7 PKS-NRPS hybrid enzymes were found to be encoded in the genome, and the gene expression levels were determined from RNA-sequencing analysis (**Table 1**). First, we compared the expression levels of the 51 core genes between APU10-199A and APU10-199A_P to evaluate the influence of the totivirus and/or chrysovirus on the secondary metabolism of *M. oryzae*. We filtered the core genes differently expressed in APU10-199A and APU10-199A_P under the following conditions: the ratio of transcripts per million (TPM) > 10 or <0.1, and TPM > 1/10 mean TPM (>7.66). Three core genes, MGG_10671, MGG_14767, and *TAS1* (a terpene synthase plus two NRPSs) were differently expressed between APU10-199A and APU10-199A_P (**Table 1**). Whereas *TAS1* was highly expressed in APU10-199A, the other core genes, MGG_10671 and MGG_14767, were hardly expressed in APU10-199A. This suggested that the totivirus and/or chrysovirus inhibit transcription of the two core genes for secondary metabolism. This view was supported by the data that RI strains (RI-4-49 or RI-4-51) reinfected with both the totivirus and chrysovirus or only the totivirus showed lowered expressions of MGG_10671 and MGG_14767. In these RI strains, *TAS1* was as highly expressed as it was in APU10-199A. This result further confirmed that TeA was produced in a manner dependent on totivirus infection. Furthermore, the transcriptome data revealed that the expression level of *TAS2* in the RI strains was higher than that in APU10-199A_P (**Table 1**). Thus, we concluded that the totivirus enhances TeA production in *M. oryzae* by upregulating the transcription of the gene encoding TeA synthetase.

DISCUSSION

Fungi have the potential to produce various SMs with biological activities. While fungal SMs are resources for potent therapeutic agents, some fungal SMs are toxic and harmful to humans or animals. Thus, control of fungal secondary metabolism is needed for improvement of public health. To date, some knowledge on control of fungal SM production by mycoviruses has accumulated. Some mycoviruses upregulate (Okada et al., 2018; Nerva et al., 2019) or downregulate (Schmidt et al., 1986; Chu et al., 2002) mycotoxin production. However, these studies regarding SM production were based on comparison between the strains with and without viral infection. In the present study, we used reinfected strains to prove that mycovirus infection affects SM production in *M. oryzae*. Furthermore, the effect of mycovirus on biosynthetic gene expression was observed in fungi, probably for the first time. These achievements pave the way for more extensive screening for fungal bioactive compounds by taking advantage of mycovirus.

The totivirus has a monosegmented dsRNA genome (5.2 kb) encompassing two open reading frames (ORFs), each of which encodes a coat protein and a RdRp. Although the detailed molecular mechanism remains unclear, either or both of the two ORFs are possibly responsible for TeA induction. Further research is needed to determine the exact factor encoded in the genome of the totivirus that induces TeA production. The direct target that the viral factor interacts with and the signaling pathway are also still unknown. Elucidation of the signaling pathway that triggers *TAS2* activation is the main goal of our follow-up studies. In addition to induction of TeA, production of several SMs was likely to be suppressed by the chrysovirus or totivirus (**Figure 1**). Notably, different culture conditions, such as media and agitation speed, led to different mycovirus effects on SM production. This may indicate that viral effects are exerted on multiple aspects of cellular response. In this study, we could not obtain the strain that carries totivirus alone. The possibility that combination of totivirus and partitivirus or chrysovirus is required for the TeA induction cannot be ruled out at the moment. Further research is needed to clarify this question.

TeA is one of the compounds that have been identified from fungal cultures in early studies, and a variety of biological activities, including antibacterial, antiviral, and phytotoxic activities, have been reported (Miller et al., 1963; Gitterman, 1965; Chen et al., 2010). In a study of *Alternaria* species, it was proposed that TeA plays a role in fungal infection as a virulence factor (Kang et al., 2017). So far, the function of TeA in the *M. oryzae* infection process remains unclear despite its bioactivity. Yun et al. (2015) recently discovered the TeA biosynthetic gene in *M. oryzae* and reported two TeA-inducing conditions, 1% DMSO addition and deletion of an osmo-sensory MAPK-encoding gene, *OSM1*. However, there are only a few reports on TeA production in *M. oryzae,* suggesting that the TeA-producing strain is rare or that TeA is produced under limited conditions. This is because our finding that totivirus-triggered TeA production in the fungus is of great value for investigating rarely expressed fungal SMs. Viral effects induced by an endogenous genetic factor without any chemical addition or gene manipulation would allow us to activate unstudied and silent fungal secondary metabolism. Development of a viral transfer method is focus of future work.

Comprehensive sequencing of fungal genomes has revealed that fungi have many more gene clusters for SMs than the quantity estimated from the number of known SMs (Khaldi et al., 2010; Sanchez et al., 2012). However, only a few of the gene clusters are expressed under normal laboratory conditions (Brakhage and Schroeckh, 2011). In our case, out of 51 core genes encoded in the genome of *M. oryzae*, 17 genes (33.3%) were expressed in either APU10-199A or APU10-199A_P with a threshold of TPM: mean TPM × 0.1 (**Table 1**). Because of the potential of fungal cryptic gene clusters as a resource for new bioactive compounds, several strategies

TABLE 1 | Expression levels (TPM) of core genes for secondary metabolism determined by RNA-sequencing analysis.

Type	Name	Description	APU10-199A	APU10-199A_P	Ratio (199A/199A_P)	RI-4-49 (TCP)	RI-4-51 (TP)
TS	MGG_00758		**67.7**	**76.6**	0.884	**55.8**	**67.6**
	MGG_01949		0	1.11	0	0	0
	MGG_03432		0	0.0653	0	0	0.109
	MGG_03833		0.161	0.0576	2.80	0.106	0
	MGG_09239		**89.4**	**54.6**	1.64	**92.8**	**75.2**
	MGG_10671		0	**13.9**	0	0	2.01
	MGG_11702		**84.8**	**73.0**	1.16	**72.8**	**64.7**
NRPS	MGG_00022		0.0107	0.926	0.0116	0.0317	0.0670
	MGG_00385		**96.5**	**165**	0.585	**72.2**	**112**
	MGG_02351		0.197	0.176	1.12	0.187	0.420
	MGG_02611		**89.0**	**118**	0.754	**93.3**	**90.7**
	MGG_03290		**27.2**	**50.6**	0.538	**26.2**	**38.0**
	MGG_03401		**52.1**	**43.9**	1.19	**38.6**	**41.8**
	MGG_03422		0	0	-	0.0379	0
	MGG_05491		0.0407	0.261	0.156	0	0
	MGG_07803 (*TAS1*)	TeA synthetase	**163**	0.134	1220	**47.9**	**107**
	MGG_07858		0	0.0292	0	0	0
	MGG_12175	ferricrocin synthetase *SSM1* (Hof et al., 2007)	**118**	**97.4**	1.21	**73.5**	**73.7**
	MGG_14767		0.0582	**270**	0.000216	1.31	3.93
	MGG_14967		0.200	0.211	0.948	0.188	0.101
	MGG_15248		**9.23**	**7.96**	1.16	**8.31**	**8.32**
	MGG_16971		2.96	2.73	1.08	4.92	4.00
	MGG_17746		0.198	7.62	0.0260	0.893	1.05
PKS	MGG_00233		0.127	3.04	0.0418	0.216	0.359
	MGG_00241		0	0	-	0.0399	0
	MGG_00428		**15.3**	**15.6**	0.981	**18.0**	**14.6**
	MGG_04775		4.80	5.53	0.868	7.40	**9.80**
	MGG_05589		0.790	0.144	5.49	0.734	0.242
	MGG_06254		**11.5**	**11.9**	0.966	**11.8**	**13.2**
	MGG_07219	melanin synthase *ALB1* (Chumley and Valent, 1990)	0.234	0.125	1.87	0.116	0.0525
	MGG_08236		0.0332	0.142	0.234	0.197	0.164
	MGG_08281		0.0700	1.04	0.0673	0.0923	0.0209
	MGG_08285		**8.62**	6.18	1.39	**8.35**	**14.1**
	MGG_09645		0.0204	0	-	0	0
	MGG_10011		0.0564	2.64	0.0214	0	0.0169
	MGG_10912	pyriculol synthase *MoPKS19* (Jacob et al., 2017)	0.932	2.80	0.333	0.572	1.09
	MGG_11638		2.23	0.977	2.28	2.71	2.00
	MGG_12214		**16.7**	**14.6**	1.14	**16.0**	**13.7**
	MGG_12613		2.03	0.948	2.14	1.40	1.25
	MGG_13591		0	0.0200	0	0	0
	MGG_13767		2.35	0.174	13.5	0.843	1.07
	MGG_14831		0.0336	1.17	0.0287	0.598	0.346
	MGG_14945		0	0.0210	0	0	0
	MGG_15100		**172**	**133**	1.29	**170**	**991**
PKS-NRPS	MGG_03810		0.0306	6.02	0.00508	0.222	0.571
	MGG_09589		0.412	0.913	0.451	0.617	0.714
	MGG_12447	avirulence gene *ACE1* (Collemare et al., 2008)	0	0.392	0	0	0.0193
	MGG_14897		1.02	1.32	0.773	0.961	1.50
	MGG_14943		0.688	4.86	0.142	0.735	2.58
	MGG_15097		0	1.17	0	0	0
	MGG_15272		2.47	1.50	1.65	3.50	**9.08**
Transcription factor	MGG_07800 (*TAS2*)	transcription factor for TeA biosynthesis	**30.3**	**8.04**	3.77	**30.7**	**41.1**

The levels over mean TPM × 0.1 (7.66) are shown in bold.

have been employed to express cryptic genes. One of the major strategies is co-culturing of a fungus and another microorganism. For example, Schroeckh et al. (2009) revealed that interaction between *Aspergillus nidulans* and a streptomycete induces production of several fungal SMs through activation of the orselinic acid biosynthetic gene cluster. Another strategy is addition of chemical elicitors. Williams et al. (2008) discovered new compounds from two fungi using DNA methyltransferase and histone deacetylase inhibitors as an elicitor of secondary metabolism. The other strategy that increasingly draws attention from chemists who are familiar with fungal genetic manipulation is a heterologous expression system for fungal SM gene(s) (Kennedy et al., 1999; Heneghan et al., 2010; Itoh et al., 2010). Although these are powerful tools for discovery of new natural products and elucidation of biosynthetic pathways, there is no versatile method that can be applied to any gene cluster for SMs. Thus, it is important to establish a variety of alternatives for activating silent biosynthetic gene clusters. In this report, we discovered activation of the TeA biosynthetic gene by a totivirus. Some mycoviruses can be transmitted into fungal cells by hyphal anastomosis, protoplast fusion (Lee et al., 2011), or electroporation (Moleleki et al., 2003). This underscores the potential of mycoviruses as an inducer of fungal secondary metabolism.

DATA AVAILABILITY STATEMENT

The datasets generated for this study can be found in the NCBI or DDBJ DRA under accession number PRJDB9423.

AUTHOR CONTRIBUTIONS

DH conceived, supervised this study, and wrote the manuscript. SU co-designed and co-supervised this study. AN carried out the analyses and wrote the manuscript. RS performed NMR analysis. SF and HM were involved in preparation of the experimental materials. All authors read and approved the final version of the manuscript.

FUNDING

This work was supported by a grant from the Institute for Fermentation, Osaka, and the Japan Society for the Promotion of Science, KAKENHI grant 18H05999.

ACKNOWLEDGMENTS

We thank Professor Teigo Asai, The University of Tokyo, for helpful discussions.

SUPPLEMENTARY MATERIAL

The Supplementary Material for this article can be found online at: https://www.frontiersin.org/articles/10.3389/fmicb.2020.01641/full#supplementary-material

REFERENCES

Bennett, J. W., and Klich, M. (2003). Mycotoxins. *Clin. Microbiol. Rev.* 16, 497–516.

Bérdy, J. (2005). Bioactive microbial metabolites. *J. Antibiot.* 58, 1–26.

Blin, K., Shaw, S., Steinke, K., Villebro, R., Ziemert, N., Lee, S. Y., et al. (2019). antiSMASH 5.0: updates to the secondary metabolite genome mining pipeline. *Nucleic Acids Res.* 47, W81–W87.

Bode, H. B., Bethe, B., Höfs, R., and Zeeck, A. (2002). Big effects from small changes: possible ways to explore nature's chemical diversity. *Chembiochem* 3, 619–627.

Brakhage, A. A., and Schroeckh, V. (2011). Fungal secondary metabolites – Strategies to activate silent gene clusters. *Fungal Genet Biol.* 48, 15–22. doi: 10.1016/j.fgb.2010.04.004

Carrasco, L., and Vazquez, D. (1973). Differences in eukaryotic ribosomes detected by the selective action of an antibiotic. *Biochim. Biophys. Acta* 319, 209–215. doi: 10.1016/0005-2787(73)90011-7

Chen, S., Yin, C., Qiang, S., Zhou, F., and Dai, X. (2010). Chloroplastic oxidative burst induced by tenuazonic acid, a natural photosynthesis inhibitor, triggers cell necrosis in *Eupatorium adenophorum* Spreng. *Biochim. Biophys. Acta* 1797, 391–405. doi: 10.1016/j.bbabio.2009.12.007

Chu, Y. M., Jeon, J. J., Yea, S. J., Kim, Y. H., Yun, S. H., Lee, Y. W., et al. (2002). Double-stranded RNA mycovirus from *Fusarium graminearum*. *Appl. Environ. Microbiol.* 68, 2529–2534. doi: 10.1128/aem.68.5.2529-2534.2002

Chumley, F., and Valent, B. (1990). Genetic analysis of melanin-deficient, nonpathogenic mutants of *Magnaporthe grisea*. *Mol. Plant Microb. Interact.* 3, 135–143.

Collemare, J., Pianfetti, M., Houlle, A. E., Morin, D., Camborde, L., Gagey, M. J., et al. (2008). *Magnaporthe grisea* avirulence gene ACE1 belongs to an infection-specific gene cluster involved in secondary metabolism. *New Phytol.* 179, 196–208. doi: 10.1111/j.1469-8137.2008.02459.x

Ghabrial, S. A., Castón, J. R., and Jiang, D. (2015). 50-plus years of fungal viruses. *Virology* 479–80, 356–368. doi: 10.1016/j.virol.2015.02.034

Gitterman, C. O. (1965). Antitumor, cytotoxic, and antibacterial activities of tenuazonic acid and congeneric tetramic acids. *J. Med. Chem.* 8, 483–486. doi: 10.1021/jm00328a015

Heneghan, M. N., Yakasai, A. A., Halo, L. M., Song, Z., Bailey, A. M., Simpson, T. J., et al. (2010). First heterologous reconstruction of a complete functional fungal biosynthetic multigene cluster. *Chembiochem* 11, 1508–1512. doi: 10.1002/cbic.201000259

Higashiura, T., Katoh, Y., Urayama, S., Nibert, M., and Suzuki, N. (2019). *Magnaporthe oryzae* chrysovirus 1 strain D confers growth inhibition to the host fungus and exhibits multiform viral structural proteins. *Virology* 535, 241–254. doi: 10.1016/j.virol.2019.07.014

Hof, C., Eisfeld, K., Welzel, K., Antelo, L., Foster, A. J., and ANke, H. (2007). Ferricrocin synthesis in *Magnaporthe grisea* and its role in pathogenicity in rice. *Mol. Plant Pathol.* 8, 163–172. doi: 10.1111/j.1364-3703.2007.00380.x

Itoh, T., Tokunaga, K., Matsuda, Y., Fujii, I., Abe, I., Ebizuka, Y., et al. (2010). Reconstitution of a fungal meroterpenoid biosynthesis reveals the involvement of a novel family of *Terpene cyclases*. *Nat. Chem.* 2, 858–864. doi: 10.1038/nchem.764

Jacob, S., Grötsch, T., Foster, A. J., Schüffler, A., Rieger, P. H., Sandjo, L. P., et al. (2017). Unravelling the biosynthesis of pyriculol in the rice blast fungus *Magnaporthe oryzae*. *Microbiology* 163, 541–553. doi: 10.1099/mic.0.000396

Kang, Y., Feng, H., Zhang, J., Chen, S., Valverde, B. E., and Qiang, S. (2017). TeA is a key virulence factor for *Alternaria alternata* (Fr.) Keissler infection of its host. *Plant Physiol. Biochem.* 115, 73–82. doi: 10.1016/j.plaphy.2017.03.002

Kennedy, J., Auclair, K., Kendrew, S. G., Park, C., Vederas, J. C., and Hutchinson, C. R. (1999). Modulation of polyketide synthase activity by accessory proteins

during lovastatin biosynthesis. *Science* 284, 1368–1372. doi: 10.1126/science.284.5418.1368

Khaldi, N., Seifuddin, F. T., Turner, G., Haft, D., Nierman, W. C., Wolfe, K. H., et al. (2010). SMURF: genomic mapping of fungal secondary metabolite clusters. *Fungal Genet. Biol.* 47, 736–741. doi: 10.1016/j.fgb.2010.06.003

Lee, K.-M., Yu, J., Son, M., Lee, Y. W., and Kim, K. H. (2011). Transmission of *Fusarium boothii* mycovirus via protoplast fusion causes hypovirulence in other phytopathogenic fungi. *PLoS One* 6:e21629. doi: 10.1371/journal.pone.0021629

Miller, F. A., Rightsel, W. A., Sloan, B. J., Ehrlich, J., French, J. C., Bartz, Q. R., et al. (1963). Antiviral activity of tenuazonic acid. *Nature* 200, 1338–1339. doi: 10.1038/2001338a0

Moleleki, N., van Heerden, S. W., Wingfield, M. J., Wingfield, B. D., and Preisig, O. (2003). Transfection of *Diaporthe perjuncta* with diaporthe RNA virus. *Appl. Environ. Microbiol.* 69, 3952–3956. doi: 10.1128/aem.69.7.3952-3956.2003

Nerva, L., Chitarra, W., Siciliano, I., Gaiotti, F., Ciuffo, M., Forgia, M., et al. (2019). Mycoviruses mediate mycotoxin regulation in *Aspergillus ochraceus*. *Environ. Microbiol.* 21, 1957–1968. doi: 10.1111/1462-2920.14436

Nolte, M. J., Steyn, P. S., and Wessels, P. L. (1980). Structural investigations of 3-acylpyrrolidine-2,4-diones by nuclear magnetic resonance spectroscopy and X-ray crystallography. *J. Chem. Soc. Perkin. Trans.* 10, 1057–1065.

Nukina, M. (1999). The blast disease fungi and their metabolic products. *J. Pesticide Sci.* 24, 293–298.

Nuss, D. L. (2005). Hypovirulence: mycoviruses at the fungal–plant interface. *Nat. Rev. Microbiol.* 3, 632–642. doi: 10.1038/nrmicro1206

Okada, R., Ichinose, S., Takeshita, K., Urayama, S. I., Fukuhara, T., Komatsu, K., et al. (2018). Molecular characterization of a novel mycovirus in *Alternaria alternata* manifesting two-sided effects: down-regulation of host growth and up-reguration of host plant pathogenicity. *Virology* 519, 23–32. doi: 10.1016/j.virol.2018.03.027

Rosett, T., Sankhala, R. H., Stickings, C. E., Taylor, M. E. U., and Thomas, R. (1957). Biochemistry of microorganisms. CIII. Metabolites of *Alternaria tenuis* auct.: culture filtrate products. *Biochem. J.* 67, 390–400. doi: 10.1042/bj0670390

Sanchez, J. F., Somoza, A. D., Keller, N. P., and Wang, C. C. C. (2012). Advances in *Aspergillus* secondary metabolite research in the post-genomic era. *Nat. Prod. Rep.* 29, 351–371.

Schmidt, F. R., Lemke, P. A., and Esser, K. (1986). Viral influences on aflatoxin formation by *Aspergillus flavus*. *Appl. Microbiol. Biotechnol.* 24, 248–252. doi: 10.1007/bf00261546

Schroeckh, V., Scherlach, K., Nützmann, H. W., Shelest, E., Schmidt-Heck, W., Schuemann, J., et al. (2009). Intimate bacterial–fungal interaction triggers biosynthesis of archetypal polyketides in *Aspergillus nidulans*. *Proc. Natl. Acad. Sci. U.S.A.* 106, 14558–14563. doi: 10.1073/pnas.0901870106

Sugui, J. A., Pardo, J., Chang, Y. C., Zarember, K. A., Nardone, G., Galvez, E. M., et al. (2007). Gliotoxin is a virulence factor of *Aspergillus fumigatus*: gliP deletion attenuates virulence in mice immunosuppressed with hydrocortisone. *Eukaryot. Cell* 6, 1562–1569. doi: 10.1128/ec.00141-07

Williams, R. B., Henrikson, J. C., Hoover, A. R., Liu, F., Selvaraj, J. N., Liu, L., et al. (2008). Epigenetic remodeling of fungal secondary metabolome. *Organ. Biomol. Chem.* 6, 1895–1897.

Yaegashi, H., Sawahata, T., Ito, T., and Kanematsu, K. (2011). A novel colony-print immunoassay reveals differential patterns of distribution and horizontal transmission of four unrelated mycoviruses in *Rosellinia necatrix*. *Virology* 409, 280–289. doi: 10.1016/j.virol.2010.10.014

Yun, C.-S., Motoyama, T., and Osada, H. (2015). Biosynthesis of the mycotoxin tenuazonic acid by a fungal NRPS-PKS hybrid enzyme. *Nat. Commun.* 6:8758.

Yun, C.-S., Motoyama, T., and Osada, H. (2017). Regulatory mechanism of mycotoxin tenuazonic acid production in *Pyricularia oryzae*. *ACS Chem. Biol.* 12, 2270–2274. doi: 10.1021/acschembio.7b00353

Conflict of Interest: The authors declare that the research was conducted in the absence of any commercial or financial relationships that could be construed as a potential conflict of interest.

frontiers in Microbiology

REVIEW
published: 07 October 2020
doi: 10.3389/fmicb.2020.574736

Protein Acetylation/Deacetylation: A Potential Strategy for Fungal Infection Control

*Junzhu Chen[1], Qiong Liu[1], Lingbing Zeng[2] and Xiaotian Huang[1]**

[1] Department of Medical Microbiology, School of Medicine, Nanchang University, Nanchang, China, [2] The First Affiliated Hospital of Nanchang University, Nanchang, China

Protein acetylation is a universal post-translational modification that fine-tunes the major cellular processes of many life forms. Although the mechanisms regulating protein acetylation have not been fully elucidated, this modification is finely tuned by both enzymatic and non-enzymatic mechanisms. Protein deacetylation is the reverse process of acetylation and is mediated by deacetylases. Together, protein acetylation and deacetylation constitute a reversible regulatory protein acetylation network. The recent application of mass spectrometry-based proteomics has led to accumulating evidence indicating that reversible protein acetylation may be related to fungal virulence because a substantial amount of virulence factors are acetylated. Additionally, the relationship between protein acetylation/deacetylation and fungal drug resistance has also been proven and the potential of deacetylase inhibitors as an anti-infective treatment has attracted attention. This review aimed to summarize the research progress in understanding fungal protein acetylation/deacetylation and discuss the mechanism of its mediation in fungal virulence, providing novel targets for the treatment of fungal infection.

Keywords: protein acetylation, protein deacetylation, fungal infection, virulence, KDAC inhibitors

OPEN ACCESS

Edited by:
Laure Ries,
University of São Paulo, Brazil

Reviewed by:
Ingo Bauer,
Innsbruck Medical University, Austria
Özgür Bayram,
Maynooth University, Ireland

****Correspondence:***
Xiaotian Huang
xthuang@ncu.edu.cn

Specialty section:
This article was submitted to Fungi and Their Interactions, a section of the journal Frontiers in Microbiology

Received: *21 June 2020*
Accepted: *17 September 2020*
Published: *07 October 2020*

Citation:
Chen J, Liu Q, Zeng L and Huang X (2020) Protein Acetylation/Deacetylation: A Potential Strategy for Fungal Infection Control. Front. Microbiol. 11:574736. doi: 10.3389/fmicb.2020.574736

INTRODUCTION

The post-translational modification (PTM) of proteins is a major regulatory mechanism in all life forms. PTM refers to the chemical modification of amino acid residues in proteins by the addition of different chemical groups, which confer new properties on modified proteins, including changes in enzyme activity, subcellular localization, interaction partners, protein stability, and DNA binding (Mann and Jensen, 2003; Verdin and Ott, 2015). Currently, nearly 200 different types of PTMs have been identified, including acetylation, phosphorylation, alkylation, methylation, ubiquitination, and glycosylation (Garavelli, 2004). Protein acetylation, which refers to the covalent binding of an acetyl group to an amino acid residue of a protein, is the most well-known PTM besides phosphorylation (Ali et al., 2018). The most widely studied protein acetylation is that of lysine residues, although acetylation of serine and threonine side chains has also been reported (Tang and Yu, 2019). Thus, unless otherwise specified, in this review, acetylation refers only to that of lysine residues.

The acetyl group can be attached to the α-amino group on the N-terminal end of the protein or the ε-amino group on the side chain of lysine residues; therefore, acetylation can be classified as N^{α} -acetylation or N^{ε} -acetylation (Hentchel and Escalante-Semerena, 2015). At present, two mechanisms that can regulate acetylation have been identified: one mechanism is mainly regulated

by lysine acetyltransferases (KATs), while the other mechanism is non-enzymatic, which can directly introduce lysine residues through the non-enzymatic reaction of acetyl phosphate or acetyl-CoA (Wagner and Hirschey, 2014; Lee et al., 2018). In prokaryotes, acetyl phosphate can modulate bacterial virulence through non-enzymatic acetylation (Ren et al., 2019). The main contributor of non-enzymatic acetylation in eukaryotes may be acetyl-CoA in the mitochondria; however, its role still needs to be studied further and is not the focus of this review (Weinert et al., 2014).

Protein deacetylation is the reverse reaction of acetylation that is catalyzed by lysine deacetylases (KDACs), which consist of two protein families, namely, classical Zn^{2+}-dependent histone deacetylases (HDACs) and NAD^{+}-dependent sirtuins (**Table 1**; Narita et al., 2019). Although acetylation occurs in an enzymatic or non-enzymatic manner, removal of the acetyl group requires KDACs. KDACs play a vital role in numerous biological processes by allowing chromatin condensation, thereby inhibiting transcription (Rupert et al., 2016). Many eukaryotic KATs and KDACs were initially identified as histone-specific enzymes and were historically named histone acetyltransferases and HDACs. In this review, we uniformly used the more specific terms KATs and KDACs.

A substantial amount of evidence showed that acetylation and deacetylation play essential roles in modifying the chromosome structure and regulating gene expression (Nicolas et al., 2018). Acetylation and deacetylation can also modify many key cellular processes relevant to physiology and disease, such as enzymatic activity, signal transduction, DNA damage repair, cell division, metabolism, autophagy, protein stability, and protein localization and interactions (Eckschlager et al., 2017; Narita et al., 2019). Hence, protein acetylation and deacetylation can interfere with every step in a regulatory process, thereby altering cell fate and function.

Research on acetylation/deacetylation is currently focused on metabolism, tumor treatment, and other aspects, while there is less research on microbial acetylation, especially regarding microbial virulence. The development of proteomics has resulted in accumulating evidence that protein acetylation/deacetylation is related to microbial virulence and drug resistance (Hnisz et al., 2010; Li et al., 2017; Brandão et al., 2018; Ren et al., 2019). The role of acetylation in regulating bacterial virulence was summarized in a review conducted by Ren et al. (2017). However, the relationship between the specific mechanism of acetylation and fungal pathogenicity remains unclear.

Fungal pathogens have a negative impact on the global economy, food security, and human and animal welfare, not only because they have caused pestilence and famine but also because of the difficulty in treating fungal infectious diseases as well as increased resistance to antifungal drugs (Fisher et al., 2016; Motaung et al., 2017). In animals and plants, an unprecedented number of fungal and fungal-like diseases have led to some of the most serious deaths and extinctions in wild species (Fisher et al., 2016). Therefore, the virulence of pathogenic fungi must be explored. This review discusses how acetylation/deacetylation regulates fungal virulence. First, we discussed the widespread distribution of this modification in the fungal community and listed some virulence-related acetylated proteins present in fungi. Then, we highlighted recent examples to illustrate the unexpected role of acetylation/deacetylation in fungal virulence to suggest novel targets for the development of anti-infective drugs and the treatment of infectious diseases.

Acetylation/Deacetylation is Widespread in Fungi

Protein acetylation is a conserved evolutionary modification that occurs in eukaryotic and prokaryotic proteins and was first discovered in histones (Phillips, 1963; Allfrey et al., 1964). Reversible protein acetylation was studied in the context of the histones until the late 1990s. Recent advancements in high-resolution mass spectrometry and high-affinity purification technology for acetylated lysine peptides revealed that protein acetylation/deacetylation is not restricted to histones, which resulted in detailed studies of the acetylated proteome and its function (Schilling et al., 2019).

Previous studies and database searches revealed that protein acetylation is widespread in fungi. Zhou et al. detected 477 acetylated proteins (5.28%) among all 9,038 proteins of *Candida albicans*, which was the first study on acetylome in human pathogenic fungi, providing an important initiating point for further study of the functional analysis of acetylated proteins in such fungal pathogens (Zhou X. et al., 2016). The comparative analysis of fungal acetylomes plays an important role in determining the essential role of acetylation in the virulence of human fungal pathogens (Li et al., 2019). Significant differences in the number and sites of acetylated proteins were found according to the stage of human fungal pathogen growth. For example, 2,335 proteins in the mycelium growing stage were identified to be acetylated in *Trichophyton rubrum*, which was >10 times higher than that in the conidia stage, and may be explained by conidia being in a quiescent state with low metabolic activity (Xu et al., 2018). Further evidence of protein acetylation in human fungal pathogens was observed in *Histoplasma capsulatum*, *Cryptococcus neoformans*, and *Aspergillus fumigatus* (Xie et al., 2016; Brandão et al., 2018; Lin et al., 2020).

In plant pathogenic fungi, Yang et al. identified 1,313 high-confidence acetylation sites in 727 acetylated proteins in *Aspergillus flavus*, while 577 acetylated sites were reported in 364 different proteins in *Fusarium graminearum* (Zhou S. et al., 2016; Yang et al., 2019). Several published studies have described the acetylome of different fungal species, including plant pathogenic fungi *Phytophthora sojae*, *Botrytis cinerea*, and *Magnaporthe oryzae*; fungal insect pathogens, such as *Beauveria bassiana* and *Metarhizium anisopliae*; and nonpathogenic fungi species, such as *Saccharomyces cerevisiae* and *Yarrowia lipolytica*; which are considered as important resources to explore the physiological role of this modification in eukaryotes (Henriksen et al., 2012; Mukherjee et al., 2012; Li et al., 2016; Lv et al., 2016; Wang et al., 2017; Cai et al., 2018c; Liang et al., 2018).

Interestingly, most of the identified acetylated proteins were involved in the regulation of glucose, lipid, and amino acid metabolism (Wang et al., 2017). Important findings regarding

TABLE 1 | Some lysine acetyltransferases (KATs) and lysine deacetylases (KDACs) in fungi.

	KATs			KDACs			References
Classes	**Gcn5 family**	**MYST family**	**Others**	**I**	**II**	**III**	
Candida albicans	Gcn5	Esa1,Sas2, Sas3	Rtt109, Hat1, Elp3, Hpa2	Rpd31,Rpd32, Hos1, Hos2	Hda1,Hos3	Sir2, Hst1, Hst2, Hst3	Garnaud et al., 2016; Kim et al., 2018
Saccharomyces cerevisiae	Gcn5	Esa1, Sas2, Sas3	Rtt109, Hat1, Elp3, Hpa2, Hpa3	Rpd3, Hos1, Hos2	Hda1, Hos3	Sir2, Hst1, Hst2, Hst3, Hst4	Garnaud et al., 2016; Kim et al., 2018
Cryptococcus neoformans	Gcn5			Rpd3, Hos1, Hos2, Cir61, Cir62	Hda1, Hos3	Sir2, Hst1, Hst2, Hst3, Hst4, Hst5	O'Meara et al., 2010; Wassano et al., 2020
Fusarium graminearum	Gcn5	Sas2, Sas3	Rtt109, Elp3	Rpd3, Hos2	Hda1, Hos3		Li et al., 2011; Kong et al., 2018
Aspergillus nidulans	GcnE	EsaA		HosA	HdaA	SirA	Tribus et al., 2005; Reyes-Dominguez et al., 2008; Soukup et al., 2012; Itoh et al., 2017; Pidroni et al., 2018
Magnaporthe oryzae	Gcn5	Sas3	Rtt109, Hat1	Hos2	Hda1		Maeda et al., 2017; Kwon et al., 2018; Dubey et al., 2019; Lee et al., 2019; Yin et al., 2019
Aspergillus fumigatus	GcnE		Rtt109	RpdA, HosA	HdaA, HosB	SirA, SirB, SirE, SirC, SirD, HstA	Graessle et al., 2000; Lee et al., 2009; Bauer et al., 2019; Lin et al., 2020; Wassano et al., 2020

The KATs and KDACs listed in table do not represent all the KATs and KDACs of the microbe.
KAT, lysine acetyltransferase; KDAC, lysine deacetylase; MYST family, Moz, Ybf2/Sas3, Sas2, and Tip family.

the control of metabolism via protein acetylation were reported in prokaryotes (Wang et al., 2010). A large number of metabolic enzymes are also acetylated in *S. cerevisiae*, which is consistent with the enzymes that regulate central metabolism through reversible acetylation, ensuring that cells respond to environmental changes by rapidly sensing the cellular energy state and flexibly changing rates or direction (Wang et al., 2010; Henriksen et al., 2012). This result can be explained by the central role of acetyl-CoA in intermediary metabolism because acetyl-CoA acts as the acetyl-donor for both enzymatic and non-enzymatic acetylation (Trefely et al., 2019). In other words, the dynamic interplay between cellular metabolism and acetylation plays a key role in epigenetics; however, this is not the focus of this review.

In summary, protein acetylation is widely distributed in fungi. Aside from modifying many key cellular processes, such as enzymatic activity, signal transduction, cell division, and metabolism, it also controls morphological transformation, biofilm formation, acetic acid stress tolerance, and other processes, thereby affecting the entire fungal life cycle (Kim et al., 2015; Cheng et al., 2016; Narita et al., 2019; Lin et al., 2020).

ROLE OF ACETYLATION/DEACETYLATION IN FUNGAL VIRULENCE

All known bacterial KATs that have been discovered to date belong to the Gcn5-related N-acetyltransferase family; fewer deacetylases are encoded by prokaryotes, which means that acetylation and deacetylation processes in fungi are more complex with a higher proportion of acetylated proteins in eukaryotes (**Tables 1**, **2**; Hentchel and Escalante-Semerena, 2015). KATs play a vital role in the morphogenetic hyphae growth, biofilm formation, drug resistance, and virulence (Kong et al., 2018; Lin et al., 2020). In *B. bassiana*, deletion of g*cn5* led to severe defects in colony growth and loss of cuticle infection (Cai et al., 2018b). In *P. sojae*, although Δ*gcn5* mutants had a normal development, their virulence in soybean was significantly reduced (Zhao et al., 2015). KDACs are also necessary for fungal pathogenesis, which were found to be decisive regulators of genes involved in pathogenicity and fungal toxin production, regulating a number of physiological processes, including thermotolerance, capsule formation, melanin synthesis, protease activity, and cell wall integrity (Bauer et al., 2016, 2019; Brandão et al., 2018).

Many fungal phenotypes have shown a specific correlation with virulence, such as biofilm formation, capsule production, melanin formation, and the secretion of various proteins (Staniszewska et al., 2012; Alspaugh, 2015). Additionally, cellular features, such as the cell wall, hyphae formation, stress response and morphological transition, allow the rapid and effective adaptation of fungal pathogens to varying conditions, which is conducive to their survival in the environment and in infected hosts (Wang et al., 2013; Alspaugh, 2015; Kim et al., 2015). Here, we primarily focused on the KATs and KDACs to discuss the role of acetylation and deacetylation in fungal virulence (**Table 1**), particularly in *A. fumigatus*, *C. neoformans*, and *C. albicans*, which are important clinical and useful research models for studying fatal infectious fungal pathogens in humans.

Acetylation/Deacetylation Regulates Fungal Stress Response

Generally, pathogens are subjected to various environmental challenges, such as temperature variations, an acidic pH, and oxidative stress. Reversible acetylation has emerged as one of

TABLE 2 | Some representative acetylated proteins in fungi.

Species	Acetylated protein	Function	References
Candida albicans	Hsp90	Regulates stress responses and cellular signaling; mediates azole resistance.	Li et al., 2017
Saccharomyces cerevisiae	Pck1p	Controls prompt adaptation of a metabolic flux to energy status.	Lin et al., 2009
	Smc3p	Affects cohesion establishment.	Heidinger-Pauli et al., 2010
	Hsp90	Regulates stress responses and cellular signaling; mediates azole resistance.	Robbins et al., 2012
Aspergillus flavus	AflO	Affects aflatoxin production and pathogenicity.	Yang et al., 2019
Aspergillus fumigatus	Hsp90	Regulates drug resistance.	Lamoth et al., 2014
	CBP	Involved in intracellular Ca^{2+} signaling.	Xie et al., 2016
Histoplasma capsulatum	Hsp60	Interacts with CR3 molecules on host phagocytes; involved in *Histoplasma* attachment to host macrophages.	
	Hsp70	Implicated in microbial virulence.	
Magnaporthe oryzae	Atg3	Involved in autophagy during both appressorium development and nutrient starvation.	Yin et al., 2019
	Atg9	Affects development and pathogenicity of *M. oryzae.*	
Fusarium graminearum	FgFkbp12	Rapamycin toxicity.	Zhou and Wu, 2019
	FaTUA1	Virulence, hyphae growth.	
	GzOB031	Virulence.	
	GzBrom002	DON, virulence, sexual and asexual.	
	FCA6	Peroxidase activities.	
	PKR	DON, virulence, sexual and asexual.	
Trichophyton rubrum	Hsp90	Regulates drug resistance and growth in human nails *in vitro*.	Jacob et al., 2015

the processes critical to maintaining cellular homeostasis and shaping responses to environmental stimuli (O'Meara et al., 2010; Chang et al., 2015; Wang J.-J. et al., 2018). In *C. neoformans*, the loss of acetylation gene *gcn5* caused a reduction in toxicity in a murine intranasal infection model and growth defects at high temperatures (O'Meara et al., 2010). In *B. bassiana*, the deletion of *gcn5* led to a 97% reduction in the conidiation capacity as well as severe defects in the growth of fungal colonies and conidial thermotolerance (Cai et al., 2018b). Moreover, Mst2, which can specifically acetylate histone H3K14 through cooperation with Gcn5 to regulate global acetylation events in *B. bassiana*, was found to play an important role in sustaining multiple stress tolerances such as osmotic and oxidative stress tolerance, cell wall perturbing stress tolerance, thermotolerance, and UV-B resistance (Wang J.-J. et al., 2018). Furthermore, the Δ*gcn5* mutants of *S. cerevisiae* and *Schizosaccharomyces pombe* showed defects in the cellular response to many stressors, including elevated temperatures, high salt concentrations, and nutrient deprivation (Chang et al., 2015).

The absence of acetyltransferase Rtt109 in *S. cerevisiae* not only activated the transcription of stress-responsive genes but also improved the resistance to oxidative stress, which ultimately contributed to the improvement in acetic acid tolerance (Cheng et al., 2016). The KDAC sirtuin 2, played a role in starvation stress resistance in yeasts; the deacetylase gene *rpd3* was also considered essential for starvation stress resistance (Fulco et al., 2003; Nakajima et al., 2016). A previous study on *B. bassiana* suggested that Δ*rpd3* significantly reduced the conidial tolerance to wet-heat stress at 45°C but increased the conidial resistance to UV-B irradiation, and the fungal virulence was greatly attenuated in the absence of *rpd3* (Cai et al., 2018c). Studies have found that the downregulation of RPD3-type deacetylase RpdA leads to avirulence of *A. fumigatus* in a murine model for pulmonary aspergillosis (Bauer et al., 2019). In addition, KDACs also play a decisive role as virulence factors in the pathogenic fungus *Cochliobolus carbonum* and *B. bassiana* (Baidyaroy et al., 2001; Zhang et al., 2020). Although the mechanism of virulence attenuation and adverse environmental tolerance remains unclear, previous evidence suggests that acetylation/deacetylation can control the virulence level of pathogens by regulating their stress response.

Acetylation/Deacetylation Rregulates Hyphal Growth

Hyphae have a strong ability to adhere and invade the host, making it easy to maintain their colonization and escape attacks from the host immune system, probably through the release of cell type-specific virulence factors, such as adhesins (e.g., Hwp1, Als3, Als10, Fav2, and Pga55), tissue-degrading enzymes (e.g., Sap4, Sap5, and Sap6), and antioxidant defense proteins (e.g., Sod5) (Sudbery, 2011; Noble et al., 2017). Acetylation and deacetylation play critical regulatory roles in regulating the initiation and maintenance of hyphal development (Garnaud et al., 2016; Kong et al., 2018; Lee et al., 2019). Tribus et al. (2010) found that the repression of the promoter of *rpdA* knockdown strains resulted in distorted and hyperbranched hyphae and a tremendous loss of radial growth of fungal colonies. MoHOS2-mediated histone deacetylation is important for the development of *M. oryzae*. In the absence of this mechanism, *M. oryzae* exhibits defects in hyphae formation, thereby impairing its growth ability inside the host plant (Lee et al., 2019). In *B. bassiana*, the hyphal cells of Δ*hos2* mutants are significantly longer than those of the wild type strains, which was concurrent with its inability to develop intact nuclei in hyphal cells (Cai et al., 2018a). The hyphal growth defects of four acetyltransferase mutants of

F. graminearum, namely, Δ*FgGCN5*, Δ*FgRTT109*, Δ*FgSAS2*, and Δ*FgSAS3* mutants in solid medium, have also been reported (Kong et al., 2018).

In *C. albicans*, deacetylase Rpd31 and Set3C (Set3/Hos2 HDAC complex) are crucial repressors of the yeast-to-hyphae transition in *C. albicans* (Hnisz et al., 2010; Garnaud et al., 2016). The acetyltransferase activity of nucleosome acetyltransferase of H4 (NuA4) and the deacetylase activity of Hda1 have also been reported as essential for hyphal initiation and maintenance (Wang X. et al., 2018). Furthermore, NuA4 dynamically regulates hyphal growth by merging and separating with the SWR1 complex, which was mediated by the acetylation of Eaf1 at K173 (lysine residue 173) (Wang X. et al., 2018). Gcn5 was also required for the invasive and filamentous growth of *C. albicans*, while *gcn5* mutant impaired the hyphal elongation in sensing serum and attenuated the *C. albicans* virulence in a mouse systemic infection model (Chang et al., 2015). Further evidence of the association between acetylation and hyphal growth was found in the acetyltransferase Esa1, which belongs to the MYST (Moz, YBF2, Sas2p, and Tip) family. Wang et al. found that *Esa1* was not important for the general growth of *C. albicans* but was important for its filamentous growth and that *Esa1* deletion could prevent filament formation under all hyphal induction conditions (Wang et al., 2013). Overall, hyphal initiation, development, and maintenance are complex processes regulated by acetylation and deacetylation in both filamentous fungi and budding yeasts.

Acetylation/Deacetylation Regulates Morphological Transition

One of the key virulence traits of fungi is morphological plasticity (Li et al., 2017). Although some human fungal pathogens mainly exist in the form of budding yeast cells (such as *C. neoformans*) or filamentous hyphal structures (such as *Aspergillus*), *C. albicans* alternates between these and other forms, usually in response to specific environmental cues (Takagi et al., 2019). In addition to yeast-to-hyphae transition, *C. albicans* can undergo a reversible switch between two morphologies, known as the white and opaque phases. Although the white and opaque cell types share the same genome, white cells caused more severe virulent in toxicity in mouse models (Kvaal et al., 1997). The class II deacetylase Hda1 selectively inhibits white-to-opaque switches, while the class I deacetylase Rpd31 suppresses transitions in both directions (Srikantha et al., 2001). Moreover, the sirtuins Hst3 and Sir2 were repressors of the white-to-opaque switch, whereas Set3C was the key activator (**Figure 1**; Pérez-Martín et al., 1999; Hnisz et al., 2009; Stevenson and Liu, 2011). Thus, *C. albicans* requires interaction with KDACs function for its morphological plasticity, which is central to its pathogenesis.

Acetylation/Deacetylation Regulates Biofilm Formation

Biofilm formation on host tissues and indwelling medical devices is highly associated with fungal pathogenicity and drug resistance because the extracellular matrix hinders drug diffusion (Nobile et al., 2014). Fungal adhesion on both biotic and abiotic surfaces is the first phase of biofilm formation, which is closely related

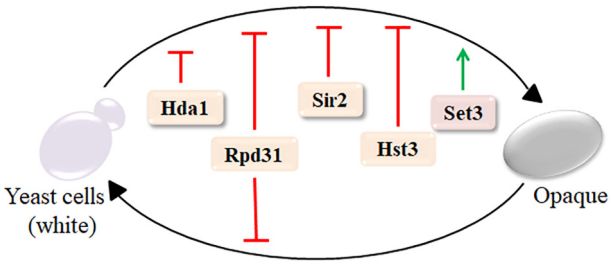

FIGURE 1 | Lysine deacetylases (KDACs) regulate the white-to-opaque switch in *C. albicans*. Set3 only activates the white-to-opaque switch; Hda1, Sir2, and Hst3 inhibit the progress; and Rpd31 suppresses transitions in both directions. Green arrows indicate activation, while red lines indicate inhibitory functions. Reproduced with the kind permission from Frontiers in Microbiology (Garnaud et al., 2016) with adjusted color scheme.

to the fungal cell wall and is critical to all later stages of biofilm development (Nett et al., 2011; Lohse et al., 2018). The relationship between biofilm resistance and the cell wall integrity pathway has been confirmed (Nett et al., 2011). In *C. albicans*, Nobile et al. (2014) found that the deletion of *set3* and *hos2* in *C. albicans* reduced biofilm formation and biomass, and these mutants appeared more resistant to yeast dispersion *in vivo*. Heat shock protein 90 (Hsp90) was a key regulator of biofilm dispersion and drug resistance and could be acetylated on lysine 27 and 270 (Robbins et al., 2012). Compromised Hsp90 function reduced the biofilm formation of *C. albicans in vitro* and impaired the dispersal of biofilm cells, blocking their capacity to serve as reservoirs of infection (Robbins et al., 2011). Moreover, Hsp90 was involved in the resistance of *A. fumigatus* biofilms to drugs (Robbins et al., 2011). Another study on *A. fumigatus* found that acetyltransferase GcnE was also required for biofilm formation (Lin et al., 2020). The list of device-associated infections caused by biofilms is expanding daily. Thus, the urgent determination of the mechanisms whereby acetylation/deacetylation participates in regulating biofilm formation is crucial.

Acetylation/Deacetylation Regulates Secondary Metabolite Production

A distinguishing feature of fungi is their ability to produce a variety of small molecules that contribute to their survival and pathogenicity. These substances include compounds such as pigments, which play a role in virulence and protect fungi from environmental damage, and toxins that kill host tissues or hinder competition from other organisms. The absence of deacetylase HdaA in *Aspergillus nidulans* caused the upregulation of carcinogenic sterigmatocystin (Shwab et al., 2007). In *A. fumigatus*, Δ*hdaA* knockout strains had a decreased production of the virulence factor gliotoxin (Lee et al., 2009). In the plant pathogenic fungus *Fusarium fujikuroi*, the deletion of *hda1* or *hda2* inhibited the production of red polyketide pigment bikaverin, plant hormone gibberellin, and mycotoxin fumaric acid; however, the deletion of *hda1* did not affect the production of mycotoxin fusarins, and the deletion of *hda2* did not affect the production of pigment fusarubin.

This finding indicated that the impact of acetylation on transcriptional regulation is usually more complex because of the functional complementarity of different KDAC genes (Studt et al., 2013).

AflO, a key enzyme in aflatoxin biosynthesis, was acetylated at lysine 241 and 384 and played a vital role in the pathogenicity of *A. flavus* (Yang et al., 2019). Six proteins involved in the virulence of *B. cinerea* were found to be acetylated (BcSak1, Hpt1, Bcchs2, CHSV, PKS, and BOS1) (Lv et al., 2016). In *F. graminearum*, 10 virulence-related proteins were also acetylated, including Kin4, Sty1, and Gpmk1 (Zhou X. et al., 2016). Deoxynivalenol (DON), a mycotoxin produced by *F. graminearum*, is a virulence factor that helps fungi colonize and spread within spikes (Kong et al., 2018). The DON production levels of Δ*FgSAS3* and Δ*FgGCN5* mutants were almost zero compared with that of wild type strain (Kong et al., 2018). Although DON is not a protein, acetylation plays an important role in its metabolism.

Melanin is a pigmented polymer that protects fungal cells against oxidative stress, phagocytosis, and antifungal drugs. It also modifies the host immune responses by reducing the susceptibility of melanized microbes to the host defense mechanisms (Brandão et al., 2015, 2018). Brandão et al. (2018) found that the change in virulence of Δ*hda1* mutants of *C. neoformans* might be due to its markedly reduced formation of capsule, melanin, and extracellular proteases, all of which are specifically required for the survival of microbes in the host. Maeda et al. (2017) found that deletion of the *HdaA* homolog in *Magnaporthe orzyae* increased the expression of melanin biosynthesis genes. Although the effect of KDAC inhibitors (KDACis) on melanin synthesis has been confirmed, the specific mechanism of acetylation in melanin formation remains unclear (Brandão et al., 2015). The abovementioned studies suggest that protein acetylation/deacetylation can affect the virulence of fungi by participating in the regulation of secondary metabolite biosynthesis.

APPLICATION OF ACETYLATION/DEACETYLATION IN ANTIFUNGAL THERAPY

Invasive infections caused by fungal pathogens are a major public health issue. More than 1.6 million people worldwide develop serious fungal diseases that have a major or fatal impact on their lives (Bongomin et al., 2017). Although the development of new antifungal drugs is an important strategy for the treatment of fungal infections, the urgent development of new infection treatment strategies in view of the uncontrolled increase in the incidence of drug-resistant fungal infections worldwide is crucial (Perlin et al., 2017). Enzymes that control chromatin modification could form a new group of antimicrobial target genes because they are involved in many pathophysiological processes that regulate virulence (Tscherner et al., 2015; Bauer et al., 2016). These results may shed new light on KATs/KDACs as a potential therapeutic target for developing an anti-infection drug (**Figure 2**).

Because KDACis can regulate reversible protein acetylation by inhibiting KDAC activity, altering gene expression; inducing cell cycle arrest, cell differentiation, and apoptosis; reducing angiogenesis; and modulating immune response; they became a new hotspot in the research of tumor-targeted therapy (Spange et al., 2009; Eckschlager et al., 2017). Currently, KDACis are broadly classified into five main groups: hydroxamates, cyclic peptides, benzamides, short-chain fatty acids, and sirtuin inhibitors (**Table 3**; von Knethen and Brüne, 2019). At present, KDACis are widely used in clinical practice; however their

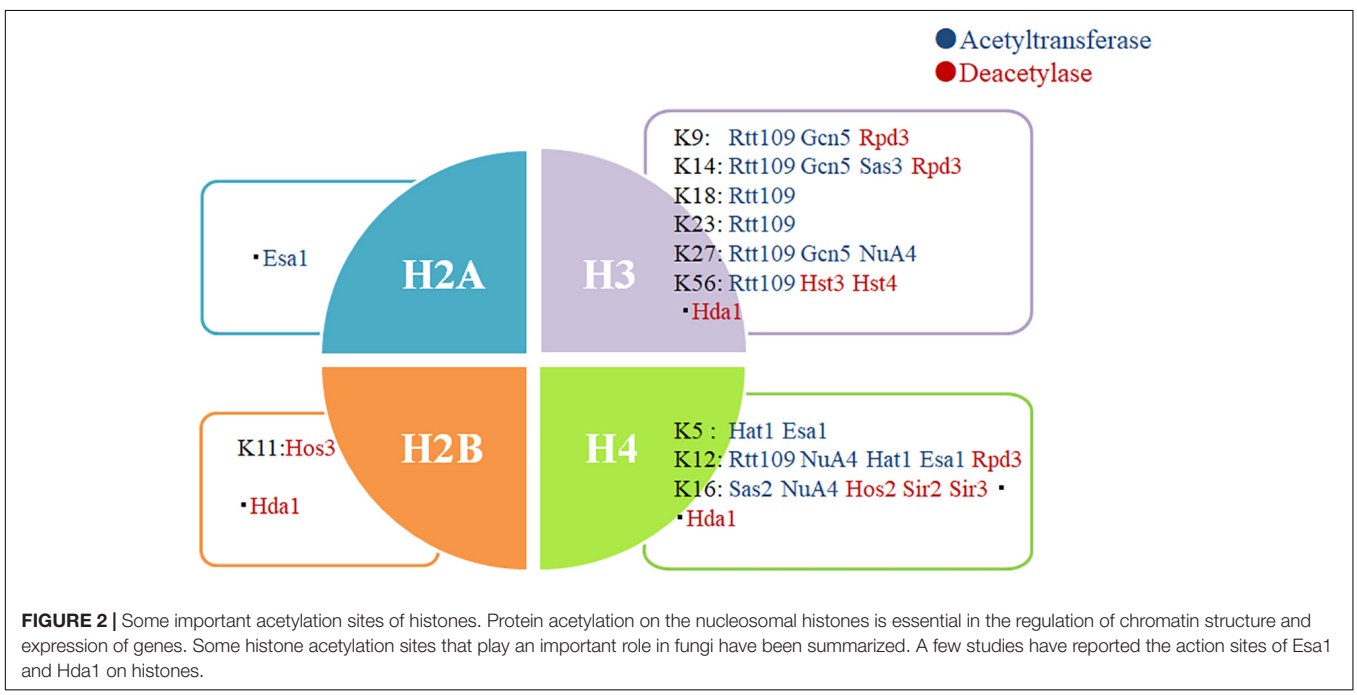

FIGURE 2 | Some important acetylation sites of histones. Protein acetylation on the nucleosomal histones is essential in the regulation of chromatin structure and expression of genes. Some histone acetylation sites that play an important role in fungi have been summarized. A few studies have reported the action sites of Esa1 and Hda1 on histones.

TABLE 3 | Classification of lysine deacetylase inhibitors.

Class	Name	KDAC specificity	Clinical trial stage
Hydroxamates	Suberoylanilide hydroxamic acid (SAHA)	Pan-KDACi	Approved in 2006 for CTCL
	Belinostat (PXD101)	Pan-KDACi	Approved in 2014 for PTCL
	Panobinostat (LBH-589)	Pan-KDACi	Approved in 2015 for MM
	Trichostatin A (TSA)	Pan-KDACi	Preclinical
	Givinostat (ITF2357)	Pan-KDACi	Phase II
	Resminostat (4SC201)	Pan-KDACi	Phase II
	Abexinostat (PCI24781	Pan-KDACi	Phase II
	Practinostat (SB939)	Class I, II,IV KDACi	Phase II
	Rocilinostat (ACY1215)	Class II KDACi	Phase I
	Pyroxamide (NSC696085)	HDAC1 inhibitor	Phase I
	CHR-3996	Class I KDACi	Phase I
	AR42	Pan-KDACi	Phase I
Cyclic peptides	Romidepsin (FK288)	Class I KDACi	Approved in 2009 for CTCL
Benzamides	Tacedinaline (CI994)	HDAC1-3 inhibitor	Phase III
	Entinostat (MS-275)	Class I KDACi	Phase II
	Mocetinostat (MGCD0103)	Class I, IV KDACi	Phase II
	4SC202	Class I KDACi	Phase I
Short chainfatty acids	Valproic acid	Class I, IIa KDACi	Phase III
	Phenylbutyric acid	Pan-KDACi	Phase II
	Butyric acid	Pan-KDAC inhibitor	Phase II
Sirtuin inhibitors	Cambinol	SIRT1,2 inhibitor	Preclinical
	Sirtinol	SIRT1,2 inhibitor	Preclinical
	EX-527	SIRT1,2 inhibitor	Phase I
	Nicotinamide (NAM)	Class III KDACi	Phase III

KDAC, lysine deacetylase; KDACi, lysine deacetylase inhibitor; CTCL, cutaneous T-cell lymphoma; PTCL, peripheral T-cell lymphoma; MM, multiple myeloma.

application value in the treatment of antifungal infections requires further investigation.

Targeting fungal deacetylases as a therapeutic strategy has a particular advantage. Inhibiting fungal KDACs may have beneficial and synergistic effects by reducing the virulence and growth of fungi, while also decreasing their tolerance and resistance to the existing antifungal drugs (Pfaller et al., 2015; Zhang and Xu, 2015). Previous studies found that KDACis could inhibit the production of toxic factors in *C. neoformans*; in *S. cerevisiae*, the deacetylase inhibitor trichostatin A (TSA) could eliminate its resistance to azole drugs by inhibiting the KDAC activity (Robbins et al., 2012; Brandão et al., 2015). Lys56 acetylation of histone H3 in *C. albicans* was an ideal target for antifungal therapy, and reduced levels of H3K56ac sensitized *C. albicans* to genotoxic and antifungal agents (**Figure 2**; Wurtele et al., 2010). In *A. fumigatus*, Hsp90 acetylation was also involved in the regulation of drug resistance (Lamoth et al., 2014). Deacetylases Hda1 and Rpd3 can regulate the function of Hsp90 to control fungal drug resistance; therefore, KDACis can block the emergence and maintenance of Hsp90-dependent azole resistance (Robbins et al., 2012). These studies demonstrate that KDACis hold great promise in the treatment of infections resistant to antifungal agents.

Little attention has been paid to acetylase inhibitors because KATs are rarely considered as drug targets. One of the reasons may be the promising application of KDACis in various diseases, and the other is that only a small number of acetylase inhibitors have been identified (Spange et al., 2009). Thus, we mainly discuss the application of KDACis in the treatment of fungal infections using several representative KDACis as examples.

Pan-KDACis

TSA is the best-known broad-spectrum KDACi. It was first isolated from a culture medium of *Streptomyces platensis* and initially appeared as an antifungal drug to inhibit the growth of *Trichophyton* and *Aspergillus* (Tsuji et al., 1976). The inhibition of RpdA activity by TSA resulted in a significant delay in the growth and germination of fungal species, such as *A. fumigatus*, *A. nidulans, Aspergillus terreus, Penicillium chrysogenum*, and *Neurospora crassa* (Bauer et al., 2016). Hnisz et al. (2010) found that TSA was involved in triggering the yeast-to-hyphae conversion of *C. albicans* by inhibiting Set3C, which controls protein kinase A signaling through Efg1. TSA also increased the susceptibility of *Candida* sp. to azole antifungals by inhibiting the biosynthesis of ergosterol (Smith and Edlind, 2002). Lamoth et al. (2014) found that the combination of TSA and azole drugs in the treatment of *A. fumigatus* also showed a promising possibility. Considering instability and rapid metabolism of TSA, the development of highly selective inhibitors is very important for mitigating potential toxicities caused by high doses (Tan and Liu, 2015). Sodium butyrate, apicidin, and suberoylanilide hydroxamic acid are also effective broad-spectrum KDACis; however, their use in antifungal therapy requires further investigation.

Selective KDACis

MGCD290, a fungal-specific Hos2 inhibitor in *Candida* sp., displayed moderate activity when used alone (Pfaller et al., 2009, 2015). However, the use of MGCD290 in combination with fluconazole, voriconazole, and posaconazole significantly increased the susceptibility of fungal species *in vitro* such as azole-resistant *Candida*, *Mucor*, and *Fusarium* sp. (Pfaller et al., 2009; Lamoth et al., 2015). When fluconazole, which had inactive activity against filamentous fungi, was used in combination with MGCD290, there was a distinctly favorable influence of the fluconazole MICs of *Aspergillus* strains, resulting in a conversion from resistance to susceptibility (Pfaller et al., 2009). Interestingly, *Hos2* was a homologous gene of *HosA* in *A. nidulans* (Pidroni et al., 2018). However, the deletion of *HosA* did not affect the efficacy of any antifungal drugs, which contradicted the specificity of MGCD290 (Pidroni et al., 2018). These contradictory results may be explained by the different biological functions of HosA-type proteins in different *Aspergillus* species, or more likely by the fact that MGCD290 does not specifically act on HosA-type enzymes in filamentous fungi (Pidroni et al., 2018). Therefore, although the specificity of MGCD290 is a debatable issue, MGCD290 has great application prospects in antifungal therapies.

Sirtuin Inhibitors

Nicotinamide (NAM), a form of vitamin B3, is a typical non-competitive inhibitor of sirtuins (Orlandi et al., 2017). NAM possesses an antibacterial activity, inhibits cell proliferation and enhances the antiproliferative effect of cytostatic drugs (Xing et al., 2019). NAM's potential to inhibit the growth of *Mycobacterium tuberculosis*, *Plasmodium falciparum*, and HIV has been demonstrated in clinical trials (Murray, 2003; Tcherniuk et al., 2017). Furthermore, NAM displayed broad-spectrum activity against multiple clinical isolates, including *C. parapsilosis*, *C. tropicalis*, *C. glabrata*, *C. krusei*, *C. neoformans*, and fluconazole-resistant *C. albicans* (Xing et al., 2019). NAM also reduced the kidney burden in a mouse model of disseminated candidiasis (Wurtele et al., 2010). Moreover, two different *Aspergillus* species, *A. fumigatus*, and *A. nidulans*, were very sensitive to NAM (Wurtele et al., 2010). NAM also reduced the activity of some enzymes produced by fungi, such as *C. albicans*, *T. rubrum*, and *Trichophyton mentagrophytes*, which supports the use of NAM as an antifungal drug (Ciebiada-Adamiec et al., 2010). In addition to NAM, sirtuin inhibitors include the specific SIRT1 and SIRT2 inhibitors sirtinol, cambinol and EX-527, but their value in the treatment of infection is unclear (Eckschlager et al., 2017).

OUTLOOK AND CONCLUSION

As a common PTM, protein acetylation plays an essential role in metabolism, virulence, transcription, and translation, among other processes. Acetylation is primarily catalyzed by specific acetyltransferases but can also occur due to the non-enzymatic reactions of acetyl phosphates. At present, only a few studies have reported on the latter, and the relationship between the two different acetylation processes in the regulation of microbial virulence remains unclear. Furthermore, it is unknown whether other non-enzymatic/enzymatic acetylation mechanisms exist and how these (de)acetylation mechanisms cooperate.

Additionally, fungal virulence is a complex phenotype involving multiple factors, making it difficult to explain by analyzing a single type of PTM because there may be multiple PTMs on the same protein, and one protein usually has multiple acetylated lysine residues. How do multiple PTMs cooperate in response to different environmental changes? Besides acetylation, are there other types of acylation that affect the regulation of acetylation, such as malonylation, glutarylation, succinylation, methylation, propionylation, and butyrylation? Do these acetylation modifications have an effect on fungal virulence? These questions need to be addressed in future studies.

At present, research on acetylation and deacetylation mainly focuses on human metabolism, tumors, and other aspects. By contrast, studies on microbial acetylation/deacetylation are limited and mainly focus on a few microbial species, such as *Escherichia coli*, *Salmonella typhimurium*, *M. tuberculosis*, *S. cerevisiae*, and *C. albicans*; and studies on human fungal pathogens mainly focus on *C. albicans*, *C. neoformans*, and *A. fumigatus* (Brandão et al., 2018; Bauer et al., 2019; Lin et al., 2020). With the rapid development of protein detection technology, such as high-resolution mass spectrometry, and the broad application of the protein chip, developments in these fields will greatly enrich the investigations on the role of acetylation/deacetylation in regulating microbial physiological process, especially that of microbial pathogenesis and immunity. Therefore, further study of other pathogens is important to reveal the effect of protein acetylation/deacetylation on fungal toxicity and its potential mechanism and may provide some novel potential drug targets for drug development. Finally, in most cases, the effect of the regulation of protein acetylation in host cells by specific pathogens on the quality of immune responses to a broad range of pathogens has not been studied. Future investigations need to be rationally designed to analyze both the pathogen itself and the host's immune status to avoid excessive damage to the host's tissues.

AUTHOR CONTRIBUTIONS

All authors contributed to the critical analysis of the collected data and writing of the manuscript. All authors approved the final manuscript.

FUNDING

This study was supported by the National Natural Science Foundation of China (32060040, 31760261, and 31660035), the Science and Technology Research Project of Jiangxi Provincial Education Department (60224), the Key Research and Development Projects of Jiangxi Natural Science Foundation (20192BBG70067, 20202BAB206062, and 20202BAB216045), and the Key Projects of Jiangxi Province Science Foundation for Youths (20192ACBL21042).

ACKNOWLEDGMENTS

We would like to thank Enago (www.enago.cn) for the English language editing.

REFERENCES

Ali, I., Conrad, R. J., Verdin, E., and Ott, M. (2018). Lysine acetylation goes global: from epigenetics to metabolism and therapeutics. *Chem. Rev.* 118, 1216–1252. doi: 10.1021/acs.chemrev.7b00181

Allfrey, V. G., Faulkner, R., and Mirsky, A. E. (1964). Acetylation and methylation of histones and their possible role in the regulation of RNA synthesis. *Proc. Natl. Acad. Sci. U.S.A.* 51, 786–794. doi: 10.1073/pnas.51.5.786

Alspaugh, J. A. (2015). Virulence mechanisms and *Cryptococcus neoformans* pathogenesis. *Fungal Genet. Biol.* 78, 55–58. doi: 10.1016/j.fgb.2014.09.004

Baidyaroy, D., Brosch, G., Ahn, J. H., Graessle, S., Wegener, S., Tonukari, N. J., et al. (2001). A gene related to yeast HOS2 histone deacetylase affects extracellular depolymerase expression and virulence in a plant pathogenic fungus. *Plant Cell* 13, 1609–1624. doi: 10.1105/tpc.010168

Bauer, I., Misslinger, M., Shadkchan, Y., Dietl, A.-M., Petzer, V., Orasch, T., et al. (2019). The Lysine Deacetylase RpdA Is Essential for Virulence in *Aspergillus fumigatus*. *Front. Microbiol.* 10:2773. doi: 10.3389/fmicb.2019.02773

Bauer, I., Varadarajan, D., Pidroni, A., Gross, S., Vergeiner, S., Faber, B., et al. (2016). A Class 1 Histone Deacetylase with Potential as an Antifungal Target. *mBio* 7:e00831-16. doi: 10.1128/mBio.00831-16

Bongomin, F., Gago, S., Oladele, R. O., and Denning, D. W. (2017). Global and Multi-National Prevalence of Fungal Diseases-Estimate Precision. *J. Fungi* 3:57. doi: 10.3390/jof3040057

Brandão, F., Esher, S. K., Ost, K. S., Pianalto, K., Nichols, C. B., Fernandes, L., et al. (2018). HDAC genes play distinct and redundant roles in *Cryptococcus neoformans* virulence. *Sci Rep.* 8:5209. doi: 10.1038/s41598-018-21965-y

Brandão, F. A., Derengowski, L. S., Albuquerque, P., Nicola, A. M., Silva-Pereira, I., and Poças-Fonseca, M. J. (2015). Histone deacetylases inhibitors effects on *Cryptococcus neoformans* major virulence phenotypes. *Virulence* 6, 618–630. doi: 10.1080/21505594.2015.1038014

Cai, Q., Tong, S.-M., Shao, W., Ying, S.-H., and Feng, M.-G. (2018a). Pleiotropic effects of the histone deacetylase Hos2 linked to H4-K16 deacetylation, H3-K56 acetylation, and H2A-S129 phosphorylation in *Beauveria bassiana*. *Cell Microbiol.* 20:e12839. doi: 10.1111/cmi.12839

Cai, Q., Wang, J.-J., Fu, B., Ying, S.-H., and Feng, M.-G. (2018b). Gcn5-dependent histone H3 acetylation and gene activity is required for the asexual development and virulence of *Beauveria bassiana*. *Environ. Microbiol.* 20, 1484–1497. doi: 10.1111/1462-2920.14066

Cai, Q., Wang, Z.-K., Shao, W., Ying, S.-H., and Feng, M.-G. (2018c). Essential role of Rpd3-dependent lysine modification in the growth, development and virulence of *Beauveria bassiana*. *Environ. Microbiol.* 20, 1590–1606. doi: 10.1111/1462-2920.14100

Chang, P., Fan, X., and Chen, J. (2015). Function and subcellular localization of Gcn5, a histone acetyltransferase in *Candida albicans*. *Fungal Genet. Biol.* 81, 132–141. doi: 10.1016/j.fgb.2015.01.011

Cheng, C., Zhao, X., Zhang, M., and Bai, F. (2016). Absence of Rtt109p, a fungal-specific histone acetyltransferase, results in improved acetic acid tolerance of *Saccharomyces cerevisiae*. *FEMS Yeast Res.* 16:fow010. doi: 10.1093/femsyr/fow010

Ciebiada-Adamiec, A., Małafiej, E., and Ciebiada, I. (2010). Inhibitory effect of nicotinamide on enzymatic activity of selected fungal strains causing skin infection. *Mycoses* 53, 204–207. doi: 10.1111/j.1439-0507.2009.01696.x

Dubey, A., Lee, J., Kwon, S., Lee, Y.-H., and Jeon, J. (2019). A MYST family histone acetyltransferase, MoSAS3, is required for development and pathogenicity in the rice blast fungus. *Mol. Plant Pathol.* 20, 1491–1505. doi: 10.1111/mpp.12856

Eckschlager, T., Plch, J., Stiborova, M., and Hrabeta, J. (2017). Histone deacetylase inhibitors as anticancer drugs. *Int. J. Mol. Sci.* 18:1414. doi: 10.3390/ijms18071414

Fisher, M. C., Gow, N. A. R., and Gurr, S. J. (2016). Tackling emerging fungal threats to animal health, food security and ecosystem resilience. *Philos. Trans. R. Soc. Lond. B. Biol. Sci.* 371:20160332. doi: 10.1098/rstb.2016.0332

Fulco, M., Schiltz, R. L., Iezzi, S., King, M. T., Zhao, P., Kashiwaya, Y., et al. (2003). Sir2 regulates skeletal muscle differentiation as a potential sensor of the redox state. *Mol. Cell.* 12, 51–62. doi: 10.1016/s1097-2765(03)00226-0

Garavelli, J. S. (2004). The RESID Database of Protein Modifications as a resource and annotation tool. *Proteomics* 4, 1527–1533. doi: 10.1002/pmic.200300777

Garnaud, C., Champleboux, M., Maubon, D., Cornet, M., and Govin, J. (2016). Histone deacetylases and their inhibition in candida species. *Front. Microbiol.* 7:1238. doi: 10.3389/fmicb.2016.01238

Graessle, S., Dangl, M., Haas, H., Mair, K., Trojer, P., Brandtner, E. M., et al. (2000). Characterization of two putative histone deacetylase genes from *Aspergillus nidulans*. *Biochim. Biophys. Acta* 1492, 120–126. doi: 10.1016/s0167-4781(00)00093-2

Heidinger-Pauli, J. M., Onn, I., and Koshland, D. (2010). Genetic evidence that the acetylation of the Smc3p subunit of cohesin modulates its ATP-bound state to promote cohesion establishment in *Saccharomyces cerevisiae*. *Genetics* 185, 1249–1256. doi: 10.1534/genetics.110.116871

Henriksen, P., Wagner, S. A., Weinert, B. T., Sharma, S., Bacinskaja, G., Rehman, M., et al. (2012). Proteome-wide analysis of lysine acetylation suggests its broad regulatory scope in *Saccharomyces cerevisiae*. *Mol. Cell. Proteomics* 11, 1510–1522. doi: 10.1074/mcp.M112.017251

Hentchel, K. L., and Escalante-Semerena, J. C. (2015). Acylation of biomolecules in prokaryotes: a widespread strategy for the control of biological function and metabolic stress. *Microbiol. Mol. Biol. Rev.* 79, 321–346. doi: 10.1128/MMBR.00020-15

Hnisz, D., Majer, O., Frohner, I. E., Komnenovic, V., and Kuchler, K. (2010). The Set3/Hos2 histone deacetylase complex attenuates cAMP/PKA signaling to regulate morphogenesis and virulence of *Candida albicans*. *PLoS Pathog.* 6:e1000889. doi: 10.1371/journal.ppat.1000889

Hnisz, D., Schwarzmüller, T., and Kuchler, K. (2009). Transcriptional loops meet chromatin: a dual-layer network controls white-opaque switching in *Candida albicans*. *Mol. Microbiol.* 74, 1–15. doi: 10.1111/j.1365-2958.2009.06772.x

Itoh, E., Shigemoto, R., Oinuma, K.-I., Shimizu, M., Masuo, S., and Takaya, N. (2017). Sirtuin A regulates secondary metabolite production by *Aspergillus nidulans*. *J. Gen. Appl. Microbiol.* 63, 228–235. doi: 10.2323/jgam.2016.11.002

Jacob, T. R., Peres, N. T. A., Martins, M. P., Lang, E. A. S., Sanches, P. R., Rossi, A., et al. (2015). Heat Shock Protein 90 (Hsp90) as a Molecular Target for the Development of Novel Drugs Against the Dermatophyte *Trichophyton rubrum*. *Front. Microbiol.* 6:1241. doi: 10.3389/fmicb.2015.01241

Kim, J., Lee, J.-E., and Lee, J.-S. (2015). Histone deacetylase-mediated morphological transition in *Candida albicans*. *J. Microbiol.* 53, 805–811. doi: 10.1007/s12275-015-5488-3

Kim, J., Park, S., and Lee, J.-S. (2018). Epigenetic Control of Oxidative Stresses by Histone Acetyltransferases in *Candida albicans*. *J. Microbiol. Biotechnol.* 28, 181–189. doi: 10.4014/jmb.1707.07029

Kong, X., van Diepeningen, A. D., van der Lee, T. A. J., Waalwijk, C., Xu, J., Xu, J., et al. (2018). The Histone Acetyltransferases Are Important for Morphogenesis, DON Biosynthesis, and Pathogenicity. *Front. Microbiol.* 9:654. doi: 10.3389/fmicb.2018.00654

Kvaal, C. A., Srikantha, T., and Soll, D. R. (1997). Misexpression of the white-phase-specific gene WH11 in the opaque phase of *Candida albicans* affects switching and virulence. *Infect. Immun.* 65, 4468–4475. doi: 10.1128/iai.65.11.4468-4475.1997

Kwon, S., Lee, J., Jeon, J., Kim, S., Park, S.-Y., Jeon, J., et al. (2018). Role of the Histone Acetyltransferase Rtt109 in Development and Pathogenicity of the Rice Blast Fungus. *Mol. Plant Microbe Interact.* 31, 1200–1210. doi: 10.1094/MPMI-01-18-0015-R

Lamoth, F., Juvvadi, P. R., Soderblom, E. J., Moseley, M. A., Asfaw, Y. G., and Steinbach, W. J. (2014). Identification of a key lysine residue in heat shock protein 90 required for azole and echinocandin resistance in *Aspergillus fumigatus*. *Antimicrob. Agents Chemother.* 58, 1889–1896. doi: 10.1128/AAC.02286-13

Lamoth, F. D. R., Juvvadi, P. R., and Steinbach, W. J. (2015). Histone deacetylase inhibition as an alternative strategy against invasive aspergillosis. *Front. Microbiol.* 6:96. doi: 10.3389/fmicb.2015.00096

Lee, I., Oh, J.-H., Shwab, E. K., Dagenais, T. R. T., Andes, D., and Keller, N. P. (2009). HdaA, a class 2 histone deacetylase of *Aspergillus fumigatus*, affects germination and secondary metabolite production. *Fungal Genet. Biol.* 46, 782–790. doi: 10.1016/j.fgb.2009.06.007

Lee, J., Lee, J.-J., and Jeon, J. (2019). A histone deacetylase, MoHOS2 regulates asexual development and virulence in the rice blast fungus. *J. Microbiol.* 57, 1115–1125. doi: 10.1007/s12275-019-9363-5

Lee, S.-Y., Choi, Y.-S., Kim, E.-H., Cheong, H.-K., Lee, Y.-J., Lee, J.-G., et al. (2018). Nonenzymatic acetylation of ubiquitin Lys side chains is modulated by their neighboring residues. *FEBS J.* 285, 1277–1289. doi: 10.1111/febs.14404

Li, D., Lv, B., Tan, L., Yang, Q., and Liang, W. (2016). Acetylome analysis reveals the involvement of lysine acetylation in diverse biological processes in Phytophthora sojae. *Sci Rep.* 6:29897. doi: 10.1038/srep29897

Li, X., Robbins, N., O'Meara, T. R., and Cowen, L. E. (2017). Extensive functional redundancy in the regulation of *Candida albicans* drug resistance and morphogenesis by lysine deacetylases Hos2, Hda1, Rpd3 and Rpd31. *Mol. Microbiol.* 103, 635–656. doi: 10.1111/mmi.13578

Li, Y., Li, H., Sui, M., Li, M., Wang, J., Meng, Y., et al. (2019). Fungal acetylome comparative analysis identifies an essential role of acetylation in human fungal pathogen virulence. *Commun. Biol.* 2:154. doi: 10.1038/s42003-019-0419-1

Li, Y., Wang, C., Liu, W., Wang, G., Kang, Z., Kistler, H. C., et al. (2011). The HDF1 histone deacetylase gene is important for conidiation, sexual reproduction, and pathogenesis in *Fusarium graminearum*. *Mol. Plant Microbe Interact.* 24, 487–496. doi: 10.1094/MPMI-10-10-0233

Liang, M., Zhang, S., Dong, L., Kou, Y., Lin, C., Dai, W., et al. (2018). Label-Free Quantitative Proteomics of Lysine Acetylome Identifies Substrates of Gcn5 in Magnaporthe oryzae Autophagy and Epigenetic Regulation. *mSystems* 3, e00270-18. doi: 10.1128/mSystems.00270-18

Lin, C.-J., Hou, Y.-H., and Chen, Y.-L. (2020). The histone acetyltransferase GcnE regulates conidiation and biofilm formation in *Aspergillus fumigatus*. *Med. Mycol.* 58, 248–259. doi: 10.1093/mmy/myz043

Lin, Y.-Y., Lu, J.-Y., Zhang, J., Walter, W., Dang, W., Wan, J., et al. (2009). Protein acetylation microarray reveals that NuA4 controls key metabolic target regulating gluconeogenesis. *Cell* 136, 1073–1084. doi: 10.1016/j.cell.2009.01.033

Lohse, M. B., Gulati, M., Johnson, A. D., and Nobile, C. J. (2018). Development and regulation of single- and multi-species *Candida albicans* biofilms. *Nat. Rev. Microbiol.* 16, 19–31. doi: 10.1038/nrmicro.2017.107

Lv, B., Yang, Q., Li, D., Liang, W., and Song, L. (2016). Proteome-wide analysis of lysine acetylation in the plant pathogen Botrytis cinerea. *Sci Rep.* 6:29313. doi: 10.1038/srep29313

Maeda, K., Izawa, M., Nakajima, Y., Jin, Q., Hirose, T., Nakamura, T., et al. (2017). Increased metabolite production by deletion of an HDA1-type histone deacetylase in the phytopathogenic fungi, Magnaporthe oryzae (Pyricularia oryzae) and Fusarium asiaticum. *Lett. Appl. Microbiol.* 65, 446–452. doi: 10.1111/lam.12797

Mann, M., and Jensen, O. N. (2003). Proteomic analysis of post-translational modifications. *Nat. Biotechnol.* 21, 255–261. doi: 10.1038/nbt0303-255

Motaung, T. E., Saitoh, H., and Tsilo, T. J. (2017). Large-scale molecular genetic analysis in plant-pathogenic fungi: a decade of genome-wide functional analysis. *Mol. Plant Pathol.* 18, 754–764. doi: 10.1111/mpp.12497

Mukherjee, K., Fischer, R., and Vilcinskas, A. (2012). Histone acetylation mediates epigenetic regulation of transcriptional reprogramming in insects during metamorphosis, wounding and infection. *Front. Zool.* 9:25. doi: 10.1186/1742-9994-9-25

Murray, M. F. (2003). Nicotinamide: an oral antimicrobial agent with activity against both Mycobacterium tuberculosis and human immunodeficiency virus. *Clin. Infect. Dis* 36, 453–460. doi: 10.1086/367544

Nakajima, E., Shimaji, K., Umegawachi, T., Tomida, S., Yoshida, H., Yoshimoto, N., et al. (2016). The Histone Deacetylase Gene Rpd3 Is Required for Starvation Stress Resistance. *PLoS One* 11:e0167554. doi: 10.1371/journal.pone.0167554

Narita, T., Weinert, B. T., and Choudhary, C. (2019). Functions and mechanisms of non-histone protein acetylation. *Nat. Rev. Mol. Cell Biol.* 20, 156–174. doi: 10.1038/s41580-018-0081-3

Nett, J. E., Sanchez, H., Cain, M. T., Ross, K. M., and Andes, D. R. (2011). Interface of *Candida albicans* biofilm matrix-associated drug resistance and cell wall integrity regulation. *Eukaryot. Cell* 10, 1660–1669. doi: 10.1128/EC.05126-11

Nicolas, D., Zoller, B., Suter, D. M., and Naef, F. (2018). Modulation of transcriptional burst frequency by histone acetylation. *Proc. Natl. Acad. Sci. U.S.A.* 115, 7153–7158. doi: 10.1073/pnas.1722330115

Nobile, C. J., Fox, E. P., Hartooni, N., Mitchell, K. F., Hnisz, D., Andes, D. R., et al. (2014). A histone deacetylase complex mediates biofilm dispersal and drug resistance in *Candida albicans*. *mBio* 5, e01201-14. doi: 10.1128/mBio.01201-14

Noble, S. M., Gianetti, B. A., and Witchley, J. N. (2017). *Candida albicans* cell-type switching and functional plasticity in the mammalian host. *Nat. Rev. Microbiol.* 15, 96–108. doi: 10.1038/nrmicro.2016.157

O'Meara, T. R., Hay, C., Price, M. S., Giles, S., and Alspaugh, J. A. (2010). *Cryptococcus neoformans* histone acetyltransferase Gcn5 regulates fungal adaptation to the host. *Eukaryot. Cell* 9, 1193–1202. doi: 10.1128/EC.00098-10

Orlandi, I., Pellegrino Coppola, D., Strippoli, M., Ronzulli, R., and Vai, M. (2017). Nicotinamide supplementation phenocopies SIR2 inactivation by modulating carbon metabolism and respiration during yeast chronological aging. *Mech. Ageing Dev.* 161, 277–287. doi: 10.1016/j.mad.2016.06.006

Pérez-Martín, J., Uría, J. A., and Johnson, A. D. (1999). Phenotypic switching in *Candida albicans* is controlled by a SIR2 gene. *EMBO J.* 18, 2580–2592. doi: 10.1093/emboj/18.9.2580

Perlin, D. S., Rautemaa-Richardson, R., and Alastruey-Izquierdo, A. (2017). The global problem of antifungal resistance: prevalence, mechanisms, and management. *Lancet Infect. Dis.* 17, e383–e392. doi: 10.1016/S1473-3099(17)30316-X

Pfaller, M. A., Messer, S. A., Georgopapadakou, N., Martell, L. A., Besterman, J. M., and Diekema, D. J. (2009). Activity of MGCD290, a Hos2 histone deacetylase inhibitor, in combination with azole antifungals against opportunistic fungal pathogens. *J. Clin. Microbiol.* 47, 3797–3804. doi: 10.1128/JCM.00618-09

Pfaller, M. A., Rhomberg, P. R., Messer, S. A., and Castanheira, M. (2015). In vitro activity of a Hos2 deacetylase inhibitor, MGCD290, in combination with echinocandins against echinocandin-resistant Candida species. *Diagn. Microbiol. Infect. Dis.* 81, 259–263. doi: 10.1016/j.diagmicrobio.2014.11.008

Phillips, D. M. (1963). The presence of acetyl groups of histones. *Biochem. J.* 87, 258–263. doi: 10.1042/bj0870258

Pidroni, A., Faber, B., Brosch, G., Bauer, I., and Graessle, S. (2018). A Class 1 Histone Deacetylase as Major Regulator of Secondary Metabolite Production in *Aspergillus nidulans*. *Front. Microbiol.* 9:2212. doi: 10.3389/fmicb.2018.02212

Ren, J., Sang, Y., Lu, J., and Yao, Y. F. (2017). Protein acetylation and its role in bacterial virulence. *Trends Microbiol.* 25, 768–779. doi: 10.1016/j.tim.2017.04.001

Ren, J., Sang, Y., Qin, R., Su, Y., Cui, Z., Mang, Z., et al. (2019). Metabolic intermediate acetyl phosphate modulates bacterial virulence via acetylation. *Emerg. Microbes Infect.* 8, 55–69. doi: 10.1080/22221751.2018.1558963

Reyes-Dominguez, Y., Narendja, F., Berger, H., Gallmetzer, A., Fernandez-Martin, R., Garcia, I., et al. (2008). Nucleosome positioning and histone H3 acetylation are independent processes in the *Aspergillus nidulans* prnD-prnB bidirectional promoter. *Eukaryot. Cell* 7, 656–663. doi: 10.1128/EC.00184-07

Robbins, N., Leach, M. D., and Cowen, L. E. (2012). Lysine deacetylases Hda1 and Rpd3 regulate Hsp90 function thereby governing fungal drug resistance. *Cell Rep.* 2, 878–888. doi: 10.1016/j.celrep.2012.08.035

Robbins, N., Uppuluri, P., Nett, J., Rajendran, R., Ramage, G., Lopez-Ribot, J. L., et al. (2011). Hsp90 governs dispersion and drug resistance of fungal biofilms. *PLoS Pathog.* 7:e1002257. doi: 10.1371/journal.ppat.1002257

Rupert, C. B., Heltzel, J. M. H., Taylor, D. J., and Rusche, L. N. (2016). Sporadic Gene Loss After Duplication Is Associated with Functional Divergence of Sirtuin Deacetylases Among Candida Yeast Species. *G3* 6, 3297–3305. doi: 10.1534/g3.116.033845

Schilling, B., Meyer, J. G., Wei, L., Ott, M., and Verdin, E. (2019). High-resolution mass spectrometry to identify and quantify acetylation protein targets. *Methods Mol. Biol.* 1983, 3–16. doi: 10.1007/978-1-4939-9434-2_1

Shwab, E. K., Bok, J. W., Tribus, M., Galehr, J., Graessle, S., and Keller, N. P. (2007). Histone deacetylase activity regulates chemical diversity in *Aspergillus*. *Eukaryot. Cell* 6, 1656–1664. doi: 10.1128/EC.00186-07

Smith, W. L., and Edlind, T. D. (2002). Histone deacetylase inhibitors enhance *Candida albicans* sensitivity to azoles and related antifungals: correlation with reduction in CDR and ERG upregulation. *Antimicrob. Agents Chemother.* 46, 3532–3539. doi: 10.1128/aac.46.11.3532-3539.2002

Soukup, A. A., Chiang, Y.-M., Bok, J. W., Reyes-Dominguez, Y., Oakley, B. R., Wang, C. C. C., et al. (2012). Overexpression of the *Aspergillus nidulans* histone 4 acetyltransferase EsaA increases activation of secondary metabolite production. *Mol. Microbiol.* 86, 314–330. doi: 10.1111/j.1365-2958.2012.08195.x

Spange, S., Wagner, T., Heinzel, T., and Krämer, O. H. (2009). Acetylation of non-histone proteins modulates cellular signalling at multiple levels. *Int. J. Biochem. Cell Biol.* 41, 185–198. doi: 10.1016/j.biocel.2008.08.027

Srikantha, T., Tsai, L., Daniels, K., Klar, A. J., and Soll, D. R. (2001). The histone deacetylase genes HDA1 and RPD3 play distinct roles in regulation of high-frequency phenotypic switching in *Candida albicans*. *J. Bacteriol.* 183, 4614–4625. doi: 10.1128/JB.183.15.4614-4625.2001

Staniszewska, M., Bondaryk, M., Piłat, J., Siennicka, K., Magda, U., and Kurzatkowski, W. (2012). [Virulence factors of *Candida albicans*]. *Przegl. Epidemiol.* 66, 629–633.

Stevenson, J. S., and Liu, H. (2011). Regulation of white and opaque cell-type formation in *Candida albicans* by Rtt109 and Hst3. *Mol. Microbiol.* 81, 1078–1091. doi: 10.1111/j.1365-2958.2011.07754.x

Studt, L., Schmidt, F. J., Jahn, L., Sieber, C. M. K., Connolly, L. R., Niehaus, E. M., et al. (2013). Two histone deacetylases, FfHda1 and FfHda2, are important for Fusarium fujikuroi secondary metabolism and virulence. *Appl. Environ. Microbiol.* 79, 7719–7734. doi: 10.1128/AEM.01557-13

Sudbery, P. E. (2011). Growth of *Candida albicans* hyphae. *Nat. Rev. Microbiol.* 9, 737–748. doi: 10.1038/nrmicro2636

Takagi, J., Singh-Babak, S. D., Lohse, M. B., Dalal, C. K., and Johnson, A. D. (2019). *Candida albicans* white and opaque cells exhibit distinct spectra of organ colonization in mouse models of infection. *PLoS One* 14:e0218037. doi: 10.1371/journal.pone.0218037

Tan, S., and Liu, Z.-P. (2015). Natural products as zinc-dependent histone deacetylase inhibitors. *ChemMedChem* 10, 441–450. doi: 10.1002/cmdc.201402460

Tang, Y., and Yu, W. (2019). SIRT1 and p300/CBP regulate the reversible acetylation of serine-threonine kinase NDR2. *Biochem. Biophys. Res. Commun.* 518, 396–401. doi: 10.1016/j.bbrc.2019.08.069

Tcherniuk, S. O., Chesnokova, O., Oleinikov, I. V., and Oleinikov, A. V. (2017). Nicotinamide inhibits the growth of *P. falciparum* and enhances the antimalarial effect of artemisinin, chloroquine and pyrimethamine. *Mol. Biochem. Parasitol.* 216, 14–20. doi: 10.1016/j.molbiopara.2017.06.004

Trefely, S., Doan, M. T., and Snyder, N. W. (2019). Crosstalk between cellular metabolism and histone acetylation. *Methods Enzymol.* 626, 1–21. doi: 10.1016/bs.mie.2019.07.013

Tribus, M., Bauer, I., Galehr, J., Rieser, G., Trojer, P., Brosch, G., et al. (2010). A novel motif in fungal class 1 histone deacetylases is essential for growth and development of Aspergillus. *Mol. Biol. Cell* 21, 345–353. doi: 10.1091/mbc.E09-08-0750

Tribus, M., Galehr, J., Trojer, P., Brosch, G., Loidl, P., Marx, F., et al. (2005). HdaA, a major class 2 histone deacetylase of *Aspergillus nidulans*, affects growth under conditions of oxidative stress. *Eukaryot. Cell* 4, 1736–1745. doi: 10.1128/EC.4.10.1736-1745.2005

Tscherner, M., Zwolanek, F., Jenull, S., Sedlazeck, F. J., Petryshyn, A., Frohner, I. E., et al. (2015). The *Candida albicans* histone acetyltransferase Hat1 regulates stress resistance and virulence via distinct chromatin assembly pathways. *PLoS Pathog.* 11:e1005218. doi: 10.1371/journal.ppat.1005218

Tsuji, N., Kobayashi, M., Nagashima, K., Wakisaka, Y., and Koizumi, K. (1976). A new antifungal antibiotic, trichostatin. *J. Antibiot.* 29, 1–6. doi: 10.7164/antibiotics.29.1

Verdin, E., and Ott, M. (2015). 50 years of protein acetylation: from gene regulation to epigenetics, metabolism and beyond. *Nat. Rev. Mol. Cell Biol.* 16, 258–264. doi: 10.1038/nrm3931

von Knethen, A., and Brüne, B. (2019). Histone deacetylation inhibitors as therapy concept in sepsis. *Int. J. Mol. Sci.* 20:346. doi: 10.3390/ijms20020346

Wagner, G. R., and Hirschey, M. D. (2014). Nonenzymatic protein acylation as a carbon stress regulated by sirtuin deacylases. *Mol. Cell* 54, 5–16. doi: 10.1016/j.molcel.2014.03.027

Wang, G., Guo, L., Liang, W., Chi, Z., and Liu, L. (2017). Systematic analysis of the lysine acetylome reveals diverse functions of lysine acetylation in the oleaginous yeast *Yarrowia lipolytica*. *AMB Express* 7:94. doi: 10.1186/s13568-017-0393-2

Wang, J.-J., Cai, Q., Qiu, L., Ying, S.-H., and Feng, M.-G. (2018). The histone acetyltransferase Mst2 sustains the biological control potential of a fungal insect pathogen through transcriptional regulation. *Appl. Microbiol. Biotechnol.* 102, 1343–1355. doi: 10.1007/s00253-017-8703-9

Wang, X., Zhu, W., Chang, P., Wu, H., Liu, H., and Chen, J. (2018). Merge and separation of NuA4 and SWR1 complexes control cell fate plasticity in *Candida albicans*. *Cell Discov.* 4:45. doi: 10.1038/s41421-018-0043-0

Wang, Q., Zhang, Y., Yang, C., Xiong, H., Lin, Y., Yao, J., et al. (2010). Acetylation of metabolic enzymes coordinates carbon source utilization and metabolic flux. *Science* 327, 1004–1007. doi: 10.1126/science.1179687

Wang, X., Chang, P., Ding, J., and Chen, J. (2013). Distinct and redundant roles of the two MYST histone acetyltransferases Esa1 and Sas2 in cell growth and morphogenesis of *Candida albicans*. *Eukaryot. Cell* 12, 438–449. doi: 10.1128/EC.00275-12

Wassano, N. S., Leite, A. B., Reichert-Lima, F., Schreiber, A. Z., Moretti, N. S., and Damasio, A. (2020). Lysine acetylation as drug target in fungi: an underexplored potential in Aspergillus spp. *Braz. J. Microbiol.* 51, 673–683. doi: 10.1007/s42770-020-00253-w

Weinert, B. T., Iesmantavicius, V., Moustafa, T., Schölz, C., Wagner, S. A., Magnes, C., et al. (2014). Acetylation dynamics and stoichiometry in *Saccharomyces cerevisiae*. *Mol. Syst. Biol.* 10:716. doi: 10.1002/msb.134766

Wurtele, H., Tsao, S., Lépine, G., Mullick, A., Tremblay, J., Drogaris, P., et al. (2010). Modulation of histone H3 lysine 56 acetylation as an antifungal therapeutic strategy. *Nat. Med.* 16, 774–780. doi: 10.1038/nm.2175

Xie, L., Fang, W., Deng, W., Yu, Z., Li, J., Chen, M., et al. (2016). Global profiling of lysine acetylation in human histoplasmosis pathogen Histoplasma capsulatum. *Int. J. Biochem. Cell Biol.* 73, 1–10. doi: 10.1016/j.biocel.2016.01.008

Xing, X., Liao, Z., Tan, F., Zhu, Z., Jiang, Y., and Cao, Y. (2019). Effect of nicotinamide against *Candida albicans*. *Front. Microbiol.* 10:595. doi: 10.3389/fmicb.2019.00595

Xu, X., Liu, T., Yang, J., Chen, L., Liu, B., Wang, L., et al. (2018). The First Whole-Cell Proteome- and Lysine-Acetylome-Based Comparison between *Trichophyton rubrum* conidial and mycelial stages. *J. Proteome Res.* 17, 1436–1451. doi: 10.1021/acs.jproteome.7b00793

Yang, G., Yue, Y., Ren, S., Yang, M., Zhang, Y., Cao, X., et al. (2019). Lysine acetylation contributes to development, aflatoxin biosynthesis and pathogenicity in Aspergillus flavus. *Environ. Microbiol.* 21, 4792–4807. doi: 10.1111/1462-2920.14825

Yin, Z., Chen, C., Yang, J., Feng, W., Liu, X., Zuo, R., et al. (2019). Histone acetyltransferase MoHat1 acetylates autophagy-related proteins MoAtg3 and MoAtg9 to orchestrate functional appressorium formation and pathogenicity in *Magnaporthe oryzae*. *Autophagy* 15, 1234–1257. doi: 10.1080/15548627.2019.1580104

Zhang, L., and Xu, W. (2015). Histone deacetylase inhibitors for enhancing activity of antifungal agent: a patent evaluation of WO2014041424(A1). *Expert Opin. Ther. Pat.* 25, 237–240. doi: 10.1517/13543776.2014.981256

Zhang, N., Yang, Z., Zhang, Z., and Liang, W. (2020). BcRPD3-Mediated Histone Deacetylation Is Involved in Growth and Pathogenicity of Botrytis cinerea. *Front. Microbiol.* 11:1832. doi: 10.3389/fmicb.2020.01832

Zhao, W., Wang, T., Liu, S., Chen, Q., and Qi, R. (2015). The histone acetyltransferase PsGcn5 mediates oxidative stress responses and is required for full virulence of *Phytophthora sojae*. *Microb. Pathog.* 87, 51–58. doi: 10.1016/j.micpath.2015.07.015

Zhou, S., and Wu, C. (2019). Comparative acetylome analysis reveals the potential roles of lysine acetylation for DON biosynthesis in *Fusarium graminearum*. *BMC Genomics* 20:841. doi: 10.1186/s12864-019-6227-7

Zhou, S., Yang, Q., Yin, C., Liu, L., and Liang, W. (2016). Systematic analysis of the lysine acetylome in *Fusarium graminearum*. *BMC Genomics* 17:1019. doi: 10.1186/s12864-016-3361-3

Zhou, X., Qian, G., Yi, X., Li, X., and Liu, W. (2016). Systematic Analysis of the Lysine Acetylome in *Candida albicans*. *J. Proteome Res.* 15, 2525–2536. doi: 10.1021/acs.jproteome.6b00052

Conflict of Interest: The authors declare that the research was conducted in the absence of any commercial or financial relationships that could be construed as a potential conflict of interest.

frontiers in Microbiology

ORIGINAL RESEARCH
published: 07 October 2020
doi: 10.3389/fmicb.2020.562063

Discovery of Pyranoviolin A and Its Biosynthetic Gene Cluster in *Aspergillus violaceofuscus*

*Xingxing Wei[1], Lin Chen[1], Jian-Wei Tang[2] and Yudai Matsuda[1,3]**

[1] Department of Chemistry, City University of Hong Kong, Kowloon, Hong Kong, China, [2] Department of Ocean Science and Division of Life Science, Hong Kong University of Science and Technology, Clear Water Bay, Hong Kong, China, [3] City University of Hong Kong Shenzhen Research Institute, Shenzhen, China

A new polyketide-non-ribosomal peptide hybrid molecule, pyranoviolin A (**1**), was discovered from the genome-sequenced fungus *Aspergillus violaceofuscus* CBS 115571 and was characterized to be the first pyranonigrin analog harboring the C-3 methoxy group. Examination of the genome sequence of the fungus identified a putative biosynthetic gene cluster of **1**, which was designated as the *pyv* cluster. The gene deletion experiment of the polyketide synthase (PKS)-non-ribosomal peptide synthetase (NRPS) hybrid gene in the cluster confirmed the involvement of the *pyv* cluster in the pyranoviolin A biosynthesis. Finally, a plausible biosynthetic route leading to **1** has been proposed based on the bioinformatic analysis. Our study indicates that metabolite analysis of genome-sequenced microorganisms whose metabolites have been largely unexplored facilitates the discovery of new secondary metabolites along with their biosynthetic gene clusters.

Keywords: *Aspergillus violaceofuscus*, natural products, biosynthesis, fungal secondary metabolites, polyketide-non-ribosomal peptides

OPEN ACCESS

Edited by:
Koon Ho Wong,
University of Macau, China

Reviewed by:
Yit-Heng Chooi,
The University of Western Australia, Australia
Li Li,
Fujian Normal University, China
Liyan Wang,
Shenzhen University, China

****Correspondence:***
Yudai Matsuda
ymatsuda@cityu.edu.hk

Specialty section:
This article was submitted to Fungi and Their Interactions, a section of the journal Frontiers in Microbiology

Received: *14 May 2020*
Accepted: *16 September 2020*
Published: *07 October 2020*

Citation:
Wei X, Chen L, Tang J-W and Matsuda Y (2020) Discovery of Pyranoviolin A and Its Biosynthetic Gene Cluster in Aspergillus violaceofuscus. Front. Microbiol. 11:562063. doi: 10.3389/fmicb.2020.562063

INTRODUCTION

Filamentous fungi have been rich sources for naturally occurring organic compounds and thus provided many pharmaceutical drugs, as exemplified by penicillins, cyclosporin, and lovastatin. However, since a large number of natural products have been isolated and characterized over the past century, it is becoming challenging to obtain novel natural products only with traditional methodologies. As more and more microbial genomes have been sequenced, many researchers have been seeking to obtain novel metabolites by activating silent and unexploited biosynthetic gene clusters. This approach, generally described as "genome mining," has been widely utilized, leading to the discovery of many new natural products (Brakhage and Schroeckh, 2011; Rutledge and Challis, 2015; Zarins-Tutt et al., 2016; Yan et al., 2020). To activate a specific gene cluster, several different strategies could be used, including the overexpression of the pathway-specific transcriptional factor and heterologous expression of the gene cluster. Nevertheless, these strategies do not always work, probably due to the presence of "dead," rather than "silent," gene clusters (Montiel et al., 2015).

Meanwhile, we can now access the genome sequences of many microbial organisms whose metabolites have not been, or rarely, investigated. Thus, it is suggested that the metabolomic analysis of these microbial organisms leads to the rapid identification of new natural products. Additionally, because of the known genome sequences, the biosynthetic gene cluster of the

new metabolite could be readily identified, and the biosynthetic study can be performed quickly after the isolation of the compound (Cacho et al., 2015). Importantly, the rapid linking of secondary metabolites to their biosynthetic gene clusters facilitates biosynthetic engineering of important compounds and mining of other related natural products.

In this study, to examine this concept, we investigated the metabolites produced by the fungus *Aspergillus violaceofuscus* CBS 115571 (Vesth et al., 2018), and isolated and characterized one new polyketide-non-ribosomal peptide hybrid molecule named pyranoviolin A (**1**). Furthermore, the biosynthetic gene cluster of **1** was readily identified in the genome of the fungus, and a plausible biosynthetic pathway of **1** has been proposed, suggesting the usefulness of the concept to obtain new natural products together with their biosynthetic information.

MATERIALS AND METHODS

General

Organic solvents were purchased from Anaqua (Hong Kong) Co. Ltd., and other chemicals were purchased from Wako Chemicals Ltd., Thermo Fisher Scientific, Sigma-Aldrich, or J&K Scientific Ltd., unless noted otherwise. Oligonucleotide primers were purchased from Tech Dragon Limited. Polymerase chain reaction (PCR) was performed using a T100 Thermal Cycler (Bio-Rad Laboratories, Inc.) with the Phusion High-Fidelity DNA Polymerase (Thermo Fisher Scientific) or the Plant Direct PCR Kit (Vazyme Biotech Co., Ltd). Analytical LC/HR-ESI-MS analysis was performed on a Dionex Ultimate 3000 UHPLC system (Thermo Fisher Scientific) with a micrOTOF-Q II mass spectrometer (Bruker Daltonics), using a COSMOSIL 2.5Cholester packed column (2.0 i.d. × 100 mm; Nacalai Tesque, Inc.). Flash chromatography was performed using an Isolera Spektra One flash purification system (Biotage). Preparative HPLC was performed on a Waters 1525 Binary HPLC pump with a 2998 photodiode array detector (Waters Corporation), using an XBridge BEH C18 OBD Prep Column (100 Å, 5 μm, 19 i.d. × 250 mm; Waters Corporation). NMR spectra were obtained 600 MHz (^{1}H)/150 MHz (^{13}C)/60 MHz (^{15}N) with a Bruker Ascend Avance III HD spectrometer, and chemical shifts were recorded with reference to solvent signals [^{1}H NMR: DMSO-d_6 2.49 ppm; ^{13}C NMR: DMSO-d_6 39.5 ppm; ^{15}N NMR: 78.98 ppm (^{15}N urea as an external reference)]. Optical rotations were measured with P-2000 Digital Polarimeter (JASCO Corporation). CD spectra were obtained with J-1500 Circular Dichroism Spectrophotometer (JASCO Corporation). X-ray diffraction data were collected on a Bruker D8 Venture Photon II diffractometer. The glufosinate solution for the fungal transformation was extracted from Basta (Bayer) as previously described (Chooi et al., 2010) and used at a 50 μL/mL concentration.

HPLC Analysis

Analytical HPLC was performed with a solvent system of 20 mM formic acid (solvent A) and acetonitrile containing 20 mM formic acid (solvent B), at a flow rate of 0.4 mL/min and a column temperature of 40°C. The separation was performed using a linear gradient from 10:90 (solvent B/solvent A) to 100:0 for 10 min, 100:0 for the following 3 min, and a linear gradient from 100:0 to 10:90 within the following 2.5 min.

Production and Purification of Pyranoviolin A (1)

Aspergillus violaceofuscus CBS 115571 was purchased from the Westerdijk Fungal Biodiversity Institute, inoculated on 100 YES agar plates [*ca.* 2 L; 20 g/L yeast extract, 150 g/L sucrose, 0.5 g/L $MgSO_4{\cdot}7H_2O$, 20 g/L agar supplemented with 1mL/L of a trace element solution (10 g/L $ZnSO_4{\cdot}7H_2O$, 5 g/L $CuSO_4{\cdot}5H_2O$), pH 6.5], and cultivated for 9 days at 25°C. The resultant fungal cultures including agar were crushed into small pieces and extracted with ethyl acetate twice using an ultrasonic bath. The crude extract was subjected to flash chromatography with Biotage® SNAP KP-Sil cartridge (100 g) and eluted stepwise using chloroform:ethyl acetate gradient (100:0 to 0:100). Fractions that contained **1** were concentrated and further purified by reverse-phase preparative HPLC (40% aqueous acetonitrile containing 0.05% trifluoroacetic acid, 10 mL/min) to yield 64.9 mg of colorless crystals.

Calculation of the ECD Spectrum of Pyranoviolin A (1)

Initially, an exhaustive conformation space search of (7*R*)-**1** and (7*S*)-**1** were conducted by Conformer-Rotamer Ensemble Sampling Tool (CREST) version 2.8 (Pracht et al., 2020). Fifteen conformers for (7*R*)-**1** and (7*S*)-**1**, respectively, were obtained with relative energies in 5 kcal/mol. All conformers were then optimized in Gaussian 09 software package (Frisch et al., 2010) at M062x/def2tzvp level with PCM in methanol. The optimized conformers with the Boltzmann distribution >1% were further calculated for the ECD by using TDDFT at cam-b3lyp/tzvp level with PCM in methanol. The ECD spectrum was obtained by weighing the Boltzmann distribution rate of each geometric conformation in Multiwfn 3.6 (Lu and Chen, 2012).

The ECD spectrum is simulated by overlapping Gaussian functions for each transition according to:

$$\Delta\varepsilon(E) = \frac{1}{2.297\times10^{-39}} \times \frac{1}{\sqrt{2\psi}} \sum_{i}^{A} \Delta E_i R_i e^{-[(E-E_i)/(2\sigma)]^2}$$

Where σ represents the width of the band at 1/*e* height, and ΔE_i and R_i are the excitation energies and rotational strengths for transition *i*, respectively. σ = 0.5 eV and $R^{velocity}$ have been used in this work.

The optimized conformation geometries, thermodynamic parameters, key transitions, oscillator strengths, and rotatory strengths in the ECD spectrum and populations of all conformations were provided in **Supplementary Tables 1–16**.

Gene Deletion Experiment of *pyvA*

The gene deletion of *pyvA* was performed by CRISPR-Cas9-mediated target gene break and repair with a microhomology

repair template, as previously described for *Aspergillus fumigatus* (Al Abdallah et al., 2017). The components for the dual Cas9-gRNA system, namely Cas9 protein, CRISPR RNAs (crRNAs), and transactivating CRISPR RNA (tracrRNA), were purchased from Integrated DNA Technologies; two separate crRNAs were designed at 5′- and 3′-end regions of *pyvA*, respectively (protospacer sequences: 5′-AAAGGCACCACACAAGACGG-3′; 5′-CGGAACCAAGTCCACGACGA-3′). The Cas9 ribonucleoprotein (RNP) complexes were assembled as reported (Al Abdallah et al., 2017). The microhomology repair template for the fungal transformation was amplified from pBARI (Matsuda et al., 2014) using the primers pyvA_bar-F (5′-CCGGAATCTCCTTGGAGGAGATGAACGGCTCACGCACC TTTGGTGATTGGAATAACTGAC-3′) and pyvA_bar-R (5′-GGAGCGCCGTGAGATAGTTGACCGGAACCAAGTCC ACGACGTGACGATGAGCCGCTCTTG-3′), generating the glufosinate-resistant gene (*bar*) flanked by microhomology arms targeting *pyvA*. The transformation of *A. violaceofuscus* and selection of transformants were performed as previously described for *Aspergillus oryzae* (Matsuda et al., 2018) except that the lysing enzymes from *Trichoderma harzianum* (Sigma-Aldrich) was used as fungal cell lytic enzymes at a concentration of 40 mg/mL. The successful deletion of *pyvA* was confirmed by colony-direct PCR of the transformant using the primers pyvA-check-F (5′-CATCGAACAGAAGGATGTGAGGCGCAAAC-3′) and PptrA-check-R (5′-CTATCATCTGTTAGCCATTCCATCAACAGG-3′) (**Supplementary Figure S10**).

Analytical Data

Pyranoviolin A (**1**): Colorless crystal; $[\alpha]^{24}_D$ + 61.3 (*c* 1.00, MeOH); CD (*c* 0.025, MeOH) λ, nm (Δε) 200 (−5.9), 210 (−3.4), 219 (−4.1), 244 (+1.8), 271 (+4.6), 334 (−0.3); for NMR spectra see **Supplementary Figures 1–7**; HRMS (ESI) *m/z*: $[M + Na]^+$ Calcd. for $C_{13}H_{15}NO_5Na$ 288.0842; Found 288.0850.

Crystallographic data for pyranoviolin A (**1**): $C_{13}H_{15}NO_5$, M = 265.26, a = 9.7800(2) Å, b = 18.8599(3) Å, c = 20.9282(4) Å, α = 90°, β = 90°, γ = 90°, V = 3860.20(12) Å^3, T = 213(2) K, space group $P2_12_12_1$, Z = 12, μ(Cu Kα) = 0.893 mm^{-1}, 43 655 reflections measured, 7883 independent reflections (R_{int} = 0.0435). The final R_1 values were 0.0345 ($I > 2\sigma(I)$). The final $wR(F^2)$ values were 0.0918 ($I > 2\sigma(I)$). The final R_1 values were 0.0389 (all data). The final $wR(F^2)$ values were 0.0961 (all data). The goodness of fit on F^2 was 1.022. Flack parameter = 0.00(5). The crystallographic information file (CIF) for this crystal structure was submitted to The Cambridge Crystallographic Data Centre (CCDC), under reference number 2003775.

RESULTS AND DISCUSSION

Search for a New Metabolite in *Aspergillus violaceofuscus* CBS 115571

Aspergillus violaceofuscus CBS 115571 is one of the *Aspergillus* fungi whose genomes have been recently sequenced and published (Vesth et al., 2018). Analysis of the genome of the *A. violaceofuscus* strain using antiSMASH (Blin et al., 2019) suggested that the fungus harbors ∼80 biosynthetic gene clusters for secondary metabolites; however, only a few natural products have been isolated from this species (Myobatake et al., 2014; Liu et al., 2018), implying the potential of *A. violaceofuscus* to produce new natural products. The fungus produced several major metabolites, which are predicted to be calbistrins (Brill et al., 1993), eupenoxide (Mehta and Roy, 2004), and himeic acid A (Tsukamoto et al., 2005) based on their molecular formulas and UV spectra (**Supplementary Figure 8**). The ethyl acetate extract of the fungus cultivated on YES agar plate revealed the presence of one major product

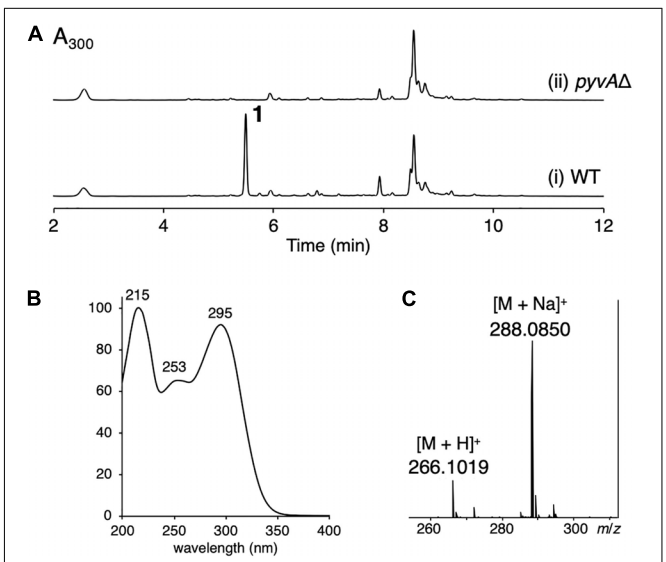

FIGURE 1 | (A) HPLC profile of the ethyl acetate extract of (i) the wild type (WT) and (ii) the *pyvA*Δ mutant of *A. violaceofuscus* CBS 115571. The chromatograms were monitored at 300 nm. **(B)** The UV spectrum of **1**. **(C)** The mass spectrum of **1**.

TABLE 1 | NMR data of **1**.

Position	δ_C, type	δ_N	δ_H, mult. (*J* in Hz)
2	154.1, C		
3	143.7, C		
4	169.9, C		
4a	113.9, C		
5	164.6, C		
6-NH		129.2	8.63, brs
7	74.9, CH		5.73, dd (9.2, 1.5)
7a	174.8, C		
8	60.3, CH_3		3.76, s
1′	117.2, CH		6.57, d (15.8)
2′	139.7, CH		6.61, dd (15.8, 5.9)
3′	34.5, CH_2		2.27, m
4′	21.4, CH_2		1.48, sext (7.3)
5′	13.6, CH_3		0.91, t (7.3)
7-OH			6.81, d (9.2)

^{1}H NMR, 600 MHz; ^{13}C NMR, 150 MHz; ^{15}N NMR, 60 MHz (in DMSO-d_6).

1 (**Figure 1A**, trace i). Compound **1** exhibited UV maxima at 215 nm, 253 nm, and 295 nm (**Figure 1B**), and its molecular formula was determined to be $C_{13}H_{15}NO_5$ by HR-ESI-MS analysis (**Figure 1C**). The database search indicated that **1** is a previously unreported metabolite. Thus, the *A. violaceofuscus* strain was cultivated on a large scale, and **1** was successfully purified by a series of chromatographic procedures.

Characterization of Pyranoviolin A

As mentioned above, the molecular formula of **1** was established as $C_{13}H_{15}NO_5$, indicating seven degrees of unsaturation. The ^{13}C NMR spectrum revealed 13 signals (**Table 1**), consisting of two methyls, including one methoxy (C-8), two methylenes, three methines, including one oxymethine (C-7) and two olefinic methines (C-1′ and C-2′), four olefinic quaternary carbons (C-2, C-3, C-4a, C-7a), and two carbonyls (C-4 and C-5). Additionally, interpretation of ^1H and ^{15}N NMR spectra illuminated the presence of one hydroxy group (7-OH: δ_H 6.81) and one amide nitrogen (6-NH: δ_H 8.63; δ_N 129.2). Altogether, it was indicated that **1** possesses a bicyclic structure.

The ^1H-^1H COSY spectrum then revealed the spin systems of 6-NH/H-7/7-OH and H-1′/H-2′/H_2-3′/H_2-4′/H_3-5′ (**Figures 2A,B**). Furthermore, the HMBC correlations of H-1′ (δ_H 6.57) and H-2′ (δ_H 6.61) to C-2, 6-NH (δ_H 8.63) to C-4a, C-5, C-7, and C-7a, H-7 (δ_H 5.73) to C-4a, C-5, and C-7a, 7-OH (δ_H 6.81) to C-7 and C-7a, and H-8 (δ_H 3.76) to C-3 established the connections of C-1′ to C-2, C-5 to C-4a and N-6, C-7a to C-7 and C-4a, and C-3 to C-8 via one oxygen atom (**Figure 2B**). In the course of the structural determination, we noted that the NMR spectra of **1** highly resemble those of another fungal metabolite pyranonigrin F isolated from *Penicillium brocae* (Meng et al., 2015), except that the signal for the methoxy group is missing in pyranonigrin F [Note that two distinct natural products are individually named "pyranonigrin F" (Meng et al., 2015; Yamamoto et al., 2015) (**Supplementary Figure 9**)]. The comparison of the NMR spectra elucidated the presence of γ-pyrone in **1**, thus establishing the planar structure of **1**, which is a methylated analog of pyranonigrin F and hereby named pyranoviolin A. Pyranoviolin A is the first example of a pyranonigrin analogs with the C-3 methoxy group.

To determine the absolute configuration of **1** at C-7 position, we obtained the calculated electron circular dichroism (ECD) spectra of (7*R*)- and (7*S*)-**1** and compared them with the experimental ECD spectrum of **1** (**Figure 2C**), which suggested the absolute configuration of **1** to be 7*R*. To further confirm the predicted structure, we performed single-crystal X-ray diffraction

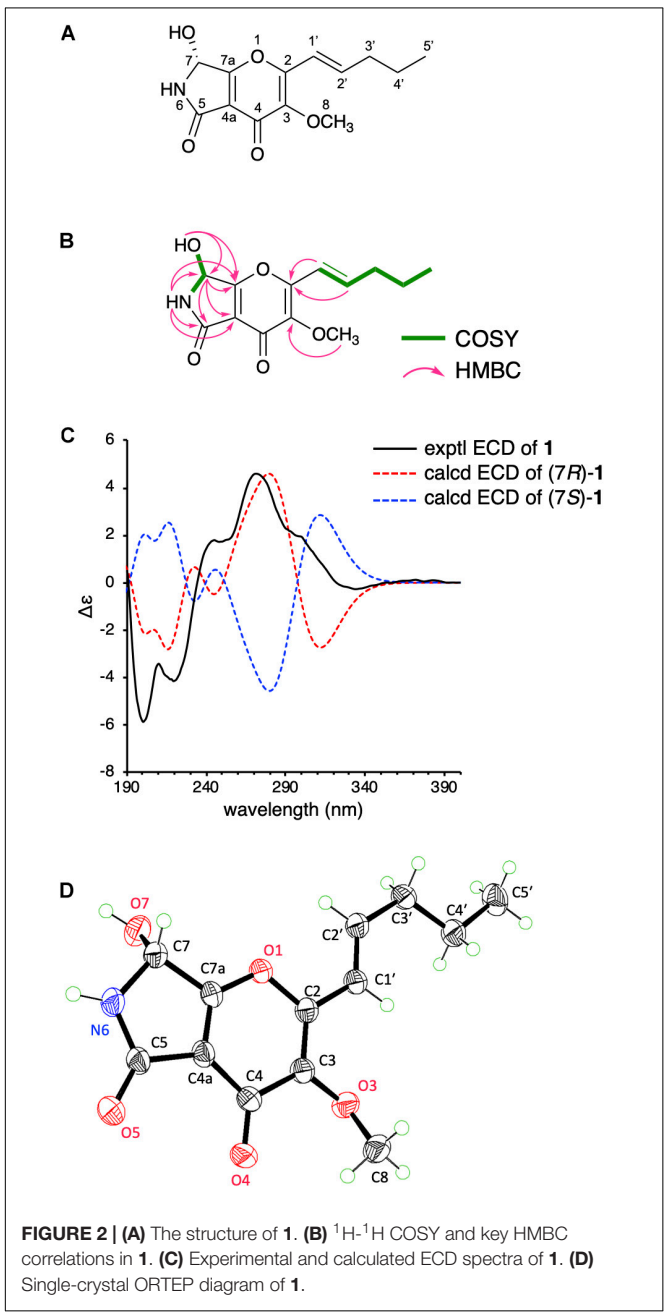

FIGURE 2 | (A) The structure of **1**. **(B)** ^1H-^1H COSY and key HMBC correlations in **1**. **(C)** Experimental and calculated ECD spectra of **1**. **(D)** Single-crystal ORTEP diagram of **1**.

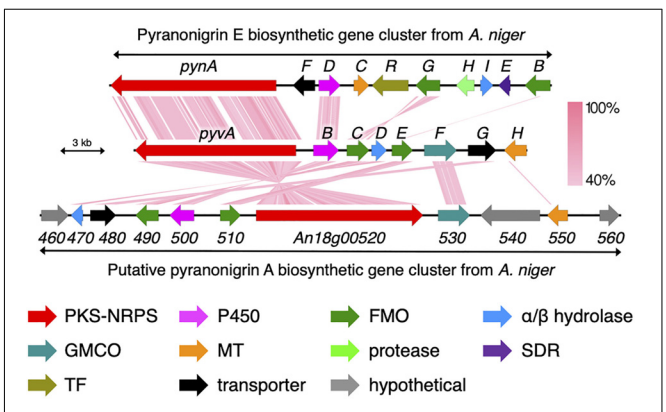

FIGURE 3 | Schematic representation of the *pyv* cluster and tblastx comparison with the biosynthetic gene clusters for pyranonigrins A and E. PKS-NRPS, polyketide synthase-non-ribosomal peptide synthetase; P450, cytochrome P450 monooxygenase; FMO, flavin-dependent monooxygenase; GMCO, glucose–methanol–choline family of oxidoreductase; MT, methyltransferase; SDR, short-chain dehydrogenase/reductase; TF, transcription factor.

analysis of **1** using Cu Kα radiation and successfully determined the crystal structure of **1** with a Flack parameter of 0.00(5) (**Figure 2D**), which is consistent with the structure deduced from the NMR data and the calculation. Collectively, the structure of **1** has been unambiguously established, revealing that **1** possesses the same absolute stereochemistry as those of pyranonigrins A and F.

We then investigated the biological activity of **1**. Since the demethylated analog of **1**, pyranonigrin F, reportedly displays potent activity against some bacteria (Meng et al., 2015), including *Staphylococcus aureus*, we evaluated the antibacterial property of **1** using the previously described method (Zhao et al., 2018). However, **1** unfortunately did not show any antibacterial activity against the six tested strains, namely *Staphylococcus aureus* ATCC 6538, *Pseudomonas aeruginosa* ATCC 7700, *Escherichia coli* ATCC 10536, *Staphylococcus epidermidis* ATCC 12228, *Bacillus cereus*, and *Salmonella typhimurium* TA100. Given that the structural difference of **1** from pyranonigrin F is only the presence of the methyl group, it could be reasoned that the C-3 hydroxy group is critical for the biological activity.

Investigation on the Biosynthesis of Pyranoviolin A

We next sought to identify the biosynthetic gene cluster of pyranoviolin A (**1**) in the genome of *A. violaceofuscus* CBS 115571. Given the structural similarity of **1** and pyranonigrins, the biosynthetic gene cluster of **1** should be somewhat homologous to those of pyranonigrins (Awakawa et al., 2013; Yokoyama et al., 2017; Tang et al., 2018). Examination of the genome sequence identified one candidate gene cluster

TABLE 2 | Annotation of each gene in the *pyv* cluster.

Gene (Accession code)	Amino acid (Base pairs)	Protein homolog [origin]	Similarity/identity (%)	Proposed function
pyvA (PYI13694.1)	3940 (11971)	ANI_1_982164 [*Aspergillus niger*]	73/60	Polyketide synthase-non-ribosomal peptide synthetase
pyvB (PYI13693.1)	487 (1644)	ANI_1_978164 [*Aspergillus niger*]	78/65	Cytochrome P450 monooxygenase
pyvC (PYI13692.1)	427 (1603)	ANI_1_976164 [*Aspergillus niger*]	84/70	Flavin-dependent monooxygenase
pyvD (PYI13691.1)	245 (934)	ANI_1_972164 [*Aspergillus niger*]	79/67	α/β hydrolase
pyvE (PYI13690.1)	452 (1431)	ANI_1_980164 [*Aspergillus niger*]	83/74	Flavin-dependent monooxygenase
pyvF (PYI13689.1)	629 (2323)	ANI_1_984164 [*Aspergillus niger*]	62/45	Glucose-methanol-choline family oxidoreductase
pyvG (PYI13688.1)	543 (1894)	ANI_1_974164 [*Aspergillus niger*]	78/65	Major facilitator superfamily transporter
pyvH (PYI13687.1)	426 (1559)	PaMT [*Diaporthe amygdali*]	55/36	*O*-methyltransferase

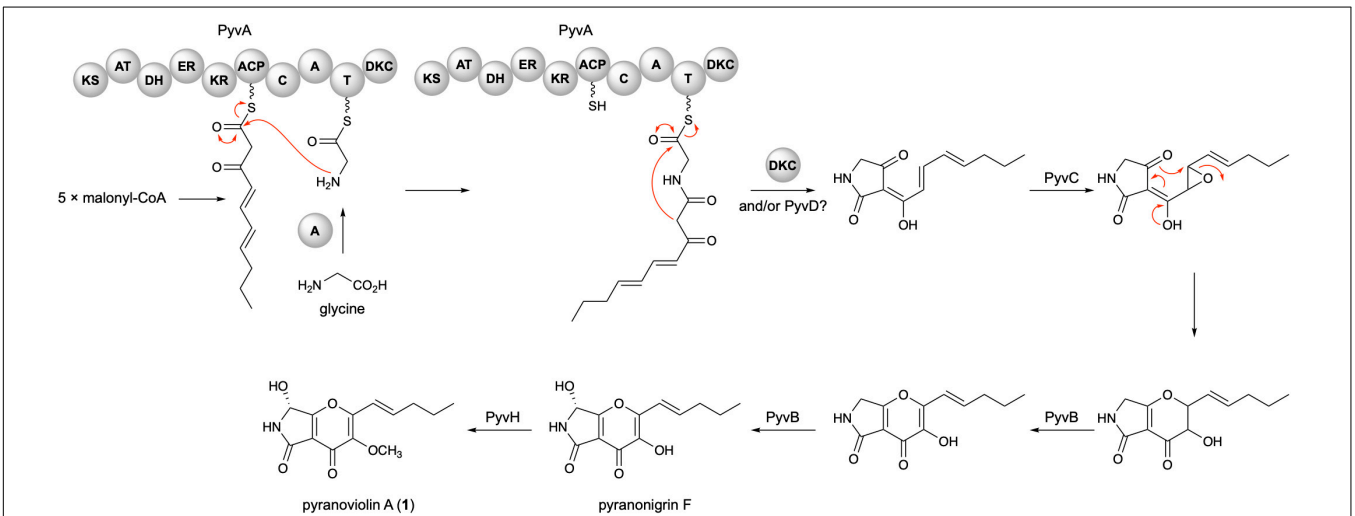

FIGURE 4 | Predicted biosynthetic pathway of **1**.

for the pyranoviolin A biosynthesis (**Figure 3** and **Table 2**), which was designated as the *pyv* cluster (DDBJ/EMBL/GenBank accession number: BR001648). The *pyv* cluster encodes a polyketide synthase (PKS)-non-ribosomal peptide synthetase (NRPS) hybrid PyvA, a cytochrome P450 monooxygenase PyvB, two flavin-dependent monooxygenases (FMOs) PyvC and PyvE, an α/β hydrolase PyvD, glucose–methanol–choline (GMC) family of oxidoreductase PyvF, and *O*-methyltransferase PyvH. Among these proteins, homologous enzymes of PyvA, PyvB, and PyvC are involved in the biosynthesis of pyranonigrins A and E (**Figure 3**), which are known to be responsible for the construction of the backbone skeleton of pyranonigrins (Yamamoto et al., 2015; Tang et al., 2018). Meanwhile, close homologs of PyvD, PyvE, and PyvF are encoded by the biosynthetic gene clusters of pyranonigrin A; PyvD might be engaged in the Dieckmann condensation to release the polyketide-non-ribosomal peptide chain, whereas the PyvE and PyvF homologs in the pyranonigrin A pathway have no apparent function in the biosynthesis. The *O*-methyltransferase gene *pyvH* is specifically found in the *pyv* cluster, which is consistent with the observation that C-3 methoxy group is only present in pyranoviolin A (**1**).

To confirm the involvement of the *pyv* cluster in the biosynthesis of pyranoviolin A (**1**), we deleted the PKS-NRPS hybrid gene *pyvA* by means of CRISPR-Cas9-based genome editing technology (Al Abdallah et al., 2017). The disruption of *pyvA* completely abolished the production of **1** (**Figure 1A**, trace ii), thus demonstrating that the *pyv* cluster is indeed responsible for the pyranoviolin A biosynthesis.

On the basis of the bioinformatic analysis and previous biosynthetic studies on pyranonigrins, the biosynthetic route leading to pyranoviolin A (**1**) can be proposed as follows (**Figure 4**). Initially, the PKS portion of PyvA synthesizes C_{10} carbon chain from five molecules of malonyl-CoA, which is then condensed with the thiolation (T) domain-bound glycine activated by the adenylation (A) domain. The subsequent chain release by Dieckmann condensation (DKC) could be catalyzed by the DKC domain present at the C-terminus of PyvA and/or the α/β hydrolase PyvD, installing the tetramic acid moiety. The FMO PyvC next epoxidizes one of the olefins of the polyketide part, and the epoxide ring-opening induces the dihydro-γ-pyrone ring formation. The P450 PyvB would be responsible for the two consecutive reactions, in which the dihydro-γ-pyrone is oxidized to γ-pyrone and C-7 is hydroxylated to yield pyranonigrin F. Finally, the *O*-methyltransferase PyvH, which is specifically found in the pyranoviolin A pathway, methylates the C-3 hydroxy group to complete the biosynthesis.

CONCLUSION

In this study, we discovered a new polyketide-non-ribosomal peptide hybrid molecule pyranoviolin A (**1**) from *Aspergillus violaceofuscus* CBS 115571 and identified the biosynthetic gene cluster of **1** in the genome of the fungus. Compound **1** possesses a methoxy group at C-3, which had not been reported in this family of natural products. Our study indicates that working on genome-sequenced microorganisms whose metabolic profiles have not, or poorly, been investigated can readily discover new natural products and link the metabolites with their biosynthetic gene clusters. Given that many microbial genomes have been or being sequenced, this approach would accelerate the discovery of new natural products and characterization of their biosynthetic enzymes, which expands the natural product diversity and repertoire of unusual biosynthetic enzymes.

DATA AVAILABILITY STATEMENT

The datasets presented in this study can be found in online repositories. The names of the repository/repositories and accession number(s) can be found in the article/**Supplementary Material**.

AUTHOR CONTRIBUTIONS

XW, LC, and YM performed the experiments and analyzed the data. J-WT performed the ECD calculation. YM designed the research and wrote the manuscript. All authors approved the manuscript.

FUNDING

This study was supported by the grants from City University of Hong Kong (Project Nos. 7200579 and 9610412) and the National Natural Science Foundation of China (Project No. 21907083).

ACKNOWLEDGMENTS

The authors thank Dr. Man-Kit Tse (City University of Hong Kong), Dr. Shek-Man Yiu (City University of Hong Kong), and Dr. Wei-Guang Wang (Yunnan Minzu University) for their assistance in NMR/CD spectra acquisition, X-ray diffraction data collection and analysis, and ECD calculation, respectively.

SUPPLEMENTARY MATERIAL

The Supplementary Material for this article can be found online at: https://www.frontiersin.org/articles/10.3389/fmicb.2020.562063/full#supplementary-material

REFERENCES

Al Abdallah, Q., Ge, W., and Fortwendel, J. R. (2017). A simple and universal system for gene manipulation in *Aspergillus fumigatus*: *in vitro*-assembled Cas9-guide RNA ribonucleoproteins coupled with microhomology repair templates. *mSphere* 2:e00446-17. doi: 10.1128/mSphere.00446-17

Awakawa, T., Yang, X.-L., Wakimoto, T., and Abe, I. (2013). Pyranonigrin E: a PKS-NRPS hybrid metabolite from *Aspergillus niger* identified by genome mining. *ChemBioChem* 14, 2095–2099. doi: 10.1002/cbic.201300430

Blin, K., Shaw, S., Steinke, K., Villebro, R., Ziemert, N., Lee, S. Y., et al. (2019). antiSMASH 5.0: updates to the secondary metabolite genome mining pipeline. *Nucleic Acids Res.* 47, W81–W87. doi: 10.1093/nar/gkz310

Brakhage, A. A., and Schroeckh, V. (2011). Fungal secondary metabolites–strategies to activate silent gene clusters. *Fungal Genet. Biol.* 48, 15–22. doi: 10.1016/j.fgb.2010.04.004

Brill, G. M., Chen, R. H., Rasmussen, R. R., Whittern, D. N., and Mcalpine, J. B. (1993). Calbistrins, novel antifungal agents produced by *Penicillium restrictum*. II. Isolation and elucidation of structure. *J. Antibiot.* 46, 39–47. doi: 10.7164/antibiotics.46.39

Cacho, R. A., Tang, Y., and Chooi, Y.-H. (2015). Next-generation sequencing approach for connecting secondary metabolites to biosynthetic gene clusters in fungi. *Front. Microbiol.* 5:774. doi: 10.3389/fmicb.2014.00774

Chooi, Y.-H., Cacho, R., and Tang, Y. (2010). Identification of the viridicatumtoxin and griseofulvin gene clusters from *Penicillium aethiopicum*. *Chem. Biol.* 17, 483–494. doi: 10.1016/j.chembiol.2010.03.015

Frisch, M. J., Trucks, G. W., Schlegel, H. B., Scuseria, G. E., Robb, M. A., Cheeseman, J. R., et al. (2010). *Gaussian 09, Revision E.01*. Wallingford, CT: Gaussian Inc.

Liu, J., Gu, B., Yang, L., Yang, F., and Lin, H. (2018). New anti-inflammatory cyclopeptides from a sponge-derived fungus *Aspergillus violaceofuscus*. *Front. Chem.* 6:226. doi: 10.3389/fchem.2018.00226

Lu, T., and Chen, F. (2012). Multiwfn: a multifunctional wavefunction analyzer. *J. Comput. Chem.* 33, 580–592. doi: 10.1002/jcc.22885

Matsuda, Y., Bai, T., Phippen, C. B. W., Nødvig, C. S., Kjærbølling, I., Vesth, T. C., et al. (2018). Novofumigatonin biosynthesis involves a non-heme iron-dependent endoperoxide isomerase for orthoester formation. *Nat. Commun.* 9:2587. doi: 10.1038/s41467-018-04983-2

Matsuda, Y., Wakimoto, T., Mori, T., Awakawa, T., and Abe, I. (2014). Complete biosynthetic pathway of anditomin: nature's sophisticated synthetic route to a complex fungal meroterpenoid. *J. Am. Chem. Soc.* 136, 15326–15336. doi: 10.1021/ja508127q

Mehta, G., and Roy, S. (2004). Enantioselective total synthesis of (+)-eupenoxide and (+)-phomoxide: revision of structures and assignment of absolute configuration. *Org. Lett.* 6, 2389–2392. doi: 10.1021/ol0492288

Meng, L.-H., Li, X.-M., Liu, Y., and Wang, B.-G. (2015). Polyoxygenated dihydropyrano[2,3-c]pyrrole-4,5-dione derivatives from the marine mangrove-derived endophytic fungus *Penicillium brocae* MA-231 and their antimicrobial activity. *Chin. Chem. Lett.* 26, 610–612. doi: 10.1016/j.cclet.2015.01.024

Montiel, D., Kang, H.-S., Chang, F.-Y., Charlop-Powers, Z., and Brady, S. F. (2015). Yeast homologous recombination-based promoter engineering for the activation of silent natural product biosynthetic gene clusters. *Proc. Natl. Acad. Sci. U.S.A.* 112, 8953–8958. doi: 10.1073/pnas.1507606112

Myobatake, Y., Takemoto, K., Kamisuki, S., Inoue, N., Takasaki, A., Takeuchi, T., et al. (2014). Cytotoxic alkylated hydroquinone, phenol, and cyclohexenone derivatives from *Aspergillus violaceofuscus* Gasperini. *J. Nat. Prod.* 77, 1236–1240. doi: 10.1021/np401017g

Pracht, P., Bohle, F., and Grimme, S. (2020). Automated exploration of the low-energy chemical space with fast quantum chemical methods. *Phys. Chem. Chem. Phys.* 22, 7169–7192. doi: 10.1039/C9CP06869D

Rutledge, P. J., and Challis, G. L. (2015). Discovery of microbial natural products by activation of silent biosynthetic gene clusters. *Nat. Rev. Microbiol.* 13:509. doi: 10.1038/nrmicro3496

Tang, M.-C., Zou, Y., Yee, D., and Tang, Y. (2018). Identification of the pyranonigrin A biosynthetic gene cluster by genome mining in *Penicillium thymicola* IBT 5891. *AIChE J.* 64, 4182–4186. doi: 10.1002/aic.16324

Tsukamoto, S., Hirota, H., Imachi, M., Fujimuro, M., Onuki, H., Ohta, T., et al. (2005). Himeic acid A: a new ubiquitin-activating enzyme inhibitor isolated from a marine-derived fungus, *Aspergillus* sp. *Bioorgan. Med. Chem. Lett.* 15, 191–194. doi: 10.1016/j.bmcl.2004.10.012

Vesth, T. C., Nybo, J. L., Theobald, S., Frisvad, J. C., Larsen, T. O., Nielsen, K. F., et al. (2018). Investigation of inter- and intraspecies variation through genome sequencing of *Aspergillus* section *Nigri*. *Nat. Genet.* 50, 1688–1695. doi: 10.1038/s41588-018-0246-1

Yamamoto, T., Tsunematsu, Y., Noguchi, H., Hotta, K., and Watanabe, K. (2015). Elucidation of pyranonigrin biosynthetic pathway reveals a mode of tetramic acid, fused γ-pyrone, and *exo*-methylene formation. *Org. Lett.* 17, 4992–4995. doi: 10.1021/acs.orglett.5b02435

Yan, Y., Liu, N., and Tang, Y. (2020). Recent developments in self-resistance gene directed natural product discovery. *Nat. Prod. Rep.* 37, 879–892. doi: 10.1039/C9NP00050J

Yokoyama, M., Hirayama, Y., Yamamoto, T., Kishimoto, S., Tsunematsu, Y., and Watanabe, K. (2017). Integration of chemical, genetic, and bioinformatic approaches delineates fungal polyketide–peptide hybrid biosynthesis. *Org. Lett.* 19, 2002–2005. doi: 10.1021/acs.orglett.7b00559

Zarins-Tutt, J. S., Barberi, T. T., Gao, H., Mearns-Spragg, A., Zhang, L., Newman, D. J., et al. (2016). Prospecting for new bacterial metabolites: a glossary of approaches for inducing, activating and upregulating the biosynthesis of bacterial cryptic or silent natural products. *Nat. Prod. Rep.* 33, 54–72. doi: 10.1039/C5NP00111K

Zhao, Z.-Z., Zhao, K., Chen, H.-P., Bai, X., Zhang, L., and Liu, J.-K. (2018). Terpenoids from the mushroom-associated fungus *Montagnula donacina*. *Phytochemistry* 147, 21–29. doi: 10.1016/j.phytochem.2017.12.015

Conflict of Interest: The authors declare that the research was conducted in the absence of any commercial or financial relationships that could be construed as a potential conflict of interest.

frontiers in Microbiology

ORIGINAL RESEARCH
published: 23 October 2020
doi: 10.3389/fmicb.2020.564350

Global Proteomic Analysis of Lysine Crotonylation in the Plant Pathogen *Botrytis cinerea*

Ning Zhang, Zhenzhou Yang, Wenxing Liang and Mengjie Liu**

Key Lab of Integrated Crop Pest Management of Shandong Province, College of Plant Health and Medicine, Qingdao Agricultural University, Qingdao, China

Lysine crotonylation (Kcr), a recently discovered post-translational modification, plays a key role in the regulation of diverse cellular processes. *Botrytis cinerea* is a destructive necrotrophic fungal pathogen distributed worldwide with broad ranging hosts. However, the functions of Kcr are unknown in *B. cinerea* or any other plant fungal pathogens. Here, we comprehensively evaluated the crotonylation proteome of *B. cinerea* and identified 3967 Kcr sites in 1041 proteins, which contained 9 types of modification motifs. Our results show that although the crotonylation was largely conserved, different organisms contained distinct crotonylated proteins with unique functions. Bioinformatics analysis demonstrated that the majority of crotonylated proteins were distributed in cytoplasm (35%), mitochondria (26%), and nucleus (22%). The identified proteins were found to be involved in various metabolic and cellular processes, such as cytoplasmic translation and structural constituent of ribosome. Particularly, 26 crotonylated proteins participated in the pathogenicity of *B. cinerea*, suggesting a significant role for Kcr in this process. Protein interaction network analysis demonstrated that many protein interactions are regulated by crotonylation. Furthermore, our results show that different nutritional conditions had a significant influence on the Kcr levels of *B. cinerea*. These data represent the first report of the crotonylome of *B. cinerea* and provide a good foundation for further explorations of the role of Kcr in plant fungal pathogens.

Keywords: crotonylome, *Botrytis cinerea*, LC-MS/MS, fungal pathogenicity, lysine crotonylation

OPEN ACCESS

Edited by:
Chengshu Wang, Chinese Academy of Sciences, China

Reviewed by:
Wolfgang Buckel, University of Marburg, Germany
Wende Liu, Chinese Academy of Agricultural Sciences, China

****Correspondence:***
Wenxing Liang
wliang1@qau.edu.cn
Mengjie Liu
mjlliu@qau.edu.cn

Specialty section:
This article was submitted to Fungi and Their Interactions, a section of the journal Frontiers in Microbiology

Received: *21 May 2020*
Accepted: *08 October 2020*
Published: *23 October 2020*

Citation:
Zhang N, Yang Z, Liang W and Liu M (2020) Global Proteomic Analysis of Lysine Crotonylation in the Plant Pathogen Botrytis cinerea. Front. Microbiol. 11:564350. doi: 10.3389/fmicb.2020.564350

INTRODUCTION

Post-translational modifications (PTMs), in which functional groups are covalently introduced to amino acid residues, play important roles in regulating diverse biological processes (Khoury et al., 2011). With the application of liquid chromatography-mass spectrometry (LC-MS/MS)-based proteomics, an array of novel PTMs have been identified. Particularly, lysine residues are targeted by numerous PTMs, including acetylation, succinylation, butyrylation, propionylation, 2-hydroxyisobutyrylation, glutarylation, malonylation, lactylation, and crotonylation (Chen et al., 2007; Tan et al., 2011; Dai et al., 2014; Hirschey and Zhao, 2015; Zhang et al., 2019). Currently, there is a lack of research on the identification of substrates of these PTMs and elucidation of their functional impacts.

Lysine crotonylation (Kcr) was first identified on histones and its role in regulation of gene transcription has been well investigated (Tan et al., 2011). HDAC1, a member of the class I histone

deacetylases (HDACs), was found to catalyze histone decrotonylation in mammalian cells (Wei et al., 2017a). Therefore, it is presumed that both protein crotonylation and acetylation are regulated by histone acetyltransferases (HATs) and HDACs. Other than histone proteins, crotonylation is newly discovered targeting non-histone proteins, regulating protein stability, enzymatic activity, protein localization, and many other cellular processes (Wei et al., 2017b; Xu et al., 2017). Advancements in novel enrichment strategies (LC-MS/MS) have made it possible to investigate Kcr on a proteomic level and large number of crotonylated proteins have been identified. Up to now, several organisms or cell lines have been reported with respect to Kcr, including *Carica papaya* (Liu K. et al., 2018), *Nicotiana tabacum* (Sun et al., 2017), *Oryza sativa* (Liu S. et al., 2018), *Danio rerio* (Kwon et al., 2018), and four human cell lines (Wei et al., 2017b; Wu et al., 2017; Xu et al., 2017; Huang et al., 2018). However, the understanding of the features of Kcr is still insufficient. Particularly in plant fungi, global identification of this kind of PTM has not been well reported.

Botrytis cinerea is an worldwide economically important fungal pathogen that can cause gray mold disease on a wide variety of hosts (Williamson et al., 2007). In recent years, extensive research has been conducted to interpret transcriptional regulation of virulence genes in *B. cinerea* (Weiberg et al., 2013; Brandhoff et al., 2017; Wang et al., 2017, 2018; Porquier et al., 2019). However, gaps in the protein level studies limited a deeper understanding of the molecular basis of *B. cinerea* pathogenesis. In this study, we conducted the first proteome-wide Kcr analysis in *B. cinerea*. In total, 3967 Kcr sites in 1041 proteins were identified. The crotonylated proteins were distributed in multiple compartments and associated with diversified biological processes. Particularly, 26 crotonylated proteins were found to be associated with virulence of *B. cinerea*. These proteins participates in diverse pathogenesis pathways including signal transduction, redox homeostasis, plant cell wall degrading, secretory of virulence factors, and secondary metabolites biosynthesis. This work provides an extensive dataset for further investigating the physiological role of Kcr in *B. cinerea* and other filamentous fungal pathogens.

MATERIALS AND METHODS

Protein Extraction From *B. cinerea*

The *B. cinerea* strain B05.10 was cultured on PDA plates (2% dextrose, 20% potato, and 1.5% agar) at 25°C for 10 days, and then the conidia were collected and transferred into YEPD medium (2% glucose, 1% yeast extract, and 2% peptone) with shaking at 180 rpm for 14 h. The protein extraction was performed as previously described (Zhou et al., 2016). Briefly, the harvested mycelia were ground into powder in liquid nitrogen. Then the powder sample was suspended by lysis buffer (50 mM nicotinamide, 8 M urea, 65 mM dithiothreitol, 1% Triton-100, 0.1% protease inhibitor cocktail, 2 mM EDTA, and 3 μM Trichostatin A) and then sonicated. After centrifugation at 15,000 × *g* at 4°C for 15 min, 15% cold TCA was used to precipitate the proteins at −20°C for 2 h. The precipitates were washed three times with cold acetone after centrifugation at 4°C for 15 min. Finally, the target protein was re-dissolved in 8 M urea supplemented with 100 mM NH_4CO_3 (pH 8.0) and 2-D Quant kit (GE Healthcare) was used to determine protein concentration according to the manufacturer's instructions.

Affinity Enrichment of Lysine Crotonylated Peptides

For affinity enrichment, the *B. cinerea* proteins were firstly digested into peptides by trypsin. The digestion reaction was performed with a previously described experimental approach (Zhou et al., 2016), briefly, the trypsin was added at 1:50 trypsin-to-protein mass ratio at the first time overnight and added again at 1:100 trypsin-to-protein mass ratio for another 4 h. The sample was separated into fractions by high PH reverse-phase HPLC using Agilent 300 Extend C18 column (5 μM particles, 4.6 mm ID, and 250 mm length) (Liu L. et al., 2016). The peptides were separated firstly into 80 fractions with a gradient of 2 to 60% acetonitrile in 10 mM $(NH_4)_2CO_3$ (PH 10.0). Then, the peptides were combined into 8 fractions and dried by vacuum centrifuging. For Kcr peptides enrichment, the tryptic peptides were dissolved in NETN buffer (1 mM EDTA, 100 mM NaCl, 0.5% NP-40, and 50 mM Tris–HCl pH 8.0) and then separated into several fractions. Each fraction was incubated with pan anti-Kcr antibody (PTM-502, PTM Biolabs) conjugated agarose beads overnight at 4°C with gentle shaking. Then the peptides bound with beads were eluted with 0.1% trifluoroacetic acid after washing with NETN buffer and then the acquired peptides were cleaned with C18 Zip Tips (Millipore) (Sun et al., 2019).

LC-MS/MS Analysis

Liquid chromatography-mass spectrometry analysis of the crotonylated peptides was performed as described (Li et al., 2016; Liu L. et al., 2016; Lv et al., 2016; Zhou et al., 2016) by Micrometer Biotech Company (Hangzhou, China). Briefly, The Kcr peptides were separated using a reversed-phase analytical column (Acclaim PepMap RSLC C18 column, Thermo Scientific) on UPLC system. The gradient was composed of an increase from 2% formic acid (0.1%) to 10% formic acid (0.1% in 98% acetonitrile) for 6 min, 10 to 20% for 45 min, 20% climbing to 80% in 7 min and then holding at 80% at least for 4 min, all maintaining a flow rate of 250 nl/min. The peptides were subjected by to ESI/NSI sources followed by MS/MS in Q Exactive™ Plus (Thermo Scientific) coupled online to UPLC. The Orbitrap was used to detect whole peptides and ion fragments at a resolution of 70,000 and 17,500, respectively, with NCE set at 30. The electrospray voltage was set at 2.0 kV. Automatic gain control (AGC) was used to avoid ion trap overfilling. The m/z range was from 350 to 1800 for MS scans. The MS fixed first mass was set at 100 m/z.

Generation of Bcpck1-GFP Strains

To generate Bcpck1-GFP overexpression construct, CDS (coding domain sequence) of *Bcpck1* was cloned into pOPT-GFP vector that contains *oliC* promoter, *niaD* terminator, hygromycin phosphotransferase and optimized C-terminal

eGFP sequence (Leroch et al., 2011). The constructed plasmid was then transformed into the B05.10 strain using protoplast transformation of *B. cinerea* (Gronover et al., 2001). The resulting transformants were selected by 100 μg/ml hygromycin B.

Immunoprecipitation and Western Blot Analysis

Total proteins were extracted using lysis buffer (0.5 mM EDTA, 150 mM NaCl, 0.5% NP-40, and 10 mM Tris–HCl pH 7.5) from mycelium of *B. cinerea* cultivated in liquid YEPD or MM (10 mM K_2HPO_4, 10 mM KH $_2PO_4$, 4 mM $(NH_4)_2SO_4$, 2.5 mM NaCl, 2 mM $MgSO_4$, 0.45 mM $CaCl_2$, 9 mM $FeSO_4$, 50 mM glucose, and 1 L water, pH 6.5) with shaking at 180 rpm for 14 h. Anti-GFP agarose beads (KTSM1301, KT HEALTH) were subsequently added and the mixture was incubated for 2 h. The beads were washed 3 times with 500 μl of lysis buffer, and the bound proteins were eluted with SDS-PAGE loading buffer.

The obtained proteins were then separated by 12% SDS-PAGE and immunoblotted using anti-GFP antibody (ab290, Abcam) and anti-Kcr antibody, respectively. Proteins were visualized using Immobilon Western Chemiluminescent HRP Substrate (Millipore) according to the manufacturer's protocol.

Database Search

MaxQuant and Andromeda search engine (v.1.5.1.8) were used to analyze the raw data of MS/MS (Cox and Mann, 2008; Cox et al., 2009). The tandem mass spectra collected were searched against *B. cinerea* B05.10 database from UniProt. Mass errors of fragment ions and precursor were set as 0.02 Da and 10 ppm, respectively. Trypsin/P was specified as cleavage enzyme allowing up to 4 missing cleavage, 5 charges and 5 modifications per peptide. Carbamidomethylation on Cysteine was specified as fixed modification and crotonylation on lysine was fixed as variable modification. The minimal peptide was set to seven, and the false discovery rate (FDR) threshold for modification sites and peptides were set as 1%. The Kcr site localization probability of <0.75 was exclude (Zhou et al., 2016; Yang et al., 2018).

Bioinformatics Analysis

Gene ontology (GO) of crotonylation proteome was performed from the UniProt-GOA database based on three categories: cellular component, molecular function, and biological process according to Zhou et al. (2016). The soft WoLF PSORT was used to predict the subcellular localization of the crotonylated protein (Horton et al., 2007). Proteins secondary structures (β-strand, α-helix, coil) were analyzed by the online tool NetSurfP (Chou and Schwartz, 2011). Soft MoMo (motif-x algorithm) was used to analyze the sequences model of crotonylated proteins composed of amino acids in distinct positions of modify-21-mers (10 amino acids up- and downstream of the Kcr site) in all protein sequences. To define the conservation of crotonylation, the BLASTP was used to compare the crotonylated protein sequences of *B. cinerea* with *Carica papaya* (Liu K. et al., 2018), *Nicotiana tabacum* (Sun et al., 2017), *Oryza sativa* (Liu S. et al., 2018), *Danio rerio* (Kwon et al., 2018), and four human cell lines including *Human peripheral blood*, *Human Hela cells*, *Human H1299 cells*, and *Human A549 cells* (Wei et al., 2017b; Wu et al., 2017; Xu et al., 2017; Huang et al., 2018). InterProScan was used to perform the protein domain functional annotation based on protein alignment method and the InterPro domain database. Kyoto Encyclopedia of Genes and Genomes (KEGG) database was employed to annotate protein pathway description (Kanehisa et al., 2004). Cytoscape software was used to analyze the protein-protein interactions which was obtained from the STRING database (Shannon et al., 2003; Szklarczyk et al., 2015). A two-tailed Fisher's exact test was used to verify the enrichment of lysine crotonylated proteins against all database proteins. All projects with a corrected p-valve < 0.05 is considered significant.

RESULTS

Identification and Analysis of Lysine-Crotonylated Sites and Proteins in *B. cinerea*

Lysine crotonylation is a newly discovered PTM which is poorly studied in *B. cinerea*, one of the most important plant fungi pathogen in the world. To extensively characterize protein crotonylation in *B. cinerea*, a proteome-wide analysis of Kcr was carried out. Proteins extracted from mycelium were digested by trypsin and the crotonylation peptides were enriched using anti-crotonyl lysine antibody, followed by high-resolution LC-MS/MS analysis. An overview of the experimental procedures was demonstrated in **Supplementary Figure S1A**. Mass errors of the identified peptides were checked first to confirm the dependability of the MS data. As shown in **Supplementary Figure S1B**, the distribution of mass errors was near zero, most were less than 10 PPM, indicating that the mass accuracy fits the requirement. Moreover, the length of most lysine-crotonylated peptides were between 7 and 20, which is consistent with tryptic peptides (**Supplementary Figure S1C**). The above results demonstrated that the sample preparation meets the standard.

After a global lysine crotonylome analysis using LC-MS/MS, 4913, 4839, and 4922 Kcr sites in 1242, 1230, and 1253 crotonylated proteins, respectively, were identified within three independent biological repeats. Moreover, 3967 Kcr sites and 1041 crotonylated proteins were overlapped in the individual triplicate experiments (**Supplementary Figure S2** and **Supplementary Table S1**). MS/MS spectra of three crotonylated peptides were shown in **Supplementary Figure S3**. The number of crotonylated sites in the identified proteins was then calculated. As shown in **Supplementary Figure S4**, 371 (35%) proteins contained only one crotonylation site, whereas 670 (65%) proteins had multiple crotonylation sites.

Pattern Analysis of Crotonylated Sites

To evaluate the properties of Kcr sites in *B. cinerea*, we examined the sequence motif flanking the identified peptides. A total of nine conserved amino acid sequences from −10 to +10 around the crotonylated lysine were extracted from 3196 peptides (**Figure 1A**). Particularly, motifs YKcrE, FKcr, and KcrE were strikingly conserved. Among them, FKcr and KcrE have been

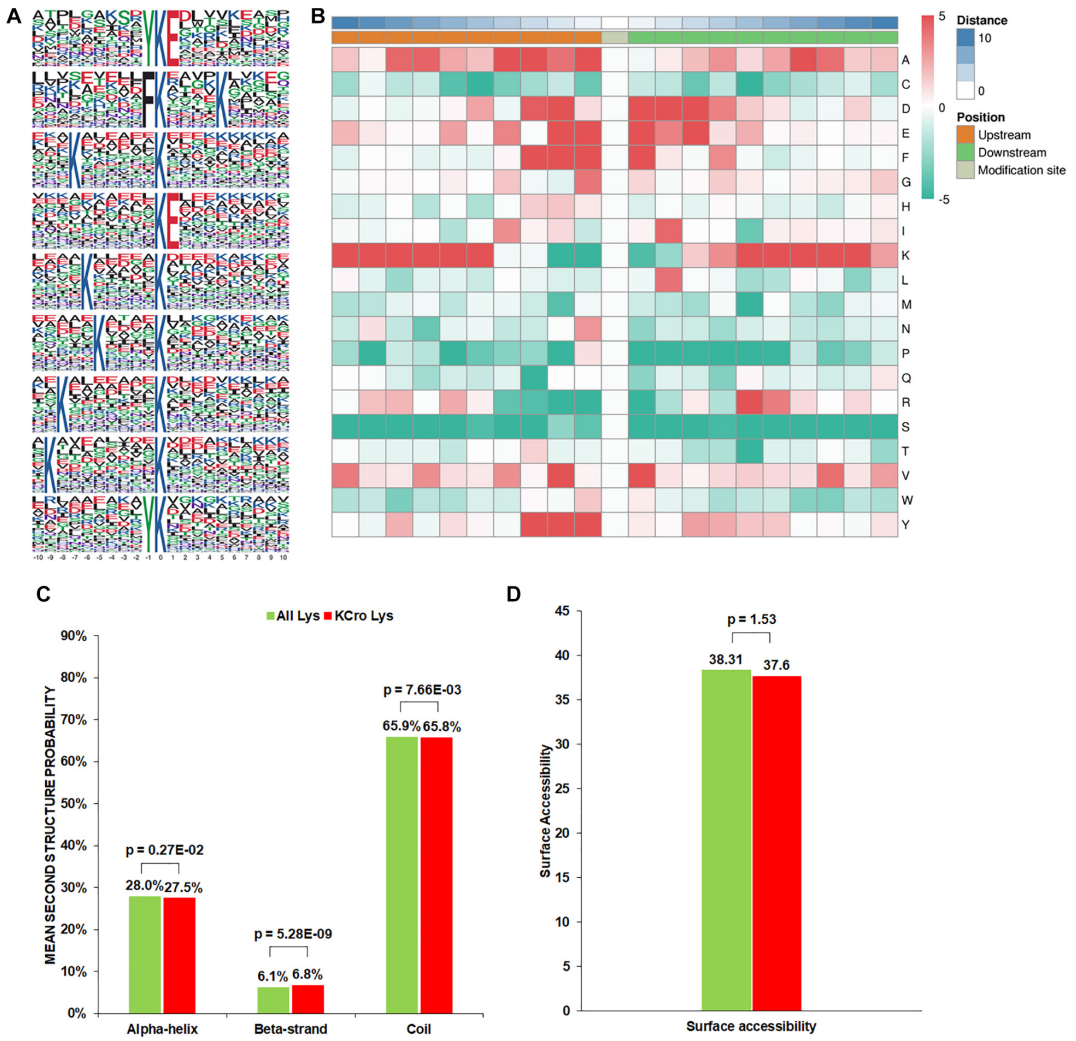

FIGURE 1 | Properties of the Kcr peptides in *B. cinerea*. **(A)** Crotonylation sequence motifs for ±10 amino acids surrounding the Kcr sites. **(B)** Heatmap of the amino acid compositions of the Kcr sites demonstrating the frequency of certain amino acids around the modified lysine. Red indicates high frequency and green means low frequency. **(C)** Probabilities of Kcr in the structures of beta-strand, alpha-helix, and coil. **(D)** Predicted surface accessibility of Kcr sites.

identified as crotonylation motifs previously, while YKcrE was firstly found in our study, which may represent a characteristic feature of crotonylation in *B. cinerea*. To further analyze these motifs, heatmaps of the amino acid sequences surrounding the crotonylation sites were generated. The results showed that certain amino acid residues surrounding the Kcr were markedly enriched. K residues were observed to be enriched in the −10 to −5 and +5 to +9 positions, while residues A, D, E, F, Y were significantly enriched in −4 to −1, −3 to +3, −2 to +3, −3 to +1, and −3 to −1 positions, respectively (**Figure 1B**).

In order to clarify the relationship between crotonylation and the presence of protein structures in *B. cinerea*, a structure analysis of the crotonylated proteins was performed. As shown in **Figure 1C**, 34.3% of the crotonylated sites were located in regions with ordered secondary structures. Among them, 27.5% were located in alpha-helix, and 6.8% were in a beta-strands. The residual 65.8% of the crotonylated sites were distributed in disordered protein regions. However, considering the distribution patterns of crotonylated lysines and all lysines are similar, there was no tendency of Kcr in *B. cinerea*. The surface accessibility of Kcr sites was further evaluated. The results showed that the exposure of crotonylation sites on the protein surface is close to that of all lysine residues (**Figure 1D**). Therefore, Kcr may not be affected by the surface properties of proteins in *B. cinerea*.

Conservation Analysis of Lysine Crotonylated Proteins

Increasing studies in recent years have revealed improved number of crotonylated proteins in various species or cell lines (Sun et al., 2017; Wei et al., 2017b; Wu et al., 2017; Xu et al., 2017; Huang et al., 2018; Kwon et al., 2018; Liu K. et al., 2018; Liu S. et al., 2018). However, the conservation of Kcr in these organisms is unknown. As such, we compared

the crotonylated proteins in *B. cinerea* with those in eight organisms or cell lines that have determined crotonylomes. Totally, 3019 orthologs of the crotonylproteins in *B. cinerea* were identified in these organisms (**Supplementary Table S2**). As shown in **Figure 2A**, 790 crotonylated proteins have orthologs in *Oryza sativa* (359 proteins), *Nicotiana tabacum* (301 proteins), *Human peripheral blood* (225 proteins), *Human Hela cells* (182 proteins), *Human H1299 cells* (522 proteins), *Human A549 cells* (682 proteins), *Danio rerio* (129 proteins), and *Carica papaya* (619 proteins), which account for 75.9% (790/1041 proteins) of the total crotonylproteins in *B. cinerea*. We further classified the crotonylated proteins of *B. cinerea* depending on the number of the orthologous proteins in these organisms. The data demonstrated that the percentage of completely conserved proteins (have 8 orthologs), well-conserved proteins (have 6 to 7 orthologs), conserved proteins (have 3 to 5 orthologs) and poorly conserved proteins (have 1 to 2 orthologs) were 3.9% (41/1041 proteins), 12.1% (126/1041 proteins), 36.9% (384/1041 proteins), and 22.9% (239/1041 proteins) (**Figure 2B**), respectively. Furthermore, 24.1% (251/1041 proteins) of the crotonylated proteins in *B. cinerea* was characterized as novel proteins since no orthologs were found in these organisms (**Figure 2B**). These results suggest that Kcr plays both common and specific roles in different species.

Functional Annotation and Cellular Localization of Crotonylated Proteins in *B. cinerea*

To obtain a comprehensive overview of potential roles of crotonylated proteins in *B. cinerea*, we conducted the Gene Ontology (GO) functional classification analysis of all crotonylated proteins based on their biological process, cellular component, and molecular function (**Figure 3** and **Supplementary Table S3**). The result of biological process analysis showed that crotonylated proteins were widely distributed within different kinds of metabolic and cellular processes (**Figure 3A**). For cellular component analysis, crotonylated proteins were distributed among various cellular compartments, mostly in intracellular (21%), intracellular organelle (19%), and membrane-bounded organelle (16%) (**Figure 3B**). Within the molecular function category, the majority of the modified proteins were composed of those related to heterocyclic compound binding (15%), organic cyclic compound binding (15%), protein binding (8%), ion binding (8%), and hydrolase activity (8%) (**Figure 3C**).

Subcellular localization analysis of the crotonylated proteins was also performed. As shown in **Figure 3D**, a large number of the crotonylated proteins in *B. cinerea* were distributed in the cytoplasm (35%), mitochondria (26%), and nucleus (22%). These data demonstrated that the crotonylated proteins, with diversified cellular distribution, are involved in various biological processes in *B. cinerea*.

Functional Enrichment Analysis of Crotonylated Proteins

To better elucidate the characteristics of crotonylaed proteins in *B. cinerea*, enrichment analyses of GO (Gene Ontology), protein domain and KEGG pathway were conducted. The enrichment analysis of biological process revealed that the majority of crotonylaed proteins were related to cytoplasmic translation (**Figure 4A** and **Supplementary Table S4**). In support of these observations, large numbers of the modified proteins were involved in structural constituent of ribosome in molecular function enrichment analysis (**Figure 4B** and **Supplementary Table S4**). Based on cellular component enrichment analysis, proteins located to cytosolic part were more likely to be crotonylated (**Figure 4C** and **Supplementary Table S4**).

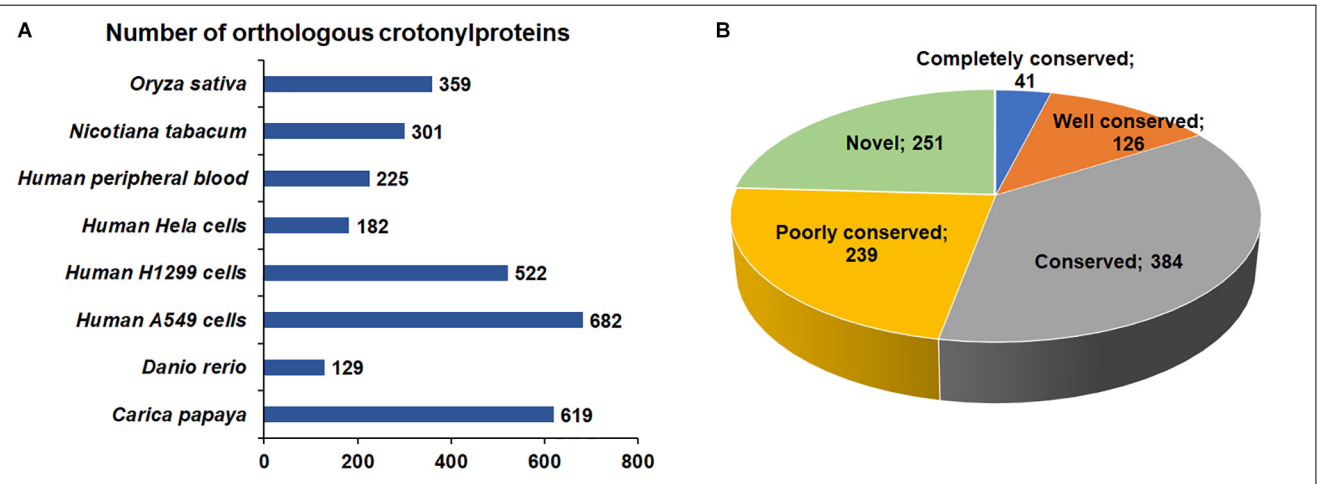

FIGURE 2 | Conservation analysis of lysine crotonylated proteins. **(A)** Number of orthologous crotonylproteins in eight organisms or cell lines with reported crotonylomes. **(B)** A pie chart of conservation of crotonylproteins in *Oryza sativa*, *Nicotiana tabacum*, *Human peripheral blood*, *Human Hela cells*, *Human H1299 cells*, *Human A549 cells*, *Danio rerio*, and *Carica papaya*. Classification was performed as follows: Completely conserved group, 8 orthologs; Well conserved group, 6 to 7 orthologs; Conserved group, 3 to 5 orthologs; Poorly conserved group, 1 to 2 orthologs; Novel group, 0 orthologs.

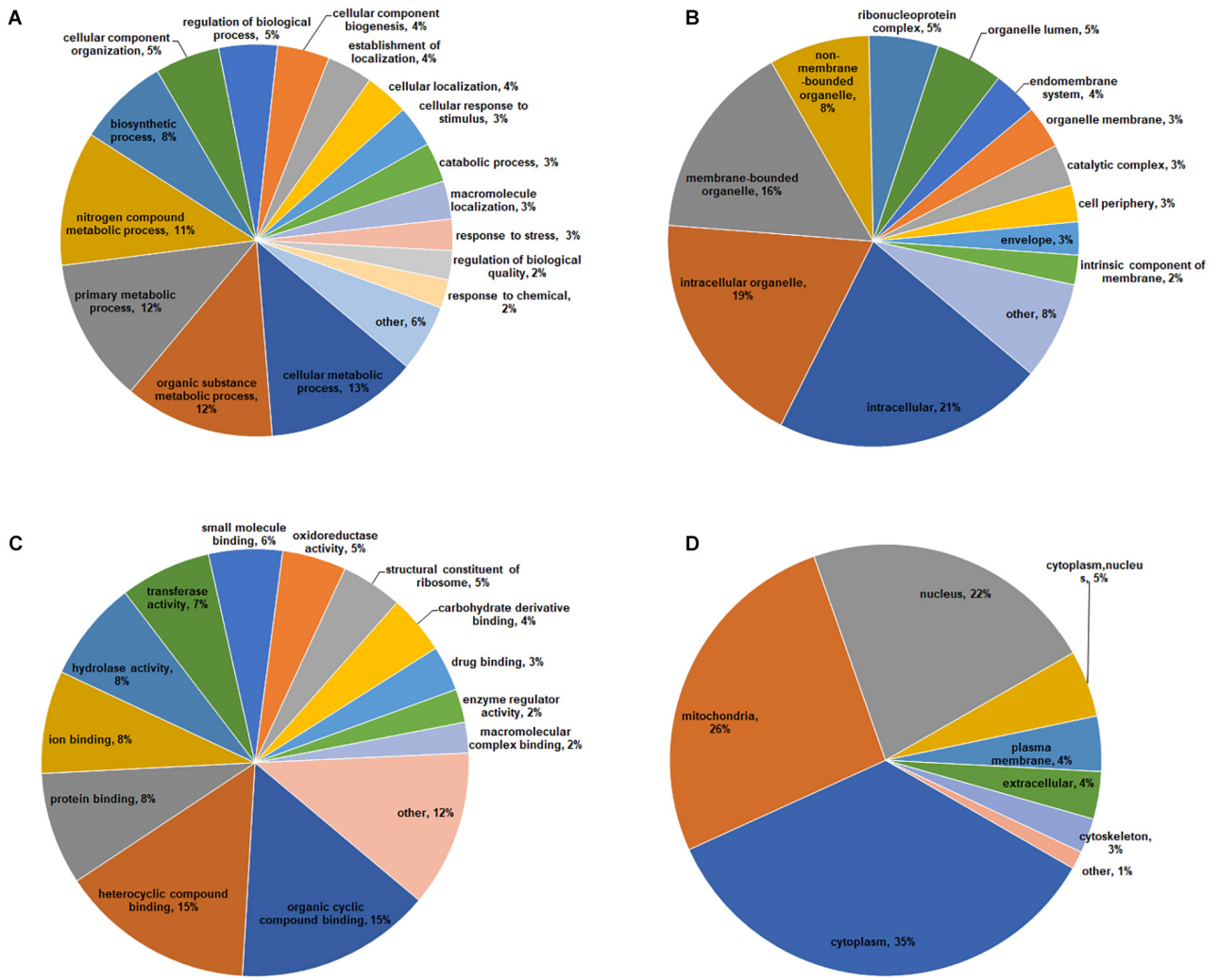

FIGURE 3 | Functional classification of lysine crotonylated proteins based on GO and subcellular location in *B. cinerea*. GO classification of crotonylated proteins based on biological process **(A)**, cellular component **(B)**, and molecular function **(C)**. **(D)** Subcellular localization classification of the crotonylated proteins.

Further enrichment analyses of protein domain and KEGG pathway obtained similar results. The protein domain enrichment analysis demonstrated that the proteins with domains of proteasome subunit were more likely to have crotonylation (**Supplementary Figure S5A** and **Supplementary Table S5**). Consistent with these findings, enrichment analysis of KEGG pathway indicated that a large proportion of crotonylated proteins were associated with ribosome (**Supplementary Figure S5B** and **Supplementary Table S6**). Overall, our data indicate that lysine crotonylated proteins are widely distributed and involved in various pathways, suggesting important roles of crotonylation in cell metabolism.

Analysis of Crotonylated Proteins Related to Fungal Pathogenicity

To further understand the pathogenesis regulated by crotonylation in *B. cinerea*, we summarized the crotonylated proteins reported to be involved in fungal pathogenicity and listed in **Table 1** and **Supplementary Table S7**. A total of 26 proteins were identified, with diversified numbers of Kcr sites varied from one to eight. These proteins participate in diverse pathogenesis pathways including signal transduction (6 proteins), redox homeostasis (6 proteins), plant cell wall degrading (4 proteins), secretory of virulence factors (3 proteins), and secondary metabolites biosynthesis (7 proteins), indicating that Kcr has a broad range of effects on pathogenicity of *B. cinerea*. Importantly, most of the crotonylated sites were located or near to the functional domains of these proteins. For example, cytochrome P450 reductase (Bccpr1) was found to be crotonylated at K290, which is next to R292, one of the conserved key sites of flavin adenine dinucleotide (FAD) domain of Cytochrome P450 reductase (Ebrecht et al., 2019; **Figure 5A**). Glutathione reductase (Bcglr1) carried the crotonylated K379 which is spatially close to one of the key sites of this enzyme, R371 (Yu and Zhou, 2007; **Figure 5B**). These data suggests

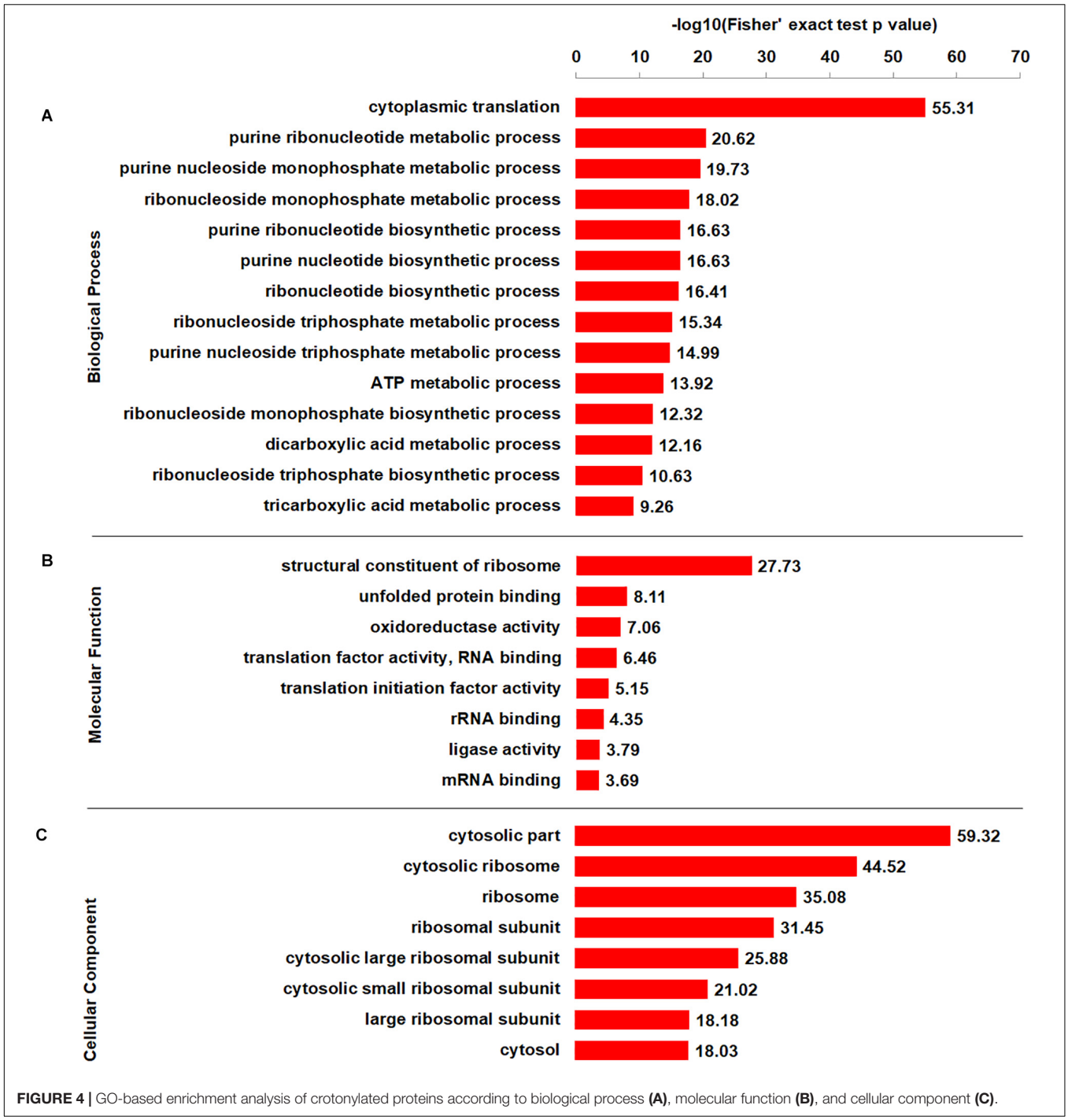

FIGURE 4 | GO-based enrichment analysis of crotonylated proteins according to biological process **(A)**, molecular function **(B)**, and cellular component **(C)**.

that Kcr may have effect on the adjacent key domain sites, and thus regulate the function of these proteins involved in pathogenicity.

PPI Network of Crotonylated Proteins in *B. cinerea*

To better investigate the cellular processes regulated by crotonylation in *B. cinerea*, a PPI network of all identified crotonylated proteins was assembled using Cytoscape software. As shown in **Figure 6** and **Supplementary Table S8**, 783 crotonylated proteins were mapped to the PPI network, exhibiting an overview of diverse pathways modulated by these proteins in *B. cinerea*. Five greatly interconnected clusters of crotonylated proteins were retrieved, including ribosome, carbon metabolism, proteasome, oxidative phosphorylation, and aminoacyl-tRNA biosynthesis (**Figure 6** and **Supplementary Table S8**). These findings indicate

TABLE 1 | Crotonylated proteins associated with pathogenicity in *B. cinerea*.

Protein name	Protein description	Functional Classification
Bclga1	Dihydrodipicolinate synthase	
Bcgar1	Aldo/keto reductase	Plant cell wall degrading
Bclgd1	Galactonate dehydratase	
Bcpg1	Glycosyl hydrolase	
Bctrx1	Thioredoxin	
Bctrx2	Thioredoxin	
Bctrr1	Thioredoxin reductase	
Bcglr1	Glutathione reductase	Redox homeostasis
Bcpdi1	Protein disulfide-isomerase	
Bcsod1	Superoxide dismutase [Cu-Zn]	
Bmp1	Mitogen-activated protein kinase	
Bmp3	Mitogen-activated protein kinase	
Bcptc3	Serine/threonine protein phosphatase	Signal transduction
Bcras1	Ras-related GTPase	
Bcpka1	cAMP-dependent protein kinase	
Bcg1	G-protein alpha subunit	
Bcbrn1	Tetrahydroxynaphthalene Reductases	
Bcbrn2	Tetrahydroxynaphthalene Reductases	
Bcscd1	Scytalone dehydratase	
Bcp1	Peptidyl-prolyl *cis-trans* isomerase	Secondary metabolites
Bcpck1	Phosphoenolpyruvate carboxykinase	Biosynthesis
Bccpr1	NADPH–cytochrome P450 reductase	
Bcser2	Subtilisin-related protease	
Bcsas1	Rab GTPase	Secretory of virulence
BcactA	Actin and related proteins	Factors
Bcsec31	Vesicle coat complex COPII	

that physiological interactions among these complexes may conduce to their harmonization and cooperation in *B. cinerea*.

Kcr Levels of *B. cinerea* Under Different Metabolic Conditions

To test whether the crotonylome differs under different physiological conditions, we carried out immunoblotting of the crotonylated proteins of *B. cinerea* cultivated in YEPD or MM (minimal medium), representing rich or limited nutrient condition. As shown in **Figure 7A**, the whole protein Kcr levels were increased in YEPD than in MM. Moreover, the Kcr level of Bcpck1, a critical enzyme in the nutrient-starvation adaptation before host invasion (Liu J.K. et al., 2018), was also elevated in YEPD (**Figure 7B**). Thus the above results suggested that Kcr may participate in nutrient metabolic regulation and it will be interesting to characterize the function of crotonylated substrates under different metabolic conditions.

DISCUSSION

Histone crotonylation is a newly discovered PTM which plays critically important roles for gene transcription in mammalian cells (Tan et al., 2011; Wei et al., 2017a). Other than histones, recent findings on global profiling of crotonylated proteins in various species have expanded the repertoire of modified proteins (Sun et al., 2017, 2019; Wei et al., 2017b; Wu et al., 2017; Xu et al., 2017; Liu J.K. et al., 2018; Liu K. et al., 2018; Liu S. et al., 2018; Yang et al., 2018), which exhibited widely distributed cellular localization and diversified biological function. However, study of Kcr is surprisingly lacking and has not yet been studied in plant fungi. In this study, we performed a global Kcr analysis in *B. cinerea* to bridge this knowledge gap in fungal pathogens.

A total of 1041 crotonylated proteins with 3967 Kcr sites were identified, which exceeds the Kcr levels of most reported organisms or cell lines including *Danio rerio*, *Oryza sativa*, *Nicotiana tabacum*, *Human Hela cells*, *Human peripheral blood*, *Human H1299 cells*, and less than *Human A549 cells* and *Carica papaya*. These data indicate that Kcr is a widespread PTM among organisms. Further functional annotation and enrichment analysis demonstrated that the crotonylated proteins were widely distributed and involved in diverse cellular processes. The identification of specific lysine motifs indicates substrate preference of Kcr in *B. cinerea*. Furthermore, PPI network analysis showed that a mass of protein interactions are regulated by crotonylation. These data represents the first proteome-wide view of the crotonylome in *B. cinerea* and fungal pathogens.

Recently, proteomic studies into crotonylation have indicated that abundant proteins are crotonylated in various organisms, suggesting that crotonylation is a common mechanism of metabolic regulation. However, it remains unclear whether such biochemical changes play crucial roles in physiological processes. In this study, we found that the crotonylome of *B. cinerea* differs under different nutrient conditions (**Figure 7**). Moreover, the crotonylation of Bcpck1, a PEP-carboxykinase which is important in gluconeogenesis, changed significantly under different metabolic conditions. Future studies are needed to uncover the effects of crotonylation on regulating protein functions and to interpret the underlying mechanisms behind protein crotonylation's ability to modulate diverse physiological processes.

In our study, 85 ribosomal proteins were crotonylated, accounting for 8% of the total crotonylated proteins, suggesting that Kcr of ribosomal proteins may have effect on protein translational control and ribosome assembly. Afterward, 26 crotonylated proteins were reported to be associated with pathogenicity in *B. cinerea*, participating in various pathogenesis processes (**Table 1** and **Supplementary Table S7**). The infection process of *B. cinerea* is regulated by a complicated signal transduction network, such as Mitogen-activated protein kinases (MAPKs), the cAMP-dependent signal cascade, and small GTPases. In our study, several components involved in these signaling pathways were identified to be crotonylated including MAPKs bmp1 (K298), bmp3 (K72), cAMP-dependent protein kinase Bcpka1 (K205), G-protein alpha subunit Bcg1 (K51,141), and Ras-related small GTPase Bcras1 (K153). Mutants in genes encoding MAPK bmp1 and bmp3 showed defects in germination, vegetative growth, and pathogenicity (Zheng et al., 2000; Rui and Hahn, 2007). Bcpka1 and Bcg1 play important roles in growth and virulence in *B. cinerea*, regulating invasive process of plant tissue via a cAMP-independent pathway

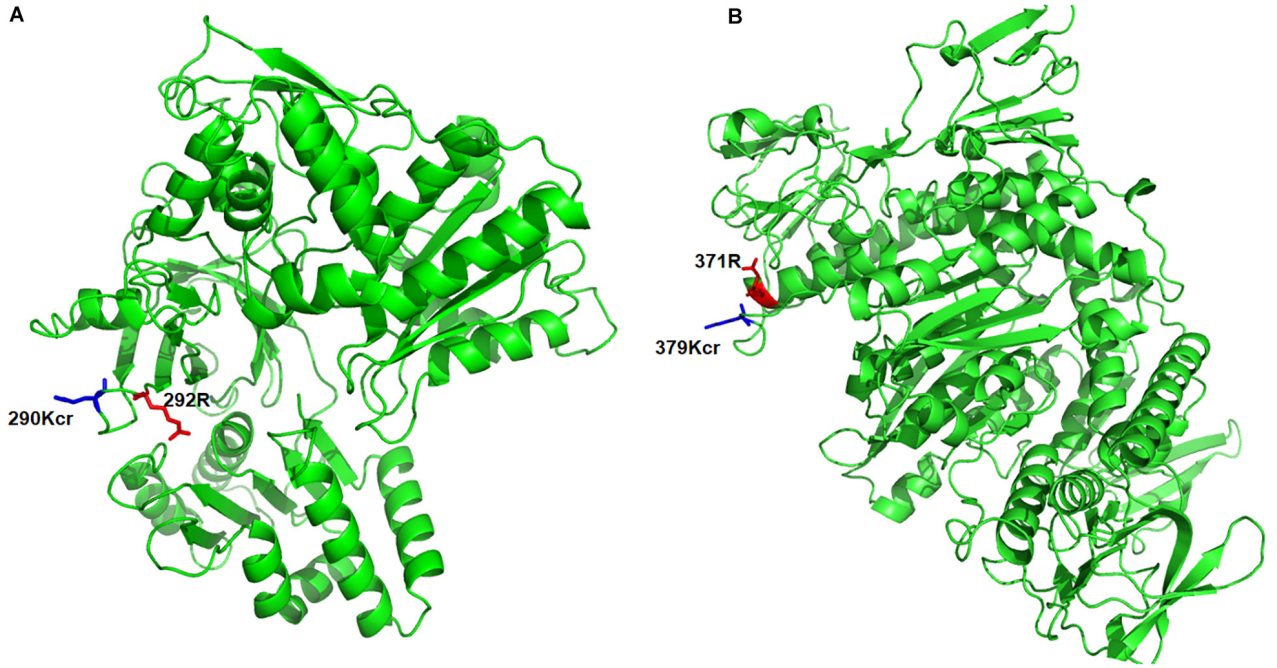

FIGURE 5 | Three-dimensional structure of Bccpr1 **(A)** and Bcglr1 **(B)** with identified crotonylation site. The structure was derived from PDB database. The crotonylated lysine residues and adjacent arginine residues were indicated by blue and red colored sticks, respectively.

(Schumacher et al., 2008a,b). Bcras1, which influences both MAPK and cAMP-dependent signal transduction, is necessary for development and virulence in *B. cinerea* (Minz Dub et al., 2013). These data indicates that Kcr might play a role in signal transduction and thus modulate multiple steps of fungal growth and pathogenicity.

The rapid production of reactive oxygen species (ROS) and maintaining a balanced redox homeostasis are crucial for colonization process of necrotrophic pathogen *B. cinerea*. Cu-Zn superoxide dismutase Bcsod1, an important virulence factor through stimulating ROS generation in *B. cinerea* (López-Cruz et al., 2017), was found to be crotonylated at K89, K106, and K129 sites. Thioredoxin and glutathione are two major cellular redox systems to keep redox homoeostasis during stage of infection for *B. cinerea*. Thioredoxins Bctrx1 (K74, K114), and Bctrx2 (K57), thioredoxin reductase Bctrr1 (K331), and glutathione reductase Bcglr1 (K72, K275, K379) were found to be crotonylated in this study. Knock out mutants of these enzymes showed retarded growth and impaired virulence (Viefhues et al., 2014). In addition, protein disulfide-isomerase Bcpdi1, a new interaction partner of NADPH oxidase complexes which is essential for the conservation of the redox homeostasis in *B. cinerea* (Marschall and Tudzynski, 2017), was identified to be crotonylated at multiple sites in our study.

D-galacturonic acid, one of the major components of plant cell wall, is an important carbon source for filamentous fungi. The mutants in each step of the catabolic pathway of converting D-galacturonic acid of plant to pyruvate and l-glyceraldehyde showed reduced virulence (Zhang et al., 2011). In our study, a group of D-galacturonate catabolic enzymes were identified to be crotonylated including galacturonate reductase Bcgar1 (K276, K286), galactonate dehydratase Bclgd1 (K173, K186, K410), and 2-keto-3-deoxy-l-galactonate aldolase Bclga1 (K247, K307). In addition, endopolygalacturonase Bcpg1, which function as a cell-wall-degrading enzyme and is required for full virulence of *B. cinerea* (ten Have et al., 1998), was found to be crotonylated at multiple sites in this study.

To colonize the host tissue, *B. cinerea* usually secretes a battery of virulence factors to the extracellular environment. The Rab GTPase Bcsas1, reported to play a critical role in the secretion of polygalacturonases, polysaccharide hydrolases, xylanases and proteases (Zhang et al., 2014), was identified to be crotonylated at K172. Deletion of gene encoding vesicle coat complex protein Bcsec31 resulted in a reduction in the protein secretion and virulence of *B. cinerea* (Zhang et al., 2016). This protein was found to be crotonylated at K444 and K571 sites in our study. In addition, actin protein BcactA was found crotonylated at multiple sites, which was recently discovered to influence the secretome of *B. cinerea* and is crucial for extracellular virulence factors regulation (Li et al., 2020).

The secondary metabolites play critical roles in fungal survival and host killing. In our study, several key enzymes responsible for the committed biosynthetic steps were found to be crotonylated. DHN melanin has different effects during the life cycles of the fungus, particularly, contributing to the invading process of the penetration structures and the longevity of the reproduction structures (Zhang et al., 2015; Schumacher, 2016). In this study, three key enzymes of melanogenesis pathway, tetrahydroxynaphthalene reductases

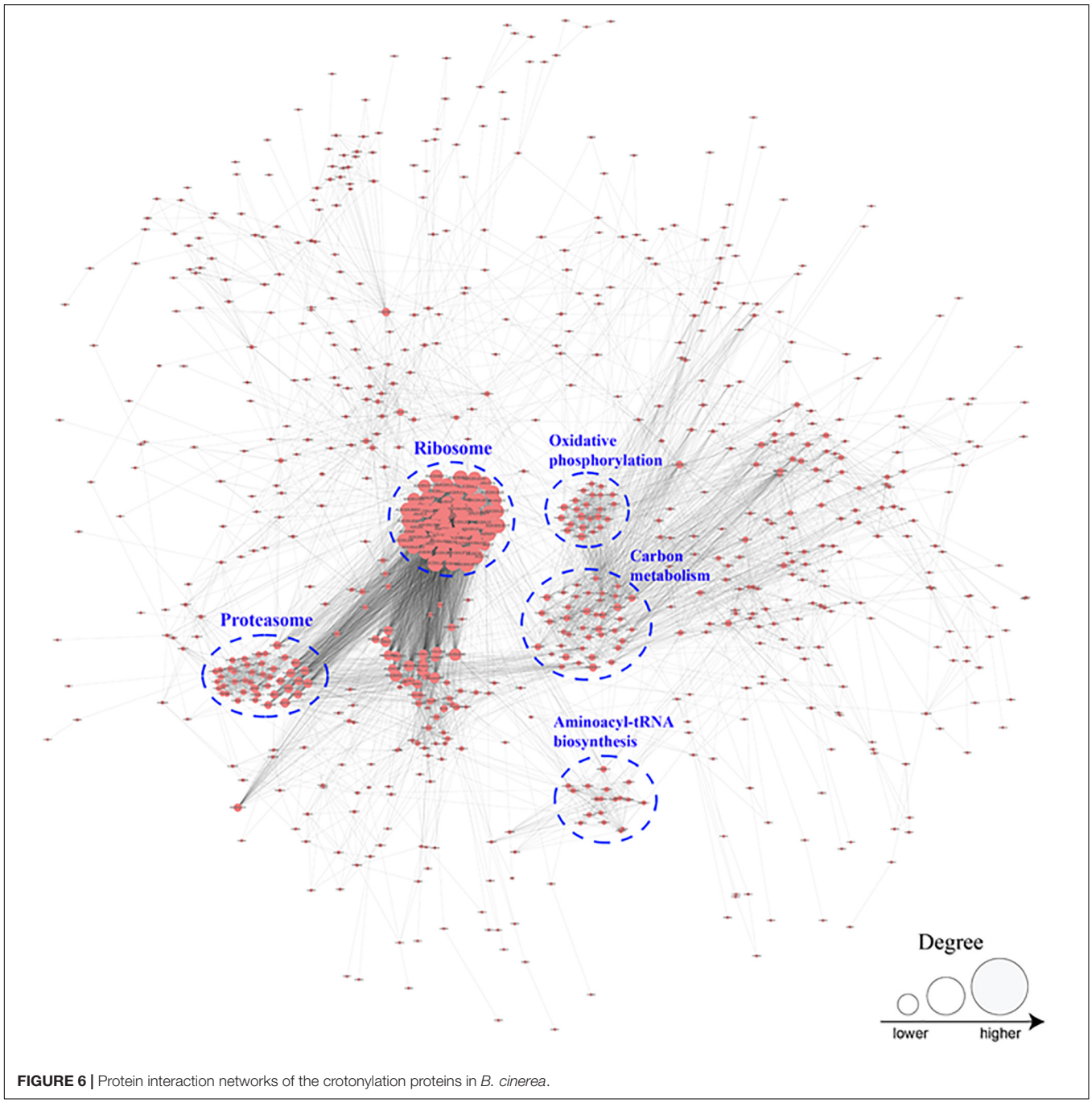

FIGURE 6 | Protein interaction networks of the crotonylation proteins in *B. cinerea*.

Bcbrn1, Bcbrn2, and scytalone dehydratase Bcscd1, were found to be crotonylated at multiple sites. Besides, the phosphoenolpyruvate carboxykinase Bcpck1, which was identified to be crotonylated at multiple sites in our study, plays an important role in gluconeogenesis and is critical in the nutrient-starvation adaptation before host invasion (Liu J.K. et al., 2018). Furthermore, Bccpr1, which function as a cytochrome P450 oxidoreductase regulating the fungal ABA production (Siewers et al., 2004), was identified to be a crotonylated protein with multiple modified sites. Further studies are needed to explore the functions of crotonylation of these substrate proteins to deeply understand mechanisms of *B. cinerea* pathogenesis at protein level.

CONCLUSION

We have conducted the first crotonyl-proteome of *B. cinerea*, an important plant fungal pathogen, showing abundant Kcr among a large number of proteins. The lysine crotonylome in this study provides a good resource for in-depth exploration of the functions of Kcr in the growth, development and pathogenicity

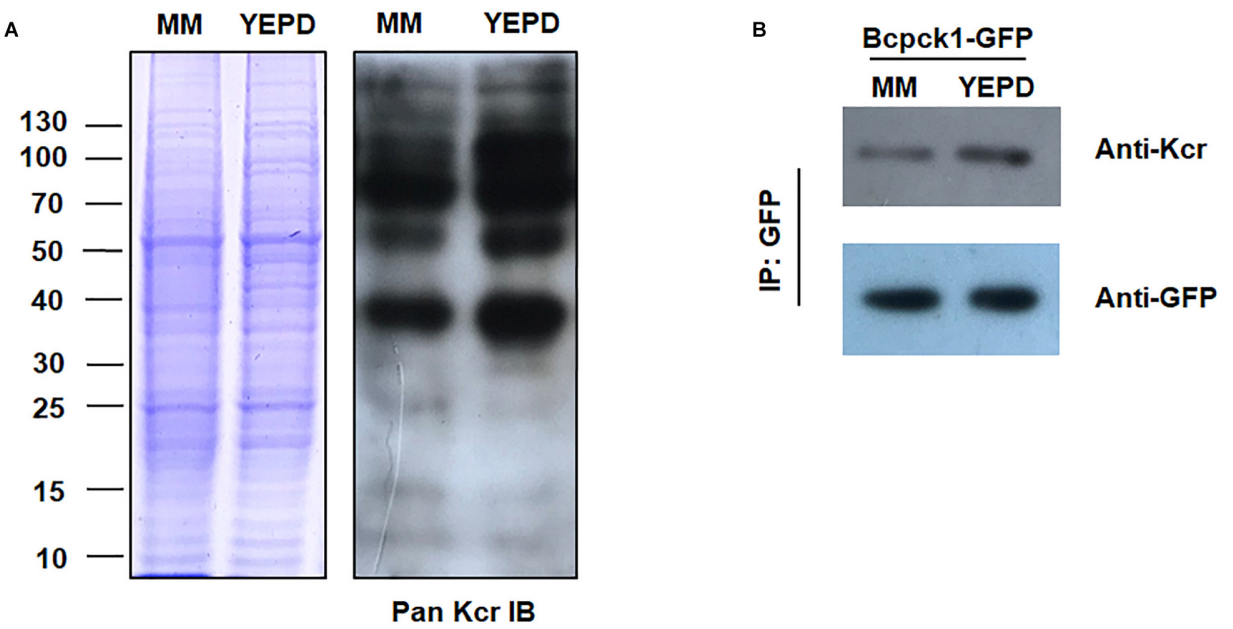

FIGURE 7 | Kcr levels of *B. cinerea* under different physiological conditions. **(A)** Immunoblot analysis of crotonylated proteins with pan anti-Kcr antibody of *B. cinerea* cultivated in liquid YEPD or MM. The loading control by Coomassie blue staining was used to ensure that equal amounts of protein were loaded in each lane. **(B)** Protein extracts containing Bcpck1-GFP were immunoprecipitated (IP) using anti-GFP beads. The isolated proteins were resolved by SDS-PAGE. Anti-GFP and anti-Kcr antibodies were used to detect Bcpck1-GFP and its crotonylated isoform, respectively.

of *B. cinerea* and other filamentous fungi. Investigating the functions of the crotonylation of the target proteins may help to design drugs with high specificity and low toxicity to prevent and control gray mold disease.

DATA AVAILABILITY STATEMENT

The mass spectrometry proteomics data have been deposited to the ProteomeXchange Consortium via the PRIDE partner repository with the dataset identifier PXD019358.

AUTHOR CONTRIBUTIONS

NZ, WL, and ML generated the hypothesis and planned the experiments. NZ and ZY performed the experiments. NZ and WL wrote the manuscript. All other authors provided comments on the manuscript.

FUNDING

This research was supported by the Ministry of Agriculture of China (2016ZX08009003-001), the National Natural Science Foundation of China (31722044 and 31972213), the Shandong Provincial Natural Science Foundation (ZR2019BC070), Shandong Postdoctoral Innovation Program (201903081), Taishan Scholar Construction Foundation of Shandong Province (tshw20130963) and "First class grassland science discipline" program in Shandong Province, China.

SUPPLEMENTARY MATERIAL

The Supplementary Material for this article can be found online at: https://www.frontiersin.org/articles/10.3389/fmicb.2020.564350/full#supplementary-material

Supplementary Figure 1 | (A) Systematic analysis of Kcr in *B. cinerea*. **(B)** Mass error distribution of the Kcr peptides. **(C)** Distribution of Kcr peptides based on their length.

Supplementary Figure 2 | Overlaps of three individual MS/MS spectra of the crotonylated peptides.

Supplementary Figure 3 | MS/MS spectra of three crotonylated peptides: A0A384J6Z0 (Pyruvate kinase), A0A384K3A6 (Bcrpl5), and A0A384K3C6 (Ribosomal protein L15).

Supplementary Figure 4 | Number of crotonylation sites per protein in *B. cinerea*.

Supplementary Figure 5 | Enrichment analyses of protein domain **(A)** and KEGG pathway **(B)**.

Supplementary Table 1 | The identified Kcr sites in *B. cinerea*.

Supplementary Table 2 | Conservation analysis of Kcr proteins.

Supplementary Table 3 | Protein GO terms distribution.

Supplementary Table 4 | GO enrichment based on molecular function, cellular component, and biological process.

Supplementary Table 5 | Enrichment analysis of KEGG protein pathway.

Supplementary Table 6 | Enrichment analysis of protein domain.

Supplementary Table 7 | Crotonylated proteins associated with pathogenicity in *B. cinerea*.

Supplementary Table 8 | Protein interaction network of the crotonylated proteins.

REFERENCES

Brandhoff, B., Simon, A., Dornieden, A., and Schumacher, J. (2017). Regulation of conidiation in *Botrytis cinerea* involves the light-responsive transcriptional regulators BcLTF3 and BcREG1. *Curr. Genet.* 63, 931–949. doi: 10.1007/s00294-017-0692-9

Chen, Y., Sprung, R., Tang, Y., Ball, H., Sangras, B., Kim, S. C., et al. (2007). Lysine propionylation and butyrylation are novel post-translational modifications in histones. *Mol. Cell Proteomics* 6, 812–819. doi: 10.1074/mcp.M700021-MCP200

Chou, M. F., and Schwartz, D. (2011). Biological sequence motif discovery using motif-x. *Curr. Protoc. Bioinformatics* Chapter 13:Unit1315–24. doi: 10.1002/0471250953.bi1315s35

Cox, J., and Mann, M. (2008). MaxQuant enables high peptide identification rates, individualized p.p.b.-range mass accuracies and proteome-wide protein quantification. *Nat. Biotechnol.* 26, 1367–1372. doi: 10.1038/nbt.1511

Cox, J., Matic, I., Hilger, M., Nagaraj, N., Selbach, M., Olsen, J. V., et al. (2009). A practical guide to the MaxQuant computational platform for SILAC-based quantitative proteomics. *Nat. Protoc.* 4, 698–705. doi: 10.1038/nprot.2009.36

Dai, L., Peng, C., Montellier, E., Lu, Z., Chen, Y., Ishii, H., et al. (2014). Lysine 2-hydroxyisobutyrylation is a widely distributed active histone mark. *Nat. Chem. Biol.* 10, 365–370. doi: 10.1038/nchembio.1497

Ebrecht, A. C., Van Der Bergh, N., Harrison, S. T. L., Smit, M. S., Sewell, B. T., and Opperman, D. J. (2019). Biochemical and structural insights into the cytochrome P450 reductase from Candida tropicalis. *Sci. Rep.* 9:20088. doi: 10.1038/s41598-019-56516-6

Gronover, C. S., Kasulke, D., Tudzynski, P., and Tudzynski, B. (2001). The role of G protein alpha subunits in the infection process of the gray mold fungus *Botrytis cinerea*. *Mol. Plant Microbe Interact.* 14, 1293–1302. doi: 10.1094/mpmi.2001.14.11.1293

Hirschey, M. D., and Zhao, Y. (2015). Metabolic regulation by lysine malonylation, succinylation, and glutarylation. *Mol. Cell Proteomics* 14, 2308–2315. doi: 10.1074/mcp.R114.046664

Horton, P., Park, K. J., Obayashi, T., Fujita, N., Harada, H., Adams-Collier, C. J., et al. (2007). WoLF PSORT: protein localization predictor. *Nucleic Acids Res.* 35, W585–W587. doi: 10.1093/nar/gkm259

Huang, H., Wang, D. L., and Zhao, Y. (2018). Quantitative crotonylome analysis expands the roles of p300 in the regulation of lysine crotonylation pathway. *Proteomics* 18:e1700230. doi: 10.1002/pmic.201700230

Kanehisa, M., Goto, S., Kawashima, S., Okuno, Y., and Hattori, M. (2004). The KEGG resource for deciphering the genome. *Nucleic Acids Res.* 32, D277–D280. doi: 10.1093/nar/gkh063

Khoury, G. A., Baliban, R. C., and Floudas, C. A. (2011). Proteome-wide post-translational modification statistics: frequency analysis and curation of the swiss-prot database. *Sci. Rep.* 1:90. doi: 10.1038/srep00090

Kwon, O. K., Kim, S. J., and Lee, S. (2018). First profiling of Kcr of myofilament proteins and ribosomal proteins in zebrafish embryos. *Sci. Rep.* 8:3652. doi: 10.1038/s41598-018-22069-3

Leroch, M., Mernke, D., Koppenhoefer, D., Schneider, P., Mosbach, A., and Doehlemann, G. (2011). Living colors in the gray mold pathogen *Botrytis cinerea*: codon-optimized genes encoding green fluorescent protein and mCherry, which exhibit bright fluorescence. *Appl. Environ. Microbiol.* 77, 2887–2897. doi: 10.1128/aem.02644-10

Li, D., Lv, B., Tan, L., Yang, Q., and Liang, W. (2016). Acetylome analysis reveals the involvement of lysine acetylation in diverse biological processes in Phytophthora sojae. *Sci. Rep.* 6:29897. doi: 10.1038/srep29897

Li, H., Zhang, Z., Qin, G., He, C., Li, B., and Tian, S. (2020). actin is required for cellular development and virulence of *Botrytis cinerea* via the mediation of secretory proteins. *mSystems* 5:e00732-19. doi: 10.1128/mSystems.00732-19

Liu, J. K., Chang, H. W., Liu, Y., Qin, Y. H., Ding, Y. H., Wang, L., et al. (2018). The key gluconeogenic gene PCK1 is crucial for virulence of *Botrytis cinerea* via initiating its conidial germination and host penetration. *Environ. Microbiol.* 20, 1794–1814. doi: 10.1111/1462-2920.14112

Liu, K., Yuan, C., Li, H., Chen, K., Lu, L., Shen, C., et al. (2018). A qualitative proteome-wide Kcr profiling of papaya (*Carica papaya* L.). *Sci. Rep.* 8:8230. doi: 10.1038/s41598-018-26676-y

Liu, S., Xue, C., Fang, Y., Chen, G., Peng, X., Zhou, Y., et al. (2018). Global involvement of lysine crotonylation in protein modification and transcription regulation in rice. *Mol. Cell Proteomics* 17, 1922–1936. doi: 10.1074/mcp.RA118.000640

Liu, L., Wang, G., Song, L., Lv, B., and Liang, W. (2016). Acetylome analysis reveals the involvement of lysine acetylation in biosynthesis of antibiotics in Bacillus amyloliquefaciens. *Sci. Rep.* 6:20108. doi: 10.1038/srep20108

López-Cruz, J., Óscar, C. S., Emma, F. C., Pilar, G. A., and Carmen, G. B. (2017). Absence of Cu-Zn superoxide dismutase BCSOD1 reduces *Botrytis cinerea* virulence in *Arabidopsis* and tomato plants, revealing interplay among reactive oxygen species, callose and signalling pathways. *Mol. Plant Pathol.* 18, 16–31. doi: 10.1111/mpp.12370

Lv, B., Yang, Q., Li, D., Liang, W., and Song, L. (2016). Proteome-wide analysis of lysine acetylation in the plant pathogen *Botrytis cinerea*. *Sci. Rep.* 6:29313. doi: 10.1038/srep29313

Marschall, R., and Tudzynski, P. (2017). The protein disulfide isomerase of *Botrytis cinerea*: an ER protein involved in protein folding and redox homeostasis influences NADPH oxidase signaling processes. *Front. Microbiol.* 8:960. doi: 10.3389/fmicb.2017.00960

Minz Dub, A., Kokkelink, L., Tudzynski, B., Tudzynski, P., and Sharon, A. (2013). Involvement of *Botrytis cinerea* small GTPases BcRAS1 and BcRAC in differentiation, virulence, and the cell cycle. *Eukaryot Cell* 12, 1609–1618. doi: 10.1128/ec.00160-13

Porquier, A., Moraga, J., Morgant, G., Dalmais, B., Simon, A., Sghyer, H., et al. (2019). Botcinic acid biosynthesis in *Botrytis cinerea* relies on a subtelomeric gene cluster surrounded by relics of transposons and is regulated by the Zn(2)Cys(6) transcription factor BcBoa13. *Curr. Genet.* 65, 965–980. doi: 10.1007/s00294-019-00952-4

Rui, O., and Hahn, M. (2007). The Slt2-type MAP kinase Bmp3 of *Botrytis cinerea* is required for normal saprotrophic growth, conidiation, plant surface sensing and host tissue colonization. *Mol. Plant Pathol.* 8, 173–184. doi: 10.1111/j.1364-3703.2007.00383.x

Schumacher, J. (2016). DHN melanin biosynthesis in the plant pathogenic fungus *Botrytis cinerea* is based on two developmentally regulated key enzyme (PKS)-encoding genes. *Mol. Microbiol.* 99, 729–748. doi: 10.1111/mmi.13262

Schumacher, J., Kokkelink, L., Huesmann, C., Jimenez-Teja, D., Collado, I. G., Barakat, R., et al. (2008a). The cAMP-dependent signaling pathway and its role in conidial germination, growth, and virulence of the gray mold *Botrytis cinerea*. *Mol. Plant Microbe Interact.* 21, 1443–1459. doi: 10.1094/mpmi-21-11-1443

Schumacher, J., Viaud, M., Simon, A., and Tudzynski, B. (2008b). The Galpha subunit BCG1, the phospholipase C (BcPLC1) and the calcineurin phosphatase co-ordinately regulate gene expression in the grey mould fungus *Botrytis cinerea*. *Mol. Microbiol.* 67, 1027–1050. doi: 10.1111/j.1365-2958.2008.06105.x

Shannon, P., Markiel, A., Ozier, O., Baliga, N. S., Wang, J. T., Ramage, D., et al. (2003). Cytoscape: a software environment for integrated models of biomolecular interaction networks. *Genome Res.* 13, 2498–2504. doi: 10.1101/gr.1239303

Siewers, V., Smedsgaard, J., and Tudzynski, P. (2004). The P450 monooxygenase BcABA1 is essential for abscisic acid biosynthesis in *Botrytis cinerea*. *Appl. Environ. Microbiol.* 70, 3868–3876. doi: 10.1128/aem.70.7.3868-3876.2004

Sun, H., Liu, X., Li, F., Li, W., Zhang, J., Xia, Z., et al. (2017). First comprehensive proteome analysis of Kcr in seedling leaves of Nicotiana tabacum. *Sci. Rep.* 7:3013. doi: 10.1038/s41598-017-03369-6

Sun, J., Qiu, C., Qian, W., Wang, Y., Sun, L., Li, Y., et al. (2019). Ammonium triggered the response mechanism of lysine crotonylome in tea plants. *BMC Genomics* 20:340. doi: 10.1186/s12864-019-5716-z

Szklarczyk, D., Franceschini, A., Wyder, S., Forslund, K., Heller, D., Huerta-Cepas, J., et al. (2015). STRING v10: protein-protein interaction networks, integrated over the tree of life. *Nucleic Acids Res.* 43, D447–D452. doi: 10.1093/nar/gku1003

Tan, M., Luo, H., Lee, S., Jin, F., Yang, J. S., Montellier, E., et al. (2011). Identification of 67 histone marks and histone Kcr as a new type of histone modification. *Cell* 146, 1016–1028. doi: 10.1016/j.cell.2011.08.008

ten Have, A., Mulder, W., Visser, J., and Van Kan, J. A. (1998). The endopolygalacturonase gene Bcpg1 is required for full virulence of *Botrytis cinerea*. *Mol. Plant Microbe Interact.* 11, 1009–1016. doi: 10.1094/mpmi.1998.11.10.1009

Viefhues, A., Heller, J., Temme, N., and Tudzynski, P. (2014). Redox systems in *Botrytis cinerea*: impact on development and virulence. *Mol. Plant Microbe Interact.* 27, 858–874. doi: 10.1094/mpmi-01-14-0012-r

Wang, M., Weiberg, A., Dellota, E. Jr., Yamane, D., and Jin, H. (2017). Botrytis small RNA Bc-siR37 suppresses plant defense genes by cross-kingdom RNAi. *RNA Biol.* 14, 421–428. doi: 10.1080/15476286.2017.1291112

Wang, Y., Zhou, J., Zhong, J., Luo, D., Li, Z., Yang, J., et al. (2018). Cys(2)His(2) zinc finger transcription factor BcabaR1 positively regulates abscisic acid production in *Botrytis cinerea*. *Appl. Environ. Microbiol.* 84:AEM.00920-18. doi: 10.1128/aem.00920-18

Wei, W., Liu, X., Chen, J., Gao, S., Lu, L., Zhang, H., et al. (2017a). Class I histone deacetylases are major histone decrotonylases: evidence for critical and broad function of histone crotonylation in transcription. *Cell Res.* 27, 898–915. doi: 10.1038/cr.2017.68

Wei, W., Mao, A., Tang, B., Zeng, Q., Gao, S., Liu, X., et al. (2017b). Large-scale identification of protein crotonylation reveals its role in multiple cellular functions. *J. Proteome Res.* 16, 1743–1752. doi: 10.1021/acs.jproteome.7b00012

Weiberg, A., Wang, M., Lin, F. M., Zhao, H., Zhang, Z., Kaloshian, I., et al. (2013). Fungal small RNAs suppress plant immunity by hijacking host RNA interference pathways. *Science* 342, 118–123. doi: 10.1126/science.1239705

Williamson, B., Tudzynski, B., Tudzynski, P., and Van Kan, J. A. (2007). *Botrytis cinerea*: the cause of grey mould disease. *Mol. Plant Pathol.* 8, 561–580. doi: 10.1111/j.1364-3703.2007.00417.x

Wu, Q., Li, W., Wang, C., Fan, P., Cao, L., Yang, J., et al. (2017). Ultradeep lysine crotonylome reveals the crotonylation enhancement on both histones and nonhistone proteins by SAHA treatment. *J. Proteome Res.* 16, 3664–3671. doi: 10.1021/acs.jproteome.7b00380

Xu, W., Wan, J., Zhan, J., Li, X., He, H., Shi, Z., et al. (2017). Global profiling of crotonylation on non-histone proteins. *Cell Res.* 27, 946–949. doi: 10.1038/cr.2017.60

Yang, Q., Li, Y., Apaliya, M. T., Zheng, X., Serwah, B. N. A., Zhang, X., et al. (2018). The response of rhodotorula mucilaginosa to patulin based on lysine crotonylation. *Front. Microbiol.* 9:2025. doi: 10.3389/fmicb.2018.02025

Yu, J., and Zhou, C. Z. (2007). Crystal structure of glutathione reductase Glr1 from the yeast *Saccharomyces cerevisiae*. *Proteins* 68, 972–979. doi: 10.1002/prot.21354

Zhang, C., He, Y., Zhu, P., Chen, L., Wang, Y., Ni, B., et al. (2015). Loss of bcbrn1 and bcpks13 in *Botrytis cinerea* not only blocks melanization but also increases vegetative growth and virulence. *Mol. Plant Microbe Interact.* 28, 1091–1101. doi: 10.1094/mpmi-04-15-0085-r

Zhang, D., Tang, Z., Huang, H., Zhou, G., Cui, C., Weng, Y., et al. (2019). Metabolic regulation of gene expression by histone lactylation. *Nature* 574, 575–580. doi: 10.1038/s41586-019-1678-1

Zhang, L., Thiewes, H., and Van Kan, J. A. (2011). The D-galacturonic acid catabolic pathway in *Botrytis cinerea*. *Fungal Genet. Biol.* 48, 990–997. doi: 10.1016/j.fgb.2011.06.002

Zhang, Z., Li, H., Qin, G., He, C., Li, B., and Tian, S. (2016). The MADS-Box transcription factor Bcmads1 is required for growth, sclerotia production and pathogenicity of *Botrytis cinerea*. *Sci. Rep.* 6:33901. doi: 10.1038/srep33901

Zhang, Z., Qin, G., Li, B., and Tian, S. (2014). Knocking out Bcsas1 in *Botrytis cinerea* impacts growth, development, and secretion of extracellular proteins, which decreases virulence. *Mol. Plant Microbe Interact.* 27, 590–600. doi: 10.1094/mpmi-10-13-0314-r

Zheng, L., Campbell, M., Murphy, J., Lam, S., and Xu, J. R. (2000). The BMP1 gene is essential for pathogenicity in the gray mold fungus *Botrytis cinerea*. *Mol. Plant Microbe Interact.* 13, 724–732. doi: 10.1094/mpmi.2000.13.7.724

Zhou, S., Yang, Q., Yin, C., Liu, L., and Liang, W. (2016). Systematic analysis of the lysine acetylome in *Fusarium graminearum*. *BMC Genomics* 17:1019. doi: 10.1186/s12864-016-3361-3

Conflict of Interest: The authors declare that the research was conducted in the absence of any commercial or financial relationships that could be construed as a potential conflict of interest.

frontiers in Microbiology

ORIGINAL RESEARCH
published: 26 November 2020
doi: 10.3389/fmicb.2020.559975

Mitochondrial Complex I Core Protein Regulates cAMP Signaling via Phosphodiesterase Pde2 and NAD Homeostasis in *Candida albicans*

Xiaodong She[1,2†], Lulu Zhang[2,3†], Jingwen Peng[1], Jingyun Zhang[1], Hongbin Li[2,4], Pengyi Zhang[2,5], Richard Calderone[2], Weida Liu[1,6] and Dongmei Li[2*]*

[1] Institute of Dermatology, Chinese Academy of Medical Sciences (CAMS) & Peking Union Medical College (PUMC), Nanjing, China, [2] Department of Microbiology & Immunology, Georgetown University Medical Center, Washington, DC, United States, [3] Department of Dermatology, Jiangsu Province Hospital of Traditional Chinese Medicine, Nanjing, China, [4] Department of Dermatology, The First Affiliated Hospital of Kunming Medical University, Kunming, China, [5] Sport Science Research Center, Shandong Sport University, Jinan, China, [6] Center for Global Health, School of Public Health, Nanjing Medical University, Nanjing, China

OPEN ACCESS

Edited by:
Fernando Rodrigues, University of Minho, Portugal

Reviewed by:
Todd B. Reynolds, The University of Tennessee, Knoxville, United States
Zeeshan Fatima, Amity University Gurugram, India

***Correspondence:**
Weida Liu
liumyco@hotmail.com
Dongmei Li
dl33@georgetown.edu

† These authors have contributed equally to this work

Specialty section:
This article was submitted to Fungi and Their Interactions, a section of the journal Frontiers in Microbiology

Received: *07 May 2020*
Accepted: *29 October 2020*
Published: *26 November 2020*

Citation:
She X, Zhang L, Peng J, Zhang J, Li H, Zhang P, Calderone R, Liu W and Li D (2020) Mitochondrial Complex I Core Protein Regulates cAMP Signaling via Phosphodiesterase Pde2 and NAD Homeostasis in Candida albicans. Front. Microbiol. 11:559975. doi: 10.3389/fmicb.2020.559975

The cyclic adenosine 3′,5′-monophosphate (cAMP)/protein kinase A (PKA) pathway of *Candida albicans* responds to nutrient availability to coordinate a series of cellular processes for its replication and survival. The elevation of cAMP for PKA signaling must be both transitory and tightly regulated. Otherwise, any abnormal cAMP/PKA pathway would disrupt metabolic potential and ergosterol synthesis and promote a stress response. One possible mechanism for controlling cAMP levels is direct induction of the phosphodiesterase *PDE2* gene by cAMP itself. Our earlier studies have shown that most single-gene-deletion mutants of the mitochondrial electron transport chain (ETC) complex I (CI) are hypersensitive to fluconazole. To understand the fluconazole hypersensitivity observed in these mutants, we focused upon the cAMP/PKA-mediated ergosterol synthesis in CI mutants. Two groups of the ETC mutants were used in this study. Group I includes CI mutants. Group II is composed of CIII and CIV mutants; group II mutants are known to have greater respiratory loss. All mutants are not identical in cAMP/PKA-mediated ergosterol response. We found that ergosterol levels are decreased by 47.3% in the *ndh51*Δ (CI core subunit mutant) and by 23.5% in *goa1*Δ (CI regulator mutant). Both mutants exhibited a greater reduction of cAMP and excessive trehalose production compared with other mutants. Despite the normal cAMP level, ergosterol content decreased by 33.0% in the CIII mutant *qce1*Δ as well, thereby displaying a cAMP/PKA-independent ergosterol response. While the two CI mutants have some unique cAMP/PKA-mediated ergosterol responses, we found that the degree of cAMP reduction correlates linearly with a decrease in total nicotinamide adenine dinucleotide (NAD) levels in all mutants, particularly in the seven CI mutants. A mechanism study demonstrates that overactive *PDE2* and cPDE activity must be the cause of the suppressive cAMP-mediated ergosterol response in the *ndh51*Δ

and *goa1*Δ. While the purpose of this study is to understand the impact of ETC proteins on pathogenesis-associated cellular events, our results reveal the importance of Ndh51p in the regulation of the cAMP/PKA pathway through Pde2p inhibition in normal physiological environments. As a direct link between Ndh51p and Pde2p remains elusive, we suggest that Ndh51p participates in NAD homeostasis that might regulate Pde2p activity for the optimal cAMP pathway state.

Keywords: mitochondrial complex I, ergosterol synthesis, NADH/NAD$^+$ redox state, PDE2 regulation, *Candida albicans*

INTRODUCTION

Candidiasis is the fourth most common cause of bloodstream infections (BSI) in United States hospitals (Berman and Sudbery, 2002). Other types of candidiasis are mucosal oral or vaginal candidiasis, whose predisposing factors differ from those associated with BSI. For several reasons, including azole resistance and poor diagnosis assays, candidemia remains a disease with high mortality. A strategy for the development of novel antifungals has been to identify new antifungals that act against fungal- or even *Candida*-specific targets (Gintjee et al., 2020; Li et al., 2020). The current antifungal pipeline on specific metabolic targets includes olorofim (nucleic acid synthesis) (Oliver et al., 2016), fosmanogepix (MGX) [glycosylphosphatidylinositol (GPI) synthesis] (Alkhazraji et al., 2019), and arylamidine T2307 (mitochondria) (Yamashita et al., 2019).

Our recent efforts have focused on the identification of mitochondrial targets that have specificity for fungi – almost exclusively subunit proteins of electron transport chain (ETC) complex I (CI). To this end, we have identified two CI subunit proteins, Nuo1p and Nuo2p, as well as a CI regulator, Goa1p, that are fungal specific or CTG specific. The CTG clade contains a few opportunistic pathogenic yeasts (mostly *Candida* spp. but not *Saccharomyces cerevisiae*) that encode the CUG codon as a serine instead of a leucine. Other CTG-specific subunits of ETC CIII and CIV have also been recently reported (Sun et al., 2019). Fungal specificity, once established, should lead to the identification of functions that relate to the contribution of these proteins to host immune responses and pathogenesis. We have constructed knockout strains in the genes encoding the proteins described above. Among functional assignments, ETC mutants have a number of defects related to oxidative metabolism [ATP synthesis, oxygen consumption, reactive oxygen species (ROS) sensitivity], aging, survival in phagocytes, and virulence in mice and *Drosophila melanogaster*. We identified functions of the fungal-specific CI subunits that include cell wall polysaccharide synthesis. A third subunit protein of interest to us is a CI protein that is broadly conserved among species: Ndh51p. The use of this knockout strain has allowed us to categorize conserved functions and compare them to those having fungal-specific functions.

Genomic comparisons of *Candida albicans* and *S. cerevisiae* reveal many similar signaling pathways that regulate cellular processes, including cell cycle, morphogenesis, stress adaptation, and energy metabolism. The equilibrium between energy-generating and energy-depleting biosynthetic events is modulated by several conserved signal pathways, including Snf1 (Ulery et al., 1994; Mayer et al., 2011) and cyclic adenosine 3′,5′-monophosphate (cAMP)-activated protein kinase A (PKA). The Snf1 kinase pathway of *C. albicans* is a homolog of the mammalian AMPK for energy regulation. We have demonstrated that Snf1 is phosphorylated either during mitochondrial ATP insufficiency or during the addition of cAMP (Zhang et al., 2018). In contrast to the stress-responding Snf1 kinase pathway, the cAMP/PKA pathway functions mainly to regulate nutrient metabolism by coordinating energy consumption with cell activities such as fungal germination, cell cycling, and ergosterol biosynthesis under physiological conditions. However, mitochondrial ETC features of *C. albicans* are different from those of *S. cerevisiae* since the latter yeast species entirely lacks a mitochondrial CI. Also, *S. cerevisiae* is a Crabtree-positive organism that undergoes fermentation in the presence of oxygen, while *C. albicans* is Crabtree negative and uses oxygen for energy production.

The essential role of the Ras-cAMP-PKA chain has been conserved evolutionarily since the progenitors of yeasts and mammals diverged (Kataoka et al., 1985). It is initiated by carbon-sensing proteins Ras1/2p and Gpr1/Gpa2p. Once the GTP-bound form of Ras1/2p is activated by the guanine nucleotide exchange factor (GEF) Cdc25p, adenylate cyclase (Cyr1p) converts ATP into cAMP that initiates PKA (Tpk1p/Tpk2p) activation. The cAMP/PKA pathway regulates mitochondrial CI but not CII respiration in isolated liver (Lark et al., 2015). However, the coordination of cAMP/PKA signaling with CI function is not well understood in *C. albicans*. A number of studies have suggested a link between the cAMP/PKA pathway and mitochondrial oxidative phosphorylation (OXPHOS) in *S. cerevisiae* (Dejean et al., 2002; Hlavatá et al., 2008), in which enzyme content, ROS, the antioxidant defense system, and mitochondrial protein import are all significantly disrupted by cAMP/PKA dysfunction (Chevtzoff et al., 2005; Feliciello et al., 2005; Schmidt et al., 2011). As *S. cerevisiae* lacks CI, one can imagine that cAMP/PKA regulation of energy production in *C. albicans* would be different from *S. cerevisiae*. Structurally, *C. albicans* contains two Ras homologs Ras1p and Ras2p with redundant functions, and Ras2p has been further identified as part of the feedback inhibition of PKA (Zhu et al., 2009; Dong and Bai, 2011). In contrast to the multiple effectors in

mammalian cells, Ras1p and Ras2p appear to have a single effector (Cyr1p) in *C. albicans*. To avoid an overreaction in cAMP/PKA production, cAMP conversion to AMP is catalyzed by the enzyme phosphodiesterases (PDE) Pde1p and Pde2p in *C. albicans*. When mitochondrial activity is positively regulated by the RAS/PKA pathway (Dejean et al., 2002), the activity of this pathway is largely dependent on the cAMP levels in the cells (Chevtzoff et al., 2005). Intracellular cAMP levels are constantly maintained but still spike during the lag phase in both *S. cerevisiae* and *C. albicans* (van der Plaat, 1974; Nikawa et al., 1987) – perhaps as a precursor to the acceleration of carbon metabolism.

We have chosen to focus upon ergosterol synthesis because of its contributions to cell membrane stability and because ergosterol synthesis is the target of the triazole antifungals. We noted that 10 out of 12 ETC CI mutants, including *ndh51*Δ (Sun et al., 2013), are hypersensitive to fluconazole (FLC). Unlike those fungal-specific proteins mentioned above, conserved Ndh51p in all eukaryotes is a core protein of CI that exerts the critical function of NADH oxidation by binding to NADH and participating in electron transfer (Gabaldón et al., 2005). Downregulated ERG and efflux pump activity have been used to explain azole sensitivities in *goa1*Δ and *ndh51*Δ (Sun et al., 2013; She et al., 2016). While *ERGs* are also seen to be downregulated in two other CI mutants, *nuo1*Δ and *nuo2*Δ, but to a lesser extent, the expressions of *FLU1* and *MDR1* (the major facilitator gene superfamily) were unexpectedly increased. It should be noted that the CIII and CIV mutants are also sensitive to FLC (Sun et al., 2019). However, the expression of *ERG* genes and drug efflux pumps *CDR1* and *CDR2* (ABC family members) have been seen to be normal in CIII and CIV mutants (Sun et al., 2019). These results suggest that the mechanisms for FLC sensitivity in these respiration mutants are different.

In order to determine the contribution of ergosterol synthesis to FLC sensitivity and to understand how cAMP/PKA-mediated ergosterol synthesis was affected by the mitochondrial ATP-generating process, we compared cAMP content and ergosterol abundance in two groups of ETC mutants with variable respiration defects and *ERG* profiles. In addition, trehalose and coenzyme nicotinamide adenine dinucleotide (NAD) content were used to estimate the degree of metabolic disorder due to abnormal cAMP pathway and NADH oxidation in the mitochondria. We employed two distinct testing models: the first is based on using gene-deleted strains of ETC [CI subunit mutants compared to that of wild type (WT) and other ETC complex mutants] during the early stationary phase of YP-glucose and YP-glycerol growth; the second model measures the effects caused by a cAMP antagonist and agonist versus untreated controls. Through the expression of genes in the cAMP pathway and PDE activities in the ETC mutants, we are able to demonstrate the molecular mechanism of a CI subunit protein that affects cAMP regulation. Our broad objective is to understand the impact of ETC proteins on cAMP/PKA-mediated ergosterol synthesis. **Figure 1** describes key events in cAMP/PKA-mediated ergosterol synthesis. For each mutant used, we focused upon ergosterol levels, NAD content, cAMP levels, PDE activity, and trehalose synthesis, all of which are related to CI activity in *C. albicans* in **Figure 1**.

MATERIALS AND METHODS

Culture Media

Media and Chemicals

YPD (2% glucose, 2% peptone, and 1% yeast extract) and YPG (2% glycerol, 2% peptone, and 1% yeast extract) were used. Compounds purchased from Sigma-Aldrich include bucladesine (BuC) and MDL-12330A [MDL, *cis-N*-(2-phenylcyclopentyl)-azacyclotridec-1-en-2-amine hydrochloride] and were dissolved in DMSO for a stock preparation. The working solutions were diluted with medium or phosphate-buffered saline (PBS) (pH 7.0).

Strains

SN250 was used as the parental strain (WT) for nine mitochondrial ETC subunit mutants tested in this study. ETC mutant strains include CI subunit mutants (*nuo1*Δ, *nuo2*Δ, *ndh51*Δ, *mt3290*Δ, *mt4758*Δ, and *mt7590*Δ), CI regulator *goa1*Δ, and one gene each for CIII and CIV (Noble and Johnson, 2005; Bambach et al., 2009; She et al., 2015). CI mutants and CI regulator *goa1*Δ are denoted as CI mutants throughout the text and experiments described below. The mutant strain *qce1*Δ and mutant strain *pet111*Δ are derived from the CIII subunit gene *QCE1* and CIV subunit *PET111*, respectively (Sun et al., 2019). Each of these mutants displayed a compromised respiration and was unable to assemble in the individual ETC complex (Li et al., 2011; She et al., 2015; Sun et al., 2019).

Growth Conditions

All cultures were streaked on a YPD agar plate from −80°C stocks. One colony was added to 5 ml of YPD broth to initiate overnight yeast cultures (200 rpm, 30°C). Cultures in YPD at 12 h were centrifuged at 4°C, and cell lysates were prepared from 200 ml medium for metabolite measurement. Cells were washed twice with cold PBS and stored at −80°C. For the YPG medium, as the ETC mutants are incapable of growing in non-fermentable glycerol, cells from a YPD culture at 10 h were collected, washed with PBS, and then incubated in YPG broth for an additional 2 h before being harvested. The cells were washed and stored at −80°C. For other experiments, cells grown in YPD for 10 h were supplemented with each compound at the concentration indicated in the results section. After a 2- or 4-h treatment according to each individual experiment, cells were washed with cold PBS twice and stored at −80°C until analysis (see below).

Ergosterol Measurements

Sample Preparation

Cells were thawed at room temperature (RT), then sonicated for 10 min at 4°C, and were treated with 25 ml of 400 g/L KOH methanol (85–90°C for 2 h) (Abidi, 2001). After cooling, samples were shaken for 1 min in 6 g of sodium phosphate. The upper

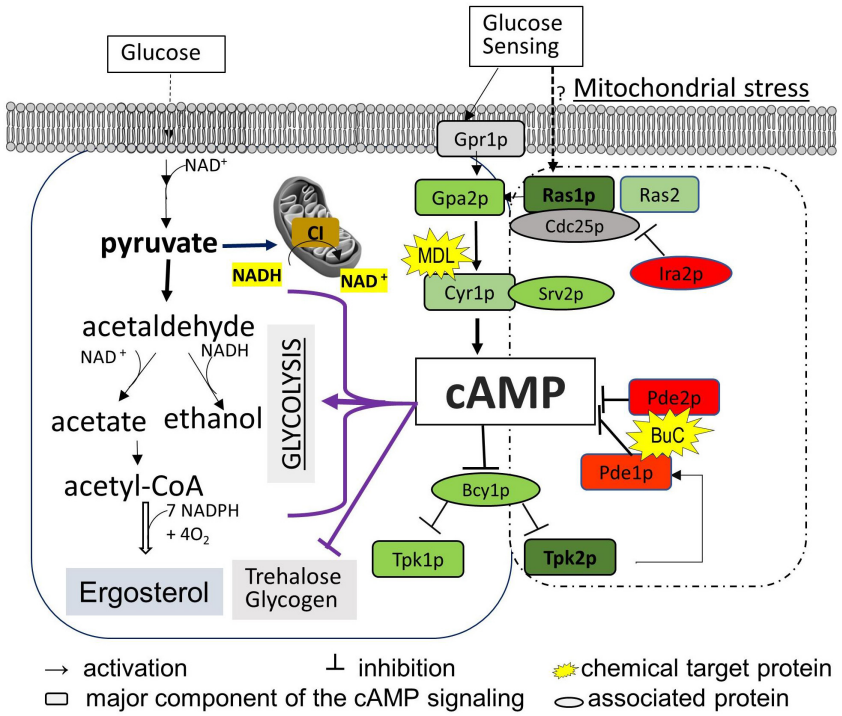

FIGURE 1 | Diagram of the cAMP/PKA nutrient signaling pathway and two downstream effectors (ergosterol synthesis and trehalose accumulation) in *C. albicans*. Glucose metabolism in the mitochondria and cytosol depends on total NAD, which is constantly monitored by the cAMP/PKA pathway (left box). The major events in glycolysis that also require the NAD coenzyme are shown to highlight the possible affected steps for cAMP reduction observed in mitochondrial CI mutants such as *ndh51*Δ. We assume that Ras1-Tpk2 (in bold) activation harmonizes mitochondrial NAD metabolism and also actuates Pde1 to avoid an overactive cAMP/PKA response. The cAMP/PKA proteins are presented in green, and feedback control proteins are marked in red. MDL represents MDL-12330, which inhibits adenylyl cyclase for cAMP synthesis; BuC represents bucladesine, a cell membrane-soluble cAMP analog. Ergosterol content undergoes a change under either of BuC or MDL.

layer was adjusted to 25 ml with MeOH/acetone/*n*-hexane (2:2:1) (Nagy et al., 2006) and then subjected to filtration with a 0.45-μm Millipore filter. The filtrate was dried at RT under nitrogen, and the residue was dissolved in 50 μl MeOH for HPLC-mass spectrometry (MS) analysis.

Sterols in 10-μl aliquots were separated on a C18 (250 mm × 4.6 mm, 5 μm) chromatographic column (Shiseido, Japan) at 30°C. The solvent gradient used in the mobile phase is MeOH/H_2O (97:3, v/v) at a flow rate of 1.0 ml/min. Detection of ergosterol was achieved at 280 nm (Kesselmeier et al., 1985) using HPLC (Agilent-1260, Agilent Technologies, Santa Clara, CA, United States). Samples were compared to commercial ergosterol (Sigma). The quantitation of total sterol content was calculated as follows: sterol content = C × N × V/M (C, concentration; V, volume; N, dilution factor; and M, dry weight of cell lysate).

Determination of cAMP, NADH, and NAD^+ in *C. albicans* Lysates by HPLC-MS/MS

Sample Preparation

Samples were lyophilized and then ground into powders. Approximately 100 mg of sample from each strain was dissolved in 1 ml of water. The suspension was vigorously vortexed for about 30 min at 4°C and then centrifuged at 13,200 rpm for 4 min. A 50-μl aliquot of supernatant of each strain was mixed with 150 μl of acetonitrile. A mixture of 50 μl was aspirated and subjected to HPLC-MS/MS analysis.

Instrument and Reagents

All the standard compounds and chemicals for HPLC-MS/MS including methanol and acetonitrile were purchased from Sigma. The HPLC-MS/MS system consisted of Shimadzu LC-20AD and API 3200MD TRAP. MS was performed in electrospray positive ionization mode with mass ranges of 124–1,000 and 8–1,000 Da. Experimental parameters for HPLC and tandem MS are as follows.

Liquid-Phase Conditions

The column temperature was maintained at 35°C. Each 10 μl of the samples was injected onto a MSLab 45 + AA-C18 column (4.6 × 150 mm, 5-μm particle diameter) at a flow rate of 0.75 ml/min. Metabolites were separated by a linear gradient of an aqueous phase solution A, water (ammonium acetate), and organic phase solution B, acetonitrile (ammonium acetate, ammonia, and water). The gradient was as follows: 1–2 min, 100% A; 3–4 min, 90% A; 5–6 min, 50% A; 7–8 min, 5% A; and 9–10 min, equilibration with 100% A. The fraction collected

from the HPLC was coordinated as 0–1, 1.1–3.0, 3.01–5.0, 5.01–8.0, and 8.01–11.0 min. The total analysis time, including the equilibration, was 12 min for each analysis.

MS Conditions

Sciex API 3200, a fully integrated triple quadrupole mass spectrometer with ESI electrospray ion source was used and multiple-reaction monitoring (MRM) was operated for quantitative metabolite analysis. Samples were infused continuously at 5 μl/min. An atomizing gas (50 psi) and auxiliary gas (60 psi) were used as the nebulizing gas with collision gas (CAD) in the medium. A constant flow of curtain gas (20 psi) around the electrospray needle was supplied for reducing surface tension. The collision chamber injection voltages for exit potential (CXP) and entrance potential (EP) were −3.0 and −10 V, respectively. The electrospray needle voltage was set to −4.0 kV, and the heated capillary tube was kept at 350°C.

Quantitative Analysis of Metabolites

Metabolites of samples were identified by their retention time and mass spectral analyses (MS and MS/MS spectra); concentrations of metabolites were based on accurate mass, retention time, and MS/MS information in accordance with the published guidelines for metabolomics studies (Sumner et al., 2007; Wang et al., 2018).

RAS and *PDE* Gene Expression in *C. albicans*

The expressions of *RAS1*, *RAS2*, *PDE1*, and *PDE2* were measured by RT-PCR. All strains of *C. albicans* (WT and complex mutants) were prepared in YPD mid-log phase growth at 30°C. RNAs were obtained from each strain following glass bead shaking and phenol extraction at 65°C. The quality and concentration of RNAs were measured with a nano-spectrophotometer, and approximately 0.8 μg of RNA was used to prepare cDNA and the real-time PCR procedure of QIAGEN (OneStep RT-PCR Kit). The transcription level of each gene was normalized to 18S rRNA gene level. Data are presented as means ± standard deviations (SD). The $2^{-\Delta\Delta CT}$ (where CT is the threshold cycle) method of analysis was used to determine the fold change in gene transcription (She et al., 2013).

cAMP PDE (cPDE) Activity Assay

The cPDE activity assay kit from BioVision Inc. (Milpitas, CA, United States) is normally used to measure the PDE activity in mammalian cells. We modify the manufacturer's protocol in order to apply the method to fungal cells with cell walls. The assay specifically targets PDEs that degrade cAMP molecules. When AMP produced by cPDE activity in the sample is metabolized by the enzyme mix provided in the kit, a newly formed intermediate compound will react with a fluorescent probe to generate a fluorescent signal at Ex/Em = 538/587. Measurement of fluorescence [relative fluorescence units (RFU)] was assessed in kinetic mode for 30 min at 37°C, and the results were plotted for calculation of cPDE activity.

The cells were harvested from 12 h of growth in YPD or YPG broth by centrifugation at 5,000 × *g* for 10 min. After washing twice with PBS, 2×10^6 cells in each strain were suspended in 200 μl of cPDE assay buffer supplemented with 200 μl of glass beads. Cell lysate was achieved by rigorous shaking at 4°C for 3 min and subsequent centrifugation. An aliquot of 20 μl of cell lysate (optimal concentration of cPDE in preliminary experiment) was used to measure cPDE activity in a black 96-well plate with a flat bottom. For each experimental set, an appropriate standard curve for cPDE activity was generated by plotting the resulting RFU values against AMP concentrations from 20 to 100 nM, and positive and negative controls are included in each assay. The calculation of cPDE activity (the difference of ΔRFU_S between two time points) of each sample was based on the observed slope (the linear portion of the plotted RFU post 12 min of substrate addition). The testing well without substrate (background control) for each sample was set up in parallel. After subtraction of the background control (ΔRFU_{bk}) for the same time interval, the RFU changes between two time points (ΔRFU_S value) were applied in standard curve to determine the AMP generation (con_{AMP}). The cPDE activity (pmol/min/ml, or μU/ml) was then calculated according to the following formula: cPDE activity = $(con_{AMP}/\Delta T \times V) \times D$, in which ΔT represents the time interval chosen for the ΔRFU_S value (in minutes), V is the sample volume (ml), and D is the dilution factor. The cPDE activity in each strain was also normalized by protein concentration in each testing sample and was presented as μU/ml/mg protein. Protein concentration was determined by the Bradford reagent assay.

Statistical Analysis

All the data were analyzed by SPSS Statistics 17.0. For each assay, three replicates were analyzed with one-way analysis of variance (ANOVA) along with Dunnett's test to calculate the statistical difference between means. The comparisons were performed against WT *C. albicans* in the YPD condition or each strain without treatment if not indicated otherwise. Significance was established at $p = 0.05$.

RESULTS

Variations in Ergosterol Reduction in Respiratory Mutants

Fluconazole is an inhibitor of ergosterol synthesis. Inhibition of CI and CIII–CV in *C. albicans* increases the susceptibility to FLC in strains found in clinical settings, lab isolates, and even in strains with an FLC resistance phenotype (Sun et al., 2013). The ETC deletion mutants chosen in this study fall in two classes based on their O_2 consumption rates (OCRs) (Sun et al., 2019). All CI mutants are categorized as Class I, which sustains a 30–35% level of WT OCR that is no longer sensitive to rotenone (CI inhibitor) but is still sensitive to the CIV inhibitor KCN. This means that the residual OCR in Class 1 mutants is not a product of CI respiration. The CIII mutant (*qce1*Δ) and CIV mutant (*pet111*Δ) belong to Class II – characterized by maintaining only ∼7% of WT OCR levels, where this residual OCR is no

longer sensitive to KCN. Both classes of respiratory mutants are hypersensitive to FLC (Sun et al., 2013). However, there seem to be mutant-specific mechanisms for the FLC susceptibility because of their variable efflux pump activities (Sun et al., 2013, 2019; She et al., 2015). In contrast to other CI mutants, the *ndh51*Δ mutant exhibits more pronounced changes in *ERGs* for ergosterol synthesis (Sun et al., 2013).

To determine the correlation between cell energy and azole susceptibility or ergosterol synthesis, we compared the ergosterol content in Class I mutants (three CI mutants: *nuo1*Δ, *nuo2*Δ, and *ndh51*Δ), the CI regulator mutant *goa1*Δ, and two Class II mutants (*qce1*Δ and *pet111*Δ). The ergosterol content was measured by HPLC in cellular lysates collected from early stationary phase growth. When compared to those in WT, significant reductions in ergosterol of 47.3, 32.8, and 23.7% were observed in *ndh51*Δ, *qce1*Δ, and *goa1*Δ (p values of <0.001 and <0.01), respectively, as shown in **Figure 2A**. Like GOA1, QCE1 is also a CTG lineage-specific protein. By contrast, ergosterol abundance remained relatively undisturbed upon deletion of the other two CI mutants (*nuo1*Δ and *nuo2*Δ) and *pet111*Δ. These results exhibit a lack of correlation between ergosterol synthesis and respiration activities. Apparently, mutant-specific ergosterol changes with one or more MFS (major facilitator superfamily) or CDR efflux pumps give rise to the common FLC sensitivity in these respiratory mutants. Furthermore, the greatest loss of ergosterol in *ndh51*Δ validates the greatest downregulation of the *ERG* gene family.

Intracellular cAMP Levels Decrease in ETC Mutants, Especially in the CI Core Subunit Mutant *ndh51*Δ

The impact of cAMP levels on azole sensitivity (Jain et al., 2003) and ergosterol biosynthesis is well documented (Sardari et al., 2003). To confirm whether the reduction of ergosterol content in *ndh51*Δ, *qce1*Δ, or *goa1*Δ is correlated with cAMP levels in these mutants, cAMP levels in each of the six ETC mutants having variable ergosterol levels were assessed during early stationary phase growth in YPD (2% glucose). As shown in **Figure 2B**, the intracellular cAMP content of WT in overnight YPD culture was 1.47 ng/mg cell lysate. With the same carbon source and growth conditions, the cAMP level in *ndh51*Δ was 0.74 ng/mg cell lysate – 48% of the WT cAMP level ($p < 0.001$). In the other three CI mutants, an approximate 25% reduction was shown in *goa1*Δ ($p < 0.01$), and reductions of approximately 15% and 12% were found in *nuo1*Δ ($p < 0.05$) and *nuo2*Δ, respectively. At the same time, cAMP loss was less than 10% in the CIII mutant *qce1*Δ or the CIV mutant *pet111*Δ when compared to WT. The significantly reduced cAMP levels and losses in ergosterol in *ndh51*Δ and *goa1*Δ (**Figure 2A**) perhaps suggest a defect of cAMP-mediated ergosterol occurrence in these two CI mutants. However, this is not the case for ergosterol loss in *qce1*Δ .

cAMP Agonist BuC Partially Restores Ergosterol Content in CI Mutants

To explain whether reduced cAMP is the cause of ergosterol reduction in *ndh51*Δ and *goa1*Δ shown above, we measured the ergosterol contents in each respiratory mutant under treatments of BuC and adenylyl cyclase inhibitor MDL-12330A (MDL) that have opposite effects on cAMP levels. BuC is a cAMP agonist that targets a PDE to increase cAMP in mammalian cells as shown in **Figure 1**. At 4 h post treatment with 50 μM BuC, cAMP slightly increased by 12–15% in all the mutants, which resulted in a significant restoration of ergosterol in *goa1*Δ ($p > 0.05$) and partial restoration of ergosterol levels in *ndh51*Δ and *qce1*Δ through 1.89- and 1.3-fold increases, respectively (**Figure 2C**). Under the same treatment, BuC unexpectedly decreased endogenous cAMP by 15% in WT, which leads to no change in its ergosterol level. Further studies showed that this cAMP reduction in WT remained over a range of BuC concentrations from 10 to 200 μM and does not operate in a dose-dependent manner (data not shown). These results suggest that a compensatory response, i.e., through an inhibition of cAMP generation or activation of cAMP degradation, may suppress the cAMP spike when PDE activity is inhibited by BuC. However, CI function-related PDE activity plays an important role in maintaining cAMP/PKA-mediated ergosterol or other downstream effectors.

When tested with cyclase inhibitor, MDL effectively decreased cAMP levels in mutants and WT, showing a dose-dependent manner over a range of 50 to 200 μM in WT (data not shown). We used 50 μM MDL to suppress cAMP in respiratory mutants. Contrary to our expectations, ergosterol levels were increased in WT strain under 50 μM MDL treatment, which was also evident in the two CI mutants *goa1*Δ and *nuo2*Δ and the CIII and CIV mutants (**Figure 2C**). On the other hand, ergosterol content was not further reduced in *ndh51*Δ under MDL treatment (p value > 0.05) but significantly decreased in MDL-treated *nuo1*Δ (p value < 0.01) when compared with each untreated baseline (**Figure 2C**). These results indicate that other pathways acted to oppose the downregulation of the cAMP-mediated ergosterol pathway in WT and most respiratory mutants. The insensitivity of *ndh51*Δ and apparent ergosterol reduction in *nuo1*Δ under MDL treatment suggest their possible roles in such compensatory responses for ergosterol biosynthesis under cAMP inhibition.

Suppression of cAMP in *ndh51*Δ Increases Trehalose in *C. albicans*

Trehalose is a stress protectant, along with glycogen, both acting to prepare yeast cells to enter the stationary growth phase under nutrient stresses. Trehalose also controls glycolytic flux and mitochondrial activity in yeast via the cAMP/PKA pathway to balance glycolysis with OXPHOS for ATP synthesis (Noubhani et al., 2009). In WT *Candida* cells, the trehalose level was seen to be slightly lower in YPG than in YPD (**Figure 3A**), which correlates with a 12% (1.29/1.47) cAMP reduction (**Figure 3B**). The lower trehalose levels under non-fermentable glycerol culture may help WT cells to increase mitochondrial activity during ATP synthesis, but this does not appear to be the case for mutants. For *ndh51*Δ grown in YPD, trehalose levels were sevenfold higher than for WT ($p < 0.001$) while cAMP was reduced by 48% in this

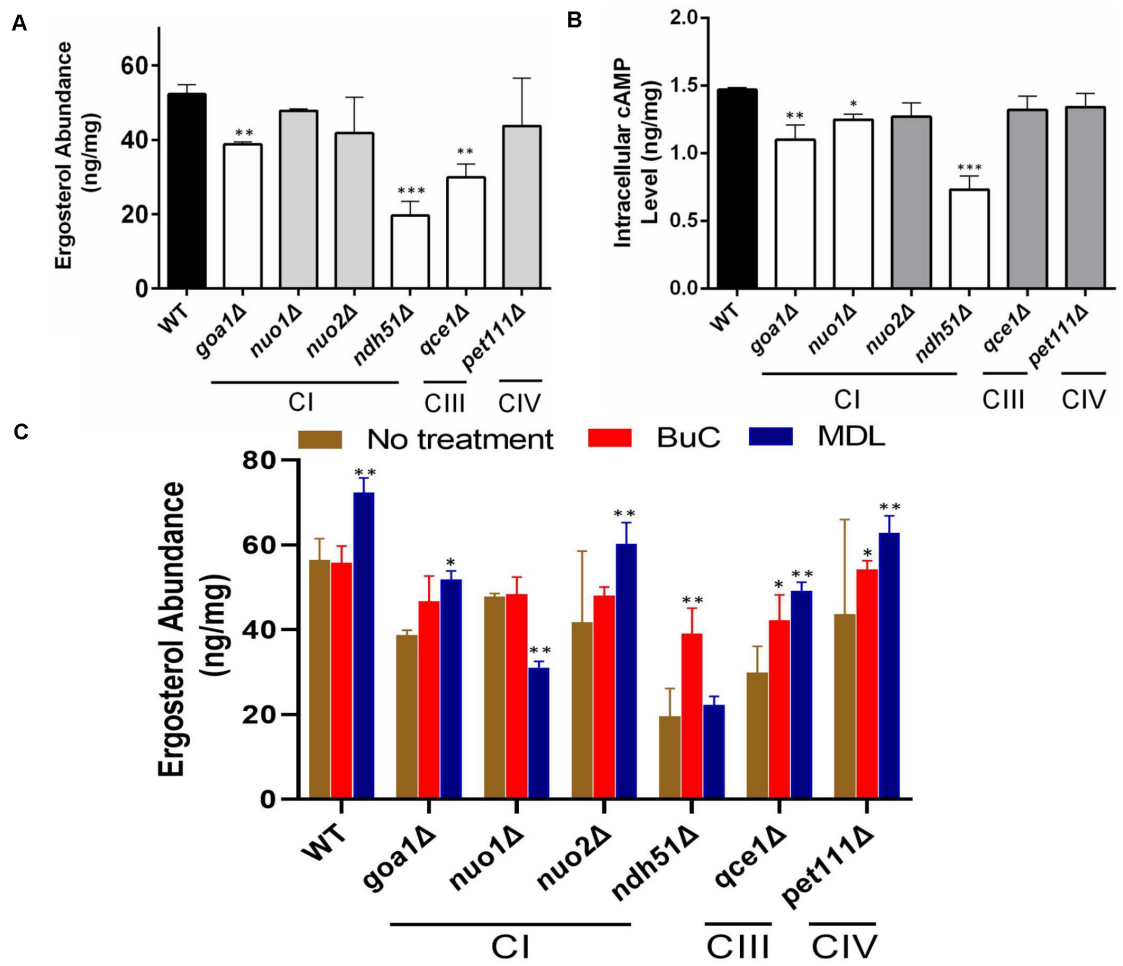

FIGURE 2 | Reduction of ergosterol and cAMP levels varies with each respiration mutant, denoted by their affected ETC complexes: CI, CIII, or CIV null mutants. Ergosterol measurements from cell lysates extracted after 12-h growth in YPD at 30°C of HPLC **(A)** and cAMP levels from HPLC-MS/MS **(B)**. The ergosterol and cAMP content are presented in units of ng/mg cell lysate for each of the CI, CIII, and CIV mutants and compared with WT strain SN250. First, ergosterol reduction is more pronounced (than in WT) in the CI mutant *ndh51*Δ ($p < 0.001$), the CI regulator mutant *goa1*Δ ($p < 0.01$), and the CIII mutant *qce1*Δ ($p < 0.01$). Second, cellular cAMP concentration is markedly reduced in *ndh51*Δ ($p < 0.001$) but less reduced in *goa1*Δ ($p < 0.01$) and CI mutant *nuo1*Δ ($p < 0.05$). Third, the CIII mutant *qce1*Δ shows a 33% lower ergosterol level (compared to WT), but its cAMP reduction is less than 10%, while the CIV mutant *pet111*Δ shows a normal ergosterol level, with less than 10% cAMP reduction. **(C)** Ergosterol measurement under an agonist and an antagonist of cAMP suggests a negative feedback regulation of ergosterol synthesis upon inhibition of the cAMP/PKA pathway. Under a 4-h treatment with 50 μM BuC, the ergosterol reductions seen in the CI regulator mutant *goa1*Δ are restored ($p > 0.05$ versus WT). While no significant change occurs in WT, ergosterol increases 1.89- and 1.3-fold in the CI mutant *ndh51*Δ and CIII mutant *qce1*Δ, respectively, compared with their untreated baselines. However, the adenylyl cyclase inhibitor MDL at 50 μM concentration slightly elevates ergosterol content in WT and in most mutants (except for *ndh51*Δ and *nuo1*Δ). On the other hand, MDL suppresses ergosterol levels in *nuo1*Δ ($p < 0.01$) versus WT but that treatment cannot further suppress ergosterol levels in *ndh51*Δ. All experiments run in triplicate, with error bars generated from the triplicate data. *p* values are shown as "****" for <0.001, "**" for <0.01, and "*" for <0.05.

mutant (**Figures 3A,B**). Withdrawal of glucose also appears to decelerate trehalose accumulation in the *ndh51*Δ strain; we observed a threefold higher trehalose level in YPG with only a slight cAMP elevation (**Figure 3B**). However, the increase in trehalose (2- to 2.5-fold) is marginally changed in other mutants such as CIV mutant *pet111*Δ under YPD and *goa1*Δ and *nuo2*Δ under YPG. Trehalose behavior under either medium for mutants is generally contrary to WT, betraying their metabolic disorders even in glucose-rich media. Nevertheless, there is no direct correlation between cAMP reduction and trehalose accumulation. The massive trehalose level in *ndh51*Δ is likely one of the consequent effectors of the suppressive cAMP/PKA pathway.

NAD and cAMP Levels in Mitochondrial Mutants

The pyridine nucleotide cofactors NAD and NAD phosphate (NADP) are primary redox carriers in mitochondrial tricarboxylic acid (TCA) cycle, mitochondrial CI, and ergosterol biosynthesis. NAD represents the total pyridine nucleotide pool, while NAD^+ and NADH are used to denote the specific

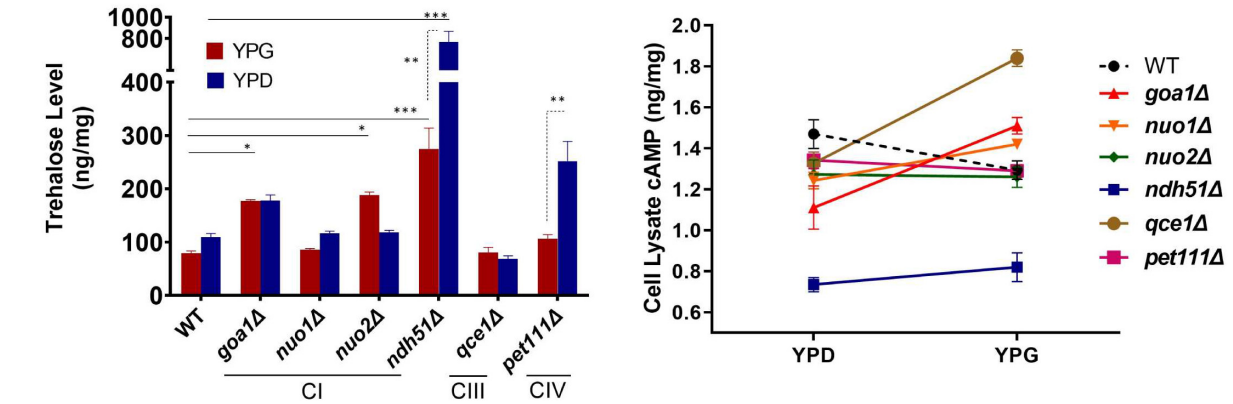

FIGURE 3 | Metabolite disorders associated with the severity of cAMP reduction under mitochondrial stress. Growth conditions for YPG in ETC mutants initiated with 10-h YPD (2% glucose) culture due to their inability to utilize non-fermentable carbon sources. After washing twice with PBS, the cells from mutants and WT were transferred to YP-2% glycerol medium for 2 h before cell lysate preparation. **(A)** Trehalose content in *ndh51*Δ increases sevenfold (YPD) and threefold (YPG) over WT, which correlates with the greatest cAMP reduction in this mutant. Significant increases in trehalose are also shown in the CI regulator *goa1*Δ and *nuo2*Δ (under YPG) and in *pet111*Δ (under YPD). **(B)** Non-fermentable glycerol (YPG) growth represses cAMP levels and slightly decreases trehalose content in WT when compared with YPD. A contrary impact on the cAMP levels is seen in most ETC mutants during YPG growth. The changes in cAMP level between YPD and YPG in each mutant do not correlate with trehalose production in panel **(A)**. $^{*}p < 0.05$, $^{**}p < 0.01$, $^{***}p < 0.001$.

respective oxidized and reduced forms. In the mitochondria, the electron donor NADH is oxidized by mitochondrial CI forming NAD^+, which is then converted to NADH via the TCA cycle. To estimate whether dysfunctional CI affects the turnover of NADH, we measure NADH and NAD^+ in all respiratory mutants described above. To further validate the correlation of NADH dehydrogenases of CI with cAMP and NAD, three additional CI mutants were included. The *mt7590*Δ and *mt4758*Δ are deletion mutants of ortholog core subunits NDUFS1 and NDUFS8 in humans (Lazarou et al., 2009), respectively. The *mt3290*Δ, which encodes the human ortholog NDUFS4, is not an enzymatic core subunit in any eukaryotic cell. The function of CI is carried by three domains: the electron transfer site, quinone-binding site, and proton translocation site. All three additional CI proteins, like Ndh51p, come from the electron transfer site. In addition, Ndh51p is one of the proteins to bind the NADH substrate (Gabaldón et al., 2005). We were not surprised to find that the operative structures of three mutants are similar, particularly to the role of Ndh51p. As shown in **Figure 4A**, reduction of cAMP levels in these additional CI mutants was greater than what we saw in *qce1*Δ and *pet111*Δ. We found that *mt4758*Δ and *mt7590*Δ showed 32 and 20% reductions, respectively, while the cAMP level in the non-core CI mutant *mt3290*Δ had a 17.5% reduction. In our previous study, *mt3290*Δ was one of the few CI subunit mutants that showed an MIC to FLC similar to that of WT cells (Sun et al., 2013).

For WT grown in 12 h YPD, a baseline level of 1.47 ng/mg cAMP correlated to 48.34 ng NAD per milligram of cell lysate with a 2.63 ratio of NAD^+/NADH. In conjunction with a 12% reduction of cAMP in YPG, the total NAD molecules are reduced by 30% in WT, and the ratio of NAD^+/NADH is significantly reduced to 0.96. Under the same 12-h YPD cultures, results for respiratory mutants showed that the relatively low levels of cAMP – especially in CI mutants – correspond numerically to a decreased total NAD (**Figure 4B**), of which *ndh51*Δ shows the greatest reduction in total NAD (48%) with the lowest cAMP level and an intermediate amount of total NAD reduction in other CI mutants corresponding to a respective intermediate reduction of cAMP level. The correlation coefficient is 0.8559 among all mutants as shown in **Figure 4B**.

The linear correlation between total NAD and cAMP content is less evident in each mutant when adjudged by changes of NAD^+, NADH, or NAD^+/NADH ratio as shown in **Table 1**. Although the cellular NAD^+ level is one of the key factors regulating glycolytic speed, we found the greater reduction of NAD^+ in all CI mutants and in the CIII mutant *qce1*Δ as well. As for NADH, we find that it is higher in those mutants with a more modest cAMP change, while the decreases only appear for the top three CI mutants (**Table 1**). The same suppression of NAD^+ and NADH response in these top three CI mutants is also shown in WT under YPG conditions, suggesting that healthy electron transfer (in NADH metabolism) between CI and CIII releases a positive signal to activate the cAMP/PKA pathway to accelerate glycolysis and increase redox capability.

*ndh51*Δ Elicits an Unusually Strong Phosphatase PDE2 Response

The contribution of two RAS isomers and two isomers of PDE in the context of mitochondrial metabolic state is not known. The microarray data (**Table 2**) showed that CYR1 (adenylyl cyclase) expression was not affected in all mutants and that the overall downregulated cAMP/PKA pathway was more evident in CI mutants *ndh51*Δ and *goa1*Δ. Meanwhile, it also suggests that

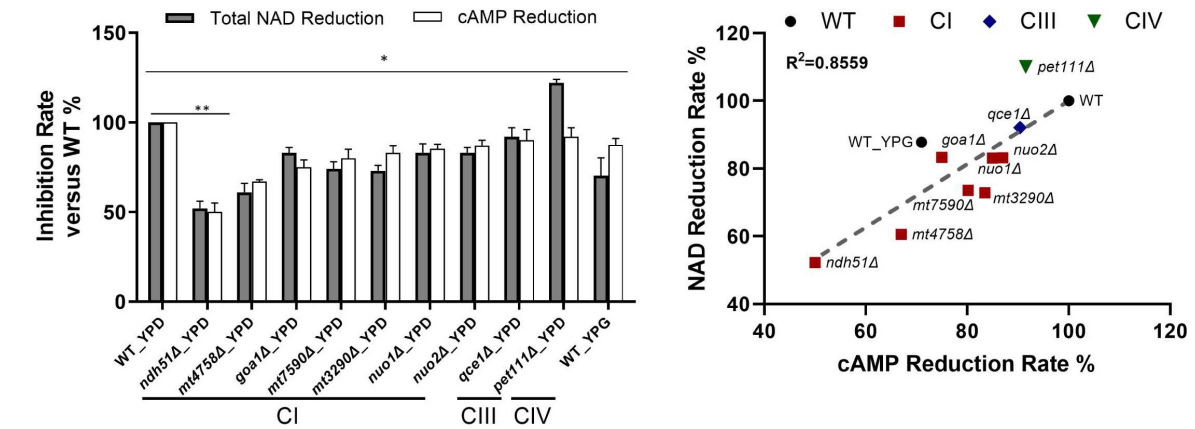

FIGURE 4 | Direct correlation of total NAD with cAMP reduction levels. **(A)** The greatest NAD in the CI mutant *ndh51*Δ grown in YPD corresponds to a ∼50% cAMP reduction. The moderate NAD reductions shown in the CI mutant *mt4758*Δ and in the CI regulator mutant *goa1*Δ correspond to 32 and 25% cAMP reductions, respectively. A cAMP reduction of less than 10% in the CIII and CIV mutants reflects their respective abilities to maintain normal or even higher-than-normal NAD concentrations. **(B)** A strong direct (and linear) relationship between total NAD and cAMP reduction levels among CI, CIII, and CIV mutants (R^2 = 0.8559). These results suggest a close relationship for ETC proteins with NAD metabolism and cAMP/PKA state during NADH oxidation in *C. albicans* mitochondria. Data are taken in triplicate, and comparisons are done between WT and each mutant in panels **(A,B)** under the same culture conditions. *p* values <0.001 are denoted as "**" for <0.01 and "*" for < 0.05.

TABLE 1 | Correlation of cAMP reduction with % changes in NAD^+, NADH, and NAD^+/NADH ratio in ETC mutants versus WT strain in YPD.

Strain (Complexes Mutant)	cAMP Change	NAD^+ Change	NADH Change	NAD^+/NADH ratio
*ndh51*Δ (CI)	−48.0%	−50.5%	−26.8%	1.04
*mt4758*Δ (CI)	−32.3%	−31.3%	−44.9%	1.41
*goa1*Δ (CI)	−25.1%	−13.1%	−24.2%	1.14
*nuo1*Δ (CI)	−15.0%	−36.9%	+ 34.5%	0.53
*nuo2*Δ (CI)	−12.3%	−24.3%	+ 9.4%	0.69
*mt3290*Δ (CI)	−17.5%	−35.4%	−7.5%	0.70
*mt7590*Δ (CI)	−19.8%	−36.2%	−2.9%	0.66
*qce1*Δ (CIII)	−9.5%	−38.8%	+ 71.4%	0.41
*pet111*Δ (CIV)	−8.2%	+ 29.8%	+0.4%	1.47
WT-YPG	−12.3%	−53.4%	+ 35.7%	0.43

two RAS proteins and PDE proteins have opposite patterns in coordination with mitochondrial stress occurring in respiration mutants. Together with respiration defects observed in *ras1*Δ and *tpk2*Δ (data not shown), we proposed that Ras1p/Tpk2-activated Pde1 is a dominant axis relevant to the cAMP/PKA regulation for glycolysis in the cytosol and mitochondria under physiological conditions (**Figure 1**).

In *S. cerevisiae*, Pde1p is involved in cAMP signaling induction, and Pde2p controls basal levels of cAMP, governing resistance of cells to various stresses, such as heat shock, nutritional starvation, and oxidative stress (Ma et al., 1999). To better explain cAMP reduction in CI mutants, the gene expressions of *RAS1*, *RAS2*, *PDE1*, and *PDE2* were analyzed in *ndh51*Δ and *goa1*Δ with the greatest (intermediate) reduction of cAMP using RT-PCR. The results were compared with those for *nuo1*Δ and *nuo2*Δ, which were predicated to have only minor effets on cAMP levels at transcription levels in the cAMP/PKA pathway. As seen in **Figure 5A**, the gene expressions of *RAS1*, *RAS2*, and even *PDE1* were significantly downregulated in the four CI mutants. However, *PDE2* was highly expressed (more than 25-fold) in *ndh51*Δ and only mildly enhanced (twofold) in *goa1*Δ, while it downregulated in *nuo1*Δ and *nuo2*Δ. Indeed, the net cAMP response in each of the four CI mutants matched their *RAS* and *PDE* expression patterns. For example, the highly upregulated *PDE2* repressed cAMP levels in *ndh51*Δ. The downregulated *PDE1* and *PDE2* and the reduced downregulated *RAS1* and *RAS2* help *nuo1*Δ and *nuo2*Δ to maintain a more compatible cAMP level. Together with the more modest *PDE2* upregulation, strongly downregulated *PDE1* and *RAS1* in *goa1*Δ compensate for and block further cAMP loss of the sort seen in *ndh51*Δ. The overactive *PDE2* mRNA in *ndh51*Δ is supported by a filamentous defect in *ndh51*Δ described previously (McDonough et al., 2002), as the *pde2*Δ mutant is hyperfilamentous and the constitutive overexpression of *PDE2* blocks bud-hypha transitions (Bahn et al., 2003).

Elevation of PDE Activity in *ndh51*Δ

More than 10 PDEs with varying selectivity of cAMP and other cyclic nucleotides have been identified in mammals, where PDE4 is a predominant enzyme for cAMP degradation. Intracellular cAMP is synthesized from ATP by adenylyl cyclase and is inactivated by the hydrolytic cPDE superfamily enzyme. The cPDE activity assay kit used in this study is specific to cAMP-degrading enzymes. In *C. albicans*, two genes (*PDE1* and *PDE2*) are responsible for cAMP inactivation. At 12 h

TABLE 2 | Fold changes in gene expression in the cAMP pathway.

Genes	Systematic name	ETC mutant cAMP level (WT 1.47 ng/mg)					
		0.74	1.10	1.25	1.29	1.33	1.35
		*ndh51*Δ	*goa1*Δ	*nuo1*Δ	*nuo2*Δ	*qce1*Δ	*pet111*Δ
RAS1	*Orf*19.1760	–	–	−3.96	−3.93	–	
CDC25	*Orf*19.6926	−2.0	−2.0	–	–	–	–
IRA2	*Orf*19.5219	–	−2.78	2.96	2.4	–	
RAS2	*Orf*19.5902	−13.26	−2.78	33.93	45.30	−5.14	−5.68
GPR1	*Orf*19.1944	−2.05	−3.08	–	–	–	–
GPA2	*Orf*19.1621	–	–	−2.86	−2.28	–	–
CYR1	*Orf*19.5148	–	–	–	–	–	–
SRV2	*Orf*19.505	–	–	–	−2.31	–	–
BCY1	*Orf*19.2014	–	−2.07	−2.66	−2.32	–	–
TPK1	*Orf*19.4892	–	–	2.96	2.47	–	–
TPK2	*Orf*19.2277	–	−2.50	−3.47	−2.01	–	–
PDE1	*Orf*19.4235	–	−3.67	–	–	–	–
PDE2	*Orf*19.2972	–	–	3.05	2.12	–	−2.21

"–": change less than twofold.

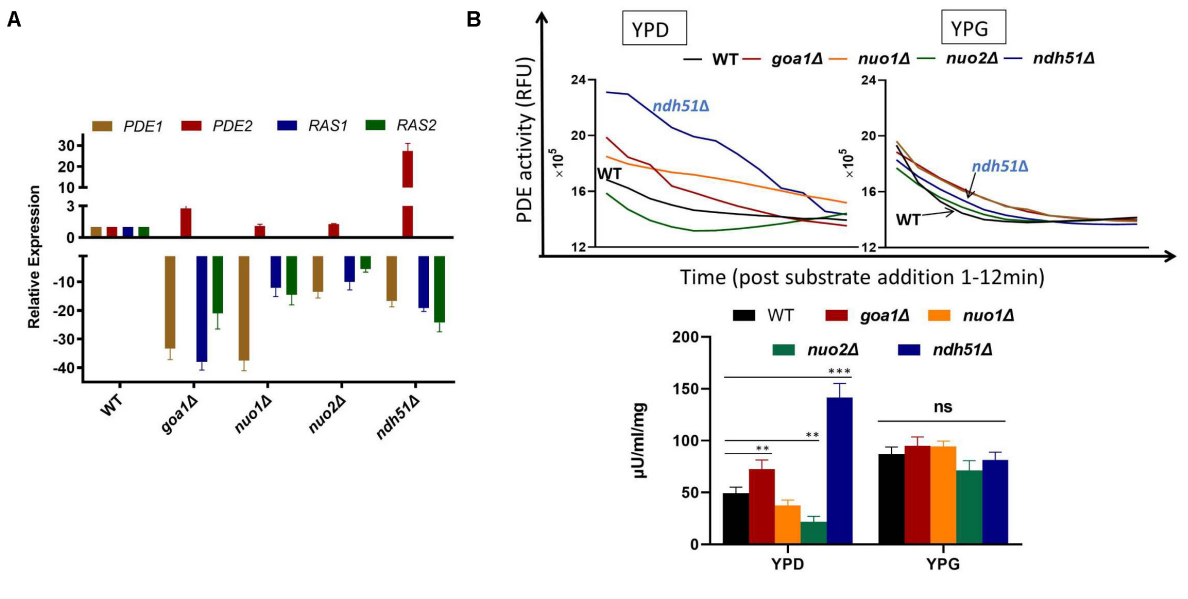

FIGURE 5 | Validation of gene expression of two major G-proteins (*RAS1*/*RAS2*) and phosphodiesterases *PDE1*/*PDE2* by RT-PCR **(A)** and cPDE activity **(B)** in four CI mutants. **(A)** The four genes' expression profiles illuminate the cAMP patterns in the four CI mutants. The relatively normal cAMP levels found in two of the CI mutants (*nuo1*Δ and *nuo2*Δ) correlate with a smaller scale of downregulation in *RAS1*, *RAS2*, and *PDE1* along with a normal *PDE2* expression. A severe cAMP reduction in *ndh51*Δ results from a >25-fold increase in *PDE2* expression while the other three genes are downregulated. A less than threefold increase in *PDE2* expression in *goa1*Δ, together with a significant level of downregulation for *PDE1*, results in a moderate cAMP reduction in this mutant. **(B)** Variation of cAMP-phosphodiesterase (cPDE) activity in four CI mutants in YPD; *ndh51*Δ shows the greatest activity. cPDE activity (slope of RFU change within 12 min after substrate addition) example shown in the top panel. An increased cPDE activity is shown for the mutants in YPD, but not in YPG. The bottom panel represents the cPDE activity from three experiments normalized to μU/ml/mg protein. A threefold higher cPDE activity is shown in *ndh51*Δ with *PDE2* upregulation and a 1.5-fold higher activity in *goa1*Δ versus WT. *p* values <0.001 are denoted as "***" and <0.01 as "**".

in YPD culture, we found that the total cPDE activity in *ndh51*Δ was threefold higher than in WT as shown in **Figure 5B**, which is correlated with the greatest upregulation of *PDE2* in **Figure 5A**. While the cPDE activity was also elevated in *goa1*Δ (1.5-fold), it was reduced in *nuo1*Δ and *nuo2*Δ by a factor of 1.3–2.3-fold. However, the divergent cPDE responses in these CI mutants become uniform upon glucose withdrawal. As seen in **Figure 5B**, the cPDE activity in each mutant turned out to be identical to that in WT in YPG. The total cPDE activities in these strains may be a result of the high-affinity Pde2p protein, which is supported by other observations. In particular, Pde1p of *C. albicans*

hydrolyzes cGMP with a higher affinity than it did cAMP (Hoyer et al., 1994), suggesting a more important role for Pde1p in degrading cGMP than cAMP.

Taken together, the overexpression of *PDE2* and hyperactive cPDEs particularly in *ndh51*Δ and in *goa1*Δ to a lesser extent restricts the optimal level of cAMP during glucose metabolism. The highest ergosterol reduction and trehalose elevation seen in *ndh51*Δ reflect the downstream outcomes of suppressive cAMP/PKA. Therefore, the inhibition of PDE by BuC alleviates an originally low set of cAMP baselines, which leads to ergosterol restoration in *ndh51*Δ and *goa1*Δ. Given the metabolic disturbances in NAD levels seen in *ndh51*Δ and *goa1*Δ, we propose a CI protein Ndh51p-mediated Pde2p-cAMP regulation mode via an as-yet-undetermined NAD regulation mechanism. Furthermore, Goa1p likely utilizes the Ras1-PKA regulation model in order to coordinate TCA and lipid metabolism in *C. albicans*.

DISCUSSION

In eukaryotic cells, biochemical and genetic evidence strongly suggests a connection between mitochondrial status and activity of the cAMP pathway to regulate catabolism and anabolism. The interaction between the cAMP/PKA pathway and others harmonizes energy production with cellular activities according to nutrient availability and mitochondrial stresses. Through the use of a set of mitochondrial ETC complex mutants of *C. albicans*, the downstream responses of the cAMP pathway under disruption of NADH oxidation are investigated in this study. Through their different responses during cAMP-mediated ergosterol biosynthesis, cellular redox state, and glycolytic metabolites under different carbon sources, we uncover the roles of the ETC subunits on cAMP signaling in *C. albicans* that have not been well studied previously.

The Ras1-cAMP-PKA signaling pathway is critical for *C. albicans* animal model virulence (Rocha et al., 2001) in response to host ATP depletion and elevated CO_2 levels (Tao et al., 2017). Loss of virulence is also one of the most common phenotypes of mitochondrial ETC CI mutants (Bambach et al., 2009; She et al., 2013, 2015; Huang et al., 2017). Using an array of respiratory mutants in this study, we observed a similar trend of cAMP reduction in CI mutants. All seven CI mutant (Class I) showed greater cAMP reduction than *qce1*Δ and *pet111*Δ (Class II) although Class II mutant has greater loss of respiration (Sun et al., 2019). Apparently, the ATP crisis is not a complete explanation for the severity of cAMP reduction.

The notion that Pde2p-mediated cAMP regulation is specific to Ndh51p arises from two observations in this study. First, *PDE2* expression increased >25-fold and cPDE activity increased three times in *ndh51*Δ. Second, the PDE inhibitor BuC partially restores cAMP ergosterol in mutants, including *ndh51*Δ. The PDE-regulated cAMP response is also supported by others' observation that PDE inhibitors reverse the antifungal activity of azole drugs (Sardari et al., 2003). In *S. cerevisiae*, on the other hand, *pde1*Δ causes no change in cAMP levels, but *pde2*Δ reduces cAMP levels (Crauwels et al., 1997). In this study, the expression patterns of *RAS1*, *RAS2*, *PDE1*, and *PDE2* in four of the CI mutants showed that *PDE1* expression is in concordance with downregulation of *RAS1* and *RAS2* in all cases. It seems likely that Pde1p acts in parallel with Ras1p-PKA activation in terms of regulation of mitochondrial ATP synthesis. Since the *PDE2* response is opposite to that of *PDE1* in *ndh51*Δ or *goa1*Δ, two Pde1/Pde2 proteins in *C. albicans* may involve different regulation modes.

A high expression of *PDE2* in *ndh51*Δ explains the severe loss of cAMP in this mutant; moreover, a more downregulated *PDE1* moderates the degree of cAMP reduction due to slightly elevated *PDE2* and cPDE activities in *goa1*Δ. The severe or moderate cAMP reduction in *ndh51*Δ and *goa1*Δ explain the corresponding decrease in their ergosterol content. However, we are unable to apply the same reasoning to the 33% ergosterol reduction in *qce1*Δ. The smaller change in cAMP level in this CIII mutant thus suggests a cAMP-independent ergosterol biosynthesis mechanism where Qce1p might be involved. The elevation of ergosterol content in WT under MDL treatment (cAMP inhibitor) also supports the existence of this mechanism. As with ergosterol reduction, the trehalose accumulation is not corelated with cAMP content. A correlation coefficient greater than 0.85 between total NAD and cAMP in all nine tested mutants, on the other hand, justifies a linear correlation between NAD and cAMP. The correlation coefficient is even better when the CIV mutant is not included. These results suggest that total NAD is perhaps a bioenergetic marker to modulate the Ras1-cAMP-PKA regulation pathway in *C. albicans*. Indeed, the metabolism of NAD has emerged as a key regulator of cellular homeostasis (Nikiforov et al., 2015). Being a major component of both bioenergetic and signaling pathways, total NAD is ideally suited to regulate metabolism and major cellular events. In an early study, constant NAD levels in *C. albicans* were sustained during exponential growth and into the stationary growth phase (Chaffin et al., 1979). We assume that the unexplained persistence of high NAD after cessation of protein synthesis also implies that the NAD is upstream of cAMP, rather than being a downstream step in the cAMP pathway. In this case, when the depletion of glucose causes a slowdown in the turnover of NAD (metabolism) in the stationary phase, the accumulated NAD in turn would repress the cAMP response.

In this study, changes in NAD^+ alone, or in NADH alone, or in the NAD^+/NADH ratio do not correspond to any cAMP reduction in any mutant. This is somewhat noteworthy, since in mammalian cells, the NAD^+/NADH ratio is an important marker to reflect the redox state of a cell for the metabolic activities during both catabolism and anabolism. Both the oxidized and reduced forms of NAD are maintained at significant concentrations, with the high NAD^+/NADH ratio favoring the oxidative reaction through regulation of several key enzymes, including glyceraldehyde 3-phosphate dehydrogenase and pyruvate dehydrogenase. In conjunction with a range of 3–10 for the NAD^+/NADH

ratio in mammals, we observe a 2.63 ratio in the YPD growth in WT *C. albicans*, which then dropped to 0.9 in the non-fermentable glycerol medium due to the decrease in NAD^+. The low NAD^+/NADH ratio in the mutants indicates their insufficient glycolysis.

Our data exhibit a similar level of NAD^+ decrease in all CI and CIII mutants, but not in the CIV mutant. The NAD^+ reservoir is well known as a prerequisite condition for continued glycolysis in the cytosol. The significant reduction of NAD^+ in the CI and CIII mutants represents a downregulated metabolic activity, perhaps including reduced ergosterol synthesis in CI mutants and the CIII mutant. In terms of NADH content, more than twofold decreases are seen in the top three CI mutants (*ndh51*Δ, *mt4758*Δ, and *goa1*Δ in **Table 2**), which had severe or intermediate cAMP reductions. The NADH reservoir is an important determinant not only for catabolic processes but also for some anabolic reactions, such as gluconeogenesis (Sistare and Haynes, 1985). Shortage of NADH suggests an additional role for the CI regulators Goa1p or NDUFS8 ortholog beyond their "major" CI enzymatic function. Perhaps, two proteins participate in NADH generation processes, i.e., the TCA cycle in the mitochondria, a process that utilizes non-fermentable carbon sources (such as amino acids and lipids) to generate ATP in the mitochondria. This hypothesis requires further investigation; however, the downregulated acryl-CoA carrier genes and the glycogenesis pathway in *goa1*Δ described in our previous study highlight possible roles of Goa1p in the regulation of NADH metabolism (Li et al., 2016).

Apparently, high levels of *PDE2* and cPDE activity are the causes of cAMP reduction in *ndh51*Δ; however, the invocation of a direct interaction (i.e., Ndh51p inhibiting Pde2p) seems somewhat contrived due to the different locations for the two proteins. The NAD-mediated model is suggested by the linear correlation evident between total NAD and cAMP. However, the current study cannot determine if the NAD loss in *ndh51*Δ is suffered in the cytosol or in the mitochondria. Whether NAD serves as a signal to link Ndh51p activity for NADH oxidization in the mitochondria with cytosol phosphodiesterase activity for controlling cAMP levels requires further investigation. To date, the knowledge of NAD synthesis or breakdown in *C. albicans* remains limited. Genomic BLAST suggests that this organism possesses a functional pathway for the endogenous synthesis of NAD from tryptophan and a salvage pathway from nicotinamide. BLAST analysis also identified an *NDT1* (mitochondrial NAD^+ transporter of *S. cerevisiae*) ortholog – orf19.1393 – with an *E* value of 2.0e-91. Deletion of *NDT1* in *S. cerevisiae* decreases NAD^+ and NADH content in mitochondria and reduces activity of mitochondrial NAD^+-requiring enzymes (Todisco et al., 2006). Although the link between CI proteins and each NAD-maintaining mechanism above remains elusive, the report by Sporty et al. (2009) might offer an interesting area for future research, since they found that a functional salvage pathway is more important than the absolute NAD^+ or NADH levels for life span extension under calorie restriction (CR) conditions. It should be noted that decreased life span is one common phenotype of CI mutants in our earlier studies (Chen et al., 2012; She et al., 2015).

CONCLUSION

In conclusion, mitochondrial CI interacts with the cAMP/PKA signaling pathway that governs NADH metabolism in the mitochondria and redox potential in the cytosol, which promotes ergosterol synthesis and other virulence-related processes in *C. albicans*. A conserved mitochondrial CI subunit (Ndh51p) is required for maintenance of a high NAD potential and optimal concentration of cAMP via Pde2p inhibition. With regard to CI subunits, our data indicate a high degree of functional specificity. It is not surprising that the broadly conservative Ndh51p plays such an important role in cell membrane synthesis, when the fungal-specific subunits are so closely involved with cell wall assembly. This model also has implications in higher eukaryotes for cholesterol synthesis, since Ndh51p is a conserved protein in mammalian cells. The data we collect from ETC mutants also tempt us to explore an improved regimen for fungal infection by synergizing ergosterol inhibitors with cAMP antagonists.

DATA AVAILABILITY STATEMENT

The original contributions presented in the study are included in the article/supplementary material, further inquiries can be directed to the corresponding authors.

ETHICS STATEMENT

No ethical clearance is required as no human or animal studies are presented in this study. All the experiments followed established biosecurity and institutional safety and ethical guidelines.

AUTHOR CONTRIBUTIONS

XS, DL, RC, and WL designed the experiments. XS, LZ, JP, JZ, PZ, and HL performed the experiment and collected the data. XS and DL designed and performed the analysis. DL, RC, and WL wrote the manuscript. All authors contributed to the article and approved the submitted version.

FUNDING

This study was supported by the National Natural Science Foundation of Jiangsu Province, China (BK20191137), the scholarship from China Scholarship Council (CSC, 201908110198) to XS, the scholarship from China Scholarship Council (CSC, 201908320117) to LZ, and the Scientific and Technological Innovation Project of Medicine and Health of Chinese Academy of Medical Sciences (2016-I2M-3-021) to WL.

ACKNOWLEDGMENTS

We wish to thank Dr. Deborah A. Hogan and Dr. William Fonzi for the generous gift of several mutant strains, and we thank Dr. Joseph Bellanti for his suggestions in writing this manuscript. We thank Sensichip Tech@infor Co. Ltd. and Qingdao Sci-tech Innovation Quality Testing Co. Ltd. for technical support.

REFERENCES

Abidi, S. L. (2001). Chromatographic analysis of plant sterols in foods and vegetable oils. *J. Chromatogr. A* 935, 173–201. doi: 10.1016/S0021-9673(01)00946-3

Alkhazraji, S., Gebremariam, T., Alqarihi, A., Gu, Y., Mamouei, Z., Singh, S., et al. (2019). Fosmanogepix (APX001) is effective in the treatment of immunocompromised mice infected with invasive pulmonary scedosporiosis or disseminated fusariosis. *Antimicrob. Agents Chemother,* 64:e01735-19. doi: 10.1128/AAC.01735-19

Bahn, Y.-S., Staab, J., and Sundstrom, P. (2003). Increased high-affinity phosphodiesterase PDE2 gene expression in germ tubes counteracts CAP1-dependent synthesis of cyclic AMP, limits hypha production and promotes virulence of *Candida albicans*: regulation of cAMP signalling and virulence of *C. albicans*. *Mol. Microbiol.* 50, 391–409. doi: 10.1046/j.1365-2958.2003.03692.x

Bambach, A., Fernandes, M. P., Ghosh, A., Kruppa, M., Alex, D., Li, D., et al. (2009). Goa1p of *Candida albicans* localizes to the mitochondria during stress and is required for mitochondrial function and virulence. *Eukaryotic Cell* 8, 1706–1720. doi: 10.1128/EC.00066-09

Berman, J., and Sudbery, P. E. (2002). *Candida albicans*: a molecular revolution built on lessons from budding yeast. *Nat. Rev. Genet.* 3, 918–931. doi: 10.1038/nrg948

Chaffin, W. L., Barton, R. A., Jacobson, E. L., and Jacobson, M. K. (1979). Nicotinamide adenine dinucleotide metabolism in *Candida albicans*. *J. Bacteriol.* 139, 883–888. doi: 10.1128/jb.139.3.883-888.1979

Chen, H., Calderone, R., Sun, N., Wang, Y., and Li, D. (2012). Caloric restriction restores the chronological life span of the goa1 null mutant of *Candida albicans* in spite of high cell levels of ROS. *Fungal Genet. Biol.* 49, 1023–1032. doi: 10.1016/j.fgb.2012.09.007

Chevtzoff, C., Vallortigara, J., Avéret, N., Rigoulet, M., and Devin, A. (2005). The yeast cAMP protein kinase Tpk3p is involved in the regulation of mitochondrial enzymatic content during growth. *Biochim. Biophys. Acta Bioenerget.* 1706, 117–125. doi: 10.1016/j.bbabio.2004.10.001

Crauwels, M., Donaton, M. C. V., Pernambuco, M. B., Winderickx, J., de Winde, J. H., and Thevelein, J. M. (1997). The Sch9 protein kinase in the yeast *Saccharomyces cerevisiae* controls cAPK activity and is required for nitrogen activation of the fermentable-growth-medium-induced (FGM) pathway. *Microbiology* 143, 2627–2637. doi: 10.1099/00221287-143-8-2627

Dejean, L., Beauvoit, B., Bunoust, O., Guérin, B., and Rigoulet, M. (2002). Activation of Ras cascade increases the mitochondrial enzyme content of respiratory competent yeast. *Biochem. Biophys. Res. Commun.* 293, 1383–1388. doi: 10.1016/S0006-291X(02)00391-1

Dong, J., and Bai, X. (2011). The membrane localization of Ras2p and the association between Cdc25p and Ras2-GTP are regulated by protein kinase A (PKA) in the yeast *Saccharomyces cerevisiae*. *FEBS Lett.* 585, 1127–1134. doi: 10.1016/j.febslet.2011.03.057

Feliciello, A., Gottesman, M. E., and Avvedimento, E. V. (2005). cAMP-PKA signaling to the mitochondria: protein scaffolds, mRNA and phosphatases. *Cel. Signal.* 17, 279–287. doi: 10.1016/j.cellsig.2004.09.009

Gabaldón, T., Rainey, D., and Huynen, M. A. (2005). Tracing the evolution of a large protein complex in the eukaryotes, NADH:ubiquinone oxidoreductase (Complex I). *J. Mol. Biol.* 348, 857–870. doi: 10.1016/j.jmb.2005.02.067

Gintjee, T. J., Donnelley, M. A., and Thompson, G. R. (2020). Aspiring antifungals: review of current antifungal pipeline developments. *JoF* 6:28. doi: 10.3390/jof6010028

Hlavatá, L., Nachin, L., Ježek, P., and Nyström, T. (2008). Elevated Ras/protein kinase A activity in *Saccharomyces cerevisiae* reduces proliferation rate and lifespan by two different reactive oxygen species-dependent routes. *Aging Cell* 7, 148–157. doi: 10.1111/j.1474-9726.2007.00361.x

Hoyer, L. L., Cieslinski, L. B., Mclaughlin, M. M., Torphy, T. J., Shatzman, A. R., and Livi, G. P. (1994). A *Candida albicans* cyclic nucleotide phosphodiesterase: cloning and expression in *Saccharomyces cerevisiae* and biochemical characterization of the recombinant enzyme. *Microbiology* 140, 1533–1542. doi: 10.1099/13500872-140-7-1533

Huang, X., Chen, X., He, Y., Yu, X., Li, S., Gao, N., et al. (2017). Mitochondrial complex I bridges a connection between regulation of carbon flexibility and gastrointestinal commensalism in the human fungal pathogen *Candida albicans*. *PLoS Pathog.* 13:e1006414. doi: 10.1371/journal.ppat.1006414

Jain, P., Akula, I., and Edlind, T. (2003). Cyclic AMP signaling pathway modulates susceptibility of *Candida* Species and *Saccharomyces cerevisiae* to antifungal azoles and other sterol biosynthesis inhibitors. *AAC* 47, 3195–3201. doi: 10.1128/AAC.47.10.3195-3201.2003

Kataoka, T., Powers, S., Cameron, S., Fasano, O., Goldfarb, M., Broach, J., et al. (1985). Functional homology of mammalian and yeast RAS genes. *Cell* 40, 19–26. doi: 10.1016/0092-8674(85)90304-6

Kesselmeier, J., Eichenberger, W., and Urban, B. (1985). High performance liquid chromatography of molecular species from free sterols and sterylglycosides isolated from oat leaves and seeds1. *Plant Cell Physiol.* 26, 463–471. doi: 10.1093/oxfordjournals.pcp.a076930

Lark, D. S., Reese, L. R., Ryan, T. E., Torres, M. J., Smith, C. D., Lin, C.-T., et al. (2015). Protein kinase a governs oxidative phosphorylation kinetics and oxidant emitting potential at complex I. *Front. Physiol.* 6:322. doi: 10.3389/fphys.2015.00332

Lazarou, M., Thorburn, D. R., Ryan, M. T., and McKenzie, M. (2009). Assembly of mitochondrial complex I and defects in disease. *Biochim. Biophys. Acta Mol. Cell Res.* 1793, 78–88. doi: 10.1016/j.bbamcr.2008.04.015

Li, D., Chen, H., Florentino, A., Alex, D., Sikorski, P., Fonzi, W. A., et al. (2011). Enzymatic dysfunction of mitochondrial complex i of the *Candida albicans* goa1 mutant is associated with increased reactive oxidants and cell death. *Eukaryotic Cell* 10, 672–682. doi: 10.1128/EC.00303-10

Li, D., She, X., and Calderone, R. (2016). Functional diversity of complex I subunits in *Candida albicans* mitochondria. *Curr. Genet.* 62, 87–95. doi: 10.1007/s00294-015-0518-6

Li, D., She, X., and Calderone, R. (2020). The antifungal pipeline: the need is established. are there new compounds? *FEMS Yeast Res.* 20:foaa023. doi: 10.1093/femsyr/foaa023

Ma, P., Wera, S., Van Dijck, P., and Thevelein, J. M. (1999). The PDE1 -encoded Low-affinity phosphodiesterase in the yeast *Saccharomyces cerevisiae* has a specific function in controlling agonist-induced cAMP signaling. *MBoC* 10, 91–104. doi: 10.1091/mbc.10.1.91

Mayer, F. V., Heath, R., Underwood, E., Sanders, M. J., Carmena, D., McCartney, R. R., et al. (2011). ADP regulates SNF1, the *Saccharomyces cerevisiae* homolog of AMP-activated protein kinase. *Cell Metab.* 14, 707–714. doi: 10.1016/j.cmet.2011.09.009

McDonough, J. A., Bhattacherjee, V., Sadlon, T., and Hostetter, M. K. (2002). Involvement of *Candida albicans* NADH dehydrogenase complex I in filamentation. *Fungal Genet. Biol.* 36, 117–127. doi: 10.1016/S1087-1845(02)00007-5

Nagy, K., Jakab, A., Pollreisz, F., Bongiorno, D., Ceraulo, L., Averna, M. R., et al. (2006). Analysis of sterols by high-performance liquid chromatography/mass spectrometry combined with chemometrics. *Rapid Commun. Mass Spectrom.* 20, 2433–2440. doi: 10.1002/rcm.2606

Nikawa, J., Cameron, S., Toda, T., Ferguson, K. M., and Wigler, M. (1987). Rigorous feedback control of cAMP levels in *Saccharomyces cerevisiae*. *Genes Dev.* 1, 931–937. doi: 10.1101/gad.1.9.931

Nikiforov, A., Kulikova, V., and Ziegler, M. (2015). The human NAD metabolome: functions, metabolism and compartmentalization. *Crit. Rev. Biochem. Mol. Biol.* 50, 284–297. doi: 10.3109/10409238.2015.1028612

Noble, S. M., and Johnson, A. D. (2005). Strains and strategies for large-scale gene deletion studies of the diploid human fungal pathogen *Candida albicans*. *Eukaryotic Cell* 4, 298–309. doi: 10.1128/EC.4.2.298-309.2005

Noubhani, A., Bunoust, O., Bonini, B. M., Thevelein, J. M., Devin, A., and Rigoulet, M. (2009). The trehalose pathway regulates mitochondrial respiratory chain content through hexokinase 2 and cAMP in *Saccharomyces cerevisiae*. *J. Biol. Chem.* 284, 27229–27234. doi: 10.1074/jbc.M109.029454

Oliver, J. D., Sibley, G. E. M., Beckmann, N., Dobb, K. S., Slater, M. J., McEntee, L., et al. (2016). F901318 represents a novel class of antifungal drug that inhibits dihydroorotate dehydrogenase. *Proc. Natl. Acad. Sci. U.S.A.* 113, 12809–12814. doi: 10.1073/pnas.1608304113

Rocha, C. R. C., Schröppel, K., Harcus, D., Marcil, A., Dignard, D., Taylor, B. N., et al. (2001). Signaling through adenylyl cyclase is essential for hyphal growth and virulence in the pathogenic fungus *Candida albicans*. *MBoC* 12, 3631–3643. doi: 10.1091/mbc.12.11.3631

Sardari, S., Mori, Y., Kurosawa, T., and Daneshtalab, M. (2003). Modulatory effect of cAMP on fungal ergosterol level and inhibitory activity of azole drugs. *Can. J. Microbiol.* 49, 344–349. doi: 10.1139/w03-045

Schmidt, O., Harbauer, A. B., Rao, S., Eyrich, B., Zahedi, R. P., Stojanovski, D., et al. (2011). Regulation of mitochondrial protein import by cytosolic kinases. *Cell* 144, 227–239. doi: 10.1016/j.cell.2010.12.015

She, X., Calderone, R., Kruppa, M., Lowman, D., Williams, D., Zhang, L., et al. (2016). Cell wall N-Linked mannoprotein biosynthesis requires Goa1p, a putative regulator of mitochondrial complex I in *Candida albicans*. *PLoS One* 11:e0147175. doi: 10.1371/journal.pone.0147175

She, X., Khamooshi, K., Gao, Y., Shen, Y., Lv, Y., Calderone, R., et al. (2015). Fungal-specific subunits of the *C andida* albicans mitochondrial complex I drive diverse cell functions including cell wall synthesis: defective colonization in host tissues by mitochondrial mutants. *Cell Microbiol.* 17, 1350–1364. doi: 10.1111/cmi.12438

She, X., Zhang, L., Chen, H., Calderone, R., and Li, D. (2013). Cell surface changes in the *Candida albicans* mitochondrial mutant goa1 Δ are associated with reduced recognition by innate immune cells: *GOA1* and recognition by macrophages and epithelial cells. *Cell Microbiol.* 15, 1572–1584. doi: 10.1111/cmi.12135

Sistare, F. D., and Haynes, R. C. (1985). The interaction between the cytosolic pyridine nucleotide redox potential and gluconeogenesis from lactate/pyruvate in isolated rat hepatocytes. Implications for investigations of hormone action. *J. Biol. Chem.* 260, 12748–12753.

Sporty, J., Lin, S.-J., Kato, M., Ognibene, T., Stewart, B., Turteltaub, K., et al. (2009). Quantitation of NAD + biosynthesis from the salvage pathway in *Saccharomyces cerevisiae*. *Yeast* 26, 363–369. doi: 10.1002/yea.1671

Sumner, L. W., Amberg, A., Barrett, D., Beale, M. H., Beger, R., Daykin, C. A., et al. (2007). Proposed minimum reporting standards for chemical analysis: chemical analysis working group (CAWG) metabolomics standards initiative (MSI). *Metabolomics* 3, 211–221. doi: 10.1007/s11306-007-0082-2

Sun, N., Fonzi, W., Chen, H., She, X., Zhang, L., Zhang, L., et al. (2013). Azole susceptibility and transcriptome profiling in *Candida albicans* mitochondrial electron transport chain complex I mutants. *Antimicrob. Agents Chemother.* 57, 532–542. doi: 10.1128/AAC.01520-12

Sun, N., Parrish, R. S., Calderone, R. A., and Fonzi, W. A. (2019). Unique, diverged, and conserved mitochondrial functions influencing *Candida albicans* Respiration. *mBio* 10:e00300-19. doi: 10.1128/mBio.00300-19

Tao, L., Zhang, Y., Fan, S., Nobile, C. J., Guan, G., and Huang, G. (2017). Integration of the tricarboxylic acid (TCA) cycle with cAMP signaling and Sfl2 pathways in the regulation of CO2 sensing and hyphal development in *Candida albicans*. *PLoS Genet.* 13:e1006949. doi: 10.1371/journal.pgen.1006949

Todisco, S., Agrimi, G., Castegna, A., and Palmieri, F. (2006). Identification of the Mitochondrial NAD + Transporter in *Saccharomyces cerevisiae*. *J. Biol. Chem.* 281, 1524–1531. doi: 10.1074/jbc.M510425200

Ulery, T. L., Jang, S. H., and Jaehning, J. A. (1994). Glucose repression of yeast mitochondrial transcription: kinetics of derepression and role of nuclear genes. *Mol. Cell. Biol.* 14, 1160–1170. doi: 10.1128/MCB.14.2.1160

van der Plaat, J. B. (1974). Cyclic 3',5'-adenosine monophosphate stimulates trehalose degradation in baker' s yeast. *Biochem. Biophys. Res. Commun.* 56, 580–587. doi: 10.1016/0006-291X(74)90643-3

Wang, H., Hu, J., Liu, C., Liu, M., Liu, Z., and Sun, L. (2018). LC-MS based cell metabolic profiling of tumor cells: a new predictive method for research on the mechanism of action of anticancer candidates. *RSC Adv.* 8, 16645–16656. doi: 10.1039/C8RA00242H

Yamashita, K., Miyazaki, T., Fukuda, Y., Mitsuyama, J., Saijo, T., Shimamura, S., et al. (2019). The novel arylamidine T-2307 selectively disrupts yeast mitochondrial function by inhibiting respiratory chain complexes. *Antimicrob. Agents Chemother.* 63:e00374-19. doi: 10.1128/AAC.00374-19

Zhang, P., Li, H., Cheng, J., Sun, A. Y., Wang, L., Mirchevska, G., et al. (2018). Respiratory stress in mitochondrial electron transport chain complex mutants of *Candida albicans* activates Snf1 kinase response. *Fungal Genet. Biol.* 111, 73–84. doi: 10.1016/j.fgb.2017.11.002

Zhu, Y., Fang, H.-M., Wang, Y.-M., Zeng, G.-S., Zheng, X.-D., and Wang, Y. (2009). Ras1 and Ras2 play antagonistic roles in regulating cellular cAMP level, stationary-phase entry and stress response in *Candida albicans*: *C. albicans* Ras1 and Ras2. *Mol. Microbiol.* 74, 862–875. doi: 10.1111/j.1365-2958.2009.06898.x

Conflict of Interest: The authors declare that the research was conducted in the absence of any commercial or financial relationships that could be construed as a potential conflict of interest.

frontiers in Microbiology

ORIGINAL RESEARCH
published: 07 December 2020
doi: 10.3389/fmicb.2020.527389

Whole Transcriptome Analysis Provides Insights Into the Molecular Mechanisms of Chlamydospore-Like Cell Formation in *Phanerochaete chrysosporium*

*Lei Liu[1], Huihui Li[1], Yanyan Liu[1], Yi Li[1] and Hailei Wang[1,2]**

[1] College of Life Sciences, Henan Normal University, Xinxiang, China, [2] Advanced Environmental Biotechnology Center, Nanyang Environment and Water Research Institute, Nanyang Technological University, Singapore, Singapore

Phanerochaete chrysosporium is a white rot fungus naturally isolated from hardwoods and widely used in environmental pollution control because it produces extracellular peroxidases. It forms chlamydospores during nitrogen starvation, which naturally occurs in the habitat of *P. chrysosporium*. Chlamydospores protect fungi against many stresses; the molecular basis underlying chlamydospore formation in basidiomycetes is poorly explored. Chlamydospores in *P. chrysosporium* have a different cell wall compared with hyphae, as confirmed by cell wall digestion and microscopy. Furthermore, this study investigated the transcriptome of *P. chrysosporium* in different life stages, including conidium, hypha, and chlamydospore formation, through RNA sequencing. A total of 2215 differentially expressed genes were identified during these processes. The expression patterns of genes involved in several molecular events critical for chlamydospore formation, including starch and sucrose metabolism, phosphatase and kinase, and transcription factors, were determined. This study serves as a basis for further investigating the function of chlamydospore formation in the biotechnologically relevant fungus *P. chrysosporium*.

Keywords: *Phanerochaete chrysosporium*, chlamydospore, transcriptome (RNA-seq), *TEC1*, signaling pathways

OPEN ACCESS

Edited by:
Fernando Rodrigues, University of Minho, Portugal

Reviewed by:
Khajamohiddin Syed, University of Zululand, South Africa
Laure Ries, University of São Paulo, Brazil

****Correspondence:***
Hailei Wang
whl@htu.cn

Specialty section:
This article was submitted to Fungi and Their Interactions, a section of the journal Frontiers in Microbiology

Received: *16 January 2020*
Accepted: *09 November 2020*
Published: *07 December 2020*

Citation:
Liu L, Li H, Liu Y, Li Y and Wang H (2020) Whole Transcriptome Analysis Provides Insights Into the Molecular Mechanisms of Chlamydospore-Like Cell Formation in Phanerochaete chrysosporium. Front. Microbiol. 11:527389. doi: 10.3389/fmicb.2020.527389

INTRODUCTION

Phanerochaete chrysosporium is a typical representative of white rot fungi belonging to Phanerochaetaceae under Polyporales, Agaricomycetidae, and Basidiomycota. This fungus has been extensively studied and used in environmental pollution control because of its ability to degrade a wide variety of non-phenolic and phenolic compounds by producing ligninolytic enzymes (Gao et al., 2010). *P. chrysosporium* can be identified by the morphological characteristics of membranaceous, crust-like fruiting bodies and the microscopic characteristics of conidial structure and hyphae. Thick-walled chlamydospores appear in the middle or at the end of hyphae, and they vary in size from 50 μm to 60 μm. Chlamydospores are morphological structures observed in fungi with enlarged, thick-walled vegetative cells and a condensed cytoplasm; this structure forms in the middle or top of the hyphae and can

be used as a morphological identification of many fungal species (Barran et al., 1977; Ohara and Tsuge, 2004; Spraker et al., 2016). Environmental cues that trigger chlamydospore formation in fungi are usually species specific and include nutrients, osmolarity, light, pH, temperature, air, drug treatment, and plant stimulants.

Chlamydospores can be found in a number of fungi, including ascomycetes, saccharomycetes, and basidiomycetes. This life stage emerges under unfavorable conditions in some pathogenic fungi and promotes survival. Chlamydospores exhibit better stress resistance than conidia; as such, the former preserve, germinate, and survive easily (Jiménez-Tobon et al., 2003; Chung et al., 2005). Chlamydospores can be induced to form on hyphal tips via suspensor cells under nutrient-poor oxygen-limited conditions at low temperatures in *Candida albicans* (Calderone, 2002), whose natural habitats are humans and warm-blooded animals; this species has been widely studied because of its capacity to grow in several distinct morphological forms. Its chlamydospores are three to four times larger than those of yeast cells. In addition to *Candida* species, other fungal species belonging to *Cryptococcus*, *Trichoderma*, *Phytophthora*, *Fusarium*, *Ralstonia*, and *Clonostachys* genus can form chlamydospores (Lewis and Papavizas, 1984). Chlamydospores in *Cryptococcus neoformans* are rich in glycogen, suggesting that they play a role in energy storage (Lin and Heitman, 2005). Chlamydospores of *Trichoderma harzianum* and *Gliocladium roseum* can be induced by antifungal compounds produced by *Bacillus subtilis* (Li et al., 2005). Chlamydospores of *Phytophthora cinnamomi* are produced within plant roots during drought, are transported in root fragments or soil, and germinate to cause infections under warm and moist conditions (McCarren et al., 2005). Chlamydospores of *Fusarium* species promote long-term survival during unfavorable periods in soil, thereby resulting in the intercalary production of macroconidia and hyphae with a thickened wall or hyphal tips with a comparatively thin wall (Bandara and Wood, 1978). They play an important role as inoculum, with a greater potential of infecting plants than when compared to hyphae (Couteaudier and Alabouvette, 1990). Fusarium wilt, which is particularly difficult to control in strawberries, is also partly due to the ability of chlamydospores formed by pathogens to persist in soil for years (Cha et al., 2015). In another study, ralsolamycin, a diffusible metabolite produced by *Ralstonia solanacearum*, can facilitate its invasion of fungal hyphae. The fungi close to a *R. solanacearum* colony form distinct hyphal swellings that resemble chlamydospores, and the chlamydospores formed may provide a specific niche for bacterial colonization and enhance the survival of the symbiotic fungus (Spraker et al., 2016). Conversely, this structure can work as an antagonist that enables the biocontrol ability of fungi. The efficiency of the chlamydospores of *Clonostachys rosea* strain 67-1 to control the cucumber fusarium wilt exceeds 65% when chlamydospores are mixed with cucumber seeds at a concentration of 10^6 spores/mL (Dong et al., 2014).

Chlamydospore formation in basidiomycetes has not been comprehensively studied. As one of the numbers of basidiomycetes, *P. chrysosporium* belongs to white rotting fungus and lives in rotted wood, which lacks nitrogen and experiences nitrogen starvation. Preliminary studies showed that a nitrogen-limited medium can induce chlamydospore formation in *P. chrysosporium* possibly to overcome this unfavorable environment. However, the genetic control of chlamydospore formation in *P. chrysosporium* remains to be studied. In the present study, RNA sequencing (RNA-seq) was conducted to investigate the changes in the expression of all genes involved in the chlamydospore formation of *P. chrysosporium* and to explore the mechanisms and molecular events associated with this process. RNA-seq is a high-throughput, deep-sequencing technology commonly used in genomic research to analyze the functional complexity of transcriptomes. It has a sufficient sensitivity and generates ultrahigh-throughput data, including several low-abundance genes; therefore, RNA-seq is more suitable and affordable for comparative gene expression than microarrays. Our findings provided important insights into the gene expression landscape of the chlamydospore formation of *P. chrysosporium* and provided a basis for identifying specific functional genes contributing to chlamydospore formation in other species.

MATERIALS AND METHODS

Fungal Culture and Sample Preparation

Phanerochaete chrysosporium (ATCC24725) was obtained from the Henan Province Engineering Laboratory for Bioconversion Technology of Functional Microbes, China. It was incubated on potato dextrose agar (PDA) plates and subcultured for 3 days at 30°C. Subsequently, conidial suspensions (5×10^7 spores/mL) were prepared in sterile water. For hyphal formation, the suspensions (2.0 mL/flask) were inoculated into 500-mL flasks containing 300 mL of PDA. The flasks were placed in a shaking incubator at 180 rpm and 37°C. For chlamydospore formation, the suspensions (5.0 mL/flask) were inoculated in 500-mL flasks containing a liquid medium (300 mL) composed of the following: 10.0 g/L glucose, 2.5 g/L $(NH4)_2SO_4$, 1.0 g/L KH_2PO_4, 0.8 g/L $MgSO_4$, 0.5 g/L $CaCl_2$ (Sigma-Aldrich, United States), and 0.7% trace element solution comprising 0.5 g/L glycine, 0.1 g/L $FeSO_4{\cdot}7H_2O$, 0.1 g/L $CoSO_4$, 0.1 g/L $ZnSO_4$, 0.1 g/L $MnSO_4{\cdot}H_2O$, 10 mg/L $CuSO_4{\cdot}5H_2O$, 10 mg/L $AlK(SO_4)_2{\cdot}12H_2O$, 10 mg/L H_2BO_3, and 10 mg/L $Na_2MoO_2{\cdot}2H_2O$ (Sangon Biotech, China). The sampling interval was 12 h, and the samples cultured for 36 and 72 h were taken out from the fermentation broth in a laminar flow bench after their morphological characteristics were observed under a microscope. The fungal biomass was freeze-dried before weighing. Cell wall thickness was determined via transmission electron microscopy (TEM) to measure the different parts of the cell wall with a scale mark from different hyphae and chlamydospores in accordance with a previously described protocol (Ferguson et al., 2005). Data were presented as mean ± standard error of the mean. The samples were washed twice with phosphate-buffered saline (PBS), stored, and then frozen in liquid nitrogen.

On the basis of preliminary experiments, the conidial structure (0 h, CK0) and the hyphae cultured in PDA at 36 h (CK36)

and 72 h (CK72) were taken as the control group, while chlamydospore formation included two stages, namely, 36 h (T36) and 72 h (T72), were taken as the treatment group to understand the pattern of differential gene expression between the hyphae and the chlamydospores (**Table 1**). Then, 100 mg of the conidia, hyphae, and chlamydospores was separately added to 1.5-mL centrifuge tubes after 8000 r/min for 10 min and washed twice with PBS.

Cell walls were stained with calcofluor white (Sigma-Aldrich, United States) at a final concentration of 1 mg/mL for 1 min before microscopy, and lipid bodies were stained by submerging the fungal sections in 10 μg/mL Nile red (Sigma-Aldrich, United States) for 5 min and then washed with 0.1 M PBS (Sangon Biotech, China). Coomassie brilliant blue (Njjcbio, China) was used to stain for 15 min to detect whether or not proteins were present in the cell wall. Excitation and emission filters were 350 and 400 nm, respectively. Images were observed under a fluorescence microscope (Leica DM2500, Germany) and a laser scanning confocal microscope (Zeiss LSM 800, Germany). The cell wall thickness of the chlamydospores was also measured using TEM (JEM-100CXII, Japan).

Enzymatic Hydrolysis of Cell Wall Components

The chlamydospores were washed twice with PBS, acquired from the fermentation broth, and separated from the hyphae through an ultrasonic treatment for 20 min. They were pretreated by grinding in liquid nitrogen and then processed through Soxhlet extraction to eliminate interference from lipid bodies. The powders were ground in liquid nitrogen for 5 min, ultrasonically treated for 60 min, and then centrifuged at 10,000 rpm for 10 min to obtain a purified cell wall. The cell wall of the hypha was obtained via the same method. β-Glucanase powder (400 mg; Solarbio, China) was dissolved in 20 mL of sodium acetate buffer solution (pH 4.5) to obtain 20 mg/mL β-glucanase buffer with filtration. Samples were taken every 6 h for a total of 42 h for enzymatic hydrolysis by glucanase. Cellulase powder (320 mg; Sigma-Aldrich, United States) was dissolved in 20 mL of sodium acetate buffer solution (pH 4.5) to obtain 16 mg/mL cellulase buffer with filtration. Samples were collected every 6 h for a total of 30 h for enzymatic hydrolysis by cellulase. Chitinase powder (100 mg; Sigma-Aldrich, United States) was dissolved in phosphate buffer (pH 6.4) to obtain 20 mg/mL chitinase buffer with filtration. The sampling interval was 2 h for a total of 10 h for enzymatic hydrolysis by cellulase. The supernatant (100 μL) of enzymatic hydrolysis liquid was tested with the 3,5-dinitrosalicylic acid method to measure the resulting sugars (Frankeberger and Johanson, 1983).

TABLE 1 | Details of each sample.

Sample	Time	Description
CK0_1	0 h	Conidia
CK0_2	0 h	Biological replicate of CK0_1
CK36_1	36 h	36 h hyphae
CK36_2	36 h	Biological replicate of CK36_1
CK72_1	72 h	72 h hyphae
CK72_2	72 h	Biological replicate of CK72_1
T36_1	36 h	Chlamydospore starting produced from hyphae
T36_2	36 h	Biological replicate of T36_1
T72_1	72 h	Chlamydospores massively produced (>96%)
T72_2	72 h	Biological replicate of T72_1

Preparation of the cDNA Library for RNA-Seq

All samples were immediately frozen in liquid nitrogen after preparation and then stored at −80°C until their RNA was isolated. Total RNA was extracted using a Trizol reagent in accordance with the manufacturer's protocol (Invitrogen, China) and treated with DNase to remove DNA contamination. RNA degradation and contamination were monitored on 1% agarose gels. The purity of the RNA samples was checked with a NanoPhotometer spectrophotometer (Implen, CA, United States) at absorbance wavelengths of 260 and 280 nm. RNA concentration was measured with a Qubit RNA assay kit in a Qubit 2.0 fluorometer (Life Technologies, CA, United States), and RNA integrity was assessed using the RNA Nano 6000 assay kit of the Bioanalyzer 2100 system (Agilent Technologies, CA, United States). Exactly 3 μg of RNA per sample was used as the input material for the RNA sample preparations. Sequencing libraries were generated using a NEBNext Ultra RNA library prep kit for Illumina (NEB, United States) in accordance with the manufacturer's recommendations, and index codes were added to the attribute sequences of each sample. mRNA was isolated and enriched from the total RNA by using oligo (dT) magnetic beads (Illumina, CA, United States). Then, mRNA was divided into short fragments to be used as templates for the random hexamer-primed synthesis of first-strand cDNA in a fragmentation buffer. The second-strand cDNA was synthesized using the buffer, deoxyribonucleotide triphosphate, RNase H, and DNA polymerase I. The remaining overhangs were converted into blunt ends via exonuclease/polymerase activities. The NEBNext Adaptor with a hairpin loop structure was ligated to prepare for hybridization after the adenylation of the 3′-ends of the DNA fragments. Library fragments were purified with an AMPure XP system (Beckman Coulter, Beverly, MA, United States) to select cDNA fragments with a length of 150–200 bp. Then, 3 μL of uracil-specific excision reagent enzyme (NEB, United States) was used with a size-selected adaptor-ligated cDNA at 37°C for 15 min, followed by 5 min at 95°C before quantitative real-time polymerase chain reaction (qRT-PCR). PCR was performed with Phusion High-Fidelity DNA polymerase, universal PCR primers, and the index (X) primer. The PCR products were purified (AMPure XP system), and the quality of the library was assessed on an Agilent Bioanalyzer 2100 system. The index-coded samples were clustered on a cBot Cluster Generation System by using the TruSeq PE Cluster Kit v3-cBot-HS (Illumina) in accordance with the manufacturer's instructions. After cluster generation, the prepared library was sequenced on an Illumina Hiseq platform to generate 125 bp paired-end reads.

Transcriptome Data Processing and Sequencing Data Assembly

Raw sequence data were transformed by base calling into sequence data and stored in FASTQ format. Raw reads were cleaned by removing adapter sequences, empty reads, and low-quality sequences and deposited in the NCBI Sequence Read Archive[1] under the SRA accession number SRP153122. The clean reads generated through RNA sequencing were mapped to the reference genome of *P. carnosa*, which has a close phylogenetic relationship to *P. chrysosporium*. An index of the reference genome was built using Bowtie v2.2.3 (Langmead and Salzberg, 2012), and paired-end clean reads were aligned to the reference genome via TopHat v2.0.12 (Trapnell et al., 2009). TopHat was selected as the mapping tool because it can generate a database of splice junctions based on the gene model annotation file and produce better mapping results than other non-splice mapping tools.

Normalized Expression Levels of Genes From RNA-Seq

The gene expression levels based on the read counts obtained via HTSeq v0.6.1 were normalized through transformations with fragments per kilo base per million mapped reads (FPKM) to eliminate the influence of different gene lengths and sequence discrepancies on expression calculations (Anders et al., 2015). Transcripts with FPKM < 1 were filtered out, and the filtered transcripts were used as a reference for downstream analysis (Huang et al., 2015). The calculated gene expression levels could be used for the direct comparison of the samples. Expression values were standardized across the dataset to combine the data from different genes.

Analysis of Differentially Expressed Genes (DEGs), Gene Ontology (GO), and Kyoto Encyclopedia of Genes and Genomes (KEGG)

The two conditions or groups (two biological replicates per condition) were subjected to differential expression analysis by using the DESeq R package (1.18.0; Wang et al., 2010). DESeq R provides statistical functions to determine differential expression in digital gene expression data via a model based on the negative binomial distribution. The resulting p-values were adjusted with the Benjamini–Hochberg method to control the false discovery rate (FDR) via the sequentially modified Bonferroni correction for testing multiple hypotheses (Benjamini and Hochberg, 1995). Positive and negative log2FoldChange (log2FC) values indicated significantly upregulated and downregulated genes, respectively. $|\log 2\ \mathrm{FC}| > 1$ and FDR < 0.01 were considered as the cutoff values for DEG screening. The genes screened were subjected to GO enrichment analysis in GOseq R package. In this method, the gene length bias was corrected. The GO terms with the corrected $p < 0.05$ were considered significantly enriched by DEGs. The KEGG database was used to assign and predict the putative functions and pathways associated with the assembled sequences (Kanehisa and Goto, 2000). KOBAS software was utilized to test the statistical enrichment of DEGs in the KEGG pathways (Mao et al., 2005).

RT-qPCR

RNA was isolated using the Ezgene^{TM} Fungal RNA Miniprep kit (Biomiga, San Diego, CA, United States). In this procedure, 50 ng of RNA was transcribed to cDNA by using Omniscript RT kit (Qiagen, Hilden, Germany) in accordance with the manufacturer's instructions. Six genes were chosen to validate the RNA-seq differential gene expression data via qRT-PCR. The primers were designed with Primer version 5.0 based on the assembled transcriptome used for amplification. The product annotations are listed in **Supplementary Table S1**. β-Actin was used as an internal reference gene, and the relative gene expression levels were calculated using the comparative Ct method with the formula $2^{-\Delta\Delta Ct}$ (Livak and Schmittgen, 2001). RT-qPCR analyses were run in triplicate with three biological replicates. Then, RT-qPCR results were compared with the transcriptome data to detect the correlation of each gene expression.

Statistical Analysis

Statistical analysis was conducted in GraphPad Prism 8 (GraphPad Software Inc., San Diego, CA, United States) for Windows. The means ± standard error of the mean (SEM) were used between the treatments. A *t*-test was performed to evaluate the statistical significance of independent groups. The correlation coefficient (r) between RNA-Seq and qPCR was calculated using two-tailed p-value with a confidence interval of 95%.

RESULTS

Morphological Characteristics of the Conidia, Hyphae, and Chlamydospores

The hyphae and the chlamydospores were observed and recorded in different culture phases to investigate the phenotypic changes between them. The maximum biomass of the hyphae and the chlamydospore reached 4.63 and 2.2 g/L, respectively, after cultivation for 72 h (**Figure 1A**). Three types of cells, namely, CK0 (conidia, **Figure 1B**), CK36 (hyphae, 36 h growth, **Figure 1C**), CK72 (hyphae, 72 h growth, **Figure 1D**), T36 (chlamydospores, 36 h, **Figure 1E**), and T72 (chlamydospores, 72 h, **Figure 1F**) were analyzed via light microscopy. The remarkable characteristics of the thickened cell wall were observed for the chlamydospores in comparison with the hyphae (**Figures 2A–D**). The thickness of the cell wall increased with prolonged culture time, and the overall thickness of the entire wall of 60 hyphae and mature chlamydospores was measured. The maximum thickness of the cell wall of the chlamydospores reached 6.7 μm (**Figure 2E**). Optical microscopy confirmed that the cell walls of the cultured chlamydospores (**Figure 2B**) were thicker than those of the hyphae (**Figure 2A**). After the samples were stained with calcofluor white, laser confocal scanning

[1] https://www.ncbi.nlm.nih.gov/sra

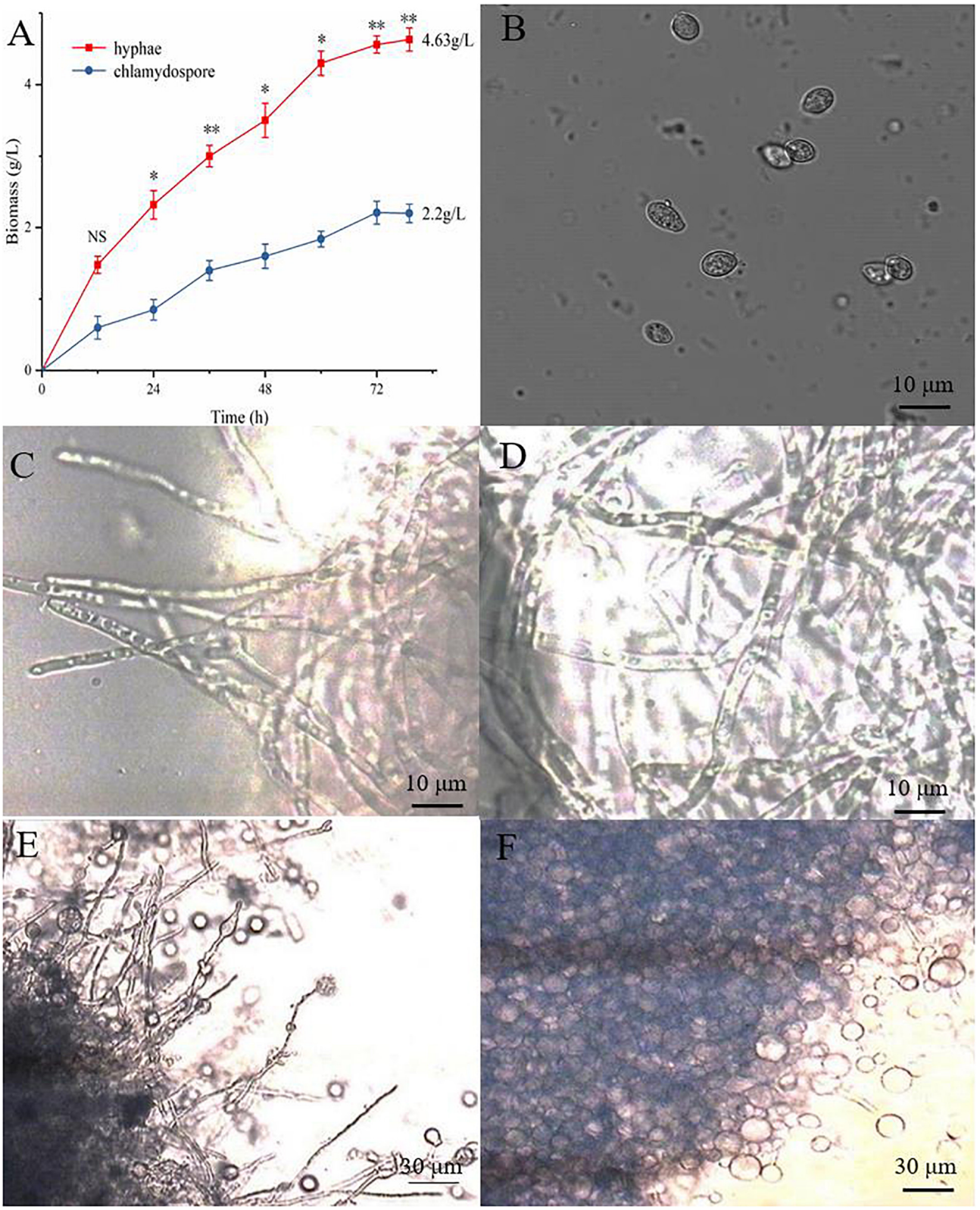

FIGURE 1 | Different growth statuses of the hyphae and chlamydospores of *P. chrysosporium* under a light microscope. **(A)** The biomass of hyphae and chlamydospores cultured from 0 h to 72 h. **(B)** *P. chrysosporium* conidia (CK0). **(C)** Hyphae cultured for 36 h (CK36). **(D)** Hyphae cultured for 72 h (CK72). **(E)** Chlamydospore cultured for 36 h (T36) and **(F)** chlamydospore cultured for 72 h (T72). (Student's *t*-test. Asterisks represent significant differences, $^{**}p < 0.01$ and $^{*}p < 0.05$).

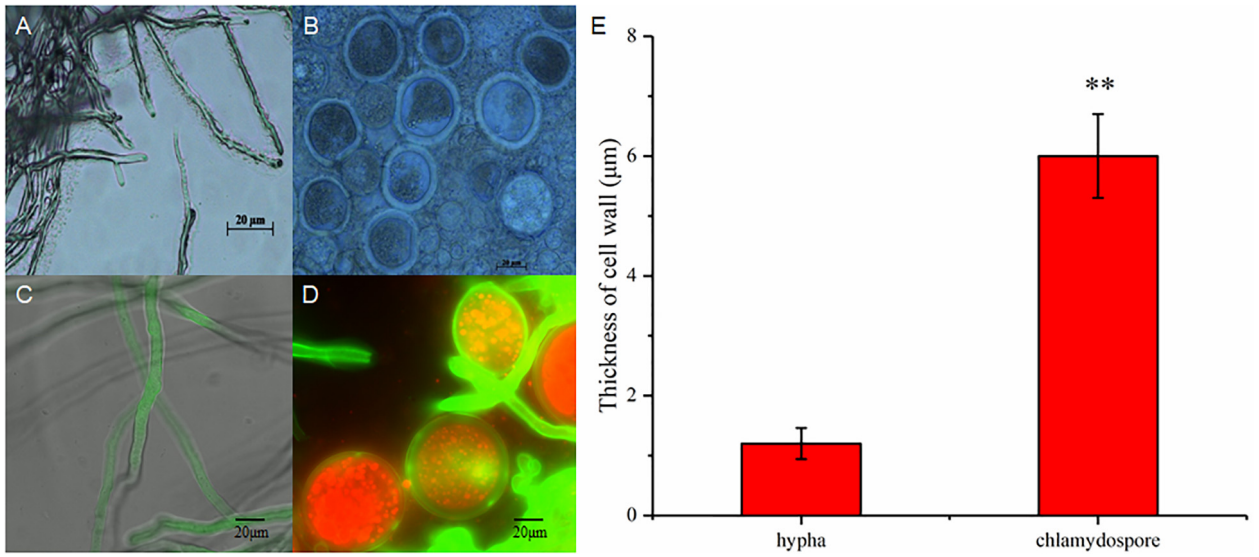

FIGURE 2 | Different morphological characteristics of hyphae and chlamydospores. **(A)** Light microscopy of the hyphae at 72 h. **(B)** Light microscopy of the chlamydospores at 72 h. **(C)** Laser scanning confocal microscope (LSCM) of the hyphae at 72 h. **(D)** LSCM of the chlamydospores at 72 h. **(E)** measurement of the thickness of the cell wall between the hyphae and the chlamydospores. Asterisk indicates that the thickness of the cell wall was significantly different between hyphae and chlamydospores (Student's *t*-test, $^{**}p < 0.01$).

microscopy revealed that the fluorescence intensities of the cell wall of the chlamydospores (**Figure 2D**) were stronger than those of the cell wall of the hyphae (**Figure 2C**). Nile red staining also showed that the chlamydospores contained large lipid bodies (**Figure 2D**). The thickened part of the cell wall was not stained with Coomassie brilliant blue, indicating that this part rarely contained or did not have proteins (**Supplementary Figure S1**).

Enzymatic Hydrolysis by Glucanase, Cellulase, and Chitinase

Enzymatic hydrolysis by glucanase, cellulose, and chitinase was experimentally studied to further understand the different compositions of polysaccharides between the hyphae and the chlamydospores. β-Glucans are natural polysaccharides with a molecular weight of over 6400 daltons and composed of β-(1-3)-glucans, β-(1-4)-glucans, or β-(1-6)-glucans. β-Glucanase can specifically hydrolyze glucan into glucose as the final enzymatic hydrolysate. As such, the reducing sugar in the hydrolysate of 20 mg of the cell wall of the chlamydospores was tested after β-glucanase treatment. An equivalent amount of the cell wall of the hyphae was used as the control. Before the experiment, the reducing sugar content was tested, and the result indicated that neither the samples nor the enzymes contained a reducing sugar before processing (**Figure 3A**). In the first 18 h of enzymatic hydrolysis, the reducing sugar content in the enzymatic hydrolysates of the hyphae and the chlamydospores increased. The reducing sugar content in the hyphal enzymatic hydrolysate was slightly higher than that in the chlamydospore enzymatic hydrolysate. After 18 h, the reducing sugar content in the hyphal enzymatic hydrolysate no longer changed, and the maximum content was 0.480 mg/mL. However, the reducing sugar content detected in the chlamydospore enzymatic hydrolysate continued to increase and reached the peak concentration of 0.598 mg/mL at 30 h (**Figure 3A**). This phenomenon may be attributed to the relatively dense thickened part of the chlamydospore cell wall, thereby causing low-efficiency catalysis. Glucan in the cell wall was gradually digested by the enzyme as enzymatic hydrolysis continued. The results indicated that the glucan content in the chlamydospore cell wall was higher than that in the hyphal cell wall at equal mass. However, it might have also resulted from the different organizations of the polysaccharides of the cell walls of the chlamydospores and the hyphae. Consequently, more β-glucans were exposed to β-glucanase in the chlamydospores.

Cellulose is another polysaccharide and important component of the fungal cell wall. It can be degraded generally by cellulase to generate glucose. The cellulose contents in the substrate of the chlamydospores and the hyphae can be determined by measuring and comparing the glucose contents before and after enzymatic hydrolysis. In this study, 20 mg of hyphae and 20 mg of chlamydospores were used in enzymatic hydrolysis (**Figure 3B**). The degradation rate of cellulose in the chlamydospore cell wall was high, and its glucose content was slightly higher than that in the hyphal cell wall in the first 6 h. Nevertheless, the enzymatic hydrolysis of the chlamydospore group tended to be stable, and the hydrolysate content reached the maximum of 0.215 mg/mL at 18 h. Similarly, the hydrolysate content in the hyphal group reached the maximum of 0.244 mg/mL at 18 h. Subsequently, the glucose content was maintained at a stable level. The glucose content in the hyphal group remained higher than that in the chlamydospore group from 6 h to the end of the experimental period. The cellulose concentration in the chlamydospore cell wall was lower than that in the hyphal cell wall. However, the

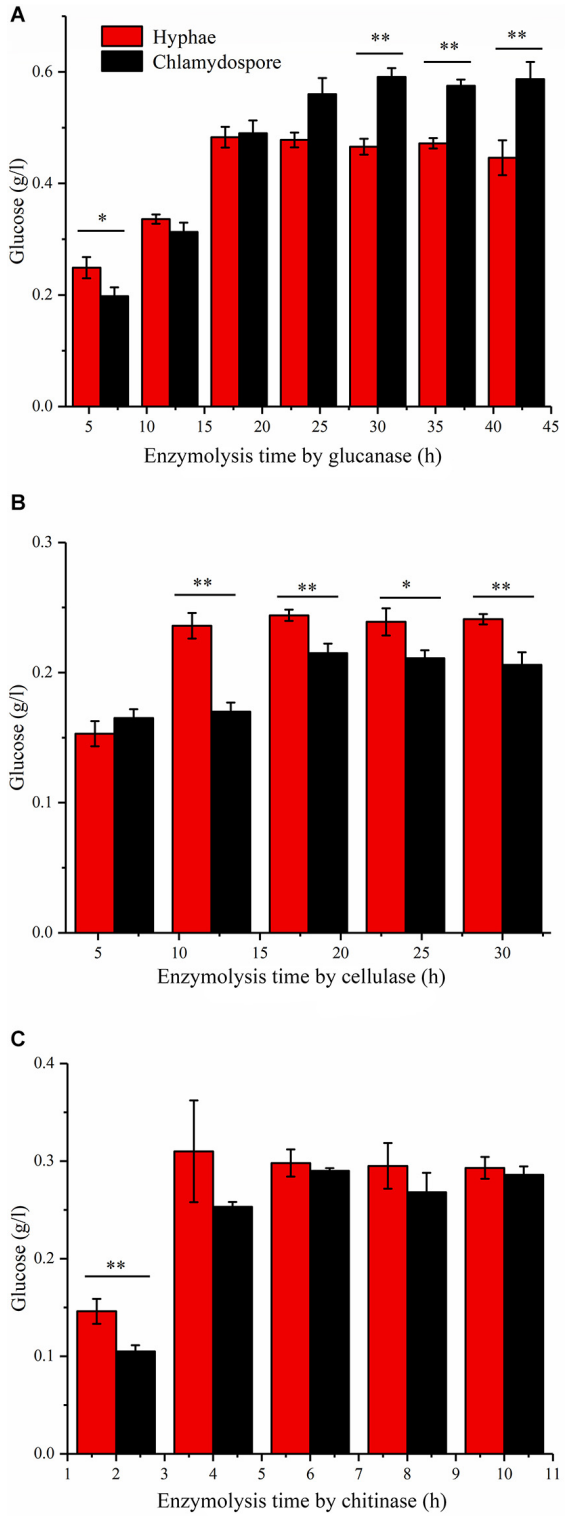

FIGURE 3 | Analysis of the polysaccharide composition of the cell wall of the hyphae and chlamydospores through the enzymatic hydrolysis of the extract. **(A)** Enzymatic hydrolysis by glucanase. **(B)** Enzymatic hydrolysis by cellulase. **(C)** Enzymatic hydrolysis by chitinase. All data are presented as the means ± standard error and evaluated using Student's *t*-test. Asterisks represent significant differences (**$p < 0.01$ and *$p < 0.05$).

organization of cell wall polysaccharides of the chlamydospores might differ from that of the hyphae likely because the amount of cellulose exposed to cellulase in the chlamydospores was lower than that in the hyphae.

Chitin is a straight-chain macromolecule composed of *N*-acetylglucosamine residues linked by β-1,4-glycosidic bonds. It widely exists in crustaceans and in the cell wall of filamentous fungi and some green algae. In this experiment, 5 mg of hyphal cell wall was digested by the enzyme at an equal rate and reached the maximum chitin concentration of 0.313 mg/mL in the first 4 h of enzymatic hydrolysis. The chitinase hydrolysis rate of the chlamydospore cell wall with the same quantity was lower than that of the hyphal cell wall at the initial stage. Afterward, it increased gradually possibly because of the weak combination between the enzyme and the thick dense cell wall of the chlamydospores. The enzymatic hydrolysis of the hyphae stopped after 6 h, whereas the enzymatic hydrolysis of the chlamydospores continued at a slow rate at 6 h and stopped at 8 h (**Figure 3C**). The enzymatic hydrolysis of the chlamydospores yielded the maximum chitin concentration of 0.290 mg/mL. Therefore, the chitin contents in the cell walls of the hyphae and the chlamydospores were basically consistent. Consequently, the results of all above enzymatic hydrolysis supported the microscopic observation and suggested significant differences in cell wall structure and organization between the chlamydospores and the hyphae in *P. chrysosporium*.

RNA-Seq and DEGs (Differentially Expressed Genes) Analyses at Different Stages

The hyphae and the chlamydospores at different stages were subjected to RNA-seq analysis in order to identify the transcriptional patterns associated with chlamydospore development. The sequencing results are summarized in **Table 2**. The proportion of the clean reads to the raw reads in the 10 cDNA libraries ranged from 96.06% to 96.67%. Overall, 76.68% to 80.96% of the clean reads were aligned against the *P. carnosa* genome, and the uniquely mapped reads ranged from 76.23% to 80.44%. The average guanine–cytosine content of the clean reads from the 10 libraries was 59.82. The proportion of the reads with the Phred quality value of Q20 among the clean reads ranged from 97.46% to 97.82%, and the Q30 among the clean reads ranged from 94.02% to 94.58%. The error rate of a single base was 0.01%.

The clean reads were assembled to understand the DEGs associated with chlamydospore formation. The results revealed 32,016 genes, which were used in sequential DEG analyses. Subsequently, a global view of the gene expression pattern of DEGs was generated through hierarchical cluster analysis (**Figure 4**). In the first 36 h, 805 differentially expressed mRNAs were obtained through the pairwise comparison of T36 vs. CK36 vs. CK0. Results showed the following: 736 DEGs between the Ck36 and Ck0 groups, i.e., 323 upregulated genes and 413 downregulated genes; 213 DEGs between the T36 and CK0 groups, i.e., 94 upregulated genes and 119 downregulated genes; and 82 DEGs between T36 and CK36, i.e., 28 upregulated genes

TABLE 2 | The quality of transcriptome sequencing data.

Sample name	Raw reads	Clean reads	Clean base (G)	Error rate (%)	Q20 (%)	Q30 (%)	GC (%)
CK0_1	35441486	34065626	4.2	0.01	97.46	94.02	59.94
CK0_2	36137676	34880668	4.36	0.01	97.68	94.40	60.00
CK36_1	30940888	29733958	3.72	0.01	97.54	94.15	60.36
CK36_2	28013254	26973044	3.37	0.01	97.67	94.36	60.06
CK72_1	29965294	28968620	3.62	0.01	97.82	94.58	59.49
CK72_2	32299912	31179170	3.90	0.01	97.72	94.39	59.82
T36_1	37415538	36022412	4.50	0.01	97.72	94.48	59.99
T36_2	20588054	29565202	3.70	0.01	97.73	94.40	58.59
T72_1	33169438	31960838	4.00	0.01	97.54	94.09	60.11
T72_2	33871300	32666572	4.08	0.01	97.72	94.45	59.85

and 54 downregulated genes (**Figure 5A**). From 36 h to 72 h, only 130 differentially expressed mRNAs were obtained after the three groups were compared (T72 vs. CK72 vs. T36 vs. CK36). Furthermore, two DEGs, namely, one upregulated gene and one downregulated gene, were found between the CK72 and CK36 groups, and 51 DEGs, i.e., 38 upregulated genes and 13 downregulated genes, were observed between the T72 and T36 groups (**Figure 5B**). These results indicated the difference in the gene expression levels between the samples.

Formation of Relevant Differential Gene KEGG (Kyoto Encyclopedia of Genes and Genomes) Enrichment Pathways With Chlamydospores

The DEGs were searched against the KEGG database to understand the potential molecular pathways underlying chlamydospore formation. Chlamydospore formation was related to the regulation of biomacromolecule synthesis and decomposition, which involved carbohydrate, lipid, and protein metabolism. Comparison of the enrichments revealed that most of the DEGs were involved in various pathways (**Table 3**), including ribosome, ascorbate, and aldarate metabolism in T36 vs. CK36 (**Figure 6A**); secondary metabolite biosynthesis, arginine and proline metabolism, MAPK signaling pathway, and metabolic pathways in T72 vs. T36 (**Figure 6B**); and secondary metabolite biosynthesis, fatty acid degradation, starch and sucrose metabolism, glycolysis/gluconeogenesis, galactose metabolism, tryptophan metabolism, and pentose and glucuronate interconversions in T72 vs. CK72 (**Figure 6C**). These pathways indicated that the large-scale assembly of carbohydrates might participate in chlamydospore formation.

Two sugar metabolism-related genes were differentially regulated in *P. chrysosporium*. Uridine triphosphate (UTP)–glucose-1-phosphate uridylyltransferase gene (*UGP*; log2FoldChange = −1.8348) and β-glucosidase gene (*GLU*; log2FoldChange = −3.2038) were greatly downregulated in the starch and sugar metabolism of the enrichment pathways in the T72 vs. CK72 groups (**Figure 7A**). *UGP*, also known as glucose-1-phosphate uridylyltransferase or uridine diphosphate (UDP)–glucose pyrophosphorylase, is an enzyme involved in carbohydrate metabolism. *UGP* synthesizes UDP–glucose from glucose-1-phosphate and UTP. The downregulation of this gene might cause the partition of the sugar flux toward cell wall synthesis, including cellulose and 1,4-β-D-glucan syntheses. *GLU* belongs to glycoside hydrolase family 1, which encodes a wide range of enzymes that hydrolyze the glycosidic bond between two or more carbohydrates or between a carbohydrate and a non-carbohydrate moiety. *GLU* expression can catalyze the hydrolysis of 1,4-β-D-glucan into β-D-glucose. The downregulation of this gene in T72 might result in the accumulation of 1,4-β-D-glucan in cells (**Figure 7A**). The glycogen phosphorylase gene (*GP*), which helps remove glucose from glycogen, can produce glucose-1-phosphate, which can be used to produce ATP. However, it was significantly regulated only during the hyphal growth (CK36 vs. CK0, CK72 vs. CK0) and the initial stage of chlamydospore formation (T36 vs. CK0). Therefore, *GP* might not play a key role in chlamydospore formation (**Figure 7A**).

Mitogen-activated protein kinase (MAPK) pathways control the reproduction, spore morphology, and expression of the pathogenic toxicity factor and is vital in the synthesis and integrity of the fungal cell wall (Mehrabi et al., 2006). In *Schizosaccharomyces pombe*, the loss of any of the kinases in this pathway results in the appearance of rounded cells instead of rod-like cells that are sensitive to β-glucanase; this finding suggests that this pathway is involved in cell wall maintenance (Nobel et al., 2000). MAPKs coordinate and execute cellular responses to environmental signals (Pearson et al., 2011). External stimuli, such as oxygen pressure, hunger, osmotic pressure, heavy metals, and low temperature, can activate MAPK signaling pathways. Most fungi always have four major MAPK pathways, including the Fus3/Kss1, Kss1, Slt2, and Hog1 pathways. In the pheromone response pathway, Fus3 and Kss1 MAPKs regulate the mating processes. For filamentous growth pathways, KSS1 is the final kinase in the signal transduction cascade regulating activation/repression of the filamentation induced by nitrogen/carbon limitation. The Slt2 cell integrity pathway monitors cell wall integrity and promotes cell wall biosynthesis, and the high-osmolarity glycerol (Hog 1) response pathway is required for growth under hyperosmotic conditions (Zhao et al., 2007). The synthesis of chlamydospores started from 36 h, and hyphae were basically transformed into chlamydospores at 72 h. According to the enrichment of the T72 vs. T36 groups, the Kss1 (starvation) pathway showed a

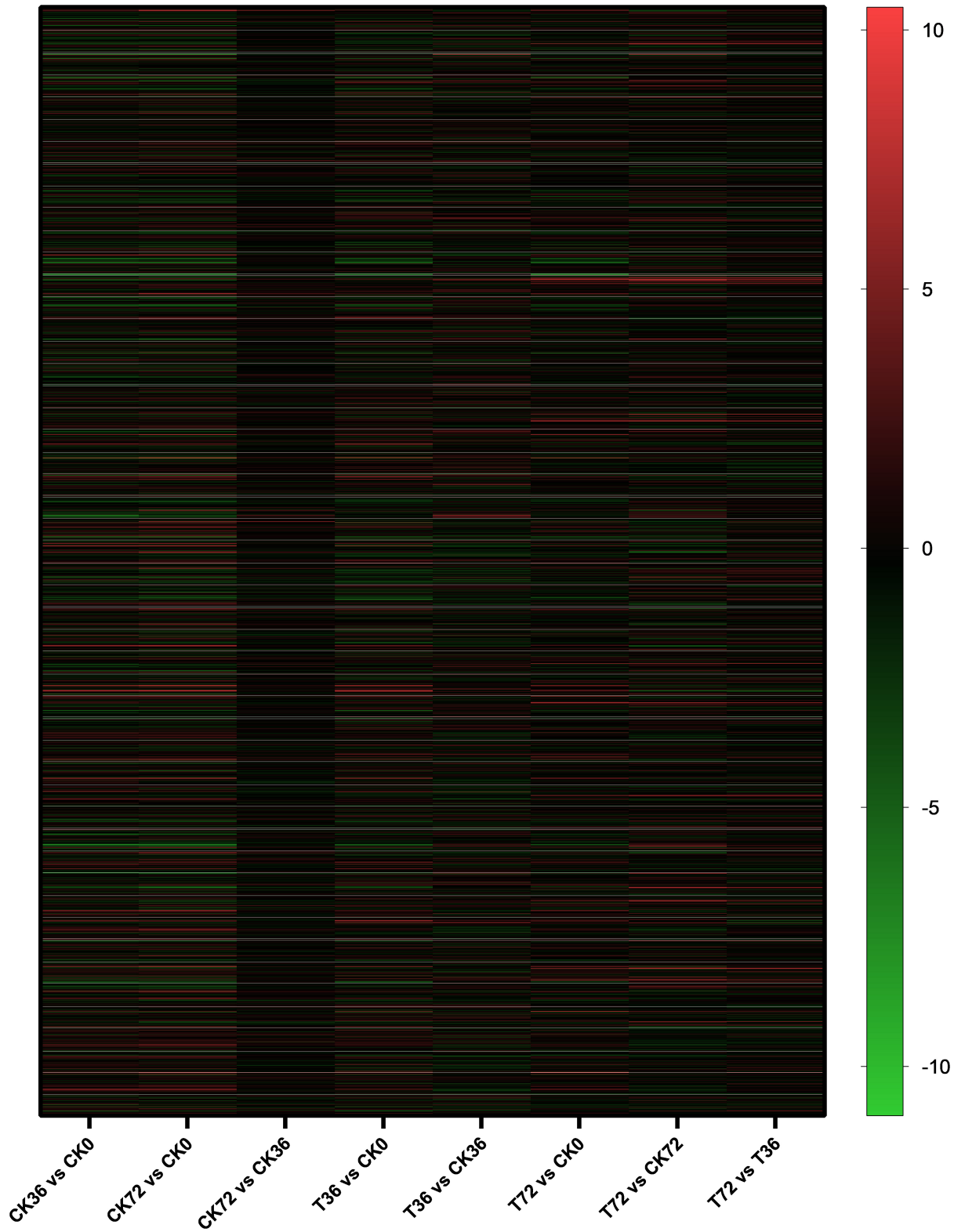

FIGURE 4 | Hierarchical cluster analysis of the gene expression based on the log ratio RPKM data of *P. chrysosporium* in terms of its chlamydospore formation. Red represented a relatively high expression level, and blue corresponded to a relatively low expression level. Each column showed an experimental condition (CK0-T72), and each row indicated a gene.

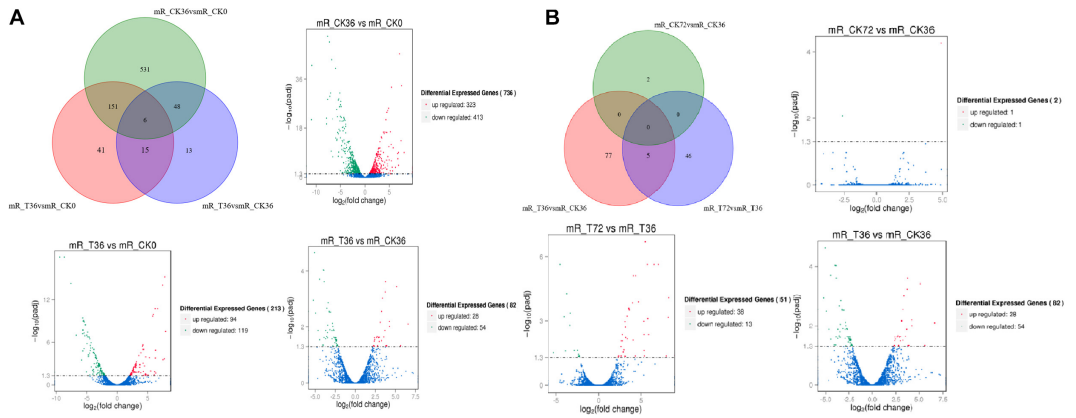

FIGURE 5 | Venn chart of unique and common differentially expressed genes (DEGs) between different stages of chlamydospore formation. **(A)** The grouping of the gene lists responding to T36 vs. CK36 vs. CK0. **(B)** The grouping of the gene lists responding to T72 vs. CK72 vs. T36 vs. CK36.

TABLE 3 | Significantly changed Kyoto Encyclopedia of Genes and Genomes (KEGG) pathways.

Developmental stages	Pathway	*P*-value (<0.05)	Gene name	Blast swiss prot	Up/Down
T36 vs. CK0	Galactose metabolism	0.0197392327084	Unknown	UTP–glucose-1-phosphate uridylyltransferase	Up
			Unknown	Aldose 1-epimerase	Up
	Fatty acid degradation	0.0247110569989	Unknown	Alcohol dehydrogenase, propanol-preferring	Down
			Unknown	Cytochrome P450/NADPH-cytochrome P450 reductase	Down
T36 vs. CK36	Ribosome	0.00317042906325	S15e	Small subunit ribosomal protein S15e	Up
			LP1, LP2	Large subunit ribosomal protein LP1, LP2	Up
	Ascorbate and aldarate metabolism	0.00621469206944	Unknown	Inositol oxygenase	Down
			Unknown	Aldehyde dehydrogenase family 7 member A1	Down
T72 vs. CK0	Fatty acid degradation	0.0230827057547	Unknown	Alcohol dehydrogenase, propanol-preferring	Down
			Unknown	Cytochrome P450/NADPH-cytochrome P450 reductase	Down
T72 vs. CK72	Fatty acid degradation	0.0298625776715	Unknown	Acyl-CoA oxidase	Up
			Unknown	Aldehyde dehydrogenase family 7 member A1	Up
	Alpha-Linolenic acid metabolism	0.043461306319	ACX	Acyl-CoA oxidase	Up
	Starch and sucrose metabolism	0.00637655688167	Unknown	Beta-glucosidase	Down
			Unknown	UTP–glucose-1-phosphate uridylyltransferase	Down
T72 vs. T36	MAPK signaling pathway - yeast	0.0293679603427	Tec1	Transcriptional enhancer factor	Up

remarkable enrichment that plays an important role in cell cycle regulation. The transcriptional enhancer factor Tec1 functions by assembling with another transcription factor Ste12 in the Kss1 pathway in yeast (Shock et al., 2009). Ste12 and Tec1 factors activate genes involved in biofilm/filamentation programs (van der Felden et al., 2014). Ste12–Tec1 heterodimers bind cooperatively to a distinct DNA sequence called the filamentation and invasion response element present in the promoter region of genes that regulate invasive or pseudohyphal growth (Wang and Dohlman, 2006). *TEC1* was substantially upregulated in the targets of the T72 vs. T36 groups (log2FoldChange = 5.3222) and conserved with Ste12, which might promote hyphal growth (**Figure 7B**). *P. chrysosporium* chlamydospores were produced primarily within the hyphal cells or at the end of hyphae, and upregulating *TEC1* might positively promote hyphal elongation, which induced the formation of additional chlamydospores. *TEC1* in *P. chrysosporium* had low amino acid sequence identity (27.94%, e-value = 4e − 06) compared with *Saccharomyces cerevisiae*, which may indicate divergence of function. Moreover, it has not been studied in other species closely related to *P. chrysosporium*. Thus, its significance and role in basidiomycete chlamydospore formation remain enigmatic but present an interesting target for studies aiming to understand chlamydospore formation in this fungus.

Other genes, such as those encoding transcription factors, phosphatases, and kinases, and development/morphology-related components, may play important roles in chlamydospore formation. Functional annotation revealed the differential expression of eight transcription factors (**Figure 7C**), seven phosphatase and kinase genes (**Figure 7D**), and seven genes involved in development/morphology (**Figure 7E**). Most transcription factor, phosphatase, and kinase genes were significantly upregulated during chlamydospore production (T72 vs. T36), but these genes remain uncharacterized in fungi

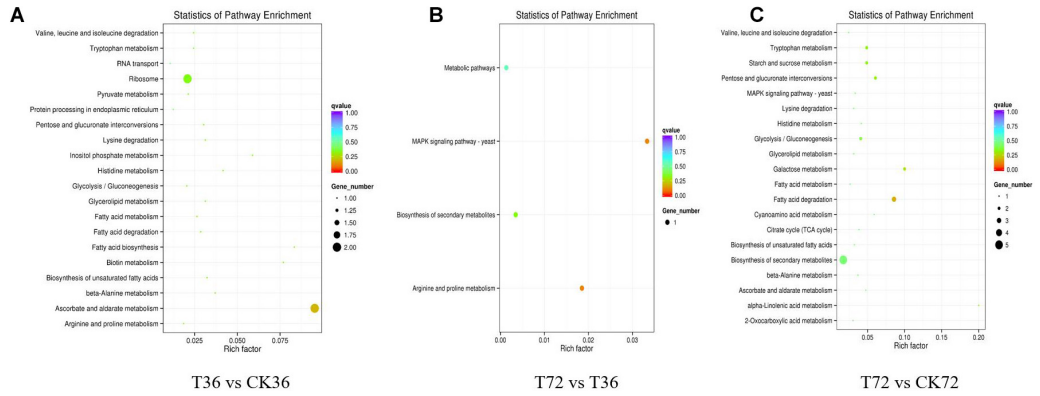

FIGURE 6 | KEGG pathway enrichment analysis of the differentially expressed genes (DEGs) of chlamydospore formation. **(A)** T36 vs. CK36, **(B)** T72 vs. T36, and **(C)** T72 vs. CK72.

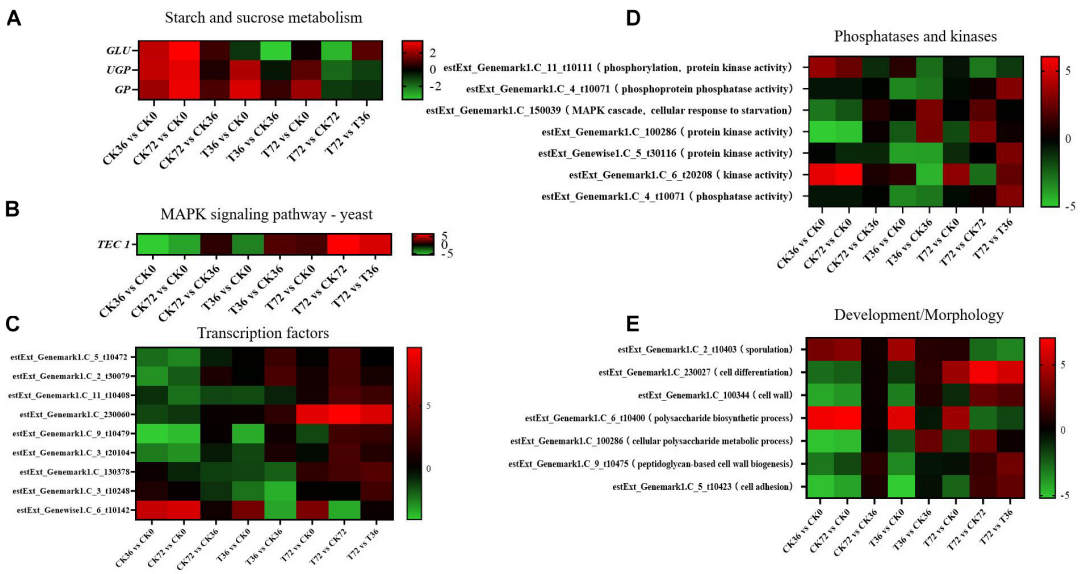

FIGURE 7 | Heatmap of the genes regulated at different stages of chlamydospore formation. The bar represents log2 (fold change) between different groups. Red represents upregulation, and green shows downregulation. **(A)** *GLU*, *UGP*, and *GP*. **(B)** *TEC* 1. **(C)** Transcription factor genes. **(D)** phosphatase and kinase genes. **(E)** Development/morphology genes.

to date. Further verification through deletion of these genes is needed to clarify their functions in chlamydospore formation.

qRT-PCR results are shown in **Supplementary Figure S2** to validate the reliability of DEGs obtained from RNA-seq analysis. r was calculated between the RNA-seq and qRT-PCR data of six genes. The expression patterns of the six genes determined through qRT-PCR were consistent with the RNA-seq data, indicating the reliability and accuracy of the RNA-seq data (**Figure 8**).

DISCUSSION

Early research found that the cell wall of *Aspergillus flavus* chlamydospores could stain calcofluor white, which demonstrated that chlamydospore cell walls are thicker than normal hyphal cell walls (Spraker et al., 2016). In *C. neoformans*, the diameter of chlamydospores is greater than 10 μm, which is significantly larger than the almost uniform 2–5 μm round blastospores or 1.5–3 μm oval basidiospores (Lin and Heitman, 2005). In the current work, hypertrophic structures in thick-walled chlamydospores were observed by cell wall-specific staining and demonstrated that chlamydospore cell walls are thicker than normal hyphal cell walls. Enzymatic hydrolysis also suggested the differences in polysaccharide compositions of the cell walls between chlamydospores and hyphae. Some essential genes for chlamydospore formation have been determined through specific mutation in *C. albicans* (Staib and Morschhäuser, 2007; Böttcher et al., 2016; Noble et al., 2016) and *Gibberella zeae* (Son et al., 2012), but genes

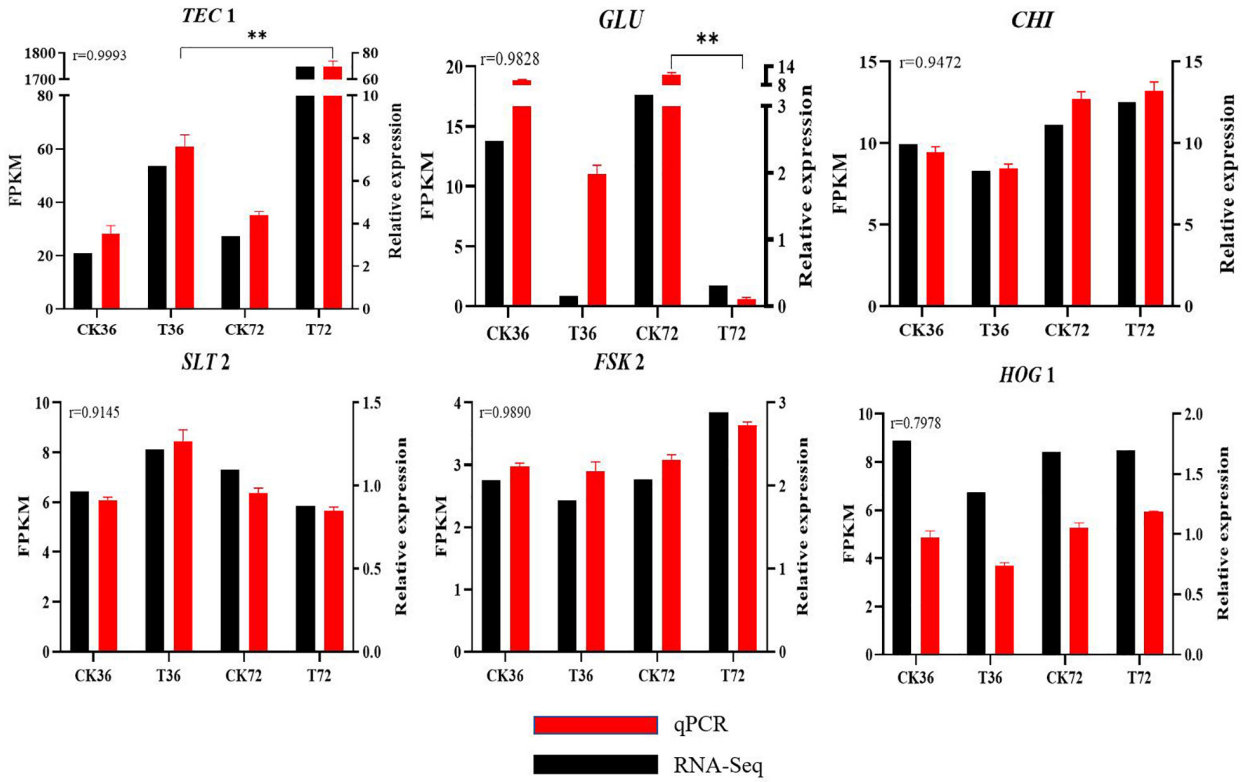

FIGURE 8 | Real-time qPCR validation showing the relative expression levels of *GLU*, *TEC* 1, *CHI*, *SLT* 2, *FKS* 2, and *HOG* 1. (Student's *t*-test. Asterisks represent significant differences, $^{**}p < 0.01$).

in the chlamydospore formation of *P. chrysosporium* have not been investigated. Efg1p, which is the first discovered regulatory factor and encoded by *EFG* for chlamydospore formation in *C. albicans*, can regulate morphogenesis and induce mycelial growth (Stoldt et al., 1997). *HOG1* in the MAPK pathway is another gene related to the formation of chlamydospores in *C. albicans* (Alonso-Monge et al., 2003). *C. albicans HOG1* is activated in response to hydrogen peroxide and an increase in external osmolarity. Chlamydospores, which are round and have thick walls, have been observed in wild-type *HOG1*, whereas chlamydospore formation is completely abolished in *HOG1* mutants (Staib and Morschhäuser, 2007). The colonies display the hyperfilamentous phenotype of *HOG1* mutants, and some structures at some hyphal tips slightly resemble chlamydospores (Alonso-Monge et al., 2003). *Ole1* is not universal in filamentous fungi, but it may be an important inducer of some signaling pathways for specialized developmental structures. *Ole1* can make saturated fatty acids from unsaturated ones through dehydrogenation. The wild-type expression levels of *OLE1* and the corresponding levels of oleic acid favor chlamydospore formation in *C. albicans* (Krishnamurthy et al., 2004). *NRG1* encodes one universal transcription inhibitor and regulates chlamydospore formation (Staib and Morschhäuser, 2005). However, the genes mentioned above had no significant differential expression levels or were not found in the transcriptome of *P. chrysosporium*. Therefore, the molecular mechanism of chlamydospore formation might vary in different fungi.

KEGG analyses illustrated 17 significantly changed genes enriched in seven pathways, which were involved in galactose metabolism; fatty acid degradation; ribosome, ascorbate, and aldarate metabolism; alpha-linolenic acid metabolism; starch and sucrose metabolism; and MAPK signaling pathway. Two major KEGG enrichment pathways involved in the change in the cell wall are the starch and sucrose metabolism and the Kss1 MAPK signaling pathway. β-Glucan has extensive distribution. It mainly exists in the cell walls of fungi and advanced plants (Barsanti et al., 2011) and has different chemical bonding modes compared with those of other sugars. β-1,3-Glucosidic bonds are the main chain in β-glucan, and β-1,6-glucosidic bonds as the branched chain are observed in yeast and fungi. In *Saprolegnia monoica*, which belongs to Oomycetes, high substrate concentrations of UDP–glucose in the membrane promote mycelial homogenate and microfibril production, and β-1,3-linked glucans are mainly produced; meanwhile, β-1,4-linked glucans are the only polysaccharide synthesized at low substrate concentrations in the presence of $MgCl_2$ (Fèvre and Rougier, 1981). Starch and sucrose metabolism analysis showed that the expression of *UGP* was evidently downregulated when T72 was compared with CK72 and resulted in low UDP–glucose accumulation. The downregulation of *UGP* could promote sugar flux to produce 1,4-β-D-glucan, and downregulating *GLU*

could reduce the hydrolysis of 1,4-β-D-glucan into β-D-glucose. The resulting 1,4-β-D-glucan accumulation was speculated as the major component of the thickened part of the cell wall in the chlamydospores. In compliance with this speculation, the enzymatic hydrolysis experiment revealed that the glucan content in the chlamydospore cell wall was higher than that in the hyphal cell wall. However, the cell wall organization may differ substantially between both structures, thereby masking polysaccharides that lie underneath and causing difficulty in accessing enzymes to it, resulting in more or less detected glucan/cellulose/chitin. Moreover, calcofluor white stained chitin and cellulose in the cell wall, but the contents of chitin and cellulose were not greater in the chlamydospores than in the hyphae via the enzymatic hydrolysis experiment. This finding also proved the complicated organization of the thickened cell wall. Therefore, additional experiments are needed to clarify this problem. Proteins are also found in the thick inner layer of the cell wall of *C. albicans* (Jansons and Nickerson, 1970), but these proteins were not detected in our study. MAPK cascade functions include induction of enzymes necessary for hyphal fusions by regulating different genes. Upregulation of transcription factors Tec1 in the MAPK signaling pathway might promote the extension of hypha and facilitate chlamydospore formation on it.

Although chlamydospore formation started at 36 h and peaked at 72 h, most transcriptional changes should occur earlier so that the cells have time to accommodate these changes and induce a corresponding result. Thus, a low number of DEGs were found between some conditions, and a more pronounced transcriptional response was observed at earlier time points.

Nitrogen limiting or starvation is a key factor triggering chlamydospore formation in *P. chrysosporium*. Further hyphal extension would be inhibited during the transportation of nutrients along the long vegetative hyphae. In this circumstance, the hyphae would grow because of the carbon sources stored in the chlamydospore structure rather than because of long-distance transportation. The fungal cell wall is made of polysaccharides and can be stored as energy; thus, the formed chlamydospores for energy storage could supply a stable energy for germination. This process could be completed by controlling the transfer and decomposition of stored nutrients.

CONCLUSION

The cell wall of the chlamydospores was thicker than that of the hyphae, and more β-glucans were exposed to β-glucanase in the chlamydospores than in the hyphae by enzymatic hydrolysis. Thus, the cell wall structure and organization of the chlamydospores and the hyphae significantly differed. Chlamydospore formation in *P. chrysosporium* was characterized using RNA-seq. The results provided a basic understanding of the molecular mechanisms under this process, including MAPK, phosphatases, and transcription factors. The chlamydospore formation in P. chrysosporium was encoded by a large number of genes subject to strict patterns of temporal regulation. These comprehensive analyses provide molecular evidence that could promote the understanding of morphological variation in chlamydospore formation and serve as a potential blue print for future research on this process in basidiomycetes and other fungi. The genes mentioned in this process will be tested via gene knockout in our future work.

DATA AVAILABILITY STATEMENT

The datasets generated for this study can be found in the SRA, SRP153122.

AUTHOR CONTRIBUTIONS

LL, HL, and YYL performed the experiments and wrote the main text of the manuscript. HW designed and directed the experiments. YL analyzed the data. All authors have read and approved the manuscript.

FUNDING

This work was supported by the National Science Foundation of China (31700435 and U160411067), Plan for Scientific Innovation Talent of Henan Province (18HASTIT039), the Ph.D. Research Startup Foundation (5101049170143) of Henan Normal University, the Young Scholar's Foundation (2015QK17) of Henan Normal University, and the Foundation of Henan Educational Committee (14B180022).

ACKNOWLEDGMENTS

We are grateful to the editor and the reviewers for their comments and suggestions.

SUPPLEMENTARY MATERIAL

The Supplementary Material for this article can be found online at: https://www.frontiersin.org/articles/10.3389/fmicb.2020.527389/full#supplementary-material

REFERENCES

Anders, S., Pyl, P. T., and Huber, W. (2015). HTSeq–a Python framework to work with high-throughput sequencing data. *Bioinformatics* 31, 166–169.

Bandara, J. M. R. S., and Wood, R. K. S. (1978). Soil factors influencing chlamydospore formation by *Fusarium solani* f. sp. *phaseoli*. *Ann. Appl. Biol.* 90, 169–177. doi: 10.1111/j.1744-7348.1978.tb02624.x

Barran, L. R., Schneider, E. F., and Seaman, W. L. (1977). Requirements for the rapid conversion of macroconidia of *Fusarium sulphureum* to chlamydospores. *Can. J. Microbiol.* 23, 148–151. doi: 10.1139/m77-021

Barsanti, L., Passarelli, V., Evangelista, V., Frassanito, A. M., and Gualtieri, P. (2011). Chemistry, physico-chemistry and applications linked to biological activities of β-glucans. *Nat. Prod. Rep.* 28, 457–466. doi: 10.1039/C0NP00018C

Benjamini, Y., and Hochberg, Y. (1995). Controlling the false discovery rate: a practical and powerful approach to multiple testing. *J. R. Stat. Soc. B* 57, 289–300. doi: 10.2307/2346101

Böttcher, B., Pöllath, C., Staib, P., Hube, B., and Brunke, S. (2016). Candida species rewired hyphae developmental programs for chlamydospore formation. *Front. Microbiol.* 7:1697. doi: 10.3389/fmicb.2016.01697

Calderone, R. A. (2002). *Candida and Candidiasis*. Washington, DC: American Society for Microbiology.

Cha, J. Y., Han, S., Hong, H. J., Cho, H., Kim, H., Kwon, Y., et al. (2015). Microbial and biochemical basis of a Fusarium wilt-suppressive soil. *ISME J.* 10, 119–129. doi: 10.1038/ismej.2015.95

Chung, E., Oh, J., Hwang, S., Ahn, I. S., and Yoon, Y. J. (2005). Enhanced production of manganese peroxidase from immobilized *Phanerochaete chrysosporium* due to the increased autolysis of chlamydospore-like cells. *Biotechnol. Lett.* 27, 477–481. doi: 10.1007/s10529-005-2224-9

Couteaudier, Y., and Alabouvette, C. (1990). Survival and inoculum potential of conidia and chlamydospores of *Fusarium oxysporum* f. sp. lini in soil. *Can. J. Microbiol.* 36, 551–556. doi: 10.1139/m90-096

Dong, P. P., Sun, M. H., Li, S. D., Peng, Y., and Luo, M. (2014). Biological characteristics of chlamydospores of *Clonostachys rosea* 67-1. *Mycosystema* 33, 1242–1252.

Ferguson, D. J., Henriquez, F. L., Kirisits, M. J., Muench, S. P., Prigge, S. T., Rice, D. W., et al. (2005). Maternal inheritance and stage-specificvariation of the apicoplast in *Toxoplasma gondii* during development in the intermediate and definitive host. *Eukaryot. Cell* 4, 814–826. doi: 10.1128/EC.4.4.814-826.2005

Fèvre, M., and Rougier, M. (1981). β-1-3- and β -1-4-glucan synthesis by membrane fractions from the fungus *Saprolegnia*. *Planta* 151, 232–241. doi: 10.1007/BF00395174

Frankeberger, W. T., and Johanson, J. B. (1983). Method of measuring invertase activity in soils. *Plant Soil* 74, 301–311. doi: 10.1007/bf02181348

Gao, D. W., Du, L. N., Yang, J. L., Wu, W. M., and Liang, H. (2010). A critical review of the application of white rot fungus to environmental pollution control. *Crit. Rev. Biotechnol.* 30, 70–77. doi: 10.3109/07388550903427272

Huang, S., Wang, J., Yue, W. C., Chen, J., Gaughan, S., Lu, W. Q., et al. (2015). Transcriptomic variation of hepatopancreas reveals the energy metabolism and biological processes associated with molting in Chinese mitten crab, *Eriocheir sinensis*. *Sci. Rep.* 5:14015. doi: 10.1038/srep14015

Jansons, V. K., and Nickerson, W. J. (1970). Chemical composition of chlamydospores of *Candida albicans*. *J. Bacteriol.* 104, 922–932. doi: 10.1128/JB.104.2.922-932.1970

Jiménez-Tobon, G., Kurzatkowski, W., Rozbicka, B., Solecka, J., Pocsi, I., and Penninckx, M. J. (2003). In situ localization of manganese peroxidase production in hyphael pellets of *Phanerochaete chrysosporium*. *Microbiology* 149, 3121–3127. doi: 10.1099/mic.0.26451-0

Kanehisa, M., and Goto, S. (2000). KEGG: kyoto encyclopedia of genes and genomes. *Nucleic Acids Res.* 28, 27–30. doi: 10.1093/nar/28.1.27

Kang, Y., Mi, R. K., Kim, K. H., Lee, J., and Lee, S. H. (2016). Chlamydospore induction from conidia of *Cylindrocarpon destructans* isolated from ginseng in Korea. *Mycobiology* 44, 63–65. doi: 10.5941/MYCO.2016.44.1.63

Krishnamurthy, S., Plaine, A., Albert, J., Prasad, T., Prasad, R., and Ernst, J. F. (2004). Dosage-dependent functions of fatty acid desaturase Ole1p in growth and morphogenesis of *Candida albicans*. *Microbiology* 150, 1991–2003. doi: 10.1099/mic.0.27029-0

Langmead, B., and Salzberg, S. L. (2012). Fast gapped-read alignment with Bowtie 2. *Nat. Methods* 9, 357–359. doi: 10.1038/nmeth.1923

Lewis, J. A., and Papavizas, G. C. (1984). Chlamydospore formation by *Trichoderma* spp. in natural substrates. *Can. J. Microbiol.* 30, 1–7. doi: 10.1139/m84-001

Li, L., Qu, Q., Tian, B., and Zhang, K. Q. (2005). Induction of chlamydospores in *Trichoderma harzianum* and *Gliocladium roseum* by antifungal compounds produced by *Bacillus subtilis* C2. *J. Phytopathol.* 153, 686–693. doi: 10.1111/j.1439-0434.2005.01038.x

Lin, X. R., and Heitman, J. (2005). Chlamydospore formation during hyphal growth in *Cryptococcus neoformans*. *Eukaryot. Cell* 4, 1746–1754. doi: 10.1128/EC.4.10.1746-1754.2005

Livak, K. J., and Schmittgen, T. D. (2001). Analysis of relative gene expression data using real-time quantitative PCR and the $2-\Delta\Delta CT$ method. *Methods* 25, 402–408. doi: 10.1006/meth.2001.1262

Mao, X., Cai, T., Olyarchuk, J. G., and Wei, L. (2005). Automated genome annotation and pathway identification using the KEGG Orthology (KO) as a controlled vocabulary. *Bioinformatics* 21, 3787–3793. doi: 10.1093/bioinformatics/bti430

McCarren, K. L., McComb, J. A., Shearer, B. L., St, J., and Hardy, G. E. (2005). The role of chlamydospores of *Phytophthora cinnamomi* – a review. *Australas. Plant Path.* 34, 333–338. doi: 10.1071/ap05038

Mehrabi, R., Van der Lee, T., Waalwijk, C., and Gert, H. J. K. (2006). MgSlt2, a cellular integrity MAP kinase gene of the fungal wheat pathogen *Mycosphaerella graminicola*, is dispensable for penetration but essential for invasive growth. *Mol. Plant Microbe Interact.* 19, 389–398.

Monge, R. A., García, F. N., Román, E., Negredo, A. I., Eisman, B., Nombela, C., et al. (2003). The Hog1 mitogen-activated protein kinase is essential in the oxidative stress response and chlamydospore formation in *Candida albicans*. *Eukaryot. Cell* 2, 351–361. doi: 10.1128/EC.2.2.351-361.2003

Nobel, H. D., Ende, H. V., and Klis, F. M. (2000). Cell wall maintenance in fungi. *Trends Microbiol.* 8, 344–345. doi: 10.1016/S0966-842X(00)01805-9

Noble, S. M., Gianetti, B. A., and Witchley, J. N. (2016). *Candida albicans* cell-type switching and functional plasticity in the mammalian host. *Nat. Rev. Microbiol.* 15, 96–108. doi: 10.1038/nrmicro.2016.157

Ohara, T., and Tsuge, T. (2004). FoSTUA, encoding a basic helix-loop-helix protein, differentially regulates development of three kinds of asexual spores, macroconidia, microconidia, and chlamydospores, in the fungal plant pathogen *Fusarium oxysporum*. *Eukaryot. Cell* 3, 1412–1422. doi: 10.1128/EC.3.6.1412-1422.2004

Pearson, G., Robinson, F., Beers Gibson, T., Xu, B. E., Karandikar, M., Berman, K., et al. (2011). Mitogen-activated protein (MAP) kinase pathways: regulation and physiological functions. *Endocr. Rev.* 22, 153–183. doi: 10.1210/edrv.22.2.0428

Peck, R. J. (1947). *The Lipids of Fungi with Special Reference to Pathogenic Fungi*. New York, NY: Ronald Press.

Raudonis, B. M., and Smith, A. G. (1982). Germination of the chlamydospores of *Candida albicans*. *Mycopathologia* 78, 87–91. doi: 10.1007/BF00442631

Shock, T. R., Thompson, J., Yates, J. R., and Madhani, H. D. (2009). Hog1 mitogen-activated protein kinase (MAPK) interrupts signal transduction between the Kss1 MAPK and the Tec1 transcription factor to maintain pathway specificity. *Eukaryot. Cell* 8, 606–616. doi: 10.1128/EC.00005-09

Son, H., Lee, J., and Lee, Y. W. (2012). Mannitol induces the conversion of conidia to chlamydospore-like structures that confer enhanced tolerance to heat, drought, and UV in *Gibberella zeae*. *Microbiol. Res.* 167, 608–615. doi: 10.1016/j.micres.2012.04.001

Spraker, J. E., Sanchez, L. M., Lowe, T. M., Dorrestein, P. C., and Keller, N. P. (2016). *Ralstonia solanacearum* lipopeptide induces chlamydospore development in fungi and facilitates bacterial entry into fungal tissues. *ISME J.* 10, 2317–2330. doi: 10.1038/ismej.2016.32

Staib, P., and Morschhäuser, J. (2005). Differential expression of the Nrg1 repressor controls species-specific regulation of chlamydospore development in *Candida albicans* and *Candida dubliniensis*. *Mol. Microbiol.* 55, 637–652. doi: 10.1111/j.1365-2958.2004.04414.x

Staib, P., and Morschhäuser, J. (2007). Chlamydospore formation in *Candida albicans* and *Candida dubliniensis*– an enigmatic developmental programme. *Mycoses* 50, 1–12. doi: 10.1111/j.1439-0507.2006.01308.x

Stoldt, V. R., Sonneborn, A., Leuker, C. E., and Ernst, J. F. (1997). Efg1p, an essential regulator of morphogenesis of the human pathogen *Candida albicans*, is a member of a conserved class of bHLH proteins regulating morphogenetic processes in fungi. *EMBO J.* 16, 1982–1991. doi: 10.1093/emboj/16.8.1982

Trapnell, C., Pachter, L., and Salzberg, S. L. (2009). TopHat: discovering splice junctions with RNA-Seq. *Bioinformatics* 25, 1105–1111. doi: 10.1093/bioinformatics/btp120

van der Felden, J., Weisser, S., Brückner, S., Lenz, P., and Mösch, H. U. (2014). The transcription factors Tec1 and Ste12 interact with coregulators Msa1 and Msa2 to activate adhesion and multicellular development. *Mol. Cell. Biol.* 34, 2283–2293. doi: 10.1128/MCB.01599-13

Wang, H. L., Li, L., Li, P., Li, H., Liu, G. S., and Yao, J. M. (2011). The acceleration of sludge granulation using the chlamydospores of *Phanerochaete* sp. HSD. *J. Hazard. Mater.* 192, 963–969. doi: 10.1016/j.jhazmat.2011.05.076

Wang, L., Feng, Z., Wang, X., Wang, X., and Zhang, X. (2010). DEGseq: an R package for identifying differentially expressed genes from RNA-seq data. *Bioinformatics* 26, 136–138. doi: 10.1093/bioinformatics/btp612

Wang, Y. Q., and Dohlman, H. G. (2006). Pheromone-regulated sumoylation of transcription factors that mediate the invasive to mating developmental switch in yeast. *J. Biol. Chem.* 281, 1964–1969. doi: 10.1074/jbc.M508985200

Xu, P., Zeng, G. M., Huang, D. L., Liu, L., Zhao, M. H., Lai, C., et al. (2016). Metal bioaccumulation, oxidative stress and antioxidant defenses in *Phanerochaete chrysosporium* response to Cd exposure. *Ecol. Eng.* 87, 150–156. doi: 10.1016/j.ecoleng.2015.11.029

Zhao, X., Mehrabi, R., and Xu, J. R. (2007). Mitogen-activated protein kinase pathways and fungal pathogenesis. *Eukaryot. Cell* 6, 1701–1714. doi: 10.1128/ec.00216-07

Conflict of Interest: The authors declare that the research was conducted in the absence of any commercial or financial relationships that could be construed as a potential conflict of interest.

frontiers in Fungal Biology

ORIGINAL RESEARCH
published: 18 January 2021
doi: 10.3389/ffunb.2020.629510

Volatile Organic Compounds Produced by Human Pathogenic Fungi Are Toxic to *Drosophila melanogaster*

Hadeel S. Almaliki[1,2], *Astrid Angela*[1], *Nayab J. Goraya*[1], *Guohua Yin*[1]* and *Joan W. Bennett*[1]

[1] Department of Plant Biology, Rutgers, The State University of New Jersey, New Brunswick, NJ, United States, [2] Technical Institute of Samawa, Al-Furat Al-Awsat Technical University, Samawa, Iraq

Volatile organic compounds (VOCs) are low molecular mass organic compounds that easily evaporate at room temperature. Fungi produce diverse mixtures of VOCs, some of which may contribute to "sick building syndrome," and which have been shown to be toxigenic in a variety of laboratory bioassays. We hypothesized that VOCs from medically important fungi might be similarly toxigenic and tested strains of *Aspergillus fumigatus*, *Candida albicans*, *Cryptococcus neoformans*, *Cryptococcus gattii*, and *Saccharomyces cerevisiae* in a *Drosophila melanogaster* eclosion bioassay. Fungi were grown in a shared microhabitat with third instar larvae of *D. melanogaster* such that there was no physical contact between flies and fungi. As the flies went through metamorphosis, the numbers of larvae, pupae, and adults were counted daily for 15 days. After 8 days, ∼80% of controls had eclosed into adults and after 15 days the controls yielded 96–97% eclosion. In contrast, eclosion rates at 8 days were below 70% for flies exposed to VOCs from six different *A. fumigatus* strains; the eclosion rate at 15 days was only 58% for flies exposed to VOCs from *A. fumigatus* strain SRRC 1607. When flies were grown in a shared atmosphere with VOCs from *S. cerevisiae*, after 15 days, 82% of flies had eclosed into adults. Exposure to the VOCs from the medically important yeasts *Candida albicans*, *Cryptococcus neoformans*, and *Cryptococcus gattii* caused significant delays in metamorphosis with eclosion rates of 58% for *Candida albicans*, 44% for *Cryptococcus neoformans*, and 56% for *Cryptococcus gattii*. Using gas chromatography-mass spectrometry, the VOCs from the most toxic and least toxic strains of *A. fumigatus* were assayed. The two most common VOCs produced by both strains were 1-octen-3-ol and isopentyl alcohol; however, these compounds were produced in 10-fold higher concentrations by the more toxic strain. Our research demonstrates that gas phase compounds emitted by fungal pathogens may have been overlooked as contributing to the pathogenicity of medically important fungi and therefore deserve more scrutiny by the medical mycology research community.

Keywords: ***Aspergillus fumigatus*, *Candida albicans*, *Cryptococcus neoformans*, *Cryptococcus gattii*, *Drosophila melanogaster*, Virulence, volatile organic compounds**

OPEN ACCESS

Edited by:
Chengshu Wang,
Shanghai Institutes for Biological Sciences (CAS), China

Reviewed by:
Xuemei Niu,
Yunnan University, China
Alexander Idnurm,
The University of Melbourne, Australia

***Correspondence:**
Guohua Yin
guohuayin1997@gmail.com

Specialty section:
This article was submitted to Fungi-Animal Interactions, a section of the journal Frontiers in Fungal Biology

Received: *15 November 2020*
Accepted: *21 December 2020*
Published: *18 January 2021*

Citation:
Almaliki HS, Angela A, Goraya NJ, Yin G and Bennett JW (2021) Volatile Organic Compounds Produced by Human Pathogenic Fungi Are Toxic to Drosophila melanogaster. Front. Fungal Biol. 1:629510. doi: 10.3389/ffunb.2020.629510

INTRODUCTION

Volatile organic compounds (VOCs) are low molecular mass organic substances that are easily vaporized at room temperature (Herrmann, 2010). The best-known VOCs are synthetic chemicals used as solvents, cleaning agents and so forth; many of these industrial VOCs have toxigenic effects and their emissions have been subject to government regulation (Bennett and Inamdar, 2015). Less is known, however, about the toxigenic potential of biogenic VOCs emitted by fungi and other organisms as part of their normal metabolism. Fungal VOCs are released as mixtures of chemical compounds; different species growing on different substrates produce unique mixtures of VOCs (Korpi et al., 2009; Hung et al., 2015). VOC "signatures" provide rapid, inexpensive, and non-destructive indicators for recognizing the presence of agricultural or indoor mold contamination (Gao et al., 2002; Polizzi et al., 2009; Cabral, 2010; Pennerman et al., 2016). Similarly, researchers have sought to diagnose invasive aspergillosis by the detection of VOCs emitted in breath when the fungus is growing on the human host (Heddergott et al., 2014; Licht and Grasemann, 2020; Martínez et al., 2020). Fungal VOCs often have odors similar or identical to toxic industrial compounds and have been associated with symptoms of poor health such as headaches, dizziness, faintness, and irritation of the eyes and mucous membranes of the nose and throat (Takigawa et al., 2009; Araki et al., 2010, 2012). Many researchers have hypothesized that fungal VOCs have negative effects on human health with reference to processes like composting (Herr et al., 2003). In particular, it is thought that these VOCs may contribute to the symptoms of a poorly understood health condition called "sick building syndrome" (Mølhave et al., 1993; Hodgson, 1999; Heseltine and Rosen, 2009; Mølhave, 2009; Hosseini et al., 2020; Zuo et al., 2020).

Relatively little is known about the biological activity of VOCs associated with human fungal pathogens. *Aspergillus fumigatus*, for example, is not only an opportunistic human pathogen (Agarwal, 2009; Latgé and Steinbach, 2009) but it has been isolated from buildings whose occupants have complained of building-related illness as well as from the homes of asthmatic children (Schwab and Straus, 2004). *Candida albicans*, another opportunistic human pathogen, has been isolated as one of the contaminants present in hospital air (Pantoja et al., 2016). Known volatiles emitted by *A. fumigatus* and *C. albicans* include ethanol, acetaldehyde, acetone, methanethiol, 2-butenal, isoamyl alcohol, phenethyl alcohol, and cyclohexane as determined by ion mobility spectrometry and selected ion flow tube-mass spectrometry (SIFT-MS) (Scotter et al., 2005; Perl et al., 2011).

Our laboratory has adapted *D. melanogaster* as a model for studying the toxigenic potential of fungal volatiles. Flies are well-suited for toxigenic studies because the fly immune system is highly conserved with mammals. Furthermore, immune deficient flies have been used as models for studying aspergillosis and other human mycoses (Lionakis and Kontoyiannis, 2012). Here, we used an eclosion assay (the emergence of the adult insect from the pupal case during metamorphosis) that did not involve direct contact between fungi and flies (Inamdar et al., 2013; Rand et al., 2014). Third instar larvae of *Drosophila* were placed in a common atmosphere with VOCs produced by six different *A. fumigatus* strains, as well as one strain each of *Candida albicans*, *Cryptococcus neoformans*, *Cryptococcus gattii*, and *Saccharomyces cerevisiae* as a non-pathogen control. The numbers of larvae, pupae, and adults were counted daily for 15 days in order to determine effects of VOCs on the developmental process and/or eclosion into adults. Using a somewhat different version of this fly toxicity test, previous experiments in our laboratory showed that VOCs emitted by molds isolated from contaminated building materials after Hurricane Katrina and Superstorm Sandy caused developmental defects and death (Inamdar and Bennett, 2015; Zhao et al., 2017). Here we hypothesized that volatiles emitted by medically important fungi would have similar toxigenic properties. The long-term goal of our research is to learn whether VOCs emitted by fungi have physiological effects that can contribute to the severity of human disease. The specific aim of this study was to use the *Drosophila* larval bioassay to test the volatiles produced by medically important fungi to determine if they had toxicological impacts on fly metamorphosis.

MATERIALS AND METHODS

Fungal Strains, Culture Conditions, Measurement of Biomass/Dry Weight

A. fumigatus strains were obtained from Dr. Geromy Moore, Southern Regional Research Laboratories, U. S. Department of Agriculture, New Orleans, Louisiana, USA. The *A. fumigatus* strain numbers and their original sources were listed in **Table 1**. Stock cultures were maintained on potato dextrose agar (PDA, Difco). For all *Drosophila* exposure experiments, the fungi were grown on 25 mL of PDA in 6 oz. *Drosophila* stock bottles (Genesee Scientific, CA). When fungi serve as human pathogens, they grow at 37°C. However, *Drosophila* flies do not grow at this temperature. Therefore, fungi were pre-grown for 3 days at 37°C, but when the fungal colonies were affixed to the bottles containing fly larvae, the 15-day exposure experiment was conducted at 25°C. Parallel experiments were conducted with fungi pre-grown at 25°C for 5 days in order to determine if fungal growth temperature was associated with different VOC profiles and associated toxicological effects. In order to determine if there was a difference in biomass, different strains of *A. fumigatus* grown at 25°C for 5 days or at 37°C for 3 days were compared. Spore suspensions of the different *A. fumigatus* strains were inoculated into 50 mL of Potato Dextrose Broth (PDB) and were incubated at 120 rpm at 25°C for 5 days or at 37°C for 3 days. The resultant mycelial pellets were filtered using Whatman filter paper No. 1 and dried at 50°C for 4 days in an air incubator to measure the biomass/dry weight of fungus (Singh et al., 2012). Three replicates were performed for each fungal strain and repeated two times.

Exposure of *Drosophila* 3rd Instar Larvae to VOCs Produced by Fungi

White-eyed *Drosophila* flies ($w^{1,118}$; y^{1}) with a wild type immune system were maintained in Ward's Instant *Drosophila* medium (WARD's Natural Science, NY) before exposure studies with 3rd

TABLE 1 | The details about toxicity and the origins of different fungal strains used in this study.

Species	Origins	VOCs toxicity ranking*
Cryptococcus neoformans H99	Serotype A, Public Health Research Institute Center, New Jersey Medical School-Rutgers, Newark, NJ, USA	10
Cryptococcus gattii R265	Wild type, Public Health Research Institute Center, New Jersey Medical School-Rutgers, Newark, NJ, USA	9
Aspergillus fumigatus SRRC1607	Damp indoor environment	8
Candida albicans ATCC 90028	Wild type, Public Health Research Institute Center, New Jersey Medical School-Rutgers, Newark, NJ, USA	7
Aspergillus fumigatus SRRC46	A penguin at the Brookfield Zoo, Chicago, IL	6
Aspergillus fumigatus SRRC323	Chicken lung	5
Aspergillus fumigatus SRRC2569	Clinical isolate from the University of Manchester, Manchester, UK	4
Saccharomyces cerevisiae BY4741	Public Health Research Institute Center, New Jersey Medical School-Rutgers, Newark, NJ, USA	3
Aspergillus fumigatus SRRC51	Human chest cavity lining	2
Aspergillus fumigatus SRRC1592	Rain forest soil	1

**The most toxic strains are labeled with high values. All the strains are ranked based on their VOCs toxicities of the eclosion adult flies on the 10th and 15th days at 37°C.*

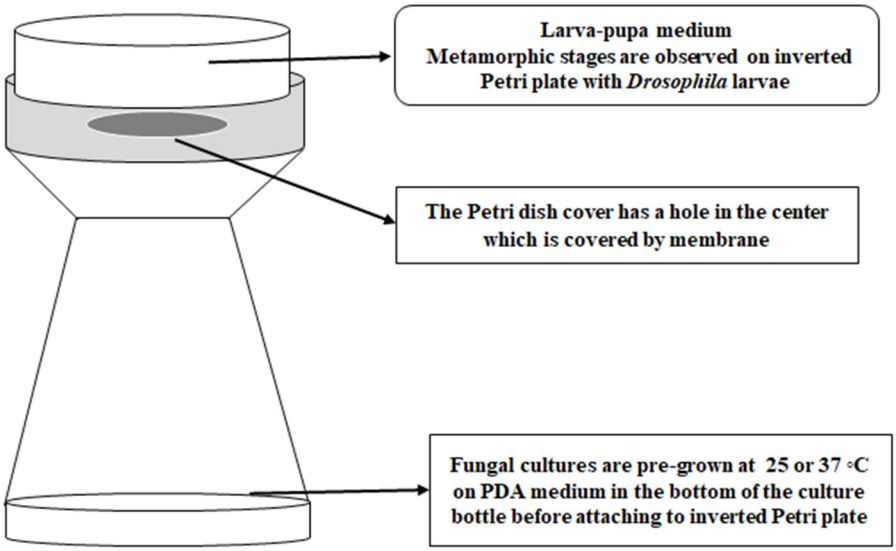

FIGURE 1 | The bottle-plate microhabitat for placing *Drosophila* developmental stages and fungal cultures in a shared atmosphere without physical contact between the flies and fungi.

stage of instar larvae. Third instar fly larvae were exposed to VOCs following a modified version of the method of Inamdar et al. (2012). Instead of using a double-Petri plate set up, a *Drosophila* bottle with fungal cultures was used and attached via masking tape to a Petri plate cover that had been punctured with a flame-hot pipe to make a tri-circular opening and paired with a Petri plate of larval medium. Fifteen larvae were placed onto each larva-pupa medium plate, so that there were 15 larvae present in each "bottle-plate" microhabitat. Each Petri plate was secured on top of the bottle with a strip of clear tape across the edges of the plate (**Figure 1**). Different fungal strains pre-grown at 25°C for 5 days or at 37°C for 3 days were placed in the microhabitat with fifteen 3rd instar larvae, with three replicates for each temperature. The experiment was conducted in duplicate for a total of six bottles of larvae per strain and temperature. Control larvae were exposed to PDA medium without any fungi. All the bottle-plate microhabitats were incubated at 25°C with rotation at 50 rpm for 15 days. The numbers of larvae, pupae, and adult flies were counted daily. The differences in metamorphic stages and eclosion between controls and VOC-exposed strains were analyzed for significance by using Student *t*-test on the 4th day for the larvae, the 8th day for the pupal stage, and the 15th day for the adult flies.

Gas Chromatography-Mass Spectrometry Analysis of *A. fumigatus* Volatiles

The VOCs from the most toxic (*A. fumigatus* SRRC 1607) and the least toxic (*A. fumigatus* SRRC 1592) strains were analyzed using Purge and Trap-Thermal Desorption-GC-MS (Hung et al., 2013; Zhao et al., 2017). Sterile PDA media and a blank containing only air were used as the negative controls. The fungi were grown either at 25°C for 5 days or at 37°C for

3 days on PDA in 250 mL flasks closed with plastic stoppers and sealed with Parafilm. Compounds were identified by comparison of spectra obtained from the *Aspergillus* samples with those from the reference library (NIST 08). Three replicates were performed for each fungal strain. The Tenax traps were spiked with 1.0 μg of benzene-d6, toluene-d8, and naphthalene-d8 as the internal standards.

RESULTS

Effects of VOCs Produced by *Aspergillus fumigatus* Strains on *Drosophila* Metamorphosis

To evaluate the effects of VOCs emitted from six *A. fumigatus* strains, the numbers of larvae (**Figures 2A,B**), pupae (**Figures 2C,D**), and adults (**Figures 2E,F**) were counted daily for 15 days. The data in **Figures 2A,C,E**, show percentages of larval, pupal, and adult stages over 15 days when exposed to fungal cultures that had previously been grown at 25°C; the data in **Figures 2B,D,F** show the different metamorphic stages when the fungi had previously been grown at 37°C. Note, however, that in all cases, the 15-day exposure period of flies to VOCs was conducted at 25°C. Data are calculated as percentages of a given metamorphic stage during the *Drosophila* metamorphic cycle; thus, as numbers of larvae go down, the numbers of pupae increase. Similarly, numbers of pupae decrease when the flies eclose into adults. Some flies never eclose into adults, which reflects the percent toxicity from exposure to the VOCs (**Figures 2G,H**).

Normally, the larvae have pupated after 4 days and indeed, for control larvae, over 90% had pupated at this time. Significant delays in pupation were observed for all VOCs-exposed flies, with the most significant delays for larvae exposed to VOCs from *A. fumigatus* SRRC 46 and SRRC 1607, with fewer significant delays for larvae exposed to the VOCs released by *A. fumigatus* strains SRRC 2569 and 1592. On the 8th day, these delays were similar for fungi pre-grown at either temperature (**Figures 2C,D**). For example, nearly 38 and 56% of total flies remained in the pupal stage when exposed to VOCs emitted from *A. fumigatus* strain SRRC 1607 pre-grown at 25 and 37°C, respectively; however, only 13 and 16% were in the pupal stage for control treatments (**Figures 2C,D**).

The pupal stage usually lasts 3.5–4.5 days and then flies eclose into adults. Indeed, by the 10th day for the controls, 80–84% of the pupae had emerged as adults. However, for VOC-exposed flies, significant developmental delays were seen for the length of time spent in the pupal stage (**Figures 2E,F**). The numbers of adult flies on the 7th, 10th, and 15th days were compared and shown in **Figures 2G,H**. For strains SRRC 1607 and SRRC 46 pre-grown at 37°C, 44% had eclosed on the 10th day; only 58 and 60%, respectively, had eclosed on the 15th day; however, the larvae exposed to the VOCs released by SRRC 51 and SRRC 1592 had over 86% eclosion into adults; for strains SRRC 323 and 2569, eclosion rates were about 78% on the 15th day (**Figure 2H**). Overall, the toxic effects of *A. fumigatus* VOCs on the developmental stages of fruit flies were more significant when the fungi originally grew at 37°C than grew at 25°C. Exposure to a common atmosphere with VOCs from *A. fumigatus* strains SRRC 1607 and 46 significantly delayed the metamorphosis more than those exposed to VOCs from all the other strains (SRRC 51, 323, 2569, and 1952) which showed fewer significant differences compared to control treatments. Exposure to a common atmosphere with strain SRRC 1607 also yielded the most delays in metamorphosis and imposed the highest level of toxicity (**Figure 2**).

In order to determine if the greater toxicity seen with fungi pre-grown at 37°C was due to higher biomass, the six strains of *A. fumigatus* were measured for the dry weight cultivated at different temperatures. There were almost no differences in biomass at the two different temperatures (37 vs. 25°C) for any of the strains; however, SRRC 1607, which emitted the most toxic VOCs, had a lower biomass than the other five strains (**Supplementary Figure 1**).

Effects of VOCs Emitted From *Candida albicans*, *Cryptococcus neoformans*, *Cryptococcus gattii*, and *Saccharomyces cerevisiae*

Using the ecolosion assay to evaluate the effects of VOCs emitted from three medically important yeast strains and one *S. cerevisiae* strain, the numbers of larvae (**Figures 3A,B**), pupae (**Figures 3C,D**), and adults (**Figures 3E,F**) were counted daily for 15 days. The eclosion adult fly rates on the 7th, 10th, and 15th days are shown in **Figures 3G,H**. For sterile PDA media as the control, 85% of larvae had pupated by the 4th day and 95.5–97% of flies completed metamorphosis and eclosed by the 10th day (**Figures C,D,G,H**). For *S. cerevisiae* as a biological control, on the 10th day, the temperature of pre-incubation (25 or 37°C) was associated with no significant differences in the timing of metamorphosis and 67% of flies had eclosed into adults. On the 15th day, the eclosion adult rate was 87% for *S. cerevisiae* pre-grown at 25°C and 82% for those pre-grown at 37°C (**Figures 3G,H**). In contrast, the three medically important yeast species all emitted VOCs that caused delays in metamorphosis as well as toxicity. Delays in metamorphosis were observed for flies exposed to yeasts pre-grown at both 25 and 37°C; however, the delays were greater for larvae exposed to VOCs from yeasts pre-grown at the higher temperature. On the 4th day, 85% of controls had pupated; however, the percent pupation was 69, 61.2, 53.3, and 48.9% for those grown in a common atmosphere with VOCs emitted from *Cryptococcus gattii*, *Candida albicans*, *S. cerevisiae*, and *Cryptococcus neoformans*, respectively, pre-grown at 37°C (**Figures 3A,B**).

For *Candida albicans*, eclosion rates were 62.2 and 55.5% when exposed to VOCs from yeast cultures pre-grown at 25°C and at 37°C, respectively. For *Cryptococcus gattii*, the eclosion rates were 51.1% at both temperatures. For *C. neoformans*, the eclosion rates were 55.5 and 33.3% when exposed to VOCs from cultures pre-grown at 25°C and at 37°C, respectively. On the 15th day, for yeast strains pre-grown at 25°C, the eclosion rates were 55.7% for *Cryptococcus gattii*, and 73.3% for both *Candida albicans* and *Cryptococcus neoformans* (**Figures 3E–H**).

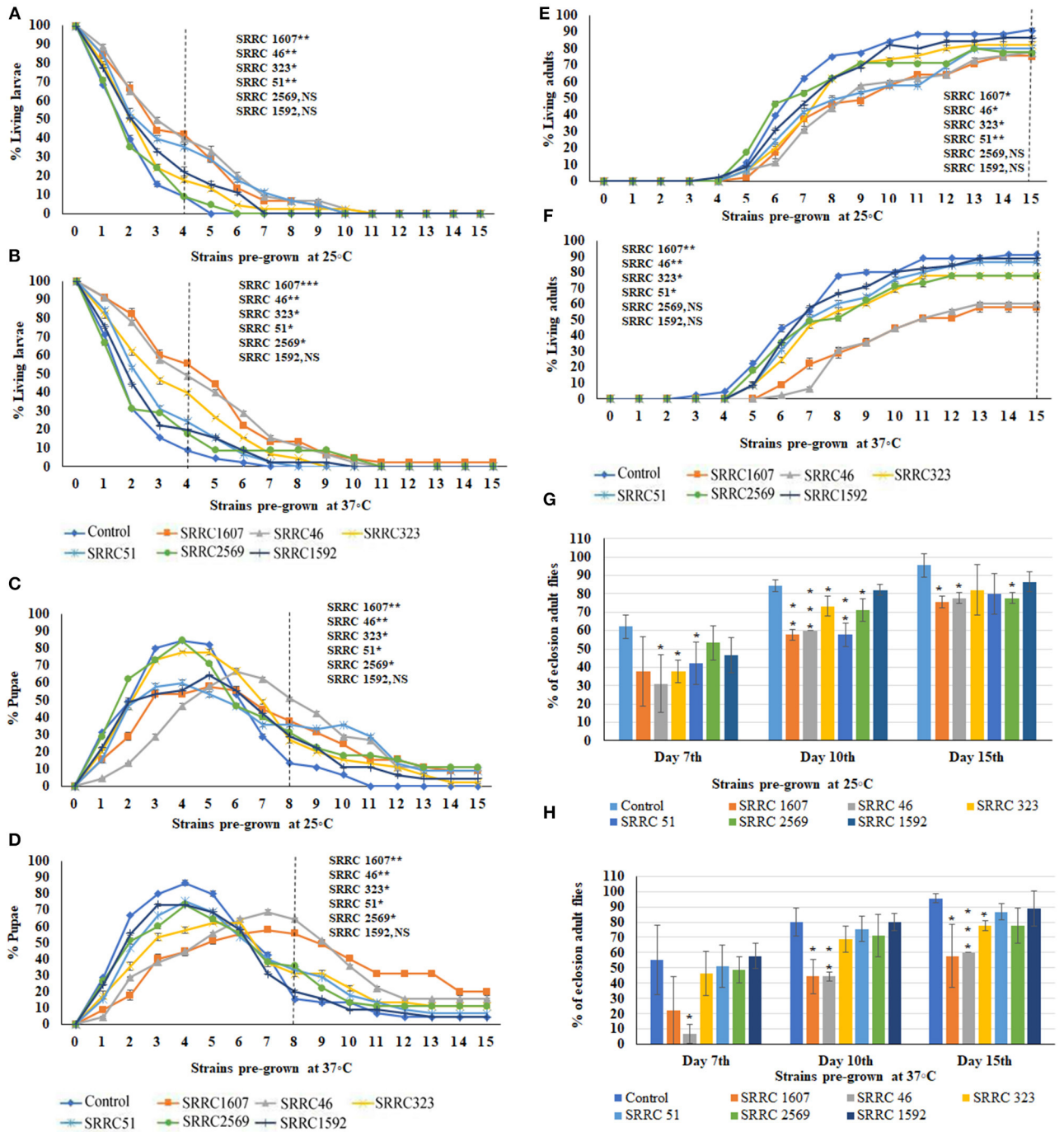

FIGURE 2 | Percent living larval, pupal, and adult stages of 15 days of continuous exposure to VOCs emitted by six strains of *A. fumigatus*. The numbers of VOC-exposed larvae were compared to controls and the statistical differences were calculated on the 4th day: **(A)** Fungi were pre-grown at 25°C, **(B)** Fungi were pre-grown at 37°C. Where *represents the significant difference between controls and *A. fumigatus* exposed flies (*$P < 0.05$, **$P < 0.005$, ***$P < 0.0005$ and NS = Non-significant). A dashed vertical line denotes the day for statistical analysis. The numbers of VOC-exposed pupae were compared to controls and the statistical differences were calculated on the 8th day: **(C)** Fungi were pre-grown at 25°C, **(D)** Fungi were pre-grown at 37°C. The numbers of VOC-exposed adults were compared to controls and the statistical differences were calculated on the 15th day: **(E)** Fungi were pre-grown at 25°C; **(F)** Fungi were pre-grown at 37°C. Comparative analysis of percent of eclosion adult flies treated by VOCs emitted from six different strains of *A. fumigatus* (N = 90) at 7th, 10th, and 15th days at either 25°C **(G)** or 37°C **(H)**.

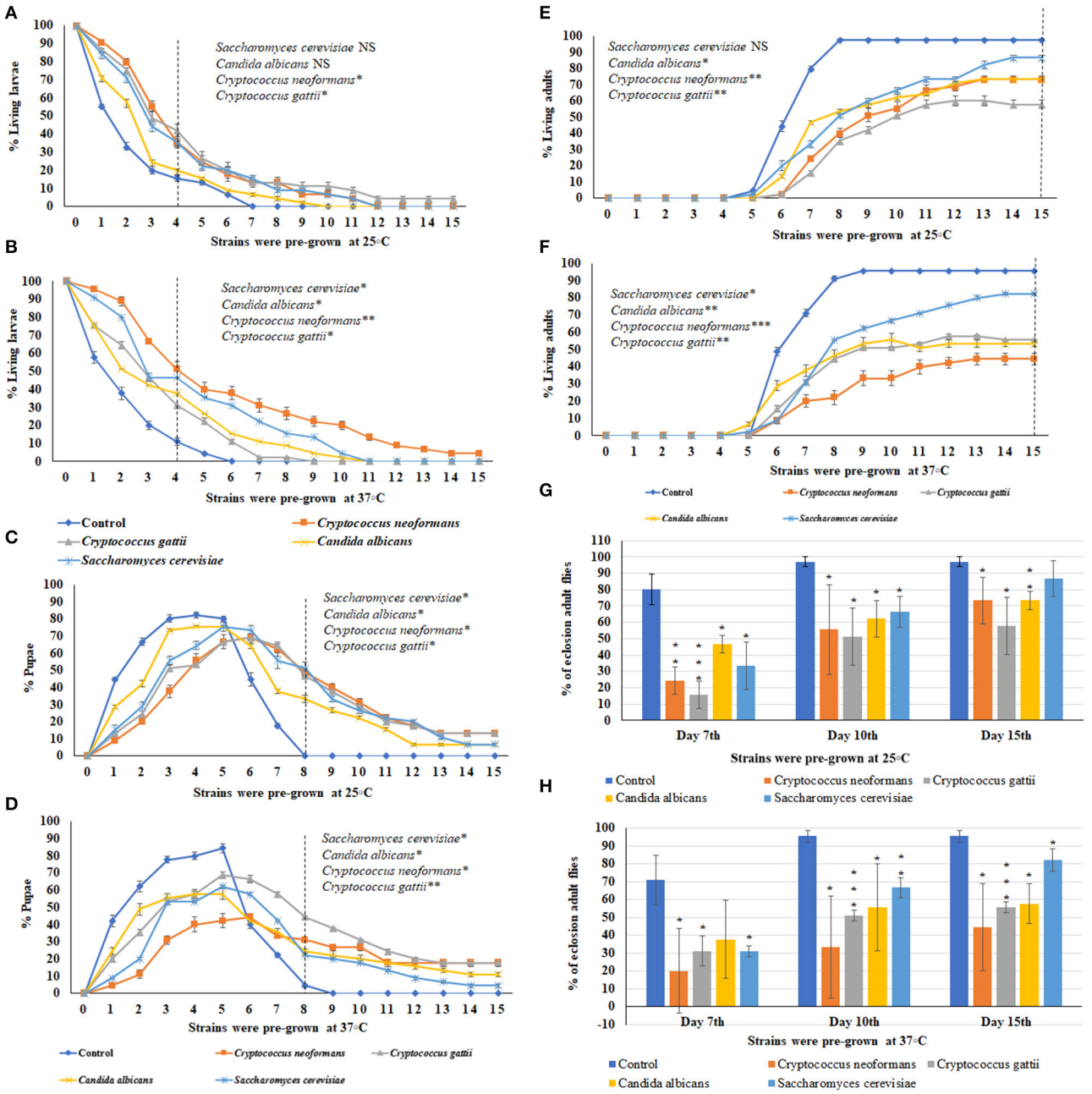

FIGURE 3 | Percent larval, pupal, and adults of 15 days of continuous exposure to VOCs emitted by three yeast species and one *S. cerevisiae* strain. The numbers of VOC-exposed larvae were compared to controls and the statistical differences were calculated on the 4th day: **(A)** different strains were pre-grown at 25°C, **(B)** different strains were pre-grown at 37°C. Where *represents the significant difference between controls and VOC-exposed flies (*$P < 0.05$, **$P < 0.005$, ***$P <$ 0.0005 and NS = Non-significant). A dashed vertical line denotes the day for statistical analysis. The numbers of VOC-exposed pupae were compared to controls and the statistical differences were calculated on the 8th day: **(C)** different strains were pre-grown at 25°C, **(D)** different strains were pre-grown at 37°C. The numbers of VOC-exposed adults were compared to controls and the statistical differences were calculated on the 15th day: **(E)** different strains were pre-grown at 25°C, (**F)** different strains were pre-grown at 37°C. Comparative analysis of percent of eclosion adult flies treated by VOCs emitted by three yeast species and one *S. cerevisiae* strain (N = 90) grown at 7th, 10th, and 15th days at either 25°C **(G)** or 37°C **(H)**.

On the 15th day for yeast strains pre-grown at 37°C, the eclosion rates were 57.7% for *Candia albicans*, 55.5% for *Cryptococcus gattii*, and 44.4% for *Cryptococcus neoformans* (**Figures 3G,H**). Overall, the flies exhibited more toxic effects and a longer delay in metamorphosis when exposed to the yeast strains pre-grown at 37°C than at 25°C.

Comparative VOCs Toxicity From Different Strains and Morphology of VOCs Exposed Flies

Comparisons among VOCs emitted from *A. fumigatus* strains and *Candida albicans*, *Cryptococcus neoformans*, *Cryptococcus gattii*, and *Saccharomyces cerevisiae* pre-grown at 37°C were performed based on the 10th and 15th days of the eclosion rates and the toxicity rankings were listed in **Table 1**. The most toxic strains are *Cryptococcus* spp. and *A. fumigatus* SRRC1607, and their eclosion rates are below 58%; the least toxic strains are *Saccharomyces cerevisiae* and *A. fumigatus* SRRC1592 and their eclosion rates reach over 82% (**Figures 2**, **3** and **Table 1**).

We also observed certain morphological abnormalities in VOC-exposed *Drosophila* larval, pupal, and adult stages compared to control treatments. Dead larvae and pupae displayed dark pigmentation. VOC-exposed adults had wing and leg abnormalities. These morphological abnormalities were more pronounced when fly developmental stages were exposed to VOCs emitted from *A. fumigatus* than with the tested yeasts (**Supplementary Figure 2**).

Purge and Trap-Thermal Desorption-GC-MS

Two strains of *A. fumigatus*, the most toxic SRRC 1607 strain and the least toxic SRRC 1592 strain, were selected for GC-MS analysis. These data were shown in **Supplementary Table 1**. Each strain had its own profile of VOCs at different temperatures. Both *A. fumigatus* strains produced 1-octen-3-ol, isopentyl alcohol, 1,3-octadeiene. *A. fumigatus* SRRC 1607 released higher amounts of different VOCs when it was pre-grown at 37°C (1978.8 ng) than at 25°C (684.5 ng). The most abundant VOC detected from both strains was 1-octen-3-ol, which was 521.4 ng (76.2%) at 25°C and 1544.7 ng (78.1%) at 37°C for the most toxigenic SRRC 1607 strain, and 164.5 ng (95.4%) at 25°C and 384 ng (61.2%) at 37°C for the least toxigenic SRRC 1592 strain (**Figure 4** and **Supplementary Table 1**). SRRC 1607 also produced high amounts of isopentyl alcohol (13.3 ng, 1.9%) and acetic acid (67.7 ng, 9.9%) at 25°C; at 37°C, it produced 231.7 ng of isopentyl alcohol (11.7%) and 39.8 ng of 1,3-octadeiene (2.0%). Similarly, SRRC 1592 also produced high amounts of isopentyl alcohol (33.8 ng, 5.4%) and 1-butanol (26.4 ng, 4.2%); moreover, it produced more different VOCs including diacetyl, 7-oxabicyclo.heptane, 3-oxiranly, trans-2-undecenal, decanoic acid, lauric acid, and myristic acid (**Figure 4** and **Supplementary Table 1**).

DISCUSSION

Filamentous fungi do not normally produce infections in healthy people and of the many species of known fungi, only a few cause diseases in humans and other animals. However, when patients are immunocompromised, opportunistic species including *A. fumigatus*, *Candida albicans*, *Cryptococcus gattii*, and *Cryptococcus neoformans* can cause infections. Modern medical practice has increased the number of immunocompromised patients and, concomitantly, fungal diseases such as invasive aspergillosis, invasive candidiasis, and cryptococcosis have become a more important cause of human mortality (Chamilos et al., 2007; Latgé and Steinbach, 2009; Casadevall, 2018; Almeida et al., 2019). Here, we hypothesized that the VOCs emitted by medically important fungi might be contributing to the virulence of opportunistic fungal infections and used a *Drosophila* model to test our hypothesis.

Past research with *Drosophila* models in medical mycology has utilized toll deficient mutant flies and infection by direct contact between the fungal pathogens and the flies (Alarco et al., 2004; Apidianakis et al., 2004; Chamilos et al., 2007; Hamilos et al., 2012; Lionakis and Kontoyiannis, 2012). In our studies, we used an eclosion assay. We placed third instar larvae from a white-eyed *Drosophila* strain with a wild-type immune system into a shared atmosphere with fungi that had been pre-grown at either 25 or 37°C such that there was no physical contact between the fungi and the flies. The numbers of larva, pupa, and adult flies were counted over 15 days of exposure to VOCs from six strains of *A. fumigatus*, and the pathogenic yeasts *Cryptococcus neoformans*, *Cryptococcus gattii*, and *Candida albicans*. The non-pathogenic yeast *S. cerevisiae* served as a biological control. In the eclosion assay, larvae exposed to VOCs from *S. cerevisiae* showed some delays in metamorphosis, but after 15 days, 82–87% of the flies nevertheless had eclosed into adults. In contrast, exposure to fungal VOCs from human pathogens delayed the time it took larvae to encapsulate into pupae, and then once at the pupal stage, delayed the time it took for pupae to eclose into adult flies. These effects were more pronounced when the fungal strains were pre-grown at 37°C, the temperature at which human infections occur, than when pre-grown at 25°C. For the *Aspergillus* strains, strain SRRC 1607 pre-grown at 37°C caused the greatest developmental delays, as well as displaying the highest mortality rate compared to the other *Aspergillus* strains. In a preliminary report using the *Drosophila* eclosion assay, we found similar toxicity of *A. fumigatus* strain SRRC 1607 VOCs to *Drosophila* larvae and hypothesized that volatiles might serve as virulence factors in aspergillosis (Al-Maliki et al., 2017). Furthermore, in previous research using a somewhat different version of this bioassay, we have showed that VOCs emitted by fungi isolated after hurricane events, and by chemical standards of 1-octen-3-ol and other eight carbon volatiles, caused toxicity and death in *Drosophila* larvae and adults (Inamdar et al., 2013; Inamdar and Bennett, 2014; Yin et al., 2015; Zhao et al., 2017). When several oxylipin volatiles were tested for their effects on *Drosophila* metamorphosis, body color of larvae and pupae became darker in the presence of 1-octen-3-ol and adult flies had abnormal wings (Yin et al., 2015). Here, similar morphological changes were observed when fly larvae were exposed to VOCs emitted by growing *A. fumigatus* cultures but not by exposure to VOCs emitted by the yeast species tested.

GC-MS analysis on the VOCs produced by the most toxic and the least toxic *A. fumigatus* strains was performed. Each strain produced a different VOCs signature; however, the single most abundant VOC detected was 1-octen-3-ol (**Figure 4** and **Supplementary Table 1**). Other abundant compounds emitted by *A. fumigatus* strains pre-grown at 37°C included 2-butanone +diacetyl, 1,3-octadeiene, 2-octen-1-ol, isopentyl alcohol, and

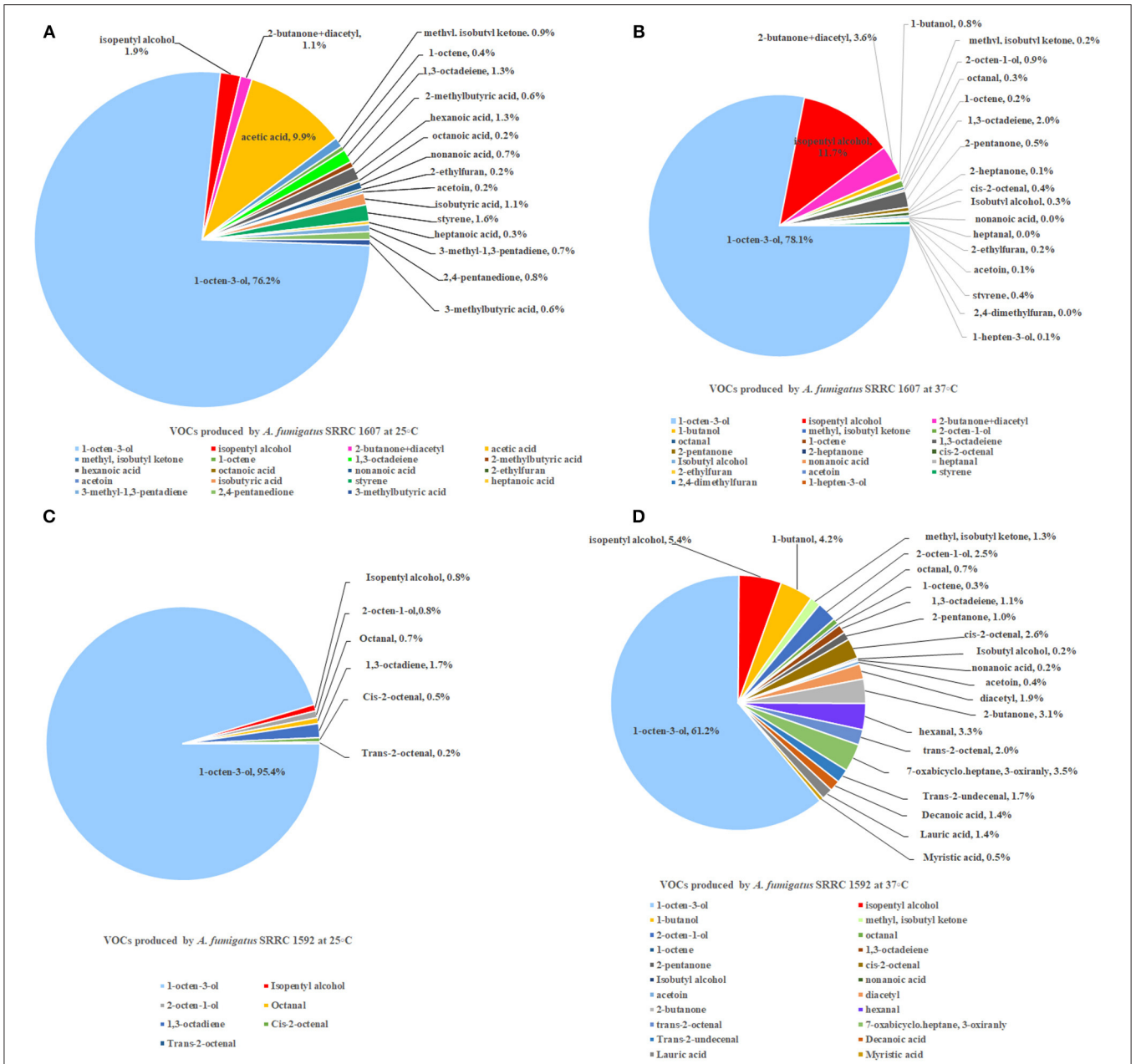

FIGURE 4 | GC-MS analyses of VOCs from *A. fumigatus* strains SRRC 1607 and 1592. **(A)** VOCs emitted by SRRC 1607 cultivated for 5 day at 25°C. **(B)** VOCs emitted by SRRC 1607 cultivated for 3 day at 37°C. **(C)** VOCs emitted by SRRC 1592 cultivated for 5 day at 25°C. **(D)** VOCs emitted by SRRC 1592 cultivated for 3 days at 37°C.

isobutyl alcohol. Many previous studies on the composition of fungal VOC mixtures show that 1-octen-3-ol is usually the single most abundant VOCs produced by molds and mushrooms (Combet et al., 2006). Moreover, in the past research, 1-octen-3-ol has been associated with numerous interspecific physiological effects. For example, in a study of filamentous fungi isolated after Hurricane Sandy, *Aspergillus niger* was the single most toxic mold. By solid-phase micro extraction-gas chromatography-mass spectrometry (SPME) analysis, high concentrations of 1-octen-3-ol were also found from this strain (Zhao et al., 2017). This aliphatic eight carbon alcohol is a degradation product of linoleic acid and is known to inhibit spore germination and growth in several fungal species (Chitarra et al., 2005; Combet et al., 2006; Noble et al., 2009; Herrero-Garcia et al., 2011; Berendsen et al., 2013). In animal systems, it is the natural ligand of bovine odorant-binding protein (Ramoni et al., 2001) and there is evidence that it is highly neurotoxic in human tissue culture lines as well as the cause of movement

disorders in fruit flies (Inamdar et al., 2013). Furthermore, in human embryonic stem cells, 1-octen-3-ol is eighty times more toxic than toluene (Inamdar et al., 2012). When tested for fumigant properties, chemical standards of 1-octen-3-ol limit colony growth in *Saccharomyces cerevisiae* (Morath et al., 2017) and in *Pseudogymnoascus destructans,* the causative agent of white nose syndrome, it also inhibits mycelial growth (Padhi et al., 2017). In a transcriptome study on the effect of 1-octen-3-ol on *Penicillium chrysogenum*, genes for transporters and other membrane constituents were enriched, indicating that 1-octen-3-ol may be involved in membrane trafficking in fungi (Yin et al., 2019). Moreover, in recent work using a *Drosophila* model, Macedo et al. showed that mitochondria were a crucial target of 1-octen-3-ol toxicity, and caused alterations in levels of antioxidant enzymes, electron transport chain inhibition and apoptosis (Macedo et al., 2020). Using the yeast *Saccharomyces cerevisiae* as a host, a research group cloned the cDNA genes of lipoxygenase and hydroperoxide lyase from *Tricholoma matsutake* and biosynthesized (R)-(-)-1-octen-3-ol (Lee et al., 2020).

It is generally believed that pathogenic fungi possess virulence factors that allow them to grow in animals and cause diseases. Current known virulence factors include the ability to grow at 37°C, the capacity to evade host defenses, and the production of various toxins, adhesion factors or other metabolites that can cause host damages (Calderone and Clancy, 2011; Brunke et al., 2016). We suggest that VOCs emitted by pathogenic species of fungi may also serve as virulence factors. Scientists who study "sick building syndrome" have shown that there is a possible association between the presence of fungal VOCs and individuals who experience negative health effects when exposed to damp and moldy indoor environments (Mølhave, 2009). Toxicity depends on the chemical nature of the VOC and the level and length of exposures (Morath et al., 2012; Bennett and Inamdar, 2015). In one Brazilian study, colonies of *A. fumigatus*, *C. albicans*, *C. neoformans*, and *C. gattii* could be sub-cultivated from hospital air. When VOCs were assayed from this air, 1-pentanol, 1-octen-3-ol, 3-methyl-1-butanol, 3-octanol and 2-methyl-1-butanol were found in low concentrations while 2-heptanone and 2-methyl-1-propanol were present in high concentrations (Pantoja et al., 2016). In our study, *Cryptococcus* spp showed higher toxicity than *A. fumigatus* strain SRRC 1607 while the latter imposed more pronounced wing and leg abnormalities in flies than the former. The VOCs from *Cryptococcus* spp and the underlying mechanism that caused the differences will be investigated in our future experiments.

In summary, the data reported here demonstrate that in a *Drosophila* toxicity test, the VOCs emitted by growing cultures of *A. fumigatus*, *Candida albicans*, *Cryptococcus gattii*, and *Cryptococcus neoformans* cause significant delays in metamorphosis, along with significant lethality. In future research, it will be essential to determine which individual compounds such as 1-octen-3-ol, isopentyl alcohol, 1-butanol, in the VOC mixtures are causing the toxic effects and are therefore related to pathogenicity. VOCs from human pathogenic fungi, especially 1-octen-3-ol, may be previously unrecognized virulence factors that enhance the ability of these fungi to cause human disease. The *Drosophila* eclosion model provides a powerful reductionist method for studying the impact of fungal VOCs not only with respect to indoor air contamination, but also for shedding new light on factors that may enhance fungal pathogenesis and contribute to the differential virulence of medically important fungi. In future research, it will be important to analyze the VOCs emitted by pathogenic and non-pathogenic yeasts, as well as to use mammalian models to corroborate these data about the negative impact of fungal volatile compounds in certain fungal-animal interactions.

DATA AVAILABILITY STATEMENT

The original contributions presented in the study are included in the article/**Supplementary Material**, further inquiries can be directed to the corresponding author/s.

AUTHOR CONTRIBUTIONS

HA drafted the manuscript. AA and NG helped do some of the experiments. HA, GY, and JB discussed and revised the whole manuscript. All authors contributed to the article and approved the submitted version.

FUNDING

This work was funded by a scholarship and stipend to HA by the Higher Committee for Education Development in Iraq (HCED) for a graduate fellowship. Partial funding came from a USDA-ARS Cooperative Agreement (58-2030-6-053).

ACKNOWLEDGMENTS

We thank Dr. Moore for providing the isolates of *A. fumigatus* and Emina Drazanin for her technical help. Dr. Arati Inamdar developed an earlier *Drosophila* bioassay from which our protocol was developed and Dr. Sunita Kramer gave us helpful advice about maintaining our fly colonies. Drs. Sally Padhi and Kayla Pennerman provided insights about the toxigenic effects of biogenic volatile compounds. We thank Dr. Chaoyang Xue from the Public Health Research Institute Center, New Jersey Medical School-Rutgers, Newark, NJ, USA, who provided us with cultures of *Saccharomyces cerevisiae* (BY4741), *Cryptococcus neoformans* (H99 serotype A), *Cryptococcus gattii* wild type (R265), and *Candida albicans* wild-type (ATCC 90028). We also gratefully acknowledge a travel grant that was awarded to HA by the Medical Mycological Society of the America to present this work at the annual meeting of the American Society for Microbiology (Microbe) in San Francisco, California in 2019.

SUPPLEMENTARY MATERIAL

The Supplementary Material for this article can be found online at: https://www.frontiersin.org/articles/10.3389/ffunb.2020.629510/full#supplementary-material

Supplementary Figure 1 | Dry weights of six *A. fumigatus* strains grown on potato dextrose broth at 25°C for 5 days or at 37°C for 3 days. There were no

significant differences in dry weights between pairs of individual strains grown at the different temperatures; however, there was a significant difference in amount of growth between *A. fumigatus* strain SRRC 1607 and the other five strains ($^*P < 0.05$).

Supplementary Figure 2 | The morphological effects of *Drosophila* exposed to VOCs from different strains. **(A)** larvae exposed to VOCs from control treatment for 4 days. **(B)** larvae exposed to VOCs from *Candida albicans* and *Cryptococcus* spp for 4 days. **(C)** larvae exposed VOCs from *A. fumigatus* strains for 10 days. **(D)** pupae exposed to VOCs from control treatments for 15 days. **(E)** pupae exposed to VOCs from *Candida albicans* and *Cryptococcus* spp for 15 days. **(F)** pupae exposed to VOCs from *A. fumigatus* strains for 15 days. **(G)** flies exposed to VOCs from control treatments for 15 days. **(H)** flies exposed to VOCs from *Candida albicans* and *Cryptococcus* spp for 15 days **(I)** flies exposed to VOCs from *A. fumigatus* strains for 15 days. The red arrows highlight the morphological abnormalities of larvae, pupae, and adults affected by VOCs from *A. fumigatus* strains.

Supplementary Table 1 | Major VOCs produced by two *A. fumigatus* strains (SRRC 1607 and 1592) grown at either 25 or 37°C.

REFERENCES

Agarwal, R. (2009). Allergic bronchopulmonary aspergillosis. *Chest* 135, 805–826. doi: 10.1378/chest.08-2586

Alarco, A. M., Marcil, A., Chen, J., Suter, B., Thomas, D., and Whiteway, M. (2004). Immune-deficient *Drosophila melanogaster*: a model for the innate immune response to human fungal pathogens. *J. Immunol.* 172, 5622–5628. doi: 10.4049/jimmunol.172.9.5622

Al-Maliki, H. S., Martinez, S., Piszczatowski, P., and Bennett, J. W. (2017). *Drosophila melanogaster* as a model for studying *Aspergillus fumigatus*. *Mycobiology* 45, 233–239. doi: 10.5941/MYCO.2017.45.4.233

Almeida, F., Rodrigues, M. L., and Coelho, C. (2019). The still underestimated problem of fungal diseases worldwide. *Front. Microbiol.* 10:214. doi: 10.3389/fmicb.2019.00214

Apidianakis, Y., Rahme, L. G., Heitman, J., Ausubel, F. M., Calderwood, S. B., and Mylonakis, E. (2004). Challenge of *Drosophila melanogaster* with *Cryptococcus neoformans* and role of the innate immune response. *Eukaryotic Cell* 3, 413–419. doi: 10.1128/EC.3.2.413-419.2004

Araki, A., Kanazawa, A., Kawai, T., Eitaki, Y., Morimoto, K., Nakayama, K., et al. (2012). The relationship between exposure to microbial volatile organic compound and allergy prevalence in single-family homes. *Sci. Total Environ.* 423, 18–26. doi: 10.1016/j.scitotenv.2012.02.026

Araki, A., Kawai, T., Eitaki, Y., Kanazawa, A., Morimoto, K., Nakayama, K., et al. (2010). Relationship between selected indoor volatile organic compounds, so-called microbial VOC, and the prevalence of mucous membrane symptoms in single family homes. *Sci. Total Environ.* 408, 2208–2215. doi: 10.1016/j.scitotenv.2010.02.012

Bennett, J. W., and Inamdar, A. A. (2015). Are some fungal volatile organic compounds (VOCs) mycotoxins? *Toxins* 7, 3785–3804. doi: 10.3390/toxins7093785

Berendsen, R. L., Kalkhove, S. I., Lugones, L. G., Baars, J. J., Wösten, H. A., and Bakker, P. A. (2013). Effects of the mushroom-volatile 1-octen-3-ol on dry bubble disease. *Appl. Microbiol. Biotechnol.* 97, 5535–5543. doi: 10.1007/s00253-013-4793-1

Brunke, S., Mogavero, S., Kasper, L., and Hube, B. (2016). Virulence factors in fungal pathogens of man. *Curr. Opin. Microbiol.* 32, 89–95. doi: 10.1016/j.mib.2016.05.010

Cabral, J. P. (2010). Can we use indoor fungi as bioindicators of indoor air quality? Historical perspectives and open questions. *Sci. Total Environ.* 408, 4285–4295. doi: 10.1016/j.scitotenv.2010.07.005

Calderone, R. A., and Clancy, C. J. (2011). *Candida and Candidiasis*. Washington, DC:American Society for Microbiology Press. doi: 10.1128/9781555817176

Casadevall, A. (2018). Fungal diseases in the 21st century: the near and far horizons. *Pathog. Immun.* 3:183. doi: 10.20411/pai.v3i2.249

Chamilos, G., Lionakis, M. S., Lewis, R. E., and Kontoyiannis, D. P. (2007). Role of mini-host models in the study of medically important fungi. *Lancet Infect. Dis.* 7, 42–55. doi: 10.1016/S1473-3099(06)70686-7

Chitarra, G. S., Abee, T., Rombouts, F. M., and Dijksterhuis, J. (2005). 1-Octen-3-ol inhibits conidia germination of *Penicillium paneum* despite of mild effects on membrane permeability, respiration, intracellular pH, and changes the protein composition. *FEMS Microbiol. Ecol.* 54, 67–75. doi: 10.1016/j.femsec.2005.02.013

Combet, E., Henderson, J., Eastwood, D. C., and Burton, K. S. (2006). Eight-carbon volatiles in mushrooms and fungi: properties, analysis, and biosynthesis. *Mycoscience* 47, 317–326. doi: 10.1007/S10267-006-0318-4

Gao, P. F., Korley, F., Martin, J., and Chen, B. T. (2002). Determination of unique microbial volatile organic compounds produced by five *Aspergillus* species commonly found in problem buildings. *AIHAJ* 63, 135–140. doi: 10.1080/15428110208984696

Hamilos, G., Samonis, G., and Kontoyiannis, D. P. (2012). Recent advances in the use of *Drosophila melanogaster* as a model to study immunopathogenesis of medically important filamentous fungi. *Int. J. Microbiol.* 2012:583792. doi: 10.1155/2012/583792

Heddergott, C., Calvo, A., and Latgé, J. (2014). The volatome of *Aspergillus fumigatus*. *Eukaryotic Cell* 13, 1014–1025. doi: 10.1128/EC.00074-14

Herr, C. E., Zur Nieden, A., Bodeker, R. H., Gieler, U., and Eikmann, T. F. (2003). Ranking and frequency of somatic symptoms in residents near composting sites with odor annoyance. *Int. J. Hyg. Environ. Health* 206, 61–64. doi: 10.1078/1438-4639-00182

Herrero-Garcia, E., Garzia, A., Cordobés, S., Espeso, E. A., and Ugalde, U. (2011). 8-carbon oxylipins inhibit germination and growth, and stimulate aerial conidiation in *Aspergillus nidulans*. *Fungal Biol.* 115, 393–400. doi: 10.1016/j.funbio.2011.02.005

Herrmann, A. (2010). Volatiles–an interdisciplinary approach. *Chem. Biol. Volatiles* 1–10. doi: 10.1002/9780470669532.ch1

Heseltine, E., and Rosen, J. (2009). *WHO Guidelines for Indoor Air Quality: Dampness and Mould*. Copenhagen:WHO Regional Office Europe.

Hodgson, M. (1999). Sick building syndrome. *Occup. Med.* 15, 571–585.

Hosseini, M. R., Fouladi-Fard, R., and Aali, R. (2020). COVID-19 pandemic and sick building syndrome. *Indoor Built Environ.* 29, 1181–1183. doi: 10.1177/1420326X20935644

Hung, R., Lee, S., and Bennett, J. W. (2013). *Arabidopsis thaliana* as a model system for testing the effect of *Trichoderma* volatile organic compounds. *Fungal Ecol.* 6, 19–26. doi: 10.1016/j.funeco.2012.09.005

Hung, R., Lee, S., and Bennett, J. W. (2015). Fungal volatile organic compounds and their role in ecosystems. *Appl. Microbiol. Biotechnol.* 99, 3395–3405. doi: 10.1007/s00253-015-6494-4

Inamdar, A. A., and Bennett, J. W. (2014). A common fungal volatile organic compound induces a nitric oxide mediated inflammatory response in *Drosophila melanogaster*. *Sci. Rep.* 4:3833. doi: 10.1038/srep03833

Inamdar, A. A., and Bennett, J. W. (2015). Volatile organic compounds from fungi isolated after hurricane Katrina induce developmental defects and apoptosis in a *Drosophila melanogaster* model. *Environ. Toxicol.* 30, 614–620. doi: 10.1002/tox.21933

Inamdar, A. A., Hossain, M. M., Bernstein, A. I., Miller, G. W., Richardson, J. R., and Bennett, J. W. (2013). Fungal-derived semiochemical 1-octen-3-ol disrupts dopamine packaging and causes neurodegeneration. *Proc. Natl. Acad. Sci. U.S.A.* 110, 19561–19566. doi: 10.1073/pnas.1318830110

Inamdar, A. A., Moore, J. C., Cohen, R. I., and Bennett, J. W. (2012). A model to evaluate the cytotoxicity of the fungal volatile organic compound 1-octen-3-ol in human embryonic stem cells. *Mycopathologia* 173, 13–20. doi: 10.1007/s11046-011-9457-z

Korpi, A., Jarnberg, J., and Pasanen, A. L. (2009). Microbial volatile organic compounds. *Crit. Rev. Toxicol.* 39, 139–193. doi: 10.1080/10408440802291497

Latgé, J. P., and Steinbach, W. J. (2009). *Aspergillus fumigatus and Aspergillosis*. Washington, DC: ASM Press, 568.

Lee, N.-Y., Choi, D.-H., Kim, M.-G., Jeong, M.-J., Kwon, H.-J., Kim, D.-H., et al. (2020). Biosynthesis of (R)-(-)-1-Octen-3-ol in recombinant *Saccharomyces cerevisiae* with lipoxygenase-1 and hydroperoxide lyase genes from *Tricholoma matsutake*. *J. Microbiol. Biotechnol.* 30, 296–305. doi: 10.4014/jmb.2001.01049

Licht, J.-C., and Grasemann, H. (2020). Potential of the electronic nose for the detection of respiratory diseases with and without infection. *Int. J. Mol. Sci.* 21:9416. doi: 10.3390/ijms21249416

Lionakis, M. S., and Kontoyiannis, D. P. (2012). *Drosophila melanogaster* as a model organism for invasive aspergillosis. *Methods Mol. Boil.* 845, 455–468. doi: 10.1007/978-1-61779-539-8_32

Macedo, G. E., de Brum Vieira, P., Rodrigues, N. R., Gomes, K. K., Martins, I. K., Franco, J. L., et al. (2020). Fungal compound 1-octen-3-ol induces mitochondrial morphological alterations and respiration dysfunctions in *Drosophila melanogaster*. *Ecotoxicol. Environ. Saf.* 206:111232. doi: 10.1016/j.ecoenv.2020.111232

Martínez, R. A. S., Hernández, J. M. P., Torrado, Ó. Y., Díaz, M. C., de Diego Puente, T., Vinaixa Crevillent, M., et al. (2020). Exhaled volatile organic compounds analysis in clinical pediatrics: a systematic review. *Pediatr. Res.* 1–12. doi: 10.1038/s41390-020-01116-8

Mølhave, L. (2009). "Volatile organic compounds and sick building syndrome: Chapter 8" in *Environmental Toxicants, Human Exposures and Their Health Effects*, ed M. Lippmann (Hoboken, NJ:John Wiley & Sons Ltd), 241–256.

Mølhave, L., Liu, Z., Jørgensen, A. H., Pedersen, O. F., and Kjægaard, S. K. (1993). Sensory and physiological effects on humans of combined exposures to air temperatures and volatile organic compounds. *Indoor Air* 3, 155–169. doi: 10.1111/j.1600-0668.1993.t01-1-00002.x

Morath, S. U., Boland, C. E., and Bennett, J. W. (2017). *Saccharomyces cerevisiae* as a model for screening the effects of volatile organic compounds. *Curr. Biotechnol.* 6, 245–251. doi: 10.2174/2211550105666160530104622

Morath, S. U., Hung, R., and Bennett, J. W. (2012). Fungal volatile organic compounds: a review with emphasis on their biotechnological potential. *Fungal Biol. Rev.* 26, 73–83. doi: 10.1016/j.fbr.2012.07.001

Noble, R., Dobrovin-Pennington, A., Hobbs, P. J., Pederby, J., and Rodger, A. (2009). Volatile C8 compounds and pseudomonads influence primordium formation of *Agaricus bisporus*. *Mycologia* 101, 583–591. doi: 10.3852/07-194

Padhi, S., Dias, I., and Bennett, J. W. (2017). Two volatile-phase alcohols inhibit growth of *Pseudogymnoascus destructans*, causative agent of white-nose syndrome in bats. *Mycology* 8, 11–16. doi: 10.1080/21501203.2016.1269843

Pantoja, L. D. M., Do Nascimento, R. F., and Nunes, A. B. D. (2016). Investigation of fungal volatile organic compounds in hospital air. *Atmos. Pollut. Res.* 7, 659–663. doi: 10.1016/j.apr.2016.02.011

Pennerman, K., Al-Maliki, H., Lee, S., and Bennett, J. (2016). "Fungal volatile organic compounds (VOCs) and the genus *Aspergillus*," in *New and Future Developments in Microbial Biotechnology and Bioengineering*, (ed) V. Gupta (Chennai:Elsevier), 95–115. doi: 10.1016/B978-0-444-63505-1.00007-5

Perl, T., Junger, M., Vautz, W., Nolte, J., Kuhns, M., Zepelin, M. B. V., et al. (2011). Detection of characteristic metabolites of *Aspergillus fumigatus* and *Candida* species using ion mobility spectrometry-metabolic profiling by volatile organic compounds. *Mycoses* 54, E828–E837. doi: 10.1111/j.1439-0507.2011.02037.x

Polizzi, V., Delmulle, B., Adams, A., Moretti, A., Susca, A., Picco, A. M., et al. (2009). JEM Spotlight: Fungi, mycotoxins and microbial volatile organic compounds in mouldy interiors from water-damaged buildings. *J. Environ. Monit.* 11, 1849–1858. doi: 10.1039/b906856b

Ramoni, R., Vincent, F., Grolli, S., Conti, V., Malosse, C., Boyer, F.-D., et al. (2001). The insect attractant 1-octen-3-ol is the natural ligand of bovine odorant-binding protein. *J. Biol. Chem.* 276, 7150–7155. doi: 10.1074/jbc.M010368200

Rand, M. D., Montgomery, S. L., Prince, L., and Vorojeikina, D. (2014). Developmental toxicity assays using the *Drosophila* model. *Curr. Protoc. Toxicol.* 59, 1.12. 11–11.12.20. doi: 10.1002/0471140856.tx0112s59

Schwab, C. J., and Straus, D. C. (2004). The roles of *Penicillium* and *Aspergillus* in sick building syndrome. *Adv. Appl. Microbiol.* 55, 215–240. doi: 10.1016/S0065-2164(04)55008-6

Scotter, J. M., Langford, V. S., Wilson, P. F., Mcewan, M. J., and Chambers, S. T. (2005). Real-time detection of common microbial volatile organic compounds from medically important fungi by selected ion flow tube-mass spectrometry (SIFT-MS). *J. Microbiol. Methods* 63, 127–134. doi: 10.1016/j.mimet.2005.02.022

Singh, K., Nizam, S., Sinha, M., and Verma, P. K. (2012). Comparative transcriptome analysis of the necrotrophic fungus *Ascochyta rabiei* during oxidative stress: insight for fungal survival in the host plant. *PLoS ONE* 7:e33128. doi: 10.1371/journal.pone.0033128

Takigawa, T., Wang, B. L., Sakano, N., Wang, D. H., Ogino, K., and Kishi, R. (2009). A longitudinal study of environmental risk factors for subjective symptoms associated with sick building syndrome in new dwellings. *Sci. Total Environ.* 407, 5223–5228. doi: 10.1016/j.scitotenv.2009.06.023

Yin, G., Padhi, S., Lee, S., Hung, R., Zhao, G., and Bennett, J. W. (2015). Effects of three volatile oxylipins on colony development in two species of fungi and on *Drosophila* larval metamorphosis. *Curr. Microbiol.* 71, 347–356. doi: 10.1007/s00284-015-0864-0

Yin, G., Zhang, Y., Fu, M., Hua, S. S. T., Huang, Q., Pennerman, K. K., et al. (2019). Influence of R and S enantiomers of 1-octen-3-ol on gene expression of *Penicillium chrysogenum*. *J. Ind. Microbiol. Biotechnol.* 46, 977–991. doi: 10.1007/s10295-019-02168-4

Zhao, G., Yin, G., Inamdar, A. A., Luo, J., Zhang, N., Yang, I., et al. (2017). Volatile organic compounds emitted by filamentous fungi isolated from flooded homes after Hurricane Sandy show toxicity in a *Drosophila* bioassay. *Indoor Air* 27, 518–528. doi: 10.1111/ina.12350

Zuo, C., Luo, L., and Liu, W. (2020). Effects of increased humidity on physiological responses, thermal comfort, perceived air quality, and sick building syndrome symptoms at elevated indoor temperatures for subjects in a hot-humid climate. *Indoor Air.* 1–17. doi: 10.1111/ina.12739

Conflict of Interest: The authors declare that the research was conducted in the absence of any commercial or financial relationships that could be construed as a potential conflict of interest.

Advantages of publishing in Frontiers

OPEN ACCESS
Articles are free to read for greatest visibility and readership

FAST PUBLICATION
Around 90 days from submission to decision

HIGH QUALITY PEER-REVIEW
Rigorous, collaborative, and constructive peer-review

TRANSPARENT PEER-REVIEW
Editors and reviewers acknowledged by name on published articles

Frontiers
Avenue du Tribunal-Fédéral 34
1005 Lausanne | Switzerland

Visit us: www.frontiersin.org
Contact us: frontiersin.org/about/contact

REPRODUCIBILITY OF RESEARCH
Support open data and methods to enhance research reproducibility

DIGITAL PUBLISHING
Articles designed for optimal readership across devices

FOLLOW US
@frontiersin

IMPACT METRICS
Advanced article metrics track visibility across digital media

EXTENSIVE PROMOTION
Marketing and promotion of impactful research

LOOP RESEARCH NETWORK
Our network increases your article's readership